CONTEMPORARY PROBLEMS OF POWER ENGINEERING AND ENVIRONMENTAL PROTECTION

EDITORS :
KRZYSZTOF PIKOŃ
MAGDALENA BOGACKA

Silesian University of Technology

Edited by Krzysztof Pikoń and Magdalena Bogacka

CONTEMPORARY PROBLEMS OF POWER ENGINEERING AND ENVIRONMENTAL PROTECTION 2020

Gliwice, 2021

Scientific Editors: Krzysztof Pikoń, Magdalena Bogacka

Technical Editors: Mohamad Kasem, Abdulkarim Mira, Ahmed Saber

Cover design: Kamila Tukenova

List of Reviewers:

PhD Eng. Magdalena Bogacka
Prof. PhD Eng. Zbigniew Malinowski
Prof. PhD Eng. Adam Szurlej
Prof. PhD Eng. Małgorzata Wilk
Prof. PhD Leszek Czepirski
PhD Wafaa Saleh
Prof. PhD Eng. Andrzej Szlęk
PhD Eng. Grzegorz Jodłowski
PhD Eng. Sebastian Werle
PhD Rui Pedro da Costa Neto
PhD Diana C Martinez C
PhD Tomasz Szulc
PhD Piotr Noga
Prof. Teresa Grzybek
Prof. PhD Anna Grobelak
PhD Eng. Grzegorz S. Jodłowski
Prof. PhD Eng. Mariusz Dudziak
Prof. PhD Eng. Katarzyna Szymańska,
PhD Shelemei Oksana Petrivna
Prof. PhD Eng. Jacek Kalina
PhD Eng. Wojciech Adamczyk
PhD Eng. Waldemar Ścierski
PhD Eng. Katarzyna Kowalska
PhD Eng. Zbigniew Buliński
PhD Eng. Dominika Wrońska-Wałach

ISBN 978-83-950087-9-5

Published by Department of Technologies and Installations for Waste Management,

Silesian University of Technology

Available online: waste.polsl.pl

Copyright Notice

Contemporary Problems of Power Engineering and Environmental Protection

The technological advancement, industrial developments, development of the civilizations, and the increase in population lead to the higher demand for energy and power globally from different sources of fossil fuel and renewables. Governments focus on energy developments and efficiency due to the restrictions on environmental aspects from emissions as greenhouse gases and consumption of natural resources. On the other hand, renewable energy is becoming more popular, advanced, and acceptable by societies due to its low emission to the environment. furthermore, improvements in energy efficiency, clean energy alternatives, and new technological processes have taken the attention of research topics to lower the impacts on the environment. This book has a collection of a variety of topics in the fields related to Environmental Protection and Energy, been devoted by young scientists and students to make our world brighter and cleaner.

The monograph "Contemporary Problems of Power Engineering and Environmental Protection" is the eight-volume of its scientific edition. This monograph consists of scientific articles written by students, scholars, and young scientists from different fields of studies and different countries, where all these topics were presented during the 8th edition of the Environmental Protection and Energy Conference. The conference was devoted to three categories environment, energetics, and technological advances. Under these categories, plentiful topics arise as industrial and bio-waste, recycling and materials, waste management, renewables, bio-energy, industrial progression, air and water protection, and computer-aided engineering in technological advances. The conference took place through the Zoom platform and Facebook online streaming on the 11th of December 2020 operated by the Silesian University of Technology, Gliwice, Poland. The challenge was tremendous to held an online conference, where previously was operated on-site at Silesian University Campus in former editions. An experience that will not be forgotten, and proves the conscientiousness and persistence of students, academic staff, and all organizers.

The conference was an excellent occasion to share knowledge and innovative ideas of student and scientists who wants to make difference in the sector of energy and environment and make the world a better place to live. Moreover, the event was completely organized by students of the Silesian University of Technology as a part of the Project Management course to emphasize the idea of "learning by doing".

Master's in Energy Transition objective to prepare students to lead the implementations of energy systems and circular economy strategies to shape the future of clean energy resources and sustainable economy. The program is perfectly structured starting from conventional generation and bio-fuels through smart grids and renewables. Alongside with engineering and business management courses.

We are proud of the achievement of organizing an online conference that was dedicated to share the knowledge of students and young scientists and to demonstrate the challenges of the energy and environment sectors. A big success has been done using virtual rooms due to the pandemic situation of COVID-19. We appreciate the support of the academic staff of Silesian University of Technology, and the industrial sponsors, and for InnoEnergy for supporting the MSc Energy Transition program and the 8th Conference on Environmental Protection and Energy.

Abdulkarim Abdulmalek Mira

Table of Contents

The concept of an interactive shower panel in terms of the assumptions of Industry 4.0

Leszek Remiorz[1], Adrian Czajkowski[1,2], Sebastian Pawlak[1], Eryk Remiorz[1], Jakub Szyguła[1], Gabriel Drabik[1], Dariusz Marek[1], Oleg Antemijczuk[1], Jarosław Paduch[1], Grzegorz Baron[1], Marcin Paszkuta[1]

[1]*Silesian University of Technology, e-mail:* adriczaj@gmail.com
[2]*Miscea.pl Engineering Sp. z o.o.*

Abstract

The aim of this article was to present the developed concept of a multifunctional shower panel, which was designed to minimize water consumption. This is accomplished by providing dynamic feedback to the user on the information of water consumption, which is displayed in the form of a personalized visualization on an integrated liquid crystal screen. In this graphical way, the necessary information is provided in real-time, promoting water-saving when taking a shower, and further, the recorded data in the form of statistics of water consumption are sent to the user's personal mobile device. The article discusses a technologically advanced shower panel, which consists of the following components: a hydraulic system (including electrically-operated valves), a flow meter system recording water consumption, a control system via a touch screen (or indirectly via a mobile device with built-in WiFi), an electronically controlled dispenser system, and a data processing system. The innovation of the device consists in the integration of the above-mentioned systems and their cooperation with a multimedia device in the form of a tablet or smartphone. The concept of the device presented in the article meets the critical assumptions of the Industry 4.0 concept and significantly contributes to rational water management.

Keywords: Industry 4.0, multifunctional shower device, multimedia, graphical user interface, smart home

1. Introduction

The continuous development of civilization, raising living standards, the need to introduce automated solutions, with simultaneous emphasis on environmental issues, seems to be endless. It is obvious that devices that have been on the market for years must be adapted to the current reality [1]. An example of such a product is a technologically advanced shower panel, which is practically completely different from other bathroom sanitary products commonly available on the market. The innovative product described in this article combines modern technical solutions, built into the shower panel, where the following components are integrated:

- a water supply system
- a dispensing system for selected liquids (such as liquid soap, shampoo, disinfectant)
- a multi-functional interface with a large colour touch screen

This device can be installed directly in the shower cabin or above the bathtub. The most important and at the same time the most innovative part of the device, i.e. the touch interface, performs many functions, ranging from displaying information about instantaneous water consumption, and regulating the temperature and water flow rate through the time of shower and the moment of its on/off, ending with a whole range of functionalities, i.e. Internet access, e-mail, multimedia, TV, music etc. The device can be integrated with the software of the smart home. Thanks to the possibility of remote control of its operation via a smartphone/tablet, the user can manage its functions remotely or download the data (e.g. statistics of water consumption for each user separately). Based on extensive, dedicated user interface software, it is possible to create profiles in the field of the preferred water temperature, water stream intensity, time of water spray, and the moment of starting water flow from various nozzles. An integral part of the device is an electronic dosing system, which enables the application of various liquids in precisely measured amounts from the same place

(nozzles are located in one place of the panel), in accordance with the preferences of users [2]. An important element of the shower panel described in the article is its adaptation to the current and changing trends towards more ecological solutions because it is equipped with innovative technology to control water and energy consumption, which allows reducing operating costs. Electronically controlled water valves and temperature sensors controlled by embedded intelligent software prevent the appearance of legionella bacteria and other bacteria that multiply in conditions of high humidity
and temperature [3].

2. Problem areas

The interactive shower panel described in this work, due to its level of innovation and technological advancement, required the development of integrated elements solving problem areas, such as:

1. Water flows control technology.
2. Fluid dispenser system control technology.
3. User interface technology.
4. Technology for control water system.
5. Technology for measuring the level (or volume) of fluids.
6. Multimedia technology.

2.1. Water flow control technology

To control the water flows, a module consisting of two parts (hardware and software) was created. The hardware part is based on a microcontroller that enables simultaneous control of four motors (electrically controlled valves), mechanically connected to the water flow regulating valves, and communication with the device via the I2C bus. Dedicated software enables the user to control all four connected motors simultaneously, along with the control of the exact position of the valve (from fully closed to fully open). Figure 1 shows the discussed engine control module.

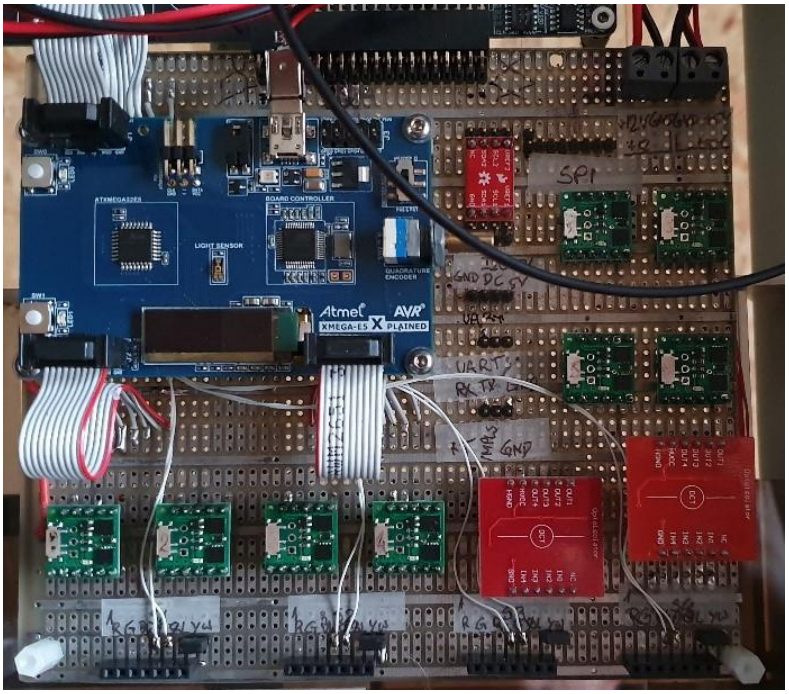

Fig. 1. Motor control module.

2.2. **Fluid dispenser system control technology**

A module consisting of two parts (hardware and software) was created to control the dispenser system. The hardware part is based on a microcontroller, which allows the simultaneous control of four peristaltic pumps (DC electric motors), flexible tubes connected to containers of the dispenser, reading the filling level of containers with liquids, communication with the device via the I2C bus and contactless starting of dosing. The dedicated software allows the user to choose one of the four dispensers and to read the level of their filling (on a colour LCD screen). The software allows selecting a specific dispenser via the I2C bus. After selecting a container with a given fluid, the dispensing is activated immediately (or with a set delay) after bringing the hand to the sensor. The software allows to set the amount of dispensed liquid and prevents spontaneous dripping of liquid from the dispenser (through a short back-rotation of the pump motor).

The software, along with the designed communication using the I2C bus has been adapted to all the needs and functionalities required for the trouble-free operation of the designed shower panel. Figure 2 shows the dispensers system control module.

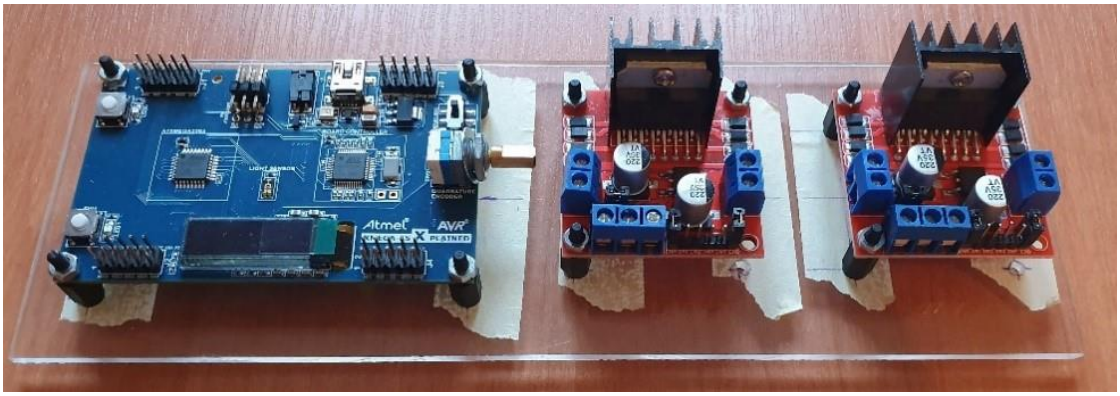

Fig. 2. The dispenser system control module.

2.3. **User interface technology**

The VAR-DT8M CustomBoard evaluation kit dedicated to DART-MX8M (Variscite) with the i.MX8M (NXP) processor in the form of an SoM (System-on-Module) module was used to build the main multimedia unit on which the user interface is based [4]. The module has 3 GB of fast LPDDR4 RAM memory and 16 GB of eMMC permanent memory, which can be additionally extended with an SD card with a capacity of up to 256 GB. The i.MX 8M processor has four 1.5 GHz Cortex ™ -A53 cores. The module also provides WiFi communication in the 802.11 ac/a/b/g/n standard and Bluetooth 4.2/BLE. The multimedia module works with the screen (HDMI connection, resolution 1920x1080) with a touch overlay [5]. The touch module communicates via the USB <-> I2C converter. In the current configuration, it can support up to 10 touch points at the same time (due to the need to ensure resistance to water splashes - the functionality of handling multiple touchpoints has been programmatically limited to 2 points, and in the event of a splash of water on the screen to 1 point). The sound subsystem is based on the digital amplifier TAS5755M (Texas Instruments) controlled directly from the DART-MX8M (Variscite) module [4], via the I2C/I2S SPDIF bus.

2.4. **Technology for control water system**

The water and temperature control module is a low-level controller that integrates other elements of the system, such as the multimedia module, valve control module and dosing module. It is also responsible for measuring

the temperature and flow of water and for stabilizing the temperature of the water supplied to the outlet nozzles. Figure 3 shows a diagram of the inlet and outlet water temperature measurement module.

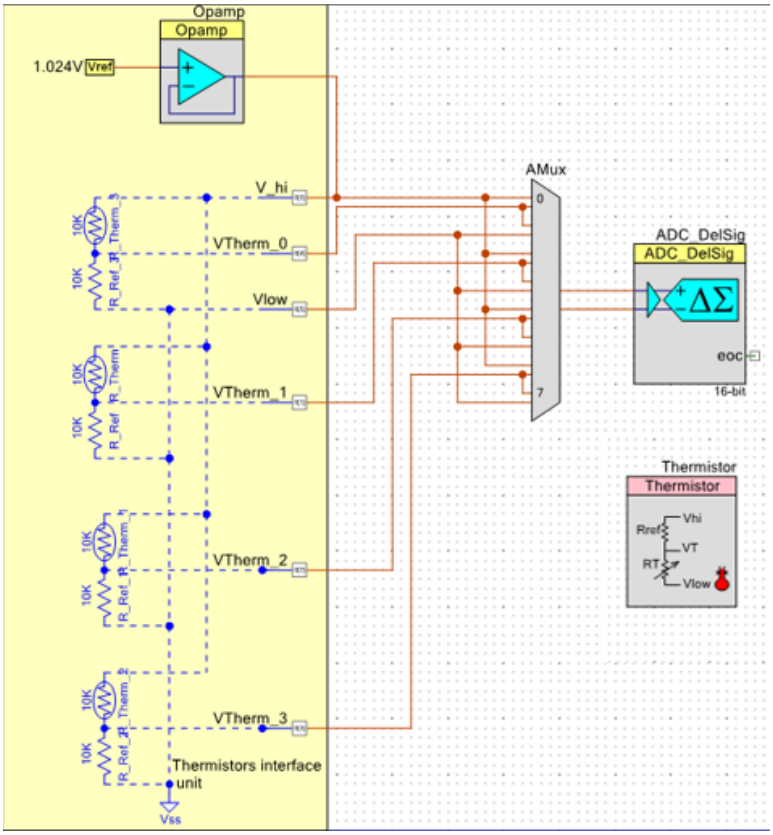

Fig. 3. Diagram of the temperature measurement module.

The water and temperature control module is also responsible for regulating the temperature of the outlet water stream. Based on the temperature measurement results and data obtained from the multimedia module, the discussed module controls the mixing valve with the help of a software-implemented PID controller, the inputs of which are supplied with cold and hot water from an external network.

2.5. **Fluid level measurement technology**

The fluid levels in the dispenser tanks are read by measuring the pressure of the container on the FSR402 sensor. Four sensors with the necessary repeaters are connected to the inputs of the analogue-to-digital converter. The selection of the location of the sensor, its type and measurement threshold values were selected based on the series of measurements. Dedicated software enables the measurement of the current pressure force value for each container, it is averaging and comparison with the stored value, the calibration value for an empty container. Figure 4 shows view of the FSR402 pressure sensors mounted under the containers of the dispenser.

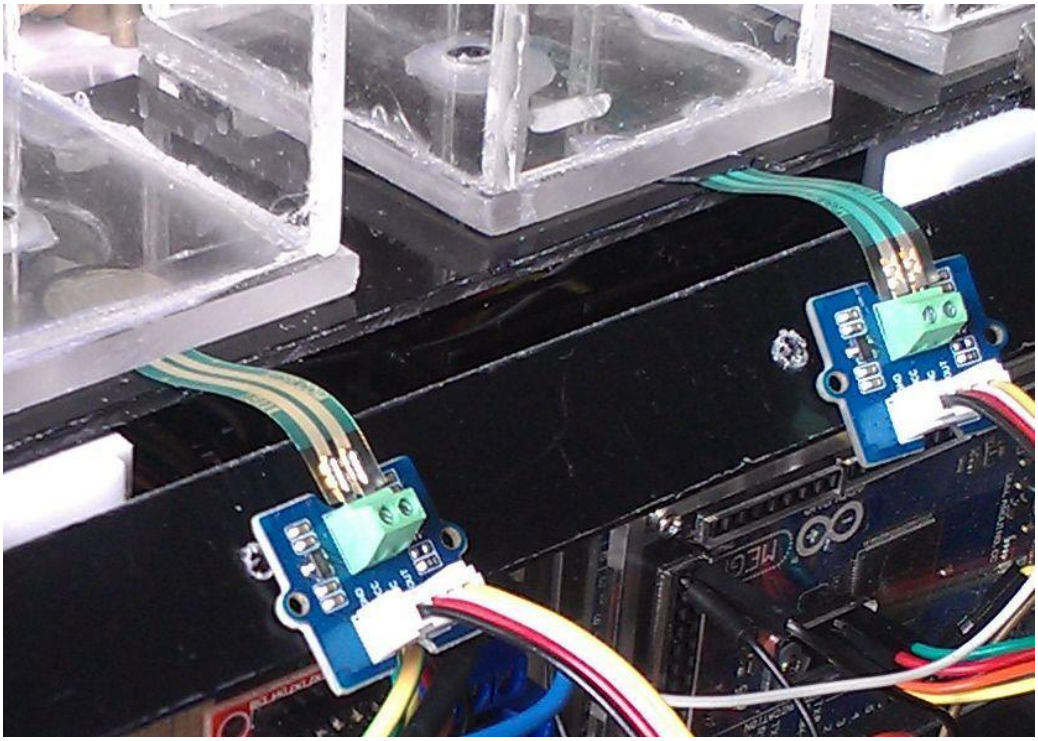

Fig. 4. View of the FSR402 pressure sensors mounted under the containers of the dispenser.

2.6. **Multimedia technology**

A program module of the user interface was developed for controlling the device. There are three modes: standard mode, simplified mode and advanced mode. The user interface was written as an Android launcher - the MUI application replaces the system startup screen application. It can display a list of all applications installed in the system and to run them. The primary screen gives quick access to control functions. Additionally, the date and time, as well as the current temperature, are displayed. Due to the application of the AIDL interface, the user can implement their control interface without the need to interfere with the hardware layers using a high-level communication mechanism. Figure 5 shows the main screen in the basic version - mode (1).

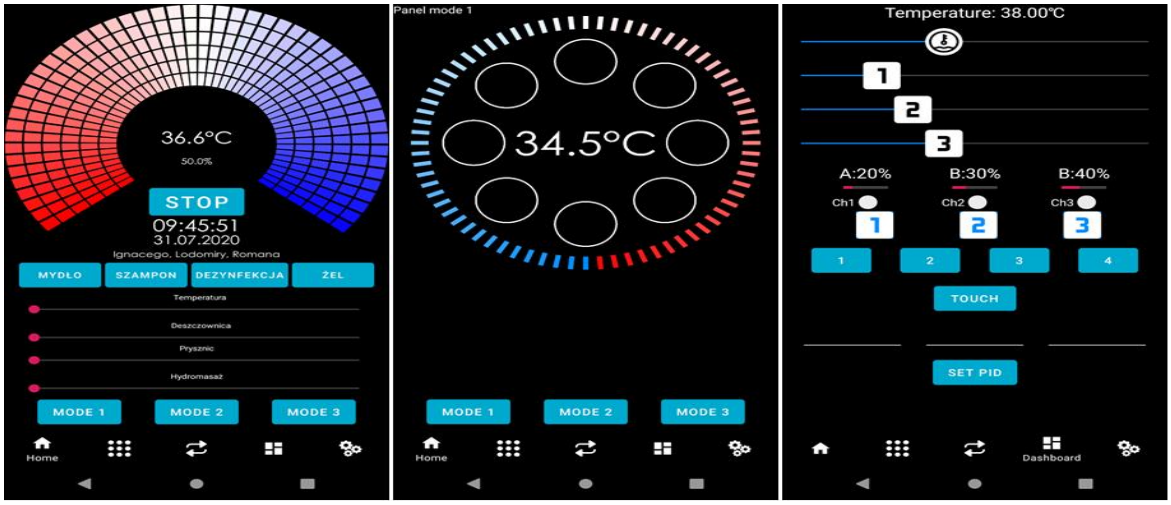

Fig. 5. View of the main screen in the basic version - mode (1, 2, 3).

This figure shows the basic version of the main screen view in three modes (Fig. 5); Mode 1 shows the primary mode, Mode 2 shows the simplified mode, Mode 3 shows the development and advanced mode.

The panel also enables the selection and control of the user's application, extending the basic functionality of the interface with the possibility of listening to music, watching videos, and when connected to the Internet, it enables voice conversations, etc.

Figure 6 shows the screen with the view of installed applications.

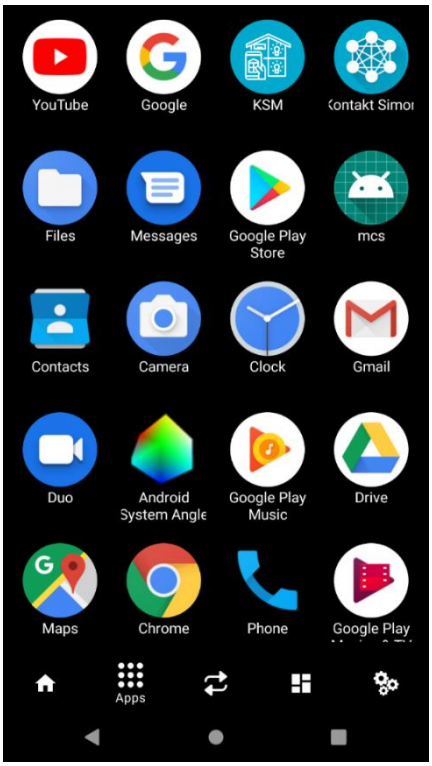

Fig. 6. View of the screen of installed applications.

3. Conclusion

The need for continuous development and the need to reconcile consumerism with the challenge of limiting climate change requires creating innovative and unconventional solutions [7]. This intensifies the trend of device management within the so-called, the Internet of Things (IoT) and striving to meet the assumptions of the Industry 4.0 concept, which requires digitization and automation to achieve its status [8, 9]. In response to this, a technologically advanced shower panel was developed to meet the current and future needs of consumers. At the same time, this device is characterized by solutions aimed at limiting the negative impact on the environment. Through research and development, many innovative elements have been prepared, which after integration, create a previously unknown product that redefines the concept of a shower and widely understood sanitary facilities.

Figure 7 shows a prototype of an innovative multi-functional shower panel, which is currently being tested.

Fig. 7a. General view.

Fig. 7b. View of the valves and dispenser system.

Fig. 7. Prototype of an innovative, multifunctional shower panel (own solution).

The device is equipped with technologies that control energy and water consumption. It also prevents the formation of microorganisms. Currently, the device is in a test and measurements phase that confirm its capabilities.

Acknowledgments

This work has been supported by the National Centre for Research and Development - Project no. POIR.01.01.01-00-0327/17, "Research and development works on an innovative multifunctional sanitary device" („Prace badawczo-rozwojowe nad innowacyjnym wielofunkcyjnym urządzeniem sanitarnym” – in Polish).

References

[1] Ryosuke Takada, Toshiyuki Ando, Buntarou Shizuki, Shin Takahashi, BaroTouch: A Technique for Touch Force Sensing Using a Waterproof Device's Built-in Barometer. Journal of Information Processing. 2019.

[2] S. Böhm, B. Timmer, W. Olthuis, P. Bergveld; *A closed-loop controlled electrochemically actuated micro-dosing system*.; Journal of Micromechanics and Microengineering, 2000, Volume 10, Number 4, Page: 498-504

[3] Cordes, L. G. Wiesenthal, A. M. Gorman, G. W. Phair, J. P. Sommers, H. M. Brown, A. Yu, V. L. Magnussen,. H. Meyer, R. D. Wolf, J. S. Shands, K. N. Fraser, D. W.; *Isolation of Legionella pneumophila from Hospital Shower Heads; Annals of Internal Medicine*, 1981, Volume 94, Issue 2, Page: 195-197

[4] Variscite DART-MX8M: NXP i.MX8M, https://www.variscite.com/product/system-on-module-som/cortex-a53-krait/dart-mx8m-nxp-imx-8m/?gclid=Cj0KCQiAk53-BRD0ARIsAJuNhptDwonswCHUftzXVCrgoE27qzDju2blnJjqmbKK-_Mziu5NGjDoDlkaAmmzEALw_wcB, available online: 02.12.2020r.

[5] NXP IMX8 family overview, https://www.solid-run.com/nxp-i-mx8m-family/?gclid=Cj0KCQiAk53-BRD0ARIsAJuNhpuEpVAxfKhiwgPUGejw3EnC9f8xwMg0l4imhcGoVRMtysq9_2d1jfgaAnR_EALw_wcB, available online: 02.12.2020r.

[6] Zestaw rozwojowy czujników, FSR402, Moduł, Grove - Round Force Sensor, https://pl.rs-online.com/web/p/narzedzia-rozwojowe-z-kategorii-czujniki/1887119/?cm_mmc=PL-PLA-DS3A-_-google-_-CSS_PL_PL_Raspberry_Pi_%26_Arduino_i_narz%C4%99dzia_rozwojowe_Whoop-_-(PL:Whoop!)+Narz%C4%99dzia+rozwojowe+z+kategorii+-+czujniki-_-1887119&matchtype=&pla-306759790208&gclid=Cj0KCQiAk53BRD0ARIsAJuNhpulC1rO5RLimw6UdAagSIj4rUDXdNoSmmLHiduZd-q8qElrEdfc9LsaAlSoEALw_wcB&gclsrc=aw.ds, available online: 02.12.2020r.

[7] Popkiewicz M., Kardaś A. Malinowski S. ; Nauka o klimacie. ISBN 978-83-8110-659-7. Warszawa 2018

[8] Ryosuke Takada, Wei Lin, Wei Lin, Toshiyuki Ando, Toshiyuki Ando, B. Shizuki, Buntarou Shizuki, Shin Takahashi, Shin Takahashi, A Technique for Touch Force Sensing using a Waterproof Device's Built-in Barometer, 2017, Pages 2140–2146

[9] Przemysł 4.0, Ministerstwo Rozwoju, Pracy i Technologii. 2019. Online: https://www.gov.pl/web/rozwoj-praca-technologia/przemysl-4-0 - available online: 02.12.2020

Influence of SO_2 poisoning on catalytic performance of modified zeolites in selective catalytic reduction of nitrogen oxides with ammonia (NH_3-SCR)

Agnieszka Szymaszek [1], Bogdan Samojeden [2], Monika Motak [3]

[1] AGH University of Science and Technology, e-mail: agnszym@agh.edu.pl
[1] AGH University of Science and Technology, e-mail: bogdan.samojeden@agh.edu.pl
[3]AGH University of Science and Technology, e-mail: motakm@agh.edu.pl

Abstract

Natural zeolite of heulandite framework (clinoptilolite) was modified with iron, promoted with copper, and tested as the catalyst for selective catalytic reduction of nitrogen oxides with ammonia (NH_3-SCR). Additionally, the materials were treated with SO_2 in order to investigate their resistance against poisoning. XRD analysis confirmed that copper can act as a structural promoter, due to the fact that crystalline structure of the zeolite can be restored after poisoning and regeneration. Nevertheless, the formation of $CuSO_4$ in the presence of SO_2 inhibited conversion of NO over the poisoned zeolite modified with Fe and Cu. It was found that when iron-doped clinoptilolite was poisoned with SO_2 and regenerated, NO conversion increased. The effect can be correlated with the formation of new Lewis and Brönsted acid centers and changes in their ratio, which facilitated the adsorption of ammonia and shifted the temperature window of the catalyst to lower values.

Keywords: clinoptilolite, selective catalytic reduction of NO_x, SO_2 poisoning

1. Introduction

Nitrogen oxides (NO_x) are one of the most hazardous pollutants of the atmosphere produced mainly by power plants, transportation and chemical industry, such as HNO_3 production [1,2]. The presence of NO_x in the atmosphere causes formation of acid rain and photochemical smog [3,4]. Nitrogen oxides also have adverse influence on human health, especially on the respiratory system [5]. The most common method used worldwide for NO_x abatement is selective catalytic reduction with ammonia [1,6]. However, despite the fact that the commercial catalyst, V_2O_5-TiO_2 promoted with MoO_3 or WO_3, exhibits satisfactory catalytic performance, it has also some significant limitations related to its narrow temperature window or toxicity of vanadium [5,7,8].

In recent decades, a number of materials have been tested as substitutes for vanadium-based catalyst, for example modified activated carbon [9,10], calcined layered double hydroxides [7,11], pillared layered clays doped with transition metals [12,13] and supported metal oxides [14,15]. Nevertheless, among the potential materials that are the most promising precursors of NH_3-SCR catalysts are zeolites. The high attention paid to catalysts supported on zeolites is mainly due to their wide temperature window and chemical composition that is neutral for the environment [16]. Generally, zeolites are porous aluminosilicates consisting of crystal structures of SiO_4 and AlO_4 connected with each other by four vertices that end with oxygen atom. Due to a partial isomorphic replacement of Si^{4+} cations by Al^{3+} cations, the zeolitic lattice has negative charge that is balanced by cations present in ion-exchange positions [17,18]. Due to that, zeolites form an open structure with ion-exchange properties and long channels that provide free motion of different molecules through their pores [19]. Zeolites can be synthesized on both laboratory and industrial scale or obtained from natural resources. There are around 40 types of recognized natural zeolites and the majority of them is a residue stored in landfills. Thus, their application in catalysis can reduce the amount of waste and act in agreement with the rules of circular economy.

The example of natural zeolite with high potential in catalysis is clinoptilolite, that belongs to heulandite (HEU) class. The chemical composition of clinoptilolite can be described by the formula: $(Na,K)_6(Al_6Si_{30}O_{72}) \cdot 20\,H_2O$. The material

combines micro-, meso-, and macroporosity and its Si/Al molar ratio oscillates around 4. Clinoptilolite structure consists of three different kinds of 2D channels confined with 8- and 10-member ring windows [20,21]. The application of clinoptilolite in NH_3-SCR was studied mainly because of its strongly acidic character, desired in the process. Additionally, high ion-exchange capacity of the zeolite provides incorporation of catalytically active metal species into its framework. Dakdareh et al. [22] synthesized nano-sized Mn_xO_y supported on clinoptilolite and tested it as a catalyst for propane-SCR. The authors proved that optimum conversion of NO of 71% was obtained at 200ºC and manganese content was strictly correlated with the catalytic activity of the material. The results of another study, carried out by Moreno-Tost et al. [16], showed that only negligible amount of N_2O was produced during SCR reaction with propane and Cu-clinoptilolite used as a catalyst. Furthermore, the studies performed by Szymaszek et al. [3] confirmed high catalytic activity of clinoptilolite modified with iron by co-precipitation method in SCR with NH_3 used as a reducing agent. The authors obtained 95% conversion of NO and ca. 3 ppm of N_2O at 275ºC. Hence, it can be concluded that modified clinoptilolite has a great potential in both NH_3- and HC-SCR.

One of the main operating problems with SCR catalysts is their sensitivity to the presence of SO_x. Sulfur oxide influences directly the catalytic performance of most of the catalysts, especially those based on zeolites [23–25]. SO_2 appears in the combustion chamber due to its content in fuel and the most severe poisoning occurs below 300ºC. The presence of SO_x results in the formation of ammonium sulphates ($(NH_4)_2SO_4$) and ammonium bisulphates (NH_4HSO_4) on the catalyst surface [1,26]. Poisoning of zeolite-supported catalysts with sulfur compounds has been recently investigated by many researchers [11,25,27,28]. Zou et al. [28] modified ZSM-5 with Fe and Mn by two different methods: co-precipitation and precipitation-chemical vapor deposition, and compared resistance of the catalysts against SO_2 under NH_3-SCR conditions. The authors found that preparation procedure had a significant impact on the activity of the catalysts in the presence of SO_2.

As it can be noticed, the type of zeolite and its modification route can play a crucial role in the catalytic performance in NH_3-SCR and resistance against SO_2. Due to that, in the presented studies we analyzed the impact of SO_2 poisoning and regeneration on the catalytic performance of iron- and copper-modified natural zeolite.

2. Experimental part

2.1. Catalysts preparation

In order to prepare the catalysts, natural zeolite (clinoptilolite) was transformed into hydrogen form by triple ion exchange with 5 vol.% HCl (with the ratio of the zeolite to the HCl solution = 5 g : 15 cm^3). Afterwards, the protonated material (H-Clin) was dried at 80ºC and modified with Fe^{2+} ions by co-precipitation method. 5 g of H-Clin was introduced into 0.05 M solution of $FeSO_4$ and mixed at 50ºC for 4 hours, maintaining pH ~ 3.0. After that time, pH of the slurry was increased to ca. 9.0 by the dropwise addition of 25 vol.% aqueous solution of NH_3, left for one more hour, and at the end washed with de-ionized water and dried for 24 hours at 105ºC. Then, the material was calcined in air for 2 hours at 450ºC. Copper as a promoter was deposited on the Fe-modified zeolite by impregnation method using the solution of $Cu(NO_3)_2$ of appropriate concentration to obtain 1 wt.% of the metal on the catalyst surface. Subsequently, the material was dried at 105ºC for 24 hours and calcined at 400ºC for 2 hours.The list of the prepared samples is given in Table 1. In order to compare the catalytic performance of fresh materials and the same samples poisoned with SO_2, the catalysts were exposed for 30 minutes to the gas mixture composed of 1000 ppm of SO_2 in helium at 300ºC. Directly afterwards, the samples were tested in NH_3-SCR. Subsequently, the catalysts after poisoning and catalytic reaction were regenerated in the atmosphere of He by increasing the temperature of the reactor from 300 to 450ºC and keeping each sample in these conditions for 30 minutes. Then, the regenerated materials were again subjected to NH_3-SCR catalytic tests. The procedure of the catalytic tests is depicted in Fig. 2. 1. All of the analyzed materials are listed in Table. 2. 1.

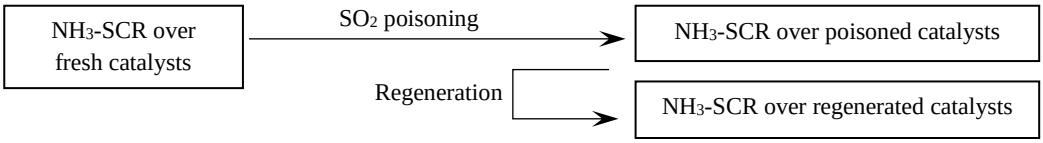

Fig. 2. 1. Experimental procedure of the catalytic tests over fresh, poisoned and regenerated catalysts

Table. 2.1. List of the analyzed materials

No.	Sample code	Description of the sample
1	Clin non-modified	Clinoptilolite before modifications
2	H-Clin	Clinoptilolite after protonation
3	Fe-Clin fresh	H-Clin modified with iron before poisoning with SO_2
4	Fe-Clin poisoned	H-Clin modified with iron after poisoning with SO_2
5	Fe-Clin regenerated	H-Clin modified with iron after regeneration
6	FeCu-Clin fresh	H-Clin modified with iron and copper before poisoning with SO_2
7	FeCu-Clin poisoned	H-Clin modified with iron and copper after poisoning with SO_2
8	FeCu-Clin regenerated	H-Clin modified with iron and copper after regeneration

2.2. Characterization of the catalysts structure

Structural properties of the catalysts were investigated by X-ray diffraction method. XRD patterns were obtained using Empyrean (Panalytical) diffractometer equipped with copper-based anode (Cu-Kα LFF HR, λ = 0.154059 nm). The diffractograms were collected in the *2θ* range of 2.0-45.0° (*2θ* step scans of 0.02° and a counting time of 1 s per step). Fourier-transform infrared spectroscopy (FT-IR) was performed to investigate characteristic chemical groups of the fresh, poisoned and regenerated catalysts. The spectra were recorded using Perkin Elmer Frontier spectrometer in the wavelength region of 1750-400 cm^{-1} with a resolution of 4 cm^{-1}. Before each measurement the analyzed sample was mixed with KBr (mass ratio 1:100) and pressed into disk.

2.3. Catalytic tests

NH_3-SCR catalytic tests over the fresh, poisoned and regenerated samples were performed under atmospheric pressure. 200 mg of the catalyst was placed in a fixed-bed flow microreactor and the reaction mixture (800 ppm of NO, 800 ppm of NH_3, 3.5 vol.% of O_2, He as an inert) was passed through the catalytic bed with the total flow rate of 100 $cm^3 \cdot min^{-1}$. The concentrations of residual NO and N_2O (the by-product of the reaction) were analysed downstream of the reactor by FT-IR detector (ABB 2000 AO series). The experimental NH_3-SCR process was conducted in the temperature range of 150-450ºC and NO conversion was calculated according to the formula represented by Equation (1):

$$NO_{conversion} = \frac{NO_{in} - NO_{out}}{NO_{in}} \quad \text{(Equation 1)}$$

where NO_{in}– inlet concentration of NO, NO_{out} - outlet concentration of NO.

3. Results and discussion

3.1. X-ray diffraction results

The results of X-ray diffraction analysis of the investigated samples are presented in Fig. 3. 1. (a-c). The pattern obtained for zeolite before modifications showed sharp and intense maxima that can be attributed to HEU-type zeolites

– heulandite and clinoptilolite. The crystalline zeolite structure is confirmed by the appearance of maxima located at *2Θ* values of 10.0, 11.4, 12.75, 19.3, 22.5, 28.1, 30.1, 32.5, 33.0, 35.25, and 35.5 [3,21,29]. Additionally, some amount of secondary phases were detected, including stilbite and SiO_2, which is typical for natural aluminosilicates. After protonation, the characteristic diffractions broadened and exhibited lower intensity. It is probably related to the incorporation of hydrogen atoms instead of cations present in the ion-exchange positions and dealumination caused by acid treatment. Hence, modification with acid caused some structural changes of clinoptilolite that led to partial amorphization of the material. These results are in agreement with those obtained by Tsitsishvili et al. [21], who modified clinoptilolite with HCl in order to test it as a catalyst for synthesis of acetylsalicylic acid. Deposition of both iron and iron with copper led to a significant decrease in the intensity of the maxima characteristic for clinoptilolite. Moreover, no evidence of the presence of metal oxides was observed on the patterns. It can be correlated either with high dispersion of the active phase and the promoter on the zeolitic support, or their amorphous state. XRD patterns obtained for Fe-Clin before and after poisoning and regeneration are presented in Fig. 3. 1. (b). The results indicated that SO_2 treatment resulted in almost complete amorphization of Fe-Clin. Additionally, the regeneration procedure performed on of the sample was insufficient to restore the initial structure of the catalyst. Nevertheless, from Fig. 3. 1. (c). it can be observed that even though the material promoted with copper lost some part of its initial crystallinity upon poisoning, the structure was almost completely rebuilt after regeneration. Therefore, copper acted as a structural promoter of iron-modified zeolite.

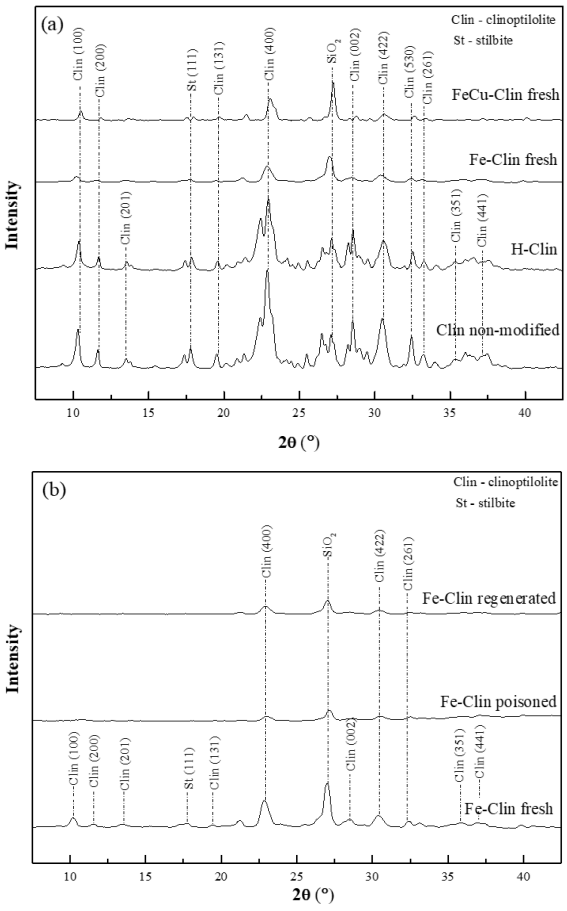

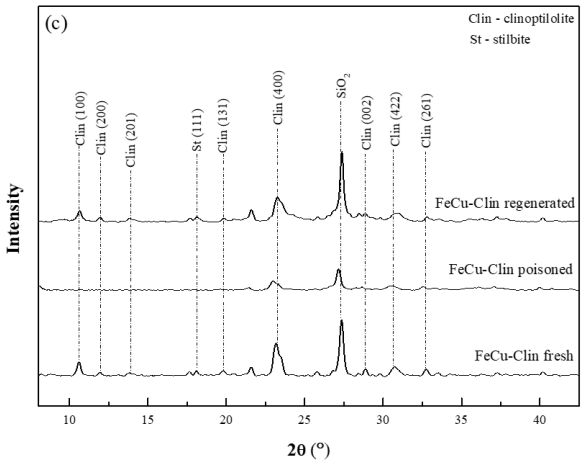

Fig. 3. 1. XRD patterns of fresh clinoptilolite samples: raw, protonated, modified with Fe, and modified with Fe and Cu (a); fresh, poisoned, and regenerated clinoptilolite modified with Fe (b); fresh, poisoned, and regenerated clinoptilolite modified with Fe and Cu (c).

3.2. **FT-IR spectroscopy results**

The results of FT-IR spectroscopy carried out over the analyzed samples are presented in Fig. 3. 2. The measurement was performed in the wavelength range of 1750-400 cm^{-1}, which is the most significant for the presence of aluminosilicate bonds and the presence of sulphates. Generally, the spectra consist of two wavelength ranges: Si-O stretching vibrations, Si-OH bending vibrations, and O-H bending vibrations from H_2O molecules (1700-700 cm^{-1}) (1), and pseudo lattice vibrations (700-450 cm^{-1}) (2) [30]. It can be observed that the spectra recorded for fresh, poisoned and modified samples exhibited similar shape and only a few bands changed their shape. It points at the fact that the structure of the modified zeolite was resistant against the harmful influence of SO_2 or the applied poisoning conditions were too lenient. The sharp peak at 1636 cm^{-1}, detected for all of the samples, is attributed to the bending vibrations of water molecules present in the internal space of the zeolite [3]. The small peaks at 1375 and 1350 cm^{-1} are characteristic for the formation of sulfate species [31]. It can be noticed that these bands are present not only for the poisoned samples, but also for Fe-Clin. It can be the result of incomplete decomposition of the precursor of the active phase which was $FeSO_4$, since the salt decomposes totally at around 680ºC [32]. Nevertheless, after deposition of copper and another calcination procedure, the peak disappeared from the spectrum. The peaks at 1212 cm^{-1} and 1048 cm^{-1} are assigned to Fe-O asymmetric stretching vibrations in tetrahedral FeO_4 groups and asymmetric O-Me-O stretching vibrations, respectively [30,33]. It can be observed that the vibration of 1213 cm^{-1} is sharper for the fresh samples and after poisoning its intensity is slightly decreased, especially for Fe-Clin. Additionally, after regeneration, in case of both samples the band was not restored. This result suggests that SO_2 promoted some reconstruction of the iron-containing chemical groups. Moreover, the peak at 1048 cm^{-1} is more intense for the fresh samples, which points at the fact that poisoning could result in partial dissolution of Si-O or Al-O structures. The broad band at 992 cm^{-1}, present for both poisoned and regenerated samples indicates the presence of sulfate groups on the catalysts. The presence of sulfates is also confirmed by the peak at 695 cm^{-1}, but, since it is present in case of both non-poisoned and poisoned samples, these groups can be the residuals from the deposition of the active phase [34]. The band divided into two peaks at 800 and 776 cm^{-1}, observed for all of the samples confirmed the presence of Si-O-Si and Al-O-Si bridges [35]. Since the shape and intensity of those peaks remain unchanged upon poisoning and regeneration, these structures are not sensitive for the presence of SO_2. Finally, the existence of the peaks at 595 cm^{-1} and 470 cm^{-1} are attributed to the heulandite phase and internal MeO_4 bending vibrations, respectively [36,37]. Additionally, comparison of the intensity of pseudolattice bands in the region of 550-650 cm^{-1} with the intensity of internal bending bands around 470 cm^{-1} can be used to determine amorphization degree in zeolites. The bands appearing in the first region are correlated with the ordered crystal structure, while those belonging to the second range do not depend on the degree of crystallization. It

can be noticed that after poisoning the band attributed to crystalline structure did not change in case of both samples, but the band independent of crystalline was broader for both poisoned and regenerated materials [35].

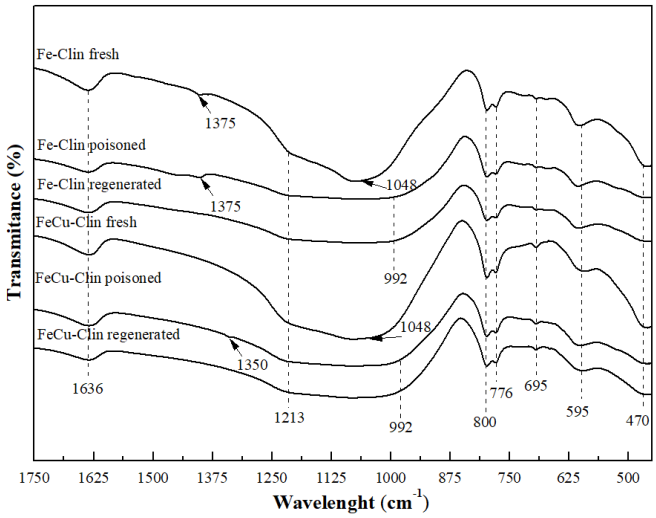

Fig. 3. 2. FT-IR spectra of fresh, poisoned and regenerated Fe-Clin and FeCu-Clin.

3.3. **Results of catalytic tests**

The results of catalytic tests carried out over non-modified clinoptilolite and fresh clinoptilolite modified with Fe or with Fe and Cu are presented in Fig. 3. 3. 1. It can be observed that raw clinoptilolite exhibits catalytic activity in NO conversion, since at 450ºC almost 60% of NO was reduced. Additionally, the introduction of copper as a promoter shifted the temperature window of Fe-Clin to a lower temperature range. The temperature of 50% conversion (t_{50}) for Fe-Clin was 250ºC, while for FeCu-Clin it was 195ºC. Thus, copper acted not only as a structural promoter, but it also increased catalytic activity of iron-modified clinoptilolite in the lower temperature range of NH_3-SCR. One of the most important practical aspects of NH_3-SCR catalysts is N_2O selectivity and its amount was measured in the gas mixture leaving the reactor. It can be observed in Fig. 3. 3. 1., that in case of Fe-Clin the amount of nitrous oxide was gradually increasing with the proceeding reaction. After the introduction of copper, the amount of the produced N_2O decreased above 350ºC, as compared to Fe-Clin. It suggests that copper prevents the occurrence of ammonia oxidation to N_2O Which can be the reaction competitive to NO reduction. Nevertheless, the drastic decrease of NO conversion above 375ºC observed for both copper-promoted and non-promoted catalysts suggests that ammonia could be oxidized to NO instead of N_2O, according to the reaction described by Equation (2) [38]:

$$4\ NH_3 + 5\ O_2 \rightarrow 4\ NO + 6\ H_2O \qquad \text{(Equation 2)}$$

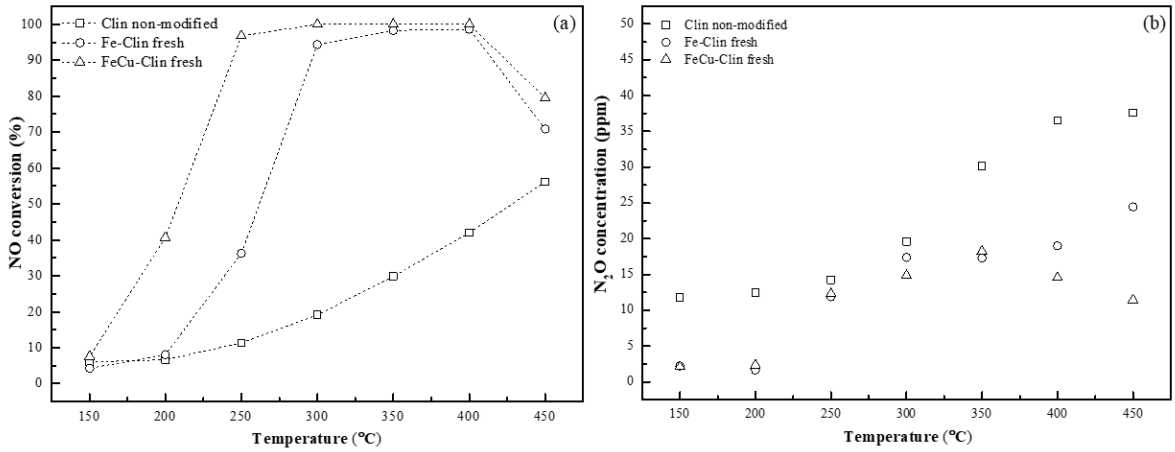

Fig. 3. 3. 1. Results of catalytic tests obtained for non-modified clinoptilolite, fresh clinoptilolite modified with iron, and fresh clinoptilolite modified with iron and copper: NO conversion (a); N_2O concentration (b).

The results of catalytic tests carried out over Fe-Clin and FeCu-Clin after poisoning with SO_2 and regeneration are presented in Fig. 3. 3. 2. and Fig. 3. 3. 3., respectively. In case of Fe-Clin, poisoning did not influence significantly the conversion of NO, since it was almost equal for the poisoned and non-poisoned sample in the entire temperature range. Therefore, the catalyst was highly resistant against SO_2. The obtained results are in agreement with literature data [31,39,40]. Shi et al. [40] investigated the effect of SO_2 on catalytic activity of Fe-ZSM-5 and it was postulated that the influence of sulphur dioxide on the catalytic performance was dependent on the temperature range of the reaction. According to their findings, ammonium sulfite/sulfates formed on the catalyst surface below 325ºC covered some of the iron active sites and inhibited SCR reaction. Nevertheless, higher catalytic activity of the poisoned and regenerated Fe-Clin suggests that the effect of SO_2 was rather promoting in case of the zeolite, or the poisoning conditions were not sufficiently severe to deactivate the material. Hence, when the appropriate conditions are applied, catalitically active surface iron sulfate species can be formed and the catalytic performance of SCR is enhanced. Similar results were obtained by Long et al. [31] who proved that Fe-ZSM-5 pretreated with SO_2 and O_2 at 400ºC increased Brönsted acidity. Consequently, the activity during SCR reaction was enhanced, especially above 350ºC. Moreover, after regeneration the temperature window of Fe-Clin was shifted to lower temperature and t_{50} decreased from 255ºC to 215ºC. It can be correlated with the introduction of highly acidic sulphur groups that acted as adsorption sites for NH_3 during the catalytic reaction. Additionally, the results of FT-IR analysis confirmed the presence of sulfate ions on the surface of Fe-Clin. These species contain covalent double bond that has strong affinity to electrons and acts as a strong Lewis acid site. It can be predicted that water molecules produced upon SCR, bond to the Lewis centre and form additional Brönsted site, simultaneously increasing the capacity of modified zeolite to adsorb ammonia [31]. The concentration of N_2O in the exhaust gas was almost identical for both Fe-Clin fresh and poisoned. Nevertheless, after regeneration the amount of the by-product increased in the entire temperature range. Hence, poisoning with SO_2 could result in the reconstruction of the Fe-active phase and formation of some species that facilitate side reactions of NH_3-SCR. On the other hand, the samples promoted with copper were more sensitive to the presence of SO_2, since the catalytic activity of FeCu-Clin slightly decreased and t_{50} parameter was shifted from 195ºC for the fresh sample to 235ºC for the poisoned one. Additionally, the regeneration procedure was insufficient to restore the initial catalytic activity of the material. The inhibiting effect on the catalytic activity of FeCu-Clin can be related to the formation of copper sulfates [41]. It was reported that SO_2 is directly oxidized to SO_3 over copper-doped catalysts under 300ºC [42]. Poisoning of the materials was performed at 300ºC, thus, it is expected that $CuSO_4$ is formed upon reactions described by Equations (3-4) [41]:

$$\text{Clinoptilolite-CuHSO}_3 + {}^1/_2\,O_2 \rightarrow \text{Clinoptilolite-CuHSO}_4 \qquad \text{(Equation 3)}$$

$$\text{Clinoptilolite-CuHSO}_3 + {}^1/_2\,O_2 \rightarrow \text{H-Clinoptilolite} + CuSO_4 \qquad \text{(Equation 4)}$$

However, $CuSO_4$ crystallites were not observed on XRD pattern obtained for FeCu-Clin. Nevertheless, XANES analysis performed by Cheng et al. [25] indicated that the species of copper sulphate are usually highly dispersed on the surface of zeolites. Similarly to the regenerated Fe-Clin, the amount of N_2O produced during the reaction was the highest for the regenerated sample, confirming the fact that SO_2 could facilitate or take part in the formation of the species that promote oxidation of ammonia. Nevertheless, in contrast to the material without Cu, a significantly decreased emission of N_2O was observed for the poisoned material.

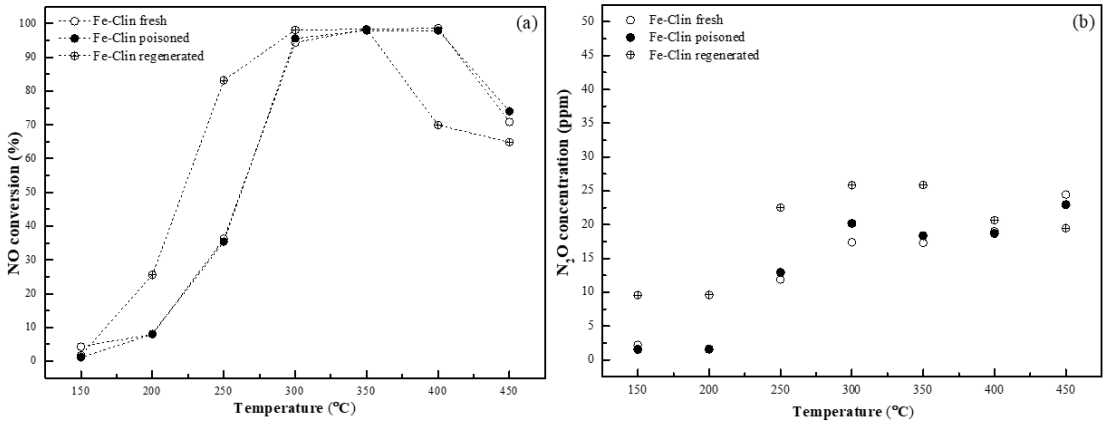

Fig. 3. 3. 2. Results of catalytic tests obtained for fresh, poisoned and regenerated clinoptilolite modified with iron: NO conversion (a); N_2O concentration (b).

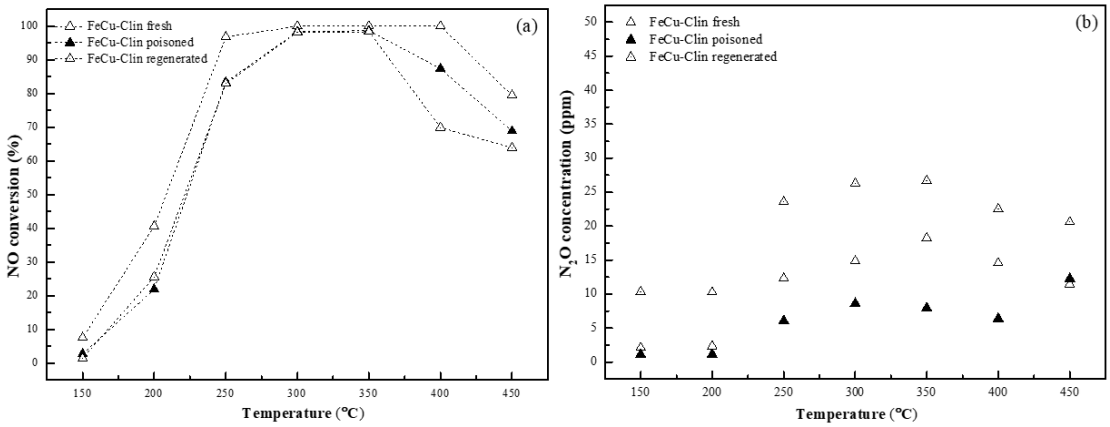

Fig. 3. 3. 3. Results of catalytic tests obtained for fresh, poisoned and regenerated clinoptilolite modified with iron and copper: NO conversion (a); N_2O concentration (b).

4. Conclusion

In the presented study, natural zeolite of the heulandite-type framework (clinoptilolite) was modified with iron and/or copper and tested as a novel catalyst of selective catalytic reduction of nitrogen oxides with ammonia. Additionally, the catalysts were treated with SO_2 in order to investigate their resistance to the poisoning. It was found that the catalytic activity of the samples doped with iron increased after poisoning and regeneration, since t_{50} was shifted from 255ºC to 215ºC. Nonetheless, despite the fact that promotion with copper improved the catalytic performance of fresh Fe-Clin, after poisoning and regeneration the catalytic activity of the material decreased. This result can be correlated with the formation and adsorption of dispersed $CuSO_4$ crystallites that block the active centers of the catalyst. However, the results of XRD confirmed that Cu can act as a structural promoter of modified clinoptilolite, since introduction of copper prevented the loss of crystallinity of the zeolitic phase.

Acknowledgment

This research was funded by AGH Subvention for Young Researchers no. 16.16.210.476.

References

[1] A. Szymaszek, B. Samojeden, M. Motak, The Deactivation of Industrial SCR Catalysts—A Short Review, Energies. 13 (2020) 3870. https://doi.org/10.3390/en13153870.

[2] A.H. Clark, R.J.G. Nuguid, P. Steiger, A. Marberger, A.W. Petrov, D. Ferri, M. Nachtegaal, O. Kröcher, Selective Catalytic Reduction of NO with NH3 on Cu−SSZ-13: Deciphering the Low and High-temperature Rate-limiting Steps by Transient XAS Experiments, ChemCatChem. 12 (2020) 1429–1435. https://doi.org/10.1002/cctc.201901916.

[3] A. Szymaszek, B. Samojeden, M. Motak, Selective catalytic reduction of NOx with ammonia (NH3-SCR) over transition metal-based catalysts - influence of the catalysts support, Physicochem. Probl. Miner. Process. 55 (2019) 1429–1441. https://doi.org/10.5277/ppmp19066.

[4] Xingxing Cheng, X.T. Bib, A review of recent advances in selective catalytic NOx reduction reactor technologies, Particuology. 16 (2014) 1–18.

[5] F. Ferella, A review on management and recycling of spent selective catalytic reduction catalysts, J. Clean. Prod. 246 (2020). https://doi.org/10.1016/j.jclepro.2019.118990.

[6] B. Samojeden, T. Grzybek, J. Kowal, A. Szymaszek, M. Jabłońska, R. Glaeser, M. Motak, The influence of holmium on catalytic properties of Fe or Cu-modified vermiculites, Physicochem. Probl. Miner. Process. 55 (2019) 1484–1495.

[7] D. Wierzbicki, R. Dębek, J. Szczurowski, S. Basąg, M. Włodarczyk, M. Motak, R. Baran, Copper, cobalt and manganese: Modified hydrotalcite materials as catalysts for the selective catalytic reduction of NO with ammonia. the influence of manganese concentration, Comptes Rendus Chim. 18 (2015) 1074–1083. https://doi.org/10.1016/j.crci.2015.06.009.

[8] M. Motak, Ł. Kuterasiński, P. Da Costa, B. Samojeden, Catalytic activity of layered aluminosilicates for VOC oxidation in the presence of NOx, Comptes Rendus Chim. 18 (2015) 1106–1113. https://doi.org/10.1016/j.crci.2015.05.005.

[9] Y. Lin, Y. Li, Z. Xu, J. Xiong, T. Zhu, Transformation of functional groups in the reduction of NO with NH3 over nitrogen-enriched activated carbons, Fuel. 223 (2018) 312–323. https://doi.org/10.1016/j.fuel.2018.01.092.

[10] B. Samojeden, T. Grzybek, The influence of the promotion of N-modified activated carbon with iron on NO removal by NH3-SCR, Energy. 116 (2016) 1484–1491.

[11] R. Wang, X. Wu, C. Zou, X. Li, Y. Du, Nox removal by selective catalytic reduction with ammonia over a hydrotalcite-derived NiFe mixed oxide, Catalysts. 8 (2018). https://doi.org/10.3390/catal8090384.

[12] P. Ziemiański, K. Kałahurska, B. Samojeden, Selective catalytic reduction of NO with NH3 on mixed alumina–iron (III) oxide pillared montmorillonite “Cheto” Arizona, modified with hexamminecobalt (III) chloride, Adsorpt. Sci. Technol. 35 (2017) 825–833. https://doi.org/10.1177/0263617417710141.

[13] S. Boxiong, M. Hongqing, H. Chuan, Z. Xiaopeng, Low temperature NH3-SCR over Zr and Ce pillared clay based catalysts, Fuel Process. Technol. 119 (2014) 121–129. https://doi.org/10.1016/j.fuproc.2013.10.026.

[14] Z. Yan, J. Yang, X. Ge, J. Yu, L. Wei, T. Yang, B. He, X. Wang, L. Liu, Manganese oxide catalysts supported on zinc oxide nanorod arrays: A new composite for selective catalytic reduction of NOx with NH3 at low temperature, Appl. Surf. Sci. 491 (2019) 579–589. https://doi.org/10.1016/j.apsusc.2019.06.185.

[15] Y. Jiang, X. Wang, Z. Xing, C. Bao, G. Liang, Preparation and characterization of CeO2-MoO3/TiO2 catalysts for selective catalytic reduction of NO with NH3, Aerosol Air Qual. Res. 17 (2017) 2726–2734. https://doi.org/10.4209/aaqr.2016.08.0352.

[16] R. Moreno-Tost, J. Santamaría-González, E. Rodríguez-Castellón, A. Jiménez-López, M.A. Autié, E. González, M.C. Glacial, C.D. Las Pozas, Selective catalytic reduction of nitric oxide by ammonia over Cu-exchanged Cuban natural zeolites, Appl. Catal. B Environ. 50 (2004) 279–288. https://doi.org/10.1016/j.apcatb.2004.01.019.

[17] Y. Li, P. Bai, Y. Yan, W. Yan, W. Shi, R. Xu, Removal of Zn2+, Pb2+, Cd2+, and Cu2+ from aqueous solution by synthetic clinoptilolite, Microporous Mesoporous Mater. 273 (2019) 203–211. https://doi.org/10.1016/j.micromeso.2018.07.010.

[18] J.F. Gelves, L. Dorkis, M.A. Márquez, A.C. Álvarez, L.M. González, A.L. Villa, Activity of an iron Colombian natural zeolite as potential geo-catalyst for NH3-SCR of NOx, Catal. Today. 320 (2019) 112–122. https://doi.org/10.1016/j.cattod.2018.01.025.

[19] E. Zanin, J. Scapinello, M. de Oliveira, C.L. Rambo, F. Franscescon, L. Freitas, J.M.M. de Mello, M.A. Fiori, J.V. Oliveira, J. Dal Magro, Adsorption of heavy metals from wastewater graphic industry using clinoptilolite zeolite as adsorbent, Process Saf. Environ. Prot. 105 (2017) 194–200. https://doi.org/10.1016/j.psep.2016.11.008.

[20] M.Z. Kussainova, R.M. Chernyakova, U.Z. Jussipbekov, S. Paşa, Structural investigation of raw clinoptilolite over the Pb 2+ adsorption process from phosphoric acid, J. Mol. Struct. 1184 (2019) 49–58. https://doi.org/10.1016/j.molstruc.2019.02.012.

[21] M. Ramishvili, V.G. Tsitsishvili, N.G. Kokiashvili, V.M. Gabunia, N.M. Inanashvili, Modified Forms of Natural Zeolites – Clinoptilolite and Heulandite as an Effective Catalysts for Synthesis of Acetylsalicylic Acid MODIFIED FORMS OF NATURAL ZEOLITES – CLINOPTILOLITE AND HEULANDITE AS AN, (2019).

[22] A.M. Dakdareh, C. Falamaki, N. Ghasemian, Hydrothermally grown nano-manganese oxide on clinoptilolite for low-temperature propane-selective catalytic reduction of NOx, J. Nanoparticle Res. 20 (2018). https://doi.org/10.1007/s11051-018-4414-0.

[23] X. Li, C. Zhang, X. Zhang, W. Li, P. Tan, L. Ma, Q. Fang, G. Chen, Study on improving the SO2 tolerance of low-temperature SCR catalysts using zeolite membranes: NO/SO2 separation performance of aluminogermanate membranes, Chem. Eng. J. 335 (2018) 483–490. https://doi.org/10.1016/j.cej.2017.10.184.

[24] S.L. Bergman, S. Dahlin, V. V. Mesilov, Y. Xiao, J. Englund, S. Xi, C. Tang, M. Skoglundh, L.J. Pettersson, S.L. Bernasek, In-situ studies of oxidation/reduction of copper in Cu-CHA SCR catalysts: Comparison of fresh and SO2-poisoned catalysts, Appl. Catal. B Environ. 269 (2020) 118722. https://doi.org/10.1016/j.apcatb.2020.118722.

[25] Y. Cheng, C. Lambert, D.H. Kim, J.H. Kwak, S.J. Cho, C.H.F. Peden, The different impacts of SO2 and SO3 on Cu/zeolite SCR catalysts, Catal. Today. 151 (2010) 266–270. https://doi.org/10.1016/j.cattod.2010.01.013.

[26] X. Du, J. Xue, X. Wang, Y. Chen, J. Ran, L. Zhang, J., Oxidation of sulfur dioxide over VO/TiO catalyst with low vanadium loading: a theoretical study, J. Phys. Chem. 122 (2018) 4517–4523. https://doi.org/10.1002/9783527809080.cataz12094.

[27] P.S. Hammershøi, A.D. Jensen, T.V.W. Janssens, Impact of SO2-poisoning over the lifetime of a Cu-CHA catalyst for NH3-SCR, Appl. Catal. B Environ. 238 (2018) 104–110. https://doi.org/10.1016/j.apcatb.2018.06.039.

[28] C. Zou, X. Wu, H. Meng, Y. Du, Z. Li, The SO2 Resistance Improvement of Mn-Fe/ZSM-5 for NH3-SCR at Low Temperature by Optimizing Synthetic Method, ChemistrySelect. 3 (2018) 13042–13047. https://doi.org/10.1002/slct.201801518.

[29] N. Mansouri, N. Rikhtegar, H.A. Panahi, F. Atami, B.K. Shahraki, Porosity, characterization and structural properties of natural zeolity - clinoptilolite - as a sorbent, Environ. Prot. Eng. 39 (2013). https://doi.org/10.1002/9780470114735.hawley03904.

[30] M. Doula, A. Ioannou, A. Dimirkou, Copper adsorption and Si, Al, Ca, Mg, and Na release from clinoptilolite, J. Colloid Interface Sci. 245 (2002) 237–250. https://doi.org/10.1006/jcis.2001.7961.

[31] R.Q. Long, R.T. Yang, Characterization of Fe-ZSM-5 catalyst for selective catalytic reduction of nitric oxide by ammonia, J. Catal. 194 (2000) 80–90. https://doi.org/10.1006/jcat.2000.2935.

[32] P. Masset, J. Poinso, J. Poignet, TG / DTA / MS STUDY OF THE THERMAL DECOMPOSITION OF FeSO 4 × 6H 2 O, J. Therm. Anal. 83 (2006) 457–462.

[33] M.K. Doula, Synthesis of a clinoptilolite-Fe system with high Cu sorption capacity, Chemosphere. 67 (2007) 731–740. https://doi.org/10.1016/j.chemosphere.2006.10.072.

[34] J. Kiefer, A. Strk, A.L. Kiefer, H. Glade, Infrared spectroscopic analysis of the inorganic deposits from water in domestic and technical heat exchangers, Energies. 11 (2018). https://doi.org/10.3390/en11040798.

[35] W. Mozgawa, M. Sitarz, M. Rokita, Spectroscopic studies of different aluminosilicate structures, J. Mol. Struct. 511–512 (1999) 251–257. https://doi.org/10.1016/S0022-2860(99)00165-9.

[36] E.P. Favvas, C.G. Tsanaktsidis, A.A. Sapalidis, G.T. Tzilantonis, S.K. Papageorgiou, A.C. Mitropoulos, Clinoptilolite, a natural zeolite material: Structural characterization and performance evaluation on its dehydration properties of hydrocarbon-based fuels, Microporous Mesoporous Mater. 225 (2016) 385–391. https://doi.org/10.1016/j.micromeso.2016.01.021.

[37] M.K. Doula, A. Ioannou, The effect of electrolyte anion on Cu adsorption-desorption by clinoptilolite, Microporous Mesoporous Mater. 58 (2003) 115–130. https://doi.org/10.1016/S1387-1811(02)00610-8.

[38] C. Paolucci, J.R. Di Iorio, F.H. Ribeiro, R. Gounder, W.F. Schneider, Catalysis Science of NOx Selective Catalytic Reduction With Ammonia Over Cu-SSZ-13 and Cu-SAPO-34, 1st ed., Elsevier Inc., 2016. https://doi.org/10.1016/bs.acat.2016.10.002.

[39] R.Q. Long, R.T. Yang, Catalytic performance of Fe-ZSM-5 catalysts for selective catalytic reduction of nitric oxide by ammonia, J. Catal. 188 (1999) 332–339.

[40] Z. Ma, X. Wu, Y. Feng, Z. Si, D. Weng, L. Shi, Low-temperature SCR activity and SO2 deactivation mechanism of Ce-modified V2O5-WO3/TiO2 catalyst, Prog. Nat. Sci. Mater. Int. 25 (2015) 342–352. https://doi.org/10.1016/j.pnsc.2015.07.002.

[41] Y. Jangjou, D. Wang, A. Kumar, J. Li, W.S. Epling, SO2 Poisoning of the NH3-SCR Reaction over Cu-SAPO-34: Effect of Ammonium Sulfate versus Other S-Containing Species, ACS Catal. 6 (2016) 6612–6622. https://doi.org/10.1021/acscatal.6b01656.

[42] A. Kumar, M.A. Smith, K. Kamasamudram, N.W. Currier, H. An, A. Yezerets, Impact of different forms of feed sulfur on small-pore Cu-zeolite SCR catalyst, Catal. Today. 231 (2014) 75–82. https://doi.org/10.1016/j.cattod.2013.12.038.

Applicable standards for low-emission low power heating devices in EU

Przyłucka Aleksandra[1], Rywotycki Marcin[2]

[1]AGH University of Science and Technology, e-mail: aprzylucka@agh.edu.pl
[2]AGH University of Science and Technology, e-mail: rywotyc@agh.edu.pl

Abstract

Air pollution increases with technological development. The paper presents the legal documents currently in force in the European Union that regulate the emissions of harmful substances. The article concerns the standards for low-emission low power solid fuels heating appliances. In the calculation part, the amounts of substances emitted by boilers meeting the Ecodesign assumptions were compared.

Keywords: ecodesign, low-emission, solid fuel

1. Introduction

Clean air is essential for the health of living organisms and the proper functioning of the environment. Since the industrial revolution, its quality has significantly deteriorated. Growing industrial and energy production, combustion of fossil fuels and biomass cause serious health problems and environmental imbalance. This contributes to an increase in health care costs, as well as reduction in the quality of work of people exposed to it. The European Union, formerly the European Economic Community, has been working on improving air quality since the 1970s. Significant progress has been made in the fight against air pollution by controlling emissions of harmful substances, improving fuels quality and interfering with environmental regulations in the transport and energy sectors. The concentrations of sulfur dioxide (SO_2), nitrogen oxides (NO_x), non-methane volatile organic compounds (NMVOC) and ammonia (NH_3) were successfully reduced. Despite the progress made, poor air quality continues to cause serious but resolvable problems [1,3].

In 2011-2013, the European Commission conducted a review of member states air behavior, which led to the adoption of the clean air policy package. As part of it, the „Clean Air for Europe" program was proposed, where the existing legislative regulations were updated and new goals were set for 2020 and 2030. The main legal basis for achieving the objectives of the above program by 2030 is directive [4]. It was introduced on December 31, 2016. This decree sets out the emission reduction commitments of member states for the five pollutants responsible for acidification, eutrophication and ground level ozone pollution. Members of European Union have been obligated to control the negative impact of harmful substances emissions on the basis of a monitoring stations network.

The main objectives of directive [4] are to achieve air purity levels, which are contained in the European Union legislation, guidelines published by the World Health Organization and to synchronize the EU air quality policy with other relevant EU policies, especially with the climate and energy policy. Its assumption is to reduce greenhouse gases emissions by 2030 by no less than 40 % compared to 1990 levels. Commitments of the countries belonging to the EU have been defined as the minimum emission reductions that should be achieved by a specific calendar year by expressing the total percentage of emissions released into the atmosphere from the reference date, i.e. 2005 [5]. Member states are obliged to reduce annual emissions According to the national limits shown in Table 1. EU territories are obliged to implement the necessary measures to reduce anthropogenic emissions of sulfur dioxide, nitrogen oxides, non-methane volatile organic compounds, ammonia and fine dust in 2025. Pollution levels are determined by a linear reduction path between 2020 and 2030 [7].

Table 1. Commitments to reduce emissions of sulfur dioxide (SO_2), nitrogen oxides (NOx), non-methane volatile organic compounds (NMVOC), ammonia (NH_3) and particulate matter ($PM_{2.5}$) [4].

Member country	SO_2 reduction compared to 2005		NO_x reduction compared to 2005		NMVOC reduction compared to 2005		NH_3 reduction compared to 2005		$PM_{2,5}$ reduction compared to 2005	
	Every year from 2020	Every year from 2030	Every year from 2020.	Every year from 2030.	Every year from 2020	Every year from 2030	Every year from 2020	Every year from 2030.	Every year from 2020	Every year from 2030.
Belgium	43 %	66%	41%	59%	21%	35%	2%	13%	20%	39%
Bulgaria	78%	88%	41%	58%	21%	42%	3%	12%	20%	41%
Czech Reublic	45%	66%	35%	64%	18%	50%	7%	22%	17%	60%
Denmark	35%	59%	56%	68%	35%	37%	24%	24%	33%	55%
Germany	21%	58%	39%	65%	13%	28%	5%	29%	26%	43%
Estonia	32%	68%	18%	30%	10%	28%	1%	1%	15%	41%
Greece	74%	88%	31%	55%	54%	62%	7%	10%	35%	50%
Spain	67%	88%	41%	62%	22%	39%	3%	16%	15%	50%
France	55%	77%	50%	69%	43%	52%	4%	13%	27%	57%
Croatia	55%	83%	31%	65%	34%	48%	1%	25%	18%	55%
Ireland	65%	85%	49%	55%	25%	32%	1%	5%	18%	41%
Italy	35%	71%	40%	34%	35%	46%	5%	16%	10%	40%
Cyprus	83%	93%	44%	51%	45%	50%	10%	20%	46%	70%
Latvia	8%	46%	32%	34%	27%	38%	1%	1%	16%	43%
Lithuania	55%	60%	48%	51%	32%	47%	10%	10%	20%	36%
Luxembourg	34%	50%	43%	83%	29%	42%	1%	22%	15%	40%
Hungary	46%	73%	34%	66%	30%	58%	10%	32%	13%	55%
Malta	77%	95%	42%	79%	23%	27%	4%	24%	25%	50%
Netherlands	28%	53%	45%	61%	8%	15%	13%	21%	37%	45%
Austria	26%	41%	37%	69%	21%	36%	1%	12%	20%	46%
Poland	59%	70%	30%	39%	25%	26%	1%	17%	16%	58%
Portugal	63%	83%	36%	63%	18%	38%	7%	15%	15%	53%
Romania	77%	88%	45%	60%	25%	45%	13%	25%	28%	58%
Slovenia	63%	92%	39%	65%	23%	53%	1%	15%	25%	60%
Slovakia	57%	82%	36%	50%	18%	32%	15%	30%	36%	49%
Finland	30%	34%	35%	47%	35%	48%	20%	20%	30%	34%
Sweden	22%	22%	36%	66%	25%	36%	15%	17%	19%	19%
United Kingdom	59%	88%	55%	73%	32%	39%	8%	16%	30%	46%
EU 28	59%	79%	42%	63%	28%	40%	6%	19%	22%	49%

At the later stage of this work, calculations of fuel consumption for hard coal, coke and wood fired boilers of the same nominal power will be presented. In addition, the emissions of certain substances emitted to the air by these devices, estimated with use of indicators will be shown.

2. Emission reduction methods for low power devices

The decision of the European Parliament and the Council of European Union recognized that despite the progress made over last decades, air pollution indicators in many areas of EU still exceed the applicable standards. To improve and regulate trade in solid fuel combustion appliances on EU market efforts have been made. The main emphasis was placed on increasing energy efficiency and the level of environmental protection, while maintaining the safety requirements in energy disposal [9]. The products predisposed to reduce emission of harmful substances include: heating devices, sets containing a solid fuel boiler, additional heaters, solar devices and temperature regulators [6]. Before the introduction of directive [2], which regulates the Ecodesign requirements, technical environmental and economic analyzes were carried out on solid fuel boilers. The research concerned facilities used in commercial premises and households. On this basis, it was found that significant environmental aspects of the device include energy consumption in the boiler use phase, emissions of nitrogen oxides, carbon monoxide, solid particles and organic gaseous compounds. Preparatory studies showed the emissions of dioxins and furans as negligible. This resulted in the exclusion from this decree of devices intended for heating only utility water, distribution of gaseous heat carriers, as well as cogeneration boilers with special properties with a power equal to or greater than 50 kW.

Specific Ecodesign requirements effective from January 1, 2020 include [2]:

- Solid fuel boilers – seasonal energy efficiency, which is the ratio of the amount of heat supplied by the device over the entire heating season to the annual Energy consumption of this device, expressed in %, cannot be less than 75% for boilers with a rated heat output of up to 20kW or not may be less than 77% for boilers with a rated heat output exceeding 20 kW.
- Emissions of nitrogen oxides (NOx) must not exceed 200 mg/m³ for biomass boilers and 350 mg/m³ for fossil fuel boilers.
- Solid fuel boilers with automatic fuel feed:
    - particulate emissions (PM) shall not exceed 40 mg/m³;
    - emissions of organic gaseous compounds (OGC) shall not exceed 20 mg/m³;
    - carbon monoxide emissions (CO) shall not exceed 500 mg/m³.
- Solid fuel boilers with manual fuel feed:
    - particulate emissions (PM) shall not exceed 60 mg/m³;
    - emissions of organic gaseous compounds (OGC) shall not exceed 30 mg/m³;
    - carbon monoxide emissions (CO) shall not exceed 700 mg/m³.

3. Calculations

3.1. Fuel consumption calculations

The amount of solid fuel consumed by a boiler of a certain power can be calculated the formulas used by devices manufacturers to determine the daily fuel consumption of the mechanism.

Initially, the power that will be obtained from the given fuel in one hour is determined

$$Q = \frac{Q_i}{\tau}$$

where:

Q_i Calorific value, $\left(\frac{m^2}{s^2}\right)$,

τ Time, (s).

The next step is to obtain performance from 1 kg of fuel w

$$w = Q \times \eta$$

where:

η boiler efficiency, (%).

To calculate the amount of fuel consumed by the boiler when operating at nominal thrust 1 hour, use the formula

$$S = \frac{P}{w}$$

where:

P nominal boiler power, $\left(\frac{kg \times m^2}{s^3}\right)$.

It is assumed that boiler will operate with nominal power about 8 hours a day. The heating season in Poland lasts 6 months, which gives 180 days. To obtain the daily fuel consumption by boiler, it is necessary to calculate the product of average hours number and the amount of fuel consumed per hour. In order to determine the annual fuel consumption (kg), the obtained value should be multiplied by the number of days

$$R = S \times 8 \times 180$$

3.2. Emission calculations

The amount of emission depends on the type of fuel burned, the amount of its consumption and parameters such as: calorific value, ash content and sulfur content in a fuel.

General formula for calculating emissions from an emission factor per unit of fuel consumed

$$\boldsymbol{E = B \times W}$$

where:

$\boldsymbol{B}$ fuel consumption, $(\boldsymbol{g})$,

$\boldsymbol{W}$ emission factor per unit of fuel consumed.

3.3. Results

For calculations of fuel consumption and emission of some substances, emission factors for hard coal, coke and wood were used, presented in tables 2, 3, 4 [8].

Table 2. Emission factors for hard coal.

Type of pollution	Unit of indicator	Fixed grate				Mechanical grate
		Nominal heat output of the boiler [MW]				
		≤ 0,5	> 0,5 ÷ ≤ 5	≤ 0,5	> 0,5 ÷ ≤ 5	> 0,5 ÷ ≤ 5
		Natural pass		Artificial pass		
Sulfur oxides (SO_x)	[g/Mg]	16000 x s				

Nitrogen oxides (NO_x)		2200	1000	2000	3000	3200
Carbon monoxide (CO)		45000		70000	20000	10000
Carbon dioxide (CO_2)		1850000	2000000	1850000	2000000	2130000
Total suspended particles (TSP)		1000 x A^r	1500 x A^r			2000 x A^r
Benzo(a)pyrene		14				3,2

where:

A^r ash content in fuel, (%),

s sulfur content in fuel, (%).

Table 3. Emission factors for coke.

Type of pollution	Unit of indicator	Fixed grate			
		Nominal heat output of the boiler [MW]			
		≤ 0,5		> 0,5 ÷ ≤ 5	
		Natural pass	Artificial pass	Natural pass	Artificial pass
Sulfur oxides (SO_x)	[g/Mg]	16000 x s			
Nitrogen oxides (NO_x)		500	1000	500	1000
Carbon monoxide (CO)		25000		20000	
Carbon dioxide (CO_2)		2360000			
Total suspended particles (TSP)		1000 x A^r	1500 x A^r	1000 x A^r	1500 x A^r
Benzo(a)piren		0,1		0,027	

where:

A^r ash content in fuel, (%),

s sulfur content in fuel, (%).

Table 4. Emission factors for wood.

Type of pollution	Unit of indicator	Fixed grate		Mechanical grate
		Nominal heat output of the boiler [MW]		
		≤ 1	> 1 ÷ ≤ 5	≤ 5
Sulfur oxides (SO_x)	[g/Mg]	110	110	20
Nitrogen oxides (NO_x)		1000	950	800
Carbon monoxide (CO)		26000	16000	11000
Carbon dioxide (CO_2)		1200000		1330000
Total suspended particles (TSP)		1500 x A^r		2500 x A^r

where:

A^r ash content in fuel, (%).

The calculations were made for ecological central heating boilers available on the market that meet Ecodesign requirements. Three boilers [10] of the same nominal power were used, differing in type of fuel. Their parameters are summarized in table 5. The obtained volumes of the emitted substances are shown in figure 1. The results concern the amount of chemical compounds produced per year.

Table 5. Parameters of 20kW boilers fueled by various fuels.

Boiler nominal power [kW]	Fuel type	Boiler efficiency [%]	Fuel calorific value [MJ/kg]	Max. ash content in fuel [%]	Max. sulfur content in fuel [%]
20	Hard coal	91	28	7	0,6
20	Coke	85	28,5	10,5	0,6
20	Wood	89	17	0,5	-

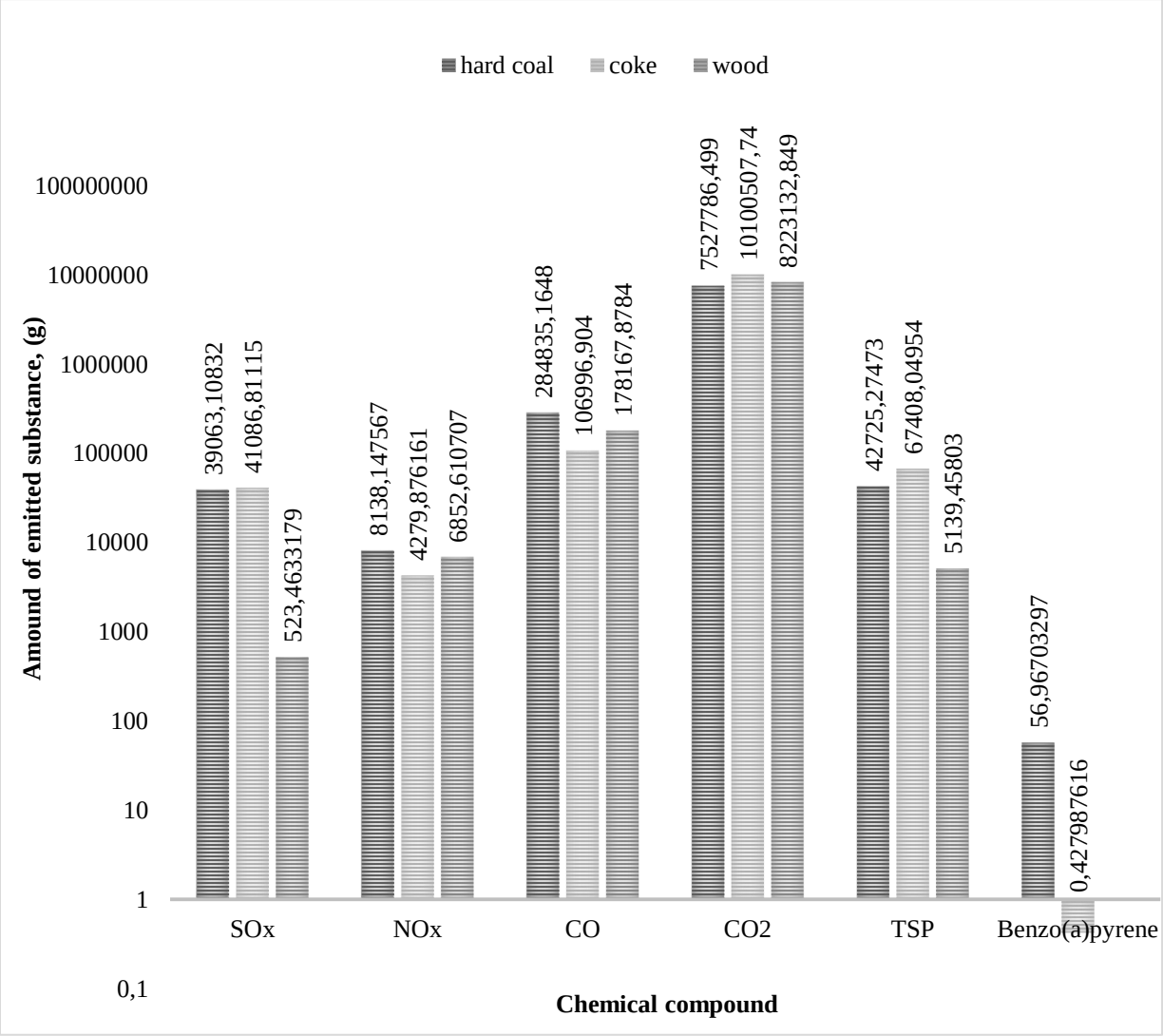

Fig 1.Substance emissions for various 20kW boilers.

The results show that the hard coal fired boiler generates the greatest amount of harmful substances. Emissions of nitrogen oxides (NOx), carbon monoxide (CO) and carbon dioxide (CO_2) using different types of fuel reach the same order of magnitude. The wood fired boiler is the best in the sheet. The amount of sulfur oxides (SOx) and total suspended particles (TSP) produced is much lower compared to other fuels.

4. Conclusion

The aim of this study was to present standards for low-emission low power heating devices in the European Union. Regulations aimed at improving quality of life on Earth and counteracting rapid climate changes were introduced. Paper presented principles according to which member states are obliged to act to achieve the air purity levels contained in this regard published by World Health Organization. In the calculation part, the emissions for boilers meeting the Ecodesign assumptions were obtained. The results depend on the type of fuel, its parameters, consumption and efficiency of the device. The effect of the accounts presents the results of the implementation of the requirements of [2] and [6]. Thus, it determines the emission reduction obtained as a result of the implementation of projects limiting or completely eliminating the combustion of solid fuels with high substance emission rates and as a result of the use of other primary and secondary methods of reducing substance emissions.

References

[1] Communication from the Commission to the European Parliament, the Council, the European Economic and Social Committee and the Committee of the Regions. Brussels, 18/12/2013 COM (2013) 918 final.

[2] Commission Regulation (EU) 2015/1189 of 28 April 2015 implementing Directive 2009/125/EC of the European Parliament and of the Council with regard to ecodesign requirements for solid fuel boilers.

[3] Commission Delegated Regulation (EU) 2015/1187 of 27 April 2015 supplementing Directive 2010/30/EU of the European Parliament and of the Council with regard to energy labelling of solid fuel boilers and packages of a solid fuel boiler, supplementary heaters, temperature controls and solar devices.

[4] Directive (EU) 2016/2284 of the European Parliament and of the Council of 14 December 2016 on the reduction of national emissions of certain atmospheric pollutants, amend Directive 2003/35 / EC and repealing Directive 2001/81 / EC.

[5] Directive 2003/35/EC of the European Parliament and of the Council of 26 May 2003 providing for public participation in respect of the drawing up of certain plans and programs relating to the environment and amending with regard to public participation and access to justice Council Directives 85/337/EEC and 96/61/EC.

[6] Directive 2009/125/EC of the European Parliament and of the Council of 21 October 2009 establishing a framework for the setting of ecodesign requirements for energy-related products.

[7] EUCO 169/14 Brussels, 24 October 2014 (OR en.).

[8] KOBiZE, Wskaźniki emisji zanieczyszczeń ze spalania paliw w kotłach o nominalnej mocy cieplnej do 5 MW, Warszawa styczeń 2015.

[9] Regulation (EU) 2017/1369 of the European Parliament and of the Council of 4 July 2017 setting a framework for energy labelling and repealing Directive 2010/30/EU.

[10] https://powietrze.malopolska.pl/ekoprojekt/ (2/12/2020)

Indium sulfide precipitation in preparation and industrial processes

Andrzej Piotrowicz[1], Stanisław Pietrzyk[2]

[1,2]AGH University of Science and Technology, e-mail: andpio@agh.edu.pl

Abstract

Indium(III) sulfide (of which few polymorphs are distinguished) are both the final product of commercial and utility value, as well as byproduct in indium production and recovery. Indium(III) sulfide has some interesting applications, most notably as a semiconductor in photoelectronic devices. Its uses depend not only on the polymorphic form, but also on the shape and dimensions of the particles (in nanometric scale). Precipitation from aqueous solutions, beside to elemental synthesis and other more complicated methods, is the simplest and most important In_2S_3 preparation method. In chemical processing, like metallurgy and wastes treatment, indium sulfide precipitation is the stage of extraction process, which main goal is to precipitate an insoluble indium compound or to separate indium from iron and copper ions. This paper presents synthesis methods and industrial processes involving indium(III) sulfide precipitation.

Keywords: indium sulfide, precipitation, indium metallurgy

1. Introduction

Among indium sulfides (or indium sulphides), indium(III) sulfide, In_2S_3, is the most common indium and sulfur compound and about it will most often be mentioned in this paper. Indium sulfides do not occur naturally in pure form; among sulfide minerals of indium only mixed sulfides are distinguished, i.e. roquesite ($CuInS_2$), laforêtite ($AgInS_2$) and others [1]. It concerns mainly sulfide ores of heavy metals, in which indium can be founded in such minerals as sphalerite, chalcopiryte, stannite and other [2], and their concentrates (as in [3,4]). Thus, indium sulfides can only be obtained by synthesis under laboratory conditions.

2. Physicochemical properties and applications of indium(III) sulfide

There are many indium-sulfur compounds, depended by composition and temperature [5-8], and the existence of some of them is postulated [5,6]. In the paper, the description is narrowed down to those that are commonly known, i.e. indium(III) sulfides. The crystal chemistry of the In_2S_3 is quite complicated: the high-temperature stable forms of the In_2S_3 can be related to standard structure; β-In_2S_3 is a defect spinel, while α-In_2S_3 has a structure like that of a cubic form of Al_2O_3; the unstable γ-In_2S_3 has a layered structure (-S-In-S-In-S-…) (see Table 2.1.) [9-11]. In_2S_3 precipitation is limited to α-In_2S_3. The β-In_2S_3 is the most stable under standard conditions, because does not absorb moisture. Sometimes α-In_2S_3 can be amorphous - it depends on the conditions under which it was synthesized or by containing of voids [12]. α-In_2S_3 is a yellow (gold-yellow if freshly precipitated) hygroscopic solid, does not dissolve in water, but dissolves in mineral acids and sodium sulfide.

However, the most important property of β-In_2S_3 is value of optical band gap, i.e. the exciton energy (bound state of an electron and hole which are held together by the Coulomb force) which determines the onset of vertical interband transitions; optical band gap value is about 2.0 eV [14,15] making it an N-type semiconductor. Generally, with the characterization of the photoelectric properties and development of production methods of In_2S_3, its use in solar cell has been suggested. This applies especially to the possibility of substituting the hazardous cadmium sulfide, constituting the buffer layer [16,17]. The processing and use in solar cells of cadmium sulfide is more harmful to the environment and human health than indium(III) sulfide. Hence, In_2S_3 has become an important precursor for the manufacturing complex semiconductor materials [13]. Other, less significant applications of In_2S_3 are: photocatalytic

hydrogen production [18], lung scanning agent for medical imaging [19], luminescence particles in phosphors [20], lithium-ion battery, photodetectors and thermoelectric materials [21].

Table. 2.1. Some physicochemical properties of In_2S_3 polymorphs [6-8,12,13]

	crystal system, space group	temperature of phase transition[1] [^{0}C]	temperature range[1] [^{0}C] and conditions of stability	energy gap[2] [eV]	density [g·cm^{-3}]	color
α-In_2S_3	cubic, Fd3m		415÷750 <415 with excess In		4.63	gold-yellow
β-In_2S_3	tetragonal, $I4_1/amd$	415	<750	1.8÷3.7	4.613	brick red
γ-In_2S_3	trigonal, P3m1	750	<1050 <415 with As or Sb in tetrahedral positions between layers	1.38÷1.88 (As) 1.42÷1.44 (Sb)	4.75 (As) 4.80 (Sb)	n.d.

1 - based on [7], 2 - depended by preparation and measurement method

3. Preparation of indium sulfides

Under conventional laboratory conditions, indium sulfides can be prepared through high-temperature or aqueous solution route. As a result of the reaction between indium oxide and hydrogen sulfide, which proceeds according to the stoichiometry [22]:

$$In_2O_{3_s} + H_2S_g \xrightarrow{500\div700^0C,several\ h} \beta In_2S_{3_s} + H_2O_g \quad (Equation\ 1)$$

high-temperature modification of In_2S_3 is formed. Sulfides with other In:S ratios, i.e. InS and In_2S, are formed as a result of direct synthesis (2) or reaction between indium(III) sulfide and indium (3) [22]:

$$In_s + S_s \xrightarrow{1100^0C} InS_s \quad (Equation\ 2)$$

$$In_2S_{3_s} + 4In \xrightarrow{700\div720^0C,high\ vacuum} 3In_2S_s \quad (Equation\ 3)$$

Preparation of the low-temperature In_2S_3, i.e. α-In_2S_3, is possible only from aqueous solution. α-In_2S_3 is precipitated from a solution containing In^{3+} cations (chlorides, sulfates, etc.) using hydrogen sulfide or S^{2-} anions (Na_2S, NaHS) (Fig. 3.1. shows the theoretical situation of precipitation by using Na_2S):

$$2In^{3+} + 3S^{2-} \rightarrow \alpha In_2S_{3_s} \quad (Equation\ 4)$$

This reaction is used in analytical chemistry to indium separation from the analytical group III and IV metals with Sn(IV) as collector. Precipitation process can be confused in many ways. It is known that indium complexing in chloride solution with chloride ions prevents the α-In_2S_3 precipitation [23]. Hence, it is desirable that the α-In_2S_3 precipitation proceed with small amount or without other ions which reduce the precipitation efficiency. As α-In_2S_3 is hygroscopic, irreversible transition to non-hygroscopic β-In_2S_3 by heating to transition temperature can be performed on it [7,22]. Practically, precipitated α-In_2S_3 is heat treated to obtain crystallized β-In_2S_3 for use in final applications.

High efficiency solar cells can indeed be achieved with In_2S_3 buffer layers grown by almost all of the deposition techniques: physical vapour deposition (PVD), chemical vapour deposition (CVD), chemical bath deposition (CBD) and their varieties, like radio frequencies sputtering, spray ions layer gas reaction (ILGAR), spray pyrolysis, spin

coating [13,21]. Although the In_2S_3 preparation for optoelectronic is possible by precipitation from an aqueous solution [25], however, PVD, CVD and CBD methods are commonly used because they allow obtaining materials of appropriate size and shape, not only bulk materials, as well as a more controlled route of In_2S_3 deposition [13]. The thickness of the indium sulfide buffer, depending on technique, is approx. 15÷500 nm. Conversion efficiencies of solar cells based In_2S_3 reach about 20 % [13,26-29] and grows with the value of optical band gap.

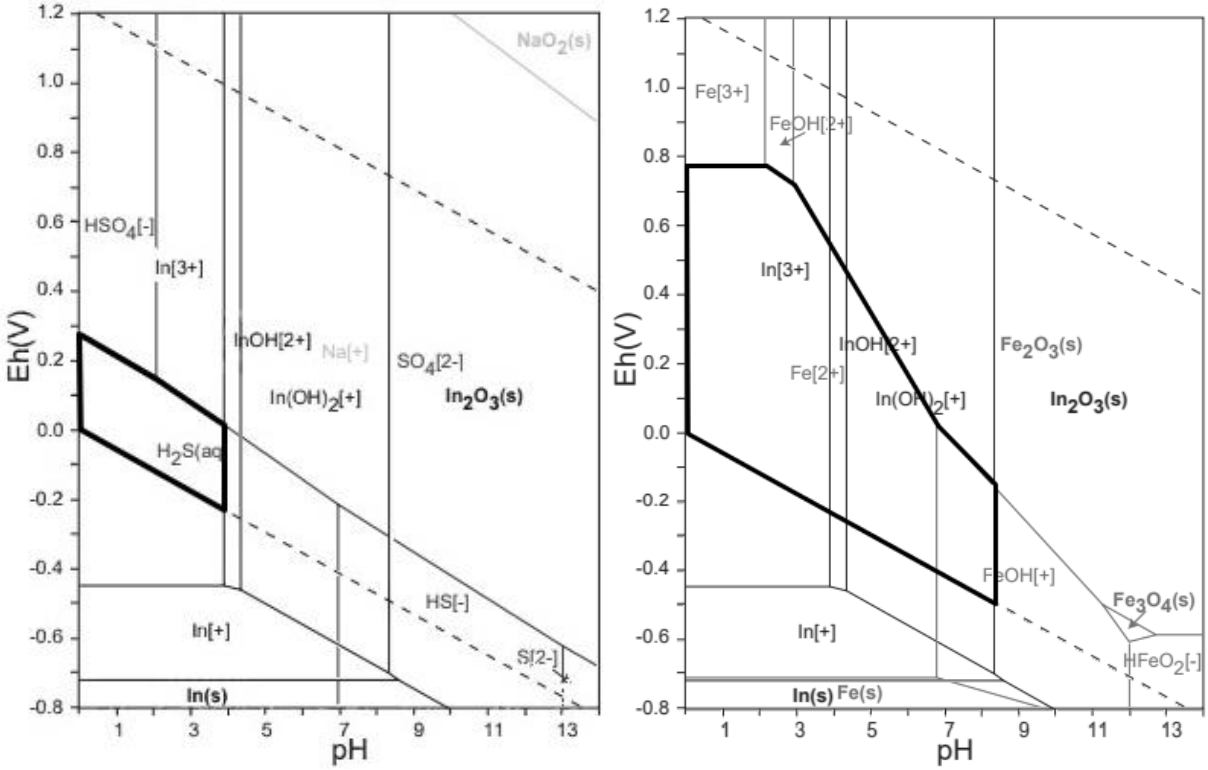

Fig 3.1. Eh-pH diagram for In-S-Na system (left) and In-Fe (right) (standard conditions), the areas of indium sulfide precipitation (left) and separation from iron (right) are marked with a thick frame (based on [24])

Deposition of In_2S_3 by the PVD method [27,29,30] is particularly important when it is possible to deposit other layers of solar cells (absorber, transparent conductive oxide) under the same conditions, which enable a significant simplification of the manufacturing process [30]. This process consists in the thermal evaporation of elemental indium and sulfur in vacuum chamber onto the substrate kept at the substrate (Na-free glass) temperature (130÷200 ^{0}C) [27,29]. An additional annealing step is required to form high-quality crystallized In_2S_3 [29,31].

CVD offers significant advantages over PVD methods: simple apparatus, mild process condition, control over composition, high deposition rates and large scale processing [32].Conventional CVD includes CVD with single-source precursors (separately indium and sulfur precursors). Basically, chemical vapour deposition of indium sulfide is classified into atomic layer chemical vapor deposition (ALCVD) [26,33] and metal organic chemical vapour deposition (MOCVD) [32,34-36]. ALCVD is based on sequential introduction of reacting precursors into the reactor and growth proceeds only via surface reactions. Reactions are controlled at the atomic layer level. The precursors are various indium and sulfur compounds such as indium acetylacetonate ($In(acac)_3$), hydrogen sulfide [26,33] and various other organic and metal-organic compounds which may include indium, sulfur and both together (e.g. $[^tBu)_2In(S^tBu)]_2$) [32,34-36]. The application of metal-organic compounds requires a higher temperature of processing (300÷850 ^{0}C) [35].

CBD is a method under aqueous conditions of preparation thin films and nanomaterials. CBD has been developed as a simple (only solution containers and substrate mounting devices) and low-cost method based on the precipitation from indium ions and sulfur source [28,37]. More details on the use of In_2S_3 precipitation in wet deposition in the next chapter.

4. Indium sulfides precipitation in chemical bath deposition

In the researches [28,37-42], chemical bath deposition was applied to form In_2S_3 by precipitation (Table 4.1.). Low-temperature wet-chemical reaction, given by [38]:

$$In^{3+} + NaHS_2 \rightarrow In_2S_{3_s} + Na^+ + 2H^+ \quad (Equation\ 5)$$

results to synthesis amorphous α-In_2S_3 powder [38]. Commonly used precursors in wet methods In_2S_3 deposition are indium(III) chloride and thioacetamide (CH_3-$CSNH_2$) [28,37,39,42]. It is suggested that In^{3+} hydrolysis occurs initially under the existence of CH_3-$CSNH_2$ leads to the formation of $In(OH)_xS_y$ [39]:

$$In^{3+} + CH_3CSNH_2 + H_2O \rightarrow In(OH)S + CH_3COOH + NH_4{}^+ + 2H^+ \quad (Equation\ 6)$$

which subsequently is converted into In_2S_3 [39]. In work [28], the difference between the dry and wet method of In_2S_3 preparation was investigated. Indium chloride and acidic CH_3-$CSNH_2$ solution as precursors and acidic additives were used. The research results shows that the type of substrate does not affect the preferential orientation of In_2S_3 and also that In_2S_3 films have less oxygen than when the high-temperature method is applied. In another study [42], the same precursors as in [28] were used, but investigation has been focused on examining the effect of temperature. At temperature 30 ^{0}C deposited layer was amorphous, and distribution of grain sizes on the surface of the film deposit is non-homogenous. With increasing temperature to 70 ^{0}C, β-In_2S_3 film get more crystalline and crystallites will be more agglomerate, but increasing to 85 ^{0}C caused the material to become amorphous and non-homogenous distributed. The higher the temperature, the higher the band gab energy (from 2,8 to 3.18 eV at 30 ^{0}C and 85 ^{0}C, respectively). The author of the yet another study [40] managed to obtain amorphous In-S compound, whose composition is changed depending on the solution pH (atomic ratio In:S were 46:58 and 36:63, respectively for pH 4 and 9). The aim of the research [41] was the co-precipitation of copper, gallium and indium sulfides using sodium sulfide as a precipitating agent (analogously to the formula 4). The dissolved metals in the acids were precipitated in few steps: 1. Homogenization in terms of bath temperature (310 K) and composition solution (stoichiometric contents of metal ions), 2. Precipitation by addition of Na_2S (10 % excess), 3. Washing and drying (373-393 K). As a result of co-precipitation of various metal sulfides, $CuIn_{0.8}Ga_{0.2}S_2$ is synthesized – a mixture in which CuS crystallizes in the hexagonal phase and In_2S_3, $CuIn_2S$ and $CuGa_2S$ in the tetragonal phase. Due to the low crystallinity, additional thermal treatment step (673 K) is required, accompanied by the evolution of sulfur(IV) oxide (a product of partial decomposition of sulfides).

Table 4.1. Examples of In_2S_3 precipitation in CBD application

ref.	indium precursor	sulfur precursor	additives	substrate	precipitation and post-treatment conditions
[38]	indium(III) chloride	sodium hydrosulfide (soln)		glass	50 ^{0}C
[39]	indium(III) chloride	thioacetamide		- glass coated tin oxide - α-Al_2O_3 plate	30 or 70 ^{0}C
[28]	indium(III) chloride	thioacetamide	- hydrochloric acid - acetic acid	- amorphous glass - glass coated tin oxide	70 ^{0}C 0÷50 min

				- crystalline Si	
[40]	indium sulfate	thioacetamide	- hydrazine hydrate - triethanolamine	- glass - glass coated indium-tin oxide	room temperature 120 min pH = 4 or 9
[42]	indium(III) chloride	thioacetamide	acetic acid	glass	35÷85 ^{0}C
[37]	indium(III) chloride	thioacetamide	aluminum chloride	glass	70 ^{0}C 45 min pH = 2
[41]	indium(III) chloride	sodium sulfide (soln)	- nitric acid - hydrochloric acid - copper nitrate - gallium nitrate		10÷120 ^{0}C 1 h

5. Indium sulfides precipitation in industrial practice

In industry, the sources of indium are:

1. ores and concentrates of indium - sulfides ore of heavy metals, especially Zn and Pb, are mining, classified and enriched (crushing, screening, flotation, feed averaging, roasting). Concentrates are directed to next extractive operations of zinc and lead metallurgical production, for example Imperial Smelting Process (ISP) and zinc refining. As a result of the production of zinc and lead, indium-bearing by-products are formed, in which the indium content is sufficient for indium recovery [1,3,4,43-46].
2. indium-bearing by-product - the sources of these materials are material flow of primary production of zinc, lead, copper and cadmium, and they are various types of ashes, slags, fumes, drosses etc. In secondary sources of indium, In content can be reached from few-hundred ppm to dozens %. Sometimes they are used as the primary mineral resource, but usually their further processing is already hydrometallurgical processes, although it may be preceded by pirometallurgical treatment (e.g. to evaporate volatile metals such as Zn) [43,44,46-53]
3. post-processing water resources - there are contaminated water or sludges which, due to the content of heavy metals such as copper, lead, thallium and mercury, must be treated. Among mentioned metals, there may also be indium, which is co-removed during purification (usually by chemical treatment) [54]. The sources of post-processing water are the mining and chemical industry (metallurgy, manufacturing, indium materials etching [43,55]) and chemical laboratories in research centers.
4. indium wastes - the most important application of indium is indium-tin oxide (ITO). Due to electrical conductivity while maintaining optical transparency, ITO is wide used in transparent conducting thin film in liquid-crystal displays (LCDs) in different electrical devices. Upon discarded, the ITO scrap, waste LCDs and rejected solar cells are valuable alternative resource for the indium recycling. [21,46,55-57].

Indium sulfide precipitation is of course related to hydrometallurgical processes and occurs in the primary production of indium, indium-containing aqueous solution treatment and in its recycling methods. For practical reasons, the indium separation from other metals, such as tin, copper and iron, in aqueous solutions is particular importance. For example, ITO waste can be treated by hydrochloric and sulfuric acid leaching and tin sulfide precipitation [56,57]. Separation of indium from iron can be carried out by precipitation of their sulfides [58]: indium sulfide is less soluble than iron sulfide. This method is not very efficient even if fractional precipitation is performed [58]. Another way of separating indium from iron is reduction to form Fe^{2+} and neutralization [44,45,47-52]. This situation is presented in Fig. 3.1 (right). The addition of S^{2-} ions into the solution (for example Na_2S) reduces

ferric (Fe^{3+}) to ferrous (Fe^{2+}); ferrous ions are stable in the wide range of pH. The neutralization (to pH 6÷10) causes the In_2S_3 precipitation [44,49-52]. In the case of indium processing, the sulfides precipitation is almost always an intermediate step followed by subsequent operations (leaching-precipitation) that allow the full separation of indium [44,47-52,59]. Table 5.1. presents results of few research in field of indium recovery with using indium sulfide precipitation (more details in the following paragraphs).

Embodiment of the indium recovery by a fractional precipitation of sulfides is below described patent [47]. Starting material is a solution obtained by acid leaching of zinc calcines or fumes (70 % Zn, 6 % Pb, 0.05 % In). Hydrogen sulfide is passed through the solution whereby sulfides precipitate. The solution from precipitation is discarded and the precipitate is leached in sulfuric acid. Due to the high acidity of the solution concentrated in indium, it must be neutralized to the appropriate level: acid concentration above 45 g H_2SO_4 per liter retards the indium precipitation, while less than about 40 g H_2SO_4 per liter promotes the precipitation of zinc. The leaching-neutralization-precipitation-solid/liquid separation sequence (Fig. 5.1.) is repeated, whereby the more soluble sulfides impurities (Cu, As, Sb, other) are removed and the precipitate is concentrated indium sulfide.

Table 5.1. Results of research about indium recovery by indium sulfide precipitation: η - efficiency, leach - leaching, prec - precipitation, conc. - concentrate, red - reduction, filtr – filtration, roast - roasting

In-bearing material ref.	initial material composition [%]	stages of processing 1 opt. factors results [%]	 2 opt. factors results [%]	 3 opt. factors results [%]	post-process In conc. [%]
copper-smelting ash [48]	Cu-10.3 Zn-8.8 Fe-2.5 Bi-2.2 S-9.5 Pb-19.1 As-4.7 Re-13 (ppm) In-278 (ppm)	roasting 250 ^{0}C, 1.5 h m_{H2SO4}/m_{slag} = 0.1 $\eta_{roast\ In}$ = 90÷95	leach. by water water 60 ^{0}C, 1 h L:S = 5 $\eta_{leach\ In}$ > 97.5	In prec. Na_2S pH = 4 $\eta_{prec\ In}$ = 99	n.d.
roasted zinc sulfide conc. [44,49,50]	Zn-68.7 SO_3-5.6 SiO_2-5.9 Fe_2O_3-6.0 LOI-8.13 MgO-1.21 Pb-1.8 In-45 (ppm)	neutral leach. pH = 3 70 ^{0}C, 75 min L:S = 7.5 $\eta_{leach\ Zn}$ = 92.5 $\eta_{leach\ In}$ = 4.2	reductive leach. of Fe^{3+} 100 g H_2SO_4 / dm^3 90 ^{0}C, 3 h M_{real}/M_{theory} Na_2S = 1.5 $\eta_{leach\ Zn}$ = 70 $\eta_{leach\ In}$ = 97.5 $\eta_{leach\ Fe}$ = 56 $\eta_{red\ Fe}$ = 67	selective In prec. ammonia pH_f = 6 90 ^{0}C, 10 min $\eta_{prec\ Zn}$ = 12 $\eta_{prec\ In}$ = 100 $\eta_{prec\ Fe}$ = 7.8	Zn-31.4 SO_3-47.4 SiO_2-3.7 Fe_2O_3-7.8 LOI-5.5 In-2650 (ppm)
In-bearing copper dross [51,52]	Pb-40 Cu-32 Sn-6 Zn-7 Fe-3 Ni-1.5 Sb-1.5 In-1150 (ppm)	oxidative leach. 1.5 M HCl L:S = 4 70 ^{0}C, 3 h T_{filtr} = 20 ^{0}C $\eta_{leach\ In}$ = 94.6	Cu prec. 70 ^{0}C, 2 h pH < 1.2 7.5 g Na_2S / dm^3 $\eta_{prec\ Cu}$ = 98 $\eta_{prec\ Sn}$ = 3 $\eta_{prec\ As}$ = 15 $\eta_{prec\ Sb}$ = 53 $\eta_{prec\ In}$ = 10	Sn-In conc. prec. NaOH 70 ^{0}C 2 h pH = 4.5	Pb-1.6 Sn-65 In-7.7

		acidic leach.	Cu prec.	Sn-In conc. prec.	
In conc. own, a similar as in [51,52]	Fe_2O_3-4 CuO-13 ZnO-10 GeO_2-7 Ag_2O-1 SnO_2-44 PbO-15 In_2O_3-5	6.5 M H_2SO_4 80 ^{0}C, 3 h L:S = 4	Na_2S 80 ^{0}C ,2 h pH_f = 0.5	NaOH pH_f = 9	SO_3-3 Fe_2O_3-24 ZnO-14 GeO_2-10 SnO_2-3 In_2O_3-40
		$\eta_{leach\ Fe}$ = 93 $\eta_{leach\ Cu}$ = 99 $\eta_{leach\ Zn}$ = 98 $\eta_{leach\ Fe}$ = 98	solid phase [%]: SO_3-44 CuO-54 GeO_2-1 In_2O_3-0.1 SnO_2-7 PbO-2	$\eta_{prec\ Fe}$ = 81 $\eta_{prec\ Zn}$ = 100 $\eta_{prec\ Cu}$ = 100 $\eta_{prec\ Ge}$ = 100 $\eta_{prec\ In}$ = 76 $\eta_{prec\ Sn}$ = 32	

Another way to recovery indium is presented in [48] (Fig. 5.2.). The initial material is copper-smelting ash (called white ash) from copper converting production. The initial material is pre-leached to remove most of the copper and zinc. The resulting leaching slag is roasted with 98 % sulfuric acid. Without the addition of sulfuric acid, only 7 % In can be recovered further, but at a mass ratio of acid to leaching slag above 0.1, it is possible to recover above 90 % In. Increasing the roasting temperature above 250 ^{0}C causes the acid to react significantly with other components, such as lead and bismuth. The optimal range of temperature and duration of roasting is 200÷250 ^{0}C and 1÷1.5 h, respectively. Then calcine is leached by water for 1 h with 5:1 of liquid:solid ratio at 60 ^{0}C. Over 90 % of indium can be leached. The filtrate form this stage is copper concentrate containing indium. After cooper extraction, from raffinate indium can be recovered by two ways: substitution by zinc or precipitation by using sodium sulfide. At pH 2, the recovery of indium is 85.3 and 97.3 %, and at pH 4, 90.3 and 99.0 % for substitution by zinc and precipitation by sodium sulfide, respectively.

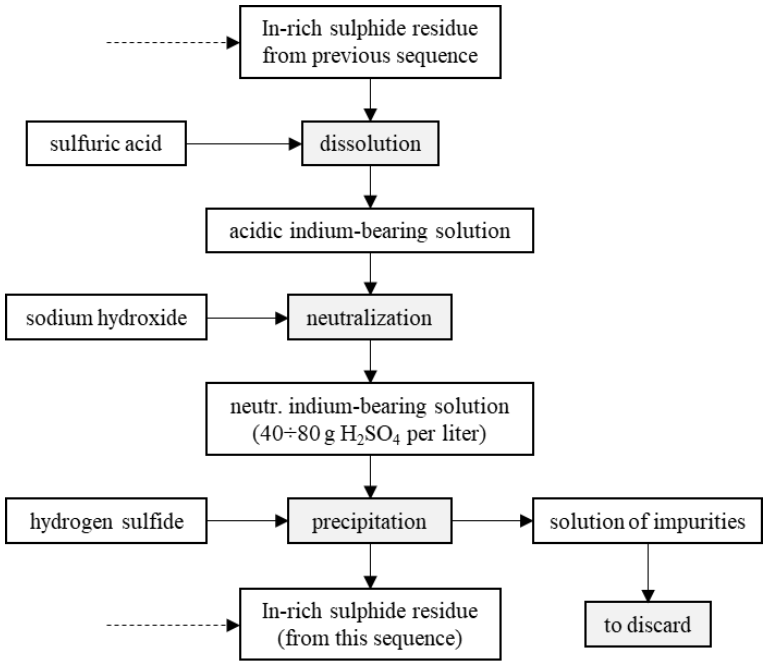

Fig. 5.1. Sequence in indium recovery method by fractional precipitation of sulfides (based on [47])

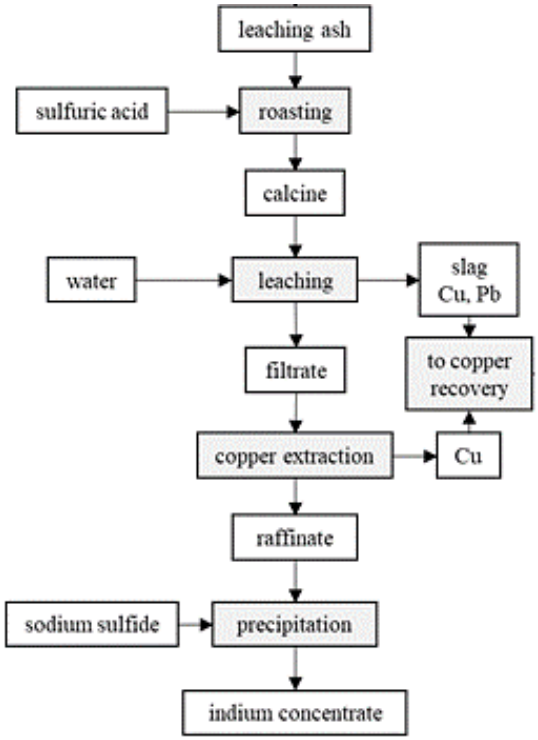

Fig. 5.2. Flow chart of the indium recovery from copper-smelting ash by using sodium sulfide (based on [48])

In the studies on the recovery of indium from zinc plant residues [44,49,50], the ferric ions reduction and selective precipitation of indium sulfide by pH change were used. The sequence of steps is as follows: 1. Leaching of material in sulfuric acid, 2. Reductive leaching of Fe^{3+} by using sulfuric acid and sodium sulfide, 3. Indium precipitation by neutralization. The most optimal conditions for acid leaching, while maintaining the maximized dissolution of zinc and the minimized dissolution of indium, are as follows: pH = 3, T = 70 ^{0}C, τ = 75 min, L:S = 7.5. Under these conditions, the dissolution efficiencies of zinc and indium are 92.5 % and less than 4.2 %, respectively. Sulfuric acid and sodium sulfide are used to reductive leaching of solid residue from acid leaching stage, and the optimal conditions for this stage are as follows: 100 g H_2SO_4 per liter, T = 90 ^{0}C, τ = 3 h. Addition amount of Na_2S is 1.5 times of theoretical amount for reducing Fe^{3+} to Fe^{2+}. For the selective precipitation of indium with using ammonia, the following parameters are used: pH_{final} = 6, T = 90 ^{0}C, τ = 10 min. Ammonia is the best selective indium precipitant taking into account the coexisting iron and zinc. Under optimum conditions, the precipitation percentage of indium, iron and zinc are 100, 7.8 and 12 %, respectively. Repeating the reductive leaching and precipitation stages on the freshly precipitant under the same technological conditions reduces the ratio of iron to indium from 680:1 to 26:1. By the way, in study [45], for reductive leaching stage can be used sphalerite concentrate (ZnS and (Zn,Fe)S) as reductant.

The studies on recovery of indium from copper drosses from lead refining were concerned [51,52]. The concept of their processing (Fig. 5.3.) is as follows: 1. Granulometric separation, 2. Leaching with hydrochloric acid, 3. Copper precipitation by using sodium sulfide, 4. Tin-indium concentrate precipitation, 5. Oxidative dissolution of concentrate, 6. Removal of residual impurities in the sulfide form, 7. Indium-tin concentrate precipitation. The main parameters of the fed material leaching operation are: 1.5 M HCl, L:S = 4, T = 70 ^{0}C, τ = 3 h. Copper sulfide precipitation is optimal according to the following parameters: T = 70 ^{0}C, τ = 2 h, pH < 1.2. Precipitation allows the effective removal of copper and also antimony and arsenic. To reduce Fe^{3+} ions, the addition of metallic iron can be used. The indium loss at this stage is less than 10 %. Elimination of tin during concentrate precipitation by using NaOH takes place at a pH about 4.5, 70 ^{0}C and after 2 h. After these steps, obtained concentrate has >5 % In. The next proposed steps for enrichment of tin-indium concentrate are: - Dissolution of concentrate

in a H_2SO_4-H_2O_2 with the parameters: L:S = 5, T = 70 ^{0}C, τ = 3 h, pH_{final} = 0.9, - Purification of the indium solution with Na_2S by precipitation of impurities (Sn, Pb, As, Sb) at temperature 70 ^{0}C, duration 2 h, final pH < 1.2, - Indium-tin concentrate precipitation by using ammonia, thanks to which the residual copper and zinc are eliminated. These additional steps should result in an indium-rich concentrate (>60 % In), which is an indium-bearing by-product for further processing.

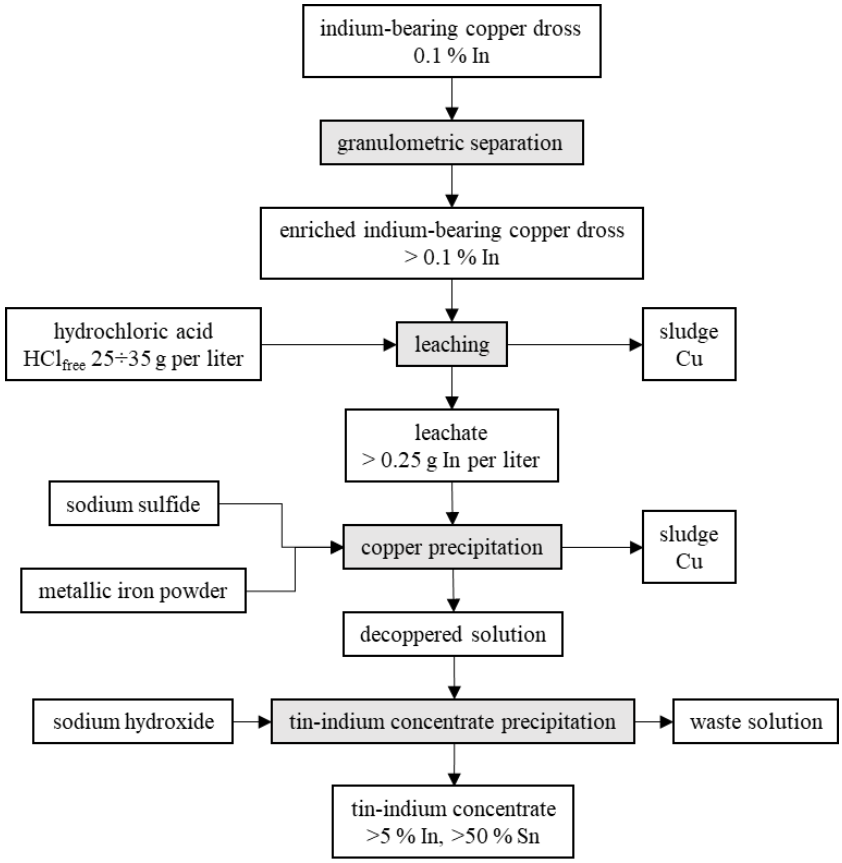

Fig. 5.3. Preliminary steps of indium recovery from copper dross by using sodium sulfide (based on [51,52])

6. Conclusion

The beta-indium sulfide has a high value of the energy gap and is therefore important in the manufacturing of solar cells, where it is an alternative of cadmium sulfide. The preparation of indium sulfide for photoelectronic applications is carried out by physical or chemical deposition. In this second, indium sulfide is prepared by precipitation from solutions of various precursors.

Indium sulfide is also by-product in various production and recovery processes, especially in heavy metal metallurgy. Sulfide precipitation method is used to separate indium from copper, tin, iron and other impurities. Indium recovery occurs either by direct indium sulfide precipitation or by precipitation of sulfides impurities and then neutralization of the solution and thus precipitation of the indium concentrate. The indium concentrate obtained in these ways is suitable for the next processing stages.

References

[1] N.J. Cook, C.L. Ciobanu, T. Williams, The Mineralogy and mineral chemistry of indium in sulphide deposits and implications for mineral processing, Hydrometallurgy, 108(3-4), 2011, 226-228

[2] J.A. Briskey, Indium in Zinc-Lead and Other Mineral Deposits - A Reconnaissance Survey of 1118 Indium Analyses Published Before 1985, USGS, 2005

[3] S. Li, M. Tang, J. He et al., Extraction of indium from indium-zinc concentrates, Transactions of Nonferrous Metals Society of China, 16(6), 2006, 1448-1454

[4] 魏昶, 李存兄, 樊刚, Method for leaching indium from indium sulfide concentrate, CN101113490A, 2010

[5] T. Goedke, K. Schubert, In the Phase Diagram InSM, Z. Metallkd., 76(5), 1985, 358-364

[6] A.Y. Zavrazhnow, A.V. Naumov, P.V. Goncharov et al., T-x phase diagram of the In-S system, Inorganic Materials, 42(12), 2006, 1294-1298

[7] H. Okamoto, In-S (Indium-Sulfur), Journal of Phase Equilibria and Diffusion, 34(2), 2012, 149-150

[8] P. Pistor, J.M.M. Alvarez, M. Leon et al., Structure reinvestigation of α-, β- and γ-In_2S_3, Acta Cryst., B72, 2016, 410-415

[9] G.A. Steigmann, H.H. Sutherland, The Crystal Structure of -In_2S_3, Acta Crystallogr., 19, 1965, 967-971

[10] M.J. Taylor, P.J. Brothers, Inorganic derivatives of the elements, in: Chemistry of Aluminium, Gallium, Indium and Thalium, edited by A.J. Downs, Blackie Academic & Professional, 1993

[11] D. Bahadur, Inorganic Materials: Recent Advances, Alpha Sciences International, Ltd., 2004

[12] O. Madelung, III2-VI3 compounds, in: Semiconductors: Data Handbook, 3rd edition, Springer, 2004

[13] N. Barreau, Indium sulfide and relatives in the world of photovoltaics, Solar Energy, 83, 2009, 363-371

[14] W. Rehwald, G. Harbeke, On the conduction mechanism in single crystal β-indium sulfide In_2S_3, J. Phys. Chem. Solids, 26, 1965, 1309

[15] K. Kambas, A. Anagnospopoulos, A. Ves et al., Optical Absorption Edge Investigation of $CdIn_2S_4$ and β-In_2S_3 Compounds, Phys. Stat. Sol., 1985, 127, 201

[16] S. Siebentritt, Alternative buffers for chalcopyrite solar cells, Solar Energy, 77(6), 2004, 767-775

[17] D. Hariskos, S. Spiering, M. Powalla, Buffer layers in Cu(In,Ga)Se_2 solar cells and modules, Thin Solid Films, 480–481, 2005, 99

[18] B. Chai, T. Peng, P. Zeng et al., Synthesis of Floriated In_2S_3 Decorated With TiO_2 Nanoparticles for Photocatalytic Hydrogen Production Under Visible Light, J. Mater. Chem., 21, 2011, 14587-14593

[19] J. Csetenyi, S.I. Szamel, M. Fyzy et al., Albumin Macroaggregates Containing ^{113m}In-sulfide (^{113m}In SMAA): Technique for the Preparation of a New Lung Scanning Agent, Proc. Int. Symp. Nucl. Med., 3, 1974, 293-301

[20] W. Chen, J. Bovin, A. Joly et al., Full-Color Emission from In_2S_3 and In_2S_3:Eu^{3+} Nanoparticles, J. Phys. Chem. B, 108, 2004, 11927-11934

[21] J. Zhang, H. Wang, X. Yuan et al., Tailored indium sulfide-based materials for solar-energy conversion and utilization, Journal of Photochemistry and Photobiology C: Photochemistry Reviews, 38, 2019, 1-26

[22] E. Doenges, Gallium, Indium, Thalium, in: Handbook of preparative inorganic chemistry, edited by G. Brauer, Academic Press, 1963

[23] N.V. Kochetkova, Y.E. Bayandina, G.M. Toptygina et al., Indium sulfide precipitation from hydrochloric acid solutions of calcium and sodium chlorides, Kompleksn. Ispol'z. Miner. Syr'ya, 5, 1988, 54-57

[24] Atlas of Eh-pH diagrams, Geological Survey of Japan Open File Report No.419, National Institute of Advanced Industrial Science and Technology Naoto TAKENO, 2005

[25] P. Rao, S. Kumar, N. Raje et al., Synthesis of binary and multinary metal sulphides by precipitation and their characterisation, Materials Research Bulletin, 79, 2016, 105-114

[26] N. Naghavi, S. Spiering, M. Powalla et al., High-efficiency copper indium gallium diselenide (CIGS) solar cells with indium sulfide buffer layers deposited by atomic layer chemical vapor deposition (ALCVD), Progress in Photovoltaics: Research and Applications, 11(7), 2003, 437–443

[27] S. Gall, Barreau N., S. Harel et al., Material analysis of PVD-grown indium sulphide buffer layers for $Cu(In,Ga)Se_2$-based solar cells, Thin Solid Films, 2005, 480-481, 138-141

[28] B. Asenjo, C. Sanz, C. Guillén, et al., Indium sulfide buffer layers deposited by dry and wet methods, Thin Solid Films, 515(15), 2007, 6041–6044

[29] N. Barreua, A. Mokrani, F. Couzinie-Devy et al., Bandgap properties of the indium sulfide thin-films grown by co-evaporation, Thin Solid Films, 517(7), 2009, 2316-2319

[30] N. Barreau, S. Marsillac, D. Albertini et al., Structural, optical and electrical properties of β-$In_2S_{3-3x}O_{3x}$ thin films obtained by PVD, Thin Solid Films, 403-404, 2002, 331-334

[31] S. Kosaraju, J.A. Marino, J.A. Harvey et al., Plasma-assisted co-evaporation of β-indium sulfide thin films, Solar Energy Materials and Solar Cells, 90(7-8), 1121-1135

[32] M.B. Power, A.N. Macinnes, A.F. Hepp et al., The Realization of Molecular Control Over Solid State Structure: Chemical Vapor Deposition of Gallium and Indium Sulfide Films, MRS Proceedings, 282, 1992, 659-664

[33] P. Genevée, F. Donsanti, G. Renou et al., Study of Growth Mechanism and Properties of Zinc Indium Sulfide Thin Films Deposited by Atomic Layer Chemical Vapor Deposition over the Entire Range of Composition, The Journal of Physical Chemistry C, 115(34), 2011, 17197-17205

[34] G. Shang, K. Kunze, M.J. Hampden-Smith et al., Low-temperature chemical vapor deposition of indium sulfide thin films using a novel single-source indium thiocarboxylate compound as precursor, Chemical Vapor Deposition, 2(6), 1996, 242–244

[35] J.A. Hollingsworth, A.F. Hepp, W.E. Buhro, Spray CVD of Copper Indium Sulfide Films: Control of Microstructure and Crystallographic Orientation, Chemical Vapor Deposition, 5(3), 1999, 105-108

[36] M. Afzaal, D. Crouch, P. O'Brien et al., Metal-organic chemical vapor deposition of β-In_2S_3 thin films using a single-source approach, Mater. Sci. - Mater. El., 14(9), 2003, 555-557

[37] M. Kilani, B. Yahmadi, N. Kamoun Turki et al., Effect of Al doping and deposition runs on structural and optical properties of In_2S_3 thin films grown by CBD, Journal of Materials Science, 46(19), 2011, 6293-6300

[38] P.N. Kumta, P.P. Phule, S.H. Risbud, Low-temperature wet-chemical synthesis of amorphous indium sulfide powders, Materials Letters, 5(10), 1987, 401-404

[39] K. Yamaguchi, T. Yoshida, H. Minoura, Structural and compositional analyses on indium sulfide thin films deposited in aqueous chemical bath containing indium chloride and thioacetamide, Thin Solid Films, 431-432, 2003, 354-358

[40] S. Bansode, R. Kapadnis, V. Wagh et al., Comparative Studies On Physico-Chemical Properties Of Indium Sulfide Films Deposited Under Different Deposition Conditions By Chemical Bath Deposition, Chemistry & Chemical Technology, 8(4), 2014, 441-444

[41] P. Rao, S. Kumar, N. Raje et al., Synthesis of binary and multinary metal sulphides by precipitation and their characterization, Materials Research Bulletin, 79, 2016, 105-114

[42] P. Esmaili, H. Kangarlou, M. Ghorannevis, Optical and Structural Properties of Indium Sulfide Thin Film Produced by CBD Method, Prot. Met. Phys. Chem., 55(6), 2019, 1097-1103

[43] A.M. Alfantazi, R.R. Moskalyk, Processing of indium: a review, Minerals Engineering, 16, 2003, 687-694

[44] S.M.J. Koleini, K. Saberian, M. Abdolahi et al, Extraction of Indium from Zinc Sulphide Concentrates, Asian Journal of Chemistry, 21(7), 2009, 5611-5620

[45] F. Zhang, C. Wei, Z. Deng et al., Reductive leaching of indium-bearing zinc residue in sulfuric acid using sphalerite concentrate as reductant, Hydrometallurgy, 161, 2016, 102-106

[46] D. Pradhan, S. Panda, L.B. Sukla, Recent advances in indium metallurgy: A review, Mineral Processing and Extractive Metallurgy Review, 39(3), 2017, 167-180

[47] H.M. Doran, Treatment of indium-bearing materials, US2052387, 1936

[48] G. Zhu, M. Zheng, G. Fan et al., Recovering indium with sulfating roasting from copper-smelting ash, Rare Metals, 26(5), 2007, 488-491

[49] S.M.J. Koleini, H. Mehrpouya, K. Saberyan et al., Extraction of indium from zinc plant residues, Minerals Engineering, 23, 2010, 51-53

[50] S.M.J. Koleyni, H. H. Mehrpouya, K. Saberyan et al., Extraction of indium from leaching residue of roasted zinc sulphide concentrate, IRJME, 5(10), 2011, 55-63

[51] G. Pietek, K. Becker, Z. Szołomicki et al., Badania możliwości odzysku indu ze szlikrów miedziowych z rafinacji ołowiu, Rudy i Metale Nieżelazne, 57(10), 2012, 688-693

[52] K. Becker, Z. Szołomicki, L. Gotfryd et al., Zbadanie możliwości odzysku indu ze szlikrów miedziowych z rafinacji ołowiu, Nowe technologie oraz nowe konstrukcje maszyn i urządzeń…, 2013, 172-182

[53] M. Drzazga, R. Prajsnar, A. Chmielarz et al., Germanium and indium recovery from zinc metallurgy by-products-dross leaching in sulphuric and oxalic acids, Metals, 8(12), 2018, 1-12

[54] A.E. Lewis, Review of metal sulphide precipitation, Hydrometallurgy, 104(2), 2010, 222-234

[55] B. Swain, C. Mishra, H.S. Hong et al., Commercial process for the recovery of metals from ITO etching industry wastewater by liquid–liquid extraction: simulation, analysis of mechanism, and mathematical model to predict optimum operational conditions, Green Chemistry, 17(7), 2015, 3979-3991

[56] W. Shukai, Recycling indium and tin by treating ITO waste with sulphuric acid and hydrochloric acid leaching-sulfide precipitation, Engineering Sciences, 9, 2009

[57] Y. Li, Z. Liu, Q. Li et al., Recovery of indium from used indium–tin oxide (ITO) targets, Hydrometallurgy, 105(3-4), 2011, 207-212

[58] F.C. Mathers, A Method For The separation of iron from indium, J. Am. Chem. Soc., 30(2), 1908, 209-211

[59] L.Q. Wei, L.X. Xiao, Comprehensive utilization of indium-substitution liquid, Nonferrous Met. Smelt. (China), 4, 1999, 29

Sustainable management of biowastes and carbon sequestration in the face of a green deal

Aneta Kowalska[1]

[1]*Czestochowa University of Technology, e-mail: aneta.kowalska@pcz.pl*

Abstract

The soil degradation, irresponsible management of environmental resources, as well as progressive climate change forced the implementation of The European Green Deal. The protection of environmental and obtaining a climatic neutral Europe is considered for ensuring prosperity for future generation. In order to achieve it, there is a necessity to fully use the soil potential to mitigate climate change and carbon sequestration. The implementation of sustainable soil management and recycling biowastes in agriculture, and for soil remediation purposes as well, will contribute to the final achievement of the ambitious goal. The biowastes recycle in soil remediation not only contribute to the soil carbon sequestration, but also improve soil quality, protect environment, and protect the biodiversity. Thus, efficiently managed recycling of biowastes in the accordance with sustainable development strategy may useful for bringing closer to the goals of the Green Deal.

Keywords: biowaste, carbon sequestration, the green deal, soil remediation, climate changes

1. Introduction

The presently occurring progressive development of many branches of industry strongly influences on the environment. Due to this, the increasing concern about the environmental effects on the plant of human activity has occurred [1]. This is the reason why it has appeared an intensified attention in the social press, in governmental agendas, and scientific literature. The changes in the surrounding environment, including its contamination, degradation, and the climate changes are the basis of many concerns for future generations. It is well known the strong negative impact of contaminants in the environment on food quality, water quality and finally on public health [2]. Thus, environmental contamination, and its long-range impact consist at the point one of the main fears worldwide. The necessity of reducing environmental contamination, the need to intensify environmental restoration, and the need to develop of greener solutions plays a very important role in the present world. Hence, the huge amount of produced biowastes forces to their proper disposal in line with the sustainable development strategy. However, the share of recycled biowastes in OECD countries is still at low level and rich only about 37% of produced biowastes [3]. To meet the sustainable development aims, in the Europe appeared The European Green Deal which assumes reaching zero net greenhouse gases emission by 2050 though transformation of the challenges connected with the climate and environmental in the new possibilities in all policy areas [4]. The Green Deal aims also at leading this transformation to be fair. The European Green Deal aims to create a modern, resource-efficient, and competitive economy [5]. Thus, the best transformation of biowaste disposal would be the one, which combines biowaste disposal, lowering environmental contamination, and reducing climate changes as well. This might be achieved by the use of biowaste as a soil additive in assisted soil remediation technique improving soil quality, and enhancing the soil carbon sequestration that allows finally to mitigate the climate changes.

2. The European Green Deal

The European Green Deal is a set of policy initiatives by the European Commission with the guiding goal of making Europe climate neutral by 2050. As intended in Green Deal, the European Union will aim to reach net-zero greenhouse gas emissions by 2050. Therefore, Green Deal aims also to prepare a new action plant for circular economy [5]. The new initiatives under Green Deal involve also:

- a strategy for a “toxic-free environment”;
- a strategy for ecosystems and biodiversity;
- EU forest strategy;
- a farm to fork strategy (F2F) which assumes reducing the use of chemical pesticides, fertilizer and antibiotics;
- a new strategy for transport sector that allows for limiting CO_2 emission by implementation sustainable alternative fuel such as biofuels and hydrogen [6].

The initiatives within the Green Deal indicate the relevance of sustainable soil management. A food safety is one of its goals under farm to fork strategy [7]. This goal cannot be achieved without healthy soils. Unfortunately, the vitality of the worldwide soils is getting worst year by year. This is caused in a large share by an excessive usage of chemical fertilizers followed by the soil contamination. Thus, chemical fertilizer should be replaced by the safer, and equally effective substitutes such as biowastes [8].

While, biowaste may help to improve soil quality and food safety, they may be also effective to move closer the main goal of the Green Deal- climatic neutrality of Europe throughout contribution to the carbon sequestration. The intensification of soil carbon sequestration processes will allow reduces CO_2 concentration in the atmosphere.

3. The Sustainable Development Strategy

The sustainable development strategy aims to discover and develop the new actions aimed to improve the quality of life thought making the sustainable communities that are able to rational manage and use of resources efficiently, and able to implement prosperity, and environmental protection as well [9]. The main goals of sustainable strategy has been shown at the figure 2.1. The creation of this strategy has been driven by the climate changes, food security and environmental protection. The definition of sustainable development refers to the way of organizing society making them possible to exist in the long term. The existence of human societies has to live and meet their needs without compromising the ability of future generation to meet their own needs. According to the Brundtland Report [10] it contains within it, two key concepts:

- the concept of needs, the world’s poor especially, to which overriding priority should be given, and
- the idea of limitations imposed by the state of technology and social organization on the environment’s ability to meet present and future needs.

Fig. 2.1. The sustainable development model

Due to the development is closely connected by a progressive transformation of economy and society, the sustainable development paths have to be regulated by a law. The current 2030 Agenda for Sustainable Development includes 17 Sustainable Development Goals (SDGs) which has been adopted on 25 September 2015. The specific feature for the 2030 Agenda is that the SDGs are global and universally applicable. The 2030 Agenda takes into account the national realities, capacities and level of development. In Sustainable Development Strategy all countries are equally responsible to achieve the assumed SDGs. Each country has an important element, and important role in striving to meet the assumptions of the 2030 Agenda. There is no less or more influential country, each of them consists an essential unit to achieve the goals. In sustainable development there is a necessity to integrate three dimensions of development including economic, social and environmental as well. Due to their inseparable integrity and interdependence, the 2030 Agenda have to be implemented as a whole, not as selected elements [11].

4. Biowaste disposal in assuming SDGs and Green Deal

A term ‘biowaste’ refers to the biodegradable food residues from a private household and food industry, green industry, municipal waste, and sewage sludge [12]. The most important specific feature of biowaste is its biodegradability, and relatively high content of organic matter. Moreover, biowaste has relatively high moisture, which usually exceeds 50% by volume. The most frequently used disposal methods are composting, biofuel production, incineration, landfilling, and biochar production [12]. According to the sustainable development, biowaste may be effectively used as a valuable source for energy production. Presently, biogas produced from the sewage sludges from municipal wastes is a heat source for office building in one of the treatment plants in Poland (Częstochowa, “Warta”). Biowaste may be also effectively used as a source of nutritive elements such as nitrogen (N), phosphorus (P), potassium (K), and carbon (C). The proportion of those elements in the biowaste composition varies in different biowastes depending on their origin. For instance, chicken manure incineration ashes contain 6 times more potassium comparing to sewage sludge ash [13]. Thus, due to the content, biowastes may be a valuable source of micro- and macroelements for plants allowing them for an intensified growth and development even in the low quality soil [14]. Nevertheless, the biowastes may pose an ecotoxicological threat not only in the context of toxic substances such as heavy metals or pathogens, but also as an excess of nutritive elements. The application of biowastes with a high concentration of phosphorus into a soil may effect in a long-term in its excessive concentration in water reservoirs leading to the eutrophication, and severe imbalance in the ecosystem [15]. Similarly, the nitrogen pollution caused by the irresponsible fertilization of

agricultural fields has a negative influence not only on human health but also on ecosystem stability, and economy. The excessive concentration of N may contaminate groundwaters throughout leaching, but also terrestrial water reservoirs [16].

The soil application as a disposal method for biowastes is widely used in agriculture but also for soil remediation purposes. The properly treated sewage sludges and compost provide the organic matter in a depleted or highly contaminated soils. The example of such soil is area in the neighborhood of zinc smelter in Poland, where high contamination with heavy metals, and lack of organic fraction is observed [12]. This way of biowaste management allows to immobilize heavy metals in organic matter structure, and lower soil toxicity. The sewage sludge application into a soil effects in pH changes, humic acids increase, cation-exchange and capacity increase as well [12, 17]. The role of biowaste as soil additive is much wider, including also such influence as reduction the lability of the harmful cations in soil by complexation or surface adsorption; improvement of soil structure [18, 19, 20]. Their impact on the soil might be essential in the case of degraded and contaminated soil. The soil degradation, besides the agricultural exclusion and ecotoxicological problems, has a impact on food safety, and that's why soil quality is emerging. In the developing countries, this problem is serious due to the highly limited areas with good quality soils. DeLong et al. (2015) has assigned the term 'global pandemic' for the soil degradation. This problem is not a specific for the selected regions, but it is rather valid for a whole world, which in the long-term may contribute to the huge poor problems worldwide. The global estimates of total degraded soils range widely in different approaches. The total soil degradation in Europe range from 65 million ha (Global Assessent of Lands Degradation and Improvement project, GLADA), up to 403 million ha (FAO TerraSTAT), while Global Assessment of Soil Degradation (GLASOD) indicated the amount of 158 million ha of degraded soils in Europe. In turn, worldwide estimations varies widely from 1216 million ha (GLASOD), thought 2740 million ha (GLADA) up to 6140 million ha for FAO TerraSTAT [28]. Soil degradation and biowastes production worldwide increase year by year.

Thus, assuming SDGs, the biowastes may be adopted as a fertilizer in agricultural application or as a soil additive in soil remediation purposes, thus limiting the amount of unused again wastes, and contributing to the improvement of soil quality.

5. Carbon sequestration and biowaste soil application

The emission of green-house gases globally, especially carbon dioxide (CO_2), have a destructive influence on climate, and global warming as well. The concentration of atmospheric CO_2 has a growing tendency, and only in three last yeast increased by 8.01 ppm achieving the amount of 411.28 in November 2020 [co2.earth]. This forces to initiate action to mitigate those changes and intensify a carbon sequestration. The soil carbon sequestration consists a long-term capturing of atmospheric carbon dioxide by photosynthesis and storing in soil organic matter (SOM) [21]. The first stage of carbon capturing by plants is its build into a plants biomass. The residues of plants are further decomposed by microorganism making the humic fraction in soil, and improving its fertility, and rising soil organic carbon. The mechanism of carbon sequestration has been described in Kowalska et al. (2020) [12]. Carbon in the soil is stored in myriad of forms, and many of them involve nitrogen (N) which is formed by microorganisms that requires nitrogen. Additionally, SOM requires more net N per unit of C in comparison to plant biomass. Due to this, the soil ability to store C is closely linked to N availability. Therefore, the major challenge for soil carbon sequestration is increasing SOM without increasing N fertilization or immobilizing N in soil influencing on plant productivity [22]. The essence of soil carbon sequestration is capturing of carbon and its stable storage in a deeper soil. The effective solutions for the maximalization of carbon sequestration in the soil requires actions without generating surplus nitrogen [22]. So far, the temperate forest and grassland soil are considered to store large amounts of C [22]. However, the large areas of degraded soils may be also used for C capturing. The assisted remediation of degraded soil may increase plant productivity via providing organic matter and nitrogen source. In the case of such areas, the carbon capturing in SOM contributes to the accelerating the improvement of soil quality driving the plant productivity, and sequestration as well. There are many studies indicating higher plant biomass production in soils treated with biowastes [23, 24]. Moreover, Placek et al. observed an increased soil organic carbon (SOC) in the soil after 18 months of sewage sludge application.

Moreover, the elevated concentration of SOC, and higher microbial biomass has been noticed as an effect of sewage sludge application [25]. Therefore, the long-term studies on the influence of hybrid application of sewage sludge and N fertilizer have shown that combine application into a soil effects in higher SOC directly by providing carbon source, and indirectly by stimulation of primary production [26]. Long-term organic fertilization in Benbi and Chang (2007) [27] study have shown increased wheat productivity by up to 33 kg ha^{-1}. Thus, application of biowastes which provides the high carbon input increases SOC, stimulates grow and development of primary production, and then, enhances carbon sequestration.

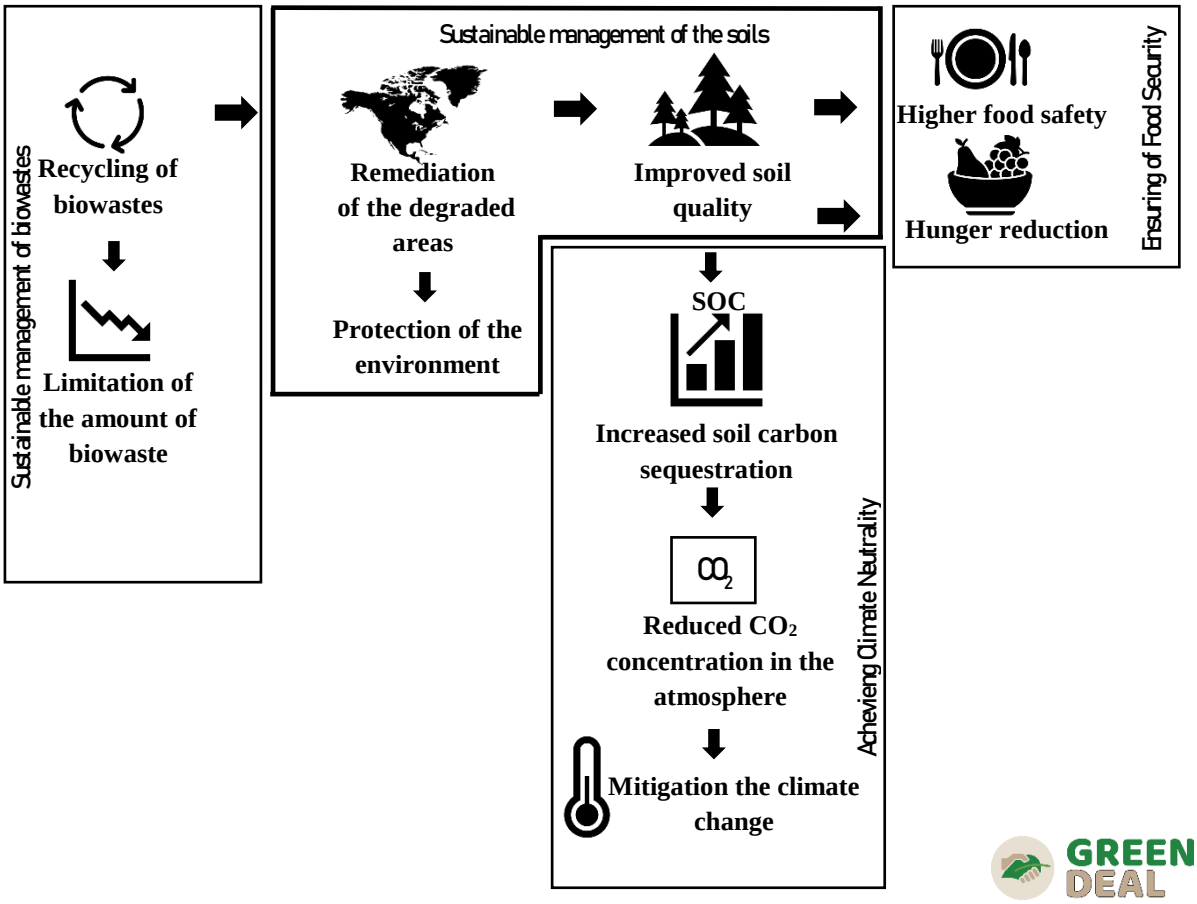

Figure 5.1. Biowaste recycling and carbon sequestration in The Sustainable Development and Green Deal

6. Conclusion

Soil application of biowastes in assisted bioremediation, besides making the assumption of sustainable development, may be useful for bringing closer to the goals of the Green Deal. An implementation of biowastes into a soils aimed to increase the efficiency of soil carbon sequestration can be one of the effective way that makes the vision of climatic neutrally Europe more realistic. Thus, the mitigation of climate changes via decarbonization and recycling of biowastes may facilitate the transition to a climate-neutral economy.

Acknowledgment

The research has been funded by Department of Infrastructure and Biotechnology, Częstochowa University of Technology, BS/MN-400-301/19.

References

[1] He, Z., Shentu, J., Yang, X., Baligar, V., Zhang, T., & Stoffella, P. (2015). Heavy metal contamination of soils: Sources, indicators, and assessment. Journal of Environmental Indicators, 9, 17–18.

[2] Pereira, Paulo; Bogunovic, Igor; Munoz-Rojas, Miriam; Brevik, Eric C. (2017). Soil ecosystem services, sustainability, valuation and management.. Current Opinion in Environmental Science & Health, (), S2468584417300326–. doi:10.1016/j.coesh.2017.12.003

[3] ISWA, 2015. Circular Economy. Carbon, Nutrients and Soil. Report 4. <https://www.iswa.org/fileadmin/galleries/Task_Forces/Task_Force_Report_4.pdf> (accessed 03.12.2020)

[4] Haines, A., Scheelbeek, P., European Green Deal: a major opportunity for health improvement, The Lancet 2020, https://doi.org/10.1016/ S0140-6736(20)30109-4, accessed 03.12.2020

[5] The Green Deal, https://eur-lex.europa.eu/legal-content/EN/TXT/?qid=1588580774040&uri=CELEX:52019DC0640, accessed 03.12.2020

[6] EU Commission – European Grean Deal. The key points, https://www.euractiv.com/section/energy-environment/news/eu-commission-unveils-european-green-deal-the-key-points/, accessed 03.12.2020

[7] Powlson, D.S., Gregory P.J.; Whalley W.R.; Quinton, J.N.; Hopkins, D.W.; Whitmore, A.P.; Hirsch, P.R.; Goulding, K.W.T. (2011). Soil management in relation to sustainable agriculture and ecosystem services. , 36(supp-S1), 0–0. doi:10.1016/j.foodpol.2010.11.025

[8] Wang, Yan; Zhu, Yuchun; Zhang, Shuoxin; Wang, Yongqiang (2018). What could promote farmers to replace chemical fertilizers with organic fertilizers?. Journal of Cleaner Production, (), S095965261832211X–. doi:10.1016/j.jclepro.2018.07.222

[9] European Commission. Sustainable Development, https://ec.europa.eu/environment/sustainable-development/strategy/index_en.htm]., accessed 03.12.2020.

[10] Brundtland Report. http://www.un-documents.net/our-common-future.pdf, accessed 03.12.2020

[11] European Commission, Sustainable Development Goals, https://ec.europa.eu/environment/sustainable-development/SDGs/index_en.htm, accessed 03.12.2020.

[12] Kowalska, A.; Grobelak, A.; Almås, Å.R.; Singh, B.R. Effect of Biowastes on Soil Remediation, Plant Productivity and Soil Organic Carbon Sequestration: A Review. Energies 2020, 13, 5813.

[13] Kaikake, K., Sekito, T., & Dote, Y. (2009). Phosphate recovery from phosphorus-rich solution obtained from chicken manure incineration ash. Waste Management, 29(3), 1084–1088. doi:10.1016/j.wasman.2008.09.008

[14] Grobelak, A.; Placek, A.; Grosser, A.; Singh, Bal Ram; Almås, Åsgeir R.; Napora, A.; Kacprzak, M. (2016). Effects of single sewage sludge application on soil phytoremediation. Journal of Cleaner Production, (), S0959652616315888–. doi:10.1016/j.jclepro.2016.10.005

[15] Farmer, A. M., Chapter 2: Phosphate pollution: A global overview of the problem, in: Schaum C. (ed.) Phosphorus: Polluter and Resource of the Future. Removal and Recovery from Wastewater, IWA Publishing, 2018, doi:10.2166/9781780408361

[16] Ahmed, M., Rauf, M., Mukhtar, Z., & Saeed, N. A. (2017). Excessive use of nitrogenous fertilizers: an unawareness causing serious threats to environment and human health. Environmental Science and Pollution Research, 24(35), 26983–26987. doi:10.1007/s11356-017-0589-7

[17] García-Gil, J. C., Plaza, C., Senesi, N., Brunetti, G., Polo, A. Effects of sewage sludge amendment on humic acids and microbiological properties of a semiarid Mediterranean soil. Biology and Fertility of Soils, 2004, 39(5), 320–328. https://doi.org/10.1007/s00374-003-0709-z

[18] Hudcová, H., Vymazal, J., & Rozkošný, M. (2019). Present restrictions of sewage sludge application in agriculture within the European Union. Soil and Water Research, (2), 104–120. https://doi.org/10.17221/36/2018-swr

[19] Mininni, G., Blanch, A. R., Lucena, F., & Berselli, S. (2015). EU policy on sewage sludge utilization and perspectives on new approaches of sludge management. Environmental Science and Pollution Research, 22(10), 7361–7374. https://doi.org/10.1007/s11356-014-3132-0

[20] Campos, Thaís, Chaer, Guilherme, Leles, Paulo dos Santos, Silva, Marcelo, & Santos, Felipe. (2019). Leaching of Heavy Metals in Soils Conditioned with Biosolids from Sewage Sludge. Floresta e Ambiente, 26(spe1), e20180399. Epub October 03, 2019.https://dx.doi.org/10.1590/2179-8087.039918

[21] Ontl, T.A., Schulte, L.A., Soil Carbon Sotrage, Nat.Educ. Knowl. 2012, 3, 35.

[22] Cotrufo, M.F., Ranalli, M.G., Haddix, M.L. et al. Soil carbon storage informed by particulate and mineral-associated organic matter. Nat. Geosci. 12, 989–994 (2019). https://doi.org/10.1038/s41561-019-0484-6

[23] Torri, S. I., Corrêa, R. S., & Renella, G. (2014). Soil Carbon Sequestration Resulting from Biosolids Application. Applied and Environmental Soil Science, 2014, 1–9. https://doi.org/10.1155/2014/821768

[24] Angelini L G, Ceccarini L, Bonari E. 2005. Biomass yield and energy balance of Giant Reed (Arundo Donax L.) cropped in central Italy as related to different management practices. Eur J Agron. 22: 375–389 https://doi.org/10.1016/j.eja.2004.05.004

[25] Börjesson, G., Kirchmann, H. & Kätterer, T. Four Swedish long-term field experiments with sewage sludge reveal a limited effect on soil microbes and on metal uptake by crops. J Soils Sediments 14, 164–177 (2014). https://doi.org/10.1007/s11368-013-0800-5

[26] Börjesson, G., Kätterer, T. Soil fertility effects of repeated application of sewage sludge in two 30-year-old field experiments. Nutr Cycl Agroecosyst 112, 369–385 (2018). https://doi.org/10.1007/s10705-018-9952-4

[27] Benbi, D.K., Chand, M. Quantifying the effect of soil organic matter on indigenous soil N supply and wheat productivity in semiarid sub-tropical India. Nutr Cycl Agroecosyst 79, 103–112 (2007). https://doi.org/10.1007/s10705-007-9100-z

[28] Gibbs, H.K., Salmon, J.M. (2015). Mapping the world's degraded lands, Applied Geography, 57, 12-21. https://doi.org/10.1016/j.apgeog.2014.11.024

,

Trees response to environmental changes in the area nearby chemical factories

Barbara Sensuła[1], Sławomir Wilczyński[2]

[1]*Silesian University of Technology, e-mail: Barbara Sensula@polsl.pl*
[2]*Agricultural University in Kraków, e-mail: slawomir.wilczynski@urk.edu.pl*

Abstract

Industrial pollution can disturb the physiological processes of trees, and in effect trees reduce their growth and change isotopic compositions of annual tree rings. In our studies we make analysis of the trees response to environmental changes in the area nearby chemical factories in Kędzierzyn- Koźle (Poland). The obtained results confirm the validity of the use of the indexes (Basal Area Increment and the degree of homogeneity of the incremental reactions, describing the incremental behavior) to identify the occurrence and to analyze the industrial pollution impact on the trees. Also industrial pollution impact on trees has been observed in changes in the C and O isotopic composition in trees due to the variability of stomata conductivity and the rate of CO2 assimilation as their response to pollution stress.

Keywords: basal area increment, growth reduction, pollution, dendroclimatology, spectrometry, isotopes

1. Introduction

The trees response to environmental changes in the area nearby chemical factories in Kędzierzyn-Koźle (Poland) was the main goal of the research. The results of the dendrochronological studies indicate that Scots pine is very sensitive to industrial pollution [1-10]. However, most of the researches base on the observation of changes in the size of radial growth, which in Scots pine are characterized by a clear downward trend with age (so-called “the age trend"). Contrary to radial growth, the current increment of the basal area increment (BAI) is characterized by a long-term upward trend, and it often culminates after several dozen years [11-12]. Therefore, decreases in the size of this incremental parameter occurring in the early phase of tree growth may prove to be a good source of the signals about the weakening of trees vitality.

Industrial pollution can disturb the physiological processes of trees, and in effect trees reduce their growth [13]. Sulfur dioxide interferes with the process of transpiration and absorption of carbon dioxide [14], while dust limit the inflow of the solar radiation assimilation apparatus and inhibit gas exchange [15], which ultimately disturbs the photosynthesis process and reduces the division activity of the vascular cambium of trees. For most plants, it is not the light but the CO_2 concentration that limits the intensity of photosynthesis, but only within certain limits. After exceeding a certain limit (for C3 plants, when the CO_2 partial pressure value is 100Pa), a further increase in CO_2 pressure not only does not increase photosynthesis, but may be harmful to plants [16].

The models proposed by researchers [17-18] describe the change in the initial isotopic composition of CO_2 taken up by the leaves of trees from the atmosphere and fractionated during many of the reactions accompanying photosynthesis and C transport in the trees. Isotope fractionation of carbon ($\delta^{13}C$) in trees is mainly related to the diffusion of atmospheric CO_2 through the stomata into the leaf and to enzymatic reactions in the plant's metabolic processes [17-18]. Carbon isotope discrimination ($\Delta^{13}C$) can be related to water transpiration in the plant. The ratio of water that the plant absorbs and uses in metabolism to the amount of water lost by the plant in the process of iWUE transpiration (intrinsic-Water-use efficiency [19-21]). Saurer and Siegwolf (2007) [22] and Scheidegger et al. (2000) [23] showed how the observed simultaneous fluctuations in $\delta^{13}C$ and $\delta^{18}O$ in the sequence of annual tree increments reflect the plant's response to external environmental factors influencing the photosynthesis. The direction of variation of the isotope composition may be synchronized for both isotopes, or it may be completely different, or it may turn out that in the studied period of time the fractionation of only one of the isotopes changes and the other remains unchanged,

which is caused by a change in the rate of CO_2 assimilation and a change in stomata conductivity. The analysis of the influence of industrial emission on trees in Kedzierzyn-Koźle has been a subject of many analysis done in the Institute of Physics at The Silesian University of Technology [9, 10,26-28]

2. Materials and methods

The research was carried out in industrial forests, particularly affected by industrial immissions from the chemical plants of Petrochemia Blachownia and Zakłady Azotowe in Kędzierzyn-Koźle.

Fig.1 Sampling sites

The amount of pollutants emitted reached its peak in the 1970s and 1980s. At the beginning of the 1990s, there was a significant reduction in emissions. In each of the 6 stands, two incremental cores were collected from the trunks of 15 pines at a height of 1 m. The annual tree-ring widths were measured using the CooRecorder and CDendro [24] programs. Results were verified using the Cofecha program [25]. The ring widths of the two cores in each tree were averaged in each year and on their basis the values of the increment in the cross-sectional area in subsequent years were calculated - BAI (basal area increment):

$BAI_i = \pi r^2_i - \pi r^2_{i-1}$ [cm^2],

where r_i - the average radius from the core to the end edge of the annual tree ring produced in the year $_i$, r_{i-1} - the radius measured to the edge of the previous tree-ring.

An individual chronology of the current section area increment (BAI_i) was constructed for each tree. Then, the BAI values of the 15 pines of each population were averaged in each year to form the standpoint BAI chronologies. Changes in the degree of homogeneity of the annual incremental reactions of pine trees were determined by calculating the average Pearson correlation coefficients of all individual pairs of the BAI chronology in 20-year intervals shifted by one year, starting from the period 1931-1950 and ending with the period 1993-2012.

The isotopic analysis has been conducted for the samples collected from the area characterized with the longest-occurring largest reductions in the width of annual tree increments. The carbon and oxygen isotope analyzes were carried out to see differences in the photosynthesis efficiency and the stomata conductivity for the period of time from 1975 to 2012. The isotopic composition of tree rings has been presented as δ notification

$\delta = (R_{sample} \backslash R_{standard} - 1) * 1000$ ‰

in alpha-cellulose extracted from annual tree-rings. δ has been expressed in per mille as the relative difference between the heavier to lighter isotope ratio in the sample and in the standard, respectively. The carbon and oxygen stable isotope compositions were measured at the Mass Spectrometry Laboratory of the Institute of Physics at Silesian University of Technology, Poland by continuous-flow isotope ratio mass spectrometry (ISOPRIME, GV Instruments, Manchester, UK) using 0,060mg of α-cellulose for δ13C measurements and 0,90 mg of α-cellulose for $\delta^{18}O$ determinations [9,10].

3. Results and Discussion

3.1. Dendrochronology

In each sampling site, it has been observed, that after the initial increase in BAI, lasting for slightly more than 20 years of pine life, BAI decreased. At the same time, BAI was the smallest at the KKS stand (Fig. 2). At the beginning of the 1960s, Scots pines began to reduce BAI growth and it continued until the beginning of the 1990s, after which the BAI size increased again. The increase in BAI coincided with a period when industrial emissions began to decline. The current increase in the area of pines reached its natural culmination between 2000 and 2010, i.e. when the pines were already over 70 years old (Fig. 2). It turns out that the greater the decline in BAI values, the more dynamic their growth followed.

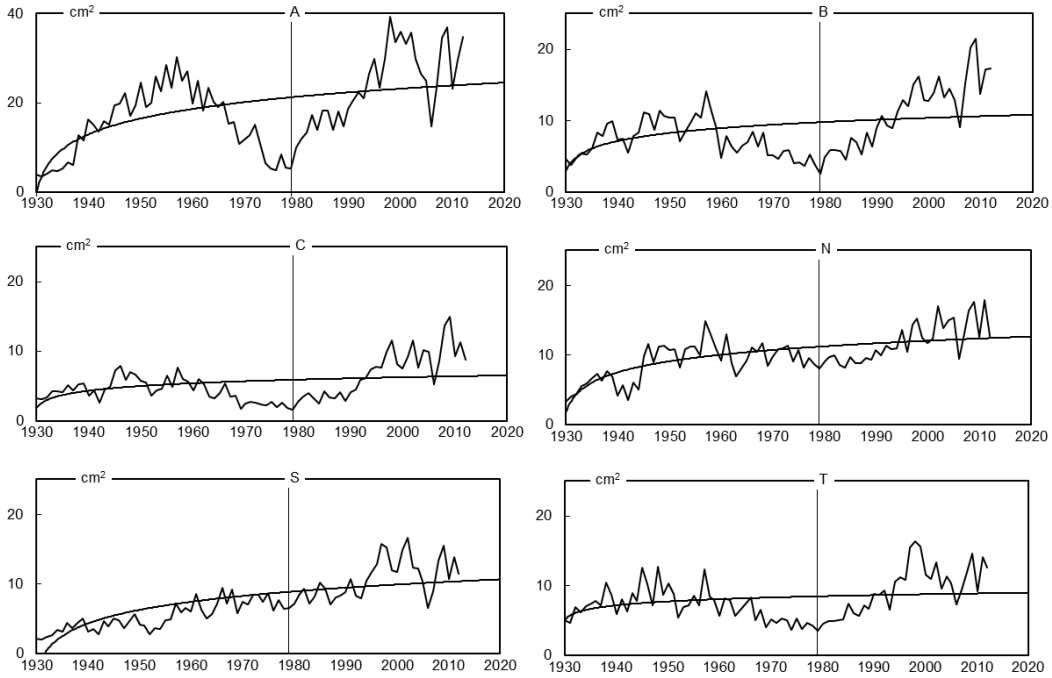

Fig. 2. The site BAI chronologies and theirs trend lines

The correlation of individual BAI chronologies of Scots pines remained at a relatively high level until the end of the 1970s, which proves the high homogeneity of incremental reactions among them. After which it decreases rapidly and reaches its minimum in the mid-1980s, and then grows again (Fig. 3).

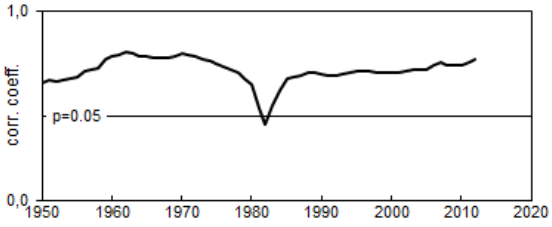

Fig.3. 20-yerar running values of mean Pearson correlation coefficient calculated between individual chronologies of all investigated pines. The first interval covers the period 1931 to 1950 and the last interval covers the period 1993 to 2012

Therefore, the deepest decrease in the homogeneity of the annual incremental reactions occurred in the years 1965-1984, i.e. the period of the culmination of industrial pollutant emissions in Poland. The current increment of the BAI wood cross-sectional area is characterized by a constant increase and a very late culmination [11,29]. In the case of Scots pine, it culminates on an average of 74 years of age [11, 12]. The situation is similar in the case of the pine populations studied in the study, in which we observe the natural culmination of BAI when they were about 75 years old.

The decrease in BAI in the young age of pines can be associated with the negative influence of pollutants immission. The results of the research conducted so far indicate that the reduction of radial increment by Scots pine in Poland lasted generally until the beginning of the 1980s [2,5,7,9,30.31]. It also turned out that the greater the reduction in the growth of wood in the examined pines, the stronger the process of their revitalization later. This is also confirmed by other studies [9,10,32-34].

An indicator informing about the occurrence of disturbances in the environment is also the degree of homogeneity of the annual growth reactions of trees [35]. The examined pines were characterized by the highest heterogeneity of annual growth reactions in the years 1965–1984. This indicates that the trees weakened by immissions were not able to respond equally to signals from the weather conditions. Similar conclusions can be drawn from other studies of Scots pine growing under the pressure of industrial pollution [5,8,34]. The increase in the correlation value of individual chronologies recorded since the mid-1980s indicates an improvement in the incremental condition of the examined pines, and the correlations reach the values recorded before the peak period of pollutant emissions.

3.2. **Analysis of the stable isotope composition**

The variability of stomatal conductivity and the variability of the maximum photosynthesis efficiency can be analyzed on the basis of changes in the stable carbon and oxygen isotopes in the plant. Isotope fractionation models [18,23] make it possible to determine which factor is decisive and how the plant reacts when an additional climatic or anthropogenic factor occurs. These analyzes are only qualitative. When the changes in $\Delta^{13}C$ are responsible for limiting the conductivity of the stomata, and the changes in photosynthesis efficiency are small, then the answer may be a positive relationship between $\delta^{13}C$ and $\delta^{18}O$ in the plant. If the changes in $\Delta^{13}C$ are only affected by the photosynthetic efficiency, no correlation between $\delta^{13}C$ and $\delta^{18}O$, as the photosynthesis efficiency does not affect the fractionation of oxygen isotopes. If the changes in $\Delta^{13}C$ are caused by the limitation of the conductivity of the stomata, and the changes in the efficiency of photosynthesis are significant, the change in $\delta^{18}O$ per unit change in $\Delta^{13}C$ will be greater than if the changes in $\Delta^{13}C$ were caused only by the limitation of the conductivity of the stomata [36]

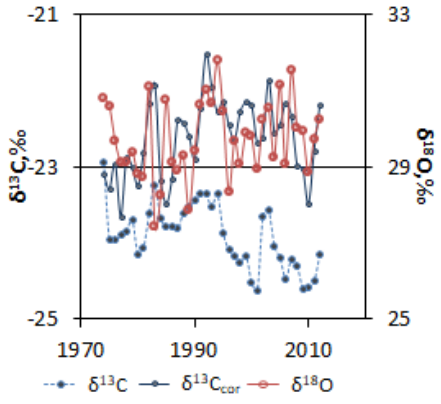

a)

$\delta^{13}C$	↑	↑	↑	↓	↓	↓	*	*
$\delta^{18}O$	↑	*	↓	↑	*	↓	↑	↓
A_{max}	*	↑	↑	↓	↓	*	↓	*
g_s	↓	*	*	*	*	↑	*	↑

b)

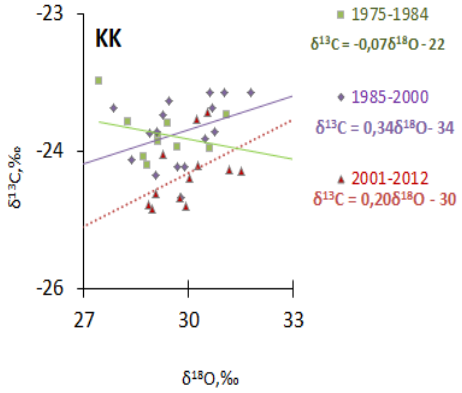

c)

Fig.4. (a) Variability of the isotopic composition of carbon (raw and corrected value according to [37]) and oxygen in annual tree increments; (b) theoretical possibilities of changes in the isotopic deltas of carbon and oxygen in plants due to the variability of stomata conductivity (g) and the rate of CO_2 assimilation (Amax) [22-23]; (an arrow pointing up or down indicates an increase or decrease in the value of a given parameter, * indicates an insignificant change; (c) Direction of isotopic deltas changes in annual tree increments.

The analysis (Fig. 4) of changes in the isotopic composition of trees shows that in the period up to the mid-1980s, the variability of CO_2 assimilation plays an important role, the plants' ability to assimilate CO_2 decreases. However, since the mid-1980s, when the emission of pollutants decreased, the rate of photosynthesis significantly depends on the conductivity of the stomata.

Acknowledgment

The authors wish to express their sincere gratitude to everyone who contributed to making these investigations possible, particularly Magdalena Opała and the technical staff of Silesian University of Technology, who helped in the sample collection and technical work. This project was a part of “Trees as bioindicators of industrial air pollution during the implementation of the pro-environmental policy in the Silesia region (BIOPOL)” funded by the National Science Centre allocated from decision number DEC-2011/03/D/ST10/05251. This research was supported by subsidies of the Ministry of Science and Higher Education for the Agricultural University of H. Kołłątaj in Krakow in 2020

References

[1] Nöjd P., Reams G.A. 1996. Growth variation of Scots pine across a pollution gradient on the Kola Peninsula, Russia. Environmental Pollution 93: 313–325.

[2] Krąpiec M., Szychowska-Krąpiec E. 2001. Tree-ring estimation of the effect of industrial pollution on pine (*Pinus sylvestris*) and fir (*Abies alba*) in the Ojców National Park (southern Poland). Nature Conservation 58(1): 33–42.

[3] Juknys R., Stravinskiene V., Vencloviene J. 2002. Tree-ring analysis for the assessment of anthropogenic changes and trends. Environmental Monitoring and Assessment 77: 81–97

[4] Stravinskiene V., Bartkevicius E., Plausinyte E. 2013. Dendrochronological research of Scots pine (Pinus sylvestris L.) radial growth in vicinity of industrial pollution. Dendrochronologia 31: 179–186.

[5] Wilczyński S. 2006. The variation of tree-ring widths of Scots pine (*Pinus sylvestris* L.) affected by air pollution. European Journal of Forest Research 125(3): 213–219. doi.org/10.1007/s10342-005-0106-2

[6] Malik I., Danek M., Marchwińska-Wyrwał E., Danek T., Wistuba M., Krąpiec M. 2012. Scots pine (*Pinus sylvestris* L.) growth suppression and adverse effects on human health due to air pollution in the Upper Silesian Industrial District (USID), southern Poland. Water, Air and Soil Pollution 223: 3345–3364.

[7] Sensuła B., Opała M., Wilczyński S., Pawełczyk S. 2015. Long- and short-term incremental response of *Pinus sylvestris* L. from industrial area nearby steelworks in Silesian Upland, Poland. Dendrochronologia 36: 1–12. DOI.org/10.1016/j.dendro.2015.08.001.

[8] Sensuła B., Wilczyński S., Piotrowska N. 2016. Zastosowanie metod dendrochronologicznych oraz spektrometrycznych w monitorowaniu drzewostanów sosnowych na obszarach przemysłowych. Sylwan 160(9): 730−740. doi.org/10.26202/sylwan.2016040.

[9] Sensuła B., Wilczyński S. 2017. Climatic signals in tree-ring width and stable isotopes composition of *Pinus sylvestris* L. growing in the industrialized area nearby Kędzierzyn-Koźle. Geochronometria 44: 240–255. doi 10.1515/geochr-2015-0070.

[10] Sensuła, B., Michczyński, A. Piotrowska, N. Wilczyński, S. 2018. Anthropogenic CO_2 Emission Records in Scots Pine Growing in the Most Industrialized Region of Poland from 1975 to 2014 Radiocarbon60(4), pp. 1041-1053

[11] Borowski M. 1974. Przyrost drzew i drzewostanów. PWRiL, Warszawa.

[12] Wilczyński S. 2020. Zapis zmian zachodzących w środowisku przez sosnę zwyczajną oraz sosnę Banksa. Sylwan 164 (7): 583−593. DOI: https://doi.org/10.26202/sylwan.2020040

[13] Percy K.E., Ferretti M. 2004. Air pollution and forest health: toward new monitoring concepts. Environmental Pollution 130(1): 113–126.

[14] L'Hirondelle S.J., Addison P.A. 1985. Effects of SO_2 on leaf conductance, Xylem tension, Fructose and sulphur levels of Jack pine seedlings. Environmental Pollution 39, seria A: 373–386.

[15] Emberson L. 2003. Air pollution impacts on crops and forests: an introduction. W: Emberson L., Ashmore M., Murray F. [red.]. Air Pollution Impacts on Crops and Forests: A Global Assessment. Imperial College Press, London. 3–29.

[16] Kopcewicz J, Lewak S. 2007. Fizjologia roślin. Warszawa. PWN.

[17] Farquhar G, Lloyd J. 1993. Carbon and Oxygen Effects in the Exchange of Carbon Dioxide between Terrestrial Plants ant Atmosphere. Eds:Ehleringer JR, Hall AE, Farquhar GD.Stable isotopes and plant carbon–water relations.New York:Academic Press 47-71.

[18] Griffiths H. (Ed.). 1998. Stable Isotopes:Integration of Biological, Ecological and Geochemical Processes. BIOS Scientific Publishers, Oxford 303–321

[19] Ehrelinger J. 1993. Carbon and Water Relations in Dessert Plants:Anisotopic Perspective in Plant Carbon and Water Relations. Wyd:Ehleringer JR, Hall AE, Farquhar GD. Stable isotopes and plant carbon–water relations.New York:Academic Press 155-172.

[20] Anderson W, Sternberg L, Pinzon M, Gann-Troxler T. 2005. Carbon isotopic composition of cypress trees from South Florida and changing hydrologic conditions. Dendrochronologia 23:1–10.

[21] Jalkanen R, Young G and, Kirchhefer A. 2011. Evidence of changing intrinsic water-use efficiency under rising atmospheric CO_2 concentrations in Boreal Fennoscandia from subfossil leaves and tree ring $\delta^{13}C$ ratios. Global Change Biology 17:1064–1072

[22] Saurer M, Siegwolf R. 2007. Human impacts on tree-ring growth reconstructed from stable isotopes. W:Stable Isotopes as Indicators of Ecological Change. Wyd:T.E. Dawson, and R.T.W. Siegwolf Terrestrial Ecology Series, Elsevier, Amsterdam, Boston 49-62.

[23] Scheidegger Y, Saurer M, Bahn M, Siegwolf R 2000. Linking stable oxygen and carbon isotopes with stomatal conductance and photosynthetic capacity:a conceptual model. Oecologia 125:350–357.

[24] www.cybis.se (2020/11/16)

[25] Holmes R. L. 1983. Computer−assisted quality control in tree-ring dating and measurement. Tree-Ring Bulletin 43: 69−78.

[26] Sensuła B., 2015. Spatial and Short-Temporal Variability of $\delta^{13}C$ and $\delta^{15}N$ and Water-Use Efficiency in Pine Needles of the Three Forests Along the Most Industrialized Part of Poland Water, Air, and Soil Pollution 226(11),362

[27] Sensuła B., 2016. $\delta^{13}C$ and Water Use Efficiency in the Glucose of Annual Pine Tree Rings as Ecological Indicators of the Forests in the Most Industrialized Part of Poland Water, Air, and Soil Pollution 227(2),68

[28] Sensuła 2016: The Impact of Climate, Sulfur Dioxide, and Industrial Dust on $\delta^{18}O$ and $\delta^{13}C$ in Glucose from Pine Tree Rings Growing in an Industrialized Area in the Southern Part of Poland Water, Air, and Soil Pollution 227(4),106

[29] Erteld W., Hengst E. 1966. Waldertragslehre. Radebeul. Neumann Verlag.

[30] Szychowska-Krąpiec E., Wiśniewski Z. 1996. Zastosowanie analizy przyrostów rocznych sosny zwyczajnej (*Pinus sylvestris*) do oceny wpływu zanieczyszczeń przemysłowych na przykładzie zakładów chemicznych „Police" (woj. szczecińskie). Kwartalnik Akademii Górniczo-Hutniczej Geologia 22(3): 281–299.

[31] Wilczyński S. 2010. Uwarunkowania przyrostu radialnego wybranych gatunków drzew z Wyżyny Kieleckiej w świetle analiz dendrochronologicznych. Zeszyty Naukowe UR w Krakowie 464 (341).

[32] Feliksik E., Wilczyński S. 2003. Tree-rings as indicators of environmental change. Electronic Journal of Polish Agricultural University 6(2) ser. Forestry.

[33] Wilczyński S., Feliksik E. 2005. Disturbances in variation of the annual ring width of Norway spruce in the Polish Western Beskid Mountains. Journal of Forest Science 51(12): 539–547.

[34] Sensuła B., Wilczyński S., Monin L., Allan M., Pazadur A., Fagel N. 2017. Variations of tree ring width and chemical composition of wood of pine growing in the area nearby chemical factories. Geochronometria 44: 226–239. DOI: 10.1515/Geochr-2015-0064.

[35] Briffa KR, Wigley TML, Jones PD 1987. Standardization and the preparation of chronologies some contrasting approaches. Towards an objective approach to standardization. W: Kairiukstis L, Bednarz Z, Feliksik E. Methods of dendrochronology. Proceedings of the Task Force Meeting on Methodology of Dendrochronology: East/West Approaches, 2-6 June, Krakow, Poland: pp. 69–86.

[36] Barbour M, Schurr U, Henry B, Wong S, Farquhar G. 2000. Variation in the Oxygen Isotope Ratio of Phloem Sap Sucrose from Castor Bean. Evidence in Support of the Peclet Effect. Plant Physiology 123:671–679.

[37] McCarroll D, Gagen M, Loader N, Robertson I, Anchukaitis K, Los S, Young G, Jalkanen R, Kirchhefer A, Waterhouse J. 2009. Correction of tree ring stable carbon isotope chronologies for changes in the carbon dioxide content of the atmosphere Geochimica et Cosmochimica Acta 73:1539–1547.

Modification of the hydrophobic properties of mineral adsorbents for the removal of petroleum pollutants

Elżbieta Vogt[1], Gabriela Chmura[1], Otmar Vogt[2]

[1]AGH University od Science and Technology, e-mail: vogt@agh.edu.pl
[2]Cracow University of Technology

Abstract

Due to their good price, availability and, above all, high adsorption capacity, mineral materials compete with other types of adsorbents used to remove petroleum pollutants. The research indicates that hydrophobization processes have a large impact on the improvement of the mineral sorbents functional properties, when sorbents are used to remove oil pollutants in the water and soil environment. The paper presents the process of hydrophobization of expanded vermiculite with the use of stearic acid vapour. The obtained results indicate a great influence of the hydrophobization processes on the improvement of the functional properties of vermiculite. Water absorption for the raw sorbent, decreased after modification from the level of 7.23 to 5.6 g/g. After the modification process, the sorption capacity of oil compounds increased twice.

Keywords: hydrophobization, mineral adsorbents, petroleum pollutants

1. Introduction

Despite incessant fears that oil sources may run out, this fuel is still the basic energy resource in the modern economy, and its extraction is still at a high level [1, 2]. High extraction is followed by the intensive development of the transport and oil processing industry, which unfortunately generate significant amount of environment pollution. Oil spills stemming from supertankers, drilling, and natural events represent a serious problem worldwide due to the potential harms to marine ecosystems and aquatic life. Much less attention is paid to the problems of pollution generated by transport or industry. Contrary to appearances, these cases pose an equally serious threat, by appearing closest to humans and require immediate reaction.

Multiple research areas have emerged in view of the deleterious impacts of oil-spills on the environment and the relative intractability of the problem per se. The dimensions mostly explored thus far, relate to the prediction of the fate of oil-spill and development of effective counter-measures [3-14]. Despite numerous challenges (related to it), long time since there is a big interest in researches into the development of effective sorbents as a remedium of oil spills. [14-18]. The mineral sorbents are especially eagerly used to remove petroleum pollutions. Mainly there are: silicate minerals, zeolites, perlite, diatomite and clay rocks [19-30]. The convenient-to-use form of granules enables the removal of pollutants from the surface of water and soil, even from hard-to-reach places. Sorption sleeves - nonwovens filled with chemical sorbents, can be used to limit the leakage zone and absorb oil as close to the source as possible.

However the most importantly is, that the sorbent materials need to be assembled in such a structure or form that they can survive the oceanic currents and other prevailing environmental conditions not losing its properties. Unfortunately, most mineral sorbents are very sensitive to moisture [31]. There absorbability may be reduced in the process of hydrophobization [32, 33]. Some producers of sorbents used to removal oil pollution offer a hydrophobic form of materials, e.g. the Perlipol (Hydroperl) company, or the Perlit-Polska company [33, 34]. However, the line of hydrophobic sorbents which is currently used to remove oil-derived pollution does not utilise the full potential of the raw material. There is a possibility to increase the range of use of this line by utilising various output materials,

modifiers and the methods of modification. The appearance of a greater amount of products which represent various costs of production and properties on the market will enhance the availability of the means of protection of this kind. The topic of the hydrofobization different material is actual and such researches could have a potential to contribute to improvements of oil waste purification processes.

2. Analysis of the modification processes of mineral adsorbents used for removal of petroleum pollutants

Table 2.1 shows the current trends in the methods of hydrophobization of mineral adsorbents in a laboratory and industrial scale are used. The variety of the analysed sorbents and hydrophobization agents indicates a wide range of research and its multidirectional nature.

Table 2.1. Trends in the methods of hydrophobization of mineral adsorbents

sorbent	modifier	modification method
magnetic adsorbents based on vermiculite-iron [27]	epoxy resin	Coating
	polystyrene improving	
dolomite [28]	palmitic acid	dip-coating
vermiculite (nanotubes) [29]	carbon nanotubes (CNT)	vapour deposition (CVD)
diatomite (IMDC) [30]	ISOBAM-104	doping and thermal treatment
perlite 180 [35]	stearic acid	vapour phase
Perlite1 180 [36]	stearic acid	coating
vermiculite fine [37]		
perlite 180 [36]	Sarsil H-15 - silicone preparation	dip-coating
vermiculite fine [37]		
perlite (Hydroperl) [33]	silicone preparation	dip-coating
diatomite (Compakt) [38, 39]	calcination	thermal treatment

The modification proses described at Table 2.1 give the materials additional properties that contribute to their better use. Adsorbent in the form of magnetic composites can be easily separated from the medium, in which they are located, by a simple magnetic process. This is particularly advantageous because it does not generate a new hazardous waste in the form of contaminated sorbent. Vermiculite modified with the method described above is characterized not only by a highly hydrophobic character, but also by structural changes leading to the form of a "sponge" (tangled nanofibers and nanotubes). This form promotes the formation of capillary forces. Modification of dolomite with palmitic acid is a very cheap and efficient method of hydrophobization. High mechanical strength, low bulk density, good chemical resistance and good thermal stability ensure that hydrophobic porous ceramics are reliable in difficult application conditions. Ceramics also show an excellent ability to regenerate for at least 10 cycles. Although these properties are very useful, but they do not define the most important feature of mineral sorbents that is necessary necessary for the removal of petroleum pollutants, which is the sorption capacity.

Table 2.2. presents the values of sorption capacity of sorbents in relation to various oil compounds.

Table 2.2. Sorption capacity of mineral adsorbents in a heterogeneous and homogeneous system with respect to petroleum-derived compounds

sorbent	sorption capacity [$g_{oil}/g_{sorbent}$]	
homogeneous system: petroleum-derived compounds		
natural zeolite – clinoptilolite [23]	Verva diesel fuel	0.31
	biodiesel fuel	0.34
synthetic zeolite Na-X [23]	Verva diesel fuel	0.91
	biodiesel	1.13
synthetic zeolite Na-P1 [23]	Verva diesel fuel	1.24
	biodiesel fuel	1.40
dolomite from Damolin A/S [24]	diesel fuel	1.06
expanded perlite 120 [24]	diesel fuel	3.16
dolomite (palmitic acid dip-coating) [28]	Dilbit oil	0.30
	Bakken oil	0.30
heterogeneous system: petroleum-derived compounds - water		
magnetic adsorbents based on vermiculite-iron [27]	N-octanol	0.27
	soybean oil	2.30
dolomite hydrophobized with palmitic acid [28]	Dilbit oil	0.50
	Bakken oil	0.53
vermiculite (nanotubes Fe1Mo0.15 (M)) [29]	diesel fuel	3.20
diatomite (IMDC) [30]	paraffin oil	1.28
	pump oil	1.70
vermiculite fine (stearic acid coating) [37]	diesel fuel	2.05
vermiculite fine (Sarsil H -15) [37]		2.17
perlite 180 (stearic acid coating) [36]		1.79
perlite180 Sarsil H – 15 [36]		1.78
perlite 180 (stearic acid vapour phase) [35]		1.67
perlite (Hydroperl) [36]		1.69
diatomite Compakt [38, 39]		0.60

Due to the variety of adsorbed substances and different conditions of hydrophobization processes, it is difficult to unequivocally assess the adsorbents listed in Table 2.1 in terms of their effectiveness. However, it can be noticed, that vermiculite and perlite are characterized by much better sorption capacity of oily substances than other sorbents, regardless of the kind of hydrophobization method and modifier that was used. Compared to the modifiers used, the stearic acid stands out from the others. There are used two methods of hydrophobization with the use of this modifier: hydrophobization from solutions (coating) and with the use of acid vapour. Based on the studies [32, 35-37], a preliminary conclusion was made that the effectiveness of stearic acid as a modifier slightly changes depending on the used method (Tab. 4.1).

3. Experimental

3.1. Composites

The tests were carried out on expanded vermiculite fine, produced by Perlipol Sp.j. The chemical composition of the material in mass percent is as follows: SiO_2: 38-46; Al_2O_3: 10-16; MgO: 16-35; Fe_2O_3: 6-13; TiO_2: 1-3; CaO: 1- 5; K_2O: 1- 6; H_2O: 8-16; others: 0.2-1.2 [33]. Physicochemical characterization of material are listed in Table 3.1.1 [33]. The grain composition of the material is presented in Table 3.1.2.

Table. 3.1.1. Physicochemical characteristic of vermiculite [33]

property	value
bulk density	60-200 kg/m^3
melting point / range	Up 1315 °C
thermal conductivity	0.062 - 0.065 W/m*K
water absorption	3.0 - 80%
compressive strength	0.14 - 0.40 MPa
chemical resistance	like glass

Table 3.1.2. The grain composition of the fine fraction of expanded vermiculite [33]

grain size	[m/m]
2.0 mm	20 – 35
1.6 mm	18 – 30
1.0 mm	20 – 40
0.5 mm	5 – 15
0.25 mm	2 – 10
bulk density	80-100 kg/m^3
moisture	max 5%

Stearic acid was used as a modifier. It is a saturated fatty acid and is a powdered white solid [40].

3.2. Vermiculite hydrophobization

Two batches of vermiculite were manufactured, the first one was hydrophobized once, the second one twice. Based on previous researches the process was carried out at 180^{o}C [41-43].

The hydrophobization process was carried out in apparatus is presented in Fig. 3.1.1. It consists in stearic acid vapour and vermiculite counter current flow and it was carried out in an installation of own design.

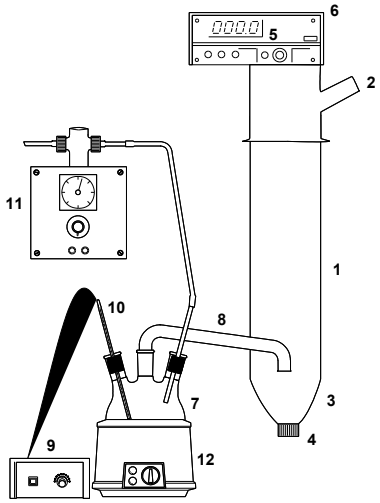

Fig. 3.1.1. The hydrophobisation apparatus scheme: 1 – hydrophobisation column, 2, 3 – hoppers, 4 - lock of hopper, 5 – control panel, 6 – feeder, 7 – boiler, 8 - ting up pipe,9 – thermoregulator, 10 – thermocouple, 11 – compressor, 12 – heater

3.3. **The study of the properties of hydrophobic materials**

In a preliminary manner, the hydrophobic properties of the materials were determined on the basis of the results of the test associated with floating on the surface of water [44]. Small amounts of material (ca. 2 cm^3) were put into small beakers filled with water. After a hydrophobization, after 24 h and after a week, one observed which part of the material floated on the water. Fig. 3.3.1 presents example photographs associated with the test which was conducted. The observations show that the hydrophobic properties of vermiculite did not improve slightly after an initial hydrophobization, therefore the material was hydrophobized again.

once hydrophobization						twice hydrophobization
after modification		a day after modification		a week after modification		a week after modification
a)	b)	a)	b)	a)	b)	a)
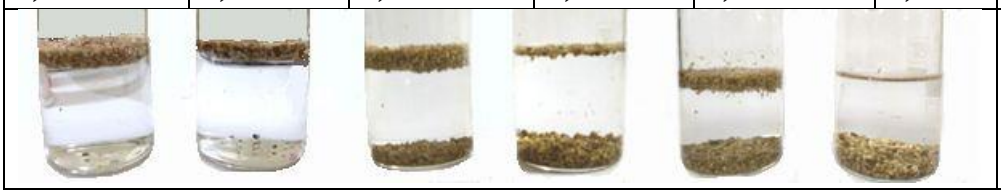						

Fig. 3.3.1. The photographs of the test of the floating of vermiculite modified (a) and raw (b) samples – on the surface of the water

3.4. **The water absorbability**

The hydrophobic properties of materials are also evaluated by measuring the absorbability, which is highly relevant in the industry, has to do with contacting a specific mass of a solid with water, and then in measuring the change of the mass after a specific period of time [45]. Research was conducted both for raw samples as well as the modified samples. 2 g of each material was contacted with 100 ml of distilled water over the period of one hour. After that time, the samples were moved to the sieves for the period of 15 min. The absorbability (N) [kg of water/kg of vermiculite] of raw and modified samples was the following: N_{raw} = 7.23; $N_{once\ hydrophobized}$ = 6.60; $N_{twice\ hydrophobized}$ = 5.98. The water absorbability decreases with the degree of modification of the materials.

3.5. **The sorption of petroleum-derived compounds**

The sorption of petroleum-derived substances from the surface of water was conducted. 25 cm^3 of the vermiculite was placed to a glass container and cm^3 of distilled water added. 30.Then 15 cm^3 diesel fuel (provided by the BP company) was added and it was extracted by shaking for 10 min. After that time, the material was separated by means of a porous plunger. The separated solution was poured to a measuring cylinder, and after diesel fuel separated from the water, the volume of the non-absorbed diesel fuel was read. The absorption of diesel fuel was calculated on the basis of a formula [46]. The results are indicated in Table 4.1.

$$ABS = \frac{15 - V_x}{25} \cdot 1000 \ \left[\frac{dm^3}{m^3}\right]$$

where: Vx – the volume of non-absorbed diesel fuel [cm^3].

4. **Conclusion**

Many different adsorbents designed for petroleum compounds removal from the water surface have been developed. A material that adsorbs petroleum pollutants can be classified as a high-class sorbent if it is displays high hydrophobicity (low water absorption), petroleum-derived compounds/water selectivity, high buoyancy, low cost. Also it should be easily available. In this work, the research was carried out on a mineral material which, after appropriate modifications, meets all these criteria. Various hydrophobization techniques were compared and own research of vermiculite hydrophobization was performed.

Among the analysed modifiers, it seems that silicone preparations stand out as stand out as cheap and easy-to-use modifier for typical minerals such as: perlite and vermiculite. Materials modified by them are characterized by a high degree of water resistance. They absorb large amounts of pollutants (Tab. 4.1 - the part of Tab. 2.2]. The sorption capacity for raw perlite is 0.86 g/g [36], and for vermiculite it is equal 0.96 g / g [37].

Hydrophobized materials can be used in both the water and soil environment as the modification processes do not significantly change their weight. The bulk density for raw perlite is 114,4 kg/m^3, after modification is 138,3 kg/m^3, and for vermiculite it is equal 113 kg/m^3, after modification is 166 kg/m^3 [37].

Table 4.1. Sorption capacity of mineral adsorbents in a heterogeneous and homogeneous system with respect to petroleum-derived compounds (part of Table 2.2)

sorbent	pollution	sorption capacity [$g_{oil}/g_{sorbent}$]
vermiculite fine (stearic acid coating) [37]	diesel fuel	2.05
vermiculite fine (Sarsil H -15) [37]		2.17
perlite 180 (stearic acid coating) [36]		1.79
Perlite180 Sarsil H – 15 [36]		1.78
perlite 180 (stearic acid vapour phase) [35]		1.67
perlite (Hydroperl) [36]		1.69
vermiculite fine (stearic acid vapour phase)		1,91

The review of other works dedicated to this problem, in which stearic acid was used as a modifier, compared with the results of our own research allow us to assume that stearic acid may be a competitive agent for silicone preparations. Materials hydrophobized with stearic acid show comparable sorption capacity as materials hydrophobized with silicone agents (Tab. 4.1).The values of diesel fuel (provided by the BP company) sorption for vermiculite hydrophobized with the use of stearic acid by various technique is showed at Table 4.1. The bulk density for raw perlite is 114,4 kg/m^3, after modification is 137,1 kg/m^3 [35], and for vermiculite it is equal 113 kg/m^3, after modification is 120 kg/m^3 [37]. Additionally hydrophobization with the use of stearic acid may compete with processes using silicone modifiers, which is due to a very small amount of acid that is sufficient for the modification. Mineral sorbent with a small addition of a modifier, does not generate harmful substances in the natural environment.

Acknowledgments

Work carried out under Research subsidy No. 16.16.210.476

References

[1] Inżynieria.com, online: https://inzynieria.com/paliwa/rankingi/56407, Wydawnictwo INŻYNIERIA sp. z o.o., December 2020.

[2] Investopedia.com, online: https://www.investopedia.com/terms/o/oil-reserves.asp, December 2020.

[3] Deschamps G., Caruel H., Vignoles Ch., *Oil removal from water by sorption on hydrophobic cotton fibres,* Environmental Science and Technology, 37, 5034-5039 (2003).

[4] Hem P.K., Laxmi K., Han J.K., *Modification of 3D plyacrylonitrile composite fiber for potential oil-water mixture separation,* Separation and Purification Technology, 229, 115840, (2019).

[5] Dmochowska A., Dmochowski D., Biedugnis S., *Charakterystyka biorekultywacji gleb skażonych produktami ropopochodnymi - metoda pryzmowania ex situ,* Środkowo-Pomorskie Towarzystwo Naukowe Ochrony Środowiska, 18, 1, 759-771 (2016).

[6] Han L., Wu W., Huang Z., Lei W., Li S., Zhang H., Jia Q., Zhang S., *Preparation and characterization of a novel fluorine-free and pH-sensitive hydrophobic porous diatomite ceramic as highly efficient sorbent for oil–water separation,* Separation and Purification Technology, 254, 1117620 (2021).

[7] Kukkar D., Rani A., KumarV., Younis S.A., Zhang M., Lee S.S., Tsang D. C.W., Kim K.H., *Recent advances in carbon nanotube sponge–based sorption technologies for mitigation of marine oil spills*, Journal of Colloid and Interface Science, 570, 15, 411- 422 (2020).

[8] Bai W., Chen K., Chen J., Xu J., Lin H., Lin J., Xu Y., Lin J., *Natural highly-hydrophobic urushiol@TiO2 coated cotton fabric for effective oil–water separation in highly acidic alkaline and salty environment*, Separation and Purification Technology, 253, 15, 117495 (2020).

[9] Yao H., Lu X., Xin Z., Zhang H., Li X., *A durable bio-based polybenzoxazine/SiO_2 modified fabric with superhydrophobicity and superoleophilicity for oil/water separation*, Separation and Purification Technology, 229, 15, 115792 (2019).

[10] Abdel-Aty A.A.R., Aziz Y.S. A., Ahmed R.M.G., ElSherbinyc I.M.A., Ulbricht S.P.M., Khalila A. S.G., *High performance isotropic polyethersulfone membranes for heavy oil-in-water emulsion separation,* Separation and Purification Technology, 253, 15, 117506 (2020).

[11] Karki H.P., Kafle L., Kim H.J., *Modification of 3D polyacrylonitrile composite fiber for potential oil-water mixture separation,* Separation and Purification Technology, 229, 15, 115840 (2019).

[12] Chen Y., Yu B., Lin J., Naidu R., Chen Z., *Simultaneous adsorption and biodegradation (SAB) of diesel oil using immobilized Acinetobacter venetianus on porous material*, Chemical Engineering Journal, 289, 1, 463-470 (2016).

[13] Nnaji N.J.N., Onuegbu T.U., Edokwe O., Ezeh G.C., Ngwu A.P., *An approach for the reuse of Dacryodes edulis leaf: Characterization, acetylation and crude oil sorption studies*, Journal of Environmental Chemical Engineering, 4, 3, 3205-3216 (2016).

[14] Bhardwaj N., Bhaskarwar A.N., *A review on sorbent devices for oil-spill control,* Environmental Pollution, 243, Part B, 1758-1771 (2018).

[15] Bigui W., Cheng Y., Jianlin L., Gang W., Liang D., Xiaosan S., Fuping W., Hua L., Qing Ch., Fabrication of superhydrophilic and underwater superoleophobic quartz sand filter for oil/water separation, *Separation and Purification Technology*, 229, 15, 115808 (2019).

[16] Galblaub O.A., Shaykhiev I.G., Stepanova S.V., Timirbaeva G.R., *Oil spill clean-up of water surface by plant-based sorbents: Russian practices*, Process Safety and Environmental Protection, 101, 88-92 (2016).

[17] Li N., Yue O., Gao B., Xu X., Su R., Yu B., *One-step synthesis of peanut hull/graphene aerogel for highly efficient oil-water separation,* Journal of Cleaner Production, 207, 764-771 (2019).

[18] Periasamy A.P., Wu W.P, Ravindranath R., Roy P., Lin G.L., Changa H.T., *Polymer/reduced graphene oxide functionalized sponges as superabsorbents for oil removal and recovery*, Marine Pollution Bulletin, 114, 2, 888-895 (2017).

[19] Ali I., Asim M., Khan A., *Low cost adsorbents for the removal of organic pollutants from wastewater*, Journal of Environmental Management, 113, 170-173 (2012).

[20] Tic W.J., Pijarowski P.M., *Charakterystyka adsorbentów stosowanych do usuwania zanieczyszczeń ropopochodnych z gleby i ścieków,* Przemysł Chemiczny, 3, 301 – 306 (2015).

[21] Pietras M., *Właściwości i zastosowanie perlitu,* Izolacje, 3, 88 – 89 (2018).

[22] Wanga S., Peng Y., *Natural zeolites as effective adsorbents in water and wastewater treatment*, Chemical Engineering Journal, 156, 11 – 24 (2010).

[23] Bandura L., Franus M., Panek R., Woszuk A., Franus W., *Charakterystyka zeolitów i ich zastosowanie jako adsorbentów substancji ropopochodnych,* Przemysł Chemiczny, 94, 3, 323-327 (2015).

[24] Pijarowski P.M., Tic W.J., *Adsorpcja na złożach mineralnych z układu homogenicznego,* Chemik, 67, 10, 995 – 1002 (2013).

[25] Rouliaa M., Chassapis K., Fotinopoulos Ch., Savvidis Th., Katakis D., *Dispersion and Sorption of Oil Spills by Emulsifier-Modified Expanded Perlite*, Spill Science & Technology Bulletin, Volume 8, 5–6, 425-431 (2003).

[26] Bastani D., Safekordi A.A., Alihosseini A., Taghikhani V., *Study of oil sorption by expanded perlite at 298.15K*, Separation and Purification Technology, 52, 2, 295-300 (2006).

[27] Machado L.C.R., Lima F.W.J., Paniago R., Ardisson J.D., Sapag K., Lago R.M., *Polymer coated vermiculite–iron composites: Novel floatable magnetic adsorbents for water spilled contaminants*, Applied Clay Science, 31, 207 – 215 (2006).

[28] Davoodi S. M., Taheran M., Brar S.K. Galvez-Cloutier R., Martel R., *Hydrophobic dolomite sorbent for oil spill clean-ups: Kinetic modeling and isotherm study*, Fuel, 251, 1, 57-72 (2019).

[29] Moura F.C.C., Lago R.M., *Catalytic growth of carbon nanotubes and nanofibers on vermiculite to produce floatable hydrophobic "nanosponges" for oil spill remediation*, Applied Catalysis B: Environmental, 90, 3–4, 436-440 (2009).

[30] Han L., Wu W., HuangZ., Lei W., Li S., Zhang H., Jia Q., Zhang S., *Preparation and characterization of a novel fluorine-free and pH-sensitive hydrophobic porous diatomite ceramic as highly efficient sorbent for oil–water separation*, Separation and Purification Technology, 254, 117620 (2021).

[31] Oszust M., Barczak M., Dąbrowski A., *Mezoporowate Materiały Krzemionkowe – Charakterystyka i Zastosowanie*, 3, 53 – 69, Rzeszów 2012.

[32] Vogt E., Płachta Ł., *The new method of modifying the hydrophobic properties of expanded perlite*, E3S Web Conf., 14, 02034 (2017).

[33] Perlipol.pl, online: https://www.Perlipol.Com.Pl/Wermikulit-Ekspandowany-Eksfoliowany, December 2020.

[34] Perlit-Polska, online: http://www.perlit-polska.pl/, December 2020.

[35] Bernaś M. *Modyfikacja właściwości powierzchniowych adsorbentów stosowanych do usuwania zanieczyszczeń ropopochodnych*, Praca Magisterska, Wydział Energetyki i Paliw AGH (2019).

[36] Smorońska A., Hyrofobizacja perlitu ekspandowanego, *Praca Magisterska*, Wydział Energetyki i Paliw, AGH (2018).

[37] Lenko S., *Hydrofobizacja wybranych mineralnych adsorbentów przemysłowych,* Praca Magisterska, Wydział Energetyki i Paliw, AGH (2018).

[38] Ospkruszwica.pl, online: http://www.ospkruszwica.pl/index.php?go=sorbenty, December 2020.

[39] Sintac.pl, online: https://www.sintac.pl/produkty/sorbenty/sorbenty-uniwersalne/sorbent-compakt/, December.2020.

[40] Standard.pl, online: http://www.standard.pl/produkty/katalog-a-z/produkt-272/kwas-stearynowy, December 2020.

[41] Vogt E., *Hydrophobized limestone powder as an antiexplosive agent*, Polish Journal of Environmental Studies, 20, 3, 801–804 (2011)

[42] Vogt E., *Effects of commercial modifiers on flow properties of hydrophobized limestone powders*, *Polish Journal of Environmental Studies,* 22, 4, 1213–1218 (2013)

[43] Vogt E., Węgrzynowicz A., Vogt O., Čablík W., *Application of krypton and nitrogen isotherms to characterisation of hydrophobized fine dispersional limestone material*, Adsorption: Journal of the International Adsorption Society, 25, 3 477–483 (2019).

[44] Vogt E., Hołownia D., *Badanie właściwości hydrofobowych modyfikowanych pyłów wapiennych*, Mineral Resource Management, 26, 2, 41-56 (2010).

[45] Wilczyński T., *Sorbenty. Podział i kryteria doboru*. BiTP, 2/4, 155 (2006).

[46] Technical Card of Hydroperl, online: https://www.perlipol.com.pl/dokumenty/Karta_Techniczna_HydroPerlu_2015.pdf., December 2020.

Demand and supply of energy for a city on example of Addis Ababa

Fasika Solomon Wolle[1]

[1]*Silesian University of Technology, e-mail: fasiwol813@student.polsl.pl*

Abstract

Number of people living in the city is increasing rapidly in the entire world. Due to this and many other reasons, cities are the most energy consuming location in one country. Measuring one city's energy consumption can be beneficial in many aspects including economical, environmental and global evaluation. The demand for energy in one city can be measured based on ISO Standard city indicators. These indicators assist to measure the energy total consumption accordingly with the renewable energy resources, this paper will assess the general steps of measuring the energy demand of a city by taking Addis Ababa as an example and how the city will fulfil the demands by indicating the energy supplies. The article will try to conceive the demand for energy of a city based on indicators and assess the supply of energy where the consumption is driven from.

Keywords: Energy demand of city, Energy supply, Electricity, Addis Ababa, Ethiopia, City indicators, Renewable sources, Energy consumption

1. Introduction

Since the world we live in is very diversified with perspectives of wide difference, Cities performance can be defined in many ways. But every definition wouldn't give sentiment unless the given definition has harmonization with mutually measurable quality. That's why an ISO standard is preferred to assess, measure and identify if the indicated performance clearly defines the city and how different perspectives can drive to conclusion.

ISO 37120 is a standard document for Sustainable development of communities, Indicators for city services and quality of life[4] . The document contains requirements that undertake to measure city performance in a comparable and verifiable manner, in regard to size and location based on indicators.

The indicators can be used to track and monitor a city's progress on city service performance and quality of life and assist cities in setting targets and monitoring achievements [4]. There are 16 city indicators listed on these document structures in classifications to appoint the service and area of application.

Energy sector is listed as one of the city indicators among the 16. This sector has 4 core indicators and 3 supporting indicators. According to the standard document core indicators means indicators that are required to demonstrate performance in the delivery of city services and quality of life and supporting indicators means indicators that are recommended to demonstrate performance in the delivery of city services and quality of life [4].

The Core indicators are

- Total residential electrical energy uses per capita (kWh/year)
- Percentage of city population with authorized electrical service
- Energy consumption of public buildings per year (kWh/m²)
- Percentage of total energy derived from renewable sources, as a share of the city's total energy consumption

The supportive indicators include

- Total electrical energy uses per capita (kWh/year)
- Average number of electrical interruptions per customer per year
- Average length of electrical interruptions (in hours)

2. Overview of Addis Ababa, Ethiopia

Addis Ababa is the capital city of Ethiopia located on the eastern horn of Africa with the largest geographical area of 527 km2 (203 sq mi). The city is considered as the political capital city of Africa. The African union Headquarter and United nation Economic Commission of Africa is based in the city which make the city the political and diplomatic significance figure for the continent and the world.

The city is located 7,726 feet above sea level which makes it one of the highest elevations of any city in the world next to Bogota, Colombia and Quito, Ecuador. This gives the city infrastructural development slightly difficult.

The city is a chartered city with a very diversified economy. The households working in Trade and commerce, Manufacturing and industry, Homeworkers, city administration, transport and communication and many more sectors. Recently, Highrise and tall buildings have been blooming under construction.

Based on the populationstat.com statistics for 2020, the city has a number of 4,877,520 population in urban area and 2,757,729 in city areas as the 10th in Africa, 87th in the world highest number of populations. Ethiopian population increased by 60% compared to 1960th. Accordingly, the economy growth of the country practiced strong, broad-based growth with average estimation of 9.8% a year from 2008/09 to 2018/19, and real gross domestic product (GDP) growth is 9% in 2018/19, based on a world bank report. Industry sectors, especially the construction, and services are considered for most of the growth.

3. Energy demand of Addis Ababa based on indicators

Ethiopian economy has been experiencing fast, strong and broad growth in the past decade. Since economic growth requires expansion, construction and urbanisation, it is a sign of system changes and upgrades. This huge change has been vividly seen in the capital city of Ethiopia (Addis Ababa).

This continuing, expanding and ongoing growth of the city demands dozens of industries, flights, logistics and transportation services, construction, and many more on the city as well as the surrounding. As these several industries require people for a job and the people from country sides choose to live in modest and better ways, Number of populations in the city is also growing as fast as the economy.

As the population starts to grow in the Addis Ababa, the number of educational, health and entertainment sectors are rapidly increasing. Because of these, there is a vivid circle between the infrastructural and service provider sectors. This economic growth indicates two basic constraints. The main constraint is all those noted sectors request accommodations for the employees and families so residential buildings have been constructed and are still under construction. The second constraint is enterprises are conceiving expansions, new services and productions.

So, both these constraints have high power and energy demand that increases daily. Based on studies, within a decade household energy consumption per capita increased by 17% from 6gigajoules (GJ) only in the city of Addis Ababa. In 2005, about 80% of the sources for energy was traditional fuel but the use of this traditional fuel increased by 10% while modern energy use increased by 50%. This shows not only generally energy is needed but the cities will start to develop many types of energy sources to fulfil the energy demand.

Table. 2.1. Primary and end use household fuel consumption per capita of Addis Ababa for year 1995 and 2015

Year	E(GJ)	Charcoal	Fuelwood	Sawdust	Dung	Electricity	LPG	Kerosene	Total
1995	Primary	0.186	4.396	0.238	0.034	0.041	0.519	0.530	5.943
	End use	0.037	0.703	0.071	0.004	0.029	0.312	0.212	1.368
2015	Primary	0.172	3.449	1.359	0.311	0.980	0.418	0.288	6.976
	End use	0.034	0.552	0.408	0.034-	0.696	0.251	0.115	2.090

□ E/E	-7%	-22%	471%	823%	2293%	-19%	-46%	17%

3.1. Core indicators: Total residential electrical energy use per capita (kWh/year)

The residential energy resource of Addis Ababa from fuel can be categorized as traditional and modern. Charcoal, sawdust, fuelwood and dung are the traditional fuels while kerosene, Liquid Petroleum Gas (LPG) and electricity derived from hydropower are the modern ones. In 1995, the per capita household energy consumption of Addis Ababa was about 6 GJ; traditional fuel shared 82% of the primary energy. In 2005, household energy consumption per capita increased by 17% (about 7 GJ); traditional fuel accounted for 76% of this consumption. Relative to 1995, traditional fuel consumption increased by 9% while the rise in modern fuel use was 55%.

3.2. Core indicators: Percentage of city population with authorized electrical service

Ethiopia's state-owned power company, Ethiopia Electric Utility (EEU) is Ethiopian state-owned power company that provides electricity to about three million customers across the country. ETHIOPIAN ELECTRIC POWER is Electrical Products Wholesalers Industry. With an estimation rate of 98%, the population of Addis Ababa is connected to the electrical service grid which numbered 0.97 million households according to the Ethiopian Electric Utility (EEU).

3.3. Core indicators: Energy consumption of public buildings per year (kWh/m²)

Buildings are the most energy consuming objects of a city. As a developing country and city and as the capital city of Africa, Addis Ababa has many buildings and many more are under construction. Even though there is lack of documented information, the consumption of the building

3.4. Core indicators: Percentage of total energy derived from renewable sources,

As a share of the city's total energy consumption Renewable energy is the most admirable way of energy implementation which makes it a better way of reducing the greenhouse emission. Calculating the usage of renewable energy in a city will promote the sustainability of the city along with the development of demand for energy conversion by supplying from renewable energy sources.

Ethiopia generates power 96% from hydro power energy, 4% wind energy, whereas 11% of production is exported to neighbouring and surrounding countries and the major share of transport energy is imported in the form of petroleum. Ethiopia is enriched with using renewable energy as priority. Hydro power takes the first place while wind, solar, geothermal and biomass are also sources. In the next chapter the detailed renewable energy source and capacity of supply will be indicated.

3.5. Supportive indicators:Total electrical energy uses per capita (kWh/year)

Electricity is the main source of development since production of goods and services of any city highly depends on it. Due to the fast economic growth, the country's usage of energy is enormously increasing with an expected rate of 10-14% per year till the year of 2037.

The total electrical energy usage per capital can be assessed by categorizing into commercial, industrial and residential consumption and dividing this overall electrical usage of the city (numerator) by the total population of the city (denominator)

Table. 3.5. Total electrical energy usage per capita.

Zone	Sum of 2012	Sum of 2015	Sum of 2017	Sum of 2020
Eastern A.A	172	341	550	797
Northern A.A	178	212	279	327
Southern A.A	320	513	744	846
Western A.A	81	146	189	252
Grand Total(mwh/year)	**751**	**6,212**	**1,762**	**2,222**

Ethiopian highly energy consuming sectors has been classified into 6 in order to measure the total energy consumption and for successful forecast. These sectors are

- Transport
- Agricultural
- Industrial
- Large scale Dwelling house expansion Programs
- Universal Electricity Access expansion Program
- Electricity export consumers

4. Supply of Energy in the city of Addis Ababa

Based on the EEU report in 2011 the overall Ethiopian electricity supply was from hydropower. The country expanded the supply of the electricity from 2,000mwh to 10,000mh in the 2010s. This power supply included the renewable resources as wind and geothermal in order to offset the difference in water level caused by seasons.
The other energy demands for cooking, heating and off-grid lighting are covered by biofuels, especially in the rural areas. The other energy resources as petroleum which the country imports, including gasoline, diesel and kerosene cover the country's 7% energy supply.
In the year of 2013, Solar photovoltaics replaced Addis Ababa's off-grid electrical and the fuel-based lighting supply.
Ethiopia is planning for a carbon-neutral status by 2025. Currently the renewable energy resources under use inorder to reach the plan are;

Hydropower
As the main source of energy, Ethiopia has built Dams that provided over 1,500 MW of capacity by 2010. In 2016, Gilgel Gibe III added 1,870 MW additionally to the four largest dams which were built between 2004-2010.
The country has a big hope behind the dam that's under construction, Grand Ethiopian Renaissance Dam (GERD) which is based on the Nile river. When the GERD is completed, the country will be able to generate 6,450 MW, which will put the biggest dam in Africa and even in the world.

Wind power
Since Ethiopian dry season is extremely windy with very little water, wind power is a good complement to hydropower. The strategic plan to generate 800 MW in 2025 has currently reached a total of 324 MW of wind power generation.
51 MW Adama I wind farm, built in 2011, the 120 MW Ashegoda Wind Farm opened in October 2013 and 153 MW Adama II wind farm which went online in May 2015 is successfully supplying energy to the country.

Solar
Ethiopia generates about 5 MW of off-grid solar energy which all the power is majorly used under telecommunication and others uses for village pumps, health care and school lighting.

Geothermal

The Aluto Langano Geothermal Pilot Plant is the only geothermal plant which currently generates 570 MW and has an expansion to generate 1000MW. The project is still under construction.

Waste to Energy Plant

The Reppie waste-to-energy plant is a waste-to-energy plant in Addis Ababa, Ethiopia, which treats waste from the city. The plant was developed by Cambridge Industries Ltd for Ethiopian Electric Power and Addis Ababa City Administration. The facility was expected to supply 50 MW of electricity to the national grid, supporting about a quarter of the city's power demand and can harvest energy from 1.4 million kilograms of waste every day.

The RWTE facility has the potential to be recycled and estimated 3.6 million kilograms of metals from the incinerated waste each year. Residue ash could also be used to produce an estimated 27,000 bricks every day.

Currently this energy plant is not working due to technical issues.

5. Conclusion

The world is changing rapidly with aim of becoming environmentally friendly, smart and having sustainable development that would not affect the environment. Living in a smart city which is convenient for its residence and suitable for living is becoming the essential measurement for many countries. In order to be considered under this measurement of the city, many criterions have been developed based on each country's way of definition of smart, sustainability and development. But as globalization is the current tool that is bringing the world into one, each country is trying to adjust itself to be measured under the global standards.

Among these global standards, ISO takes the prior position by giving quality assurance based on agreed and fixed measures. ISO 37120 is the international standard that deals with sustainable development of communities with indicators for city service and quality of life. Among many city indicators that need to be assessed, Energy is also listed and which should be given prior concern.

Even though, as a developing country, it's difficult to find well organised statical and approved reports of cities from the immediately responsible sector, more or less the data has been found on the research papers and reports of many organisations and correlate with one to another.

But based on the available information, the following main points has been observed.

- **i.** Identifying the core and supportive city indicators based on the ISO 37120.
- **ii.** Measuring the city of Addis Ababa city performance based on the identified indicators.
- **iii.** Identifying the energy supply of Ethiopia.

Based on this it has been shown that the city of Addis Ababa Electricity usage typically dependent on renewable energy. This can be a great example for many cities that are still highly dependent on non-renewable energy as fossil fuels which includes oil, natural gas.

On the other hand, the number of populations of the city is highly increasing in which in the near future, shortage of energy might be a big problem, unless a big measure is taken with wise research and developments.

It can be reached to many conclusions based on the indicators provided but the main purpose of this article is to provide clear general guidance on the possibility of measuring city performance based on standard indicators.

The remaining two supportive indicators which deal with measuring the interruption of electricity helps to analyse if the supply of the energy compensates the demand. Measuring the interruption will also help to improve the limitation with the distribution of the electricity.

Acknowledgment

I would like to thank my supervisor Prof. Tomasz Sulz for his kind appreciation, motivation and guidance throughout the entire work. Even though distance learning made the sharing of knowledge new and difficult, I would like to thank him for giving us more time for his consultation.

I would also like to thank the Silesian University of Technology for giving us opportunities to participate in an event where enormous knowledge and experience will be gained.

Finally I would like to thank my family for supporting me in every way including giving feedback and reviews for my works.

References

[1] Md Alam HossainMondal, *Ethiopian energy status and demand scenarios: Prospects to improve energy efficiency and mitigate GHG emissions*, Volume 149, 15 April 2018,

[2] Gouthami Padam, Dana Rysankova, Elisa Portale, Bryan Bonsuk Koo, Sandra Keller, Gina Fleurantin, *ETHIOPIA Beyond Connections Energy Access Diagnostic Report Based on the Multi-Tier Framework*, ©2018 International Bank for Reconstruction and Development / The World Bank 1818 H Street NW, June 2018

[3] The Resilient Cities Program, *Addis Ababa, Ethiopia Enhancing Urban Resilience*, © 2015 Global Practice on Social, Urban, Rural and Resilience The World Bank Group, July 2015

[4] ISO/TC 268, Sustainable development communities, *ISO 37120:2014, Sustainable development of communitiesIndicators for city services and quality of life*, First edition, BSI Standards Limited, 2014

[5] ETHIOPIAN ELECTRIC POWER - NARUC, https://pubs.naruc.org/pub.cfm?id=537C14D4-2354-D714-511E-CB19B0D7EBD9, 19/11/2020

[6] Ethiopia Energy Situation - energypedia.info, https://energypedia.info/wiki/Ethiopia_Energy_Situation , 23/11/2020

[7] Addis Ababa, Ethiopia Population (2020) - Population Stat, https://populationstat.com/ethiopia/addis-ababa , 26/11/2020

Oxygenic photogranules - description and investigation of potential efficiency to treat wastewater - literature review

German Smetana[1]

[1] *Czestochowa University of Technology, e-email: gerkus20123@gmail.com*

Abstract

The literature review was focused on the relatively new discovery – oxygenic photogranules, that are algae and cyanobacteria aggregations that can be formed from activated sludge illuminated by light under static conditions (in vials) or dynamic ones (in a SBR reactor) in the period of about 46 days. Their application in the wastewater treatment, in particular, the biological wastewater treatment can potentially bring such benefits as improvement of a nitrogen removal, chemical oxygen demand reduction and, most importantly, decrease in the aeration requirements that consequently decrease the operational costs of a wastewater treatment plant. In the first section there is a discussion of the conventional wastewater treatment process as well as cyclic activated sludge process, in which the SBR technology is applied. Then, there goes discussion related to biogranular wastewater process. The last section describes the oxygenic photogranules, their structure, formation as well as benefits of application in wastewater treatment.

Key words: Oxygenic photogranules, biofilms, activated sludge process, sequencing batch reactor, cyanobacteria, energy

1. Introduction

Increase in population, extensive urbanization and wastewater generation through consumption led to the diversifying of pollutants in wastewater as well as increase in its amount. These factors force to search new ways, methods and means to struggle against this pressing global problems. Also, decrease in the global fossil fuel stock and a need to switch to more renewable alternatives of energy necessitate introduction of such changes in the conventional technologies, including wastewater treatment ones, that decrease the amount of energy required in the process [1].

One of the most important methods that is used during biological wastewater treatment – activated sludge process, is extremely energy consuming (the energy consumption amounts to about 60 [%] of that available in a wastewater treatment facility). Albeit, it is effective in elimination of organic matter, great amount of energy is required during aeration process [2].

Wastewater itself is a source of an energy and if one would find means to capture this energy, wastewater treatment might become an energy producer rather than a consumer. Oxygenic photogranules (OPGs), the aggregations of cyanobacteria and algae that can be formed under photo-illumination from activated sludge, are relatively new granules that can be found applicable in biotechnology as well as wastewater treatment. Their application for the latter, can potentially reduce the need to have an external aeration [3]. OPGs can be also perceived as a potential energy storage [4]. Their application can also enhance the nitrogen, phosphorus as well as heavy metal removal [5].

This literature review was focused on the description of the activated sludge process as well as possibility to substitute it by application of oxygenic photogranules. There is presented a description, structure, way of formation as well as benefits of OPGs if applied for the wastewater treatment.

2. Wastewater treatment using biological methods

2.1. Description of activated sludge process

The waste water treatment using biological methods has been a sensitive topic and arisen an increasing interest in engineers around the globe during the last century, as they struggle to enhance them. Biological methods for the treatment of wastewater are the most popularly applicable practices which help to attain a compliance of environmental pollution discharge and waste reduction regulations or even exceed it. The activated sludge, which is used in such a treatment, is considered to be a basis of contemporary wastewater treatment and it is the most widely used component for municipal and industrial wastewaters [6].

There exist many types of activated sludge process but in this review there are mentioned the following ones [6]:

– Conventional activated sludge process system (CASPS)
– Cyclic activated sludge system (CASS).

The former one is the oldest and the most conventionally applied processes to treat municipal and industrial wastewater using activated sludge [6].

The figure 1 represents this process, wherein wastewater begins its way from the place of a primary treatment, in particular, from a receiving chamber, into which the wastewater is supplied. Primary treatment helps to remove various debris and particles which by means of gravity either settle to the bottom or float. Secondary treatment includes the activated sludge process which consists of an aeration tank and a secondary clarifier which both work in conjunction with each other [7].

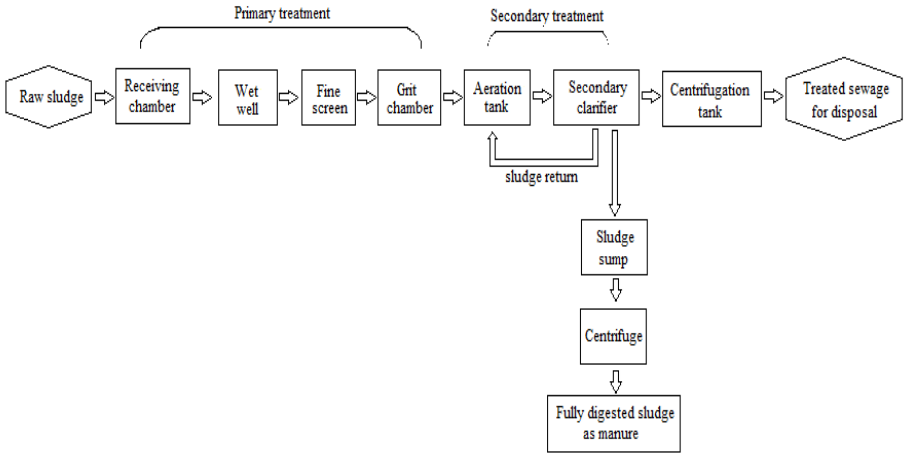

Fig. 1. Conventional activated sludge process [7, 8]

Cyclic activated sludge system principle, however, is more sophisticated and provides more benefits such as elimination of a secondary clarifier, energy optimization through nutrient removal mechanisms and overall installation and exploitation cost reduction [7–9]. The next figure shows a layout of a wastewater treatment plant with a sequencing batch reactor (SBR) that substitutes the conjunction of an aeration tank plus a secondary clarifier, for SBR is an aerator and a clarifier itself. In this system, the biological treatment stage is divided into cycles, during which the necessary biological treatment processes are applied, and each of them has its own duration, for example, 3 – 5 hours [6].

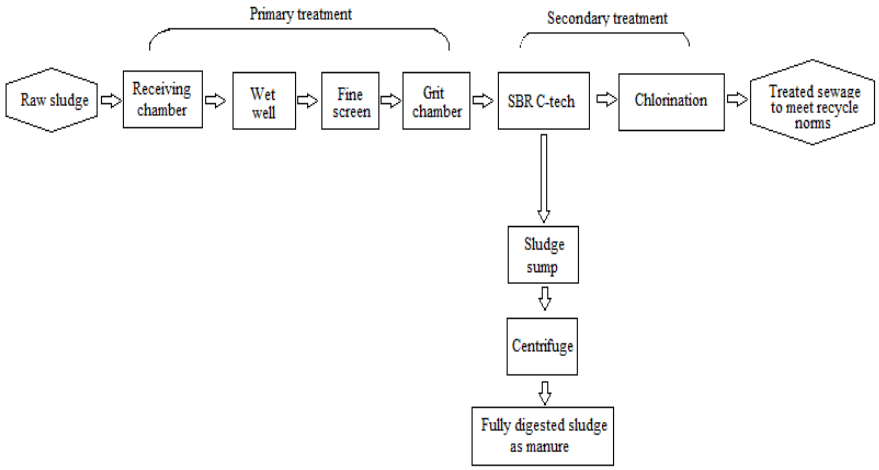

Fig. 2. Cyclic activated sludge process [7]

Since that very day when activated sludge was firstly used, there have been plenty of researches conducted in order to expand the original concept and designs for the purpose of achievement of higher energy and nutrient recovery, better quality of effluents, and, overall, improvement of process effectiveness [10].

Unfortunately, as the time unstoppably flows even the current technologies which proved to be effective cannot provide better results in wastewater treatment, since the variety of pollutants is deplorably diverse, and the technologies still remain to be energy consuming, for aeration process uses up to 60 [%] of the energy [5].

Recently, scientists have invented granules which are formed from activated microbial sludge and if applied can lead to superfluity of separate settling tanks which, therefore, can reduce the land requirements almost to 80 [%] and energy consumption almost to 60 [%]. The granules, whose name is oxygenic photogranules, are comprised of photosynthetic microorganisms as well as with heterotrophic bacteria. An application of the granules for the wastewater treatment can help to get rid of aeration requirements and create closed CO_2 and O_2 cycles within a single system [4].

2.2. Wastewater treatment using bio-granules

Biogranules utilized for the wastewater treatment has proved many times to be more effective than an activated sludge process over last few decades. There have been plenty of researches conducted with the granules of different kinds with different properties and there was eventually concluded that their efficiency is undeniable [2,11–13].

There can be mentioned the following beneficial properties of granules [13]:

– Microbial aggregates which are called ‘’*biofilms*’’, are comprised of microorganisms which are slow to grow, hence, the increased biomass retention in the aggregates is a major advantage over conventional suspended growth processes.
– If one would compare the conventional sludge flocs with the biogranules, the latter possess more robust, condensed and well-defined structures.
– Biogranules possess a higher settle ability which means easier separation of biomass from treated water.

Biogranules can be categorized into two groups: anaerobic and aerobic granules. The first information about the anaerobic granules was documented in 1980 and since that day, there has been conducted a lot of researches on the properties of the granules and their efficiency. The treatment of wastewater using anaerobic biogranules nowadays is only applied for municipal wastewater because the granules are very susceptive to organic load rate [14].
There should be mentioned a several disadvantages of anaerobic granules [15, 16]:

– a long period of beginning of treatment operation by the granules,
– the temperatures at which the granules operate are high, therefore an application of the anaerobic granules is energy expensive,
– the granules require a high organic load rate sustained during the granulation and operation,
– the granules provide low efficiency in removing of nitrogen and phosphorous.

Owing to the previously mentioned disadvantages, there was induced a great interest in an investigation of granular formation from aerobic bacteria in the 1990s. One way to cultivate aerobic granules is with help of sequencing batch reactors (SBRs) utilizing industrial or domestic wastewater. In the same manner as it is with an activated sludge process, aerobic granules demand presence of oxygen during the whole granulation period. But the difference of aerobic granules from activated sludge flocs is conspicuous, since they possess a dense structure and the time of settling is lower. Having such a rapid ability to settle, the application of a clarifier and polymeric flocculation agents is dispensable [17].
Apart from the advantages there are a few drawbacks of the aerobic granules [16,17]:

– a long period of beginning of treatment operation by the granules, as it was with the anaerobic granules,
– the aerobic granules only justify an application of them for industrial wastewater treatment because the oxygen demands are high.

3. Oxygenic photogranules – structure, formation and benefits of application

3.1. Structure of oxygenic photogranules

Cyanobacteria (**Cyanophyta**) - a group of bacteria which get their energy by virtue of photosynthesis, and are considered to be the only photosynthetic prokaryotes which are able to produce oxygen. The figure below represents ‘’*cyanobacteria*’’ under magnification. It is clearly noticeable that the bacteria have rather interwoven structure which gives bio-films such a dense form [18].

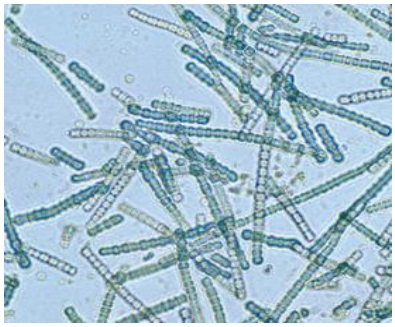

Fig. 3. Cyanobacteria (*Cylindrospermum)* under a microscope [19]

Cyanobacteria is encountered in utterly each terrestrial and aquatic environment such as oceans, pure fresh water, wet soil, volatilely moistened rocks in deserts, rock and soil, and sometimes even in Antarctic rocks. They can exist as cells of planktons or form phototrophic bio-films [20]. Cyanobacteria is an extraordinary diverse group of bacteria which are highly adaptive and contribute majorly to global cycles of carbon, oxygen, and nitrogen [21].

For example, in the regions where concentration of nitrogen is poor cyanobacteria contribute nitrogen by the fixation of atmospheric nitrogen in marine environments [22]. In those regions where the concentration is on the contrary high cyanobacteria absorb nitrogen in the form of NH_3, NO_3, or NO_2 in order to create biomass as bacteria grow and the biomass is further consumed by aquatic species [21].

In the case if cyanobacteria are exposed to light, they tend to oxygenize the environment, i.e. producing oxygen through photosynthesis. They are also able to metabolize during the absence of light by means of fermentation or glycolysis (glycogen metabolism, converting of glucose into pyruvic acid) [23]. Bacteria are facultative in their nature, meaning that they are capable but not strictly restricted to some particular mode of life, leading to the fact that they are able to exist in multiple layers of a microorganisms called microbial mats, and by virtue of gliding bacteria move throughout the microbial layers [21]. The next figure shows the microbial mat with the bacteria. As any other bacteria aggregation, an appearance, which the mat possess, has a conspicuous similarity with a fungi mould [24].

Fig. 4. The mat with cyanobacteria and algae [24]

Albeit, it is still not thoroughly known with help of which mechanism cyanobacterial aggregations can sustain their formation in a form of granules, studies performed in 2014 revealed that cohesive behaviour is attributed to the stickiness of extracellular polymeric substances, gliding actions that form stickiness patterns and which serve as a means of defence against either extreme light conditions or animals during their grazing [21, 25].

Oxygenic photogranules (OPGs) which can be produced under the laboratory conditions using activated sludge and photo-illumination have a shape of aggregates with spherical cyanobacteria which can be found in nature. OPGs have a form of microbial bio-films which are dense, spherical and interwoven. The biofilms are comprised of cyanobacteria, algae, a host of heterotrophs and autotrophs [2, 5].s

The next figure (figure 5) represents a cross-section view of an oxygenic granule. There is a noticeable layer of green filamentous cyanobacteria around a boarder of the granule and less dense bright-green layer is micro algae bio-film [2, 26].

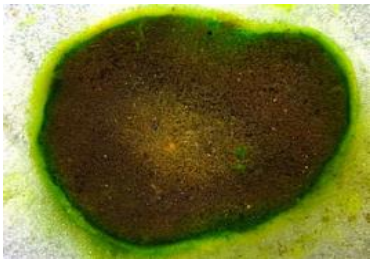

Fig. 5. Cross-section of oxygenic photogranules cultivated in a laboratory using static cultivation [27]

The oxygenic photogranules were firstly discovered by S. Dolan and C. Park in 2011 during the observation of how activated sludge is transformed when incubated under undisturbed conditions into sealed vials which further were exposed to natural light for several months. This method is called ‘*’static cultivation’’* [2]. There were observed different morphotypes of OPG during the laboratory experiments and the next figure (figure 6) represents these types [11]:

– Bald granules which have a similarity with fluvial pebbles.

– Loosely reminiscent filamentous granules and have a dreadlocks like appearance.

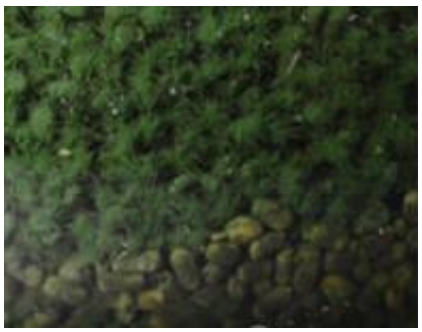

Fig. 6. Oxygenic photogranules with a bald (lower pale-brown layer) and filamentous (upper green layer) morphologies [11]

In both granule morphologies, bacteria of the order Oscillatoriales, which present in the phototrophic part of the OPG, is identified as a major contributor to the appearance the granules [2].

Oscillatoriales are known for their slender thread-like morphology and an ability to move with smooth continuous motion [2,28]. These properties are hypothesised to be major components of the structure of such a dense cloth-like phototrophic layer in OPG [28].

During the period of maturation, the net density of granules increases because of the compaction and through the precipitation of $CaCO_3$ in the interior part of the granules, in particular when OPGs grow in environments where water basins have a high hardness [2].

The table 1 represents the comparison of characteristics of OPG with flocculated activated sludge. The densities of bald OPGs can reach the value up to 1.5 [kg/L] and the percentage of volatile solids content can be around 30%, whereas the density of filamentous granules is almost equal to the density of the water and the volatile solids content is more than 70%. In these situations, bald OPGs can reach densities of up to 1.5 [kg/L] with a volatile solids content of around 30% (per total solids), whereas the density of filamentous granules is closer to that of water with volatile solid contents of more than 70 [%]. As a result, the granules have the velocity of settling ranging from 36 [m/h] for the filamentous granules, to 360 [m/h] for the bald ones [2, 4, 29, 30].

Table 1. The general physicochemical characteristics of oxygenic photogranules with flocculated activated sludge [4]

	Size	**Density [g/cm^3]**	**Settling velocity [m/h]**	**Sludge volume index [ml/g]**	**Porosity [-]**	**Water content [%]**
OPGs	0.1 – 5 [mm]	Highly variable	36 – 360	Nd*	Nd*	78 – 95
Activated sludge floc	0.5 – 1000 [μm]	1.002 – 1.006	0.6 – 15	100 – 150	> 0.95	> 99

Nd – not detected

Due to the fact that cyanobacteria and algae have very strong and versatile metabolism, it allows them to reside and prosper in a perpetually changing environment. Also, they are even supported by the non-photosynthetic bacteria within the biofilm community forming a syntrophic relationships [25].

3.2. Formation of oxygenic photogranules

It is hypothesized that both anaerobic and aerobic granule formation are induced by virtue of hydrodynamic shear forces. Oxygenic photogranules, as it was observed, actually form when exposed to hydrodynamic shear in special apparatuses called sequencing batch reactors (figure 6) and this process is called ‘*’dynamic cultivation’’* [4, 5, 27].

Fig. 6. Laboratory scale sequencing batch reactor [31]

As far as ‘’*static cultivation*’’ is concerned, oxygenic photogranules are totally formed over the period of several weeks or sometimes months from a source of activated sludge distributed to vials which are exposed to light. The result of this transformation is represented on the figure 7 [27].

Fig. 7. A gradual progression of the photogranules under ‘*’static cultivation*’’ [27]

Transformation of activated sludge into photogranules occurs with an intense formation of gliding filamentous cyanobacteria and green algae, which consequently leads to the development of mats with microorganisms which are woven with each other, and as a result the granules have such a spherical structure [4, 32]. Filamentous cyanobacteria in OPGs, due to their adaptivity to the environmental factors, can have a growth in temperatures below 10 [°C] and even above 25 [°C] [2].

The full mechanism of OPG formation under static cultivation is hitherto being investigated, albeit the presence of *Oscillatoria* bacteria, nitrogen and light are hypothesized to partake in the development of the process the most [4]. Furthermore, if one would manipulate with these variables, there will be a result in OPGs with different structural unification, densities, and settle ability [33]. The conducted researches relating the influence of shear stresses on the size of statically cultivated biomass of OPG showed that higher shear stresses promote formation of smaller granules (diameter in the range 0.5 – 1.0 [mm]), whilst lower shear stresses promote larger granules which can reach sizes greater than 4.6 [mm] [11]. Whilst hydrodynamic shear forces do not play a significant role in OPG cultivation, it does influence on hydrodynamic granulation. It was observed that larger OPG granules seem to render higher total nitrogen removal than smaller granules do. Therefore, there was found an explicit dependence of the oxygen change with the size of the granules [33].

There was also observed that OPG which were obtained in biological reactors have the following properties: creation of extracellular polymeric substances (EPSs), high hydrophobicity, high velocity of settling and high density [12, 34]. EPSs are essential for the amalgamation of microbial bio-firms and help to immobilize bacteria and provide necessary resources for formation of communities within immobilized system [34]. Hydrophobicity, which is a form of a non-covalent interaction, along with Van der Waals forces and opposite charge attraction assist greatly in the formation of the granules [12, 33]. There should be noted that under static conditions, there is no external supply of nutrients for OPGs in a closed system and this can induce starvation, whereas cultivation under hydrodynamic conditions (usage of the sequencing batch reactor) provides a possibility to adjust external supply of necessary nutrients. It was also taken into account that a periodical starvation, meaning a shortage of nutrients for growth, is a major indicator of growth of granules [11, 12]. In addition to the formerly mentioned causes of the formation of OPG, the initial presence of phototrophic communities as well as a sufficient amount of nutrients in activated sludge may increase granulation. Also, in the case of static cultivation, high ammonium concentration (20 – 30 [mg-N/L]) of activated sludge promotes the granulation, making granules more structured and settleable, whereas low concentration of ammonium (6 – 12 [mg-N/L]) renders the cultivation unsuccessful and the granules cannot take a proper granular form [35].

3.3. Benefits of application of oxygenic photogranules

Oxygenic photogranules act without external aeration and moreover they consume more CO_2, thereby reducing greenhouse emissions that overall renders the system carbon negative. Oxygenic photogranules can reduce production of sludge and their application with SBR system have a potential to supplant the conventional activated sludge that will bring great energy savings for municipal wastewater treatment [4, 5]. There exist the following benefits, besides those mentioned [23, 33, 36]:

- an improvement of nitrogen removal,
- decrease in chemical oxygen demand,
- removal of heavy metals,
- reduction of wastewater treatment carbon footprint,
- generation of bio-energy feed stock which implies minimal energy investments for the wastewater treatment purposes,
- the reduction of requirements for the mechanical aeration by improving the energy efficiency.

4. Conclusion

This literature review was focused on the relatively new discovery that is potentially applicable in biological wastewater treatment process –oxygenic photogranules. Under static conditions, activated sludge is transformed into the photogranules by means of a light source, which the photosynthetic bacteria present in the sludge, utilize for the purpose of their growth along with carbon dioxide and organic matter, which as the result renders the water denitrified and produces a great supply of oxygen [3, 5, 27].

The facts which were mentioned in the review about the structure, formation and benefits of the granules indicate their potential utility for municipal wastewater treatment, because their application and formation does not require external aeration. That feature can lead to the reduction in waste sludge generation as well as exploitation costs of wastewater treatment. Additionally, the granulation process accumulates a profound amount of bio-energy stock in the form of

granular biomass which can be further easily harvested and applied as a biofuel or for the other practical purposes [3–5]. Furthermore, granules have an advantage over an activated sludge process owing to the excellent settle ability and small footprint which implies that the technology can be a promising one if applied. The efficiency of oxygenic photogranules in removal of organic nutrients such as nitrates and phosphates etc. along with a substantial decrease in chemical oxygen demand has been shown plenty of times in the laboratory conditions by the researches about which there was a reference in the review [5]. Overall, it can be concluded that oxygenic photogranules can be utilized as a potentially beneficial measure to improve or to substitute the activated sludge process in the future [5].

The continuation of the further researches and a consequent application of such an effective a means to treat wastewater is of a great importance in aeration-free wastewater treatment as well as biotechnology which can bring the mankind one step closer towards the sustainable development and enhanced wastewater treatment practices.

References

[1] Prasse, C.; Stalter, D.; Schulte-Oehlmann, U.; Oehlmann, J.; Ternes, T.A. Spoilt for choice: A critical review on the chemical and biological assessment of current wastewater treatment technologies. *Water Res.* 2015, *87*, 237–270, doi:https://doi.org/10.1016/j.watres.2015.09.023.

[2] Butler, C.; El-Moselhy, K.M.; Park, C. The oxygenic photogranule (OPG) for aeration-free and energy-recovery wastewater treatment process. *Proc. Water Environ. Fed.* 2016, *2016*, 1–8.

[3] Stauch-White, K. The Role of Nitrification and Denitrification in Successful Cultivation of Oxygenic Photogranules for Wastewater Treatment. 2016, 5–9.

[4] Chandran, A.; Kani,] K Mophin; Anu,] Treatment of Municipal Wastewater using Oxygenic Photo granules (OPGs). *Int. J. Eng. Res. Mech. Civ. Eng.* 2018, *3*, 2456–1290.

[5] Park, C.; Dolan, S. Algal-sludge granule for wastewater treatment and bioenergy feedstock generation 2019.

[6] Arun Mittal Biological Wastewater Treatment. *FullTide* 2011, 2–9.

[7] Kumar A. Comparative study of cyclic activated sludge and conventional activated sludge process.

[8] Bhargava, A. Activated Sludge Treatment Process - Concept and System Design. *Int. J. Eng. Dev. Res.* 2016, *4*, 890–896.

[9] Wastewater Treatment Plant Operator Certification Training, Module 17: The Activated Sludge Process Part III 2014.

[10] Rittmann, B.E.; McCarty, P.L. *Environmental biotechnology: principles and applications*; Tata McGraw-Hill Education, 2012; ISBN 1259002888.

[11] Milferstedt, K.; Hamelin, J.; Park, C.; Jung, J.; Hwang, Y.; Cho, S.K.; Jung, K.W.; Kim, D.H. Biogranules applied in environmental engineering. *Int. J. Hydrogen Energy* 2017, *42*, 27801–27811, doi:10.1016/j.ijhydene.2017.07.176.

[12] Xing, B.S.; Guo, Q.; Yang, G.F.; Zhang, Z.Z.; Li, P.; Guo, L.X.; Jin, R.C. The properties of anaerobic ammonium oxidation (anammox) granules: Roles of ambient temperature, salinity and calcium concentration. *Sep. Purif. Technol.* 2015, *147*, 311–318, doi:10.1016/j.seppur.2015.04.035.

[13] Adav, S.S.; Lee, D.-J.; Show, K.-Y.; Tay, J.-H. Aerobic granular sludge: recent advances. *Biotechnol. Adv.* 2008, *26*, 411–423.

[14] Giesen, A.; de Bruin, L.M.M.; Niermans, R.P.; van der Roest, H.F. Advancements in the application of aerobic granular biomass technology for sustainable treatment of wastewater. *Water Pract. Technol.* 2013, *8*, 47–54, doi:10.2166/wpt.2013.007.

[15] Roeselers, G.; Loosdrecht, M.C.M.V.; Muyzer, G. Phototrophic biofilms and their potential applications. *J. Appl. Phycol.* 2008, *20*, 227–235, doi:10.1007/s10811-007-9223-2.

[16] Wett, B.; Omari, A.; Podmirseg, S.M.; Han, M.; Akintayo, O.; Gómez Brandón, M.; Murthy, S.; Bott, C.; Hell, M.; Takács, I.; et al. Going for mainstream deammonification from bench to full scale for maximized resource efficiency. *Water Sci. Technol.* 2013, *68*, 283–289, doi:10.2166/wst.2013.150.

[17] Sarma, S.J.; Tay, J.H. Aerobic granulation for future wastewater treatment technology: challenges ahead. *Environ. Sci. Water Res. Technol.* 2018, *4*, 9–15.

[18] Cyanobacteria : Life History and Ecology Available online: https://web.archive.org/web/20120919015239/http://www.ucmp.berkeley.edu/bacteria/cyanolh.html.

[19] Cyanobacteria - wikipedia page Available online: en.wikipedia.org/wiki/Cyanobacteria.

[20] Vaughan, T.; Ryan, J.; Czaplewski, N. *Mammalogy*; Jones & Bartlett Learning, 2011; ISBN 0763762997.

[21] Tamulonis, C.; Kaandorp, J. A model of filamentous cyanobacteria leading to reticulate pattern formation. *Life* 2014, *4*, 433–456, doi:10.3390/life4030433.

[22] Klawonn, I.; Bonaglia, S.; Brüchert, V.; Ploug, H. Aerobic and anaerobic nitrogen transformation processes in N2-fixing cyanobacterial aggregates. *ISME J.* 2015, *9*, 1456–1466, doi:10.1038/ismej.2014.232.

[23] Zhang, Z.P.; Adav, S.S.; Show, K.Y.; Tay, J.H.; Liang, D.T.; Lee, D.J.; Su, A. Characteristics of rapidly formed hydrogen-producing granules and biofilms. *Biotechnol. Bioeng.* 2008, *101*, 926–936, doi:10.1002/bit.21956.

[24] Microbial mat - wikipedia page Available online: https://en.wikipedia.org/wiki/Microbial_mat.

[25] Segawa, T.; Ishii, S.; Ohte, N.; Akiyoshi, A.; Yamada, A.; Maruyama, F.; Li, Z.; Hongoh, Y.; Takeuchi, N. The nitrogen cycle in cryoconites: naturally occurring nitrification-denitrification granules on a glacier. *Environ. Microbiol.* 2014, *16*, 3250–3262, doi:https://doi.org/10.1111/1462-2920.12543.

[26] oxygenic photogranules - wikipedia page Available online: https://en.wikipedia.org/wiki/Oxygenic_photogranules.

[27] Milferstedt, K.; Kuo-Dahab, W.C.; Butler, C.S.; Hamelin, J.; Abouhend, A.S.; Stauch-White, K.; McNair, A.; Watt, C.; Carbajal-González, B.I.; Dolan, S. The importance of filamentous cyanobacteria in the development of oxygenic photogranules. *Sci. Rep.* 2017, *7*, 1–15.

[28] Liu, L.; Fan, H.; Liu, Y.; Liu, C.; Huang, X. Development of algae-bacteria granular consortia in photo-sequencing batch reactor. *Bioresour. Technol.* 2017, *232*, 64–71, doi:10.1016/j.biortech.2017.02.025.

[29] Tiron, O.; Bumbac, C.; Patroescu, I. V; Badescu, V.R.; Postolache, C. Granular activated algae for wastewater treatment. *Water Sci. Technol.* 2015, *71*, 832–839, doi:10.2166/wst.2015.010.

[30] Kumar, R.; Venugopalan, V.P. Development of self-sustaining phototrophic granular biomass for bioremediation applications. *Curr. Sci.* 2015, *108*, 1653–1661.

[31] Aerobic granulation - wikipedia Available online: https://en.wikipedia.org/wiki/Aerobic_granulation.

[32] Pronk, M.; de Kreuk, M.K.; de Bruin, B.; Kamminga, P.; Kleerebezem, R.; van Loosdrecht, M.C.M. Full scale performance of the aerobic granular sludge process for sewage treatment. *Water Res.* 2015, *84*, 207–217, doi:https://doi.org/10.1016/j.watres.2015.07.011.

[33] Abouhend, A.S.; McNair, A.; Kuo-Dahab, W.C.; Watt, C.; Butler, C.S.; Milferstedt, K.; Hamelin, J.; Seo, J.; Gikonyo, G.J.; El-Moselhy, K.M.; et al. The Oxygenic Photogranule Process for Aeration-Free Wastewater Treatment. *Environ. Sci. Technol.* 2018, *52*, 3503–3511, doi:10.1021/acs.est.8b00403.

[34] Sheng, G.P.; Yu, H.Q.; Li, X.Y. Extracellular polymeric substances (EPS) of microbial aggregates in biological wastewater treatment systems: A review. *Biotechnol. Adv.* 2010, *28*, 882–894, doi:10.1016/j.biotechadv.2010.08.001.

[35] Stauch-White, K.; Srinivasan, V.N.; Camilla Kuo-Dahab, W.; Park, C.; Butler, C.S. The role of inorganic nitrogen in successful formation of granular biofilms for wastewater treatment that support cyanobacteria and bacteria. *AMB Express* 2017, *7*, doi:10.1186/s13568-017-0444-8.

[36] Liu, X.W.; Sheng, G.P.; Yu, H.Q. Physicochemical characteristics of microbial granules. *Biotechnol. Adv.* 2009, *27*, 1061–1070, doi:10.1016/j.biotechadv.2009.05.020.

Static mixers as multifunctional reactors for wastewater treatment

Tomasz Walica[1], Milena Kotek[1], Agata Małysiak[1], Marcin Lemanowicz[1]

[1]Silesian University of Technology, email: tomawal414@student.polsl.pl, milekot622@student.polsl.pl, Agata.Malysiak@polsl.pl, Marcin.Lemanowicz@polsl.pl

Abstract

Wastewater treatment is one of the main problems of industrialized societies. Decreasing availability of freshwater creates a need for finding new, better and more efficient ways of pollution elimination. Lately, static mixers are more often used in wastewater treatment. Variety of possible shapes and sizes of static mixers opens up the way for finding new technical solutions. In this paper the review of static mixer application as multifunctional reactors for wastewater treatment is presented. The following processes were discussed: photocatalysis, ozonation, coagulation, flocculation and membrane filtration. In each case the application of static mixers significantly enhanced the efficiency of treatment process. The huge variety of possibilities in design of static mixers makes these multifunctional reactors a very interesting and promising alternative for wastewater treatment technology.

Keywords: Static mixers, multifunctional reactors, wastewater treatment

1. Introduction

Nowadays, in the fast-growing population access to freshwater decreased significantly. To control the depletion of water resources, the renewable freshwater resources (RFR) indicator was created. When the level of the RFR is lower than intake, the water resources shrinks. Currently, the renewable freshwater resources per capita is abating every year worldwide. Since 1962 RFR has dropped over two times, compared to 2014 [1].

In order to discuss the wastewater treatment properly, key characteristics of pollutants should be defined. The most popular indicators of quality of water are:

- BOD (Biochemical Oxygen Demand)
- COD (Chemical Oxygen Demand)
- TOC (Total Organic Carbon)
- Temperature
- pH
- Conductivity
- Turbidity
- Water hardness
- Taste and odor
- Solids

The conventional ways of treating wastewaters may be divided into three types: chemical treating, biological treating, and physical treating. Usually, the treating process consists of three main stages. Primary treatment is a superficial stage, where larger solids and oils are separated from treated water. Secondary treatment is focused on the removal of the most of contaminants. Tertiary treatment is a stage where the treated water is “polished” [2]. The conventional process of water treating may be expensive. That is the motivation for searching of wastewater treatment cost reduction, enhancement of the efficiency and generally developing new methods of treating. One of the approaches is the application of static mixers. Static mixers (SMs) might be used as multifunctional apparatus, e. g. simultaneously as the heat exchanger, mass exchanger and chemical reactors reactor [3]. SMs increase the mixing efficiency and therefore

might reduce costs due to lower substrate usage [4]. Moreover, SMs need less power compared to conventional agitators [5].

Static mixer is a tool for an unconventional way of mixing, where fluid is mixed by dividing and merging streams, using motionless elements [6]. Such fluid movement increase mass and heat diffusion in cross section by creating secondary transfer flows [7]. Motionless elements may have various shapes and sizes:

- Helices, e.g. helical Kenics™ from Chemineer Inc.
- Blades e.g. LPD™ form Ross Engineering Inc.
- Plates e.g. SMV™ from Sulzer Ltd.
- Multilayer designs e.g. SMX™ from Sulzer Ltd. [8]
- And many more

Basing on patent.google.com website the number of patents dedicated to static mixers is around 140 000. Below there are few examples of industrial types of static mixers (Fig. 1 and 2).

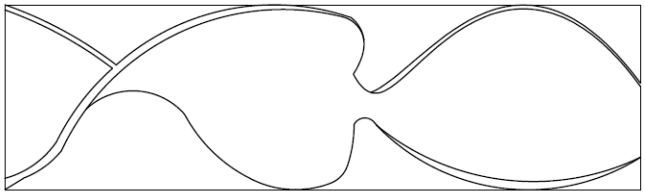

Fig. 1. Kenics static mixer

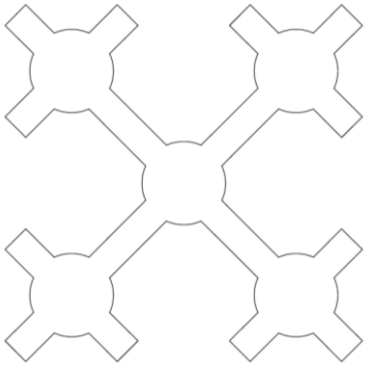

Fig. 2. NETmix static mixer

High mixing efficiency of static mixers is caused by specific profiles of mixing elements. Elements create vortexes providing local turbulences even at low flow rates. Mixing occurs due to the momentum of liquid. When liquid flows through the mixer, it hits mixing elements and the flow energy is turned into the mechanical energy. Nevertheless, achieving higher turbulences increases pressure-drop [9]. The advantages of application of static mixers in industrial processes are as follows [5]:

- Less space needed compared to conventional agitators
- Low-cost
- Low power consumption (no power needed to power agitator drive)
- Short residence time
- Attractive for continuous processes
- Possibility of establishing a plug flow
- Implement the function of various apparatus, e.g. heat exchanger, mass transporter, reactor
- Self-cleaning mixer

Static mixers have found its application in many areas of industry [3]:

- Petrochemistry, e.g. establishing water-oil emulsions
- Chemical industry, e.g. processes of emulsion polymerization
- Power engineering, e.g. dispersion of gas condensate
- Water treatment, e.g. dispersion of ozone
- Food industry, e.g. homogenization of milk products.

In this paper the review of applications of static mixers as multifunctional reactors in wastewater treatment is presented. Based on papers, the division of static mixers in wastewater treatment was proposed:

- Static mixers as photoreactors
- Static mixers in ozonation process
- Static mixers as coagulation and flocculation enhancement reactors
- Static mixers in membrane filtration process

2. Application of static mixers in wastewater treatment

2.1. Static mixers as photoreactors

Photocatalysis is a process which employs UV irradiation to degrade various wastewater contaminants. The benefit of photocatalysis lies is combination of chemical and physical phenomena. The pollutants undergo an oxidating reaction which result in achieving much simpler chemical substances. Photocatalysis can be realized by two different operations, as homogenous or heterogenous reactions. In the first case the photocatalyst and reactants are in the same phase. The main goal of this process is to generate hydroxyl radicals which may be formed due to the ozone decomposition under UV irradiation or as product of photo-Fenton reaction. Originally the catalyst in the photo-Fenton reaction was iron, nevertheless, it is possible to apply other photoactive metal catalysts, e.g. titanium. Ozone decomposition is due to the following reactions [10]:

$$O_3 + hv \rightarrow O_2 + O \quad (Equation\ 1)$$

$$O + H_2O \rightarrow OH^{\bullet} + OH^{\bullet} \quad (Equation\ 2)$$

$$O + H_2O \rightarrow H_2O_2 \quad (Equation\ 3)$$

$$H_2O_2 + hv \rightarrow OH^{\bullet} + OH^{\bullet} \quad (Equation\ 4)$$

Photo-Fenton reaction is described as follows [11]:

$$Fe^{2+} + H_2O_2 \rightarrow Fe^{3+} + OH^- + OH^{\bullet} \quad (Equation\ 5)$$

$$Fe^{3+} + H_2O \overset{hv}{\rightarrow} Fe^{2+} + H^+ + OH^{\bullet} \quad (Equation\ 6)$$

Heterogenous photocatalysis includes using photocatalyst in different phase than reactants. Heterogenous reactions are realized on the basis of two different mechanisms: transport of electrons and generation of hydroxyl radicals. Electrons in metal catalyst are photoexcited and receive excess amount of energy, what causes transition from valance band (VB) to conduction band (CB). This phenomenon creates a positive hole in the valance band, which is the main driving force in this process, according to [12]:

$$TiO_2 + hv \rightarrow {e_{CB}}^- + {h_{VB}}^+ \quad (Equation\ 7)$$

$${h_{VB}}^+ + H_2O \rightarrow OH^{\bullet} + H^+ \quad (Equation\ 8)$$

$$h_{VB}{}^{+} + OH^{-} \rightarrow OH^{\bullet} \quad (Equation\ 9)$$

$$M^{n+} + e_{CB}{}^{-} \rightarrow M^{(n-1)+} \quad (Equation\ 10)$$

$$M^{(n-1)+} + h_{VB}{}^{+} / OH^{\bullet} \rightarrow M^{n+} \quad (Equation\ 11)$$

It is possible to use static mixers in the process of photocatalysis. Catalyst might be applied in the variety of forms, from which the most popular are catalyst in suspension and catalyst supported by static mixer. On the one hand the catalyst in suspension is more efficient due to much larger active surface area. But on the other hand, one has to deal with problematic separation of catalyst from treated water and the occurrence of particle aggregation and formation of slurries. Catalyst supported by static mixer may be created in the process of spraying or dipping of mixer elements [13]. Reaction rate is usually limited by the mass transport. Application of static mixers allows one to achieve high turbulency for low flow rates which improves the mixing process. As a result the generation of hydroxyl radicals is enhanced, as well as contact between suspended catalyst and contaminants is boosted. Concluding, it becomes a cost-effective process [14]. Laminar flow reduces the consumption of the catalyst which has a large influence on the operating costs. Low flow rates extends residence time, thus higher conversion is achieved [15]. Due to these reasons, application of static mixers is very attractive. Another important issue is the choice of a proper catalyst. The most popular catalysts are iron oxide, titanium oxide and composite of both. Advantages of titanium oxide over other catalysts are high photo-reactivity, good stability, inexpensiveness and non-toxicity, but it requires UV lamps. Iron oxide can be activated with UV from sunlight, however its disadvantage is the recombination of electrons in the valence band [16]. Below we collected some examples of application of static mixers as photoreactors in wastewater treatment.

Mineralization of ibuprofen is an alternative method of its degradation. The by-products of ibuprofen mineralization are formic acid and acetic acid. This led to research for new methods of treatment. Photocatalysis with catalyst in suspension was used to degrade ibuprofen in water [15]. Catalyst used for this process was TiO_2. Static mixer was made of glass with nine semi-elliptic glass fins, placed on the rod. Lamps were the sources of UV irradiation. Main parameters that were taken into consideration during optimization of the photocatalysis were: hydrodynamic conditions and mass transport. In the experiments the laminar flow was found to be the most efficient. Static mixers help to achieve the desired intensity of turbulence what was the key parameter for tubular photoreactors. As a result of static mixer application, full degradation of ibuprofen was achieved [15]. In [14], the photocatalysis process intensification by application of static mixer was researched. Three model compounds were chosen: phenol, Cr (VI) and acid orange 7 (AO7). As in previous example, a static mixer was placed in a glass tube. There were five static mixers used in this process. Five glass tubes were mounted between two walls and connected by silicone pipes. The catalyst was $TiO_2 - P25$. In the experiments the degradation rate of phenol increased up to 150%. The decomposition rate of Cr (VI) and AO7 was boosted only after the addition of formic acid and sodium fluoride. The results show that proper method of process intensification improves reaction rates [14]. Another organic compound which may be found in wastewaters due to its poor efficiency of removal method is oxytetracycline (OTC)[13]. OTC is one of the most popular antibiotics. The usage of Kenics static mixer as a support for catalyst was proposed for removal process. The catalyst used in this method was titanium oxide and iron oxide. The static mixer was placed in a borosilicate tube connected to compound parabolic collector (CPC). Various parameters influencing the effectiveness of photocatalysis were analyzed, such as: method of coating, catalyst dosage, hydrogen peroxide concentration and number of mixing elements. It has been proven that high turbulency increased the efficiency of photocatalysis. Iron oxide turned out to be more efficient in degradation of OTC than titanium oxide, however titanium oxide was better attached to mixing elements surface. In this case, spraying was a better method of coating. The number of mixing elements did not affect the rate of degradation [13]. Alternative for CPC design is an innovative static mixer called NETmix (Fig. 2.), which can be used to treat water with organic substances, such as: ciprofloxacin, sulfamethoxazole, and trimethoprim. NETmix has a flat surface, what increases the amount of light accessible in photoreaction. Additionally, an innovative composite catalyst was applied. Titanium oxide, iron oxide and the composite of both were compared. It was proven that the application of composite catalyst resulted in joined benefits of both oxides. Also, NETmix is characterized by

high mixing and luminescence availability. Due to that fact, a higher degradation of ciprofloxacin, sulfamethoxazole and trimethoprim was achieved [11,16].

2.2. **Ozonation process**

Nowadays, ozone has become way more popular in wastewater treatment because of its high disinfection capabilities and oxidation properties. Another benefit of using ozone is that it does not produce harmful by-products (like e.g. chlorine). The ozonation process takes place in apparatuses contacting gas (ozone) with liquid (treated wastewater). The examples of these apparatuses are bubble columns, diffusers, injectors. Static mixers are great tools for ozone/water mass transfer because they can achieve efficiency up to 100% [17].

Using Back Flow Cell Model, the impact of flow rate of wastewater and ozone on efficiency of mass transfer and maximum values of concentrations in Kenics static mixers was simulated. Tests showed that the high efficiency of ozone transport was achieved for low gas to liquid flowrate ratios and high flow rates of liquid. The maximum concentration was achieved for high ratio of gas to liquid flow rates and high flow velocity of liquid [17]. Ozonation process is used for inactivation of microorganisms, for example Cryptosporidium Parvum [18] or Bacillus Subtilis [19]. Ozone is contacted with treated wastewater in static mixer, where gas is dissolved rapidly. Then gas-liquid mixture is transported into the bubble column, where undissolved gas is separated from liquid. After the bubble column liquid phase enters the system of four contact reactors to provide possibly the longest reaction time. The desired mass transport efficiency was higher than 90%, while still achieving the pressure drop as low as possible [19]. For lab – scale ozonation process was conducted in static mixer and long, narrow, empty pipe as reactor [18].

2.3. **Coagulation and flocculation enhancement reactors**

Coagulation and flocculation are the processes in which contaminants are being aggregated into bigger particles, due to the action of destabilization agents (coagulants, flocculants). In the case of coagulation solid particles are binded by the van der Waals forces forming bigger structures. The particles within the aggregates are separated with a thin film of liquid. There are many ways to achieve coagulation, e.g.: addition of colloid with opposite surface charge to primary slurry particles, addition of electrolyte, β and γ radiation, dehydration, ultra-sonification, shaking, heating, and freezing. The examples of coagulants are: $Al_2(SO_4)_3 \cdot 18H_2O$, $FeSO_4 \cdot 7H_2O$, $Fe_2(SO_4)_3 \cdot 9H_2O$, $FeCl_3 \cdot 6H_2O$. Conditions affecting coagulation are for example coagulant dosage, pH, temperature or mixing. Flocculation is a process in which the addition of flocculant destabilizes the particles leading to formation of bigger entities. Flocculant is a macromolecular polymer which aggregate particles via charge neutralization, charge patching and bridging mechanisms. The flocculation mechanism is affected among the others by molecular weight and charge density[20,21]. Static mixers in these processes are used to mix coagulant/flocculant with treated wastewater to enhance the transport of destabilization agents to the surfaces of solid particles and achieving their uniform distribution [21]. In coagulation and flocculation, the velocity of liquid cannot be too high, because shear forces may destroy created flocs. Static mixers provide high turbulence with low flow rates [22]. The choice of mixing elements depends on the desired parameters. Some elements might have good mixing efficiency, but tremendous pressure drops. For this reason there are many geometries available, such as helices, blades, plates etc.[8].

The treatment processes are interdependent, just like chain reactions. The improvement of one factor affects the rest, for example sludge recycling boost flocculation process, because it narrows particle size distribution, as well as decrease the dosage of required flocculants [23]. Static mixers improve the flocculation which influences the subsequent processing. This approach was used in processing of oil sand mature fine tailings (MTF). Previously mature fine tailings were stocked in ponds, which was a huge environmental, economic, and engineering challenge. Employment of flocculation process in dealing with this issue was proposed. Three commercial static mixers were selected: Kenics-KMS, Koflo, Komax. It is important to choose static mixer used for flocculation wisely, because this process is associated with flocs formation and small static mixers might become clogged. The MTF was mixed with flocculant in static mixer, what increased the turbulence while still preserving already created flocs due to low flow

velocity. After completed flocculation process three different methods of dehydration were considered: thin lift drying, centrifugation and rim ditch dewatering. The efficiency of these methods highly depends on the effectiveness of flocculation process. The research was realized using pilot plant [24]. Another application of static mixer in flocculation considered the treatment of mineral-processing wastewater recycling process. The application of static mixers decreases the dosage of coagulant needed. This was shown in wastewater treatment using aluminium oxide. Pilot-plant scale experiment proved that with the increasing diameter of the static mixer, the amount of coagulant needed for process decreased, compared to the empty-pipe mixer [25].

Nowadays, many countries have scarce access to fresh, clean water. It is caused by cost-prohibitive drinking water treatment. One of the possibilities is to treat using coagulation. In package surface water treatment in Iraq the static mixers with helical-shaped elements were used [26]. Alum was applied as a coagulant. Moreover, Moring oleifer was added, which reduced the amount of needed alum. In this case, water was sufficiently cleaned and the cost of process was reduced due to the smaller dosage of coagulant. Another interesting type of static mixer is a flash mixer, which may be applied in coagulation process. In this kind of mixer, a coagulant is supplied via nozzle. Such mixer was applied in full-scale and proved high efficiency in removal contaminants and dissolved organic carbon. Also, the flash mixer reduced required amount of catalyst and aluminum polychloride (PAC) [27]. To improve treatment efficiency and quality different processes may be combined. For example, coagulation process may be a pre-treatment for microfiltration. Application of coagulation may reduce fouling and improve water purification. This approach was used in treatment water from Toyohira river in Japan which is contaminated by microbes such as Cryptosporidium and Giardia. The standard pre-treatment process for filtration is an application of mechanical mixer but it involves large tanks and high energy consumption. The authors compared new method with the classic one. Coagulation process apparatus consisted of in-line static mixer and ceramic filter. PAC was used as a coagulant. Results show that efficiency of the coagulation-microfiltration process was comparable to the classic one. Dose of coagulation was lowered because of the application of in-line static mixer. This approach may be more economic water treatment technique [28].

2.4. **Membrane filtration process**

Membrane filtration is a process in which the physical phenomenon plays the key role. The most important parameters in membrane processes are pressure, osmosis, temperature, and electricity [29]. Structures that are bigger than pores of membrane are stopped at its surface and the other ones go through due to the applied pressure. This process is analogical to conventional method of filtration. The difference between these two methods is pore size of filter. In the case of membrane the pores are smaller. This process divides feed into permeate and retentate. The retentate stays at the surface of membrane and the permeate goes through. Membrane filtration might be distinguished by the pore size into several types [30]:

- microfiltration (MF), approximately pore sizes $0{,}2\ \mu m - 10\ \mu m$
- ultrafiltration (UF), approximately pore sizes $0{,}05\ \mu m - 2\ nm$
- nanofiltration (NF), approximately pore sizes $0{,}5\ nm - 2\ nm$
- reverse osmosis (RO), approximately pore sizes $0{,}2\ nm - 1\ nm$.

One of the main issues in membrane filtration is fouling. It is a phenomenon of clogging the membrane pores. It causes the decrease of filtration surface. Fouling is a complex process. It can appear due to the mechanisms like chemical reaction fouling, precipitation fouling, or solidification [31]. Membrane process might be used in wastewater treatment, due to its high contaminants' removal efficiency. Pre-treating of water is very desired in membrane process because it improves its efficiency. Moreover, in some cases it is more profitable to recover substances from wastewater and reuse them, than to remove them [32]. Static mixers may help to prevent fouling. Their application increase turbulence, what causes increase in reverse particle transport and shear tension at the membrane surface [33]. Proper choices of mixing element's shape and type of flow has a big impact on fouling effect [31].

Due to static mixer and cross flow, the reduction of fouling effect may be achieved in treating wastewater after steeping corn starch. In the process the ceramic membrane was used. Ceramic membranes have resistance for aggressive substances, good thermal and chemical stability, and long exploitation time [34]. Just as in previous examples combining different methods creates solutions which are characterized by better features – coagulation was a pre – treatment method for microfiltration and composite material as catalyst in photocatalysis process was used. In the next case, aeration and static mixer were combined. Aeration creates bubbles, which creates local vorticities. Static mixer prevents fouling. Regular Kenics static mixer and Kenics with aerating system were compared. Kenics with aerating system achieved better results. In both cases the fouling effect was decreased diametrically, and constant total resistance was achieved [35]. Static mixer may also help with formation of filtration cake. In some cases, the filtration cake may increase the filtration efficiency, by creating dynamic membrane (DM). The attractiveness of dynamic membranes lies in fact that in membrane filtration process bigger pores may be used, however the achieved purity of permeate is higher. Dynamic membrane is made of particles that did not go through the membrane. They create the resistance for other ones. Homogenous membrane formation depends on static mixer and cross flow rates. It is important to retain low flow rate, so the DM would not be destroyed. Static mixer contributed to reduce fouling, forming time, and the amount of energy required. Dynamic membrane reduces investment costs while maintaining efficiency [22].

3. Conclusion

This review paper shows benefits of application of static mixer in wastewater treatment. The great need for freshwater and lacking in resources of it, increases the attractiveness for searching new methods of treating water and sourcing it. The division into four groups of fast-growing area of static mixers in wastewater treatment was proved by multiple examples. Usually application of static mixer in already known process may increase the efficiency, lower investment costs, and overall improve process. Huge variety of possibilities in construction of static mixers makes this branch of chemical and environmental engineering attractive for new research and improvements.

Acknowledgment

This research was supported by the Polish National Science Centre (NCN) under Grant No. 2016/21/D/ST8/01714.

References

[1] Water Use and Stress, (n.d.). https://ourworldindata.org/water-use-stress#citation (accessed November 18, 2020).

[2] T.J. Gierczycki A., Kurkowski Ł., Gas cleaning and wastewater treatment for industrial and engineering chemistry students., 1st ed., Politechnika Śląska, 2011.

[3] K.A. Alekseev, A.G. Mukhametzyanova, Classification, Function, and Construction of Modern Static Mixers, Chem. Pet. Eng. 55 (2020) 934–942. https://doi.org/10.1007/s10556-020-00716-9.

[4] J.H. Kwon, J.H. Jung, H.D. Lee, Y.S. Park, D.W. Kim, Development of a hydrodynamic static mixer for mixing chemicals in ballast water treatment systems, J. Water Process Eng. 8 (2015) 209–220. https://doi.org/10.1016/j.jwpe.2015.10.006.

[5] R.K. Thakur, C. Vial, K.D.P. Nigam, E.B. Nauman, G. Djelveh, Static Mixers in the Process Industries—A Review, Chem. Eng. Res. Des. 81 (2003) 787–826. https://doi.org/https://doi.org/10.1205/026387603322302968.

[6] N. Kiss, G. Brenn, H. Pucher, J. Wieser, S. Scheler, H. Jennewein, D. Suzzi, J. Khinast, Formation of O/W emulsions by static mixers for pharmaceutical applications, Chem. Eng. Sci. 66 (2011) 5084–5094. https://doi.org/10.1016/j.ces.2011.06.065.

[7] A. Ghanem, T. Lemenand, D. Della Valle, H. Peerhossaini, Static mixers: Mechanisms, applications, and characterization methods - A review, Chem. Eng. Res. Des. 92 (2014) 205–228. https://doi.org/10.1016/j.cherd.2013.07.013.

[8] M. Ouda, O. Al-Ketan, N. Sreedhar, M.I. Hasan Ali, R.K. Abu Al-Rub, S. Hong, H.A. Arafat, Novel static mixers based on triply periodic minimal surface (TPMS) architectures, J. Environ. Chem. Eng. 8 (2020) 104289. https://doi.org/https://doi.org/10.1016/j.jece.2020.104289.

[9] S.S. Soman, C.M.R. Madhuranthakam, Effects of internal geometry modifications on the dispersive anddistributive mixing in static mixers, Chem. Eng. Process. Intensif. 122 (2017) 31–43. https://doi.org/10.1016/j.cep.2017.10.001.

[10] W. Hsin, C.-L. Chang, Decolorization of Reactive Red 2 by advanced oxidation processes: Comparative studies of homogeneous and heterogeneous systems, J. Hazard. Mater. 128 (2006) 265–272. https://doi.org/10.1016/j.jhazmat.2005.08.013.

[11] M.J. Lima, A.M.T. Silva, C.G. Silva, J.L. Faria, J.C.B. Lopes, M.M. Dias, An innovative static mixer photoreactor: Proof of concept, Chem. Eng. J. 287 (2016) 419–424. https://doi.org/10.1016/j.cej.2015.09.092.

[12] D.F.S. Morais, R.A.R. Boaventura, F.C. Moreira, V.J.P. Vilar, Advances in bromate reduction by heterogeneous photocatalysis: The use of a static mixer as photocatalyst support, Appl. Catal. B Environ. 249 (2019) 322–332. https://doi.org/https://doi.org/10.1016/j.apcatb.2019.02.070.

[13] A.M. Díez, F.C. Moreira, B.A. Marinho, J.C.A. Espíndola, L.O. Paulista, M.A. Sanromán, M. Pazos, R.A.R. Boaventura, V.J.P. Vilar, A step forward in heterogeneous photocatalysis: Process intensification by using a static mixer as catalyst support, Chem. Eng. J. 343 (2018) 597–606. https://doi.org/10.1016/J.CEJ.2018.03.041.

[14] D. Li, K. Xiong, Z. Yang, C. Liu, X. Feng, X. Lu, Process intensification of heterogeneous photocatalysis with static mixer: Enhanced mass transfer of reactive species, Catal. Today. 175 (2011) 322–327. https://doi.org/10.1016/j.cattod.2011.04.007.

[15] A. Nunez-Flores, A. Sandoval, E. Mancilla, A. Hidalgo-Millan, G. Ascanio, Enhancement of photocatalytic degradation of ibuprofen contained in water using a static mixer, Chem. Eng. Res. Des. 156 (2020) 54–63. https://doi.org/10.1016/j.cherd.7070.01.018.

[16] M.J. Lima, C.G. Silva, A.M.T. Silva, J.C.B. Lopes, M.M. Dias, J.L. Faria, Homogeneous and heterogeneous photo-Fenton degradation of antibiotics using an innovative static mixer photoreactor, Chem. Eng. J. 310 (2017) 342–351. https://doi.org/10.1016/j.cej.2016.04.032.

[17] C. Tizaoui, Y. Zhang, The modelling of ozone mass transfer in static mixers using Back Flow Cell Model, Chem. Eng. J. 162 (2010) 557–564. https://doi.org/10.1016/j.cej.2010.05.061.

[18] S.A. Craik, D.W. Smith, M.S. Chandrakanth, M. Belosevic, Efficient Inactivation of Cryptosporidium Parvum in a Static Mixer Ozone Contactor, Ozone Sci. Eng. 25 (2003) 295–306. https://doi.org/10.1080/01919510390481612.

[19] C. Mysore, J. Leparc, R. Lake, P. Agutter, M. Prévost, Comparing Static Mixer Performances at Pilot and Full Scale for Ozonation,Inactivation of Bacillus subtilis , and Bromate Formation in Water Treatment, Ozone Sci. Eng. 26 (2004) 207–215. https://doi.org/10.1080/01919510490439609.

[20] M. Lemanowicz, Sonication of flocculants and application of stimuli-responsive polymers as advanced method of dispersion systems stability influence, 1st ed., Politechnika Śląska, 2018.

[21] J.K. Edzwald, Coagulant mixing revisited: theory and practice, J. WATER SUPPLY Res. Technol. 62 (2013) 67–77. https://doi.org/10.2166/aqua.2013.142.

[22] M. Sabaghian, M.R. Mehrnia, M. Esmaieli, D. Nourmohammadi, Influence of static mixer on the formation and performance of dynamic membrane in a dynamic membrane bioreactor, Sep. Purif. Technol. 206 (2018) 324–334. https://doi.org/10.1016/J.SEPPUR.2018.06.026.

[23] J. Park, Y.-S. Han, S.-W. Ji, Investigation of Mineral-Processing Wastewater Recycling Processes: A Pilot Study, Sustainability. 10 (2018) 3069. https://doi.org/10.3390/su10093069.

[24] A. Demoz, Scaling inline static mixers for flocculation of oil sand mature fine tailings, Aiche J. 61 (2015) 4402–4411. https://doi.org/10.1002/aic.14958.

[25] S.C. Jones, A. Amirtharajah, F. Sotiropoulos, B.M. Skeens, Using static mixers to mix coagulants: CFD modeling and pilot-plant experiments, in: H. Hahn, HH and Hoffmann, E and Odegaard (Ed.), Chem. WATER WASTEWATER Treat. VI, SPRINGER-VERLAG BERLIN, HEIDELBERGER PLATZ 3, D-14197 BERLIN, GERMANY, 2000: pp. 79–88.

[26] H.J.M. Tisti, A.H. Ghawi, Performance improvement of package water treatment plant by using static mixer and natural coagulant, J. Green Eng. 10 (2020) 3717–3744.

[27] S. Byun, J. Oh, B.-Y. Lee, S. Lee, Improvement of coagulation efficiency using instantaneous flash mixer (IFM) for water treatment, Colloids Surfaces A Physicochem. Eng. Asp. 268 (2005) 104–110. https://doi.org/https://doi.org/10.1016/j.colsurfa.2005.06.027.

[28] N. Shirasaki, T. Matsushita, Y. Matsui, M. Kobuke, K. Ohno, Feasibility of in-line coagulation as a pretreatment for ceramic microfiltration to remove viruses, J. WATER SUPPLY Res. Technol. 59 (2010) 501–511. https://doi.org/10.2166/aqua.2010.102.

[29] S. Hube, M. Eskafi, K.F. Hrafnkelsdóttir, B. Bjarnadóttir, M.Á. Bjarnadóttir, S. Axelsdóttir, B. Wu, Direct membrane filtration for wastewater treatment and resource recovery: A review, Sci. Total Environ. 710 (2020) 136375. https://doi.org/https://doi.org/10.1016/j.scitotenv.2019.136375.

[30] D. Dolar, K. Košutić, Chapter 10 - Removal of Pharmaceuticals by Ultrafiltration (UF), Nanofiltration (NF), and Reverse Osmosis (RO), in: M. Petrovic, D. Barcelo, S. Pérez (Eds.), Anal. Removal, Eff. Risk Pharm. Water Cycle, Elsevier, 2013: pp. 319–344. https://doi.org/https://doi.org/10.1016/B978-0-444-62657-8.00010-0.

[31] M. Kreimer, M. Zettl, I. Aigner, T. Mannschott, P. van der Wel, J.G. Khinast, M. Krumme, Performance Characterization of Static Mixers in PrecipitatingEnvironments, Org. Process Res. Dev. 23 (2019) 1308–1320. https://doi.org/10.1021/acs.oprd.8b00267.

[32] S. Hube, M. Eskafi, K.F. Hrafnkelsdóttir, B. Bjarnadóttir, M.Á. Bjarnadóttir, S. Axelsdóttir, B. Wu, Direct membrane filtration for wastewater treatment and resource recovery: A review, Sci. Total Environ. 710 (2020) 136375. https://doi.org/https://doi.org/10.1016/j.scitotenv.2019.136375.

[33] S. Armbruster, A. Brochard, J. Lölsberg, S. Yüce, M. Wessling, Aerating static mixers prevent fouling, J. Memb. Sci. 570–571 (2019) 537–546. https://doi.org/10.1016/j.memsci.2018.10.039.

[34] L. Seres, L. Dokic, B. Ikonic, D. Soronja-Simovic, M. Djordjevic, Z. Saranovic, N. Maravic, Data-driven Modelling of Microfiltration Process with Embedded Static Mixer for Steepwater from Corn Starch Industry, Period. Polytech. Eng. 62 (2018) 114–122. https://doi.org/10.3311/PPch.10400.

[35] S. Armbruster, A. Brochard, J. Loelsberg, S. Yuece, M. Wessling, Aerating static mixers prevent fouling, J. Memb. Sci. 570 (2019) 537–546. https://doi.org/10.1016/j.memsci.2018.10.039.

Simulation analysis of a solar assisted heat pump drying system

Naeem Khalid [1], Ayaz Ahmed [2], Talal Bin Irshad [3], Rui Costa Neto[4]

[1]University of Engineering & Technology, e-mail: naeemkhalid033@gmail.com
[2]School of Energy and Environment, Southeast University, e-mail: ayaz.ahmed@sec.edu.cn
[3]University of Engineering & Technology, e-mail:talalbinirshad@gmail.com
[4]Technical University of Lisbon, e-mail: costaneto@tecnico.ulisboa.pt

Abstract

Solar assisted heat pump drying system has been proposed to improve the efficiency of energy using for drying process due to drying is an energy intensive process and solar drying is deeply influenced by local weather compared to heat pump drying. In this study, a new solar assisted heat pump dryer has been designed and investigated. The drying system consists of a compressor, evaporator-collector, air condenser, air collector, dryer, blower and dampers. This system has three kinds of working modes, including solar drying, heat pump drying and solar assisted heat pump drying according to the path of drying medium. MATLAB program has been developed to evaluate the performance of the system and the influence of different variables. Results suggest that the entire drying time of the product decreases with the increase of drying air temperature, in addition, the air temperature of each outlet varies little with the ambient temperature and solar radiation when system working with mode of solar assisted heat pump. Coefficient of performance (COP) and the specific moisture extraction rate (SMER) are two main performance indices. With the increase of ambient temperature or solar radiation, the COP slightly decreased, but the SMER increased significantly.

Keywords: Solar assisted heat pump dryer, heat pump, evaporator-collector, Coefficient of performance

1. Introduction

Drying is an energy intensive operation that easily accounts for up to 15% of all industrial energy usage, often with relatively low thermal efficiency in the range of 25–50% (Chua et al., 2001). Therefore, under the circumstances of global energy shortage and environmental pollution, it is necessary to reduce the energy consumption for drying process by using present technologies.

In the world, 97–98% of dried vegetables that traded dry with hot air under controlled conditions (Şevik et al., 2013). At present, solar drying and heat pump drying as typical hot air drying methods are widely used in the drying process. The most prominent feature of solar drying is the use of solar energy that is renewable energy, and its device construction is simple. However, its application is limited by the discontinuity and instability of solar energy. Heat pump dryers possess high coefficient of performance and potential improvements in the quality of dried products due to the ability of heat pump to operate at lower temperature (Daghigh et al., 2010).The principal advantages of heat pump dryers emerge from the ability of heat pumps to recover energy from the exhaust as well as their ability to control independently the drying gas temperature and humidity (K. J. Chua, 2002). Although heat pump drying has so many advantages, its energy consumption for same drying is higher than solar drying. Combined solar dryer and heat pump can overcome these difficulties of using solar dryer systems or solely using heat pump drying separately and satisfy important demands in industrial drying with respect to product quality control, reduced energy consumption and reduced environmental impact. Solar assisted heat pump drying systems have been studied and applied since the last decades in order to increase the quality of products where low temperature and well-controlled drying conditions are needed (Daghigh et al., 2010).

Solar assisted heat pump drying systems can be divided into several categories according to the medium flowed through solar collectors. One is based on air and water as the medium, and the other is based on refrigerant as the medium.

There is also a combination of both. Şevik S et al. (Şevik et al., 2013) proposed a solar assisted heat pump drying system with a plate collector and a water source heat pump. The hot water heated by the plate collector is used as the heat source of the evaporator to increase the energy efficiency of the system. Qiu Y et al. (Qiu et al., 2016) studied a solar assisted heat pump drying system with a heat exchanger coil. The hot water heated by the solar collector flows through the heat exchanger coil to further heat the drying medium already heated by the condenser. Li Y et al. (Li et al., 2011) studied a solar assisted heat pump in-store drying system. After the air heated by the solar collector was mixed with the air heated by the condenser, it was sent to the dryer. Yahya M et al. (Yahya et al., 2016) studied solar drying and solar assisted heat pump drying. Solar collectors assisted heat pump drying by further heating the air heated by the condenser. Mohanraj M (Mohanraj, 2014) proposed a solar-ambient hybrid source heat pump drying system, in which a solar collector was used as an evaporator. Hawlader et al (Hawlader and Jahangeer, 2006, Hawlader et al., 2003) proposed a solar-assisted heat pump system for drying and water heating. This system includes both an air collector and an evaporator-collector. The drying medium was heated by air collector after treated by the dehumidifier, so the system makes full use of solar and exhaust energy. Hawlader et al. (Rahman et al., 2013, Hawlader, 2008) also studied the performance of the air collector and evaporator-collector in this system, and the economic optimization of the two collector areas.

However, with respect to the solar assisted heat pump drying system, few people have studied the change of the drying mode by changing the air path to adapt to the change of meteorological conditions, and in the literature review, little works on the performance of the solar assisted heat pump drying system using numerical simulation. Therefore, in the study of this paper, a new solar assisted heat pump drying system was proposed. This system can not only achieve the three basic working modes, namely solar drying, heat pump drying and solar assisted heat pump drying, but also by changing the air duct to be further subdivided into open, semi-open, and closed working modes, which can greatly improve the ability of the system to adapt to environmental changes while ensuring high energy efficiency of the system; secondly, the performance of the system on working mode of solar assisted heat pump drying was studied through MATLAB programming.

2. Simulation

2.1. System design

In order to study a drying device that can change the working mode according to the external environment and operating conditions, a new solar assisted heat pump drying system was proposed, as shown in Figure 1. The system can be divided into two parts according to the flow paths of air and refrigerant. The air flowed path mainly composed of various components, including air collector, condenser, evaporator, dryer, blower, duct and valves. The refrigerant flowed path consists of a vapour compression heat pump unit and evaporator-collector. The two evaporators are connected to parallel with individual expansion valves and solenoid valves. The two flow paths are connected by evaporator and condenser.

When the solar radiation is strong, and the temperature of the air passing through the air collector is higher than the drying required temperature, the dampers 1, 3, 4 are opened, the dampers 2, 5 are closed, and the heat pump is turned off. At this moment, the energy required for drying was only provided by solar energy, which is a solar drying mode. When there is no solar radiation or at night, the heat pump is turned on, the dampers 3, 4 are closed, the dampers 2, 5 are opened, the solenoid valve 9 is closed, and the solenoid valve 8 is opened, which is a solar drying mode. In addition, the three working modes, including open, closed, semi-open, can be achieved by adjusting other dampers 1, 6, 7.

When the solar radiation is weak and the air temperature of the air collector is lower than the required temperature for drying, the heat pump is opened, the damper 3 is opened, the damper 2 is closed, and the solenoid valve 8 and 9 are opened at the same time. Similarly, according to the operating and environmental conditions, the damper can be adjusted to realize open, closed and semi-open working modes. In addition, in the middle and late stages of drying, dehumidification is mainly to remove the bound water in the dried material. Removing these waters requires a long

drying time and consumes more energy. Moreover, due to the small mass transfer coefficient between the air and the dry material, the air state at the inlet and outlet of the dryer changes little, which affects the dehumidification capacity of evaporator. In order to maintain the stability of the drying temperature, most of the energy input into the system was discharged out of the system in the form of heat energy, and the dehumidification efficiency of the system is low(Wang *et al.*, 2002). Therefore, the evaporator-collector can be used as the only evaporator in the middle and later stages of drying to improve the energy efficiency of the system.

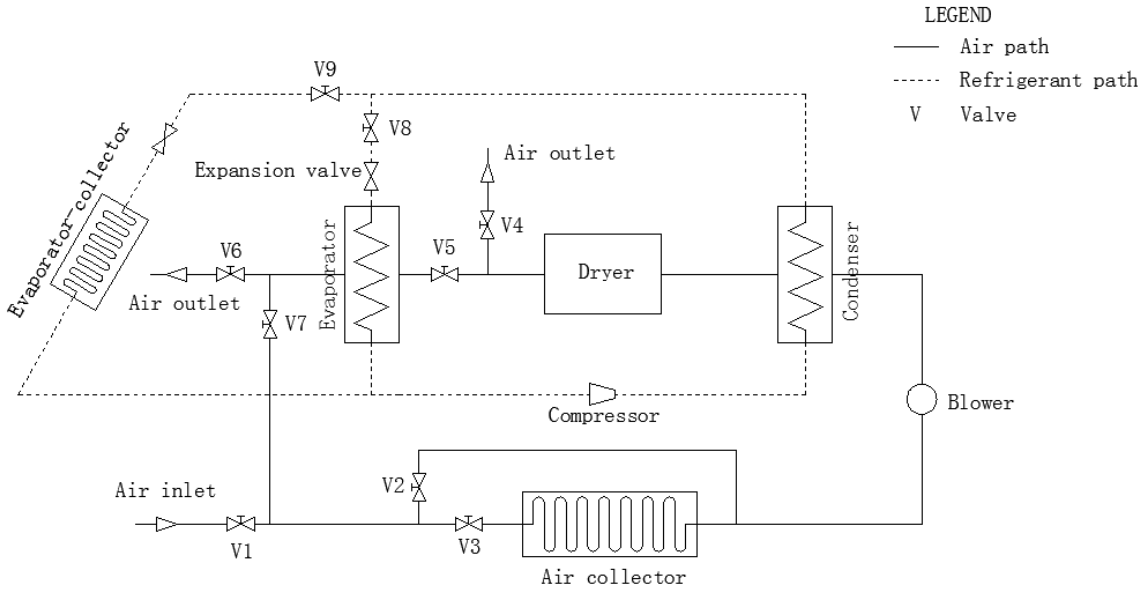

Fig. 2.1. Schematic diagram of the solar assisted heat pump drying system

2.2. **Mathematical model**

Plate collector was selected as air collector，The useful energy collected by the collector can be expressed using the following equation (Duffie *et al.*, 1980)：

$$Q_u = A_c F_R \left[I_T(\tau\alpha) - U_L \left(T_{ai} - T_a \right) \right]$$

Where:

- Q_u useful energy collected by the collector(W)
- A_c area of air collector(m^2)
- F_R collector heat removal factor (dimensionless)
- I_T Solar radiation on the collector surface (W/m^2)
- $(\tau\alpha)$ Transmittance absorptance effective product (dimensionless)
- U_L collector overall loss coefficient (W/m^2K)
- T_{ai} air temperature at inlet of collector(℃)
- T_s ambient temperature, air temperature (℃)

The collector of the evaporator-collector is in the form of a bare plate, and the useful energy collected by the evaporator-collector can be determined by the following equation(Timoumi *et al.*, 2004):

$$Q_u^{'} = A_c^{'} F^{'} \left[S^{'} - U_L^{'} \left(T_{evap} - T_a \right) \right]$$

Where:

- $Q_u^{'}$ useful energy collected by the evaporator-collector (W)
- $A_c^{'}$ area of evaporator-collector (m^2)
- $F^{'}$ collector efficiency factor (dimensionless)
- $S^{'}$ Solar radiation energy absorbed by an endothermic bare plate(W/m^2)
- $U_L^{'}$ evaporator-collector overall loss coefficient (W/m^2K)
- T_{evap} evaporating temperature(℃)
- T_a ambient temperature, air temperature (℃)

Rotary compressor was used in this study, and the refrigerant mass flow and input power can be expressed by the following equations (Zhang, 2013):

$$m_{com} = \frac{\eta_v V_{th}}{v_{suc}}$$

Where:

- m_{com} refrigerant mass flow rate of compressor (kg/s)
- η_v Volume coefficient (dimensionless)
- V_{th} theoretical Volume flow of compressor(m^3/stroke)
- v_{suc} specific volume of compressor suction(m^3/kg)

$$W = m_{com} \left(h_{dis} - h_{suc} \right) / \, f_Q$$

Where:

- W input power of the compressor(w)
- h_{dis} enthalpy of compressor discharge(J/kg)
- h_{suc} enthalpy of compressor suction (J/kg)
- f_Q heat loss coefficient(dimensionless)

The condenser model was based on the steady lumped parameter method according to different phase regions in the condenser, heat transfer equation (Zhang, 2013) is given as:

$$Q_r = UA_i \Delta T_m$$

Where:

- Q_r heat transfer rate of refrigerant side(W)
- U overall heat transfer coefficient of refrigerant side (W/m^2K)
- A_i area of refrigerant side(m^2)
- ΔT_m logarithmic mean temperature difference (℃)

With the same as condenser, the steady lumped parameter method was used in evaporator, and the heat transfer equation was also similar to condenser. However, unlike the condenser, the evaporator not only has heat transfer, but also has mass transfer. The equation for the moisture content of the humid air is given as follows(Zhang, 2013):

$$-m_a dW_a = h_d \left(W_a - W_w\right) dA_a$$

Where:

- W_a moisture content of humid air(kg/kg)
- W_w saturated moisture content of humid air at the temperature of outer tube wall(kg/kg)
- h_d mass transfer coefficient(kg/m^2)
- A_a area of air side(m^2)

In this simulation study, mushroom was selected as drying material, and its drying kinetic model was expressed by following equation (Krokida *et al.*, 2003):

$$X = X_e - (X_e - X_i)e^{-kt}$$

Where:

- X material moisture content in dry basis (kg water/kg dry solids)
- X_e equilibrium moisture content in dry basis (kg water/kg dry solids)
- X_i initial moisture content in dry basis (kg water/kg dry solids)
- K drying constant (1/min)
- T time(min)

R134a was selected as refrigerant in the system, and the calculation model of the refrigerant charge can be determined using the following equation(Zhang, 2013):

$$M = M_{TP,cond} + \int_0^{V_{SH,cond}} \rho dV + \int_0^{V_{SC,cond}} \rho dV + M_{TP,evap} + \int_0^{V_{SH,evap}} \rho dV + \rho_{com} V_{com} + M_{other}$$

Where:

- M refrigerant charge (kg)
- V volume(m^3)
- TP two phase; SH, superheat; SC, subcool; cond, condenser; evap, evaporator; com, compressor
- ρ density(kg/m^3)

In addition to the above models, the system also includes some other component models, such as the mathematical model of the expansion valve, the enthalpy of refrigerant is not changed before and after throttling. There are also some models in the system that connects the components, such as the continuity equation, mass conservation equation, energy conservation equation and momentum conservation equation. In addition, the simulation process also involves the calculation of the physical properties of refrigerant R134a, and the refrigerant properties are calculated by calling the loaded REFPROP function in MATLAB.

There are two important indices to evaluate the performance of entire system, coefficient of performance (COP) and specific moisture extraction rate (SMER). The coefficient of performance of the heat pump is defined by the following equation(Hawlader and Jahangeer, 2006):

$$COP = \frac{Thermal\ energy\ released\ by\ the\ condenser}{Electrical\ energy\ input\ to\ the\ compressor}$$

The specific moisture extraction rate can be defined as the ratio of the moisture removed in kg to the energy input in kWh(Hawlader and Jahangeer, 2006):

$$SMER = \frac{Moisture\ removed\ in\ kg}{Energy\ input\ in\ kWh}$$

2.3. **Simulation methodology**

The simulation of the system was carried out by MATLAB. The simulation algorithm mainly assumes that the evaporating temperature, condensing temperature, subcool, superheat and inlet enthalpy of compressor, and the mathematical model of each part of the system was called in turn. Adjust the hypothetical values in turn by determining the conditions until the conditions are met. After the calculation of the cycle was completed, the calculation parameters were outputted. The simulation flow chart of the system is given in Figure 2.

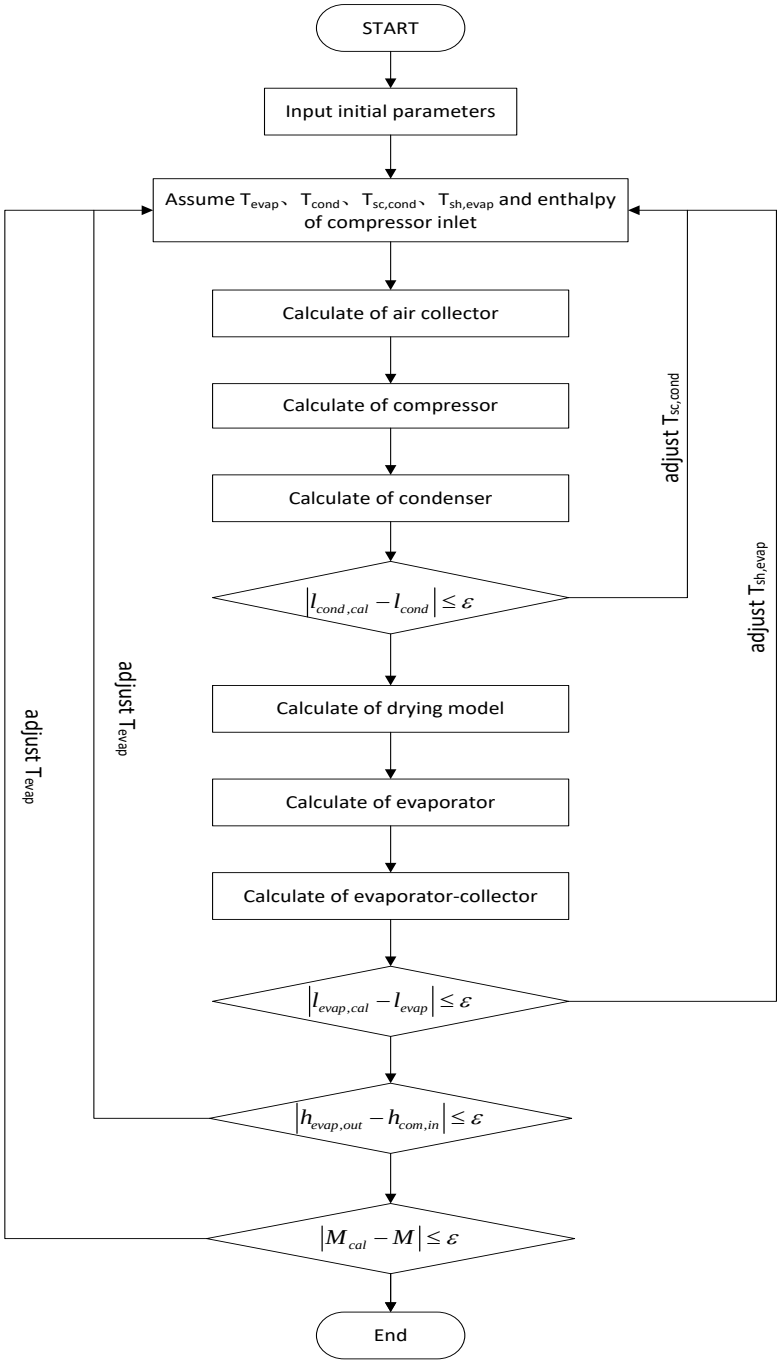

Fig. 2.2. Simulation Flow chart of the system

2.4 Simulation parameters

I Before the start of simulation, some relevant initial parameters need to be input, and in this study, solar assisted heat pump drying working modes was the primary research object. The value of each parameter is shown in Table 1 below.

According to the simulation calculation, when the solar radiation is greater than 500 W/m2, in order to achieve the solar drying mode, the area of the air collector is supposed to be about 1.5 m2. When the solar radiation is 200 W/m2,

to achieve drying requirements, and the evaporator-collector working as the only evaporator at the last drying stage, the area of the evaporator-collector should be about 1.0 m2.

As can be seen from Table 1, the refrigerant charge is small due to the small design capacity of the overall system, where the input power of the compressor is about 230 W. In addition, the heat absorbed by the refrigerant in the evaporator comes from the air with relatively high temperature and humidity discharged from the dryer, which leads to the total tube length of the evaporator small, and resulting in a lower refrigerant content in the evaporator.

Table. 2.1. Initial parameters of the system in simulation

content	symbol	unit	value
area of air collector	Ac	m2	1.5
area of evaporator-collector	Ac’	m2	1.0
solar radiation	IT	W/m2	200
ambient temperature	Ta	℃	25
refrigerant charge	M	g	143

3. Results and discussion

For mushroom drying, Figure 3 shows the variation of moisture content (dry mass) with time when the solar radiation was 200 W/m2. As can be seen from Figure 3, when the drying time is 120 minutes, the mushrooms reach safe water content (dry basis less than 0.13).

Since there is no air volume involved in the drying mathematical model, it is difficult to calculate the air state at the outlet of the dryer based on this model. In this study, a certain simplified treatment was performed to calculate the air state at the outlet of the dryer. The average value of the air state at the outlet of the dryer during the drying time was calculated at constant air volume, so the simulation of the entire system is steady state.

Figure 4 shows air temperature at different outlet under different solar radiation, as can be seen from Figure 4, with the solar radiation increases in the range shown in the figure, the air temperature of all different outlets was little change, which is due to the variation range of solar radiation was relatively small under the working mode of solar assisted heat pump drying.

Figure 5 shows the variation of SMER and COP with solar radiation. As seen from the figure, the COP decreases slightly despite an increase in solar radiation. This can be attributed to the air temperature difference between inlet and outlet of condenser decreases slightly with the increases of solar radiation, which can be seen from Figure 4, and input power of compress remains basically unchanged. It can also be seen that as the solar radiation increases, the temperature of the air at the inlet of the dryer rises, which leads to a decrease in the drying time required to reach a safe moisture content, and as a result, SMER increases.

Figure 6 shows air temperature at different outlet under different ambient temperature. With the same as solar radiation in Figure 4, ambient temperature has little influence on air temperature at different outlet.

Figure 7 shows the variation of SMER and COP with ambient temperature. From the figure, it can be seen that, with the increase of ambient temperature, the SMER increases and the COP decreases slightly. This phenomenon may be explained by the fact that, with the increase of ambient temperature, the air temperature difference between inlet and outlet of condenser decreases and the air temperature of dryer inlet increases slightly.

Figure 8 shows the variation of SMER and COP with refrigerant flow ratio of evaporator, when the ambient temperature was 27℃. As the ratio increases in the range shown in the figure, the SMER increases slightly then unchanged, and the COP remains basically unchanged.

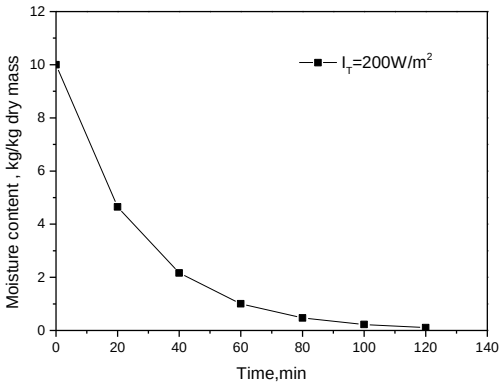

Fig.3. Variation of moisture content with time

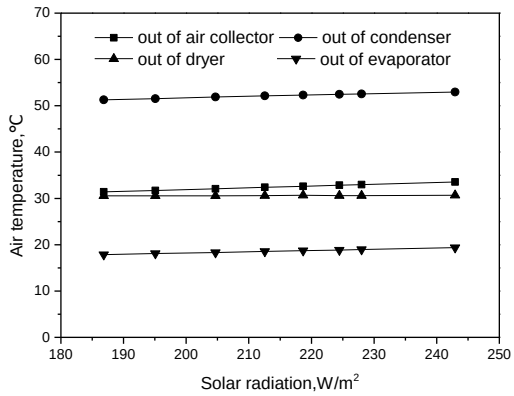

Fig.4. Air temperature at different outlet under different solar radiation

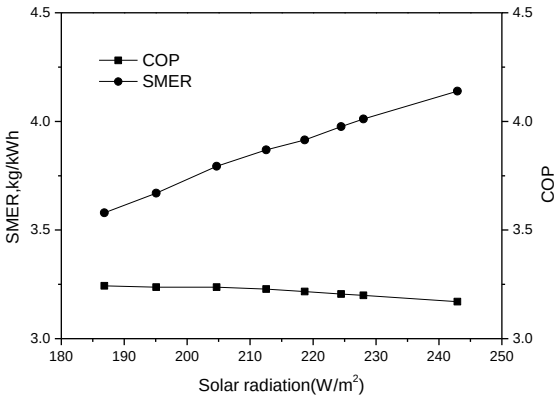

Fig.5.Variation of SMER and COP with solar radiation

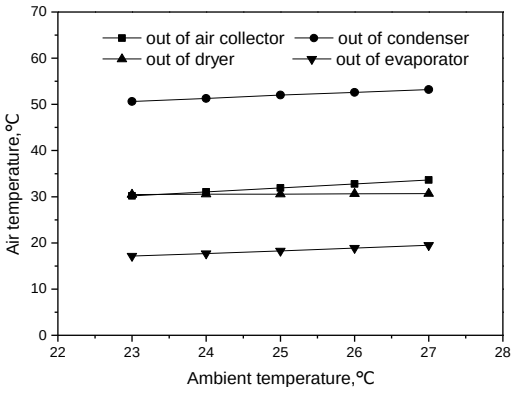

Fig.6. Air temperature at different outlet under different ambient temperature

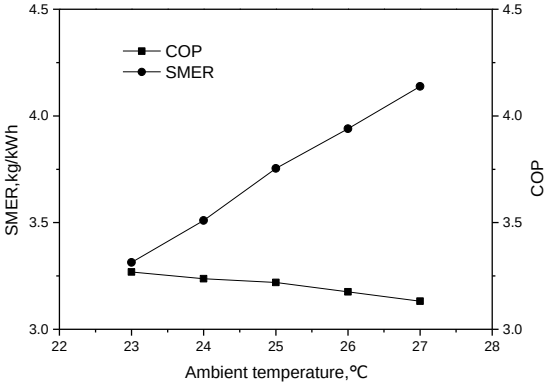

Fig.7. Variation of SMER and COP with ambient temperature

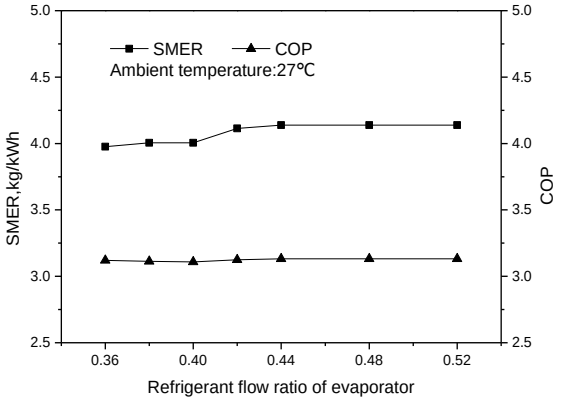

Fig.8. Variation of SMER and COP with refrigerant flow ratio of evaporator

4. Conclusion

A new designed of solar assisted heat pump drying system was proposed, and a simulation study was conducted on this system through MATLAB. In the solar assisted heat pump drying mode, the effects of solar radiation and ambient temperature on the air temperature at the outlet of each component in the system and the SMER and COP in the system were studied by simulation. According to the simulation results, the outlet air temperature of the condenser slightly increases with the increase of the solar radiation, and the value was about 52°C when the ambient temperature was 25°C and evaporator refrigerant flow ratio was 0.5. As the drying temperature increases, the drying time decreases, resulting in a significant increase in SMER with increase of solar radiation. However, the COP has slightly declined, and the value was about 3.2. Under the condition that the solar radiation was 200W/m2 and the evaporator refrigerant flow ratio was 0.5, with the increase of the ambient temperature, the variation trend of each variable similar to the variation trend that they were influenced by solar radiation. According to the simulation study of the evaporator refrigerant flow ratio, it is found that under certain environmental conditions, the SMER of the system can be improved by adjusting the evaporator refrigerant flow ratio.

References

[1] CHUA, K. J., MUJUMDAR, A. S., HAWLADER, M. N. A., CHOU, S. K. & HO, J. C. (2001), "Batch drying of banana pieces - Effect of stepwise change in drying air temperature on drying kinetics and product colour", Food Research International, Vol. 34 No. 8, pp. 721-731.

[2] DAGHIGH, R., RUSLAN, M. H., SULAIMAN, M. Y. & SOPIAN, K. (2010), "Review of solar assisted heat pump drying systems for agricultural and marine products", Renewable & Sustainable Energy Reviews, Vol. 14 No. 9, pp. 2564-2579.

[3] DUFFIE, J. A., BECKMAN, W. A. & WOREK, W. M. (1980), Solar Engineering of Thermal Processes, 2nd ed., Wiley.

[4] HAWLADER, M. N. A. & JAHANGEER, K. A. (2006), "Solar heat pump drying and water heating in the tropics", Solar Energy, Vol. 80 No. 5, pp. 492-499.

[5] HAWLADER, M. N. A., CHOU, S. K., JAHANGEER, K. A., RAHMAN, S. M. A. & EUGENE, L. K. W. (2003), "Solar-assisted heat-pump dryer and water heater", Applied Energy, Vol. 74 No. 1–2, pp. 185-193.

[6] HAWLADER, M. (2008), "Performance of evaporator-collector and air collector in solar assisted heat pump dryer", Energy Conversion & Management, Vol. 49 No. 6, pp. 1612-1619.

[7] K. J. CHUA, S. K. C. J. (2002), "HEAT PUMP DRYING: RECENT DEVELOPMENTS AND FUTURE TRENDS", Drying Technology, Vol. 20 No. 8, pp. 1579-1610.

[8] KROKIDA, M. K., KARATHANOS, V. T., MAROULIS, Z. B. & MARINOS-KOURIS, D. (2003), "Drying kinetics of some vegetables", Journal of Food Engineering, Vol. 59 No. 4, pp. 391-403.

[9] LI, Y., LI, H. F., DAI, Y. J., GAO, S. F., WEI, L., LI, Z. L., ODINEZ, I. G. & WANG, R. Z. (2011), "Experimental investigation on a solar assisted heat pump in-store drying system", Applied Thermal Engineering, Vol. 31 No. 10, pp. 1718-1724.

[10] MOHANRAJ, M. (2014), "Performance of a solar-ambient hybrid source heat pump drier for copra drying under hot-humid weather conditions", Energy for Sustainable Development, Vol. 23165-169.

[11] QIU, Y., LI, M., HASSANIEN, R. H. E., WANG, Y., LUO, X. & YU, Q. (2016), "Performance and operation mode analysis of a heat recovery and thermal storage solar-assisted heat pump drying system", Solar Energy, Vol. 137225-235.

[12] RAHMAN, S. M. A., SAIDUR, R. & HAWLADER, M. N. A. (2013), "An economic optimization of evaporator and air collector area in a solar assisted heat pump drying system", Energy Conversion & Management, Vol. 76 No. 1, pp. 377-384.

[13] ŞEVIK, S., AKTAŞ, M., DOĞAN, H. & KOÇAK, S. (2013), "Mushroom drying with solar assisted heat pump system", Energy Conversion & Management, Vol. 72 No. 72, pp. 171-178.

[14] TIMOUMI, S., MIHOUBI, D. & ZAGROUBA, F. (2004), "Simulation model for a solar drying process", Desalination, Vol. 168 No. 1, pp. 111-115.

[15] WANG, J., OUYANG, Y., ZHU, Y. & LIU, J. (2002), "Experimental study on heat pump drying system with phase change material", Acta Energiae Solaris Sinica, Vol. 78 No. 1, pp. 60-67.

[16] YAHYA, M., FUDHOLI, A., HAFIZH, H. & SOPIAN, K. (2016), "Comparison of solar dryer and solar-assisted heat pump dryer for cassava", Solar Energy, Vol. 136606-613.

[17] ZHANG, C. (2013), Fundamentals of Vapor-Compression Refrigeration and Air-Conditioning System Modeling, Chemical Industry Press.

Modelling of ammonia combustion in air using equilibrium and freely propagating flame models

Patryk Nowrot[1], Adam Klimanek[1]

[1]Silesian University of Technology, e-mail: patryk.nowrot@gmail.com; adam.klimanek@polsl.pl

Abstract

In recent years an increased interest in the use of hydrogen in transportation and power engineering is observed. Due to problems associated with hydrogen storage, mostly due to low density, its conversion to ammonia is frequently considered, whose storage and transportation is much easier and cheaper than hydrogen. Although it is possible to convert ammonia back to hydrogen gas, ammonia can be treated as the final energy carrier and fuel. Its properties are however different than typically applied today hydrocarbon fuels, therefore they have to be identified and determined for proper design of combustion systems. Furthermore reliable modelling tools should be developed. In this study an equilibrium solver was used to determine the adiabatic flame temperatures and composition of ammonia combustion products in air. Then a freely propagating flat flame model was applied to predict the flame structure and laminar flame speed. In both cases results were obtained for various excess air ratiosλ. It was shown that the maximum adiabatic flame temperature is around 2100 K andis lower than that of hydrogen and other hydrocarbon fuels due to the low lower heating value of ammonia. It was also shown that the adiabatic flame temperature is virtually independent of pressure, besides the regions of substoichiometric conditions ($\lambda < 0.4$), where it increases with pressure. The laminar flame speed at $\lambda = 1$ and $p = 1$atm was predicted to be $S_L = 0.07$ m/s, however its maximum occurs at slightly rich region ($\lambda \approx 0.9$). It was also found that considerable differences in predicted flame speed are observed for different chemical mechanisms. The laminar flame speed of ammonia is much smaller than of other fuels (~6 times for CH4 and ~36 times for H2), therefore it will have a strong influence on the application of ammonia in existing combustion systems and on design of new ones.

Keywords: ammonia, ammonia combustion, ammonia for power

1. Introduction

Development of our civilization contributes to increase of energy consumption. Most of the energy still comes from combustion of fossil fuels. Combustion of those fuels produces different types of pollution and greenhouse gases which has a great impact on climate changes. That is why renewable energy sources are becoming more popular. Each year more and more energy is obtained from renewable sources, which causes reduction of fossil fuels usage and lowering production of emissions. One of the main problems connected with some of the renewable energy sources is their intermittency and the need of energy storage. Many researchers and engineers try to develop the best storage systems for renewable energy. There are already different methods of energy storage considered and available such as: pumped-storage power plants, thermal energy storage and chemical storage. One of the best is chemical storage, where the electricity is converted to chemical energy of carriers. Electrical energy can also be stored in different types of batteries, but this method will likely not be able to satisfy large scale requirements. Therefore there is a large interest in chemical storage via hydrogen or other carbon-neutral energy carriers. Hydrogen can be obtained from electrolysis in which electricity is obtained from renewable sources, which makes its production totally carbon free. Furthermore, combustion of hydrogen is also carbon free since the only product of hydrogen oxidation is water ($2H_2 + O_2 \rightarrow 2\,H_2O$).What is more, if the oxygen produced during pyrolysis is utilized as an oxidizer instead of air, the combustion products will not generate any NOx. Hydrogen has a very high higher heating value of around 142 MJ/kg when compared to other fuels. For example HHV of natural gas is 55 MJ/kg and of propane is 50 MJ/kg. However, due to low density of H2, the heating value per unit volume or per mole is much smaller 12,7 MJ/m^3 and 244 MJ/kmol, while

for natural gas it is 39 MJ/m^3 and 802 MJ/kmol. Due to low density, hydrogen requires high pressure storage, which should be well-designed because of its ease of leaking. Thus its storage is expensive and costs around 15 $/kg of hydrogen [2]. Due to the leakage problems, as well as cost of compression, handling and transportation, other chemicals are frequently being considered as carbon free hydrogen carriers. One of the candidates is ammonia, whose storage is less complex because it is easily compressed to the liquid state at 0.8 MPa and room temperature, which makes storage cost to be around 0.54 $/kg. Ammonia can be used in combustion systems or can be treated as a hydrogen carrier. The major problems associated with ammonia is its toxicity, corrosive properties to some materials and high NO_x generation during combustion.

2. General information about ammonia

Ammonia is a colourless gas with a pungent odor. It consists of nitrogen and hydrogen and its formula is NH_3. It has no direct impact on greenhouse effect, however it plays a role in formation of atmospheric particulate matter, visibility impairment and deposition of nitrogen to ecosystems[3].Hydrogen content inside ammonia is around 17.8% of ammonia total mass, which makes ammonia one of the best possible hydrogen carriers. Its density is smaller than that of air and the value is around 0.73 kg/m^3 at 1 bar and temperature of 15°C. Boiling temperature is 239.81 K and the autoignition temperature in air is around 924K. It has a higher heating value to 22.5 MJ/kg [2].Ammonia is a toxic substance for people. Although it is produced in human body as a by-product it can become harmful. Ammonia toxicity takes place when the level of ammonia in blood will increase to the point where liver can no longer eliminate it. Ammonia process of production was invented in the early nineties thanks to Fritz Haber and Carl Bosch. This process is known as Haber-Bosch and it is used to produce most of ammonia in the world [2].The most important use of ammonia is for fertilizers. Fertilizers are used for production of food in agricultural sector. Thus this process is said to be a cause of population explosion and it has rapidly increased the grow of global population over last decades. Such a long time has contributed to the development of storage and transportation technologies of ammonia. Its transportation is distributed around the world and it is achieved by various methods such as ships, railroads and pipelines. Thus this makes ammonia a suitable replacement to fossil fuels. Combustion of ammonia is totally carbon free but it produces nitrogen oxides. The global reaction of ammonia combustion can be written as:

$$4NH_3 + 3O_2 \rightarrow 2N_2 + 6H_2O$$

Combustion of ammonia is a still developing field of research. There are several problems which needs to be solved. Those problems are associated with small value of laminar flame speed, low reactivity, high autoignition temperature, emissions of NO_x and the corrosive nature of ammonia. Values of laminar flame speed and autoignition temperature of ammonia together with other fuels is listed in Table 1.

Table 1 Laminar flame speed comparison of different fuels at 300K and 100 kPa [1], [2]

	Ammonia	Methane	Hydrogen	Methanol
Laminar flame speed (m/s)	0.07	0.38	2.50	0.36
Auto ignitron temperature (K)	930	859	773-850	712

Since its laminar flame speed is so low it still requires additional effort in development of combustion chambers in order to achieve the highest output energy and the lowest nitrogen oxides emissions. In general much higher NOx emissions can be expected and are observed due to fuel and thermal NOx mechanisms during ammonia combustion. Research is going on aiming at overcoming the NOx emission problems, however in most instances the selective catalytic reduction (SCR) needs to be applied to obtain regulatory limits. Studies show that the combusting ammonia in air with high pressures and higher concentration of ammonia inside combustion chamber reduces the amount of produced nitrogen oxides [4]. The first power plant which uses ammonia as a fuel is located in Japan. In this power plant ammonia is co-fired with coal which contributed to decrease of carbon dioxide emissions and did not affect the efficiency of power turbine [2].

3. Equilibrium modelling

In this section an equilibrium assumption was used to predict the adiabatic flame temperature and combustion products as a function of excess air ratio (λ). An open-source code Cantera [5], was applied for this purpose. The data were pre- and post-processed using Python programming language and Microsoft Excel. Equilibrium modeling provides a lot of useful information regarding the combustion process. The main drawback of this type of modeling is due to assumption of infinite process time or infinitely fast reactions. Thus results may differ for those from real experiments if the conditions are far from equilibrium. Typically for fast burning fuels the products are close to equilibrium at the outlet of the combustion chambers. However prediction of products concentrations of slow reactions, like those for example in the NO_x formation mechanism, may lead to considerably different results than in reality and thus wrong conclusions.

Equilibrium computations of ammonia combustion in air for adiabatic system were done for initial temperature of reactants of 300 K and different pressures: 0.1 MPa, 1 MPa, 10 MPa and 100 MPa. The calculations were performed in order to obtain the adiabatic flame temperature at constant pressure and composition of products. The calculations were performed using data derived from GRI 3.0 mechanism [6], which consists of 53 species. Since the species containing carbon are required, the list of species was limited to 18 species containing O, H and N elements.

In Figs 1-3 the resulting temperature and product composition are presented in the range of excess air ratios λ from 0 to 1.4. In order to normalize the range, the ratio $\boldsymbol{\lambda/(\lambda+1)}$ was shown on the abscissa, so that the stoichiometric condition corresponds to the value of $\boldsymbol{\lambda/(\lambda+1)=0.5}$. In Fig. 1 the predicted adiabatic flame temperatures at constant pressures are presented. It can be seen that highest temperatures are obtained for pressure equal 100 MPa and close to stoichiometric conditions at $\boldsymbol{\lambda=0.999}$, where the temperature is 2102.77 K. At stoichiometric conditions the temperature is just slightly reduced to 2102.45 K. For lower pressures the highest temperatures are lower and the maxima are shifted more to the rich region. This temperature reduction is associated with dissociation of products which is more favored at lower pressures. For most of excess air ratios the flame temperature is independent of pressure but in substoichiometric conditions where $\boldsymbol{\lambda}$ is in the range from 0 to 0.4. In this region faster decomposition of ammonia occurs at low pressures, which can be observed in Fig. 2 where the mole fractions of equilibrium products are presented. The decomposition reaction of $\mathbf{NH_3}$ into $\mathbf{N_2}$ and $\mathbf{H_2}$ ($\mathbf{2NH_3 \leftrightarrow 3H_2 + N_2}$) is endothermic, therefore reduction of temperature is observed for lower pressures, where the process is more pronounced due to Le Chatelier's principle. In all cases temperature increases up to $\boldsymbol{\lambda \approx 1}$and then decreases. It can be also seen from Fig. 2, as the excess air ratio increases the ammonia oxidation to the final products ($\mathbf{H_2O}$ and $\mathbf{N_2}$) occurs along with its decomposition to $\mathbf{H_2}$ na $\mathbf{N_2}$. The consumption of ammonia is complete at $\boldsymbol{\lambda=0.2}$ for $\boldsymbol{p=0.1}$ MPa and at $\boldsymbol{\lambda=0.43}$ for $\boldsymbol{p=100}$ MPa, however the complete combustion of its decomposition products occurs at $\boldsymbol{\lambda>1}$, as expected.

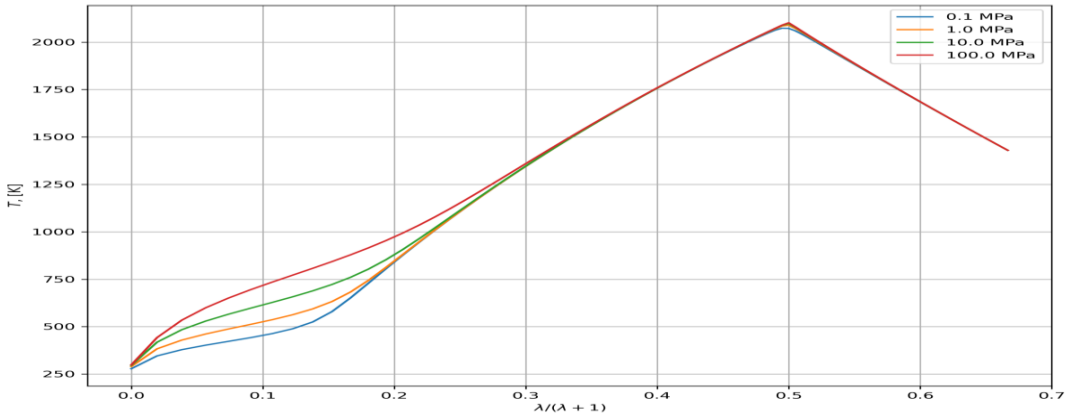

Fig 1 Adiabatic flame temperature at constant pressures

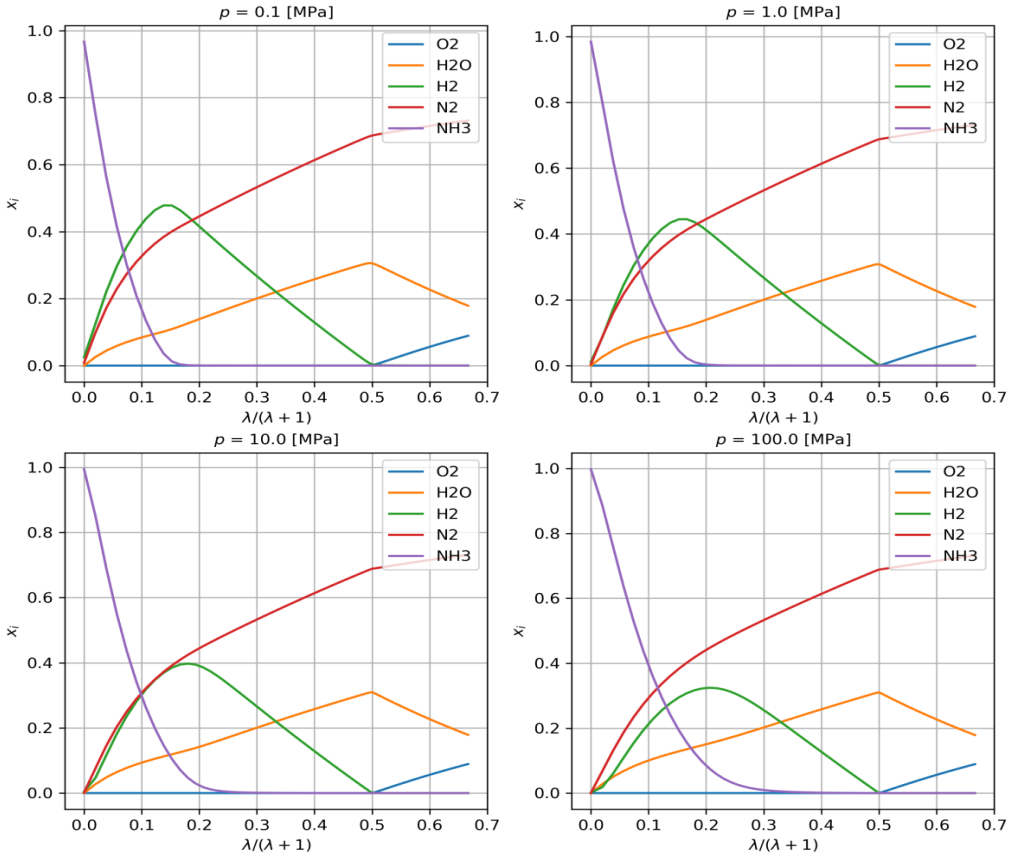

Fig 2 Mole fractions of products for various pressures

In Fig. 3 the profiles of minor species mole fractions are presented. As can be seen the dominating product is NO whose concentration is the highest at $\lambda > 1$. This is expected since formation of the oxides requires available oxygen and in the region of still high temperature due to high activation energy of $N_2 + O \rightarrow NO + N$ reaction, through which NO is formed in the thermal mechanism. The highest NO mole fraction occurs close to $\lambda = 1.18$ for both, low and high pressure and equals 1959 ppm for high pressure and 1919 ppm for low pressure. As mentioned earlier, due to the assumed infinite time of reaction in the equilibrium computations, the results are typically much higher than those occurring in real combustion systems.

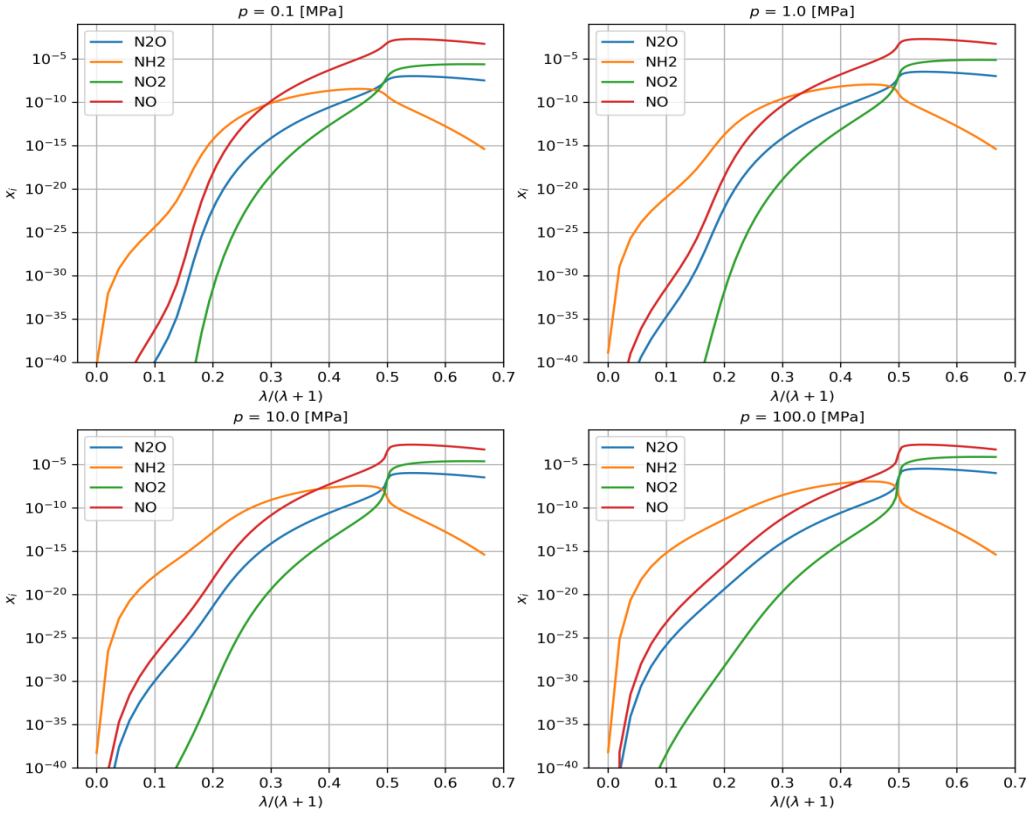

Fig 3 Molar fractions of different kinds of nitrogen compounds

4. Freely propagating flat flame

A model of freely propagating flat flame, available in the Cantera software was applied to predict the flame structure and laminar flame speed. Three reaction mechanisms were used in the computations to compare the results and assess whether the simpler mechanisms predict the flame speed with satisfactory accuracy. The first reaction mechanism applied in the study was the one derived from GRI 3.0 mechanism [6] which includes 18 chemical species and 70 chemical reactions. This mechanism does not contain any carbon species. The second mechanism is the mechanism of Nakamura et al. [7] which consists of 38 species and 232 chemical reactions. This mechanism consists mostly of species and reactions which include N, H and O elements, however 4 carbon containing species are also present. The third mechanism is of Shrestha et al. [8]consists of 32 species and 259 chemical reactions. In this mechanism a modification was added. Originally Shrestha et al. [8] mechanism consists of 121 species and 1087 chemical reactions but this mechanism includes carbon species. Thus all species and reaction which includes carbon were removed from this mechanism. Calculations for comparison of different mechanism was only performed for the pressure of 0.1 MPa.

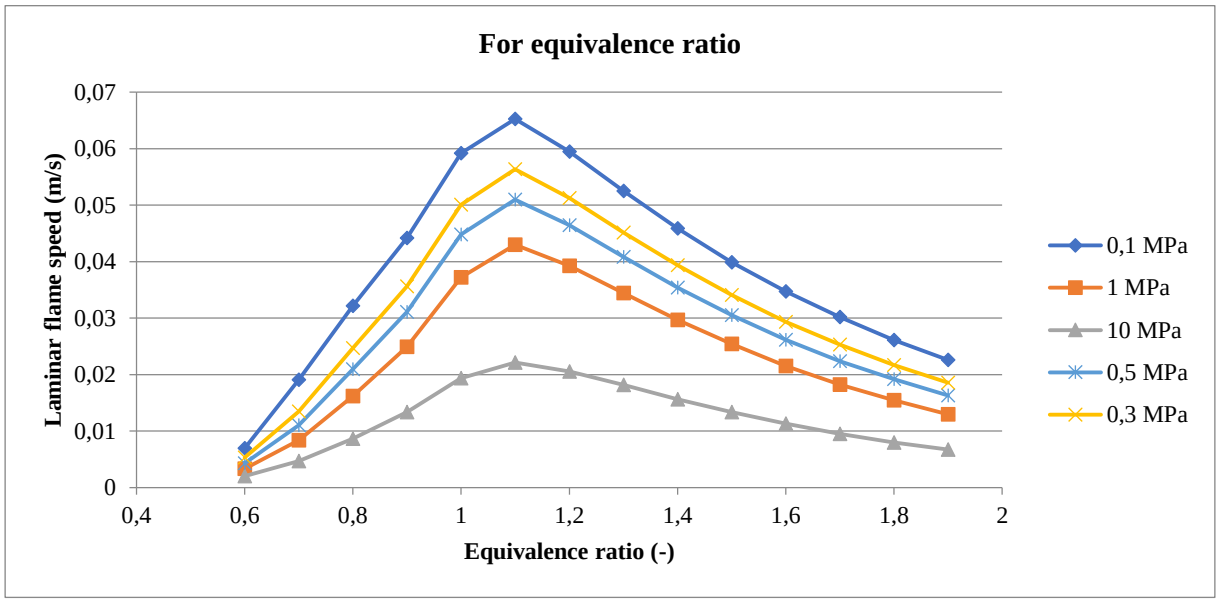

Fig 4 Laminar flame speedS_L for different pressures

Fig. 4 shows the predicted laminar flame speed for different pressures using derived from GRI 3.0 mechanism. As can be seen the flame speed depends on pressure and, as expected, is decreasing with increasing pressure. The highest laminar flame speed was obtained at equivalence ratio $\phi = 1/\lambda = 1.1$ and was equal to 6.5 cm/s at $p = 0.1$ MPa. It can be also observed that the maximum flame speeds are obtained for rich mixtures, however the location of the maxima are not affected by the pressure.

In Fig. 5 shows temperature profiles across the flame front are presented for different pressures at $\phi = 1$. From those figures it can be seen that for higher pressures the temperature gradient is higher and the overall width of the flame is smaller. This agrees with the general scaling of flame thickness with pressure $\delta \sim p^{-n/2}$, where n is the reaction order.

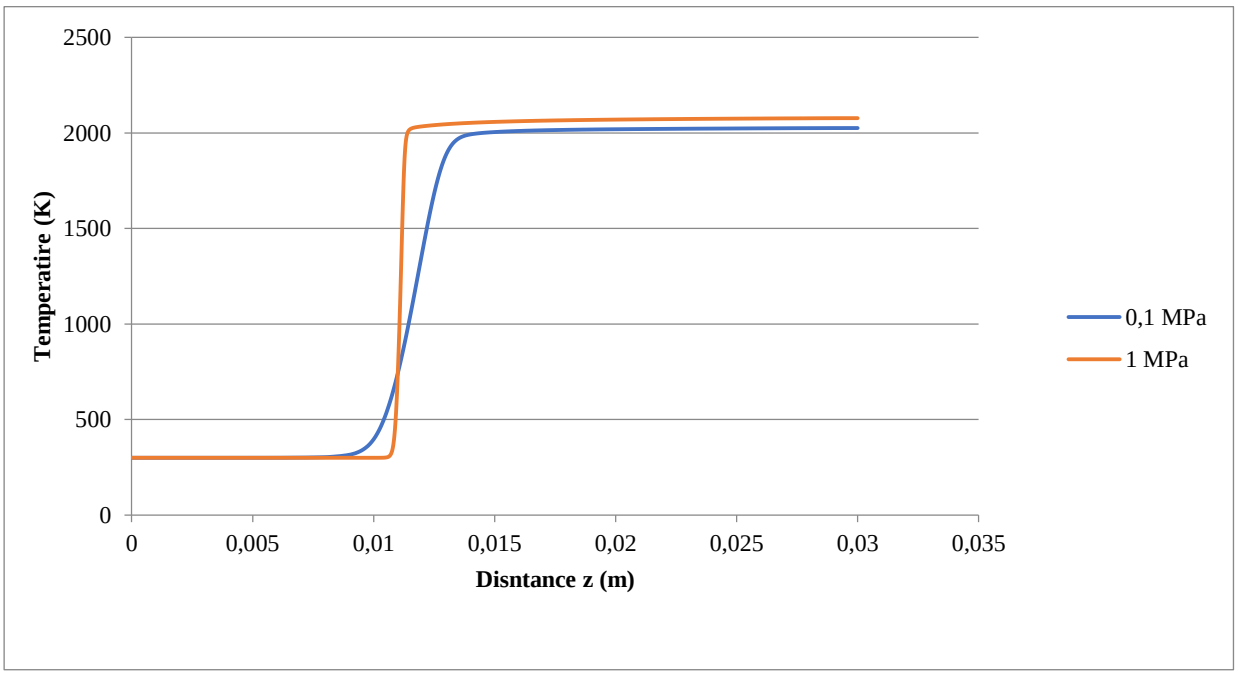

Fig 5 Temperature profile in the flame front for 0.1 MPa and 1 MPa

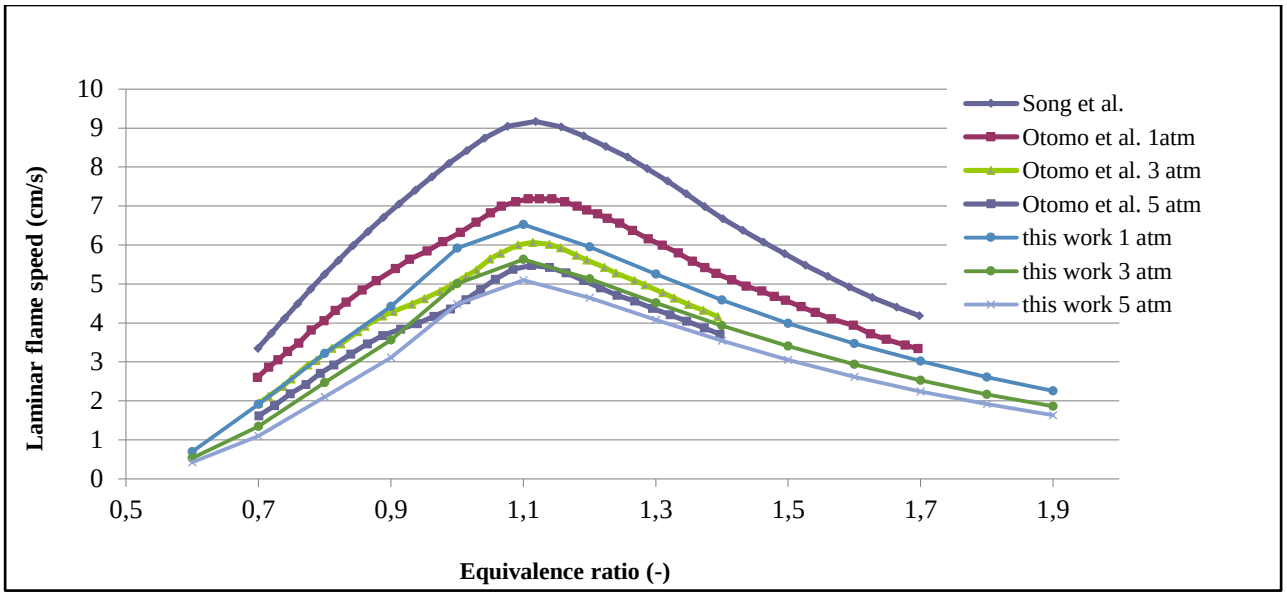

Fig 6 Comparison of obtained results with literature ones [9]

Fig. 6 shows a comparison between results of laminar flame speed obtained in this study using the derived from GRI 3.0 mechanism and results from the literature. It can be seen that laminar flame speed obtained by Song et al. [9] is much higher than those obtained in this study and by Otomo et al. [9].Comparing results by Otomo et al. and this study it can be concluded that they are very close to each other. The differences are of around 0.5 cm/s, however the flame speed obtained in [9] are systematically higher than those in this work. In both cases the proper dependence of flame speed on pressure was obtained. To examine further the results, calculations for other reaction mechanisms were also performed in this study for 0.1 MPa. The obtained results are presented in Fig. 7. The highest values of laminar flame speed were obtained for reaction mechanism by Nakamura et al. [7] and they agree well with the results presented by Song et al. [9]. These mechanisms are much more detailed (Nakamura consists of 38 species and 232 reactions and mechanism used by Song et al. of 32 species and 204 reactions) than the one derived from GRI 3.0 mechanism. It can be therefore concluded that although the simpler mechanisms have a benefit of faster computations the predicted flame speed can be considerably lower, which is unsatisfactory, since the relative difference can be as high as 29 % for equivalence ratio $\phi = 1.1$. The most detailed mechanism by Shrestha et al. [8](consisting of 32 species and 259 reactions when carbon containing species were excluded)was also applied. It can be seen that the results for this mechanism agree quite well with the mechanisms of Nakamura et al. and presented in Song et al. for high equivalence ratios, although the results were systematically higher. At low equivalence ratios the predicted flame speeds were lower and agreed much more with the results presented by Otomo et al., to increase for $\phi > 1$ nearly to the results of Song et al. and those obtained with the mechanism of Nakamura et al. [7]. It should be stressed, that as shown in Otomo et al. [9], the mechanism of Song et al. [9] slightly overpredicts the experimental data at atmospheric pressure and results obtained by Otomo et al. [9] are smaller than those from experiments. What is more, experimental data obtained by various authors are also varying considerably. Thus still further development of reaction mechanism is needed based on more reliable experimental data, in order to achieve results closer to reality.

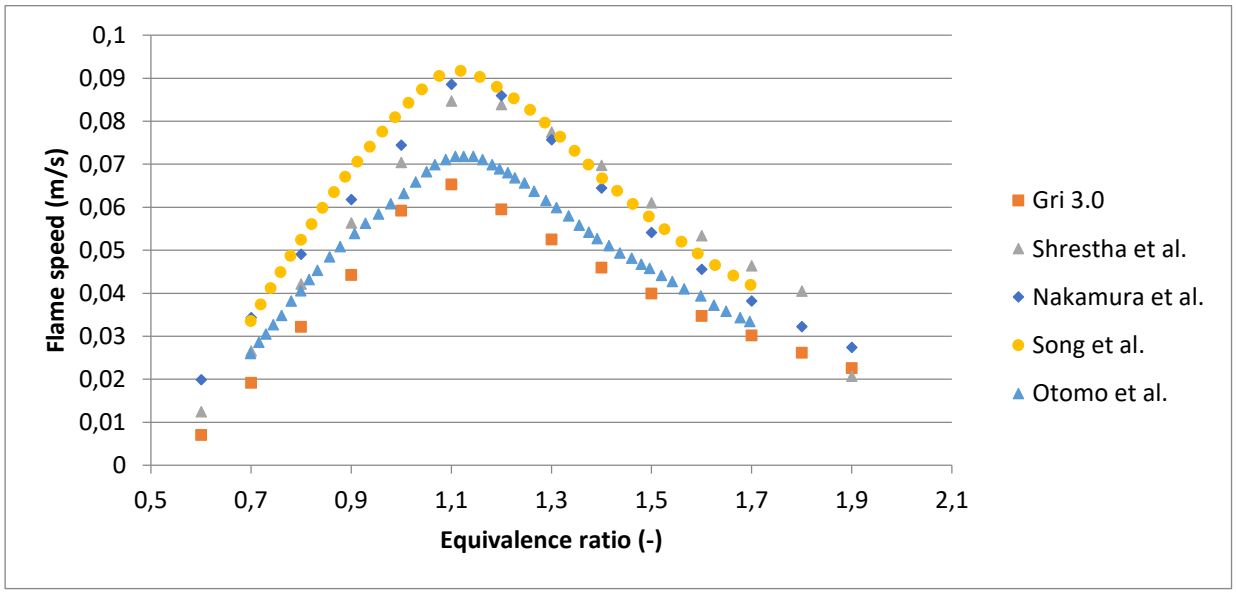

Fig 7 Comparison of calculated laminar flame speeds obtained using different reaction mechanisms and from literature at 0.1 MPa

5. Conclusion

Ammonia is currently considered as one of the possible energy carriers and hydrogen carrier in the future carbon free economy. Since its storage and transportation is much simpler than for hydrogen, it can play an important role in the use of renewable energy sources. Using ammonia for electricity production would contribute to large reduction in CO_2 emissions, however the drawbacks related to this fuel use have to be overcome first. This include the need of refurbishment of existing combustion systems for the use of ammonia due to its low flame speed and corrosive nature, as well as the requirement of solution of high NOx generation during combustion. The toxicity of ammonia has to be taken into account as well. The performed equilibrium calculations show that the adiabatic flame temperatures at constant pressure are smaller than those for the currently used hydrocarbon fuels and that it they are virtually independent on pressure for close to stoichiometric and lean conditions. Similarly the flame speed is considerably smaller for ammonia than of the currently used fuels, e.g. the flame speed is ~ 6 times smaller than for CH_4 and ~36 times smaller than H_2. The flame speeds computed with a few reaction mechanisms indicate that the differences in predictions can be as high as 29%. Similar conclusions can be drawn when comparing the experimental data, not presented in this study (see Otomo et al. [9]). Therefore it can be concluded that further studies are required to improve the quality of both experimental data and the reaction mechanisms, in particular there is a need for accurate reduced mechanisms.

Acknowledgement

This study has been supported by the statutory research fund of the Silesian University of Technology, Faculty of Energy and Environmental Engineering, Department of Thermal Engineering, Gliwice, Poland.

References

[1] A. E. Dahoe, 'Laminar burning velocities of hydrogen – air mixtures from closed vessel gas explosions', vol. 18, pp. 152–166, 2005, doi: 10.1016/j.jlp.2005.03.007.

[2] A. Valera-Medina, H. Xiao, M. Owen-Jones, W. I. F. David, and P. J. Bowen, 'Ammonia for power', *Prog. Energy Combust. Sci.*, vol. 69, pp. 63–102, 2018, doi: 10.1016/j.pecs.2018.07.001.

[3] S. N. Behera, M. Sharma, V. P. Aneja, and R. Balasubramanian, 'Ammonia in the atmosphere: A review on emission sources, atmospheric chemistry and deposition on terrestrial bodies', *Environ. Sci. Pollut. Res.*, vol. 20, no. 11, pp. 8092–8131, 2013, doi: 10.1007/s11356-013-2051-9.

[4] K. D. K. A. Somarathne, S. Colson, A. Hayakawa, and H. Kobayashi, 'Modelling of ammonia/air non-premixed turbulent swirling flames in a gas turbine-like combustor at various pressures', *Combust. Theory Model.*, vol. 22, no. 5, pp. 973–997, 2018, doi: 10.1080/13647830.2018.1468035.

[5] David G. Goodwin, Raymond L. Speth, Harry K. Moffat, Bryan W. Weber,Cantera: An Object-oriented Software Toolkit for Chemical Kinetics, Thermodynamics, and Transport Processes,Version 2.4.0,2018, (www.cantera.org), doi:10.5281/zenodo.1174508

[6] Gregory P. Smith, David M. Golden, Michael Frenklach, Nigel W. Moriarty, Boris Eiteneer, Mikhail Goldenberg, C. Thomas Bowman, Ronald K. Hanson, Soonho Song, William C. Gardiner, Jr., Vitali V. Lissianski, and Zhiwei Qin http://www.me.berkeley.edu/gri_mech/

[7] Nakamura H., Hasegawa S., Tezuka T., Kinetic modeling of ammonia/air weak flames in a micro flow reactor with a controlled temperature profile, Combustion and Flame, Vol. 185: 16-27 (2017). doi:10.1016/j.combustflame.2017.06.021

[8] Krishna P. Shrestha, Lars Seidel, Thomas Zeuch, and Fabian Mauss, Energy & Fuels 2018 32 (10), 10202-10217 DOI: 10.1021/acs.energyfuels.8b01056

[9] Junichiro Otomo, MitsuoKoshiTeruoMitsumori, Hiroshi Iwasaki,Koichi Yamada, Chemical kineticmodeling of ammonia oxidation with improved reaction mechanism for ammonia/air and ammonia/hydrogen/air combustion , International Journal of Hydrogen EnergyVolume 43, Issue 5, 1 February 2018, Pages 3004-3014

The most recently used occurring residues of antidepressants in the aquatic environment

Patryk Zdziobek [1], Kacper Stanek [1]

[1]AGH University of Science and Technology, e-mail: patrick.zdziobek@gmail.com

Abstract

The most common antidepressants found in land waters are O-desmethylvenlafaxine, venlafaxine, citalopram, sertraline, fluoxetine and citalopram. Continuous exposure to anti-depressive pharmaceuticals has a negative impact on fish and amphibians in this environment. In fish, the biggest problem is the brain impairment that prevents the food from being properly found and consumed. In amphibians, the presence of antidepressants in tissues will impair social and territorial functions and affect the mass of male animals. The most common in the aquatic environment is the metabolite of venlafaxine (O-desmethylvenlafaxine). In smaller quantities there are sertraline, citalopram, doxepin, diazepam and fluoxetine. The microbial wastewater treatment process eliminates them more effectively than O-desmethylvenlafaxine and venlafaxine. Samples for the analysis of the antidepressants content are prepared using extraction to the solid phase. The correct selection of the eluent affects the degree of recovery of the corresponding antidepressants. GC-MS and LC-MS/MS are among the most commonly used analytical devices for quantitative and qualitative analysis.

Keywords: antidepressants, emerging contaminants, pollution, pharmaceuticals, chromatography

1. Introduction

A resulting environmental pollutant are divided into gaseous, solid, liquid. Among the gases, the greatest problem is carbon dioxide (CO_2), which leads to a greenhouse effect. Nitrogen (NO_x) and sulfur oxides (SO_x) from the combustion of low-quality fuels contribute to acid rain, soil acidification and surface water. Oil spills can be among the most important pollutants. Agriculture also contributes to the introduction into the environment of a significant amount of fertilizers and pesticides. Particulate pollutants may include particulate matter, mercury and lead, which are mostly from low emissions from households and road transport [1,2]. Large access to medicines and food supplements contributes to new environmental pollution. Generally, the metabolites of medicines are not monitored and their negative effects on the environment and human beings have not been thoroughly investigated [3,4]. These include analgesics, antibiotics, diabetes medicines, anti-convulsants and psychotropic drugs. Most treated waste water entering rivers, lakes and seas contains the metabolites of pharmaceuticals. Waste water treatment plants currently do not use methods of drug degradation and enter the environment [5,6]. The presence of metabolites of antidepressants in the aquatic environment contributes to greater exposure of fish and amphibians to the attacks of predators. The very presence of antidepressive substances in animal organisms is likely to affect mood, nervous system stimulation and behavior. Due to the influence on the nervous system processes of the metabolites of psychotropic drugs, the main vital functions and the ability to feed are likely to be impaired [7]. An important issue on the residues of metabolites of medicines is to highlight the problem of the scientific. Community and the operators of waste water treatment. This publication will cover the most common antidepressants in the aquatic environment and their impact on the ecosystem, the most common methods of qualitative and quantitative analysis, and methods of preparing liquid samples for analysis.

2. Types of environmental antidepressants

A presence of pharmaceuticals and their metabolites in the aquatic environment depends mainly on the frequency and amount of medicines used. The content of individual antidepressants and their metabolites in aquatic ecosystems depends on the region of the world, as well as on the popularity and effectiveness of their elimination from waste water. Problems with the effectiveness of the removal of pharmaceuticals depend on the different levels of polarity and electrostatic activity. Pharmaceuticals with hydrophobic properties and active positive groups are better adsorbed on sewage suspension and micro-organisms than hydrophilic molecules. Among anti-depressive pharmaceuticals, a high elimination efficiency of about 90% is found in paroxetine (3S,4R)-3-(1,3-benzodioxol-5-ylxymmethyl)-4-(4-fluorophenyl)piperidine (Fig.2.1). This is likely to be directly contributed by the lipophilic amino-effect [6,8,9].

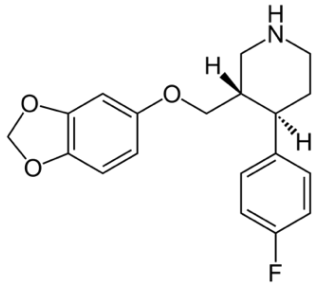

Fig. 2.1. Structure of paroxetine

Most antidepressants are removed to a much lesser extent by among others venlafaxine 1-[2-(dimethylamino)-1-(4-methoxy-phenyl)ethyl]cyclohexan-1-ol approx.25% (Fig.2.2), 40-90% fluoxetine (Fig.2.2), N-methyl-3-phenyl-3-[4-(trifluoromethyl)phenoxy]propan-1-amine approx.60-80% (Fig.2.2) [8,10].

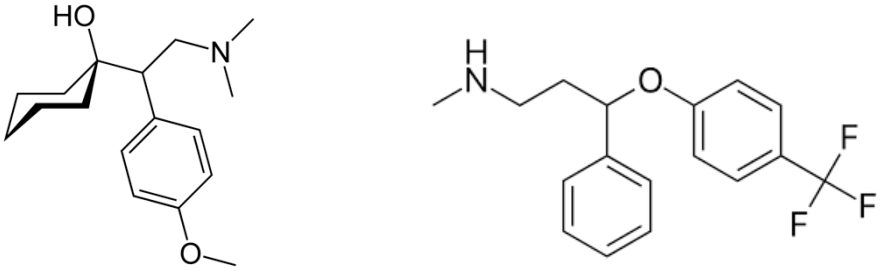

A **B**

Fig.2.2 Structure of venlafaxine (A) and fluoxetine (B).

This depends mainly on the wastewater treatment technology used. Despite efforts and work to change the biological parameters of wastewater treatment in the treatment plants, the antidepressants and their metabolites are transported in a wastewater treatment plant to the rivers and even to lakes and drinking water tanks [8,10]. The most common antidepressants and their metabolites include O-desmethylvenlafaxine, venlafaxine, citalopram, sertraline, fluoxetine, doxepin and citalopram (Table. 2.1.).

Table 2.1. Main antidepressants and their metabolites in the aquatic environment.

The name of the antidepressant	Sample presence	Concentration [ng/l]	Source
O-desmethylvenlafaxine	waste water treated (Canada)	1600	11
	river water (Germany)	640	12
	waste water treated (Germany)	1900	13
venlafaxine	waste water treated (Canada)	800	11
	waste water treated (Germany)	500	13
	river water (United Kingdom)	71.6	10
	river water (US)	600	14
	river water (Germany)	260	15
	waste water treated (Germany)	500	13
sertraline	river water (Vistula, Poland)	3.1	16
citalopram	river water (Vistula, Poland)	1.5	16
doxepin	river water (Vistula, Poland)	1.9	16
	river water (Shanghai, China)	0.8	17
diazepam	river water (Shanghai, China)	24.3	17
	river water (Tongzhou Bishui, China)	6.9	18
fluoxetine	river water (United Kingdom)	13.5	16

A concentration of the antidepressants shown in the aquatic environment in Table. 2.1. The highest concentration has a metabolite of venlafaxine (O-desmethylvenlafaxine). Low concentrations of sertraline, citalopram, doxepin, diazepam and fluoxetine confirm that they are eliminated with greater efficiency than O-desmethylvenlafaxine and venlafaxine.

3. Effects of antidepressants on aquatic organisms.

A continuous exposure of aquatic organisms to antidepressants and their metabolites causes specific adverse reactions. In fig. 3.1 a diagram of the penetration of antidepressive drugs into the brain tissue of fish is presented. In the case of fish, they may affect many of among others factors on growth, inhibit the effects of antioxidants on cells and the detoxification process of the organism, increase the peroxidation of lipids and damage the liver genetic code [19]. The main problem with fish is brain impairment, which prevents food from being properly found and consumed. Another very negative characteristic is the direct effects on reproduction. As a consequence, the anti-depressants have both characteristics. Slow reproduction significantly reduces the new fish population. In addition, the presence of antidepressants slows fire movements and impairs the mechanism of escape in the event of a predator attack [20,21,22,23]. In the dark, fish movements are passive and show uncertainty in movement. The weight of male animals is growing [24,25].

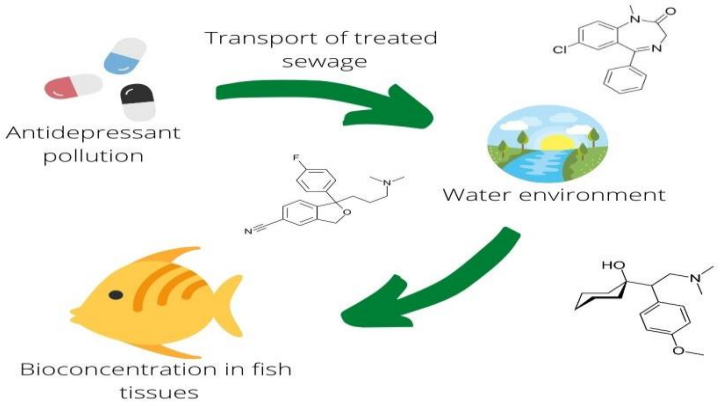

Fig. 3.1. Route of spread of antidepressants in the aquatic environment.

A small amount of information is about the impact of antidepressants on amphibians. The group Eyeck and Regnet examined the effects of fluoxetine on male amphibians. This has led to changes in social and territorial behavior. In addition, it was specified that antidepressants may affect the potential of the hypothalamus-pituitary line. In addition, Conners and his colleagues have indicated that sertraline has an impact on the reduction in the body weight of men's amphibians [26,27,28].

4. Mostly methods of analysis of antidepressants in the aquatic environment

Due to the presence of andepressants analytes in samples for treated waste water, surface water and liquid water. In Table. 4.1. Some of the most commonly used methods of analysis of antidepressants are presented together with the specific limit of detection (LOD).

Table. 4.1. Review of analytical techniques used in the analysis of antidepressants of environmental samples, human body fluids and tissues of aquatic organisms of individual antidepressants with limit of detection.

Name of analyte	Presence	Analysis technique	LOD	Source
venlafaxine	surface water	GC-MS	27 ug/ml	27
O-desmethylvenlafaxine	raw waste water, treated waste water	GC-MS	28 ng/l	13
O-desmethylvenlafaxine, venlafaxine	human blood	GC-MS	1.5 ug/l	29
fluoxetine, sertraline, O-desmethylvenlafaxine	brain, muscle, liver of river fish	GC-MS	0.01ng/g	15
setraline	plasma of human blood	GC-MS	0.1 ng/ml	31
venlafaxine, O-desmethylvenlafaxine	river water	LC-MS/MS	0.1 ng/ml	32
venlafaxine	river water	LC-MS/MS	-	33

Methods of analysis of antidepressants in aqueous samples are common both gas chromatography coupled with mass spectrometry (GC) and liquid chromatography coupled with a tandem mass spectrometer (LC-MS/MS). However, despite the close similarity of the two techniques, it can be distinguished that liquid chromatography can be used to separate all liquid soluble antidepressants. Another advantage is measurement capability in the room temperature, which allows for thermal-unstable antidepressants to be tested. On the other hand, high temperatures are used in gas chromatography, which make it impossible to analyze thermally labile compounds. An additional fact

which makes it difficult to analyze antidepressants by gas chromatography is that the compounds analyzed must show a high volatility. In order to prepare the sample for analysis, a suitable derivatization agent must be carried out. In addition, in liquid chromatography, the detectors do not affect the sample by destructive means. The main advantage of GC over LC is the analysis time. For GC, the analysis process takes a few minutes, while for LC the analysis times are much longer. The most important aspect that is taken into account during the analysis is the economic issue. The cost of conducting GC studies is significantly lower than for LC [34,35].

5. Preparation of samples for antidepressants analysis

A optimization of the solid phase extraction (SPE) relies mainly on the selection of an appropriate deposit. The most important thing is to select and maintain the correct pH of the sample and to select the eluent. Different SPE columns may be used for the extraction of venlafaxine. The Petruczynik and in employees decided to test columns C18 and HLB. Blood serum samples containing antidepressants were passed through the columns at a rate of 1ml/min. The extraction process was initiated by activating the surface of the column with methanol. However, conditioning is done with distilled water. Leaching of analytes from the column was carried out using methanol. It was shown that at higher concentrations of antidepressants samples the recovery was 95% and the process performance was up to 100%. Another example of the use of SPE is the testing of environmental samples. Samples of raw and purified waste water may be passed through the deposit (Bond Elut PPL) conditioned with methanol, methanol and acetone and distilled water. Methanol/acetone solution was used to elute the analytes [36,13].

6. Conclusion

Paroxetine shows the largest efficacy of antidepressant removal among antidepressants. It is likely that lipophilic-amino effect of paroxetine is the main cause. The remaining antidepressants, including venflaxine and fluoxetine, are removed from sewage to a much lesser extent during biological treatment of sewage. The main reason for this is the use of different wastewater treatment technologies and physico-chemical parameters of treatment processes. Despite attempts to interfere with the change in wastewater treatment parameters, the antidepressants are still present in the treated effluent. The very most common antidepressants and their metabolites occurring in aquatic environment are O-desmethylvenlafaxine, venlafaxine, citalopram, sertraline, fluoxetine, doxepin and citalopram. The highest concentrations in the aquatic environment has metabolite of venlafaxine (O-desmethylvenlafaxine). While sertraline, citalopram, doxepin, diazepam and fluoxetine are present in a smaller amount of purified sewage. It follows that they are eliminated with greater efficiency than O-desmethylvenlafaxine and venlafaxine.
The methods commonly used in the analysis of anti-depressive pharmaceuticals are liquid chromatography coupled with a tandem mass spectrometer (LC-MS/MS) and gas chromatography coupled to a single mass spectrometer (GC-MS). The extraction of anti-depressive pharmaceuticals uses columns of the SPE with different fills among others C18, HLB and Bond Elut PPL. Conditioning of the column is carried out by means of distilled water, usually. The process of elution of analytes from the stationary phase of the column is most commonly performed by methanol or methanol/acetone mixture.

References

[1] Aydın, H. and Hajlkılç, C. (2017), Air Pollution, Pollutant emissions and harmfull effects, Journal of Engineering and Technology, p. 8.

[2] Schindler, D. W. (1988), Effects of acid Rain on Freshwater Ecosystems, Science, 239(4836), p. 149-157.

[3] S. Sauvé, M. Desrosiers (2014), A review of what is an emerging conttaminants, Chemistry Central Journal, 8(1), 15

[4] M. Lei, L. Zhang, J. Lei, L. Zong, J. Li, Z. WU, Z. Wang (2015), Overview of Emerging Contaminants and associated Human Health effects, Hindawi Publishing Corporation,

[5] C. Daughton, (2004) Non-regulated water behavior: emerging research, Environmental impact Assessment Review, 24, pp.

[6] A. Zejc, M. Gorczyca, Chemia leków, PZWL Medical Publishing, 2005, ISBN: 978-83-200-3652-7.

[7] Castillo-Zacarías C., Barocio M. E. ,Hidalgo-Vázquez E., Sosa-Hernández J. E., Parra-Arroyo L., Itzel Y. López-Pacheco, Barceló D., Hafiz N.M. Iqbal, Parra-Saldívar R., (2020), Antipressant second as emerging conttaminants: Occurrence in urban and non-urban waters and analytical methods for their detection, Science of the Total Environment, p. 143722.

[8] P. Rezka, W. Balcerzak (2016), Występowanie leków przeciwdepresyjnych – ze ścieków do wody uzdatnionej, Czasopismo Techniczne Środowisko, 1-Ś

[9] Kaye, C. M., Haddock, R. E., Langley, P. F., Mellows, G., Tasker, T. C. G., Zussman, B. D., & Greb, W. H. (1989), A review of the metabolite and pharmacokinetics of paroxetine in man. ACTA Psychiatrica Scandinavia, 80(S350), 60-75.

[10] Baker, D. R. and Kasprzyk-Hordern, B. (2013) Spatial and temporal occurrence of pharmaceuticals and illicit drugs in the aqueous environment and during wastewater treatment: New developments', Science of The Total Environment, 454–455, pp. 442–456

[11] Metcalfe, C. D., Shaogang Chu, Judt C., Hongxia Li, Ken D Oakes, Mark R Servos, David M Andrews (2010), Antidepressants and their metabolites in municipal wastewater, and downstream exposure in an urban watershed', Environmental Toxicology and Chemistry, 29(1), pp. 79–89.

[12] M. P. Schlusener, P. Hardenbicker, E. Nilson, M. Schulz, C. Viergutz, T. A Ternes (2015), Occurrence of venlafaxine, other antidepressants and selected metabolites in the Rhine catchment in the face of climate change, 196, p. 247-256.

[13] P. C. Rua-Gomez, W. Puttmann (2011), Occurance and removal of lidocaine, tramadol, venlafaxine, and their metabolites in German wastewater treatment plants, Environmental Science and Pollution Research, 19(3), p. 689-699.

[14] M. M. Schultz, E. T. Furlong (2008), Trace Analysis of Antidepressant Pharmaceuticals and their Select Degras in aquatic Matrixes by LC/ESI/MS/MS, Analytical Chemistry, 80(5), p. 1756-1762

[15] B. W Brooks, C. K. Chambliss, J.K. Stanley, A. Ramirez, K. E. Banks, R.D. Johnson, R. J. Lewis (2005), Determination of Select Antidepressants in fish from an Efluent - Domented Stream, Environmental Toxicology and Chemistry, 24(2), p. 464-469

[16] J. Giebultowicz, G. Nalecz-Jawecki (2014), Occurrence of antidepressant residues in the sewage-impacula and Loss rivers and in tap water in Warsaw (Poland), Ecotoxicology and Environmental Safety, 104(1), p. 103-109.

[17] Wu, M., Xiang J., Chenjing Que, Fenfen Chen, Gang Xu (2015), Occurrence and fate of psychiatric pharmaceuticals in the urban water system of Shanghai, China, Chemosphere, 138, p. 486-493.

[18] Wang, C., Hou, L., Li J., Zeqiong Xu, Tingting Gao, Jun Yang, Huafang Zhang, Xiqing Li & Peng Du (2017), Occurrence of diazepam and its metabolites in wastwater and surface waters in Beijing, Environmental Science and Polluion Research, 24(18), p. 15379-15389.

[19] Duarte I. A, Reis-Santos P., C Novais S., Lénia D Rato, F L Lemos M., Freitas A., Ana Sofia Vila Pouca, Barbosa J., N Cabral H., F Fonseca V. (2020) Desed, hypertense and sort: Long-term effects of fluoxetine, propranolol and diclofenac exposure in a top predator fish, Science of the Total Environment, 712, p. 136564.

[20] Dorelle, L.S., da Cuña, R.H., Ganga, D.E., Rey Vázquez, G., López Greco, L., Lo Nostro, F.L., (2020) Fluoxetine exposure distruts food and energy storage in the silent fish Cichelasoma dimerus (Teleostei, Cichelformes). Chemosphere 238.

[21] Tan, H., Polverino, G., Martin, J.M., Bertram, M. G., Wales, S.C., Palacios, M.M., Bywater C.L., White, C.R., Wong, B.B.M. (2020), Chronic exposure to a passive pharmaceutical field should be used for the treatment of ammonium-individual phenotipic variation in a fish. Environ. Pollut. 263, 114450.

[22] De Abreu, M.S., Maximino, C., Cardoso, S.C., Marques, C.I., Pimentel, A.F.N., Mice, E., Winberg, S., Barcellos, L.J.G., G, Soares, M.C. (2020), Domemoranne and serotonin mediate the impact of stress on cleaner fish cooperative behavior. Hort. Behav. 125,104813.

[23] Hosain, M.S., Buřič, M., Moore, P.A., (2020), Exposure paradigm of fluoxetine impaned the Faxonius virilis agoniastic behavior differential. SCI. Total Environ. 699.

[24] Byeon, E., Park, J.C., Hagiwara, A., Han, J., Lee, J.S. (2020), Two antidepressants fluoxetine and sertraline cause growth retardation and oxidative stress in the marine rotifer Brachionus koreanus Aqua. Toxicol, 218, 105337.

[25] Ziegler, M., Knoll, S., Köhler, H.R., Tisler, S., Huhn, C., Zwiner, C., Triebskorn, R., (2020), Impact of the antidepressant citalopram on the behavioral of two differential life stages offer trout, PeerJ 2020.

[26] Sehonova, P., Svobodova, Z., Dolezelova, P., Vosmerova, P., Faggio, C. (2018) Effects of waterborne antidepressants on non-target animals living in the aquatic environment: A review', Science of The Total Environment, 631–632, pp. 789–794.

[27] Ten Eyck, G.R., Regen, E.M., (2014) Chronic fluoxetine treatment promotes submissive behavior in the territorial frog, Eleutherodactylus coqui. Pharmacol. Biochem. Behav. 124, 86–91.

[28] Conners, D.E., Rogers, E.D., Armbrust, K.L., Kwon, J.W., Black, M.C., (2009), Growth and development of tadpoles (Xenopus laevis) exposed to selective serotonin reuptake inhibitors, fluoxetine and sertraline, throughout mepamorphosis. Environ. Toxicol. Chem. 28, 2671–2676.

[29] J. P. Lamas, C. Salgado-Petite, C. Garcia-Jares, M. Lomplart, R. Cell, M. Gomez, (2004) Solid-phase microextraction–gas chromatography–mass meters for the analysis of selective serotonin reupdate inhibitors in environmental water, Journal of Chromatography A, 1046(1-2), p. 245-247

[30] I. Papoutsis, A. Khraiwesh, P. Mr Nikolaou, C. Pistos, C. Spiliopoulou, S. Athanaselis, (2012), A fully validated method for the simultaneous determination of 11 antidepressant second in whole blood block by gas chromatography-mass chemistry, Journal of Pharmaceutical and Biomedical Analysis, 70, p. 557-562.

[31] K. M. Kim, B. H. Jung, M. H. Choi, J. S. Woo, K. Paueng, B. C. Chung (2002), Rapid and sensitive determination of sertraline in human plasma using gas chromatography–mass spectrometry, Journal of Chromatography B, 769(2), pp. 333–339

[32] Lajeunesse, A., Gagnon, C. and Sauvé, S. (2008), Determination of basic antidepressants and their N-desmethyl metabolites in raw sewage and wastewater using solid-phase extraction and liquid chromatography-tandem mass spectrometry, Analytical Chemistry, 80(14), p. 5325-5333.

[33] Castillo-Zacarías C., E. Barocio M., Hidalgo-Vázquez E., Sosa-Hernández J. E., Parra-Arroyo L. , Itzel Y. López-Pacheco, Damià Barceló, Hafiz N.M. Iqbal, Parra-Saldívar R., (2020), Antidepressant drugs as emerging contaminants: Occurrence in urban and non-urban waters and analytical methods for their detection, Science of the Total Environment, p. 143722.

[34] M. Kamiński, Chromatografia cieczowa, Politechnika Gdańska, Wydział Chemii, 2004.

[35] Liquid Chromatography (LC) vs. Gas Chromatography (GC): Adventages & Disventages: http://chem-net.blogspot.com/2013/12/advantages-of-lc-vs-gc.html (access: 30.11.20).

[36] A. Petruczynik, K. Wróblewski, M. Shultka-Mlynska, B. Buszewski, H. Karakulla-Juchnowicz, J. Gajewski, J. Morillowska-Topolska, M. Waksmunzka-Hajnos (2017), Determination of venlafaxine, glazing and their main

active metabolites in human serum by HPLC-DAD and HPLC-MS, ACTA Polonia Pharmaceutical, 74(3), pp. 865-775.

Modeling of energy and environmental using variable speed drive in air-cooling towers in a steel mill

S.A. Nosherwani[1], S.U. Nausherwani[2], and M.F. Raiyaan[3]

[1]Instituto Superior Técnico, email: shahmir.nosherwani@tecnico.ulisboa.pt
[2]National University of Science and Technology, e-mail: saifullah_23@hotmail.com
[3]Instituto Superior Técnico, email: muhammad.ferdous.raiyan@tecnico.ulisboa.pt

Abstract

Industry plays a critical role in the economic development of a nation and is a major consumer of energy globally. Similarly, motors are major consumer of energy in an industry and used in a variety of function like cooling tower and pumps. Effective utilizing of energy efficient technologies can result in both significant economic growth and reduced environment emissions.

Since cooling towers consume a significant portion of the energy in a rolling steel mill, this paper presents analysis and compares the energy, economic and environmental emissions with and without Variable Frequency Drive (VFD). The air-cooling tower, in this experiment, can be used to vary the air flow entering in it by regulating the rotational speed of the motor using a VFD. This results in a significant energy savings as compared to running on full load in normal operation. Consequently, reducing the electricity bill and reducing environment emissions with a small payback period by using VFDs on these cooling towers. Moreover, the results presented in the paper are supported and compared with a modeling software for pumps and fans by Honeywell.

Keywords: Variable Frequency Drives, Energy saving, Emission reduction, Air cooling towers, Fans.

1. Introduction

Electric motors are almost found in every industry, commercial and residential sector. With different applications, electric motors consume about 40% of industry energy consumption around the global [1].Considering the global energy issue to reduce the dependence on fossil fuels and cut the energy demand, there is a lot potential to save energy in motors that is economic and environment friendly. As stated by R. Saidur et.al that greenhouse emissions (GHG) can be reduced by 20-30% by using few energy efficient alternatives [1].

In a steel rolling mill, motors are utilized in different equipment including cooling towers, shear press, pumps, compressors. However, in this paper, economic and energy analysis with and without VFD will be restricted to cooling towers on thermo mechanical treatment (TMT) circuit. TMT requires the use of impinging cool water on a hot billet resulting in rapid cooling (quenching) to a desired temperature. The amount of cooling water depends on the required strength of the final billet and diameter of the billet.

After cooling the billet, the water is cooled in an induced draft crossflow air cooling tower. Since there is no system to vary the rotation speed of cooling tower fan with the change in the flowrate of cooling water, the fan always operates at 100% load and there are significant energy loses associated with this operation. However, this energy loses can be reduced and energy efficiency can be improved using VFD.

VFD is an adjustable speed drive (ASD) operates by varying the speed and torque. This electronic system regulates and matches the speed and rotational force as per the operational requirement of the equipment in use. This results in energy savings as the fan operates at the desired speed rather than operating at full load continuously [1,2,3]. VFD can deliver savings up to 15- 20 % in HVAC operations [2].

Considering the economics, efficiency and process control, VFD is currently an effective controller that not only reduces energy consumption and energy costs but also reduces GHG emissions and maintenance costs due to less frictional losses. Moreover, it results in soft start up, improve power factor and over speed capability of the motor [1,2,3].

2. Methodology

2.1. Experimental setup and methodology

This section covers an overview of the methodology of an energy audit. This incorporates the data and mathematical expressions required to model energy usage, environmental emissions, energy savings and reduction of environmental emission by using a VFD in TMT cooling tower. TMT section is at the core of all operations in a hot rolling mill. To get the desired mechanical properties, the billet is moved across a closed bed with nozzles that are used for rapid cooling (quenching) to a specific temperature [4].

2.1.1 Energy Audit

Energy audits is a systematic approach and an effective energy management tool to understand and analyze energy consumption of an industry facility. It helps an industry by giving them in depth view of energy streams, which in turn helps them areas where they are losing energy and where there are opportunities to increase energy efficiency in a viable fashion. These savings results in reduction of electrical bill, increase the life of equipment and reduces GHG emissions. Since, the paper deals with energy management of cooling tower fan, the details of energy audit will be directed at cooling tower fan. [1,3,5,6]

2.1.2 Energy Audit Objectives

Using R Saidur et al. [5,7] approach, following are the objectives that can be considered for TMT air cooling tower audit:

- To identify the energy consumption pattern of cooling tower in the industry.
- To implement ways to reduce energy consumption in a cooling tower
- To provide a benchmark for energy usage of cooling tower for other industries.
- Identify energy wastages in cooling tower.

2.1.3 Energy Audit Process

In order to identify, implement and reap energy savings in a sustainable fashion, an energy management program is required as shown in Figure 1.

2.1.4 Data needed for a TMT Air-Cooling Tower Fan Audit

Using the approach mentioned in [1,5], following are the most important data that are needed for energy analysis:

- load factor
- production figure
- power rating
- power factor
- duty factor (hours of operation/year)
- motor load profile
- utility bill
- demand uses

- volume flow rate of water
- temperature
- pressure

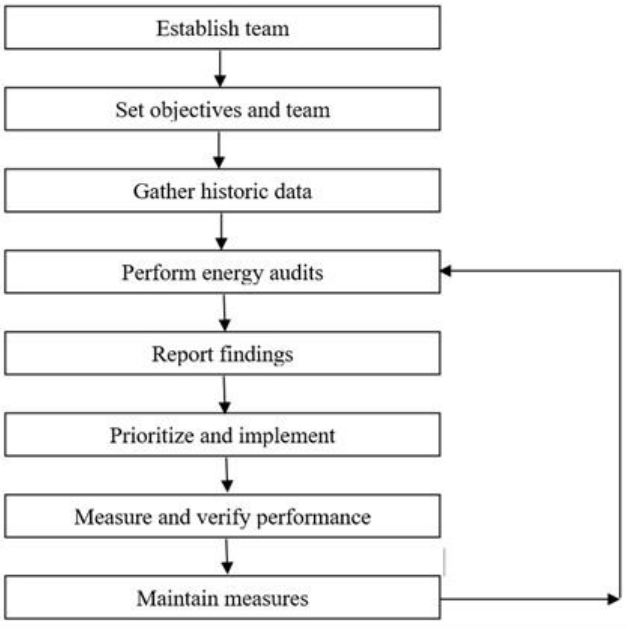

Fig.1. A typical energy management process (reproduced) [5]

2.2 Air-Cooling Tower Fan Energy Savings

There are six air-cooling towers each with its own fan. The air-cooling towers are controlled by building management system (BMS), however, there is no system control to change the speed of the motor for variable water flowrate. Furthermore, each fan has a motor of rate power of 22 hp and power is supplied by local electric company with a 3-phase AC power lines. The voltage and current rating of the motor approximately 400 V and 266 A.

Since the electric motor systems are designed to operate at a maximum load, and the time of operation at full load is less frequent. This results in energy wastage. This wastage can be reduced significantly by improving operating practices and using alternatives and energy efficient devices already available in the market [2,5,7].

According to affinity laws of turbomachinery, the power required by the motor to drive the turbomachinery depends on the cube of the speed of the motor. Hence, small reductions in speed of motor results in large energy savings. Moreover, this reduction in speed may be improve performance and life of equipment. [2,5,7]. For this experiment, the TMT cooling tower circuit is shown in Figure 2 and is operating at full load at all times, through the control system called Building Management System (BMS).

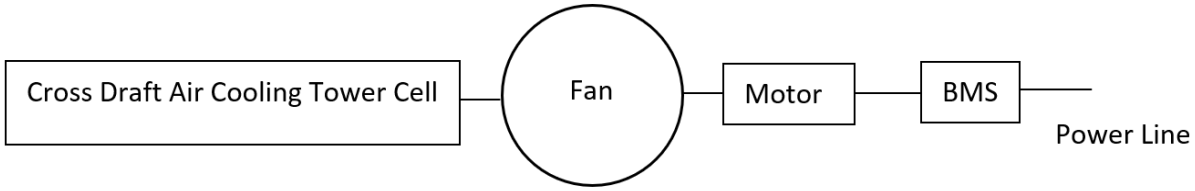

Fig.2. Schematic TMT cooling tower (Reproduced) [3]

Since the water flow varies in TMT process, VFD is the most economic and efficient way to meet the varying flow requirements. VFD can be integrated with a control system like BMS to control the speed of fan in the air cooling by regulating the speed of motor. Thus, giving more process control and energy savings instead of operating at full load always. The schematic of an air-cooling tower using VFD is shown in Figure 3.

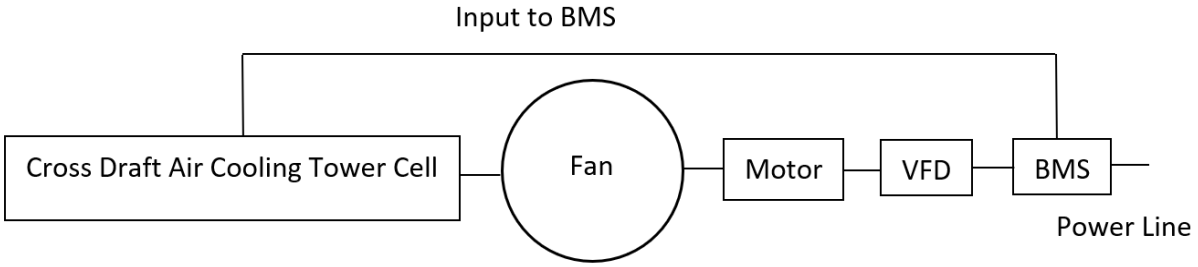

Fig.3. Schematic of TMT cooling tower operations using VFD (Reproduced) [3]

2.2. **Calculations**

As discussed, VFD is the most popular and efficient way to derive energy savings from the electric motor with frequent varying loads. From affinity law of turbomachinery shown in equation 1, It can be observed that there is a significant effect on energy consumption of an air cooling brought by a small change in electric motor speed.

$$P_2 = \left(\frac{n_2^3}{n_1^3}\right) \times P_1 \qquad \text{(Equation 1)}$$

During the energy audit, power consumption with and without VFD are calculated in order to compare and analyze the feasibility of an investment. This can be estimated using following mathematical expressions:

$$P = \frac{H \times Q \times \gamma}{3963 \times \eta} \qquad \text{(Equation 2)}$$

Where, P, H, Q, γ and Ƞ represents the air-cooling tower motor horsepower, total head, flow rate, specific gravity of working fluid and fan efficiency respectively. Pumps energy consumption using a VFD (on annual basis) can be estimated using the following equation:

$$E = P \times .746 \times (\%t) \times T \qquad \text{(Equation 3)}$$

Where, E, %t and T depicts the annual energy consumption, time utilization factor at a certain flow rate and total operating time in a year respectively.

The annual energy savings using VFD can be found by comparing the energy consumption of fan with and without VFD. These savings then can be converted into monetary terms using energy tariff. Hence a positive impact on industry's profits. Moreover, this energy savings, will also decrease environment emissions from fossil fuels used for power generation. The annual energy savings and environment emissions can be related in the following mathematical expression:

$$E_e = f \times E \times \Delta F \quad \text{(Equation 4)}$$

Where, Ee, f and ΔF represents the environment emissions, emission factor and fraction of fuel, used to generate electricity, respectively. The sum of every fuel can be calculated for total environment emissions using fossil fuels. Furthermore, the emission factor displayed in Table 1 for each fuel can be utilized to the positive change in emissions by using a VFD.

To verify the feasibility of installing a VFD on cooling tower fan, a simple payback analysis can be used to get an insight the time period to recover the investment cost. Using the mathematical expression below, simple payback period can be calculated:

$$PB = \frac{I_c}{e_t \times ES} \quad \text{(Equation 5)}$$

Where PB, I_c, e_t and ES represents the simple payback period, investment cost, energy tariff and annual energy savings respectively. The above analysis and mathematical expressions are used by R. Saidur et al. [1,3,5,7].

Table.1. Emission factor of fossil fuels used for power generation

Fuels	*Emission Factor (kg/kWh)*			
	CO2	SO2	NOx	CO
Coal	1.18	0.0139	0.0052	0.0002
Petroleum	0.85	0.0164	0.0025	0.0002
Gas	0.53	0.0005	0.0009	0.0005
Hydro	0.00	0.000	0.0000	0.0000
Others	0.00	0.000	0.0000	0.0000

3. Results and Discussion

TMT facility in this case have 6 similar air-cooling tower cells. TMT facility operates by keeping 4 cells operational and two for standby. The duty cycle observed for one fan on average is shown in Figure 4.

The fan has a motor of rate power of 22 hp with a rpm of 1800, and developing a head of 69 m and a flow rate of 180 m3/hr. Using Equations (2) and (3) annual energy consumption (E) can be calculated for the system with and without VFD, assuming the efficiency of the system to be 91% and energy tariff to be 0.22 $/kWh. The difference in annual energy consumption in both systems can be used to calculate annual energy savings (ES) and profit incurred using VFD as shown in Table 2.

Furthermore, Figure 5 depicts that using a VFD consumes 52188 kWh while current practices consumes 119720 kWh annually as it operates on full load. Hence, resulting in annual saving of around 67532 kWh. Similarly, it can be observed from Table 2 that from current practices of having no control the speed results in an annual operating cost of $26338, while using VFD incurs an annual operating cost of $ 11481. The difference in these two values is $14857 showing a marginal cost reduction in electrical bill as observed in [5,7,8].

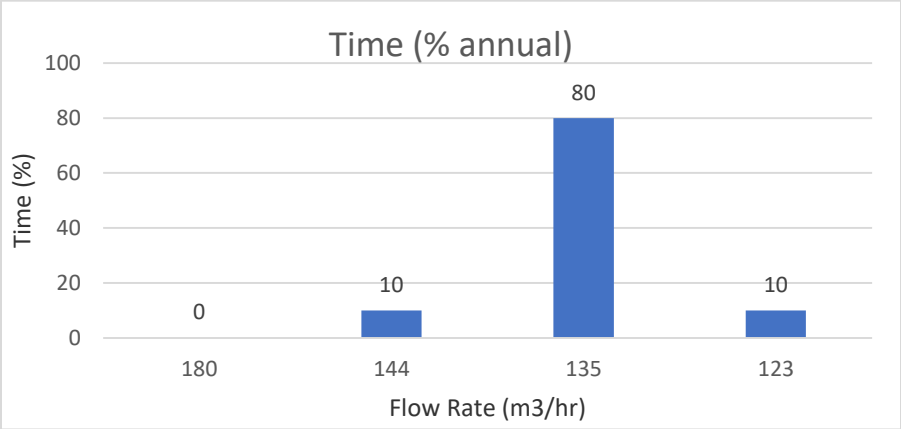

Fig.4. Time cycle of an Air-Cooling Tower Fan

Moreover, to keep business feasibility in perspective, simple payback equation (5) is used to show that VFD are a viable option to save energy as it has a small recovery period of around 10 months with an investment cost of $125000 for six fans.

Table. 2. Cost savings associated with VFD system

Type of flow control device	Annual cost of operation ($)
Current Practice	26338
VFD	11481
Annual cost savings ($)	14857

Furthermore, Honeywell VFD saver is used to verify the economic benefits presented above. Using the type of flow controlling device. Using the motor rated capacity, type of flow control device and operation time, the savings are shown in Figure 6. Honeywell VFD saver shows a saving of $ 18977 compared to previously calculated value of $14857. This change could be attributed to the assumption taken by Honeywell estimator by averaging the flow of fan to 60% and simplified approach for calculating savings.

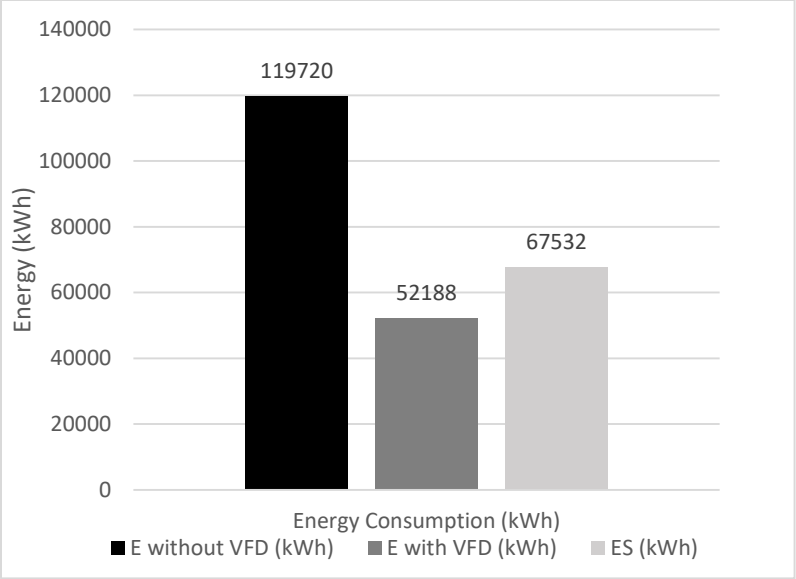

Fig.5. Comparison of Annual Energy Consumption

Finally, environment emissions and reduction in them can be calculated using values from Table 1 and equation (4). Assuming that power is generated from natural gas always, emission associated with and without VFD control system has been estimated and are tabulated in Table 3. Using VFD, a reduction of 35792 kg of CO2 is estimated on annual basis which shows 56% decrease from current practices.

Annual Energy Savings Estimator for Variable Frequency Drives (VFDs) on HVAC Applications (Fans and Centrifugal Pumps)

Compares VFD capacity control versus other types capacity control.

To make Comparisons and Estimate Savings, need to know following:

a. Motor horsepower.
b. Cost of KwH of electricity.
c. Total hours of operation per year.
d. Present method of capacity control (guide vanes, fan curves, discharge vanes, control valves, etc.) that VFD will replace.

Step 1: Converting motor Horsepower to Kw

22 HP x .746 = 16.412 Kw_A

Step 2: Multiply the Adjustable Frequency Drive Power Ratio (from table below) times Kw_A from Step 1.

0.28 Ratio x 16.412 Kw_A = 4.59536 Kw_B (using VFD)

Step 3: Multiply the Power Ratio of the presently employed control (see below) times Kw_A from Step 1.

1 Ratio x 16.412 Kw_A = 16.412 Kw_C (method now employed)

Step 4: Subtract Step 2 Kw_B from Step 3 Kw_C.

16.412 Kw_C - 4.59536 Kw_B = 11.8166 Kw_D (savings using VFD)

Step 5: Multiply Step 4 KW_D savings, times hours per year of operation, times cost of electricity per KwH.

11.8166 Kw_D x 7300 Hrs x $0.22 $/KwH = $18977.5 VFD Annual Calculated Savings

Fans at 60% of maximum flow	
Ratio	**Flow Control Method**
0.28	Variable Frequency Drive
0.62	Inlet Guide Vane
0.88	Outlet Damper
0.88	Fan Curve
1.00	Bypass Damper

Pumps at 70% of maximum flow	
Ratio	**Flow Control Method**
0.40	Variable Frequency Drive
0.94	Discharge Valve
1.00	Bypass Valve
1.00	No control

Example: A 40 Hp VAV Discharge Fan motor, with an Outlet Damper, is running 14 hours per day, six days per week (4368 hours per year). Local electric charge is $0.127 per KwH.

Step 1: 40Hp x .746 = 29.84Kw_A

Step 2: .28 Ratio x 29.84Kw_A = 8.36Kw_B

Step 3: .88 Ratio x 29.84Kw_A = 26.26Kw_C

Step 4: 26.26Kw_C - 8.36Kw_B = 17.9Kw_D

Step 5: 17.9Kw_D x 4368Hrs x $0.127/KwH = $9929.77 in annual savings

The "maximum flow" of fans and pumps is based on the accepted assumption that they operate at 60% and 70% of maximum flow or capacity rates respectively, in HVAC applications.
The same accepted assumption is true of the "Ratios" of various flow control methods.
Substantiation data may be found in the ASHRAE Handbook, HVAC Applications Volume.

Savings are based on conservative assumptions and do not include any additional savings associated with improving the Power Factor with VFDs (~.98), reducing Demand Charges, and increasing Electric Rates.

Fig.4. Modeling in Honeywell VFD Estimator

Table. 3. Comparison of Annual Environmental Emissions

Flow Controlling Device	Annual Energy Consumption (kWh)	Annual environmental emissions (kg)			
		CO2	SO2	CO	NOx
Throttling Valve	119720	63452	60	60	108
VFD	52188	27659	26	26	47
Reduction in Emissions	67532	35792	34	34	61

4. Conclusion

In this paper, it was observed that VFD is a better option when compared to current practices. VFD proves to be feasible option both economically and environmentally to control the flowrate as per demand. By reducing the operating cost by $14857, VFD delivers economic benefits for a small investment with a short payback period. Moreover, the savings are verified by Honeywell estimator. Similarly, the amount of CO2 emission of fans using VFD is 27659 kg, white it is 63452 kg without VFD showing that VFD has a positive impact on environment by reducing environment.

Notation

P = Power rating of the motor

n = rpm of the motor

H = Height provided by the fan

Q = Flowrate of the fan

Ƞ = Efficiency of the fan

γ = Specific weight of the fluid

E = Annual energy consumption

%t = Time utilization factor

T = Annual operating time

Ee = Environmental emissions

f = Emission factor

ΔF = fraction of fuel

PB = Payback period

Ic = Investment Cost

et = Energy Tariff

ES = Energy savings

References

[1] R Saidur. A review on electrical motors energy use and energy savings.Renewable and Sustainable Energy Reviews. 2010;14:877–898.

[2] Sirojiddin Khushiev, Oybek Ishnazarov. A brief review on different applications of Variable Speed Drive (VSD) in electrical motor energy savings and energy use. International Journal of Engineering Innovation & Research. 2015;4:2277 – 5668.

[3] R Saidura, S Mekhilef, MB Ali, A Safari, HA Mohammed. Applications of variable speed drive (VSD) in electrical motors energy savings. Renewable and Sustainable Energy Reviews. 2012;16:543– 550.

[4] J Hoffmann, M Rieth, M Klimenkov, S Baumgärtne. Improvement of EUROFER's mechanical properties by optimized chemical compositions and thermo-mechanical treat ments. Nuclear Materials and Energy. 2018;16:88–94.

[5] R Saidur, NA Rahim, M Hasanuzzaman. A review on compressed-air energy use and energy savings. Renewable and Sustainable Energy Reviews. 2010;14:1135-1153.

[6] Wayne C Turner, Steve Doty. Energy Management Handbook 7th edition. Fairmont Press. 2009.

[7] R Saidur, M Hasanuzzaman, TMI Mahlia, NA Rahim, HA Mohammed. Chillers energy consumption, energy savings and emission analysis in an institutional buildings. Energy. 2011;36:5233-5238.

[8] R Saidur, M Hasanuzzaman. Energy and environmental analysis of electrical motor in industrial boilers. Proceedings of 3rd International Conference on Energy and Environment, Malacca, Malaysia: 2009. p. 427-435.

[9] David E Rice. A suggested energy-savings evaluation method for AC Adjustable-Speed Drive applications. IEEE transactions on industry applications. 1988;24:1107-1117.

[10] Honeywell. quick vfd estimator (accessed on 8 July 2020). Available from https://customer.honeywell.com/en-US/support/commercial/se/vfdq/Pages/default.aspx

[11] Neetha John, Mohandas R, Suja C Rajappan. Energy saving mechanism using Variable Frequency Drives. International Journal of Emerging Technology and Advanced Engineering. 2013;3:784-790.

[12] Seouk Park. Fully numerical analysis for effects of cooling water flow rate and plate running speed on steel plate cooling in very high temperature region. ISIJ International. 2011;51:1864–1869.

[13] M Benhaddadi, G Olivier, B Dima. Energy savings by means of generalization Adjustable Speed Drive utilization. Proceedings of Canadian Conference on Electrical and Computer Engineering. Vancouver, Canada:2007. p.389-392.

[14] Brune R Munson, Donald F Young, Wade W Huebsch. Fundamentals of fluid mechanics 7th edition. John Wiley and Sons. 2013.

A numerical analysis of pcm based heat sink with triangular and rectangular pin-fins

Talal Bin Irshad[1], Yousif Muhammad[2], Rui Costa Neto[3]

[1]University of Engineering and Technology, e-mail: talalbinishad@gmail.com
[2]Technical University of Lisbon, e-mail: Muhammad.yousif@tecnico.ulisboa.pt
[3]Technical University of Lisbon, e-mail: costaneto@tecnico.ulisboa.pt

Abstract

This study uses numerical methodology to emphasize the improvisation in passive cooling techniques of integrated circuit using PCM (Phase Change Material) based pin fin heat sinks acting as the TCE (Thermal Conductivity Enhancer). This investigation uses variation in pin-fin cross section by introduction of triangular and rectangular geometries in aluminum heat sinks. Three different PCMs namely RT-54, RT-44, and RT-35 HC with varying melting temperatures, latent heats and heat capacities are used for their heat absorbing trait. Furthermore, heat input is varied between the range of 4 and 8 W. The data deduced from the simulation is analyzed for the effect of PCM on a heat sink. Triangular pin fins achieve the maximum heat transfer with RT-35HC at 5W and RT-54 at 8W. All numerical computations were performed using COMSOL Multiphysics 5.5.

Keywords: phase change material, heat sink, numerical analysis

1. Introduction:

Consumer electronic devices have gained a considerable amount of recognition in past 3 decades. Integrated Circuits in these electronic devices are repeatedly producing immense heat and have been proved to function best in a specified temperature range. This concern calls for an effective technology to be designed for removal of the unwanted heat. Power consumption and noise production by active cooling methods renders them unsuitable for modern electronics. As a substitute, submissive cooling technique using PCMs has been largely considered due to its advantage of high latent heat of fusion and specific heat, making it feasible for application in realtime devices like laptops, mobile phones, hand held and portable devices. This shall increase its reliability, enhance functionality, make operations more efficient and provide protection against damages in ICs due to thermal stresses. Many numerical and practical investigations have been carried out to eliminate such issues, providing a broad spectrum of knowledge of PCMs in the field of heat transfer.

Baby and Balaji[1] experimentally investigated the performance of PCM based heat sinks for enhancement of the operation duration against various set point temperatures and increased span of latent heat, using *Pin-fin*s as TCEs. These authors[2] also explored the thermal characteristics of heat sinks with different number of *pin-fin*s with varying volume fractions. Overall the *pin-fins* considerably stretched the operation time of the electronic device and the latent heat phase was found to be elongated. In addition, an Artificial Neural hybrid algorithm was also developed to find the *pin-fin* heat sink configuration to maximize the operating time for the two PCMs[3]. The heat sink matrix performance for system with and without PCM under constant and varying heat fluxes. The results showed that the intermittent use of heat sinks with PCM at high power levels shows significant decline in temperature[4].

Ashraf et al.[5] investigated PCM filled heat sinks with square and circular configurations for staggered and inline arrays. The volume fraction was kept constant, six PCMs were used with heat input range of 5–8W. The results suggested circular inline as the most efficient choice for a PCM based heat sink and square staggered for without PCM.

Fok et al.[6] performed experimental study on the application of PCMs at power level ranging from 3 to 5 W, for light working conditions. The results summed up that TCE with PCM was feasible option for cooling hand-held electronic devices as it enhanced their operational duration. Hu et al.[7] studied the electronic devices at intermittent thermal load focusing on the latent heat storage property of the passive cooling method. The author concluded that the selection of PCM is made on basis of specific working conditions. With the increasing values of quantity of PCM, the operational duration stretched but its uselessness for the lower power levels was also visible. Pakrouh et al.[8] presented an investigation for geometric optimization of pin fin heat sinks using RT-44HC as PCM. The Taguchi method was used to numerically simulate results. Factors like convection, PCM volume and different aspects of fins were studied for optimization. Anzar and Azeem [9] simulated the thermal analysis of various arrangements of finned heat sinks with and without PCM for different air flow conditions. The duration to control the temperature of PCM for forced convection conditions to various PCM fraction levels were recorded.

Wang et al[10] numerically evaluated the thermal properties of a PCM-based aluminum heat sinks. Results indicated increased thermal performance of the system. Soodphakdee et al.[11] worked on the heat transfer performance of different fin geometries. The pin fins are studied for inline and staggered arrays. The numerical analysis was carried out with the staggered plate fin geometry showing the highest heat dissipation for the given flow rate. Kumar et.al [12] reviewed PCM based heat sinks using pin-fins, metallic foams and nano-particles. In short, the nano-particle based heat sinks performance was ineffective for the increasing power levels. Overall the metallic foam was found to have highest thermal conductivity.

Considering all the latest studies performed on PCM based pin-fins, this work focuses on providing a practical application for cooling of consumer electronics. Square and rectangular pin-fin geometries with inline arrays are the limelight of present research work to develop most efficient passive cooling. Many PCMs are also studied giving an insight to their properties and relative effect on thermal performance of PCM based heat sink. Moreover, variations of PCMs and their heat absorbent properties are used in combination with the thermal conductivity enhancement associated with aluminum pin-fins. These characteristics account for the uniqueness of this study. Therefore, this model is intended to produce resourceful comparisons for all the factors being considered in this study and results prove this comprehensively.

2. Physical Model:

This study features the comparison of the three shapes of pin-fins, namely square, rectangular and triangular. Fig 1 shows the isometric view of Heat sink under study.

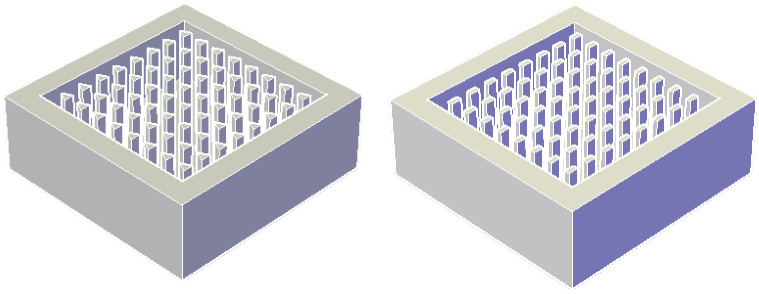

Fig 1: Isometric view of, Rectangular and Triangular pin-fin

The dimensions of rectangular fins are 1.5 x 3 mm^2 and the base of triangular fins is 1.5mm wide and 1.5mm long. The total number of fins are 64 for rectangular and triangular. The PCM is placed inside the heat sink with dimensions of 57 × 56 × 20 mm. The heat sink was equipped with an area of 50 × 50 mm with a thickness of 2 mm to accommodate electric heater. Fig 2 shows the configuration of heat sink and PCM configuration.

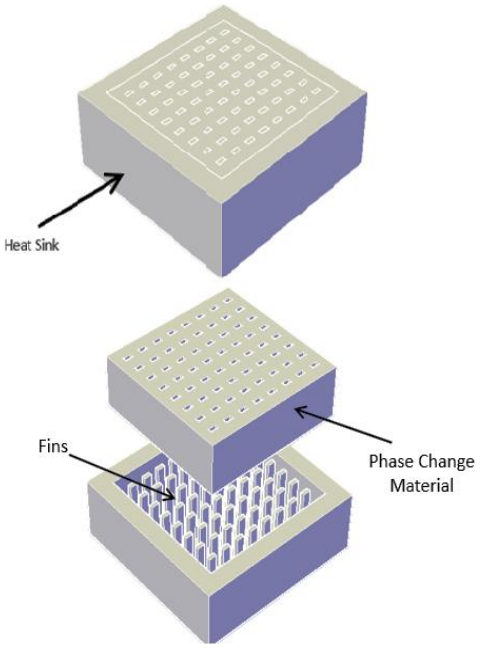

Figure 2: Heat Sink and PCM Configuration

Three PCMs are taken into consideration for this study. These PCMS are RT-54, RT44, and RT-35HC (RUBITHERM®) [13] All the selected materials have different melting temperature ranges between 34 ˚C and 54 ˚C. The thermo physical properties of aluminum heat sink and PCM are given in table 1:

Table 1: Properties of different materials involved in analysis

Material	***k (W/mK)***	***Cp (kJ/kgK)***	***L (kJ/kg)***	***Tm (˚C)***	***ρ (kg/m³)***
Aluminum	180	963	289	660.4	2700(S)
RT-54	0.2	2	200	54	800(L)
					850(S)
RT-44	0.2	2	250	44	700(L)
					800(S)
RT-35HC	0.2	3	240	34	770(L)
					880(S)

3. Governing Equation and Boundary Conditions:

Melting of PCM is a Solid-Liquid interface problem. The melting process of the PCM is modelled using enthalpy-porosity formulation. It is a single domain approach where a system of momentum and energy equations is solved in the entire physical domain.

Total specific enthalpy of the PCM is equal the sum of sensible heat and the latent heat.

$$h_{pcm} = h_s + h_l$$

Average specific heat of the PCM,

$$C = \frac{\int_0^T C_p(T)dt}{\int_0^T dt}$$

$$h_s = CT = \int_0^T C_p(T)dt$$

Latent heat is defined in piece wise function form as

$$h_l = \begin{cases} \text{If } T > T_{liquid} \\ \left[\frac{T-T_{solid}}{T-T_{Liquid}}\right] L \quad \text{If } T_{solid} < T < T_{liquid} \\ \text{If } T > T_{solid} \end{cases}$$

The Enthalpy of heat sink is measured as:

$$h_{al} = C_p T$$

The boundary conditions are applied corresponding to the experimental work.[14]

4. Results and Discussion:

In order to understand the thermal performance of heat sink, analysis is performed for a constant heat input of 5W to 8 W. To understand the effects of different PCMs, an analysis is also made with empty heat sink. The heat sink imitates the surface of chips and ICs, therefore, the temperature gain at the base section is of important consideration. Lesser temperature at this section accounts for higher heat transfer rate prolonging the life of electronic component.

4.1. Base Temperature Comparison without PCM:

This comparison is done before pouring the PCMs into the heat sink to understand the performance of PCMs effectively. All four power level are studied but for reference only 5W and 8W are discussed here. Fig. 3 shows the results for 5W and 8W respectively.

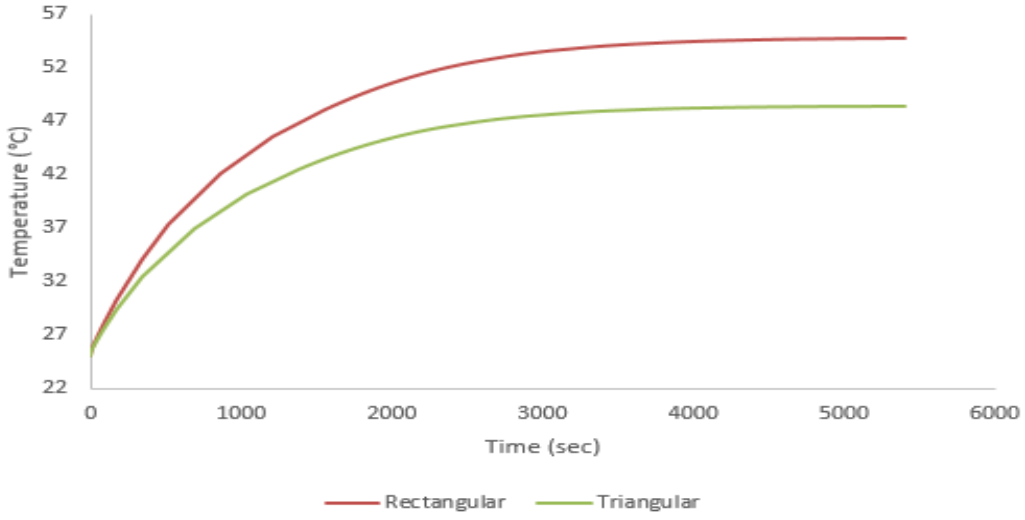

(a) At 5W

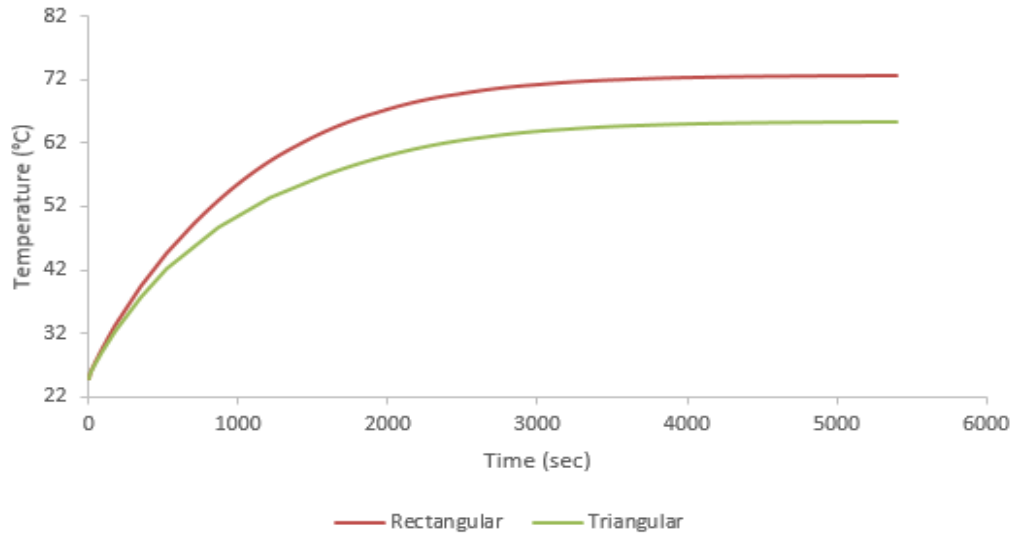

(b) At 8W

Fig. 3: Temperature distribution of different pin-fin configuration without PCM

The heat sink are studied for the operational time of 5400 seconds (90 minutes). In Fig. 3a, a clear temperature difference can be observed in between two different pin-fin configurations at a power level of 5W. The rectangular pin-fin has the temperature of 55°C and the triangular pin-fin is the most effective with maximum temperature of 48°C. Similarly, in Fig. 3b, the same trend is observed for 8W, where the maximum temperatures are 72°C and 63°C for rectangular and triangular pin-fins respectively. Hence, the triangular pin-fins proved to be dominant in heat transfer over the rectangular pin-fins which are better than the circular fin-pins.

4.2. **Base Temperature Comparison with PCM:**

This comparison is done in between heat sinks with PCM to study the base temperature of PCM. Three PCMs RT-35 HC, RT-44, and RT-54 are studied in heat sinks with Rectangular and Triangular Pin-fin configuration. This study is

also done at 5W and 8W. The Fig. 4 shows the temperature distribution of different pin-fin configuration with PCM and 5W and 8W.

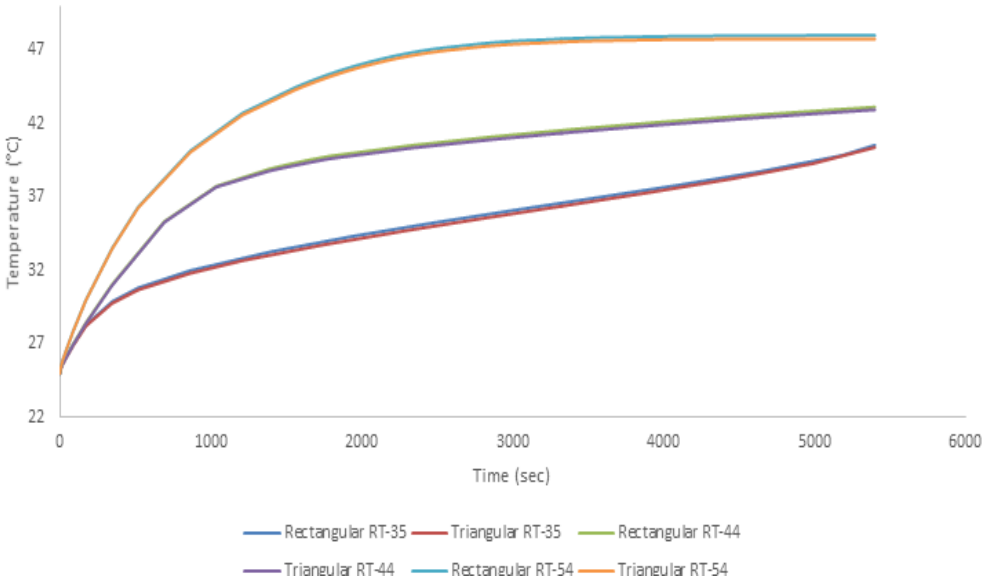

(a) At 5W

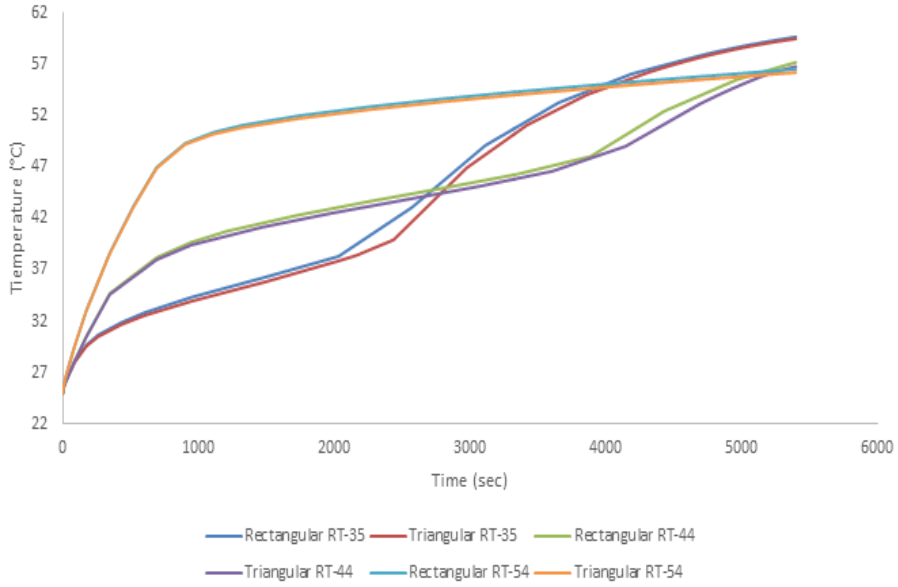

(c) At 8W

Fig. 4: Temperature distribution of different pin-fin configuration with PCM

Fig. 4a, shows the comparison of PCMs and heat sinks at 5W. The PCMs show a smooth graphical curve for all heat sinks. For RT-35 HC, Triangular pin fin configuration is most effective with the maximum temperature of 40 °C, whereas the Rectangular pin fin shows a temperature of 41°C which is less effective than Triangular pin fin configuration. Similarly, for RT-44 has a minimum temperature of 42°C for Triangular pin fin configuration and maximum temperature of 43°C for Rectangular pin fin configuration. The same trend is observed for RT-54, triangular pin fin configuration has a temperature of 47°C while the rectangular pin fin has a temperature of 48°C.

Fig. 4b, shows the temperature comparison at 8W. For RT-35 HC, first there is a constant temperature profile for some duration then a sharp curve in temperature profile can be observed. For RT-44, first there is a sharp curve, then a smooth temperature profile and again a sharp curve in temperature at the end. For RT-54, there is a sharp increase at the start and then a constant temperature profile can be observed. This trend in observed due to latent heat of the PCM, which provide a smooth profile to the temperate and maintain the constant temperature unless its phase is changed completely. After phase change a sharp increase can be observed in RT-35 HC and RT-44 because during Phase change, the temperature stays constant.

Fig. 5 shows the contours of temperature distribution inside Triangular PCM for RT-35 HC, RT-44 and RT-54 at 8W.

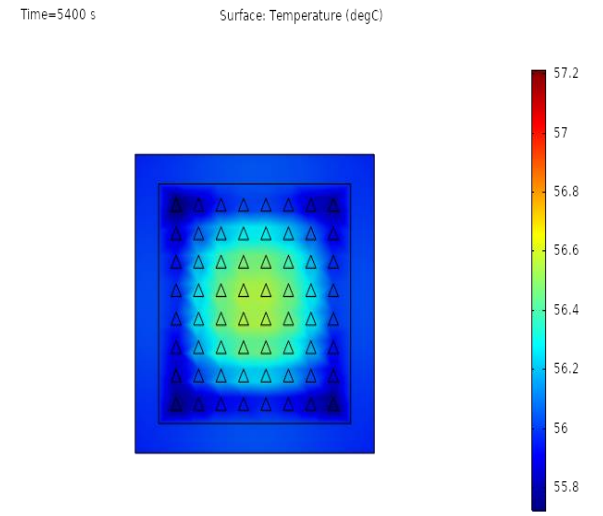

(a)

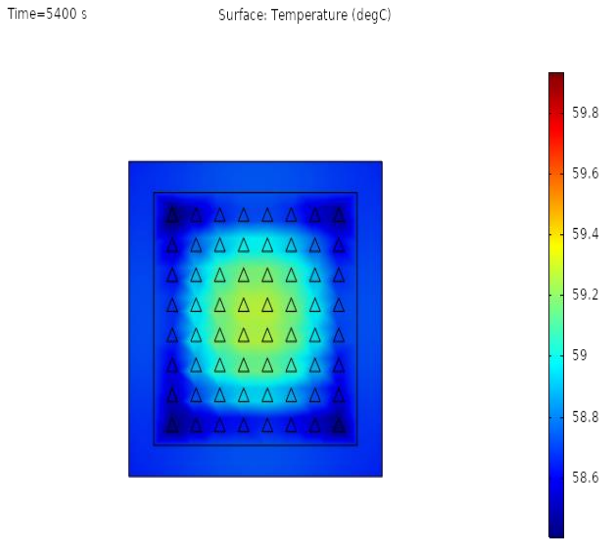

(b)

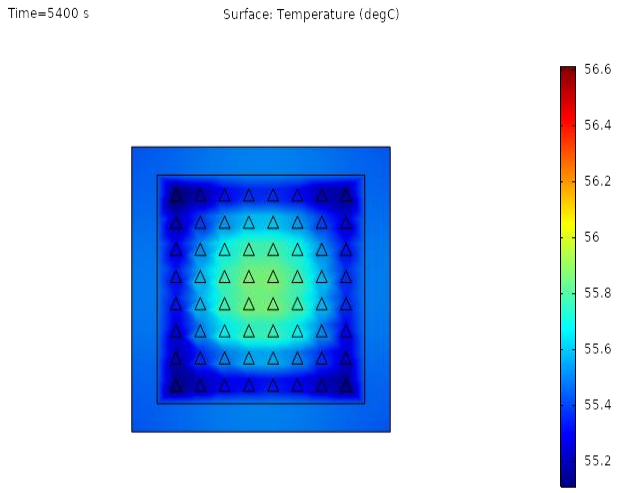

(c)

Fig. 5: Temperature variation in Triangular pin-fin configuration (a) RT-35 HC (b) RT-44 (c) RT-54 for 8W at 5400 sec

The same trend is observed for 8W study with different pin fin configuration using different PCMs as it was done for 5W. The Triangular fin-pin dominate with the maximum observed temperature of 59°C, 57°C and 55°C for RT-35 HC, RT-44, RT-55 while the Rectangular pin-fin observed the maximum temperature of 60°C, 58°C and 56°C for RT-35 HC, RT-44, RT-55 respectively.

5. Conclusion

Numerical investigation was carried out to evaluate the ideal combination for the passive cooling of ICs at constant heat load in the range of 4 W to 8 W. The pin fin configuration was varied between Triangular and Rectangular configuration. Three PCM were studied to evaluate the best results in term of minimum base temperature. Triangular pin fin has proven the best pin fin configuration for heat sink as it offer the minimum base temperature for all studied PCMs. The study of various PCMs at 5W and 8W suggested that RT-35 HC offered the minimum base temperature at 5W and RT-54 offered minimum base temperature at 8W.

References:

[1] Baby R, Balaji C. Experimental investigations on phase change material based finned heat sinks for electronic equipment cooling. *Int J Heat Mass Transf*. 2012;55(5-6):1642-1649.

[2] doi:10.1016/j.ijheatmasstransfer.2011.11.020

[3] Baby R, Balaji C. Thermal management of electronics using phase change material based pin fin heat sinks. *J Phys Conf Ser*. 2012;395(1). doi:10.1088/1742-6596/395/1/012134

[4] Baby R, Balaji C. Thermal optimization of PCM based pin fin heat sinks: An experimental study. *Appl Therm Eng*. 2013;54(1):65-77. doi:10.1016/j.applthermaleng.2012.10.056

[5] Baby R, Balaji C. Thermal performance of a PCM heat sink under different heat loads: An experimental study. *Int J Therm Sci*. 2014;79:240-249. doi:10.1016/j.ijthermalsci.2013.12.018

[6] Ashraf MJ, Ali HM, Usman H, Arshad A. Experimental passive electronics cooling: Parametric investigation of pin-fin geometries and efficient phase change materials. *Int J Heat Mass Transf*. 2017;115:251-263. doi:10.1016/j.ijheatmasstransfer.2017.07.114

[7] Fok SC, Shen W, Tan FL. Cooling of portable hand-held electronic devices using phase change materials in finned heat sinks. *Int J Therm Sci*. 2010;49(1):109-117. doi:10.1016/j.ijthermalsci.2009.06.011

[8] Hu J, Guo T, Zhu Y, Hu R, Luo X, Cheng T. Effect of melting temperature and amount of the phase change material (PCM) on thermal performance of hybrid heat sinks. In: *2014 15th International Conference on Electronic Packaging Technology*. IEEE; 2014:48-52. doi:10.1109/ICEPT.2014.6922584

[9] Pakrouh R, Hosseini MJ, Ranjbar AA, Bahrampoury R. A numerical method for PCM-based pin fin heat sinks optimization. *Energy Convers Manag*. 2015;103:542-552. doi:10.1016/j.enconman.2015.07.003

[10] Anzar, Azeem and Hafiz, PA Azeem and Ashiq, N and Shaheer M. Heat transfer analysis on PCM based heat sink incorporated with air convection. *Int J Sci Eng Res*. 2018;7(4):441-456.

[11] Wang X-Q, Yap C, Mujumdar AS. A parametric study of phase change material (PCM)-based heat sinks. *Int J Therm Sci*. 2008;47(8):1055-1068. doi:10.1016/j.ijthermalsci.2007.07.016

[12] Soodphakdee, Denpong and Behnia, Masud and Copeland DW. A comparison of fin geometries for heatsinks in laminar forced convection: Part II-Optimization of staggered plate fin heatsink. *Int J microcircuits Electron Packag*. 2001;24(1):77-83.

[13] Sahoo SK, Das MK, Rath P. Application of TCE-PCM based heat sinks for cooling of electronic components: A review. *Renew Sustain Energy Rev*. 2016;59:550-582. doi:10.1016/j.rser.2015.12.238

[14] "Rubitherm GmbH." Rubitherm GmbH, Gemany. N.p., n.d. Web. 2016; available from: https://www.rubitherm.eu/. https://www.rubitherm.eu/

[15] Ali HM, Ashraf MJ, Giovannelli A, et al. Thermal management of electronics: An experimental analysis of triangular, rectangular and circular pin-fin heat sinks for various PCMs. *Int J Heat Mass Transf*. 2018;123:272-284. doi:10.1016/j.ijheatmasstransfer.2018.02.044

Development of energy system: power generation by weight of automobile

Muhammad Azam Hafeez[1]

[1]*University of Engineering and Technology, e-mail: azam.hafeez@live.com*

Abstract

The work undertaken is a step towards a new mean of generating electric power which can contribute a substantial amount of energy towards power sector. Energy crisis across the globe has become a serious threat, particularly to under developing countries. In this scenario, there are two possibilities either to improve the performance of energy conservation methods or to discover new energy sources like renewables. The power generation using weight force is an endeavor to cope with the increased energy crisis. This method is cheap and ecofriendly. A brief concept of the plant is summarized below:

"The utilization of weight force causing an increase in the air pressure, stored in air accumulators, impinging on an impeller which is coupled to the dynamo will produce electric current". When an automobile passes over the flexible speed breaker, the force is transmitted to the air through the piston-cylinder assembly, increasing pressure of the air which is then stored in the accumulators. This high pressurized air strikes on an impeller, which is coupled with the generator shaft to produce electricity.

Keywords: Weight force, speed breaker, clean energy, power generation, mathematical modeling, Bernoulli's model for compressible flow, choked flow

1. Introduction

The article contains the innovative and advanced work in the field of mechanical engineering i.e. power generation by weight of automobile. The work is basically the design and development of pneumatic-based accumulation speed breaker. In this venture, efforts have been made to generate electricity with no carbon footprints. Motivation behind perceiving the work was to address the energy crisis and environmental issues in Pakistan. Keeping in view the present scenario, where other resources keep on lessening with the time as well as with the consumption e.g. fossil fuels therefore, it has been concluded that apart from various other sources to generate electric power, one could possibly be the weight energy. The major concern while utilizing a renewable source of energy is to develop a system that can generate continuous and substantial electricity. Development of this type of system just requires small amount of capital investment and then it can produce power for almost a year without much special care. The system would be able to generate a considerate amount of electric power, if installed properly.

Some work in this field has already been done to harvest the weight energy from moving vehicles in order to generate power. Different mechanisms for the working of speed breaker infrastructure have been proposed previously. It is pertinent to mention that several models have been reviewed along with their benefits and limitations. For instance, rack and pinion mechanism, which uses chain and sprocket system but causes friction related maintenance issues. Another one is the crank and shaft mechanism, which experiences balancing problem leading to mechanical vibrations. Additionally, piezoelectric roads terminology has been reviewed, which uses piezoelectric effect to convert mechanical strain into electrical current [1]. Moreover, researchers in Mexico has also devised a power generating speed breaker, which employs bellows to expel air by using the vehicular flow of traffic [2]. Furthermore, hydraulic accumulation system has also been considered for the model design but ultimately dropped because of expensive accumulator design and costly maintenance issues.

In view of above, pneumatic-based accumulation model for a speed breaker (i.e. air is being used as a working fluid) has been opted to formulate the work in this article because of its easier implantation and low maintenance concerns. The work in this article mainly contains the mathematical modeling using Bernoulli's Model for Compressible Flows based upon the design parameters for the development of prototype system model. In mathematical modeling, non-choked and choked behaviors of flow (i.e. flow of air) are analyzed in parallel with pressure ratio and mass flow rate.

The proposed system includes a speed breaker and a piston cylinder assembly as shown in Fig. 1.1. The speed breaker rests over a compression spring, and a small diameter cylinder which is connected by a hose system with two large diameter cylinders (i.e. accumulators). Accumulators are provided with a pipe through which high pressure jet is released on turbine (i.e. impeller) to generate mechanical energy. Impeller is coupled with motor to convert mechanical energy into electrical power.

When an automobile passes over the speed breaker, the weight force of the automobile is amplified through lever. This amplified force is transmitted to the small cylinder which is filled with air. Thus, the amplified force compresses air. This compressed air is stored in the accumulator with high pressure. The accumulator stores the pressurized air until its storing capacity is reached.

When the jet is discharged from the accumulator, it strikes the impeller. At that instant, the kinetic energy, which is extracted from the pressure energy, rotates the impeller. The shaft of impeller is coupled to electric generator. Hence, electrical energy is extracted from the mechanical energy.

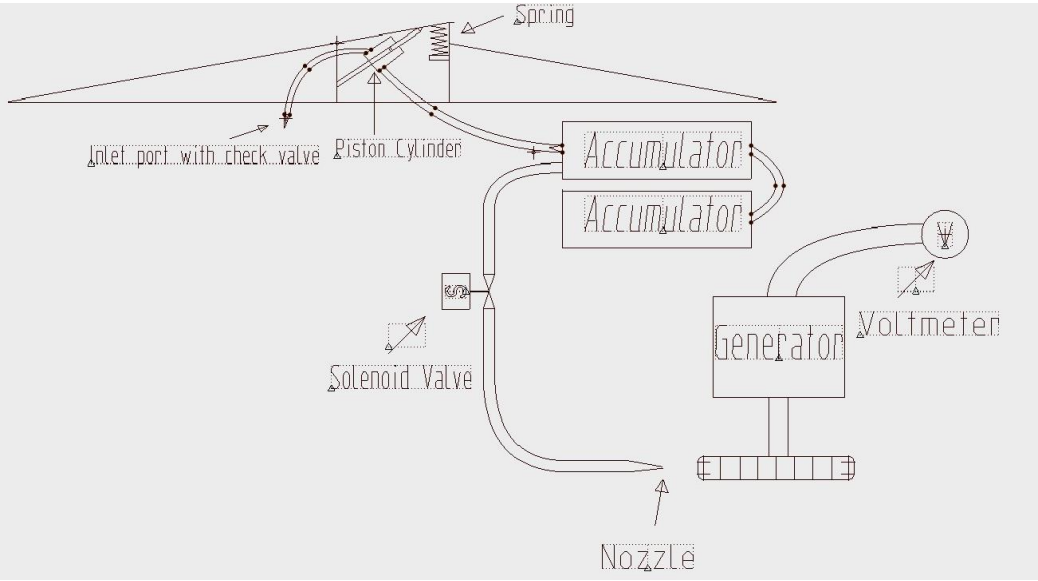

Fig. 1.1. Working Mechanism of Pneumatic-based Accumulation System Model for Speed Breaker [Formulated by using AutoCAD]

2. Basic Concepts for Pneumatic Systems

Fluid mechanics is defined as the science that deals with the behavior of fluids at rest (***fluid statics***) or in motion (***fluid dynamics***), and it also comprises the interaction of fluids with solids or other fluids at the boundaries [3]. The study of the motion of fluids that are practically incompressible (such as liquids, especially water, and gases at low speeds) is typically stated as **hydrodynamics**. **Hydraulics** is a subcategory of hydrodynamics, which deals with liquid flows in open channels as well as in pipes. **Pneumatics** is a branch of technology that deals with the study and application of pressurized gas to generate mechanical motion. **Gas dynamics** is a branch that works with the fluids' flow that goes

under the substantial density changes, like the flow of gases through nozzles at extreme velocities [3]. Pneumatic system serve as a backbone of the designed model [4].

The pneumatic machines used in the power plant are: pneumatic piston-cylinder assembly, pneumatic accumulator, and pneumatically-driven propeller generator assembly.

2.1. Governing Equations

The mathematical equations that govern the various fluid flow models for energy analysis are discussed below. Primarily, Bernoulli's equation has been stated for both compressible as well as incompressible flows. Thereafter, choked flow phenomenon relying on venturi effect has been discussed in context with the working fluid of designed model.

- **Bernoulli's Equation**

Bernoulli's equation can be derived by using the principle of conservation of energy. As, in steady flows, it formulates that, in the fluid, sum of all forms of energy is equal at every point on the streamline [5].

- **For Incompressible Flow**

$$\mathrm{P} + \frac{\rho V^2}{2} + \rho g z = constant \quad \text{(Equation 2.1)}$$

Where:

V is the fluid flow speed at a point on a streamline,
g is the acceleration due to gravity,
z is the elevation of the point above a reference plane,
P is the pressure at the chosen point, and
ρ is the density of the fluid at all points in the fluid.

- **For Compressible Flow**

Bernoulli's equation for compressible flow can be derived from Euler's Equation as [6]:

$$\mathrm{dP} = -\rho V dV \quad \text{(Equation 2.2)}$$

From Boyle's Law for adiabatic flow

$$\mathrm{P} = C\rho^{\gamma}$$

Differentiating above equation and putting this value in Equation 2.1, we get

$$C\gamma\rho^{\gamma-2}d\rho = -VdV \quad \text{(Equation 2.3)}$$

Integrating Equation 2.3, we get.

$$\left(\frac{\gamma}{\gamma-1}\right)\frac{\mathrm{P}}{\rho} + \frac{V^2}{2} = constant$$

Also,

$$\left(\frac{\gamma}{\gamma-1}\right)\frac{\mathrm{P}}{\rho} + \frac{V^2}{2} = \left(\frac{\gamma}{\gamma-1}\right)\frac{\mathrm{P_o}}{\rho_o} \quad \text{(Equation 2.4)}$$

Where;

P_O is the total pressure
ρ_O is the total density

- **Choked Flow**

Choked flow is caused because of the compressibility of the working fluid. It is a fluid dynamics condition and it corresponds with the venturi effect [7]. Whenever a fluid flows to the lower pressure environment through the throat of the nozzle, its velocity increases. Choked flow is a constraint, which takes place when there is no rise in the mass flow rate even with the further decrease in the downstream pressure [8] [9].

The minimum pressure ratios required for choked conditions to occur,

$$\frac{P_1}{P_2} \geq \left[1 + \frac{\gamma-1}{2} M^2\right]^{\frac{\gamma}{\gamma-1}} \qquad \text{(Equation 2.5)}$$

Whereas, at choked flow M = 1

$$\frac{P_1}{P_2} \geq \left[1 + \frac{\gamma - 1}{2}\right]^{\frac{\gamma}{\gamma-1}}$$

Where γ is the specific heat ratio of the gas. For air, γ = 1.4, therefore choking condition will be,

$$\frac{P_1}{P_2} \geq 1.89292$$

Thereafter, the temperature ratio is given by,

$$\frac{T_1}{T_2} = \left[1 + \frac{\gamma-1}{2} M^2\right] \qquad \text{(Equation 2.6)}$$

3. Designing Parameters of System Model

A working model has been fabricated in order to demonstrate the practicability of the power generation idea. Only a prototype of working model has been fabricated due to the financial constraint. The components used in the model system are small diameter cylinder (equipped with piston, and inlet & exhaust valves), 2 x accumulators (these are interconnected with the housing, and are serving as an energy storage device in the form of compressed air), pressure gauge, solenoid valve, nozzle, impeller & motor (max. power 60W), and electronic circuit [10]. Specifications of prototype model are given below:

Design Type	**Dimensions**
Diameter of Small cylinder (D)	0.016 m
Diameter of Accumulator (D_1)	0.11938 m
Diameter of Blue Hose (D_b)	0.005 m
Diameter of Nozzle jet (D_2)	0.002 m
Plunger Stroke (P_S)	0.01905 m
Accumulator Length (A_L)	0.2032 m
Applied Weight (model) (F)	981N (100kg)
Design Gauge Pressure of Accumulating Section	100psi = 689475.729 Pa
Design Absolute Pressure of Accumulating Section (P_1)	114.7psi = 790828.662 Pa
Density of atmospheric air (ρ_2)	1.225 kg/m^3
Atmospheric Pressure (P_2)	101325 Pa

Atmospheric Temperature (T_2)	293 K
Specific Heat ratio for air (γ)	1.4
Specific Gas constant for air (R)	287.058 J kg^{-1} K^{-1}
Maximum Motor Power	60 Watts

The area and volume of small cylinder and accumulator section is given by,

Area of small cylinder (A) $= \frac{\pi}{4}(D)^2$ = 0.000020106 m^2

Area of Accumulator (A_1) $= \frac{\pi}{4}(D_1)^2$ = 0.0112 m^2

Area of Blue Hose (A_b) $= \frac{\pi}{4}(D_b)^2$ = 0.000019634 m^2

Area of Nozzle Jet (A_2) $= \frac{\pi}{4}(D_2)^2$ = 0.000003141 m^2

Volume of small cylinder (V) $= A \times P_S$ = 0.0000038302 m^3

Volume of Accumulator (V_1) $= A_1 \times A_L$ = 0.0023 m^3

First of all, we have to check that whether the flow is choked or not, therefore using equation (2.5)

$$\frac{P_1}{P_2} = \left[1 + \frac{\gamma-1}{2} M^2\right]^{\frac{\gamma}{\gamma-1}} \qquad \text{(Equation 3.1)}$$

When flow is choked, M = 1, Therefore pressure ratio comes as,

$$\frac{P_1}{P_2} = 1.89292$$

In the designed model,

$$\frac{P_1}{P_2} = \frac{790828.662}{101325}$$

$$\frac{P_1}{P_2} = 7.805 > 1.89292$$

Therefore, it is formulated that flow will be choked. Using Bernoulli's equation between two points i.e. one is on the left side of solenoid valve, which includes the accumulator and blue hose (the condition of air on that side is stagnant) and the other point is on the right side of solenoid valve, which includes the nozzle,

$$\left(\frac{\gamma}{\gamma-1}\right)\frac{P_1}{\rho_1} + \frac{{V_1}^2}{2} = \left(\frac{\gamma}{\gamma-1}\right)\frac{P_1}{\rho_1} + \frac{{V_2}^2}{2} \qquad \text{(Equation 3.2)}$$

Since air is assumed to be stagnant on the accumulator and blue hose side therefore, the velocity $V_1 = 0$

The temperature inside accumulator can be found out by using equation (2.6)

$$\frac{T_1}{T_2} = \left[1 + \frac{\gamma-1}{2} M^2\right] \qquad \text{(Equation 3.3)}$$

[M = 1], $\frac{T_1}{T_2} = 1.2$

$$T_1 = 1.2 \times 293$$

$$T_1 = 351.6\ K$$

This is the temperature of air inside the accumulator at 790828.662 Pa.

Thus, the density at this pressure and temperature can be calculated from general gas equation,

$$\rho_1 = \frac{P_1}{RT_1} \qquad \text{(Equation 3.4)}$$

$$\rho_1 = \frac{790828.662}{287.058 \times 351.6}$$

$$\rho_1 = 7.837\ kg/m^3$$

Putting all the values in equation (3.2)

$$\left(\frac{1.4}{1.4-1}\right)\frac{790828.662}{7.837} + 0 = \left(\frac{1.4}{1.4-1}\right)\frac{101325}{1.225} + \frac{{V_2}^2}{2}$$

$$V_2 = 356.88\ m/s$$

This is the velocity at the throat of nozzle.

Velocity of air can be found by measuring the velocity of sound at that temperature because the flow is choked. Since the temperature inside the accumulator is 351.6 K and the atmospheric temperature is 293 K. Thus, the temperature of air at throat can be assumed as average of these two temperatures. By taking the average temperature as 322 K. The velocity of air can be calculated as,

$$V_2 = \sqrt{\gamma R T_{avg}}$$

$$V_2 = \sqrt{1.4 \times 287.058 \times 322}$$

$$V_2 = 359.86\ m/s$$

[This small error is because of average approximation of temperature at throat]

Now, the **mass flow rate** can be calculated from the equation,

$$\dot{m} = \rho A V \qquad \text{(Equation 3.5)}$$

$$\dot{m} = 7.837 \times 0.000003141 \times 356.88$$

$$\dot{m} = 0.008784\ kg/s$$

This is the mass flow rate across the throat of nozzle.

- **Power Output**

The peak power obtained from dynamo at 100 psi accumulator pressure (gauge) is,

Power output $\cong$ **24 W**

- **Number of Strokes**

The number of strokes of small cylinder needed to accumulate the pressure of 100 psig is given by,

$$\text{No. of stokes} = \frac{V_1}{V} = \frac{0.0023 \times 2}{0.0000038302} = 1201 \text{ strokes}$$

Therefore 1201 strokes are needed to fill the accumulator with air without compressing it, for 100psig pressure the no. of stokes needed can be obtained by multiplying it with the density ratio,

$$\text{No. of stokes} = 1201 \times \frac{\rho_1}{\rho_2} = 1201 \times \frac{7.837}{1.225}$$

$$\text{No. of stokes} = 7684 \text{ strokes}$$

3.1. MATLAB Program of the Model

MATLAB software has also been used to conduct technical computing. The main purpose of this modeling is to graphically represent, compare, and analyze the behavior of fluid flow under both un-choked as well as the choked flow conditions – Pressure inside the accumulator is used as a variable parameter. MATLAB program is shown below followed by the graphical representation of velocity at nozzle throat and mass flow rate with variable pressure ratios in Fig. 3.1. and Fig. 3.2. respectively, covering the both modes of un-choked and choked flows:

```
clear all;close all;clc;

%DESIGN OF PNEUMATIC ACCUMULATING SECTION WITH NOZZLE AT OUTLET
D = 0.016;                          %Diameter of Small Cylinder
D1 = 0.11938;                       %Diameter of Accumulator
Db = 0.005                          %Diameter of pipe at exit of accumulator
D2 = 0.002;                               %Diameter of nozzle jet
PS = 0.01905;                             %Plunger Stroke
AL = 0.2032;                              %Accumulator Length
F = 981;                                  %Applied Weight (Newton)
Po = 101325:500:191801.047;               %Pressure  of  Accumulating  Section
                                          from 14.7 to 27.827 psi
P1 = 191801.047:10000:790828.662;         %Pressure of Accumulating
                                          Section from 27.827 to 114.7 psi
d2 = 1.225;                               %Density of atmospheric air
P2 = 101325;                              %Atmospheric Pressure
T2 = 293                                  %Atmospheric Temperature
Y = 1.4;                                  %Heat Capacity Ratio
R = 287.05;                               %Specific Gas Constant

%When P1/P2 < 1.892929159, the flow is still not choked and Mach # ≠ 1
for j = 1:length(Po)
A = (pi/4)*D^2 ;                          %Area of Small Cylinder
A1 = (pi/4)*D1^2 ;                        %Area of Large Cylinder
Ab = (pi/4)*Db^2;                         %Area of Blue pipe
A2 = (pi/4)*D2^2;                         %Area of Jet from nozzle
V = A*PS ;                                %Volume of Small Cylinder
V1 = A1*AL ;                              %Volume of Large Cylinder
Mo(j) = sqrt(5*(((Po(j).^((Y-1)/Y))/(26.926))-1))     %Mach # before
                                                      choked flow
To(j) = T2*(1 + ((Y-1)/2)*Mo(j).^2);      %Temperature inside
                                          Accumulator before choked flow
do(j) = Po(j)/(R*To(j));                  %Density of air inside Accumulator
                                          before choked flow
Voj(j) = sqrt(2*((Y/(Y-1))*(Po(j)/do(j))-(Y/(Y-1))*(P2/d2)))      %Velocity
                                                        of jet before choked flow
PRo(j) = (Po(j))/P2 ;                     %Ratio of Accumulator pressure to
```

```
                                        the Atmospheric pressure
mo(j)= do(j)*A2*Voj(j)                  %Mass flowrate
end

%When P1/P2 > 1.892929159, the flow is choked
M = 1;                                  %Mach # = 1 for choked flow

for i = 1:length(P1)
A = (pi/4)*D^2 ;                        %Area of Small Cylinder
A1 = (pi/4)*D1^2 ;                      %Area of Large Cylinder
Ab = (pi/4)*Db^2;                       %Area of Blue pipe
A2 = (pi/4)*D2^2;                       %Area of Jet from nozzle
V = A*PS ;                              %Volume of Small Cylinder
V1 = A1*AL ;                            %Volume of Large Cylinder
T1 = T2*(1 + ((Y-1)/2)*M^2);            % Temperature inside Accumulator at
                                        choking condition
d1(i) = P1(i)/(R*T1);                   %Density of air inside Accumulator
                                        at choking condition
Vj(i) = sqrt(2*((Y/(Y-1))*(P1(i)/d1(i))-(Y/(Y-1))*(P2/d2))) %Choked velocity
                                                            of jet
PR(i) = (P1(i))/P2 ;                    %Ratio of Accumulator pressure to
                                        the Atmospheric pressure
m(i)= d1(i)*A2*Vj(i)                    %Mass flowrate
end

figure(1)
hold on
plot(PRo,mo,'g--','linewidth',3)
plot(PR,m,'r--','linewidth',3)
xlabel('Pressure Ratio (Stagnation Accumulator pressure to Atmospheric
pressure)');
ylabel('Mass flow rate - kg/sec');
legend('Non Choked Flow','Choked Flow');
grid on;

figure(2)
hold on
plot(PRo,Voj,'g--','linewidth',3)
plot(PR,Vj,'r--','linewidth',3)
legend('Non Choked Flow','Choked Flow');
xlabel('Pressure Ratio (Stagnation Accumulator pressure to Atmospheric
pressure)');
ylabel('Velocity of jet from nozzle - m/sec');
grid on;
```

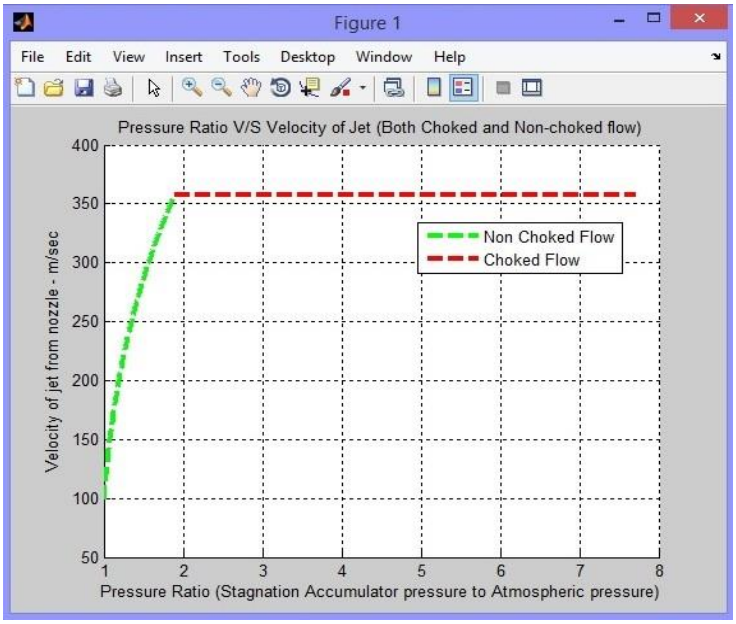

Fig. 3.1. **Pressure Ratio** vs. **Velocity of Jet from Nozzle** (Both **Non-Choked Flow** and **Choked Flow**) [Obtained from plotting the MATLAB computation]

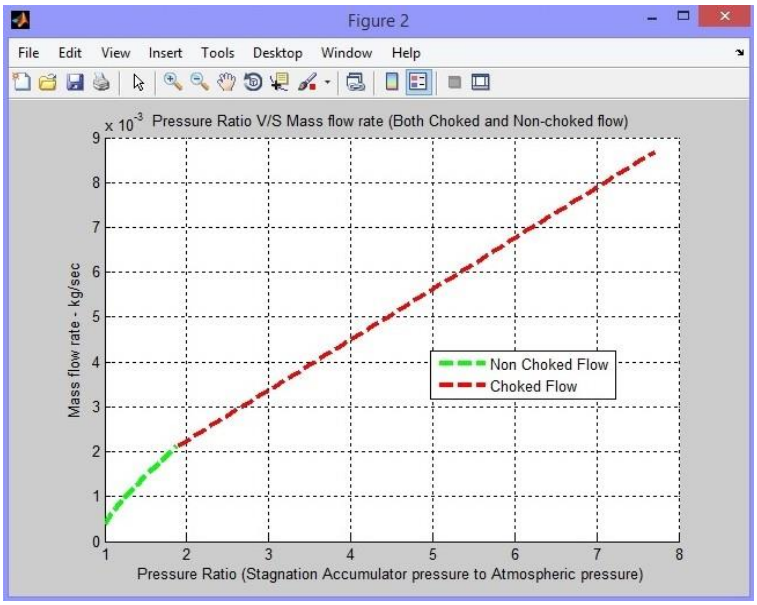

Fig. 3.2. **Pressure Ratio** vs. **Mass Flow Rate** (Both **Non-Choked Flow** and **Choked Flow**) [Obtained from plotting the MATLAB computation]

4. Conclusion

The work carried out has formulated a fluid flow model for a system that can be used to generate electric power by accumulating the weight force of vehicles (by using the speed beaker infrastructure with air operated as a working fluid). Fluid flow model has shown that when the choked flow behavior of compressible fluid is achieved, the air will be continuously striking the impeller with constant velocity hence, causing the mass flow rate to be independent of

downstream pressure. The system, when designed on practical level, can contribute an adequate amount of energy to the power sector. The system has the flexibility to work off the grid (i.e. Decentralized Energy System).

The system model requires capital investment and time to time maintenance cost, and on the other hand, it will be consuming the free source in the form of weight of vehicles (i.e. moving on the roads) and generating power with no carbon footprints. The designed energy system is recommended to give positive results, when installed in the places with high number of traffic such as parking lots, highway toll plazas, street speed breakers and other similar places.

As it has been designed to be flexible, several advancements can be made to improve the output as well as the efficiency such as, number of piston cylinder assembly or / and number of accumulators can be increased. This would decrease the required number of strokes and would result in increased quantity of accumulated air, which would result in incremental rise in power output.

References

[1] Piezoelectric road harvests traffic energy to generate electricity. https://newatlas.com/piezoelectric-road-harvests-traffic-energy-to-generate-electricity/10568/. Accessed December 3, 2013.

[2] Generating Electricity from the Weight of Cars & Pedestrians. https://cleantechnica.com/2013/12/16/generating-electricity-weight-cars-pedestrians-system-developed-exploit-energy-passing-cars/. Accessed December 20, 2013.

[3] Fluid Mechanics and Application areas of fluid mechanics, Essentials of Fluid Mechanics: Fundamentals and Applications, by Yunus A. Cengel and John Cimbala., pp. 2-5

[4] Engineering Applications of Pneumatics and Hydraulics, by EurIng Ian C Thrner

[5] Mechanical Sciences: Engineering Thermodynamics and Fluid Mechanics, by Akshoy Ranjan Paul, Sanchayan Mukherjee, Pijush Roy, pp. 306

[6] Properties of Air and Gases, Effects of compressibility & Gas Laws, Pneumatic Handbook, by Antony Barber., pp. 11-22

[7] Critical Flow, Author Holmes BJ. In: A-to-Z Guide to Thermodynamics, Heat and Mass Transfer, and Fluids Engineering (Begellhouse; 2008), doi:10.1615/atoz.c.critical_flow, Accessed December 28, 2013

[8] Two-phase critical flow by Elias E, Lellouche GS. Int J Multiph Flow, 1994;20(SUPPL. 1):91-168. doi:10.1016/0301-9322(94)90071-X, Accessed January 3, 2014

[9] Modeling Choked Flow through an Orifice, http://www.aft.com/, Accessed November 29, 2013.

[10] Compressed Air Energy Storage (CAES), (April 27, 2011), http://www.ecofriend.com/compressed-air-energy-storage-systems-could-be-the-next-big-thing-in-managing-green-energy.html, Accessed November 18, 2013

Analysis of geometry influence in $LiMn_{1.5}Ni_{0.5}O_4$ cathode/Lithium-ion battery LCA

Gildaiden Longinos-Salazar[1], Jorge Olmedo-González[2]

[1]Silesian University of Technology, e-mail: gildlon539@student.polsl.pl
[2]Universidad Autónoma Metropolitana- Iztapalapa , e-mail: jorgeolmedog@outlook.com

Abstract

The improvement of energy storage materials for lithium-ion batteries (LIB), is crucial for the proper implementation in variable renewable energies, mainly for off-grid power systems. High voltage cathode materials have proved to be a promising solution to avoid energy losses such as $LiMn_{1.5}Ni_{0.5}O_4$ (LMNO) that is quite promising for residential and mobile applications due to their high energy density and efficiency.

The present work compares the LCA for two different geometries of LMNO lithium-ion battery, coin and cylindrical, from the perspective of their mass composition. Three methods for LCA were evaluated in order to determine their impact in different categories. For the cylindrical LMNO battery, a higher impact in resources and global warming was observed due to its higher content of raw materials on its main components whilst coin LMNO battery resulted in a higher impact on human health and ecosystems due to its larger proportion of shell material within its composition. However, this does not represent the environmental impact for the energy stored in each geometry. Future research will focus on LCA that compares the functional unit (1kWh) with equivalent mass that represents 625kg in a coin battery and 20 kg in a cylindrical battery.

Keywords: LCA, Energy Storage, Li-ion Battery

1. Introduction

Greenhouse gas emissions from the energy sector represent approximately two thirds of all anthropogenic gas emissions. In a society totally dependent on technology, it is very important to innovate in sustainable energy sources capable of satisfying energy demand in a sustainable way, avoiding the emission of polluting gases and greenhouse gases such as carbon dioxide (CO_2).

Energy storage technologies (EST) allow indirect control of the generation of electrical energy from variable renewable energy (VRE) [1]. One of the most popular ESTs within electrochemical storage are lithium-ion batteries (LIB) have the best characteristics in terms of durability, coulombic efficiency, voltage and responsive time.

The design and capacity of most lithium-ion batteries (LIB) are mainly limited by the performance of the cathode, the key to improving them is the controlled design of cathodic materials with improved performance. Recently there has been an incursion into the development of new cathodic materials that provide better performance based on more abundant and cheaper transition metals such as copper, iron, manganese, and nickel, as well as aluminum and phosphorous. [2]

Previous LCA researchers have evaluated the environmental impact of lithium-ion battery from different perspectives. However, the current study will focus on the influence of battery geometry (coin and cylindrical) on the life cycle assessment of a lithium ion battery with $LiMn_{1.5}Ni_{0.5}O_4$ cathode, a material that has not been previously implemented for this type of batteries, but that its development and implementation would provide high potentials for applications where it is required to store large amounts of energy at nominal potentials of 12, 24 or 48 VDC for systems in isolated areas or electrical microgrids.

2. Methodology

Life Cycle Assessment (LCA) is a tool for quantifying the environmental performance of products taking into account the complete life cycle, starting from the production of raw materials to the final disposal of the products, including material recycling if needed. The phases of a Life Cycle Assessment are defined in the ISO standards 14040: Principles and Framework and 14044: Requirements and Guidelines. [4]

A Life Cycle Assessment consists of 4 steps [4]:

1. **Definition of Goal and Scope:** in this step, the product the product subject to analysis is defined, as well as the method in which it will be analized and how far will be the reach of the analysis.

2. **Inventory Analysis:** this refers to the data collection phase of a LCA. Data is collected and modeled into input-output flows.

3. **Impact Assessment:** this refers to the evaluation of how significant the impacts are. This is based on the Life Cycle Inventory flows from phase 2

4. **Interpretation:** after gathering all the data in place, the most reliable conclusions and recommendations can be made.

The chosen impact assessment method is the one named ReCiPe. The primary objective of the ReCiPe method is to transform the long list of life cycle inventory results into a limited number of indicator scores. These indicator scores express the relative severity on an environmental impact category. In ReCiPe we determine indicators at two levels: 18 midpoint indicators and 3 endpoint indicators. Each method (midpoint, endpoint) contains factors according to the three cultural perspectives. These perspectives represent a set of choices on issues like time or expectations that proper management or future technology development can avoid future damages. [5]

The selected database is the ecoinvent v3.0 database from SimaPro 1, which covers over 10,000 processes. This database is the result of a joint effort by different Swiss institutions to update and integrate several life cycle inventory databases.[4]

2.1. Functional Unit

As the material to be evaluated in the battery is still in a testing stage, the chosen functional unit will be 1 kWh, which ensures the comparability of carbon footprints and energy consumption of different batteries. Nevertheless, the battery is intended to be implemented to a renewable energy in a stationary application.

2.2. System boundary

The system boundary (S1) will be from the raw materials acquisition phase, the manufacture of the battery and its further usage including transportation. The recycling phase was not taken into account due to lack of regulations in Mexico for the management and disposal of Li-ion batteries.

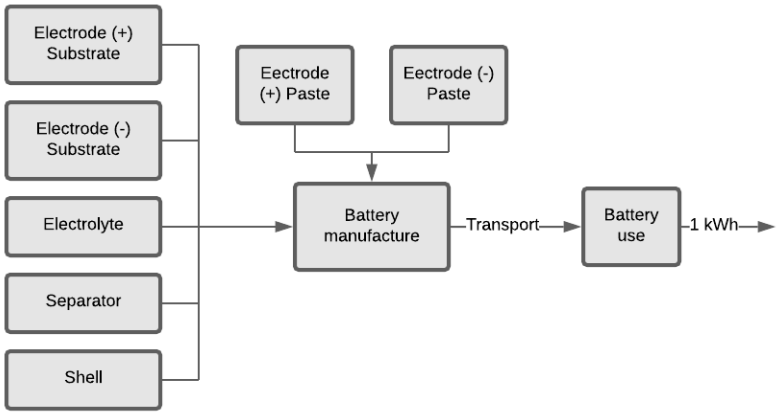

Fig 1. Life cycle process diagram and system boundary of the battery

Battery is composed by two electrodes, one positive (cathode) and one negative (anode), their flow diagrams are shown in figure 2.

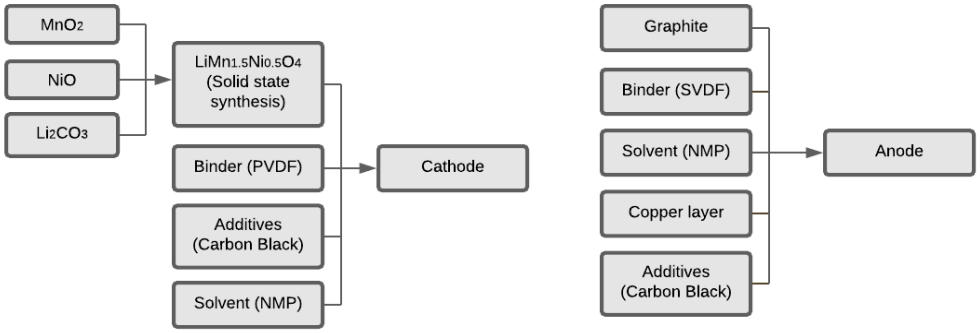

Fig 2. Flow diagrams of both electrode pastes composing the battery. Abbreviations: NMP to N-methylpyrrolidinone, PVDF to Polyvinylidene fluoride.[6]

2.3. LMNO Battery composition

To model the battery of this study, material electrochemical properties (specific capacity and voltage), and component mass breakdown were taken into account as shown in table 1.

Table 1. Electrochemical characteristics and performance of three modelled traction batteries.

Electrochemical Properties	Li-ion with LMNO cathode
Cell voltage (V)	4.7
Maximal battery capacity (mA·g-1)	130
Operative efficiency (%)	92.6

2.4. Life Cycle Analysis Inventory

The quality of the necessary battery's components was calculated when they produced exactly 1 kWh electricity, that is the way efficiency is considered, in real efficiency (~92%), more quantity of each material would be needed to

produce that 1 kWh. The cathode, anode and electrolyte materials were composed according to certain proportions, taking into account the construction of a lithium-ion coin battery and a cylindrical battery geometry.

The mass percentage in the table express the proportion of each component, cathode, anode, electrolyte, etc., within the battery itself. Also, as the battery has a limited lifetime, a fraction of the battery assembly is allocated to each charge-discharge functional unit [7]. The summary of the calculations for the masses of the inventory are shown in table 2.

The electricity considered was taken from previous analysis of Li-ion batteries which contained similar compounds in the cathode (Li, Mn, Ni, O) [7] , and adapted to the current analysis. It is evident that in a cylindrical battery can store more energy and requires less material of some components that coin battery.

Table 2. Inventory of LMNO battery production [6]–[8].

Parameter	**Raw material**	**Raw materials**	**Amount**	
Functional Unit Output (kWh)			**1**	
Material Requirements (g)			**For coin geometry**	**For cylindrical geometry**
Cathode	$LiMn_{1.5}Ni_{0.5}O_4$		1702.18	1636.58
		Li_2CO_3	361.55	334.30
		NiO	347.92	334.57
		MnO_2	1227.23	1179.99
	Aluminium layer	Aluminium	2964.96	1425.38
		Graphite	33.82	16.26
	SPC (Carbon)		212.76	102.28
	PVDF		212.76	102.28
	N-Methyl-2-pyrrolidone		8765.97	4214.21
Anode	Graphite		2835.25	1363.04
	Copper layer	Copper	5918.45	1896.84
		Graphite	36.53	11.70
	SPC (Carbon)		157.51	75.72
	PVDF		157.51	75.72
	N-Methyl-2-pyrrolidone		4867.18	4679.77
Electrolyte	LiPF6	LiPF6	6439.87	247.67
	Solvent	Ethylene carbonate (EC)	20212.85	777.38
		Dimethyl carbonate (DMC)	16384.66	630.15
		Ethyl methyl carbonate (EC)	15404.64	592.45
Separator	Glass fibber	Borosilicate glass (Coin Battery)	5073.73	
		Mono propylene (Cylinder Battery)		189.96
Shell	Stainless Steel 316	SS316	531693.35	498.67
Battery manufacture			0.0036	0.0036
Energy requirements (MJ)				
Electricity, low voltage (MX)			16.82	16.82
Emissions				
Waste heat (MJ)			16.82	16.82

In order to perform the analysis of both geometries proposed, the inventory of each component was adapted so to get 1 kg of coin and cylindrical LMNO battery, this was the functional unit used to such comparison, and for this, the mass percentages from each component within the battery were used. The inventory for 1 kg of each LMNO battery is shown in the table 3. It can be noticed that in the cylindrical battery the mass fraction of material changes with respect the coin battery, because the cylindrical battery requires less material of separator electrolyte and shell that Coin where the shell is the main material due to geometry and cell capacity.

Table 3. Inventory for 1 kg LMNO Battery assembled

Parameter	**Amount**	
Functional Unit Output	**1 kg LMNO coin battery assembled**	**1 kg LMNO cylindrical battery assembled**
Material requirements (kg)		
Cathode	0.0223	0.34
Anode	0.0224	0.35
Electrolyte	0.094	0.23
Separator	0.0081	0.019
Shell	0.8533	0.051

2.5. Life Cycle Analysis

All the inventories were introduced in the SimaPro 9 software in order to get the results of the LCA from the battery. Polyvinylidene fluoride (PVDF) binder is not included due to is not in the data base of the software, therefore the analysis was made without this element, whose thermal decomposition is considered as highly toxic and hazardous [9].

3. Results

3.1. Life Cycle Interpretation and Analysis

It is evaluated the environmental impact with the perspective of 1 kg LMNO battery for each geometry, these results allow to understand the fraction mass influence in the study. However, it does not represent the environmental impact for the energy stored in each geometry, taking in consideration that 1 kg of cylindrical battery represents 50 Wh and 1kg of coin battery can store 1.6 Wh, shown in table 2.

3.2. ReCiPe Midpoint (H) method

The comparison analysis between the two Li-ion batteries through the ReCiPe Midpoint (H) is shown in the graph below. Only the categories which are relevant for this study were taken into account. The corresponding impact categories for the graph are located in the table shown besides the graph.

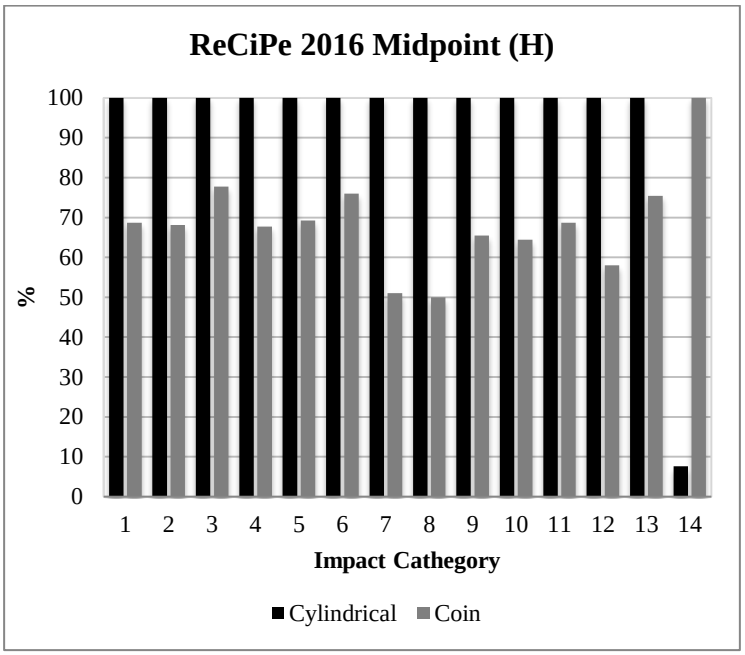

1.	Ionizing radiation
2.	Ozone formation, Human health
3.	Fine particulate matter formation
4.	Ozone formation, Terrestrial ecosystems
5.	Terrestrial acidification
6.	Freshwater eutrophication
7.	Marine eutrophication
8.	Terrestrial ecotoxicity
9.	Freshwater ecotoxicity
10.	Marine ecotoxicity
11.	Human carcinogenic toxicity
12.	Human non-carcinogenic toxicity
13.	Mineral resource scarcity
14.	Water consumption

Fig 3. Comparison of 1 kg coin and cylindrical LMNO Batteries through ReCiPe 2016 Midpoint (H) method.

As it shown in figure 3, the cylindrical LMNO battery has a higher impact in most of the categories compared with the coin shape one. Reason behind might be that, although for composition of each component from the cylindrical battery, less of the materials are needed, for overall composition of the battery, higher amounts of main components such as anode, cathode and electrolyte are needed in comparison with coin geometry.

The only category in which coin geometry had a higher impact was water consumption. In this case, the coin shape battery requires a higher amount of shell material, being stainless steel, while for cylindrical battery, less amount is needed. Stainless steel has a high chromium content, whose mining and its respective water usage is added to the impact, making it higher in the case of LMNO coin battery.

After the comparison between both geometries of the LMNO Battery, another analysis with the same method was made for the cylindrical type in order to determine the elements with the greater impact within this type of battery. Results are shown in the graph below.

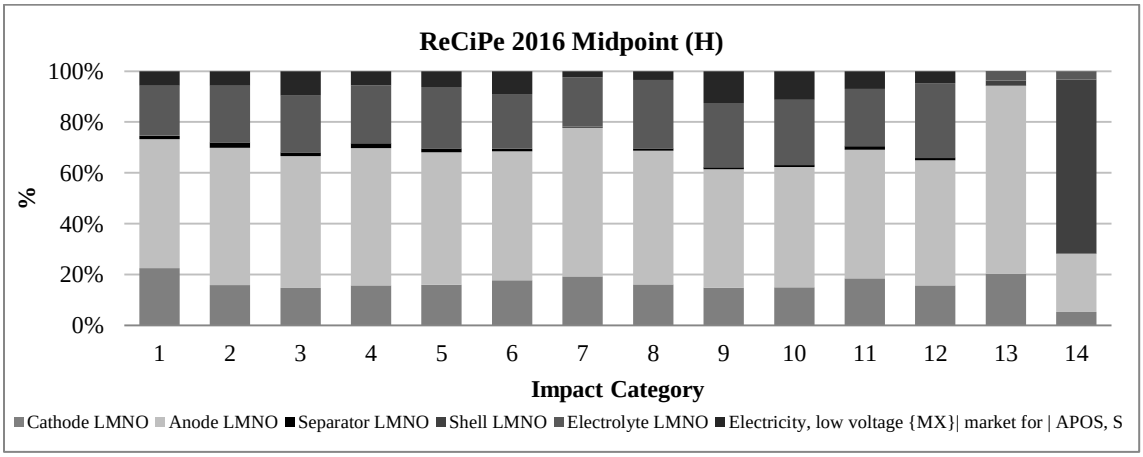

Fig 4. Analysis of 1 kWh LMNO cylindrical battery through ReCiPe 2016 Midpoint (H) method.

As shown in the graph, in most categories, the production of the anode generates the highest impact followed by the electrolyte. In the case of the anode, its composition shares common elements with the cathode, however a great difference is its demand for copper, which is needed as collector foil and might carry a significant weight of the environmental burden of the LMNO battery.

The second component with highest impact was the electrolyte due to the chemical solvents needed for its production. This process makes use of a liquid electrolyte, mostly organic, solvent based. In this kind of electrolyte, the most important consideration is the flammability; the best performing solvents have low boiling points and have flash points around 30°C. Therefore, venting or explosion of the cell and subsequently the battery pose a danger [10]. The replacement of electrolytes for Li-ion batteries is a challenge that is currently being faced, since the electrolyte has to be stable so to nor present risks due to the flammable and volatile nature of the solvents used.

Nevertheless, within the scope of the production of LMNO battery, the replacement of electrolyte is not priority, but it is the improvement of the $LiMn_{1.5}Ni_{0.5}O_4$ material performance for the cathode. Once its synthesis is completely optimized, the replacement of other components of the battery will start.

3.2.1. ReCiPe Endpoint (H) method

A second analysis was made for both batteries in order to compare their impact in human health, ecosystems and resources. The result of the analysis is shown in figure 5.

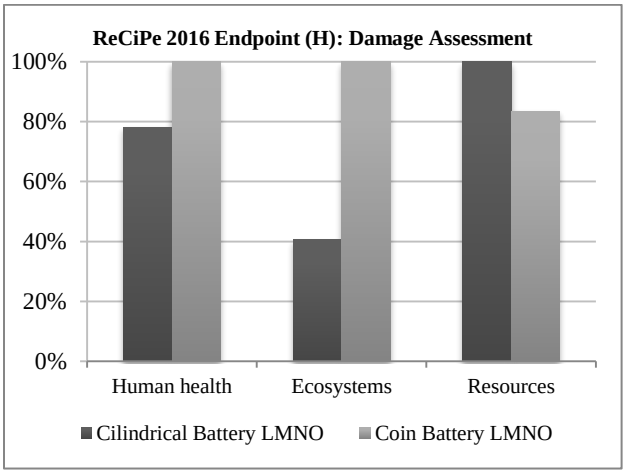

Fig. 5. Comparison of 1 kg LMNO coin and cylindrical battery through Endpoint (H) method.

In this analysis, coin LMNO battery has a higher impact in two of the three assessed categories: human health and ecosystems. The differences in the proportions for both geometries lay in the shell made from stainless steel and the electrolyte, based on a salt and organic solvents, that in case of the coin battery, for both components these proportions are higher. In order to be sure of the influece from both components mentioned above, another analysis was made only for coin LMNO battery as shown in figure 6.

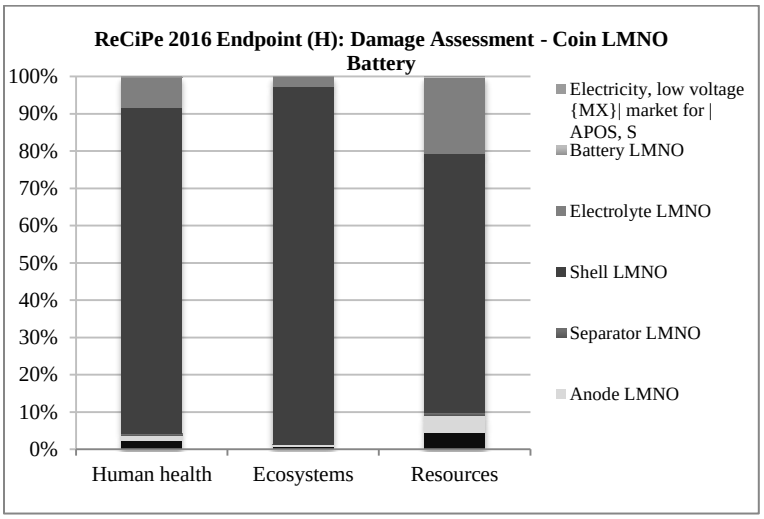

Fig. 6. ReCiPe 2016 Endpoint (H) method for 1 kWh LMNO Coin Battery.

In the three categories, the element of the process which impacts the most, is the shell of the battery made from stainless steel. Regarding the **ecosystems impact**, steel production has a number of impacts on the environment, including air emissions, wastewater contaminants, hazardous wastes, and solid wastes. [11].

Coke production is one of the major pollution sources from steel production. Air emissions such as coke oven gas, naphthalene, ammonium compounds, crude light oil, sulphur and coke dust are released from coke ovens. [11]

From the human health point of view, apart from all the pollutants previously mentioned that affect directly human health, there is also the heat exposure for the workers that has a great impact their health and productivity especially in steel industry where excessive heat exposure is a major occupational problem [12].

Finally for the resources impact, it is known that the global steel production has an overall resource efficiency of 32.9% accounting for energy and materials, which shows that this industry still has to work on the resources savings to improve its efficiency [13].

Cathode does not represent a significant amount in either of the categories.

3.2.2. IPCC 2013 GWP 100a method

A third analysis to measure the impact of LMNO coin and cylindrical batteries in Global Warming Potential was carried out, resulting in the figures 7 a) and b).

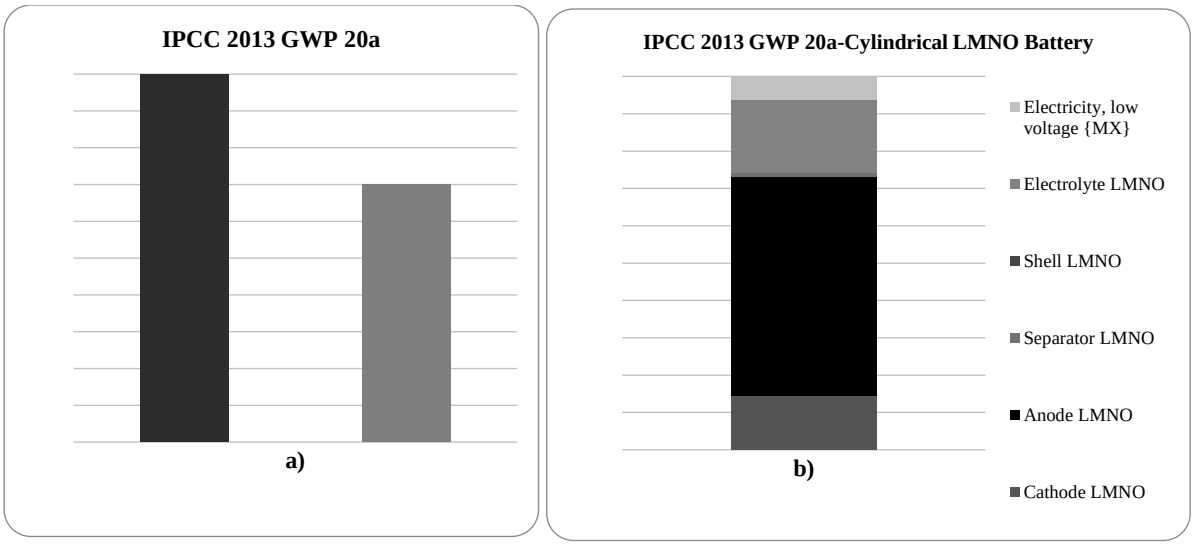

Fig7. a) IPCC GWP 20a method comparison for LMNO coin and cylindrical battery. b) IPCC GWP 100a method for LMNO cylindrical battery.

From the comparison carried out for both geometries regarding Global Warming impact, it was shown that cylindrical battery had a greater impact than coin within a time of 20 years. Looking closely to the analysis of cylindrical battery through the same method, it was the anode which represents the higher impact on Global Warming. As mentioned previously, one element which differs from the cathode is copper, which is, due to its divergent properties, an increasingly popular metal. Nevertheless, the global copper-demand increases every year, mainly due to rising Chinese imports [14], which irremediably increases the CO_2 emissions.

3.2.3. Network for a light commercial vehicle

In order to evaluate the impact of transportation of the LMNO battery, the cylindrical geometry was taken due to that, in a realistic scenario, this is the type of geometry more commonly used for energy storage applications. Geography boundaries are set to be within the country of Mexico, where the battery is produced, the distance taken was the longest that 50 batteries would have to travel in order to arrive to the furthest consumer.

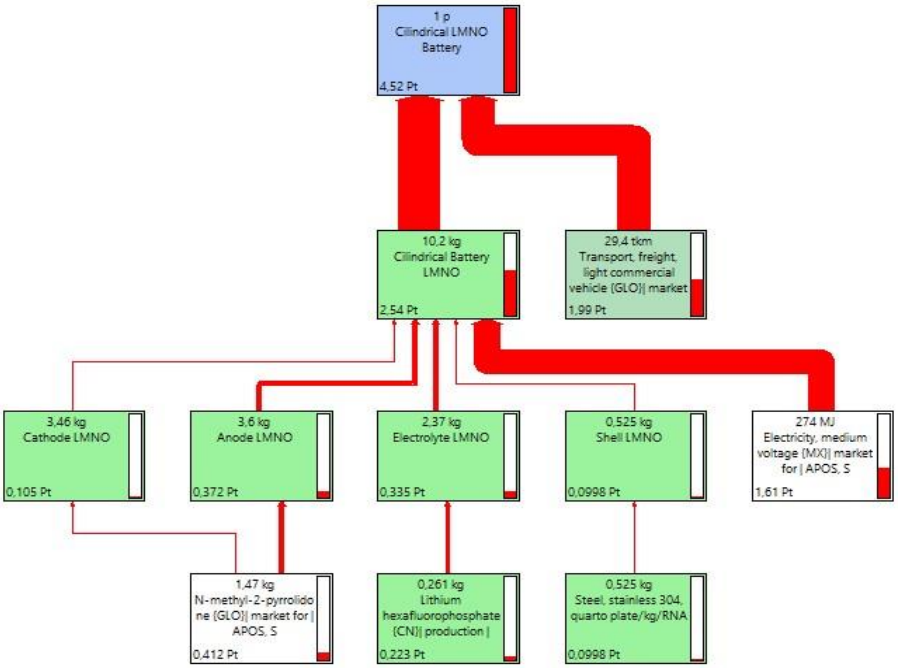

Fig 8. Network for a light commercial vehicle.

As shown in Figure 8, when taking into account the transportation of the cylindrical LMNO battery to its final destination, the impact that this action generates is almost as much as the production of the battery itself. This is understandable taking into account that the transport is done by land through a relatively long distance (2900 km). Also, it is important to note that even when SimaPro takes average parameters for transportation around the world, it might not reflect entirely that fuel for vehicles in Mexico is only produced by fossil fuels

4. Conclusion

The importance of the battery's geometry in Life Cycle Assessment was exposed within this study, showing that in the case of cylindrical LMNO battery, its impact in most of the analyzed categories was higher due to the proportion of the main components (anode, cathode, electrolyte) within the battery. However, in case of the coin shape LMNO battery, it showed a bigger impact in certain categories because higher amount of shell material was needed. This makes it possible to determine the importance of each of the materials within the battery recycling, which in case of the coin battery was the shell, and the cathode and anode in the cylindrical one.

Moreover, another goal of this analysis was the evaluation of the impact of cathode's active material ($LiMn_{1.5}Ni_{0.5}O_4$ also known as LMNO) in the battery life cycle, the different analysis carried out were focused on identifying any negative effects. However, it was found that in majority of them, the cathode in general did not have a negative significant impact in the most of the categories analyzed, being other components of the battery cell the ones that possessed higher impacts, such as the electrolyte and shell.

The future work considers a LCA that compares the functional unit (1kWh) with equivalent mass that represents 625kg in a coin battery and 20 kg in a cylindrical battery. This analysis will make it possible to determine the environmental impact that it would have with respect to the stored energy and not the mass, and to determine the importance that the type of geometry is relevant for functional units greater than 1Wh.

This is a very relevant finding for the future of the production of LMNO in a big scale, since it is currently at a researching stage and an LCA can give an idea of the impact it will have to the environment and if proceed the way it

is being produced or not. With the information obtained from this analysis and the certainty that this new cathode's active material will not represent a risk to resources, human health and global warming, the first recommendation appears by suggesting that in further steps, there can be an improvement of other components from the cell that did present a significant impact such as the electrolyte, a part of the battery than can certainly be replaced by less hazardous and toxic compounds.

Acknowledgment

Authors thank the Electrochemical Energy UAM-I group from Metropolitan Autonomous University, Mexico Dr. Guadalupe Ramos-Sanchez and the electrochemical laboratory from National Polytechnic Institute-ESIQIE, Dra. Rosa de Guadalupe González-Huerta group for the materials information support.

References

[1] IEA, "Technology Roadmap: Energy Storage," 2014.

[2] H. Kawai, M. Nagata, H. Tukamoto, and A. R. West, "High-voltage lithium cathode materials," *J. Power Sources*, vol. 81–82, pp. 67–72, 1999, doi: 10.1016/S0378-7753(98)00204-3.

[3] L. A. W. Ellingsen, C. R. Hung, and A. H. Strømman, "Identifying key assumptions and differences in life cycle assessment studies of lithium-ion traction batteries with focus on greenhouse gas emissions," *Transp. Res. Part D Transp. Environ.*, vol. 55, pp. 82–90, 2017, doi: 10.1016/j.trd.2017.06.028.

[4] M. Goedkoop, M. Oele, J. Leijting, T. Ponsioen, and E. Meijer, "Introduction to LCA with SimaPro Colophon," *Introd. to LCA with SimaPro*, no. November, 2016.

[5] L. Golsteijn, "ReCiPe," *Pre-Susyainability*, 2012. [Online]. Available: https://pre-sustainability.com/articles/recipe/. [Accessed: 04-Dec-2020].

[6] J. O. Gonzalez, "Síntesis y modificación del material catódico LMNO para baterías de ion litio y su integración en almacenamiento de energía renovable," 2020.

[7] G. M. Bettez, T. R. Hawkins, and A. H. Strømman, "Life Cycle Environmental Assessment of Lithium-Ionand Nickel Metal Hydride Batteries for Plug-in Hybridand Battery Electric Vehicles. Supporting Information.pdf," pp. 1–51.

[8] Y. Liang *et al.*, "Life cycle assessment of lithium-ion batteries for greenhouse gas emissions," *Resour. Conserv. Recycl.*, vol. 117, pp. 285–293, 2017, doi: 10.1016/j.resconrec.2016.08.028.

[9] Fluoride Action Network, "Polyvinylidene fluoride (PVDF) CAS No. 24937-79-9," *Pesticide Project*, 2005. [Online]. Available: http://fluoridealert.org/wp-content/pesticides/pvdf.page.htm. [Accessed: 20-Jun-2020].

[10] C. Daniel, "Materials and processing for lithium-ion batteries," *Jom*, vol. 60, no. 9, pp. 43–48, 2008, doi: 10.1007/s11837-008-0116-x.

[11] Greenspec, "Steel production & environmental impact." [Online]. Available: https://www.greenspec.co.uk/building-design/steel-products-and-environmental-impact/#:~:text=8 The environmental impact of,from coking and iron-making. [Accessed: 19-Jun-2020].

[12] A. karim Fahed, M. Ozkaymak, and S. Ahmed, "Impacts of heat exposure on workers' health and performance at steel plant in Turkey," *Eng. Sci. Technol. an Int. J.*, vol. 21, no. 4, pp. 745–752, 2018, doi: 10.1016/j.jestch.2018.05.005.

[13] A. Gonzalez Hernandez, L. Paoli, and J. M. Cullen, "How resource-efficient is the global steel industry?," *Resour. Conserv. Recycl.*, vol. 133, no. January, pp. 132–145, 2018, doi: 10.1016/j.resconrec.2018.02.008.

[14] W. Kuckshinrichs, P. Zapp, and W. R. Poganietz, "CO2 emissions of global metal-industries: The case of copper," *Appl. Energy*, vol. 84, no. 7–8, pp. 842–852, 2007, doi: 10.1016/j.apenergy.2007.01.014.

Biomass gasification as an alternative energy source in the forest industry in durango, Mexico

G.I. Urias Rivera[1], R. Lucho Chigo[1], D.C. Martínez Casillas[1,2], F.A. Alcázar Medina[1,2], V.J. Martínez Gómez[1,2], R. Valencia Vázquez[1,2]

[1]Durango Institute of Technology, e- mail: 19041698@itdurango.edu.mx
[2]Durango Institute of Technology, e-mail: dmartinez@itdurango.edu.mx

Abstract

The forest industry in Durango plays an essential role in the timber forest production in Mexico since two thirds of the wooded area of the state is utilized for production purposes. Pine and oak are the resources that are most exploited for products derived from lumber, sleepers, posts, plywood, firewood, and charcoal. These products are manufactured in sawmills and plywood factories, among others, where the produced waste is considered residual biomass such as sawdust, bark, chips and wood chips that, as they do not have a later use, can be used as biofuel for energy transformation in gasification technology. A proposal for the use of biomass gasification in a local industry theoretically determined that the total energy used in a sawmill can be obtained from two thirds of the total pine bark produced, saving one third of the monthly payment for electricity, demonstrating that the use of biomass for renewable energy generation is a viable alternative compared to energy from fossil fuels, providing a solution to the problem of waste disposal and reducing pollution derived from non-renewable sources.

Keywords: Forest residues, Biomass gasification, Bioenergy

1. Introduction

Energy is the ability of matter to produce change. Since ancient times, humans have used the resources in the environment to generate some type of energy, whether it is for heating food, hunting or transport purposes. The demand for these resources has increased to satisfy the needs of a growing population. As a result, the exploitation of non-renewable resources such as fossil fuels for energy generation is one of the main problems today, which has led experts to seek alternatives based on sustainable renewable.

Energy sources can be classified as renewable and non-renewable based on their origin. Renewables are those that can potentially be replenished indefinitely and come from natural energies and processes that continuously happen on Earth. Some of these natural sources include solar radiation, gravitational force, thermal energy from the interior of the earth or by the kinetic movement of fluids and biomass due to its abundance and thermal, physical or chemical energy conversion. On the other hand, the supply for non-renewable energies is limited depending on the existing reserves. The most exploited and used sources are fossil fuels, such as oil, natural gas and coal. As can be observed in Figure 1 fossil fuels dominated energy generation in more than three quarters over other energy sources in 2019 [1].

The problem that occurs with the use of fossil fuels is that when they are burned, high concentrations of greenhouse gases are released, accumulating in the atmosphere and generating a negative environmental impact, causing atmospheric, soil and water pollution as well as global warming [2].

As societies become more aware of the negative impacts of fossil fuels, renewable energies are considered to be the planet's future. Since renewable energies avoid the generation of new pollutants such as burned oils and hazardous waste, among others, their use diminishes emissions into the atmosphere also reducing global warming. Some of the most widely used renewable energies in the world are wind energy (used with wind turbines), solar energy (with

photovoltaic modules, solar heaters), biomass (used by converting biomass to energy or heat by combustion, microbial degradation, gasification, etc.) where biomass from residual organic matter in the environment is transformed into energy by biological and thermochemical methods [3].

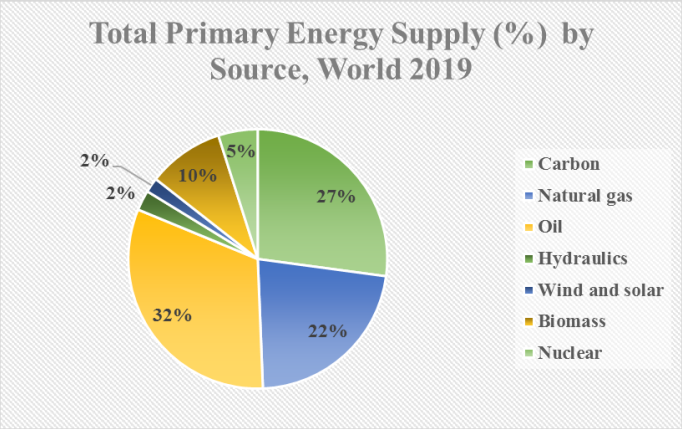

Fig 1. Total supply of energy sources worldwide

2. Forest industry

Forestry is an activity that makes use of the natural resources that come mainly from forests. The wood resources are taken as raw material for their transformation in different industrial processes from which materials such as plywood, sawn wood, wooden idlers, and cellulose are obtained for the production of paper and other products.

The forest territory in Mexico is the twelfth largest on the planet, with 138 million hectares corresponding to forest vegetation that represents 70.7% of the national territory [4], with forests being the most predominant with 22.2 million hectares of which 15 million have an economic use, followed by jungles with 12.2 million hectares [5].

Timber forest production in Mexico in 2017 was 9,012,036 m^3r, where the raw material corresponded to 73.8% from coniferous forests composed mainly of pine species, followed by tropical forests and precious woods with 13.6%, and from broadleaf forests composed of oak species with 12.6% [6,7]. The most produced out of these totals are shown in table 1 where those derived from sawn timber correspond to 62%, cellulosic 15%, firewood and bio char 6% each, plywood 5%, the wooden sleepers 4% and the poles 2% [7].

Table 1. National Timber Forest Production (m^3r) in Mexico

Products / **Genre**	**Sawn timber**	**Cellulosics**	**Plywood**	**Poles**	**Firewood**	**Coal**	**Wooden Sleepers**	**Total**
Pine and conifers forest	4,928,159	696,644	457,459	43,984	250,827	686	272,871	6,650,630
Oak and broadleaf forest	372,770	105,242	0	13,097	239,427	317,968	87,277	1,135,780
Tropical and precious forest	289,265	581,622	3,739	104,543	30,093	216,263	100	1,225,626
Total	**5,590,194**	**1,383,508**	**461,198**	**161,624**	**520,346**	**534,918**	**360,248**	**9,012,036**

SEMARNAT statistical forest yearbook, 2017

The states with the highest timber forest production in the country during 2017 were Durango with 28.5%, Chihuahua with 18.5%, Oaxaca with 8%, Tabasco with 6.7% and Michoacán with 5.5%, which contributed 67.3% of total production. In Mexico the economic contribution of the forestry sector was an average GDP of 2,050 million USD from 2013-2017, representing 0.24% of the national GDP [7].

2.1. **Region studied**

The state of Durango is located in the northwestern region of the country, bordering Chihuahua to the north, Coahuila to the northeast, Zacatecas to the southeast, Nayarit to the south and Sinaloa to the west. It is the country's fourth largest state with a forest area of 12.3 million hectares that represent 74.5% of the total area of the state, where 4.9 million hectares correspond to temperate-cold climate forests of conifers and broadleaves [8,9]. Since the Western Sierra Madre runs through almost half the state, most of the state has a cold and very dry climate. At the top of the mountains the climate is much colder with rains throughout the year, and winter with frosts and snowfalls. Figure 2 shows the geography of Durango and the area of its natural timber forest resources [10], being the one with the highest participation in forest production in the country with approximately 30% of annual production and producing more than 2 million cubic meters of wood each year [7].

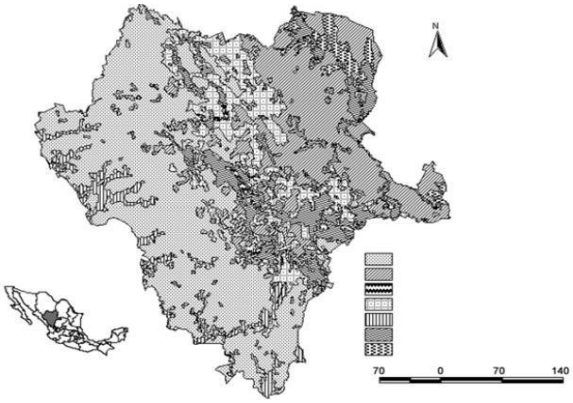

Fig 2. Area with timber forest resources in Durango

Durango's timber production corresponds to the transformation of pine and oak trees where the most widely used species are *Pinus Duranguensis* and *Quercus rugosa*, of which pine is the one that is most produced and used due to its physical manageability. Production of pine in the state during 2017 was 2,244,348 m^3r (87.7%) while the oak production in the same year was 314,948 m^3r (12.3%) [7]. For this reason, the transformation of timber resources is carried out in different industries of the state such as sawmills, plywood factories, coal producers, among others. The main products most produced in the state are those derived from sawn timber (figure 3) with 47.2% of the total, cellulosics with 23.2%, wooden sleepers and poles with 14.5%, plywood with 10.6%, and firewood and coal with 4.5% [7]. The economic value of this forest production in the state represented 30.2% of the national total, being the largest contribution with a value of 153,062,466 $ USD.

Fig 3. Pine Sawn Timber Boards

The elaboration processes of the of the products mentioned in the forest industries produce residues considered biomass since these are made of organic material. These residues can be used or discarded depending on the type or form in which they are produced. Some of the residues are sawdust, splinters and shavings that are the waste of the sawing processes of the wood, the bark and the sapwood of a trunk and scraps, which are the excesses that are cut into boards, poles, wooden sleepers, among others. Figure 4 shows different types of waste biomass generated in the forest industry.

Fig 4. Residual biomass from the forestry industry, a. Sawdust, b. bark, c. Scrap wood, d. Wood chips/shavings

Some residues can be used for the manufacturing of other products or for another activity, in the case of Durango, the sawdust and shavings that come from pine are used as food in poultry farms and as mulch for livestock and farm animals. The pine bark is put into debarking machines where the wood is separated from the bark then shredding the wood together with the scraps to be sold to factories that produce agglomerates of these residues, not making a further use of the pine bark, while the bark and oak scraps are used for the manufacture of bio char, with oak sawdust as a waste without use since it turns out to be toxic to animals.

1. Biomass gasification

Biomass gasification is the conversion of organic matter of vegetable origin through combustion in which a gasifying agent such as air or oxygen can be used to obtain a synthesis gas, in which, if it is with air, it is called gas lean and if it is with oxygen it is called rich gas. Table 2 shows the composition of the synthesis gas (syngas). The generated waste with this technology is ash, tar and residual carbon, which are considered to be by-products since they can be used in other types of processes.

Table 2. Chemical composition of syngas

Produced gas	Percentage (%)
N_2	45 – 55
CO	15 – 20
H_2	15 – 20
CO_2	8 – 12
CH_4	1 – 4

Gasification is a competitive and promising technology to produce renewable energy based on its investment and production costs. Some of the advantages of gasification when compared to other processes that produce energy from biomass include:

- Opportunity to utilize residues from forestry and agro-industries that do not serve as by-products.
- It can provide thermal and electrical energy.
- The gas generated by the combustion of biomass is used in this process as a by-product.
- Gasification can be carried out in rural communities where some types of energy might not be available; it can also be used in a small carpentry, or even at a sawmill or a plywood factory.
- The reactors consist of an austere design and easy operation.

The gasification process is mainly divided into four stages. The initial stage is drying, which consists of the water contained in the biomass evaporating at a temperature of 100 ° C. Followed by the pyrolysis stage, in which the biomass undergoes thermal decomposition at temperatures of 100 ° C to 800 ° C in the absence of oxygen. The third stage is oxidation, in which the gasifying agent is introduced, in this stage the biomass combustion occurs, igniting it with fire reaching temperatures of 700 ° C to 2000 ° C. Finally, the reduction stage, in which the biomass undergoes reactions at a high temperature, such as the reduction of the unreacted carbon and of the tar content in the gas due to the higher reaction temperature during the endothermic phases. At the end of these stages, the desired synthesis gas is obtained [11].

The gasification of the biomass is carried out in gasifiers, which consist of an equipment designed specifically for this process. In order to select the correct gasifier, you have to take into account the syngas you want to obtain, for this, you have to identify the biomass that will be the fuel used and the oxidizing agent that will enter the combustion, its costs, as well as its control, operating and physical parameters [12].

2. Biomass gasification utilization in a local sawmill proposal

The location where the gasification technology proposal would be implemented would be in a sawmill located in the municipality of Santiago Papasquiaro in the state of Durango (25 ° 08'44.0 "N 105 ° 29'27.7" W). This sawmill operates a total of 8 hours a day, 6 days per week, with pine logs being the only raw material used to work with in this particular location (mostly *Pinus Duranguensis*). The average monthly production in the sawmill is 1,280 m^3 or 960,000 kg of sawn wood (based on FAO data saying that 1 m^3 of sawn wood is equivalent to 750 kg). The processes done in the sawmill lead to the production of residual biomass in the forms of bark, sawdust and wood chips. Of these residues, the bark and the scraps are introduced into a mill to produce wood chips. It is important to note that the mill separates the bark boards into wood chips and bark to obtain by-products of better quality, and the bark produced is the final residue that usually does not have any further use. Meanwhile, sawdust is used as food in poultry farms and as mulch in stables or cattle paddocks. The scrap, sawdust, bark and chip residues that are produced in the sawmill processes are shown in Figure 5.

Fig 5. Scrap, sawdust, A. bark, B. splinter residues generated in the sawmill.

It was reported that 93% of the wood in a single wood log is used, while 7% of it is considered residual biomass that consists of 4% wood chips, 1.5% sawdust and 1.5% bark. Table 3 shows the total amount of residual biomass that is produced per month according to the production in the sawmill. According to the information above, bark is the only residual biomass that is produced monthly in quantities of almost 15,500 kg, but it is not fully used as the other residues are.

Table 3. Monthly percentages of sawn wood and residual biomass production

	Production (kg)	**Percentage (%)**
Total wood	1,032,258.065	100%
Sawn timber	960,000	93%
Wood chips	41,290.32	4%
Sawdust	15,483.87	1.5%
Bark	15,483.87	1.5%

Information on the machinery used in the sawmill and how much power each one requires was collected and reported in Table 4 the machines used in the sawmill and the power each of them requires in order to work is presented. A 300 kW electrical transformer was also used in the facilities, which supplies electricity to the sawmill.

Table 4 Inventory of sawmill machinery and the power used for their operation

Machine	**Number of motors**	**Power of each motor (kW)**	**Total machine's power (kW)**
1 Friction Machine	2	5.59	11.18
		5.59	
1 Log cutting tower	1	37.28	37.28
4 Chop saw	1	22.37	89.48
	1	22.37	
	1	22.37	
	1	22.37	
1 Pendulum	1	5.59	5.59
1 equalizer	2	5.59	11.18
		5.59	
1 Wood mizer	1	22.37	22.37
1 Double board cutter	3	22.37	50.33
		22.37	
		5.59	
1 Wood log machine	1	5.59	5.59
1 Wood chipper	5	74.57	113.72
		22.37	
		5.59	
		5.59	
		5.59	

As indicated above, the chipper is the machine that requires the most power as it has 5 built-in motors necessary for its function. Additionally, the sum of the total power used by all the equipment comes to have a value of 346,749

kW.

Besides collecting all the data needed to calculate the total power used in the sawmill, the electricity consumption reports for 3 months were also provided. The total monthly consumption and rates paid are shown on the following table.

Table 5. Electric energy consumption and fees

Month	**Consumption (kW)**	**Total fees ($USD)**
February 2020	10,761	$2,000.44
March 2020	8,422	$1,565.61
April 2020	7920	$1,472.18
Average	9,034	$1,679.39

A quotation from the company All Power Labs® was obtained for this proposal. This company currently offers two different models of gasifiers that connect directly to an electric power generator. The Power Pallet - PP30™ and the 50 kW PP Base Container™ (which consists of two PP30™ gasifiers and a more powerful generator) are convenient options since they do not have moving parts nor require turbines, power generators, condensers or any other equipment to assist the gasifiers. The quotes for both of these models and other general information about them were requested, but only the PP30's additional information was provided. Some of the most important characteristics of this gasifier are shown in Table 6.

Table 6. General conditions of the PP30™ gasifier

Parameter	**Value**
Charge	Min 3 kW Max 25 kW
Max. Continuous Operation	>16 h
Fuels	Lignocellulosic biomass
Humidity	<30%
By-products	Bio char
Particle size	1 cm - 4 cm
Residues	Ashes
Electrical power, continuous	25 kW@60 Hz / 22 kW@50 Hz
Biomass Consumption	1 kg/kWh
Hopper capacity	250 kg/m^3
Run Time per Hopper Fill	4 h - 15 kW 6 h - 10 kW 12 - 5 kW
Electrical efficiency	~23% Biomass ~28% Syngas
Electrical + Thermal Efficiency	>65% Biomass >80% Syngas

The cost of the PP30™ gasifier is $ 62,240 USD and includes:

- Power Pallet PP30™ (25 kW): 3-stage cogeneration system with the ability to connect to the electricity grid
- PP30 Operator Maintenance Kit
- Spare parts kit PP30™
- Continuous feed hopper system

- Exhaust catalytic emissions system
- A live web video conference for remote start-up

It is important to note that the maintenance costs are not shown, but a maintenance sheet was provided which includes instructions with the corresponding maintenance times and other specifications as mentioned in table 7.

Table 7. PP30™ Gasifier Maintenance Times

Maintenance practice	Frequency	Time required for each practice
Refill the hopper when it is ¼ full	1-2 times a day	1 minute
Empty cyclone dust and ash cans after shutdown.	Daily	30 minutes
Change of filters	Every 7 days	30 minutes
Clean soot and dust in the filter area	Every 7 days	30 minutes
Change of engine oil	Every 30 days	60 minutes

Based on this information the use of the PP30™ gasifier represent a convenient option for the sawmill due to the type of conditions it requires. Unlike the 50 kW PP Base Container gasifier, the PP30 produces half the energy, but it is cheaper and requires less space. According to the information obtained, the residual biomass that is produced in the sawmill and goes to waste consists mainly of pine bark, which comes to be an average amount of 15,483.87 kg each month. As this bark is not reused and finding a proper disposal for it is often a problem, using it as a biofuel in the gasification process to produce electricity for the sawmill is a convenient alternative to reduce the consumption of energy from fossil fuels and subsequently cut down the costs this service implies.

The PP30™ gasifier produces 15 kW every four hours with a load of 250 kg of residual biomass. Since the workday consists of 8 hours a day, the gasifier would end up producing 30 kW a day with two loads. The following estimations show how much residual bark biomass is needed per month to feed the gasifier and the difference between the residual biomass produced and the amount of it that could be reused to generate energy.

$$\begin{aligned} &Monthly\ residual\ biomass\ to\ use\ in\ gasifier \\ &\quad = 250\,kg * 2\,loads\,a\,day * 6\,days\,a\,week * 4\,weeks \\ &\quad = 12{,}000\,kg\ of\ residual\ biomass\ per\ month \end{aligned}$$

$$Final\ residual\ biomass = \frac{15{,}483.87\ kg\ produced}{12{,}000\ kg\ utilized} = 3{,}483.87\ kg\ of\ leftover\ biomass$$

Note that 77.5% of the bark produced in the sawmill would be used, while 22.5% would continue to be residual biomass with no further use.

Since the average monthly electricity consumption is 9,034 kW with an average monthly rate of $1,680, and the information previously obtained indicates that the gasifier would produce 30 kW per day, then knowing that a regular workday is 8 hours long and the sawmill operates 6 days a week it can be said that 5,760 kW would be produced per month (considering a month to be approximately 4 weeks long); so the difference between the monthly energy consumption and the energy that the gasifier will produce would be as follows:

$$\frac{9{,}034 kW\ consumed}{5{,}760\ kW produced} = 3{,}274 kW$$

The gasifier would potentially produce 63.75% of the total average energy needed for the sawmill to operate, reducing the consumption expenses by approximately $1070.61 USD per month. However, since regular maintenance needs to be done periodically and this would involve some costs, the prices and the amount of money required for maintenance need to also be taken into account. Such costs are described in next table.

Table 8. Costs of gasifier maintenance

Products Used Monthly	Cost per Unit ($USD)	Total Cost ($USD)
4 Air filters SA16766	$102.31	$409.23
8 Liters of engine oil 5W30	$4.87	$38.93
	Total	$448.16

The total amount of money that could be saved monthly would be $622.45 USD, which is 37.06% of what is currently spent. The cost of the gasifier itself plus the shipping expenses come to a total of $84,840 USD approximately. The total monetary investment used to adapt this technology would be covered over a period of 12 years, at the same time, 829,440 kW could be produced during this same period using a more eco-friendly approach where 1,728,000 kg of waste would be reused.

Therefore, it can be concluded that using the PP30™ gasifier in the sawmill is a viable option since it would save almost 1/3 of the payments that go towards electrical energy usage and almost 2/3 of the residual biomass produced would be reused. Additionally, adopting a new technologic approach of this kind is an opportunity to positively impact the environment by reducing the consumption of non-renewable energies.

Furthermore, it is important to note that if the gasifier that had been chosen was the 50 kW PP Base Container™, which consists of two PP30 gasifiers placed on a base that connects to a motor that generates greater power, 100% of the residual biomass could be used, potentially generating enough electrical energy for the entire sawmill. This would further reduce the current average payment of $1680 USD. Even when considering the maintenance costs, which would be twice the maintenance costs of the PP30™, the total that would be saved by implementing its use would approximately be $783 USD, making this an even more convenient alternative, however, the cost of this gasifier was not provided by All Power Labs not allowing for a more precise calculation of how much the total costs would be and how long it would take for the investment costs to be covered.

3. Conclusion

Using biomass as a renewable energy source is a viable option since natural resources are preserved by adopting a process where the forests actually get reforested to always have raw materials available, making this approach sustainable. Likewise, it provides an alternative to the consumption of energy that comes from fossil fuels. The emissions produced by the energy transformation of biomass are considered to be neutral since they take part on a biomass cycle where the CO_2 is absorbed through photosynthesis and released into the atmosphere during its combustion, contributing to the environment and reducing atmospheric pollution.

Due to the high forestry production in Durango, the disposal of residual biomass is imminent, and although residues such as the wood chips and pine sawdust produced are often reused as by-products, other waste like oak sawdust and pine bark can be used as biofuels in gasification technology as mentioned above. This proposal also explains how the implementation of this technology would be feasible since the waste itself can be used to produce the energy required for some of the sawmill's operations, saving a third of the money allocated to the payment of electricity.

There is a variety of gasifiers with different features and costs that can be used in forest industries, making biomass gasification a recommended and viable alternative to produce renewable energy in the state of Durango, which would in addition contribute to the environment by reducing the amount of residual biomass that gets disposed with no further use.

References

[1] World Energy Balances: Overview, https://www.iea.org/reports/world-energy-balances-overview, (29/11/20)

[2] Ferrari, L. *Energías fósiles: diagnóstico, perspectivas e implicaciones económicas.* Revista Mexicana de Física, pp. 36-43, 2019.

[3] Merino, L. *Las energías renovables.* Revista España: Haya Comunicación, pp. 8-20 2019.

[4] Revista electrónica de divulgación científica forestal, Comisión Nacional Forestal, http://www.conafor.gob.mx/innovacion_forestal/?edicion=74, (26/11/20).

[5] Consejo Civil Mexicano para la Silvicultura Sostenible (CMCSS), El aporte de financiera rural en el sector forestall de México, https://www.ccmss.org.mx/wp-content/uploads/El_aporte_de_financiera_rural_en_el_sector_forestal_de_Mexico.pdf, (26/11/20).

[6] Díaz, J. *Sector Forestal en México*, pp. 2-11, 2001.

[7] Secretaría de Medio Ambiente y Recursos Naturales (SEMARNAT), *Anuario Estadístico de la Producción Forestal 2017*, pp. 51, 54, 123, 162, 257. 2018.

[8] Consejo Civil Mexicano para la Silvicultura Sostenible (CCMSS), Desarrollo forestal comunitario en Durango, el camino a seguir, https://www.ccmss.org.mx/desarrollo-forestal-comunitario-durango-camino-seguir/, (27/11/2020).

[9] Secretaría de Medio Ambiente y Recursos Naturales (SEMARNAT), *Programa Estratégico Forestal 2030 Durango*, SEMARNAT, pp. 37, 2006.

[10] Pérez, G. *Los recursos forestales maderables y el desarrollo social y económico en el estado de Durango*, School of Forestry. Northern Arizona University, pp. 5, 2006.

[11] Organización de las Naciones Unidas para la Alimentación y Agricultura (FAO), *Proyecto FAO para la promoción de la energía derivada de biomasa*, Buenos Aires, 2014.

[12] Herguedas, A. *Biomasa, Biocombustibles y Sostenibilidad, Materias Primas.* Centro Tecnológico Agrario y Agroalimentario, Madrid, 2012.

[13] Almada, M. *Gasificación de Biomasa.* Organización de las Naciones Unidas para la Alimentación y la Agricultura, Ministerio de Agroindustria, Buenos Aires, 2017.

[14] Estrada, C. *Gasificación de biomasa para producción de combustibles de bajo poder calorífico y su utilización en generación de potencia y calor*. Universidad Tecnológica de Pereira. Pereira: Scientia et Technica, 2004.

[15] All Power Labs. *Power Pallet – PP30 data sheet.* http://www.allpowerlabs.com/wp-content/uploads/2019/08/PP30OneSheet8_10_19.pdf. (20/05/20).

Analysis of biodiesel production using different oils

Patrycja Trestka[1], Beata Zygmunt-Kowalska[2], Monika Kuźnia[3]

[1]AGH University of Science and Technology, e-mail: trestka@agh.edu.pl
[2]AGH University of Science and Technology e-mail: zygmunt@agh.edu.pl
[3] AGH University of Science and Technology, e-mail: kuznia@agh.edu.pl

Abstract

Due to the depletion of natural resources, new alternative fuels are sought. Biodiesel is an example of a less- toxic and promising fuel. This article presents the mechanism of production process of biodiesel from different oils (rapeseed, sunflower, and peanut) with methyl alcohol in the presence of KOH. The highest efficiency was achieved by rapeseed oil in the transesterification process. The analyzes that were carried out concerned the density, kinematic viscosity, analysis of the elements C, H and N, saponification number, acid value and iodine value.

Keywords: biodiesel, transesterification, FAME, biofuel, renewable sources, vegetable oils

1. Introduction

Nowadays fossil fuels (coal, natural gas and petroleum) are the main source of energy. Their exploitation causes global warming and reduces natural deposits [1]. The dynamic development of the transport sector and the depleting deposits of conventional raw materials energy results in interest in the market of biofuels and biocomponents. Due to this fact many researchers have been exploring alternative fuels which should be ecofriendly, economical and easily accessible [2]. Currently, the world basic liquid biofuels are: biodiesel and bioethanol. The most important is biodiesel which is obtained in the process of transesterification of vegetable oils or animal fats. This fuel is an alternative of diesel fuel, because it is made from renewable sources [3]. Another name for biodiesel is fatty acid methyl esters (FAME) [4]. Biodiesel can be used as fuel by itself or blended with petrodiesel. The main producers are countries such as Malaysia, USA, Argentina, Germany, Spain and Belgium. They provide 80% of the demand for biodiesel [5]. There are several methods to lower the viscosity of vegetable oils in order to be used as a fuel to power a diesel engine. These methods include the use of which materials as biocomponents added to diesel fuel, pyrolysis and transesterification. The last-mentioned method is the most popular and most widely used. First-generation biodiesel is produced by transesterification of triglycerides (TGs) using vegetable oils. It is a reaction of animal or vegetable oils with ethanol or methanol in the presence of alkaline catalyst. The scheme of biodiesel production in the transesterification process is shown in the Fig. 1.1.

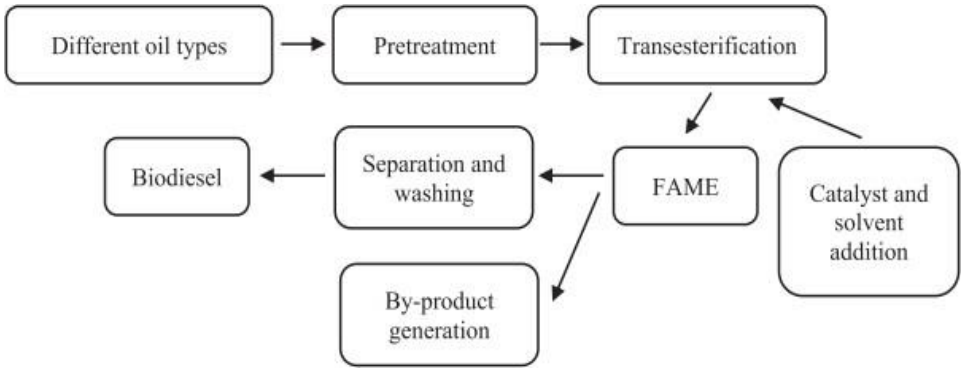

Fig. 1.1. Scheme of transesterification process of biodiesel production [5].

Biodiesel made from oils has many advantages. Biodegradability, as well as pro-ecological properties, which can lead to the reduction of the greenhouse effect, CO_2 emissions and carcinogenic compounds [6, 7]. The problems associated with the operation of this biofuel include: no possibility of long-term storage and inferior low-temperature properties compared to diesel fuel [8].

2. Materials and methods

2.1. Materials

Fatty acid methyl esters (FAME) were obtained in the process of transesterification of vegetable oils with methyl alcohol in the presence of a basic catalyst - potassium hydroxide (KOH). Rapeseed oil, sunflower oil and peanut oil were used to produce biodiesel. For the proper course of the transesterification reaction, excess alcohol and catalyst were used.

2.2. FAME manufacturing process

The transesterification reactions were divided into three main stages: stage I and stage II of vegetable oil transesterification and preliminary purification of methyl esters. Before starting the process, a mixture of the catalyst (KOH) and methyl alcohol was prepared. Then the appropriate amount of the selected vegetable oil was added to the conical flask placed on a magnetic stirrer and heated to the set temperature. The next step was to add the catalyst with alcohol and carry out the transesterification process for a certain time. Tab. 2.1. presents the parameters of the transesterification process for individual oils.

Table. 2.1. Parameters of the transesterification process.

	Oil weight [g]	Catalyst volume [ml]	Process temperature [°C]			Process time [h]
Rapeseed oil	200	43,8	40	50	60	1
Sunflower oil	200	43,8	40	50		1
Archid oil	200	43,8	40	50		1

After the specified time had elapsed, the reaction mixture was poured into a cone separator and waited for the separation of two phases, the upper fatty acid methyl ester and the lower glycerol phase, as shown in Fig. 2.1.

Fig. 2.1. Phase of methyl esters and glycerin phase.

The obtained phase of fatty acid methyl esters from the first stage was processed again using the same transesterification process. The last step is cleaning the obtained biodiesel by washing with distilled water and then drying with a drying agent.

2.3. Density

The density of methyl esters was measured in accordance with the PN - EN ISO 3104: 2004 standard using the pycnometric method [9]. In the calculations the formula (2.1) and the table water density value equal to 0,9982 $[\frac{g}{cm^3}]$ at the measurement temperature of 22 C. The formula (2.2) was also used to calculate the FAME density at 15 C.

$$\rho_{ester(22°C)} = \frac{m_{ester}}{m_{water}} * \rho_{water(22°C)} \quad (2.1)$$

$$\rho_{15\,°C} = \rho_{ester(22°C)} + 0{,}723 * (T - 15) * 10^{-3} \quad (2.2)$$

2.4. Kinematic Viscosity

Kinematic viscosity was determined for the obtained methyl esters in accordance to PN - EN ISO 3838: 2004 [10]. For this purpose Ubbelohde'a glass capillary viscometers placed in a water bath at 40°C were used.

In order to determine the kinematic viscosity of methyl esters the formula (2.3) was used:

$$\nu_{ester(40°C)} = c_{\text{capillary}} * t \quad (2.3)$$

where:

- $c_{\text{capillary}} = 0{,}00451\ \left[\frac{mm^2}{s^2}\right]$, $c_{\text{capillary}} = 0{,}00471\ \left[\frac{mm^2}{s^2}\right]$,
- t - arithmetic mean of the time the liquid flows through the calibrated part of the capillary [s].

2.5. Elemental analysis

Elemental analysis for FAME was performed using LECO CHN628. This device works by measuring the

content of the elements C, H and N in the analyzed materials. The sample is burned with pure oxygen at a temperature of 950°C. The determination of C and H is carried out using the analysis of the infrared absorption spectrum, and the determination of N through the measurement of thermal conductivity [11].

2.6. Saponification number

The saponification number was determined in accordance with the PN-83C-04043 standard by visual titration using the phenolphthalein index [12].
The following formula was used to calculate the saponification number:

$$SN = 28{,}055 \cdot \frac{(a-b)}{c} \qquad (2.4)$$

where
:

- a,b – volume of 0,5 M HCl solution used for titration of the control sample / with fat or ester [ml],
- c – mass of fat or ester [g].

2.2 Acid value

The acid number of FAME and the tested fat were determined in accordance with the PN-ISO 6618: 2011 standard by the method of titration against color indicators [13].
The following formula was used to calculate the acid number:

$$AV = 5{,}611 \cdot \frac{(a-b)}{c} \qquad (2.5)$$

where
:

- a,b – volume of 0,1 M KOH solution used to titrate the test sample with fat or ester / control [ml],
- c– mass of fat or ester [g].

2.3 Iodine value

The iodine index determination was carried out in accordance with the PN-82 C-04068 standard using the Hanus method [14].
The formula was used to calculate the iodine number:

$$IV = 1{,}269 \cdot \frac{(a-b)}{c} \qquad (2.6)$$

where
:

- a,b – volume of 0,1 M $Na_2S_2O_3$ solution used for titration of the control sample / with fat or ester [ml],
- c – mass of fat or ester [g].

3. Results and discussion

3.1. Obtaining esters of vegetable oils

The stoichiometry of the transesterification reaction shows that using 1 kg of fat is it should be possible to

obtain 1 kg of FAME and 0,1 kg of glycerine as the by-product. As a result of the conducted tests, the complete conversion of triglycerides was not achieved in any of the tested raw materials. Despite the use of an excess of catalyst and alcohol, intensive mixing and increased temperature full triglyceride conversion wasn't achieved. The reduction in the efficiency of the process was also caused by the process of purification and drying of fatty acid methyl esters. The efficiency of the transesterification process for the tested vegetable oils is shown in Fig 3.3.

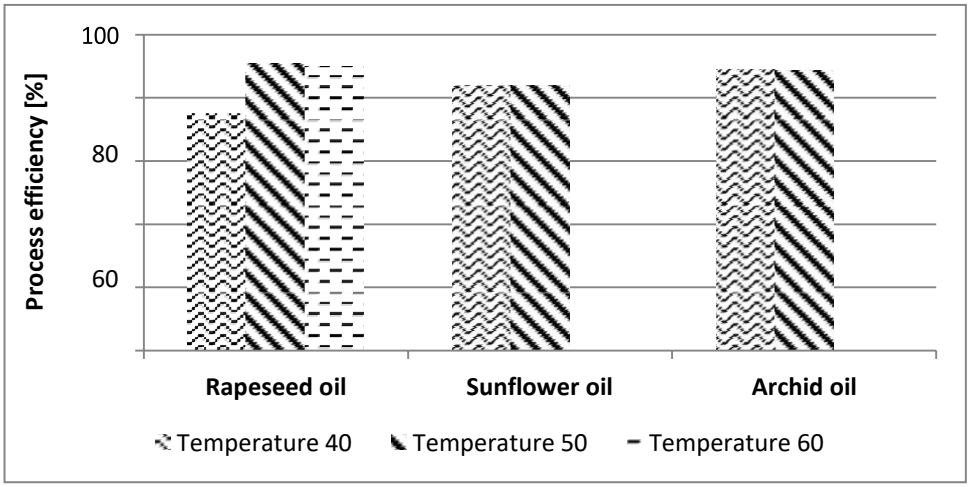

Fig. 3.3. Efficiency of the transesterification process for vegetable oils.

The transesterification process for different types of vegetable oils and different temperatures allowed to choose the best raw material for biodiesel production and the optimal process temperature. Of all the vegetable oils

tested, the highest efficiency was achieved by rapeseed oil in the transesterification process which was carried out at 50°C. This fact and the fact that rapeseed oil is the most popular raw oil material in Poland, subsequent analyses were conducted for FAME obtained from rapeseed oil.

3.2. Basic physicochemical properties

The high density and viscosity values that vegetable oils cannot be used as self-contained fuel, but are subjected to further transformation. Tab. 3.1. presents the results of the analysis, the values of density and kinematic viscosity for FAME and the required values of these parameters specified in the PN-EN 14214: 2004 specification. For comparison, the density and viscosity of crude rapeseed oil are also given.

Table. 3.1. Properties of rapeseed oil and FAME [15,16].

	Density at temperature 15°C [kg/m^3]		Kinematic viscosity [mm^2/s]	
	Measurement results	Specification PN-EN 14214:2004	Measurement results	Specification PN-EN 14214:2004
Rapeseed oil	916	900-930*	35	30-38*
FAME	881	860-900	4,278	3,5-5,0

* tabular value

As a result of the transesterification process, the density and viscosity values decreased. The measured values of density and viscosity are within the required ranges, as shown in Tab. 3.1.

3.3. Analysis of the elements C, H and N

According to the literature data in Tab. 3.2., the difference in the content of carbon in diesel fuel and methyl esters is approximately 10% and hydrogen 2%.

Table. 3.2. Content of elements C, H and N in FAME and diesel fuel [16,17].

	Fatty acid methyl esters		Diesel
	Measurement result	According to the literature	
Content C [%]	74,95	75-78	86
Content H [%]	11,48	12	14
Content N [%]	0	-	-

Small deviations of the obtained results of the analysis are related to the fact that the biodiesel is fluid. During the analysis there are losses of the tested material. In this case, the measured values can be considered within the required ranges.

3.4. Characteristic numbers

The last of the investigated properties of rapeseed oil and fatty acid methyl esters were characteristic numbers, which include: acid value, saponification number and iodine index. Results are presented in Tab. 3.3.. In the case of this parameter, an analysis of expired rapeseed oil was additionally performed in order to assess its suitability as a raw material for the production of biodiesel. Expired rapeseed oil is considered waste oil that requires disposal.

Table. 3.3. Figures characteristic for FAME and rapeseed oil [16, 17].

	Fatty acid methyl esters		Rapeseed oil		
	Measurement result	Specification PN-EN 14214:2004	Fresh	Expired	According to the literature
Saponification number [mg KOH/g]	143,20	186*	67,31	90,01	168-179
Acid value [mg KOH/g]	0,22	>0,5	1,23	1,99	max 4
Iodine value [gJ_2/100 g]	117,26	>120	92,13	75,36	94-106

* tabular value

A large difference in the saponification number can be observed between the measurement results for each analyzed sample and the required value. The deviation of the test results from the table values may be due to the fact, that here, 2% phenolphthalein solution is used, while the standard recommends a 1% phenolphthalein solution. The acid and iodine numbers for the FAME are within the required range. The acid number is often called the measure of the freshness of the test fat. The value of this number increases with the storage time of the raw material, and its growth causes a decrease in the iodine value. Due to this fact, the expired iodine number for rapeseed oil is lower than the specified range.

4. Conclusion

The article presents methods of biodiesel production from vegetable oils in laboratory conditions. The most characteristic parameters that are used to assess the quality of FAME were analyzed. Of the analyzed raw materials, rapeseed oil turned out to be the best for biodiesel production. The efficiency of the transesterification process was the highest for this raw material. Other advantages of this process include: short alcoholysis time, low process temperature, easy separation of the methyl ester phase and the glycerol phase from the reaction mixture, and high purity of the final product. The conducted analyzes of the quality of fatty acid methyl esters show that they meet the requirements and can be used as a self-contained fuel or as an additive to diesel oil. The conducted research shows the great potential of FAME as an alternative fuel to conventional fuels. The production of biodiesel and other biofuels based on oil is a multifaceted way to implement the basic assumptions of the circular bioeconomy - a priority action resulting from the economic and climate policy of the European Union.

Acknowledgment

The experimental work was done during the realization of master thesis by Patrycja Trestka: "*Analysis and comparison of the properties of biodiesel obtained from vegetable oils and low-molecular alcohols"* realized in 2019 under supervision of the PhD Monika Kuźnia at the AGH University of Science and Technology in Cracow.

References

[1] F. Yaşar: Comparision of fuel properties of biodiesel fuels produced from different oils to determine the most suitable feedstock type, *Fuel*, vol. 264, p.116817, no. March 2020, doi: 10.1016/j.fuel.2019.116817.

[2] S. Kant Bhatia *et al.*: An overview on advancements in biobased transesterification methods for biodiesel production: Oil resources, extraction, biocatalysts, and process intensification technologies, *Fuel*, vol. 285, no. August 2020, p. 119117, doi: 10.1016/j.fuel.2020.119117.

[3] H. ŞANLI: Influences of biodiesel fuels produced from highly degraded waste animal fats on the injection and emission characteristics of a CRDI diesel engine, *Int. J. Automot. Eng. Technol.*, vol. 8, pp. 11-21, no. May 2019, doi: 10.18245/ijaet.478838.

[4] N. Manojkumar, C. Muthukumaran, and G. Sharmila, A comprehensive review on the application of response surface methodology for optimization of biodiesel production using different oil sources, *J. King Saud Univ. - Eng. Sci.*, 2020, doi: 10.1016/j.jksues.2020.09.012.

[5] S. Rezania *et al.*: Review on transesterification of non-edible sources for biodiesel production with a focus on economic aspects, fuel properties and by-product applications, *Energy Convers. Manag.*, vol. 201, no. July 2019, p. 112155, doi: 10.1016/j.enconman.2019.112155.

[6] A. Pugazhendhi, A. Alagumalai, T. Mathimani, and A. E. Atabani: Optimization, kinetic and thermodynamic studies on sustainable biodiesel production from waste cooking oil: An Indian perspective, *Fuel*, vol. 273, no. August 2020, p. 117725, doi: 10.1016/j.fuel.2020.117725.

[7] A. Saydut, S. Erdogan, A. B. Kafadar, C. Kaya, F. Aydin, and C. Hamamci: Process optimization for production of biodiesel from hazelnut oil, sunflower oil and their hybrid feedstock, *Fuel*, vol. 183, no.November 2016, pp. 512–517, doi: 10.1016/j.fuel.2016.06.114.

[8] C. Kaya, C. Hamamci, A. Baysal, O. Akba, S. Erdogan, and A. Saydut: Methyl ester of peanut (Arachis hypogea L.) seed oil as a potential feedstock for biodiesel production, *Renew. Energy*, vol. 34, no. May 2009, pp. 1257-1260, doi: 10.1016/j.renene.2008.10.002.

[9] PN-EN ISO 3838:2004 Ropa naftowa i ciekłe lub stałe przetwory naftowe. Oznaczenie gęstości lub gęstości względnej.

[10] PN – EN ISO 3104:2004 Oznaczenie lepkości kinematycznej i obliczenie lepkości dynamicznej.

[11] https://pl.leco-europe.com/product/chn628-series/

[12] PN-83C-04043 Przetwory naftowe – Oznaczenie liczby zmydlania.

[13] PN-ISO 6618:2011 Przetwory naftowe i środki smarne – Oznaczenie liczby kwasowej i zasadowej – Metodą miareczkowania wobec wskaźników barwnych.

[14] PN-82C-04068 Przetwory naftowe – Oznaczenie liczby jodowej.

[15] PN-EN 14214+A1:2014-04/AC Ciekłe przetwory naftowe – Estry metylowe kwasów tłuszczowych (FAME) do użytku w silnikach samochodowych o zapłonie samoczynnym (Diesel) i zastosowaniach grzewczych – Wymagania i metody badań.

[16] J. Jakóbiec, M. Baranik, A. Duda: Wysoka jakość estrów metylowych kwasów tłuszczowych oleju rzepakowego to promocja transportu samochodowego. *Archiwum motoryzacji*, vol. 1, pp. 3-18, 2008.

[17] W. Lewandowski, M. Ryms: Biopaliwa – Proekologiczne odnawialne źródła energii, Wydawnictwo WNT, Warszawa 2013.

Cavitation technology in water and wastewater treatment

Jakub Copik[1]

[1]*Silesian University of Technology, e-mail: jakub.copik@polsl.pl*

Abstract

Due to urbanization and population increase, many undesirable pollutants are discharged into the water environment which can cause serious health effects on humans. Therefore innovative and effective techniques for water and wastewater treatment should be developed. One of the alternative to conventional processes is hydrodynamic and acoustic cavitation which are considered promising technology in many fields of industry. Literature reports proved that both ultrasonication and hydrodynamic cavitation are effective in microbial inactivation, algae and removal of low-molecular organic compounds. The effect of degradation degree depends on many different factors such as type of the pollutant, treatment time, initial concentration of pollutant, and other operational parameters. The efficiency of the pollutants removal can be enhanced by combining cavitation with other advanced oxidation processes. Recently, it is a challenge to use cavitation on an industrial scale due to its limitations, thus further research is necessary. Nevertheless, it is worth noting that some research proved the possible scalability of the cavitation process.

Keywords: ultrasound, hydrodynamic cavitation, wastewater treatment

1. Introduction

Water and wastewater treatment is one of the most important issues in terms of the sustainable use of water resources [1,2]. However, nowadays some pollutants are discharged into the water environment due to urbanization and industrialization. Many of these substances occur in low concentration but they can be very toxic and harmful for humans and the environment. A significant problem is a presence in the water environment substances such as Pharmaceuticals and Personal Care Products (PPCPs), pesticides, antibiotics, heavy metals, Disinfection by-products (DBPs), etc.[1]. The main processes of water treatment consist of sedimentation, filtration, flocculation, ion exchange, chlorination, ozonation, ultraviolet radiation, and membrane filtration [3,4]**.** Nevertheless, these processes have some limitations and problems with applications such as fouling phenomena in membrane filtration and generation of secondary pollutants during disinfection. Moreover, classical methods of water and wastewater treatment are not able to remove all types of pollutants. To improve the quality of water innovative techniques are performing. One of these methods can be the cavitation process [5].

2. Characterization of the cavitation process

Generally, two types of cavitation have been recognized – acoustic and hydrodynamic. They are basically the same in terms of principles that govern the bubbles, but the origins of local pressure drop are different [6].

Acoustic cavitation is the phenomena of the formation of bubbles caused by intensive ultrasound and their subsequent collapse in certain conditions [7].

The appearance of the tiny bubbles is related to the large pressure oscillation amplitude which is higher than the ambient pressure in the so-called rarefaction phase [2]. While the compression phase of the ultrasonic wave, these bubbles can violently collapse causing several physical and chemical effects such as shock waves, microjets, and the occurrence of shearing forces. Moreover during the collapse of the bubbles very high temperatures and pressures are generated which can reach 100 MPa and 5000 K, respectively [8]. These extreme conditions leads

also to hydroxyl radicals, hydrogen peroxide, and ozone generation similar to Advanced Oxidation Processes [9,10].

Acoustic cavitation can occur when inaudible sound frequencies (i.e. greater than 20 kHz) are used (Fig. 2.1).

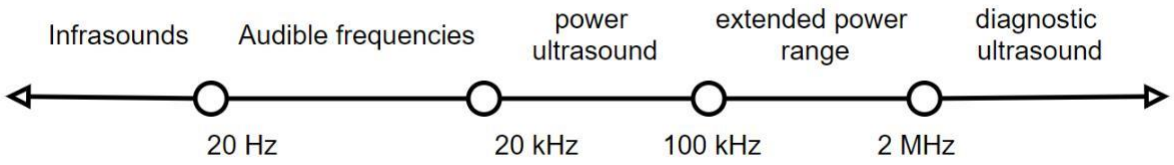

Fig. 2.1 Frequency ranges for sound [9]

For this purpose, several devices can be used [3]. In most cases, ultrasonic waves are generated using transducers composed of piezoelectric materials which can transform electrical energy into a sound (mechanical vibration) [6,11]. Some studies indicated that during acoustic cavitation more extreme conditions can be generated, however, it is difficult to expand this technology to an industrial scale [12,13].

Hydrodynamic cavitation occurs when the static pressure decrease below the vapour pressure of water due to the flow velocity increasing. That phenomenon can occur for instance while the flow passes through irregular geometries such as sharp edges. This technology is still used only on small scale due to economic issues but it is considered promising to use on an industrial scale in the future. Presently, hydrodynamic cavitation is performed in so-called hydrodynamic cavitation reactors which can be for example an orifice plate, venturi reactors, mixing blenders, or high-pressure homogenizers [14,15].

Nowadays, cavitation is considered as one of the promising methods for pollutants removal in many fields such as wastewater and drinking water treatment, chemistry, pharmacy, food processing, and cleaning (Fig.2.2) [6,14].

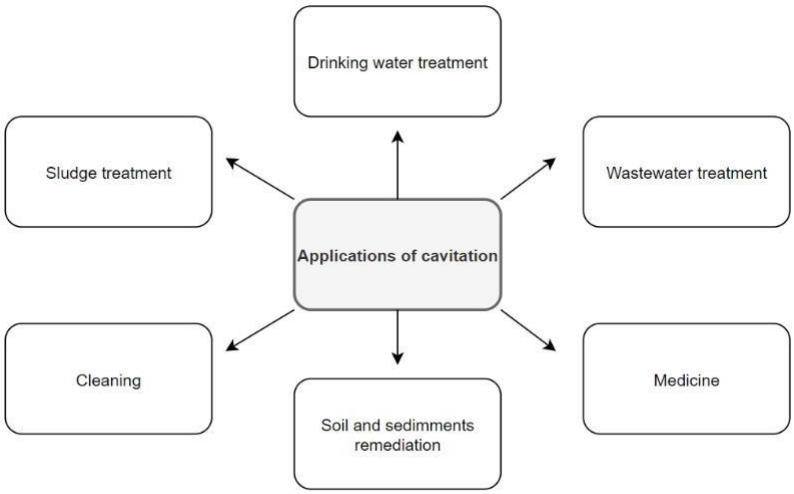

Fig. 2.2 Examples of cavitation applications [6,14,16,17]

3. Pollutants removal efficiency

As known, ultrasonic radiation can reduce the amount of pollutants in several ways. The first mechanism is related to mechanical destruction caused by violently bubble collapse, second is the oxidation of the pollutants e.g. due to hydroxyl radicals occurrence. Furthermore, pollutants can be reduced by high pressure and temperature increased during the bubble collapse [3]. Cavitation was found to be effective in many different organic pollutants removal. Microorganisms can harm human health. For example bacteria *Legionella pneumophila* which occurrence is a serious problem in warm water distribution systems causes so-called Legionnaires disease. Furthermore, Escherichia coli bacteries which are recognized as the best indicator of water fecal contamination can cause the hemolytic-uremic syndrome, bloody diarrhea, and abdominal pain [18–20].

Šarc et al. [19] performed studies on the effectiveness of the above-mentioned bacteries removal using hydrodynamic supercavitation i.e. cavitation occurs in the condition of very low pressures and high velocities [21]. They observed that after 6 cavitation passes in rotational cavitation generator, 99.98% reduction of *Legionella* occur and 99.95% reduction of *Escherichia coli* was achieved after 15 cavitation passes. While using the Venturi section setup the reduction rate was equal to 99.30% in the case of *Legionella* and 75.40% for *Escherichia Coli* during 60 and 30 cavitation passes, respectively. Jain et al**.** [22] found that also using vortex diode in hydrodynamic cavitation can be very effective in microorganisms destruction. They achieved a 99% removal rate of *Escherichia coli* during 1-hour cavitation at a very low-pressure drop of 0.5 bar. At the same conditions, *Staphylococcus Aureus* bacteria was 63% reduced but after increased pressure drop 98% reduction was achieved. Authors discovered that a vortex diode needs a lower pressure drop to be efficient in comparison with an orifice which is the most commonly use cavitating device [6]. Li et al. [23] found that using only hydrodynamic cavitation, the cultures of bacteria *Microcystic aeruginosa* from surface waters can be reduced up to 94%.

Huang et. al. study [24] have investigated the effect of ultrasonic irradiation on the behavior of extracellular organic matter (EOM) and the growth of Cyanobacteria. They found that the growth of cyanobacteria can be effectively controlled by low-frequency ultrasonic treatment and the increased intensity of treatment caused a greater release of EOM. Blooms of cyanobacteria are considered as one of the serious threats to human health and they are generated during the eutrophication process. Furthermore, the occurrence of cyanobacteria can have a negative impact on water turbidity, pH, or taste [24,25].

Some literature reports on fungi and yeast removal can be also found. Gao et al. [26] discovered a 3 log reduction of *Aureobasidium pollulans* for 60 min. low-frequency acoustic cavitation while Cameron et al. [27] determined 3.6 log reduction related to *Saccharomyces cerevisiae* during 10 min. at the 20 kHz frequency.

Some researches [26-32] demonstrated great capability and potential in persistent organic pollutants (POPs) degradation using cavitation. It is a well-known fact that these types of pollutants couldn't be removed with appropriate accuracy in conventional water and wastewater treatment systems [28]. POPs are characterized by very low hydrosolublity, high toxicity, and high resistance to degradation. Moreover, they have a very high long half-life period (up to 25 years**)** [29]. This group of substances can cause many undesirable health effects such as cancer, obesity, diabetes, cardiovascular and reproductive problems, endocrine disruption. Furthermore POPs can be more toxic in nature than was predicted in the laboratory because of synergistic effects [30]. POPs include the following substances: pesticides, polychlorinated biphenyls (PCBs), brominated compounds (BFR), furans, dioxins, and perfluorinated compounds (PFCs). These substances may have both anthropogenic and natural origin
[29]. Panda and Macikam [31] suggested that hydrodynamic cavitation is effective for dicofol (organochlorine pesticide) removal which is a DDT - type pesticide [32]. They achieved an 85 % total organic carbon removal during 60 min treatment time which proved successful mineralization of dicofol. Zhang et al. [33] found 99% destruction of 2-chlorobiphenyl, 4-chlorobiphenyl, and 2,4,5-chlorobiphenyl during 36, 47, and 29 min of sonification at 20 kHz, respectively. Moreover, Szulżyk-Cieplak [34] noted that the degradation degree of

anthracene for a single run through the hydrodynamic cavitation zone at the 7 bar inlet pressure reached 79% while the degradation degree of phenanthrene was 83%.

One of the dangerous for human health group of pollutants which occur in aquatic environment is also so-called pharmaceuticals and personal care products (PPCPs). These pollutants can have a significant impact on inducing undesirable health effects even at low doses. In general, PPCPs are used to enhance the standard of everyday life, and to cure animals and humans diseases [35]. PPCPs include substances such as caffeine, analgesics (e.g. ibuprofen, diclofenac, paracetamol), psychiatric drugs, antibiotics, antimicrobial compounds (e.g. triclosan), cosmetics, steroids, fragrances, antioxidants, and insect repellents (DEET) [36].

Vega et al. [37] reported an effective reduction of Triclosan using high-frequency ultrasound. It was 88% reduction undergo 574 kHz, 40 W L^{-1}, and 60 min sonification. They proved that the degradation rate increases as power and frequency increase. At 140 W L^{-1} Triclosan degraded completely after 25 min.

Naddeo et al. [38] found an increasing biodegradability of amoxicillin and diclofenac during low-frequency ultrasonic treatment. Furthermore, Maruyama et al. [39] performed research of ultrasonic radiation removal efficiency on hormone 17β-Estradiol. They found 62, 92, and 90% reduction at frequency 28 kHz, 580 kHz, and 1000 kHz, respectively.

Musmarra et al. [40] showed that for 60 min. hydrodynamic cavitation in venturi reactor, a 60% reduction of ibuprofen can occur. On the other hand, according to Soltani et al. [41] at 37 kHz frequency and 60 min acoustic cavitation only 13.8% but after using sonoelectroxidation the efficiency was enhanced and reached 84% ibuprofen removal. Similarly [42] improved the efficiency of ibuprofen removal from 5% (using ultrasound with frequency 1000 kHz, power density 100 40 W L^{-1} and 60 min sonification time) to 84.74% while using sonoelectroxidation with 5.26% synergy degree. Eren et al. [43] reported that effective removal of DEET (active ingredient in insect repellents) can be reached by using Dual-Frequency ultrasonic radiation. They combined 20 kHz and 640 kHz to enhanced hydroxyl radicals generation and at the same time higher efficiency of DEET removal.

4. Cavitation combined with other processes

Several studies investigated also that combined acoustic and hydrodynamic cavitation can improve the degradation of pollutants efficiency both in the same and separated reactors [12,44,45]. Yi et al. [12] for example found that the synergistic effect of the above-mentioned combined cavitation types can result in improved degradation efficiency of Rhodamine B due to enhanced collapse intensity and greater bubble formation. Furthermore, combined acoustic and hydrodynamic cavitation was more efficient in terms of energy usage, thus this technology can be considered environmentally friendly.

Nowadays, there is also a tendency to combine cavitation with advanced oxidation processes (AOPs) which can be very efficient in terms of oxidation of contaminants [15].

Čehovin et al. [46] studied the efficiency of dissolved organic carbon (DOC) removal from drinking water using AOPs processes such as O_3, H_2O_2/O_3, H_2O_2/UV, and O_3/UV combined with hybrid hydrodynamic cavitation process. Among the above-mentioned processes, the best reduction was obtained during H_2O_2/UV combined with hydrodynamic cavitation. While the most impeding impact of cavitation was achieved for O_3/UV process. Authors showed that combined H_2O_2/UV process with cavitation can improve the DOC removal efficiency up to 15%. Additionally, this improvement was obtained using relatively small doses of oxidants and a low number of cavitation passes. Mukherjee et al. [47] studied the effectiveness of total organic carbon (TOC) and chemical oxygen demand (COD) removal from greywater streams using combined hydrodynamic cavitation with AOP. They reported that using hydrodynamic cavitation combined with H_2O_2 (5g/L) after 60 min. led to 87.5% COD and 56.9% TOC reduction. While it was 6.5% and 4.3% for H_2O_2 and 11.25 and 6% for hydrodynamic cavitation used separately.

5. Factors influencing cavitation process

In general, the effect of cavitation treatment can be different according to the type of microorganism, time of the treatment, sample volumes, intensity, frequency, etc. For instance, some research suggested, that low-frequency ultrasound could be more effective than high-frequency ultrasonication in terms of bacteria removal and at the same time physical mechanism of removal could be more effective than the chemical one [48]. As the frequency of ultrasound decreases, the energy released during bubble collapse and the size of bubbles increases.While when frequency increases, more free radicals can be generated due to a greater amount of cavitation events [49,50]. However, it was also found that high-frequency ultrasonication can be very efficient in bacterial inactivation [48,51]. Koda et al. [48] for example found that inactivation of Escherichia coli and Streptococcus mutans can be slightly higher at 500 kHz than 20 kHz frequency. Whereas Nasseri et al. [52] reported that using ultrasound at frequency 35 kHz can have 24.8% removal efficiency of total chemical oxygen demand (COD) after 60 min sonification. They found also that increased at the greater frequency (130 kHz) the removal efficiency of COD in the same conditions increased to 28.2%. However, unlike total COD, the efficiency of suspended COD was higher at a lower frequency.

Some research showed also that effectiveness of the ultrasonification process could depend on internal structure of the pollutants. For example, gram-negative bacteria was found as more sensitive to ultrasound treatment in compare with gram-positive bacteria [26,27,53,54]. Moreover, it is known that the inactivation of organic pollutants can increase as the intensity and ultrasonic amplitude increases [55–57]. Koda et al. [48] proved also that the inactivation of bacteria can increases with irradiation time while Nasseri et al. [52] shown that increasing sonication time can increase the COD removal efficiency while sanitation time had no considerable effect on BOD_5 treatment.

It is also known that cavitation is connected with temperature fluctuations. In general, due to increased temperature too many bubbles could be generated and, consequently, the energy of bubble collapse and efficiency of cavitation could decrease. On the other hand, increased temperature could increase the kinetics rate of oxidation reaction thus cavitation can be more effective. Moreover, due to increased volatility, the pollutant can easier get inside the bubbles and at the same time, they could be removed easier [15,58]. Nasseri et al. [52] reported that during ultrasonic cavitation temperature can increase about 18-20 °C in 60 min. sonification. Overall, the degradation of organic pollutants is also strongly related to pH value. Mukherjee et al. [47] reported that increasing pH value corresponds to decreasing degradation efficiency. Change the pH from 3 to 10 was related to 18.23% and 5.2% reduction of TOC reduction, respectively.

The use of the cavitation process can have many advantages. It is clean technology with a high removal efficiency of many pollutants [55]. Furthermore, this technology does not require the use of chemicals, and the byproducts formed are limited. Cavitation could be also easily combined with other processes with a high synergism effect [15]**.** Although cavitation was found to be feasible on a small scale it is a challenge to develop these processes on industrial scale, mainly due to high energy requirements [59]. Nevertheless, it is worth noting that some research proved possible scalability of cavitation [60,61].

6. Conclusion

Hydrodynamic and acoustic cavitation are one of the novel methods for water and wastewater quality improvement. These techniques are an alternative to conventional processes such as sedimentation, flocculation, filtration, and chlorination which could not remove all kinds of pollutants from the aquatic environment. Recently, cavitation is considered a promising technology in wastewater and drinking water treatment, chemistry, pharmacy, cleaning, and many other industries. Literature reports indicate that both ultrasonification and hydrodynamic cavitation technology could be efficient in microbial inactivation, removal of algae and low-molecular organic

compounds which could cause many negative health effects. It could be performed in both mechanical and chemical ways due to the occurrence of so-called shock waves, hot spots, microjets, and extremely high pressure and temperature conditions. The effect of reduction depends on the type of the pollutant, treatment time, initial concentration, and other operational parameters such as inlet pressure, frequency, and intensity depending on the type of cavitation.

To improve efficiency and due to economic issues, recently there is a tendency to combine cavitation processes with other treatment methods. It was proved that cavitation can be very effective while combined with O_3, H_2O_2/O_3, O_3/UV, H_2O_2/UV, and other advanced oxidation processes.

Nowadays this is a challenge to use cavitation at a large scale because not all the cavitation generation mechanisms, scale-up effects are well understood. Moreover, research and design methods have not been established.

Additionally, cavitation technology is connected with some limitations such as high energy requirements which slows the development of industrial-scale cavitation technology. Therefore further research in theoretical, experimental, and computational aspects is necessary.

References

[1] T.J. Mason, C. Pétrier, Ultrasound processes, Adv. Oxid. Process. Water Wastewater Treat. (2004) 185–http://www.iwapublishing.com/books/9781843390176/advanced-oxidation-processes-water-and-wastewater-treatment.

[2] M. Dular, T. Griessler-Bulc, I. Gutierrez-Aguirre, E. Heath, T. Kosjek, A. Krivograd Klemenčič, M. Oder, M. Petkovšek, N. Rački, M. Ravnikar, A. Šarc, B. Širok, M. Zupanc, M. Žitnik, B. Kompare, Use of hydrodynamic cavitation in (waste)water treatment, Ultrason. Sonochem. 29 (2016) 577–588. https://doi.org/10.1016/j.ultsonch.2015.10.010.

[3] M.R. Doosti, R. Kargar, M.H. Sayadi, Water treatment using ultrasonic assistance : A review, Ecology. 2 (2012) 96–110.

[4] B. Tansel, New Technologies for Water and Wastewater Treatment: A Survey of Recent Patents, Recent Patents Chem. Eng. 1 (2010) 17–26. https://doi.org/10.2174/1874478810801010017.

[5] U.I. Gaya, A.H. Abdullah, Heterogeneous photocatalytic degradation of organic contaminants over titanium dioxide: A review of fundamentals, progress and problems, J. Photochem. Photobiol. C Photochem. Rev. 9 (2008) 1–12. https://doi.org/10.1016/j.jphotochemrev.2007.12.003.

[6] M. Zupanc, Ž. Pandur, T. Stepišnik Perdih, D. Stopar, M. Petkovšek, M. Dular, Effects of cavitation on different microorganisms: The current understanding of the mechanisms taking place behind the phenomenon. A review and proposals for further research, Ultrason. Sonochem. 57 (2019) 147–165. https://doi.org/10.1016/j.ultsonch.2019.05.009.

[7] K. Yasui, Acoustic Cavitation and Bubble Dynamics, 2018. http://www.springer.com/series/15634.

[8] M. Ashokkumar, The characterization of acoustic cavitation bubbles - An overview, Ultrason. Sonochem. (2011) 864–872. https://doi.org/10.1016/j.ultsonch.2010.11.016.

[9] N.A.H. Fetyan, T.M. Salem Attia, Water purification using ultrasound waves: application and challenges, Arab J. Basic Appl. Sci. 27 (2020) 194–207. https://doi.org/10.1080/25765299.2020.1762294.

[10] A. Warade, R. Gaikwad, Review on wastewater treatment by hydrodynamic cavitation, IOSR J. Environ. Sci. 10 (2016) 67–72.

[11] D. Chen, Applications of ultrasound in water and wastewater treatment, Handb. Appl. Ultrasound Sonochemistry Sustain. (2011) 373–405. https://doi.org/10.1201/b11012-16.

[12] C. Yi, Q. Lu, Y. Wang, Y. Wang, B. Yang, Degradation of organic wastewater by hydrodynamic cavitation combined with acoustic cavitation, Ultrason. Sonochem. 43 (2018) 156–165. https://doi.org/10.1016/j.ultsonch.2018.01.013.

[13] P.R. Gogate, G.S. Bhosale, Comparison of effectiveness of acoustic and hydrodynamic cavitation in combined treatment schemes for degradation of dye wastewaters, Chem. Eng. Process. Process Intensif. (2013) 59–69. https://doi.org/10.1016/j.cep.2013.03.001.

[14] X. Sun, S. Chen, J. Liu, S. Zhao, J.Y. Yoon, Hydrodynamic Cavitation: A Promising Technology for Industrial-Scale Synthesis of Nanomaterials, Front. Chem. 8 (2020) 1–7. https://doi.org/10.3389/fchem.2020.00259.

[15] M. Gągol, A. Przyjazny, G. Boczkaj, Wastewater treatment by means of advanced oxidation processes based on cavitation – A review, Chem. Eng. J. 338 (2018) 599–627. https://doi.org/10.1016/j.cej.2018.01.049.

[16] T.D. Pham, R.A. Shrestha, J. Virkutyte, M. Sillanpää, Recent studies in environmental applications of ultrasound, Can. J. Civ. Eng. 36 (2009) 1849–1858. https://doi.org/10.1139/L09-068.

[17] C.E. Brennen, Cavitation in medicine, Interface Focus. 5 (2015) 1–12. https://doi.org/10.1098/rsfs.2015.0022.

[18] J.P.S. Cabral, Water microbiology. Bacterial pathogens and water, Int. J. Environ. Res. Public Health. 7 (2010) 3657–3703. https://doi.org/10.3390/ijerph7103657.

[19] A. Šarc, J. Kosel, D. Stopar, M. Oder, M. Dular, Removal of bacteria Legionella pneumophila, Escherichia coli, and Bacillus subtilis by (super)cavitation, Ultrason. Sonochem. 42 (2018) 228–236. https://doi.org/10.1016/j.ultsonch.2017.11.004.

[20] M.. Karmali, Infection by verocytotoxin-producing Escherichia coli, Clin. Microbiol. 2 (1989) 15–38.

[21] D.. Stinebring, M.. Billet, J. w. Lindau, R.. Kunz, Developed Cavitation-Cavity Dynamics, (2001).

[22] P. Jain, V.M. Bhandari, K. Balapure, J. Jena, V. V. Ranade, D.J. Killedar, Hydrodynamic cavitation using vortex diode: An efficient approach for elimination of pathogenic bacteria from water, J. Environ. Manage. 242 (2019) 210–219. https://doi.org/10.1016/j.jenvman.2019.04.057.

[23] P. Li, Y. Song, S. Yu, Removal of Microcystis aeruginosa using hydrodynamic cavitation: Performance and mechanisms, Water Res. 62 (2014) 241–248. https://doi.org/10.1016/j.watres.2014.05.052.

[24] Y.R. Huang, H.Z. Li, X.M. Wei, D.H. Wang, Y.T. Liu, L. Li, The effect of low frequency ultrasonic treatment on the release of extracellular organic matter of Microcystis aeruginosa, Chem. Eng. J. 383 (2020) 123141. https://doi.org/10.1016/j.cej.2019.123141.

[25] L. Li, N. Gao, Y. Deng, J. Yao, K. Zhang, Characterization of intracellular & extracellular algae organic matters (AOM) of Microcystic aeruginosa and formation of AOM-associated disinfection byproducts and odor & taste compounds, Water Res. 46 (2012) 1233–1240. https://doi.org/10.1016/j.watres.2011.12.026.

[26] S. Gao, G.D. Lewis, M. Ashokkumar, Y. Hemar, Inactivation of microorganisms by low-frequency high-power ultrasound: 1. Effect of growth phase and capsule properties of the bacteria, Ultrason. Sonochem. 21 (2014) 446–453. https://doi.org/10.1016/j.ultsonch.2013.06.006.

[27] M. Cameron, L.D. McMaster, T.J. Britz, Electron microscopic analysis of dairy microbes inactivated by ultrasound, Ultrason. Sonochem. 15 (2008) 960–964. https://doi.org/10.1016/j.ultsonch.2008.02.012.

[28] K.O. Badmus, J.O. Tijani, E. Massima, L. Petrik, Treatment of persistent organic pollutants in wastewater using hydrodynamic cavitation in synergy with advanced oxidation process, Environ. Sci. Pollut. Res. 25 (2018) 7299–7314. https://doi.org/10.1007/s11356-017-1171-z.

[29] C.-B. Angela, The impact of persistent organic pollutants on freshwater ecosystems and human health, 2016.

[30] O.M.L. Alharbi, A.A. Basheer, R.A. Khattab, I. Ali, Health and environmental effects of persistent organic pollutants, J. Mol. Liq. 263 (2018) 442–453. https://doi.org/10.1016/j.molliq.2018.05.029.

[31] D. Panda, S. Manickam, Hydrodynamic cavitation assisted degradation of persistent endocrine-disrupting organochlorine pesticide Dicofol: Optimization of operating parameters and investigations on the mechanism of intensification, Ultrason. Sonochem. 51 (2019) 526–532. https://doi.org/10.1016/j.ultsonch.2018.04.003.

[32] Y.B. Man, K.L. Chow, Z. Cheng, Y. Kang, M.H. Wong, Profiles and removal efficiency of organochlorine pesticides with emphasis on DDTs and HCHs by two different sewage treatment works, Environ. Technol. Innov. 9 (2018) 220–231. https://doi.org/10.1016/j.eti.2017.12.004.

[33] G. Zhang, I. Hua, Cavitation chemistry of polychlorinated biphenyls: Decomposition mechanisms and rates, Environ. Sci. Technol. 34 (2000) 1529–1534. https://doi.org/10.1021/es981127f.

[34] J. Szulzyk-Cieplak, Removal of hardly bio-degradabale organic compounds from wastewater by means of reagentless methods, J. Ecol. Eng. 18 (2017) 63–71. https://doi.org/10.12911/22998993/74634.

[35] A.J. Ebele, M. Abou-Elwafa Abdallah, S. Harrad, Pharmaceuticals and personal care products (PPCPs) in the freshwater aquatic environment, Emerg. Contam. 3 (2017) 1–16. https://doi.org/10.1016/j.emcon.2016.12.004.

[36] C.R. Ohoro, A.O. Adeniji, A.I. Okoh, O.O. Okoh, Distribution and chemical analysis of pharmaceuticals and personal care products (PPCPs) in the environmental systems: A review, Int. J. Environ. Res. Public Health. 16 (2019). https://doi.org/10.3390/ijerph16173026.

[37] L.P. Vega, J. Soltan, G.A. Peñuela, Sonochemical degradation of triclosan in water in a multifrequency reactor, Environ. Sci. Pollut. Res. 26 (2019) 4450–4461. https://doi.org/10.1007/s11356-018-1281-2.

[38] V. Naddeo, S. Meriç, D. Kassinos, V. Belgiorno, M. Guida, Fate of pharmaceuticals in contaminated urban wastewater effluent under ultrasonic irradiation, Water Res. 43 (2009) 4019–4027. https://doi.org/10.1016/j.watres.2009.05.027.

[39] H. Maruyama, H. Seki, Y. Matsukawa, A. Suzuki, N. Inoue, Removal of bisphenol A and diethyl phthalate from aqueous phases by ultrasonic atomization, Ind. Eng. Chem. Res. 45 (2006) 6383–6386. https://doi.org/10.1021/ie060353s.

[40] D. Musmarra, M. Prisciandaro, M. Capocelli, D. Karatza, P. Iovino, S. Canzano, A. Lancia, Degradation of ibuprofen by hydrodynamic cavitation: Reaction pathways and effect of operational parameters, Ultrason. Sonochem. 29 (2016) 76–83. https://doi.org/10.1016/j.ultsonch.2015.09.002.

[41] R. Darvishi Cheshmeh Soltani, M. Mashayekhi, Decomposition of ibuprofen in water via an electrochemical process with nano-sized carbon black-coated carbon cloth as oxygen-permeable cathodeintegrated with ultrasound, Chemosphere. 194 (2018) 471–480. https://doi.org/10.1016/j.chemosphere.2017.12.033.

[42] B. Thokchom, K. Kim, J. Park, J. Khim, Ultrasonically enhanced electrochemical oxidation of ibuprofen, Ultrason. Sonochem. 22 (2015) 429–436. https://doi.org/10.1016/j.ultsonch.2014.04.019

[43] Z. Eren, K. O'Shea, Hydroxyl Radical Generation and Partitioning in Degradation of Methylene Blue and DEET by Dual-Frequency Ultrasonic Irradiation, J. Environ. Eng. 145 (2019) 04019070. https://doi.org/10.1061/(asce)ee.1943-7870.0001593.

[44] M. Franke, P. Braeutigam, Z.L. Wu, Y. Ren, B. Ondruschka, Enhancement of chloroform degradation by the combination of hydrodynamic and acoustic cavitation, Ultrason. Sonochem. 18 (2011) 888–894. https://doi.org/10.1016/j.ultsonch.2010.11.011.

[45] P. Braeutigam, M. Franke, R.J. Schneider, A. Lehmann, A. Stolle, B. Ondruschka, Degradation of carbamazepine in environmentally relevant concentrations in water by Hydrodynamic-Acoustic-Cavitation (HAC), Water Res. 46 (2012) 2469–2477. https://doi.org/10.1016/j.watres.2012.02.013.

[46] M. Čehovin, A. Medic, J. Scheideler, J. Mielcke, A. Ried, B. Kompare, A. Žgajnar Gotvajn, Hydrodynamic cavitation in combination with the ozone, hydrogen peroxide and the UV-based advanced oxidation processes for the removal of natural organic matter from drinking water, Ultrason. Sonochem. 37 (2017) 394–404. https://doi.org/10.1016/j.ultsonch.2017.01.036.

[47] A. Mukherjee, A. Mullick, R. Teja, P. Vadthya, A. Roy, S. Moulik, Performance and energetic analysis of hydrodynamic cavitation and potential integration with existing advanced oxidation processes: A case study for real life greywater treatment, Ultrason. Sonochem. 66 (2020) 105116. https://doi.org/10.1016/j.ultsonch.2020.105116.

[48] S. Koda, M. Miyamoto, M. Toma, T. Matsuoka, M. Maebayashi, Inactivation of Escherichia coli and Streptococcus mutans by ultrasound at 500 kHz, Ultrason. Sonochem. 16 (2009) 655–659. https://doi.org/10.1016/j.ultsonch.2009.02.003.

[49] L.A. Crum, Comments on the evolving field of sonochemistry by a cavitation physicist, Ultrason. - Sonochemistry. 2 (1995) 147–152. https://doi.org/10.1016/1350-4177(95)00018-2.

[50] S. Gao, Y. Hemar, M. Ashokkumar, S. Paturel, G.D. Lewis, Inactivation of bacteria and yeast using high-frequency ultrasound treatment, Water Res. 60 (2014) 93–104. https://doi.org/10.1016/j.watres.2014.04.038.

[51] R.V. Peterson, W.G. Pitt, The effect of frequency and power density on the ultrasonically-enhanced killing of biofilm-sequestered Escherichia coli, Colloids Surfaces B Biointerfaces. 17 (2000) 219–227. https://doi.org/10.1016/S0927-7765(99)00117-4.

[52] S. Nasseri, F. Vaezi, A. Mahvi, R. Nabizadeh, S. Haddadi, Determination of the ultrasonic effectiveness in advanced wastewater treatment, J. Environ. Heal. Sci. Eng. 3 (2006) 109–116.

[53] F.I.K. AHMED, C. RUSSELL, Synergism between Ultrasonic Waves and Hydrogen Peroxide in the Killing of Micro organisms, J. Appl. Bacteriol. 39 (1975) 31–40. https://doi.org/10.1111/j.1365-2672.1975.tb00542.x.

[54] T. Monsen, E. Lövgren, M. Widerström, L. Wallinder, In vitro effect of ultrasound on bacteria and suggested protocol for sonication and diagnosis of prosthetic infections, J. Clin. Microbiol. 47 (2009) 2496–2501. https://doi.org/10.1128/JCM.02316-08.

[55] J. Wang, Z. Wang, C.L.Z. Vieira, J.M. Wolfson, G. Pingtian, S. Huang, Review on the treatment of organic pollutants in water by ultrasonic technology, Ultrason. Sonochem. 55 (2019) 273–278. https://doi.org/10.1016/j.ultsonch.2019.01.017.

[56] S. V. Sancheti, C. Saini, R. Ambati, P.R. Gogate, Synthesis of ultrasound assisted nanostuctured photocatalyst (NiO supported over CeO2) and its application for photocatalytic as well as sonocatalytic dye degradation, Catal. Today. 300 (2018) 50–57. https://doi.org/10.1016/j.cattod.2017.02.047.

[57] A. Khataee, S. Saadi, B. Vahid, S.W. Joo, Sonochemical synthesis of holmium doped zinc oxide nanoparticles: Characterization, sonocatalysis of reactive orange 29 and kinetic study, J. Ind. Eng. Chem. (2016) 167–176. https://doi.org/10.1016/j.jiec.2015.12.028.

[58] P.R. Gogate, P.N. Patil, Combined treatment technology based on synergism between hydrodynamic cavitation and advanced oxidation processes, Ultrason. Sonochem. 25 (2015) 60–69. https://doi.org/10.1016/j.ultsonch.2014.08.016.

[59] C. Pétrier, The use of power ultrasound for water treatment, 2014. https://doi.org/10.1016/B978-1-78242-028-6.00031-4.

[60] S.M. Joshi, P.R. Gogate, Intensification of industrial wastewater treatment using hydrodynamic cavitation combined with advanced oxidation at operating capacity of 70 L, Ultrason. Sonochem. 52 (2019) 375- https://doi.org/10.1016/j.ultsonch.2018.12.016.

[61] X. Sun, C.H. Kang, J.J. Park, H.S. Kim, A.S. Om, J.Y. Yoon, An experimental study on the thermal performance of a novel hydrodynamic cavitation reactor, Exp. Therm. Fluid Sci. 99 (2018) 200–210. https://doi.org/10.1016/j.expthermflusci.2018.02.034.

Separation of methane - nitrogen mixture by adsorption

Ewelina. Brodawka[1], Mieczysław R. Bałys[1]

[1]AGH UST in Krakow, e-mail: brodawka@agh.edu.pl

Abstract

In this paper we present a new aspect of the PSA process design for the separation of methane-nitrogen mixture. This approach is based on an analysis of the impact of the gaseous mixture's composition on the design process and can be generally divided into the following two categories: (a) the enrichment of the trace of methane from ventilation air methane (VAM) and (b) the bulk separation of natural gas. The feasibility of the separation of the mixture containing different concentration of methane, with the help of computer simulations, was investigated in our research.

Keywords: pressure swing adsorption, methane-nitrogen mixture, separation processes

1. Introduction

Methane is the main component of natural gas and has a far more powerful effect on global temperatures than carbon dioxide. Its sources are both natural and artificial. One of the human sources is fossil fuels, including leakage from natural gas pipelines, oil wells, and coal mines or seams. Coal mine methane is actually referred to according to its moment of release, that is before, during and after operational mining [1]. Table. 1.1. shows the percentage of methane in coal mine methane sources according to this division.

The first major global study examining the problem of methane emission leaking from coal mines has been recently released by International Energy Agency. According to this report, mitigation of coal mine methane emission is difficult from the technical and economical points of view as the concentration of methane is frequently low and variable. Due to its environmental impact, millions of tonnes of methane must be reduced to an appropriate level before being directly discharged into the atmosphere [2].

Table. 1.1. Coal mine methane emission [1].

Coal mine streams	Percentage of methane
Ventilation air methane	0.1-1%
Coal bed methane	60-95%
Abandoned mine methane	30-95%

In recent years the natural gas upgrading was being studied for methane usage as an alternative fuel with the main objective - clean burning. Hence adsorption-based processes for the separation of nitrogen from the natural gas have become a reality in industrial practice, especially in the PSA process [3]. Despite such development in the practical applications of the PSA technology in the natural gas separation, the design and optimization of the PSA system for VAM enrichment (with the main objective - resolving the environmental crisis) still largely remains an experimental and/or simulation effort.

2. PSA process design

In order to separate methane-nitrogen mixture through the PSA process, based on their composition, it is advised to firstly select proper adsorbent based on its equilibrium and kinetic characteristics, and then select operating conditions such as pressure levels for the PSA system, cycle configuration, duration of each, and bed dimensions. Such adsorption is achieved due to the gas-solid interactions. For a methane-nitrogen separation, these 'interactions' can be dependent on two main different separation mechanisms: kinetic separation is achieved by the differences in components gas diffusion rate in the adsorbent, which is higher for the smaller nitrogen molecule compared to methane and equilibrium separation, which is obtained by the differences of the selective adsorption amount of the adsorbed components [4]. Having considered two different cases: (a) the enrichment of the trace of methane from VAM and (b) the bulk separation of natural gas it may be concluded that:

- the equilibrium separation process could be obtained for the mixture containing a low concentration of methane – case (a). Methane as a more strongly adsorbed component is at first adsorbed, then desorbed from the solid. However, the idea of the equilibrium separation process of methane (as a desorbed gas) from natural gas is known from the literature but production of purified methane as the low-pressure desorbed product during this process diminishes the energy advantage of the available high-pressure kinetic separation of natural gas [5].
- the kinetic separation process could be obtained for case (b), in which nitrogen is adsorbed on a solid adsorbent and purified methane is obtained as the high-pressure product. From an economic point of view (a very large amount of solid adsorbent is required to absorb nitrogen), this way of conducting the process is not advisable for case (a).

The flow patterns for the different separation mechanisms are schematically illustrated in Fig. 2.1.

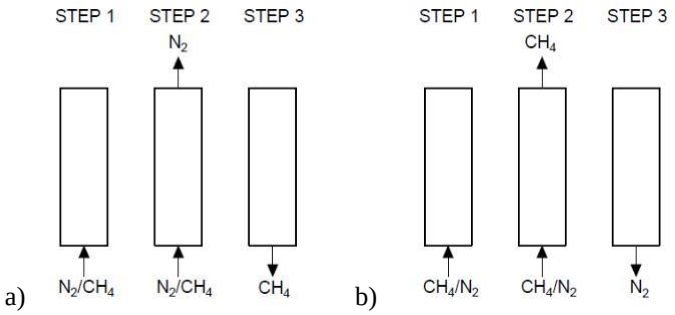

Fig. 2.1. Flow patterns for a) equilibrium separation, b) kinetic separation

3. Simulation

The removal of methane from the various feed gases composed of CH_4/N_2 the one-bed column was investigated by simulation, in order to obtain design data for future experimental measurements. For a gas mixture containing low concentration of methane a pressure swing adsorption (PSA) process has been designed and simulated by *CySim: Cycle simulator* developed at the University of Edinburgh. More information about the software used was published in [4]. For the second gas mixture, Aspen Adsorption V12 simulation program has been used to perform those simulations. Carbonaceous adsorbents with different properties were used to separate two different mixtures [5,6]. Table 2.1. shows some initial parameters. While conducting the simulation in both cases, the process consisted of the one-bed PSA unit undergoing a four-step Skarstrom cycle: (1) pressurization,
[1] high-pressure adsorption, (3) blowdown, and (3) purge at low pressure desorption. The authors are aware that as a preliminary simulation study the use of the basic Skarstrom cycle [7] is generally useful for a comparative evaluation. Yet, from an economic point of view, performing the cycle in exactly the same way is not always

beneficial in a kinetically controlled process. In that case, to improve the recovery of the product, replacing the blowdown and purge steps with the evacuation step and leaving the column open at the low pressure for some time is recommended.

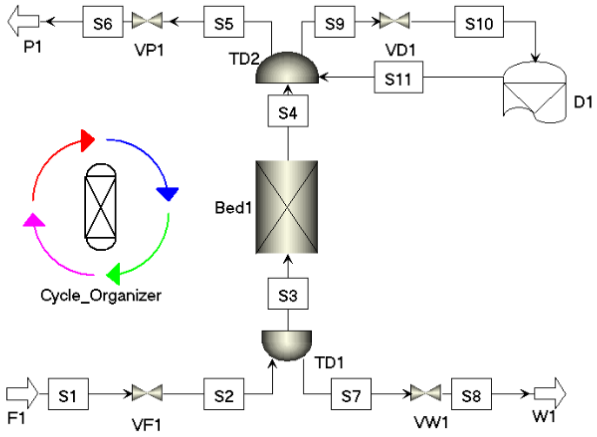

Fig. 2.1. Schematic diagram for the implementation of the one-bed PSA process within Aspen Adsorption.

Table. 2.1. The initial parameters for the simulations

No.	System	Feed gas composition	Langmuir constants		Overall resistance for components D_{c0}/r^2 (s^{-1})		Pressure range (bar)	
			CH_4	N_2	CH_4	N_2	adsorption	blowdown
1	CH_4-N_2-activated carbon [5]	CH_4 0.3% N_2 99.7%	2.51 1.12E-03	1.055 6.32E-04	-	-	1	0.05
2	CH_4-N_2-carbon molecular sieves [6]	CH_4 85% N_2 15%	3.55 5.03E-04	3.51 7.40E-04	2.77	706.31	5	1

There are two separation performance indicators: purity and recovery for the i^{th} component, where i is either CH_4 or N_2. The purity for both mixtures at the end of the k^{th} cycle is defined as follows [8]:

$$purity_{CH_4}^{k} = \frac{n_{P,CH_4}^{k} - n_{P,CH_4}^{k-1}}{\sum_{i}^{N}(n_{P,i}^{k} - n_{P,i}^{k-1})} \quad (1)$$

where N is the number of components, $n_{P,i}^{k}$ and $n_{P,i}^{k-1}$ are the cumulative amount of component i in a mole, which has been received at the end of the k^{th} or $k\text{-}1^{th}$ cycle, respectively. The purity of CH_4 we can calculate as the ratio between the amount of CH_4 and the total amount of CH_4 and N_2 components in the production step, P which: in case (a) is the blowdown and purge step, but in case (b) is the adsorption step.
The recovery is calculated as the ratio between the CH_4 recovered during the production step, P and the CH_4 introduced in the adsorption step, F:

$$recovery_{CH_4}^{k} = \frac{n_{P,CH_4}^{k} - n_{P,CH_4}^{k-1}}{n_{F,CH_4}^{k} - n_{F,CH_4}^{k-1}} \quad (2)$$

4. Results

According to simulation results for case (a), the concentration of methane increases from 0.3 vol.% (gas feed) to 0.89 vol.% - average methane concentration in product gas (desorbed + purged gas). The cyclic steady-state performance parameters are given below.

Table. 4.1. Results of simulations for case (a)

methane	product	waste
recovery (%)	36.61	63.39
purity (%)	0.89	0.27

In table. 4.1. methane waste is the amount of methane which was passed through and collected during the adsorption step.

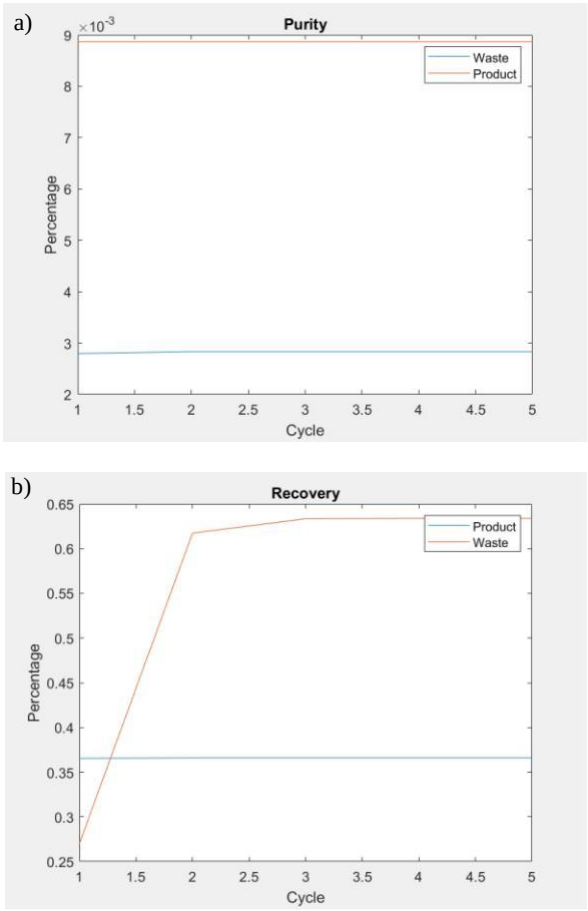

Fig. 4.1. Plot of methane a) purity and b) recovery vs. number of the cycle for case (a).

For the second case (b), the concentration of methane increases from 85 vol.% (gas feed) to around 91 vol.% - average methane concentration in the product gas. Moreover, the authors found that it is possible to reach 96% methane purity (pipeline-quality natural gas) with the carbon molecular sieves sample by decreasing blowdown pressure (table. 4.1.).

Table. 4.1. Results of simulations for case (b)

CH_4 purity (%)	CH_4 recovery (%)	Blowdown pressure (bar)
91.3	63.07	1
96.1	56.51	0.2

5. Conclusion

The product/methane purity for both cases was obtained. It has been shown that by the use of a cyclic simulator it is possible to design and calculate adsorption separation for mixtures containing different amounts of methane. The feed gas composition of methane-nitrogen mixture is a driving force to derive the rules for various decision steps in the design of PSA, including decisions on pressure levels, configuration and time of PSA cycle, thus overall used technology. More simulation results and experimental measurements in the future would help to modify the rules already proposed here and develop a more elaborate path to design methane-nitrogen separation.

Acknowledgement

The authors gratefully acknowledge financial support from the "Initiative of Excellence – Research University - IDUB, Activity no. 4" programme of AGH University of Science and Technology in Krakow, Poland.

References

[1] K. Ahmed and S. Meraj, *Coal seam methane abatement and utilization techniques with availability and feasibility criteria*, Adv. Sci. Technol. Eng. Syst., vol. 1, no. 1, pp. 1–10, 2016, doi: 10.25046/aj010101.

[2] IEA, *World Energy Outlook 2019*, Paris, 2019.

[3] C. A. Grande, *Advances in Pressure Swing Adsorption for Gas Separation*, ISRN Chem. Eng., vol. 2012, 1–13, 2012, doi: 10.5402/2012/982934.

[4] E. Brodawka, *Simulation of Kinetically Controlled Pressure Swing Adsorption Processes*, in Contemporary Problems of Power Engineering and Environmental Protection, 2019, pp. 85–91.

[5] E. Brodawka, M. Bałys, J. Szczurowski, L. Czepirski, K. Zarębska, and P. Da Costa, *Nanoporous Carbonaceous Adsorbents for Enrichment of Ventilation Air Methane (VAM) with Methane*, in Proceedings of the Nanotech France 2019 International Conference, Paris, France – June *26 - 28*, 2019, 17–20, doi: 10.26799/cp-nanotechfrance2019.

[6] S. J. Bhadra and S. Farooq, *Separation of methane-nitrogen mixture by pressure swing adsorption for natural gas upgrading*, Ind. Eng. Chem. Res., vol. 50, no. 24, pp. 14030–14045, 2011, doi: 10.1021/ie201237x.

[7] C. W. Skarstrom, *Method and apparatus for fractionating gaseous mixtures by adsorption*, US2944627, 1958.

[8] A. H. Farmahini, S. Krishnamurthy, D. Friedrich, S. Brandani, and L. Sarkisov, *From Crystal to Adsorption Column: Challenges in Multiscale Computational Screening of Materials for Adsorption Separation Processes*, Ind. Eng. Chem. Res., vol. 57, no. 45, pp. 15491–15511, 2018, doi: 10.1021/acs.iecr.8b03065.

Hydrogen-to-X application pathways overview

Karolina Zaik[1]

[1]*Silesian University of Technology, e-mail:karolina.zaik@polsl.pl*

Abstract

One of the current major research trends in the world is the development of low and carbon-free energy systems to decarbonize the global economy. The development of this energy sector indicates effective solutions to achieve the carbon reduction targets. The decarbonization of the global economy is possible today through the integration of its different sectors: electricity and fuel based on the use of renewable energy sources. Using renewable energy to produce hydrogen by electrolysis we produce a product - hydrogen, which can then be used as a zero-emission fuel or in combination with other elements as a molecular component in basic industrial raw materials. This article identifies in particular the main application paths for hydrogen produced by electrolysis and discusses the potential role of hydrogen systems in the decarbonization of the transport, industry and energy sectors.

Keywords: hydrogen, hydrogen-to-x, power-to-gas

1. Introduction

The increase in global warming and environmental pollution directly affects the need for energy transformation, focusing primarily on decarbonization. The economic "boom" that we can observe in the 21st century also influences the importance of the energy transformation process. Unfortunately, the development of the economy still based mainly on fossil fuels contributes to the increase in greenhouse gas emissions. As a consequence, we experience climate change, which affects most sectors of the economy and is also reflected in the energy security and stability of countries around the world. The direction of changes to be undertaken in order to reduce greenhouse gas emissions and strive for a "green" economy is regulated by many documents. One of the most important documents is the Paris Agreement signed in 2015, which set out the direction in which the commitment was made to limit the increase in average global temperature to well below 2°C above pre-industrial levels and to make efforts to limit this increase to 1.5°C [1]. The energy transformation assumes, among other things, reducing dependence on fossil fuels and, at the same time, minimizing emissions of harmful substances, which can be achieved through sustainable development of energy sources [2].

A frequent topic of research and analysis in this area is the development of hydrogen economy. The hydrogen economy is a system in which hydrogen is produced and used as the main energy carrier. Hydrogen has a very high potential and is recognised as an important alternative energy sector in the dynamic development of sustainable energy systems. Due to its characteristics such as lightness and environmentally friendly oxidation product (water), hydrogen appears to be an excellent energy carrier. Compared to energy production from fossil fuels, the use of hydrogen does not result in negative environmental effects. Furthermore, hydrogen has a very high calorific value (143 MJ/kg), which makes the combustion of one kilogram of hydrogen equivalent to 2.75 kg of gasoline [3].

The basic barrier to the development of hydrogen technology is the possibility of its acquisition. On Earth, in its free state, hydrogen occurs mainly in the outer layer of the atmosphere, which together with helium is the basic component. Unfortunately, access to these resources is very difficult, so currently the only possibility to obtain hydrogen in molecular form is its production. For this reason, it cannot be defined as a primary energy source but as an energy carrier, which means that its potential role is similar to that of electricity [4]. Both hydrogen and electricity can be produced using different energy sources and technologies. Both also find applications in many different applications.

On an industrial scale, hydrogen is produced mainly from natural gas in the process of steam methane reforming (SMR), which is currently the cheapest option to produce hydrogen [5], [6]. As a result of natural gas reforming, about half of the world's hydrogen supply is produced and remains the most widely used method of hydrogen production, however, it involves the production of significant amounts of CO_2 to the atmosphere. For more than 30 years scientists have been emphasizing the need to use renewable energy sources (RES) to power the hydrogen production process so that it has a real ecological and thermodynamic sense [7], [8]. In order for RES to be used, the technology and management of variable loads must be improved. Hydrogen production by water electrolysis is a promising way to compensate for the RES instability resulting from the nature of their operation. The electrolysis process can also set a zero-emission path for energy development, based on hydrogen economy.

The analysis of long-term forecasts of energy development in the world indicates that, depending on the expected level of energy consumption, the production and use of hydrogen for energy purposes in the years 2050-2100 may even exceed the current level several hundred times [9],[10],[11]. Although hydrogen has a great potential to be used in the power industry, it is currently used primarily as a raw material in industrial processes, especially in the refinery and chemical sectors to produce, among others, ammonia and methanol. Hydrogen is also used on a daily basis as a gas and liquid in the petrochemical industry and in the production of chemical, food and electrical equipment. Hydrogen gives a chance to decarbonize sectors strongly dependent on fossil fuels. Although hydrogen is one of the most promising sustainable energy carriers, it will not be able to replace fossil fuels alone. Wider use of hydrogen seems necessary.

The key to the development of a zero-emission economy may be coupled sectors - hydrogen, thanks to its storage properties and relatively cheap and efficient transmission, may become the missing link between the production of green electricity and its use in other industries, such as transport and heating [12].

2. Power to Hydrogen

The basic idea of Power-to-Hydrogen (PtH) technology is to produce gas using electricity. Usually surpluses from renewable, photovoltaic or wind sources are used for this purpose. PtH technology converts electricity into gaseous fuel through electrolysis. The gaseous fuel obtained in this process is hydrogen.

On an industrial scale, it is produced mainly from natural gas using the steam methane reforming (SMR) process, which is currently the cheapest hydrogen production option [13],[14]. In addition, commercially available technologies for the production of hydrogen from natural gas include [15]: the process of partial oxidation (POX -Partial Oxidation or CPOX - Catalytic Partial Oxidation), combining both of the above autothermal reforming (ATR), catalytic dehydrogenation, pyrolysis or electrolysis. At various stages of development are: photocatalytic processes, plasma reforming, membrane reactors and biological processes. Historical, announced data and target of low emission hydrogen production are shown in Figure 1.

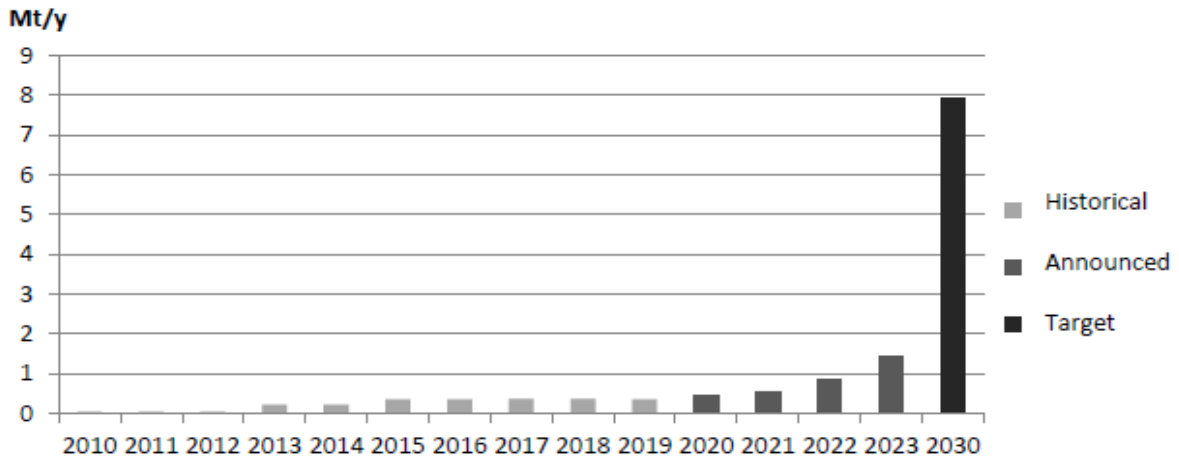

Fig. 1. Low-carbon hydrogen production, 2010-2030, historical, announced and in the Sustainable Development Scenario [17]

The decarbonization of the energy sector requires that the further development of hydrogen energy is related to the use of renewable energy for the production of hydrogen. If hydrogen is produced in a low-emission way, e.g. by electrolysis of renewable electricity or methane reforming with steam with carbon capture and storage - then the overall carbon footprint of hydrogen applications will also be reduced. Hydrogen produced from renewable energy sources can be distributed by different ways. Among other things, it can be stored and then reprocessed into electricity by using a fuel cell during periods of peak demand. It is also used in various industries, as discussed later in the article.

3. Areas of application of hydrogen

Literature indicates hydrogen for use in virtually every part of society. Currently, hydrogen is mainly used in several industrial processes, such as ammonia synthesis, nitrogen fertilizer production or oil desulphurization [18] Although hydrogen applications in the energy sector are currently carried out on a small scale, intensive research on the development of hydrogen technologies is being conducted. Currently, in the energy sector, hydrogen is used on a small scale, mainly in small installations using fuel cells. However, intensive research is being carried out on the development of hydrogen technologies.

There are also many applications of hydrogen on a smaller scale. Hydrogen, a highly reactive gas, is widely used in many industrial applications to produce various materials. In electronics, hydrogen is used on a smaller scale as a carrier gas (a gas that transports active gases) for various applications, such as the manufacture of electronic components. It offers high protection against pollution and oxidation. In the glass industry, hydrogen is essential for the production of flat glass used for the production of screens. For the production of flat glass, a float process is most often used, where high-purity hydrogen provides a protective atmosphere [19].

Due to the properties of hydrogen, there is a potential for the use of this element also for energy storage. There are many ways of storing hydrogen, but there is still research on developing appropriate solutions that could meet all safety standards [20]. Hydrogen is expected to be used in the future for all applications currently based on fossil fuels [21]. Possible main applications for hydrogen are shown in Table 1.

Table. 1. Hydrogen-to-X pathways. (based on [22])

Pathway	Acronym	Definition
Hydrogen-to-gas	HtG	Hydrogen injection into natural gas networks, directly or as synthetic methane synthesized in the methanation process
Hydrogen-to-Fuel	HtF	Hydrogen can be combined with other inputs to produce so-called hydrogen-based fuels and feedstocks.
Hydrogen-to-Industry	HtI	Hydrogen is widely used in industry, where it is mainly used in reduction and hydrogenation processes
Hydrogen-to-Chemicals	HtC	The chemical sector is currently the second and third largest source of hydrogen demand. It is closely related to HtF for the chemical industry.
Hydrogen-to-Heat	HtQ	Hydrogen is increasingly being considered in the context of its use in district heating. When hydrogen is burned with pure oxygen, the end products are heat and water - the big advantage is that no greenhouse gases such as carbon dioxide are produced.
Hydrogen-to-Power	HtP	Hydrogen can be used to store energy from renewable sources and can be used as a fuel for power generation units based, for example, on fuel cells.

3.1. **Hydrogen-to-gas**

The low energy density of hydrogen (143MJ/kg and 0.01079 MJ/dm^3 for gaseous hydrogen) means that transporting it over long distances can be expensive. However, there are many possibilities to solve this problem, e.g. by liquefaction of hydrogen (energy density for hydrogen in liquid state: 143 MJ/kg and 10.1 MJ/dm^3). Possibilities are also available to compress or integrate hydrogen into larger molecules, which can be transported more easily in liquid form. In many countries there is an extensive existing gas pipeline network that can be used to transport and distribute hydrogen after several upgrades. New infrastructure could also be developed, with dedicated pipeline networks that could potentially enable the large-scale transport of hydrogen.

Thanks to the development of P-t-H technology it is possible to integrate the energy system with the gas system by injecting hydrogen into the gas system [23]. Connecting hydrogen to the gas network, mainly by direct hydrogen injection, is one of several possible applications and has both advantages and challenges. The infrastructure of the gas system allows injecting only a limited amount of hydrogen. [24] Work in this area has already been carried out, but the overall potential, economic feasibility and constraints still need careful evaluation. Relatively low concentrations, e.g. 2-10 %, allow the injection of hydrogen into some natural gas pipeline systems with minor modifications of the supply infrastructure and/or receiving equipment [25], The reason is the insufficient strength of infrastructure elements (pipes, valves, gaskets, control systems, measuring systems). The permissible concentrations and modifications required are very dependent on pipelines and media [26]. This hydrogen supply strategy entails additional mixing and extraction costs as well as modifications to existing pipeline integrity management systems, but can significantly reduce CO_2 emissions.

3.2. **Hydrogen-to-fuel**

Hydrogen, due to its natural physical and chemical properties, is considered a very valuable fuel. It is characterized by the highest calorific value (120 MJ/kg) and combustion heat (141.9 MJ/kg) according to mass. However, due to its very low density, hydrogen has a low calorific value in comparison with other fuels, if these values are related to their volume. For this reason, hydrogen works well as a fuel for vehicles where mass plays a bigger role than volume, e.g. in spacecraft.

Unlike fossil fuels, no harmful by-products are produced when burning hydrogen, which makes it an attractive fuel in the face of the drive for decarbonization. When hydrogen combines with oxygen in a fuel cell, only energy and clean water is produced. Research on the use of hydrogen is growing steadily, but it mainly covers fuel cells. Only a few car models have ever been based on the Hydrogen Internal Combustion Engine Vehicle [27]. Hydrogen can also be converted into hydrogen-based fuels, including synthetic methane, methanol and ammonia, and synthetic liquid fuels, which have many potential transport applications. Synthetic liquid fuels produced from electrolytic hydrogen are often referred to as "power-to-liquid". In general, hydrogen-based fuels could use the existing infrastructure with limited changes in the value chain, but at the cost of loss of efficiency [28].

Hydrogen and hydrogen-based fuels, such as ammonia and synthetic natural gas, can also be used as fuels for electricity generation. Ammonia can be co-combusted e.g. in coal-fired power plants in order to reduce coal consumption and reduce the carbon footprint of these power plants. If it is low emission (taking into account the whole production process), it will also reduce overall emissions. Hydrogen and ammonia can also be used as fuels in gas turbines or fuel cells, thus providing a flexible and potentially low carbon power generation option. Hydrogen-based fuels also offer the possibility of large-scale and long-term energy storage in order to balance the variable generation of energy from renewable sources. Hydrogen fuels offer particular benefits for aviation and shipping, sectors where hydrogen or electricity is more difficult to use [28].

Hydrogen-powered vehicles are in a phase of rapid development. Experimental fuel cell vehicles have been developed by most car manufacturers and are being tested in small bus and light vehicle fleets. The development of hybrid technologies is important for the future prospects of fuel cell vehicles, as many of the electric drive technologies are similar [29].

3.3. **Hydrogen-to-industry**

Hydrogen in industry is mainly used in three industrial sectors: oil refining, chemical industry and iron and steel industry. Hydrogen production for these sectors is carried out on a commercial scale and almost entirely from natural gas, coal and oil, together with the accompanying environmental impact. However, technologies are available to avoid emissions from this fossil fuel by producing and supplying hydrogen with a low carbon footprint. Table 2 gives an overview of current industrial hydrogen applications.

Table. 2 Role of hydrogen and hydrogen-based products in basic industry fields [30]

Sector	**Current H_2 role**
Oil refining	Hydrogen is used primarily to remove contaminants (e.g. sulphur) from crude oil and to upgrade heavier oil. In smaller quantities it is used for oil sands and biofuels.
Chemical production	It is mainly used for the production of hydrogen-based fuels: ammonia and methanol, as well as in several other chemical processes on a smaller scale.
High temperature heat (excluding chemicals and iron and steel)	Virtually no hydrogen production for heat generation. Some limited use of hydrogen containing waste gases from the iron and steel and chemical sectors.

Food industry	The main application of hydrogen in the food industry is the process of hydrogenation of polyunsaturated vegetable fats, resulting in margarine. [31].
Metallurgical industry	n the metallurgical industry hydrogen is used to reduce iron ore. Hydrogen is used in a mixture with carbon monoxide, which is the source of carbon needed to produce steel from the raw iron obtained in this process. 7% of primary steel production takes place through direct iron reduction (DRI), which requires the use of hydrogen.

3.3.1 Oil refining

Hydrogen is an important part of the oil refining process. It is required, among others, in installations for desulphurization and modernization of various crude oil fractions. Currently, most refineries meet their hydrogen requirements by reforming methane vapor, which can account for up to 25% of fossil fuel CO2 emissions. It is possible to reduce this value e.g. through processes based on thermochemical biomass gasification. This thesis presents a study on the integration of processes of two different biomass-hydrogen concepts is described in detail in [32].

3.3.2. Chemical production

Hydrogen is widely used in industrial chemistry, where it has many applications. One of them is the production of ammonia by combining with nitrogen. The resulting ammonia is, among other things, the basis for artificial fertilizers. Hydrogen is also a reagent that is part of textile fibres such as nylon, polyurethane foam and many plastics. Due to the difficult, in comparison with traditional fuels, storage of hydrogen (also due to its explosive properties) the conversion of hydrogen into hydrogen-derived fuels is particularly attractive. While many industrial operators have experience in handling hazardous substances, it is safer to store hydrogen in other forms, such as ammonia [28].

3.3.3. High temperature heat (excluding chemicals and iron and steel)

In addition to the chemical and iron and steel sectors, industrial production of high-temperature heat is responsible for about 3% of carbon dioxide emissions in the energy sector [33]. There are three main temperature ranges for industrial heat: low temperature (< 100°C), medium temperature (100-400°C) and high temperature (> 400°C) [34].The industrial high-temperature heat is a potential source of future hydrogen demand growth, even though virtually no hydrogen is currently produced for this application. Hydrogen is only used in metallurgy in heat treatment atmospheres that enable the production of mechanical parts (sintering of formed parts) or change their properties (annealing of metal parts). Industry uses heat for many different purposes, including gasification, drying and mobilizing a wide range of chemical reactions. The heat can be used both directly, for example in the furnace, and indirectly, for example by first raising the water vapor and then transferring it for heating.

3.3.4 Food industry

Hydrogen is on the list of substances approved for use in the food industry and is marked with the symbol E-949. The basic legal act regulating the use of food additives in the European Union is Regulation (EC) No 1333/2008 of the European Parliament and of the Council of 16 December 2008 [35] and Commission Regulation (EU) No 1129/2011 of 11 November 2011 [36]. The main application of hydrogen in the food industry is the process of hydrogenation curing of polyunsaturated vegetable fats. . Hydrogen is also used for the synthesis of sorbitol.

3.3.5. Metallurgical industry

In the metallurgical industry, hydrogen is used in atmospheres of heat treatment, which enable the production of mechanical parts (e.g. by sintering the formed parts) or change their properties (e.g. by annealing metal parts) The process that uses hydrogen fuel is also nitriding, i.e. heating the metal in the presence of nitrogen (usually in the form of ammonia) to increase both corrosion resistance and hardness [37]. As in the chemical sector, the iron and steel sector produces large amounts of hydrogen mixed with other gases as a by-product (e.g. coke oven gas), some of which is used as part of the sector's demand and some is distributed for use in other destinations. The hydrogen production trend is also similar to other industries - practically all of this hydrogen is produced from coal and other fossil fuels. In order to reduce emissions, efforts are being made to research and test steel production using hydrogen as the main reducing agent (as opposed to fossil carbon monoxide). However, the first commercial-scale projects are not expected until 2030, so solutions are being sought for the next decade. Low-carbon hydrogen could be incorporated into existing processes, which currently rely on natural gas and coal, in order to reduce their overall CO_2 intensity [38].

3.4. Hydrogen-to-Chemicals

The chemical sector is currently the second and third largest source of hydrogen demand depending on the hydrogen fuel. For the production of ammonia, 31 MtH_2/yr is used and methanol is produced with the demand of 12 MtH_2/yr [30] The vast majority of hydrogen consumed by the chemical sector is produced using fossil fuels, which causes significant amounts of greenhouse gas emissions. Reducing the level of emissions is an important challenge for the sustainable use of energy in the sector and an important opportunity to use low-carbon hydrogen. Fossil fuels have long been a convenient and cost-effective source of hydrogen and carbon to produce ammonia and methanol. In 2018, about 270 Mtoe/year of fossil fuels were used to produce hydrogen for these two products [30].

Since production by reforming (using natural gas) is more efficient than by gasification (using coal), the former account for 65% of hydrogen production. Different regional gas and coal prices are also a key factor in the choice of the process path. Over 200 Bm^3 of natural gas and 105 MM g of coal are consumed every year to meet the global demand for hydrogen. [39].

Hydrogen has a low energy density, which makes it more difficult to store and transport than fossil fuels. However, it can be processed into hydrogen-based fuels and raw materials, such as synthetic hydrocarbons and ammonia, which can use the existing infrastructure to transport, store and distribute synthetic hydrocarbons produced from hydrogen. They can be direct substitutes for their fossil counterparts. There are many technological paths to produce these fuels and raw materials. However, many of them are still at an early stage of demonstration, which entails high costs for technology development. Ammonia production requires the separation of nitrogen from air, while the production of synthetic hydrocarbons requires the use of coal as a feedstock, which has an impact on the cost of production, and the origin of the coal also has an impact on the environmental impact and intensity of synthetic hydrocarbon consumption.

The graph describing the ammonia and synthetic hydrocarbon production pathway is shown in Fig. 2.

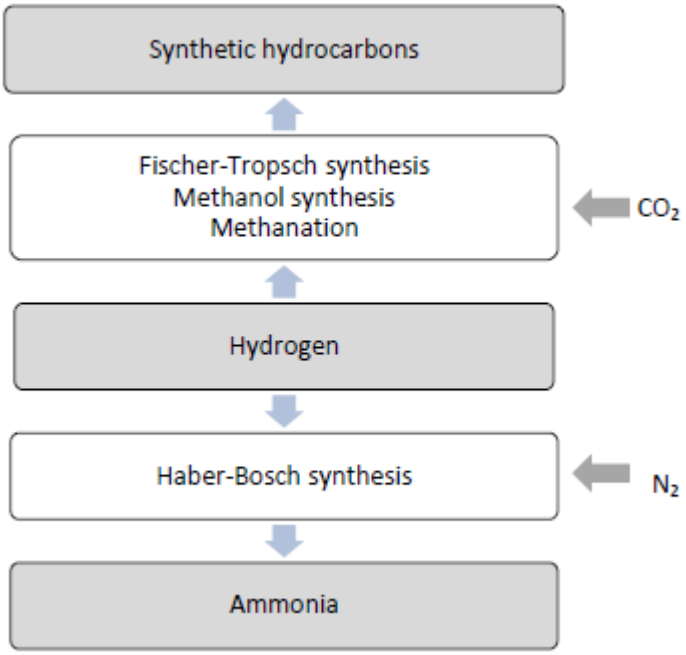

Fig. 2. Potential pathways for obtaining hydrogen-based products PtC [40]

3.4.1. Ammonia

Ammonia is a compound of nitrogen and hydrogen and therefore does not cause CO2 emissions during combustion. It is a gas at normal temperature and pressure, but can be liquefied at a temperature of -33°C, which is not too difficult to achieve. Liquid ammonia has 50% more density of volumetric energy than liquid hydrogen [33]. In principle, ammonia can be used as a fuel in various energy applications (e.g. for co-firing in coal-fired power plants), but none of these applications is currently used commercially. Ammonia is flammable (auto-ignition temperature: 630 °C). It burns with a yellowish flame on nitrogen and water [41]. Due to its thermodynamic properties, ammonia is used as a refrigerant (R717), especially in large cooling devices.

Hydrogen in combination with N_2 in Haber-Bosch synthesis produces ammonia. 90% of the world's ammonia production is obtained through this reaction [42]. The mechanism of ammonia synthesis includes the following basic stages: transport of gaseous phase reagents through the boundary layer to the surface of the catalyst, diffusion of pores to the center of the reaction, adsorption of the reagents, reaction, desorption of the product, transport of the product through the pore system back to the surface, transport of the product to the gaseous phase. Since 2018, the Haber process has been producing 230 million tons of anhydrous ammonia per year, and the resulting nitrogen fertilizers are responsible for the production of foods that keep about 1/3 of humanity alive. [43]. The Haber process consumes 3-5% of the world's natural gas production (about 1-2% of the world's energy supply) [44].

3.4.2. Synthetic hydrocarbons

Hydrogen can be combined with CO_2 to obtain synthetic hydrocarbons such as methane or synthetic liquid fuels such as methanol, diesel, gasoline and aviation fuel [45]. Some of these products have a higher energy density than hydrogen or ammonia. The production of synthetic hydrocarbons can take place through a number of different processes: through the synthesis of methanol, methanization, or Fischer-Tropsch synthesis. Synthetic methane can be produced directly by methanation with CO_2 and H_2.

For the production of synthetic diesel or kerosene you need hydrogen and carbon monoxide as raw material. Since carbon monoxide is generally not easily available, CO_2 can be used instead. In this case, carbon monoxide is first converted into carbon monoxide and then the synthesis gas is produced from carbon monoxide and hydrogen.

The Fischer-Tropsch process is quite a complicated process where many chemical reactions take place that transform a mixture of carbon monoxide and hydrogen into liquid hydrocarbons. These reactions take place in the presence of metallic catalysts, usually at 150-300°C (302-572°F) and at pressures from one to several dozen atmospheres [46].

3.5. **Hydrogen-to-Heat**

Another area where hydrogen has a chance to appear is the heating sector, which in Poland urgently needs intensive decarbonization. In an effort to modernize the heating system and to find a mechanism of low-carbon heating to combat climate change, several solutions have been proposed. One of them is to burn hydrogen instead of natural gas [47]. Hydrogen has the potential to contribute to energy transformation and long-term heat decarbonization strategies (e.g. pure hydrogen production from renewable sources). Although hydrogen is currently used very little as an energy source in the global district heating sector, various potential applications are currently being tested.

According to the IEA report, 37 demonstration projects for mixing hydrogen in the gas grid are currently underway [30]. Combustion of hydrogen in pure oxygen only produces H2O. Under normal conditions hydrogen is usually burned in air. In this case, some of the highly active oxygen atoms combine with nitrogen in the air to form NOx. In the takeij reaction there are no carbon atoms with which the oxygen atoms could bind, so most of them bind to nitrogen from the air, forming NOx. For this reason, burning hydrogen in air produces up to six times more NOx emissions than burning methane in air. Therefore, there is a much higher health risk associated with the combustion of hydrogen for heating compared to the combustion of natural gas [48].

3.6. **Hydrogen-to-Power**

According to the IEA report of June 2019, hydrogen plays a negligible role in the energy sector today. It constitutes less than 0.2% of electricity production [30]. This is mainly due to the use of gases from the steel industry, petrochemical plants and refineries. The potential for future changes in this area is noticeable. For example, co-firing of ammonia could reduce the carbon intensity of existing conventional coal-fired power plants could be a source of flexibility for power systems with an increasing share of variable renewable sources. In the form of compressed gas, ammonia or synthetic methane, hydrogen could also become a long-term storage option to offset seasonal fluctuations in power generation from renewable sources [30].

The use of hydrogen as an energy source in various branches of the economy will be based primarily on fuel cell technology. The technology does not require recharging, but only supply fuel, which may be hydrogen. Fuel cells consist of two electrodes - negative (anode) and positive (cathode) [49]. Fuel - hydrogen - is supplied to the anode and air to the cathode. The catalyst allows the decomposition of hydrogen atoms into protons and electrons, which move along separate paths to the cathode. The electrons pass through an external circuit, causing electric current to flow, while the protons through the electrolyte travel to the cathode, where they connect with electrons and oxygen molecules. The products of a fuel cell are: water; waste heat and electricity. Fuel cells can be a source of electricity for many devices, including: laptops, cars and even entire buildings.

Gas turbines, such as the so-called open-cycle gas turbines, are currently used as an alternative method of converting hydrogen into electricity (and/or heat). The technological maturity of gas turbines, which are available

on the market, makes most of them capable of using fuel consisting of a mixture of natural gas and hydrogen. It is expected that in the future, after implementation of a number of appropriate regulations, it should be possible to convert them completely into hydrogen [50].

Renewable hydrogen has a promising potential as an energy storage factor. Currently, hydrogen is an interesting medium used to produce clean energy for various applications, e.g. to power regions that are not connected to the power grid, where it can also act as an energy storage. Hydrogen storage systems (HES) offer many potential benefits in terms of decarbonization and grid resilience due to the zero-carbon potential of the entire energy production pathway.

4. Conclusion

Low-carbon" hydrogen (i.e. produced by low emission pathways) can be used in many energy-using services. It has potential importance in the electrical, gas, transport and industrial sectors. The main driving forces behind Power-to-Hydrogen and Hydrogen-to-X are the decarbonisation of the energy system and the productive ability to continuously increase the proportion of renewable energy capacity. This paper discusses the applications of hydrogen systems that are being activated or under research to decarbonize the transport, industrial and energy sectors. . The aim of the paper was to highlight the potential of hydrogen as a key factor in the transition to a low carbon economy. Development work on the already relatively mature PtG technology is announced and planned. Taking into account these plans and aiming to use the hydrogen potential, it would be necessary to focus on the development of current paths of its use, as well as to seek new solutions

Acknowledgement

The author declare that there is no conflict of interest.

References

[1] Article 2 of the Paris Agreement, ***Long-term temperature goal,*** 2015

[2] S. Shiva Kumar, V. Himabindu, *Hydrogen production by PEM water electrolysis – A review*, Materials Science for Energy Technologies, Volume 2, Issue 3, 2019, Pages 442-454,

[3] P.C Hanllenbeck.: *Fundamentals of fermentative production of hydrogen*. Water Sci.Technil 42/2005, pages 21-29

[4] B. Widera: *Renewable hydrogen implementations for combined energy storage, transportation and stationary applications* Thermal Science and Engineering Progress Volume 16, (2020),

[5] M. Melaina, J. Eichman: *Hydrogen energy storage: grid and transportation services* Natl. Renewable. Energy Lab. Denver (CO), 2015,

[6] T. Chmielniak, S. Lepszy, P. Mońka: *Energetyka wodorowa – podstawowe problemy*, Polityka Energetyczna – Energy Policy Journal, Tom 20 (3), 2017.

[7] T Chmielniak,. *Badania symulacyjne technologii wytwarzania wodoru w aspekcie emisji CO2 w cyklu– wydobycie, transport i przetwórstwo węgla*. Gliwice: Wyd. Politechniki Śląskiej,

[8] K. Liu, C. Song, V. Subramani (Eds); A John Wiley & Sons, *Hydrogen and Syngas Production and Purification Technologies*. Inc., Publication, 2010

[9] L.S. Belyaev, O.V. Marchenko, SP Filippov, SV. Solomin *Studies on competitiveness of space and terrestrial solar power plants using global energy model*. Int J Glob Energy Issues, 2006;

[10] GEA, *Global energy assessment e toward a sustainable future. International institute for applied systems analysis*. Cambridge University Press; 2012.

[11] L.S. Belyaev, O.V. Marchenko, SP Filippov, SV. Solomin, T.B Stepanova TB, A.L. Kokorin. *World energy and transition to sustainable developmen*t. Kluwer Academic Publishers; 2002

[12] M. Olczak, A. Piebalgs, *Sector coupling: the new EU Climate and Energy Paradigm?*, Florence School of Regulation 2018/17;

[13] M. EL-Shimy A.N. Afandi. *Overview of Power-to-Hydrogen-to-Power (P2H2P) Systems Based on Variable Renewable Sources.*, The 5th International Conference on Electrical, Electronics, and Information Engineering (ICEEIE 2017), 2017

[14] J.D Holladay, J. Hu, D.L. King,, Y. Wang, *An overview of hydrogen production technologies*. Catalysis Today 139, pages. 244–260. 2009.

[15] C. Acar, I. Dincer,. *Comparative assessment of hydrogen production methods from renewable and non-renewable sources*. I. Journal of Hydrogen Energy 39, pages. 1–12, 2014

[16] B.D. Solomon, A. Banerjee, *A global survey of hydrogen energy research, development and policy*. Energy Policy Vol. 34, 7, May 2006, pages. 781–7928, 2006.

[17] IEA, *Low-carbon hydrogen production, 2010-2030, historical, announced and in the Sustainable Development Scenario, 2030*, IEA, Paris https://www.iea.org/data-and-statistics/charts/low-carbon-hydrogen-production-2010-2030-historical-announced-and-in-the-sustainable-development-scenario-2030, date of access (30/11/2020)**.**

[18] V. Dupont, *Steam reforming of sunflower oil for hydrogen gas production*. Helia ;30(46):103-32, 2007

[19] J.P. Mesguen, J. Bidon, L.Lelong, ESA, 2005 https://energies.airliquide.com/resources-planet-hydrogen/uses-hydrogen, date of access 03.12.2020

[20] S. Lepszy, T. Chmielniak., P. Mońka, *System magazynowania energii z elektrowni wiatrowych z wykorzystaniem podziemnych zbiorników wodoru*, VI Konferencji Naukowo–Technicznej Energetyka Gazowa 2016, Zawiercie 20–22.04.2016

[21] Hydrogen Europe https://hydrogeneurope.eu/hydrogen-applications, date of access: 01.12.2020

[22] M. Robinius, L. Welder, D. Ryberg, C. Mansilla, P. Lucchese, O. Tlili, L.G Alain, J. Simon, M. Balan, R. Dickinson, and others, *Power-to-hydrogen and hydrogen-to-X: Which markets? Which economic potential? Answers from the literature*. 1-6. Solene. 2017.

[23] J. Jaworski, E. Kukulska-Zając, P. Kułaga, *Wybrane zagadnienia dotyczące wpływu dodatku wodoru do gazu ziemnego na elementy systemu gazowniczego*, Instytut Nafty i Gazu – Państwowy Instytut Badawczy, Nafta-Gaz 2019, nr 10, pages 625–632, DOI: 10.18668/NG.2019.10.04 2019

[24] GRTgaz, *Technical and economic conditions for injecting hydrogen into natural gas networks* , Final report, June 2019

[25] European Union Agency for the Cooperation of Energy Regulators (ACER), *ACER Report on NRAs Survey. Hydrogen, Biomethane, and Related Network Adaptations*, Evaluation of Responses Report 10 July 2020

[26] A. Lima, R. Szczerbowski, *Technologia Power to Gas w energetyce*, energia gigawat nr 4/2019 (218), pages 32-35, 2019

[27] P. Hoffmann: *Tomorrow's Energy: Hydrogen, Fuel Cells, and the Prospects for a Cleaner Planet*. London: MIT Press, 2002. ISBN 0-262-08295-0.

[28] International Energy Agency (IEA), *The Future of Hydrogen Seizing today's opportunities*. Report prepared by the IEA for the G20, Japan, 2019

[29] J. Molenda, K. Świerczek: *Fundamentalne problemy rozwoju energetyki wodorowej, E*-mobliność: wizje i scenariusze rozwoju pod redakcją Jerzego Gajewskiego, Wojciecha Paprockiego i Jany Pieriegud Publikacja Europejskiego Kongresu Finansowego, ISBN 978-83-945091-2-5, 2017

[30] IEA, https://webstore.iea.org/download/direct/2803, date of access 01.12.2020

[31] I.P. Freeman, Margarines and Shortenings, *Ullmann's Encyclopedia of Industrial Chemistry*, Weinheim: Wiley-VCH, 2005,DOI: 10.1002/14356007.a16_145

[32] J-F. Brau, *Production of Hydrogen for Oil Refining by Thermal Gasification of Biomass: Process Design, Integration and Evaluation*. 10.13140/RG.2.1.2599.6402., 2013

[33] CMS Legal 2020 https://cms.law/en/int/expert-guides/cms-expert-guide-to-hydrogen/hydrogen-in-industry, date of access 02.12.2020

[34] S. Bruckner, S. Liu, M. Laia, M. Radspieler, L. F. Cabeza and L. Eberhard, *Industrial waste heat recovery technologies: An economic analysis of heat transformation technologies*, Applied Energy, vol. 151, no. 1, pages. 157-167, 2015

[35] Rozporządzenie Parlamentu Europejskiego i Rady (WE) nr 1333/2008 z dnia 16 grudnia 2008 r.. 2008. https://eur-lex.europa.eu/legal-content/PL/TXT/PDF/?uri=CELEX:32008R1333&from=PL date of access: (03.06.2020)

[36] Rozporządzenie Komisji (UE) NR 1129/2011 z dnia 11 listopada 2011 r.. 2011 https://eur-lex.europa.eu/legal-content/PL/TXT/PDF/?uri=CELEX:32011R1129&from=PL date of access: (03.06.2020)

[37] L&L Special Furnace Co, Inc *Heat Treatment Furnace Atmospheres: Inert Gas and Hydrogen*, May 20th, 2019, https://llfurnace.com/blog/heat-treatment-furnace-atmospheres-inert-gas-and-hydrogen/ date of access 03.12.2020

[38] IRENA, *Hydrogen: a renewable energy perspective*, Report prepared for the 2nd Hydrogen Energy Ministerial Meeting in Tokyo, Japan, September 2019, International Renewable Energy Agency, Abu Dhabi

[39] R. Kaplan,M. Kopacz *Economic Conditions for Developing Hydrogen Production Based on Coal Gasification with Carbon Capture and Storage in Poland*, Energies, September 2020

[40] IEA, *Low-carbon hydrogen production, 2010-2030, historical, announced and in the Sustainable Development Scenario*, 2030, IEA, Paris https://www.iea.org/data-and-statistics/charts/low-carbon-hydrogen-production-2010-2030-historical-announced-and-in-the-sustainable-development-scenario-2030, date of access 30.11.2020

[41] A. Bielański, *Podstawy chemii inorganicznej*, Chemistry**,** ed. 5, vol. 2, Warsaw: PWN, page 651, ISBN 83-01-13654-5 2002

[42] M. Appl, *Ammonia*, Ullmann's Encyclopedia of Industrial Chemistry, Weinheim: Wiley-VCH, pages. 7-8, 2005

[43] D. W. Wolfe, *Tales from the underground. A natural history of subterranean life*, Cambridge: Perseus, 2001, ISBN 0-7382-0128-6

[44] https://rewolucjaenergetyczna.wordpress.com/2014/04/12/synteza-chemiczna-bez-paliw-kopalnych-cz-i-amoniak/ date of access 1.12.2020

[45] K. Łodygowski, Paliwa syntetyczne do zasilania silników spalinowych z zapłonem samoczynnym, Technika Transportu Samochodowego, pages 655-663. 10/2013

[46] Z. Sarbak *Reactions and catalytic processes The Fischer-Tropsch* (Part XVa) LAB process, pages 16-22 2/2019].

[47] https://globenergia.pl/wodor-jako-potencjalne-paliwo-grzewcze-przyszlosci, date of access: 29.11.2020

[48] https://www.icax.co.uk/Advantages_Burning_Hydrogen_Heating.html, date of access 1.12.2020

[49] M. Krauz, *Opracowanie technologii wytwarzania stałotlenkowych ogniw paliwowych*, PhD thesis, , Akademia Górniczo-Hutnicza im. Stanisława Staszica, Kraków 2008.

[50] M. Dorociak, M. Tomecki, *Wodorowa Alternatywa*, Raport 2019, 300GOSPODARKA, ISBN 978-83-954071-0-9

Possibilities of using gas turbine to utilize waste heat in Huta Łaziska.

Hugo Urbańczyk[1]

[1]*Silesian University of Technology, e-mail: Hugourbanczyk1@gmail.com*

Abstract

The aim of this article is to show the analysis of application of gas turbine in waste heat utilization installation at Huta Łaziska (which is a big producent of ferroalloys). Using actual data, the recovery installation layout in IPSEpro program has been modeled to determine the correct operation of the installation and find areas for potential optimization. Finally, actual performance of the installation has been compared with the designer's original assumptions on this field. At the end necessary conclusions have been drawn.

Keywords: waste heat, gas turbine, ferroalloys, heat recovery, heat, heat utilization, IPSEpro;

1. Introduction

Huta Łaziska S.A. is the largest Polish (and one of the largest in Europe) producer of ferroalloys, which are an essential addition to steel and foundry processes. Ferroalloys are iron alloys combined with other elements - the most common are silicon, manganese and chromium. They are a medium of steel alloying elements and ensure its deoxidation and degassing [1]. The side effect of the production process is a huge amount of waste heat - in form of very hot exhaust gases - which has a great potential for being re-used.

2. Production process characterization

The ferroalloy installation is equipped with several furnaces with capacity ranging from several up to dozen MVA. Furnaces are grouped in Furnace Halls I, II, III and IV (approximately 100 MVA in total). The production of ferroalloys is based on the carbothermal reduction of silicon and iron oxides (and optionally other elements) in electric arc-resistance furnaces equipped with self-sintering Soderberg electrodes.

The production process is a continuous and complex sequence of physicochemical processes taking place in the furnace bath. After proper reaction of the charge components, the tapping hole is burned through on the perimeter of the furnace with a steel rod. The obtained ferroalloy, in liquid form, is poured into ladle or directly into special tubs, in which it cools down. The product is then crushed and transported to the warehouse.

The key reaction responsible for the energy consumption in the whole process is a strongly endothermic reduction of SiO2 with carbon - in the presence of iron - which causes the temperature inside the furnace chamber to reach 2000°C. Due to such high temperatures, it is necessary to apply water cooling for furnace fittings, at the same time the production process itself must be subject to continuous control in order to maintain its appropriate parameters. A proper level of control is achieved by changing: the position of the electrodes within the furnace, the voltage of the secondary side of the supply transformer, the smelting time and the ratio of C to SiO_2. The complexity of the process increases the occurrence of uncontrolled disturbances. These disturbances, apart from the obvious failures of various installations, may be caused by variable parameters of the input materials, such as: specific conductivity, particle size distribution of raw materials and reactivity of reducing agents.

Ferroalloys production process generates a significant amount of high-temperature gases (depending on the design of the furnace), which consists mainly of SiO and CO which are being formed inside the furnace. As a result of sucking in large amounts of air and burning the gases under the furnace hood, the exhaust gases ultimately include nitrogen, oxygen, carbon dioxide, silicon dioxide, sulfur dioxide and hydrogen oxide [2].

With the use of exhaust fans, the post-process gases are directed to dedusting collector where dust is being filtered-out by "bag-house" fabric filters. Subsequently, gases are directed to the atmosphere through a 150m tall chimney. The process is a bit different, however, in case of gases from modified furnaces 17th and 18th located in Furnace Hall no. III. Those gases, prior to reaching dedusting facility, are directed to recuperators to heat the air for the waste heat utilization installation based on the UGT 2500 gas turbine. Other furnaces used in Huta Łaziska are open type, which results in:

- limited control over the post-process gas combustion,
- increased volumetric flow,
- relatively low exhaust gases temperature of 200-300ºC.

Due to these features, it is not possible to manage waste heat from open-type furnaces in an economical way [3].

3. Waste heat utilization installation

With all the furnaces turned on Huta Łaziska consumes an active power of approx. 90 MW from the power grid. Almost all that power is converted into heat in the arc-resistance furnaces. Therefore, the facility has a significant capability of managing high-temperature waste heat, however, due to a number of factors whole process is very complicated from technical standpoint. There are no recipients in the vicinity of the plant who can effectively manage this amount of heat so, at the moment, the only reasonable solution is electricity production.

3.1. Technical description

There was an investment in the Furnace Hall no. III to adapt the furnaces with a capacity of 2 x 12 MVA to cooperate with the waste heat recovery installation. This installation is based on the UGT 2500 gas turbine with an external combustion chamber of the Ukrainian production "Zorya" - "Mashproekt". The idea was to use post-process gases to heat air going into the gas turbine. Due to the high temperature of these gases (approx. 800-900 ° C), it is possible to heat the air directed to the turbine's combustion chamber up to 600-650 °C. This results in, theoretically, very low gas consumption - just to maintain correct temperature behind combustion chamber at 951ºC. The simplified layout of the installation is presented in Fig. 1.

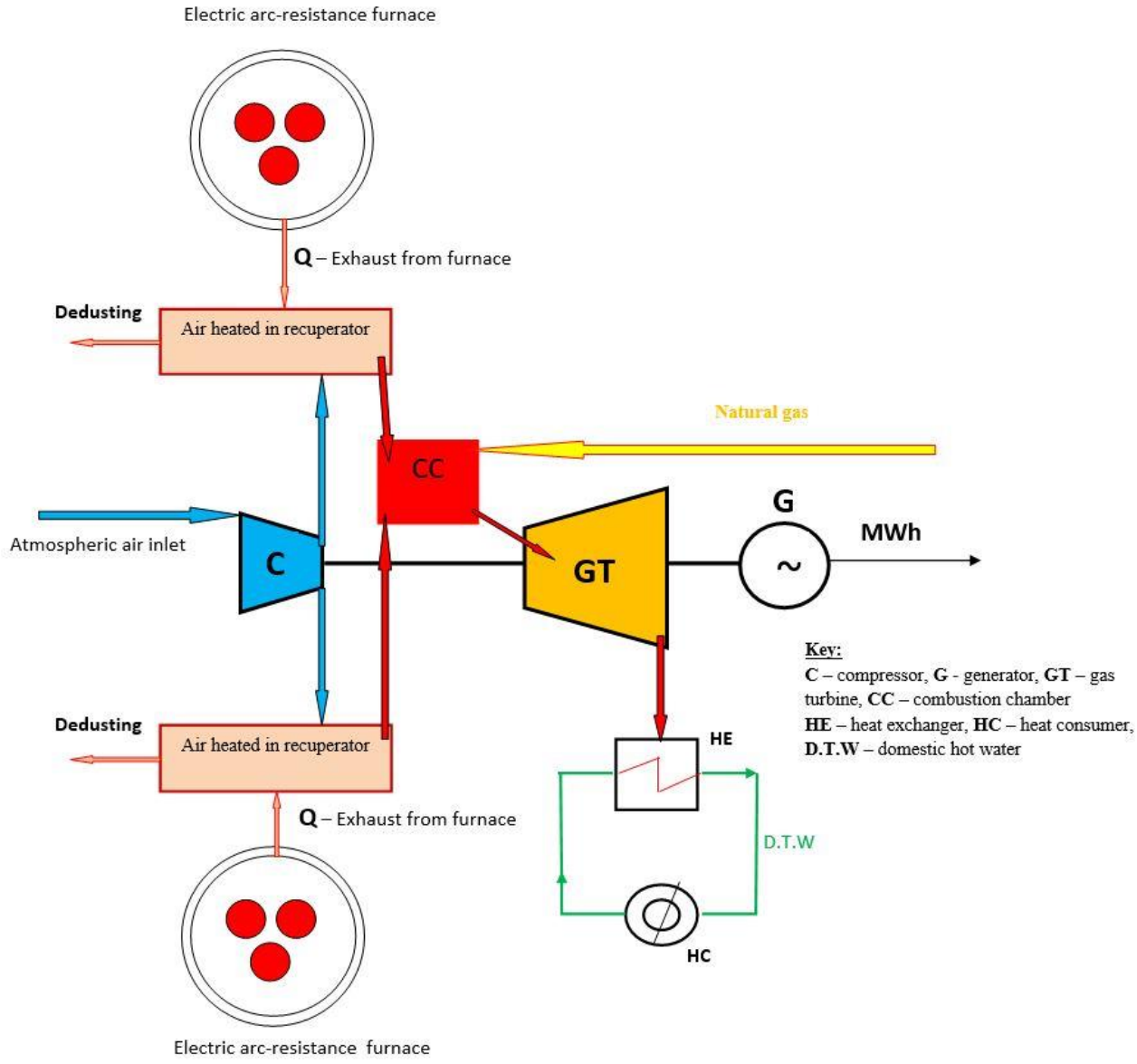

Fig. 1. Waste heat utilization installation layout.

The investment in Furnace Hall III consisted of:

- construction of a gas turbine system with a heat exchanger and other necessary installations,
- construction of furnace recuperators R17 and R18,
- modification of the furnace structure by implementing a closed housing with technological windows in order to increase the temperature of waste gases and reduce the amount of air sucked in,
- reduction of heat losses from furnaces hoods and flue gas ducts,
- modification of the cooling system to closed cooling system (water - glycol - fan cooling towers).

3.2. **IPSEpro model**

IPSEpro software is used to calculate balances and simulate thermal processes. It includes a set of software modules which are creating process models for a wide variety of applications throughout the life cycle of process plants. IPSEpro modules can also be used to predict the efficiency of designed installations, verify and validate measurements, online monitoring & optimization, and to plan modernization and modification of existing installations. [4]

The computer simulation of heat recovery installation served as the basic tool for the analysis of the real system. The model was made based on data obtained in the facility, such as postprocess exhaust gas measurements, turbine operating instructions, reports of turbine operation and others. Main data was taken from automatically generated report on April 4, 2017. On that day the installation was characterized by high and stable operating parameters, showing its actual capabilities.

For the correct operation of the model, it was necessary to define global variables such as: gaseous fuel, air, exhaust gases from furnaces, exhaust gases from turbine and water in heating system. The computer model is based on Figure 1, however, some modifications were implemented. The model in relation to the real system, due to the very similar size of streams and temperatures, assumes a simplification in the form of one recuperator and one combustion chamber (in reality, heated air streams are separated to the left and right side for 2 recuperators and mixed together just before combustion chamber). There are also no furnaces and auxiliary installations in the model.

The simulation was carried out in few variants, while variant 1 (V1) is the basis for comparison with the real system and its data from the report. The remaining variants are hypothetical variants, based, to a greater or lesser extent, on the data from the aforementioned report and the results obtained in V1. The operation of the system was also tested in accordance with the original conceptual assumptions that influenced its construction in the ferroalloys plant. The model from the IPSEpro program is shown in Figure 2. The input data for IPSEpro model is shown in Table 1.

In variant 2 (V2), the assumptions were made analogous to the first variant, with the difference in the gas flow rate (bright green in Table 2) in order to obtain the power indicated in the report (dark green in Table 2).

Variant 3, the assumptions analogous to the first variant were made as well, however, the compressed air stream (bright green, Table 2) was changed in order to obtain the reported value of the power transferred to the air on Recuperators R17 and R18 (dark green, Table 2).

Variant 4 is based on the operating parameters [5] of the installation assumed before construction including the temperature of the air supplied to the combustion chamber as well as the pressure before the turbine and the compressed air flow rate. The remaining necessary values were taken from the report.

Variant 5 assumed no combustion of gaseous fuel and the operation of the turbine only thanks to the hot air stream with parameters as in variant 4. It was assumed that the medium behind the turbine is expanded to atmospheric pressure. Compressor operating parameters are taken from the report.

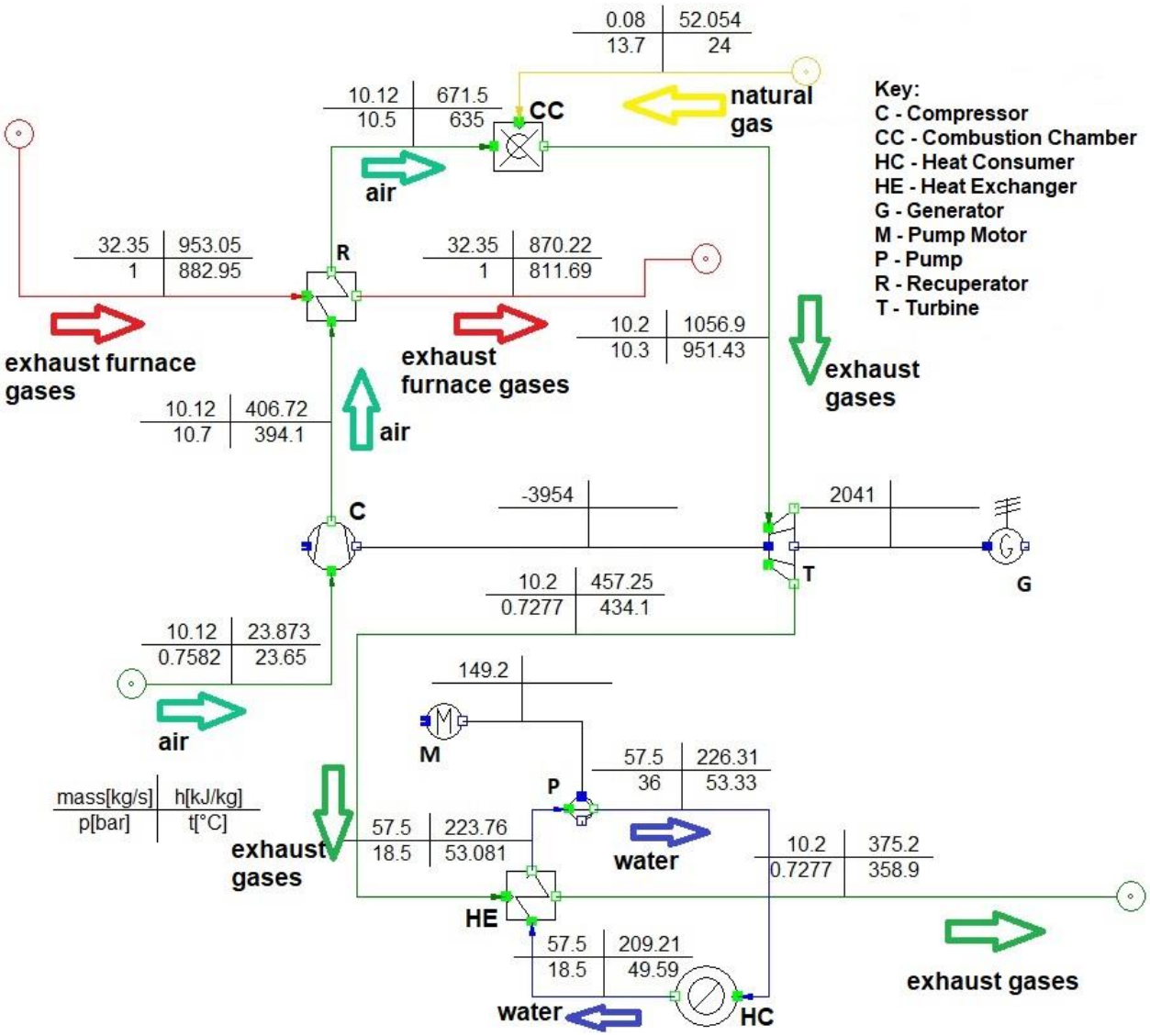

Fig. 2. IPSEpro installation scheme

4. Results

Results of the installation operation variants are shown in Table 2 and Table 3.

Results description:

- Bright blue cells in Table 1 consist of values used as a comparison for the calculations in the following variants but were no inputted to computer model.
- Results that differ significantly from the report data or which suggest possibility of failure are marked in red.
- The values which occur with * corresponds to the temperature with * in Table 1., and therefore with the value of the power transferred to the air stream. The neighboring values without * are equal to the mentioned power minus the losses between the recuperators and the combustion chamber ($\Delta T \sim 17°C$).
- Values marked with bright green are parameters that were changed to create hypothetical variants, more or less close to actual data from report or to original assumptions of the gas turbine installation
- Values marked with dark green corresponds directly to values marked with bright green.

Table 1. Input Data

Data	Value	Unit
Recuperators		
Av. Temp. in front of recuperators (ex. gases)	882,95	°C
Av. Temp. behind recupertaors (ex.gases)	***567,99***	°C
Total power from Recuperators R17 and R18	***3465,95***	kW
Ex. gases stream from Furnace Hall III	32,35	kg/s
Furnace gases density	1,266	kg/m^3
Heated air average temp.	652,57*	°C
Turbine		
Compression temp.	23,65	°C
Temperature behind compressor	391,4	°C
Temp. in front of combustion chamber	635,1	°C
Pressure behind compressor	1,07	MPa
Pressure in front of combustion chamber	1,05	MPa
Compressed air stream	10,12	kg/s
Temp. in front of turbine (nominal)	951	°C
Exhaust temp. behind turbine	434,1	°C
Generator active power	***2292***	kW
Gaseous fuel		
Gas fuel volum. flow	***596***	Nm^3/h
Gas pressure	1,37	MPa
Gas fuel temperature	24	°C
Calculated gross calorific value	40,2	MJ/m^3
Calculated gas density	0,7346	kg/m^3
Heat exchanger		
Boiler 2 - Power	***700***	kW
Water flow	207	m^3/h
Water pressure (return)	1,85	MPa
Water pressure behind heat exchanger	3,6	MPa
Water temp. in front of heat exchanger	49,59	°C
Water temp. behind heat exchanger	53,33	°C

Table 2. Results of simulation V1,V2,V3

Parameter	Variant 1		V2	V3	Unit
	reported	calculated	Calculated	calculated	
Generator active power	2292	1930,1	**2289**	**2329,4**	kW
Boiler 2 - Power	700	836,93	839,08	1009	kW
Total power from R17 i R18	3465,95	**2679,6 (2880,2*)**	2679,6 (2880,2*)	**3230,3 (3472,2*)**	kW
Av. Temp. behind recuperators (ex.gases)	567,99	**812.86**	812,86	798,36	°C
Temp. in front of turbine (nominal)	951	951,43	**981,31**	951,61	°C
Ex. gases temp. behind heat exchanger	no data	358,9	358,9	358,9	°C
Intake air pressure	no data	0,97674	0,97674	0,97674	bar
Pressure behind combustion chamber	no data	10,3	10,3	10,3	bar
Pressue behind turbine	incorrect data	0,98948	0,88297	0,9888	bar
Gas fuel volum. flow	596	**392**	**431**	473	Nm3/h
Excess air coefficient (λ)	no data	6,7	6,09	6,69	-
Compressed air stream	10,12	as in V1	as in V1	**12,2**	kg/s
Gross system efficiency electric/combined	24,16 / 31,54	28,26 / 40,46	31,63 / 43,23	28,24 / 40,47	%
Net system efficiency electric/combined	-	25,95/ 38,18	29,49 / 41,08	26,35 / 38,59	%
Compressor isentropic efficiency	-	76,5	as in V1	as in V1	%
Turbine isentropic efficiency	-	95	as in V1	as in V1	%

4.1. **Result analysis – variants 1,2,3**

Variant 1.

The obtained results show that the model is quite similar to the actual state - the calculated active power of the generator was 1930.1 kW which was the average power in longer periods of stable operation. What is particularly noteworthy is the fact that value of the calculated gas stream is 1/3 lower than in the report. It would seem that this factor is responsible for calculated power being lower than that actually obtained.
Another significant discrepancy is the temperature of gases leaving the recuperator and the power transferred to compressed air. The calculated value of this temperature is overestimated by approx. 250°C and suggests that the theoretical possibilities of heat exchange between gases from Furnace Hall III and air are much greater. The temperature given in the report, in turn, proves significant heat losses occurring in this part of the installation. According to the computer model, if cooled down to 568°C the given postproduction gases stream would be enough to heat an air stream of 23 kg/s, from 391.4 ° C to 850 ° C. This flow rate is more than twice the amount of air actually used. This gives a collectible power of 11765 kW. It is worth mentioning that such a high air stream exceeds the capacity of the installed compressor, while the heat exchange process in recuperators is constricted and interrupted due to the high dustiness of the postproduction gases.
The obtained value of the isentropic compressor efficiency is quite reliable. The isentropic efficiency of the turbine can be considered a slightly overestimated value (95%). However, this fact is affected by the lack of reliable data of the pressure behind the turbine and possibly inaccuracies in the measured temperature behind the turbine (data from several measuring points showed discrepancies of tens of °C). The atmospheric pressure on the measurement day was 0.984 bar.
The calculated power of the heat exchanger is relatively close to the power given in the report. It should be noted here that the achieved power of the exchanger depends mainly on the analyzed period of operation (season) and the flow settings which are depended on current needs of the facility. Behind the turbine, two 1500 kW heat exchangers are installed interchangeably. The achieved power value is therefore reliable for the spring period, and the visible difference may result from the inaccuracy of measuring the installation - with a flow of ~ 200 m3/h, a change in water temperature at the exchanger outlet by tenths of a °C caused the exchanger power to change by

tens of kilowatts. Due to the secondary importance and consistency of the results, the analysis of the district heating component was limited to variant 1.

The calculated efficiencies and the net power achieved by the system will in fact be lower due to the need to supply a number of auxiliary installations. The main recipient of the aforementioned power will probably be the inverter of the exhaust ventilator (approx. 200kW) which was not included in the calculations due to difficulties in determining the dependence of its power variability on other parameters of the turbine's operation.

Variant 2.

The obtained power of 2289 kW corresponds almost exactly to power achieved in the report and was obtained at the cost of increasing gas consumption by about 40 m^3/h, which is still not close to the consumption indicated in the report. What is crucial is that the temperature behind the combustion chamber / in front of the turbine rose 30 ° C above the designed value. Unlike the first variant, the temperature in front of the turbine was not fixed. Therefore, it should be stated that on April 4th 2017 the turbine could operate with the temperature at its inlet exceeding the value planned by the manufacturer. Practically whole day until it was turned off after 8 p.m., the turbine achieved enormous powers (equal to or higher than the assumed active power threshold of 2,2 MW) and burned about 600 m3/h. of gas. In addition, it is worth mentioning that the turbine emergency shutdown report includes, among others, exceeding the permissible vibrations of the front hull.

Variant 3.

Increasing the air flow rate by approx. 2 kg/s allowed to transfer from postprocess gases the power equal to the power in the report and to obtain the active power of the generator approx. 50 kW higher than indicated in the report. Due to increased air stream, it was necessary to burn more gas than in the variant 1 to maintain the correct temperature in the combustion chamber, however, the obtained value was 123 m^3/h lower than the value in the report.

4.1 Result analysis – variants 4,5

Table 3. Results of simulation V4, V5

Parameter	V4		V5		Unit
	assumed	calculated	assumed	calculated	
Generator active power	2540	2624,1	1810	1782,4	kW
Boiler 2 - Power	-	1180			kW
Total power from R17 i R18	-	7129,7 (7417,1*)	-	7129,7 (7417,1*)	kW
Av. Temp. behind recuperators (ex.gases)	-	694,71		694,71	°C
Temp. in front of turbine (nominal)	951	951,31	833	833	°C
Ex. gases temp. behind heat exchanger	-	358,9	-	357	°C
Intake air pressure	-	1,0333	-	1,0333	bar
Pressure behind combustion chamber	10,92	10,92	10,92	10,92	bar
Pressue behind turbine	-	1,0706	-	1,0846	bar
Gas fuel volum. flow	210	213	-	-	Nm3/h
Exces air coefficient (λ)		17,6	no combustion	**no combustion**	-
Gross system efficiency electric/combined		27,42/39,74		24,03	%
Net system efficiency electric/combined		25,79/38,12			%
Compressed air volum. Flow	14,5	14,5	14,5	14,5	kg/s
Heated air average temp.	850	**850***	850	850*	°C
Heated air average temp. (before CC)	833	833	833	833	°C

Variant 4.

The values calculated with the program are almost identical to the original assumptions, which allows to conclude that the model architecture is similar to that used by the designers. It is worth paying attention to the diametrically different air excess coefficient obtained in the conceptual system to the actual value measured in the report. This difference shows a completely different mode and thus the economy of the installation.

Variant 5.

The power obtained is very close to the assumed one, although the efficiency is the lowest among all considered variants, however, the generation of electricity in this variant is "free". The achieved efficiency is almost equal to the real efficiency of the system which also burns gas. Unfortunately, the system never worked without the need to burn gas.

5. Conclusion

The results of the simulation in the IPSEpro program as well as the data taken into account show that the operation of the turbine diverges from the original assumptions (characterized by a relatively low efficiency of waste heat utilization by the analyzed installation). First of all, the turbine uses too much natural gas in its operation, which affects negatively the profitability of the entire investment and the operation of the installation. The installation also produces useful heat, but only for the purposes of the ferroalloys plant, which is and will be self-sufficient in this matter. Energy prices at the time of installation analysis (2018) and today (December 2020) suggest work at the break-even point.

Waste heat in Huta Łaziska, due to the characteristics of the production line, is described by parameters that change dynamically over time. Figure 3. shows the characteristics recorded during exhaust gas tests. It can be seen that in about 30 minutes the temperature may change by as much as 300 ° C. The instability of waste heat parameters favors using an utilization solutions that are characterized by high flexibility of work, the possibility of quick adjustment, and the possibility of working in the case of low temperature of waste heat. This facts advocates for the use of gas turbines or, for example, ORC systems.

Fig. 3. Measurments of exhaust gases extraction [6]

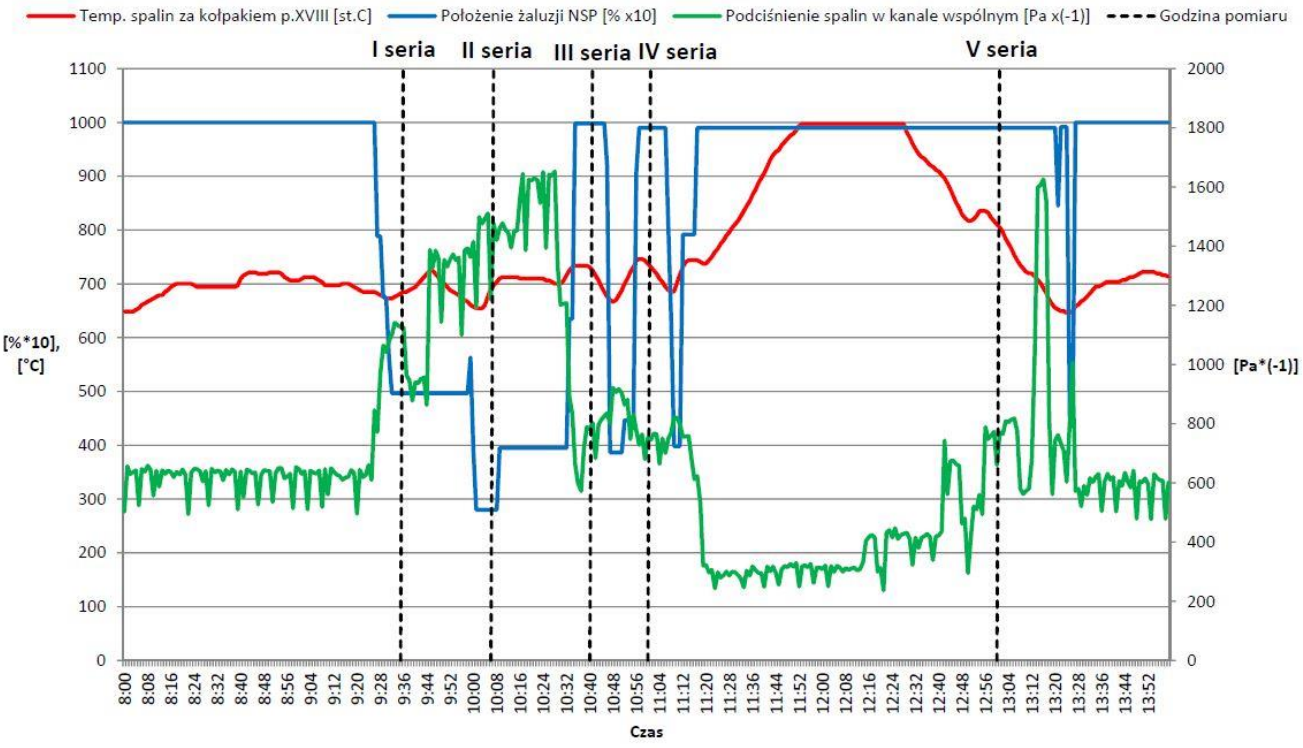

The data that served as the basis for the computer model showed the operation of the installation in the highest conditions of the recorded post-process gas temperatures. On average, the power obtained from these gases was lower, which meant that the turbine operated at lower powers. Regulation of the parameters of these gases, apart from direct control of the production process, is carried out with the degree of furnace windows closing. The less air is sucked in from around the furnace and the more closed the furnace, the higher the gas temperature can be achieved. However, this has the effect of increasing the load on the furnace cooling system, in which, after exceeding the water temperature value = 85°C, the furnace is automatically switched off in an emergency. It is imperative that the heat of the gases from the furnace heated to high temperatures is released - otherwise there is a risk of damaging the dedusting filters that can operate at temperatures up to 250°C. Despite the considerable length of the flue gas ducts, excessively heated gases may not cool down to the required temperature. In the data from the analyzed report, the gas temperature before the dedusting was 227.95 ° C, and the temperature of the cooling water at the outlet from the XVII furnace collector was 72.26 ° C. This means that the improvement of the system performance should not take place by further increasing the temperature of gases from the furnace, as it carries the risk of interrupting the continuity of the ferroalloy plant's production.

In the process of the analysis, it was found that recuperators are the installation node with the highest optimization potential. The amounts of heat exchanged in them are significantly below the design assumptions. Their work is hampered by the large amount of dust carried by the furnace gases and the failure of the vibratory cleaning system. It resulted in the necessity of their "manual" cleaning, i.e., opening them more often and as a side effect increasing the heat losses. In order to improve the operation of the installation, a different design of recuperators should be considered and the losses of heat and pressure should be minimized.

Model created in IPSEpro showed that the amount of waste heat from Furnace Hall III is sufficient for the operation of the gas turbine with low gas consumption and high excess air coefficient. Due to the nature of the program's operation and the assumed simplifications, the results obtained in the model should be treated with a certain dose of skepticism, the same should be done with the data from reports that showed visible discrepancies at various measuring points, moreover, some data was undoubtedly generated incorrectly and presented unrealistic values.

The idea of utilizing waste heat is valid only in the case of achieving a measurable economic and ecological effect. While the environmental effect can be supported by subsidies for technologies that may be sometimes financially unprofitable, in case of specialized industrial plants, the achieved economic indicators are the basis for their proper operation. The primary goal of the ferroalloys plant is the production of ferroalloys, while the utilization of waste heat is there to make this process cheaper and less harmful to the environment.

An example of an analysis of a waste heat utilization installation in Huta Łaziska based on a gas turbine has shown that, despite its large scale, the potential for managing this heat is an extremely difficult issue, causing problems both in the recovery installation itself and in the production part of the plant.

Acknowledgment

I acknowledge Dr inż. Karol Sztekler from AGH University of Science and Technology for creating friendly environment while working on case which the subject of this article.

References

[1] Huta Łaziska SA, http://hlsili.pl/, 30.11.2017

[2] Przegędza J., Analiza i krytyczna ocena aktualnego schematu technologicznego produkcji żelazostopów w piecach piecowni IV

[3] Instalacja odpylająca – instrukcja dla pracowników

[4] SimTech, http://www.simtechnology.com/CMS/index.php/ipsepro, 30.11.2017

[5] Tomeczek J., Wiśniewski T., Bialik W., Ochman J., Sprawozdanie z realizacji pracy badawczo-wdrożeniowej „Obliczenie i opracowanie wytycznych projektowych do projektu wykonawczego instalacji do produkcji energii elektrycznej z wykorzystaniem ciepła odpadowego gazów odlotowych z procesu wytopu FeSi75% w piecach 12MVA piecowni III (piec XVII i XVIII)”

[6] Parametry strugi spalin w kanałach w Piecowni III zarejestrowanych podczas pomiarów w dniu 12.09.13 r.

Oxytree – fuel property analysis

Tarun Kumar Shanmugam[1], Marcin Landrat[2]

[1]Silesian University of Technology, e-mail: tarun.1229kumar@gmail.com
[2]Silesian University of Technology, e-mail: marcin.landra@polsl.pl

Abstract

Oxytree is a fast-growing hybrid plant belonging to the Paulownia species. The fast-growing ability attributes to the increased biomass production thereby increasing the amount of energy generated through biomass. This paper aims to establish the potential of Oxytree as a biomass resource. To understand the energy potential of Oxytree, 3 samples of Oxytree were tested for the fuel properties. The results determined the calorific value of Oxytree to be 18.3 MJ/kg, a low moisture content, and elemental composition similar to other renowned hardwood energy crops, establishing the energy potential of Oxytree. The results indicate that Oxytree has a high potential to be a good biomass resource and can lead to the increase in the energy generated from biomass eventually reducing the energy generated from fossil fuels.

Keywords: Oxytree, Biomass, Fuel properties

1. Introduction

1.1. Paulownia

Paulownia, also known as the princess tree, the empress tree, or the foxglove tree belongs to the family Paulowniaceae. The scientific name for Paulownia is Paulownia tomentosa. The name Paulownia is believed to have derived from the name of the queen of the Netherlands, Anna Pavlovna (1795-1865). As it was a visually pleasing tree it was nominated to honour the queen. The origin of Paulownia is believed to be in China and is found in some other parts of East Asia. Paulownia has been cultivated for almost 3000 years.[1] Today Paulownia species can be found in many places around the world growing naturally and under cultivational conditions including Europe, North America, Central America, and Australia. Paulownia essentially grew into being a multipurpose tree finding its purpose in several areas. A few to mention are the furniture industry, musical instruments, decorative mouldings, laminated structural beams, and shipping containers. [2] Paulownia can regenerate from its existing root system. It can regenerate up to 7 times from the same existing root system.[3] This extraordinary feature made it earn the name “The Phoenix Tree”. Paulownia is also considered to be one of the fastest-growing trees in the world. A Paulownia tree can reach its maturity as early as 10 years from planting it. This astonishing growth rate and amount of wood quantity generated led people to even call this the “Magic” tree.

1.2. Oxytree

Oxytree is a hybrid tree from the Paulownia species. It is a hybrid of Paulownia elongata and Paulownia fortunei. Being a hybrid plant, its characteristics are quite similar when compared to other Paulownia species.

Fig 1.1 A picture of an Oxytree plantation.

Oxytree's rapid growth rate, diverse growing conditions, and a wide range of applications have made it one of the most valuable plants to grow. Oxytree reaches its maturity age by 8 years and can reach up to a height of 15-16 meters. The trunk diameter during maturity is estimated to be around 35 centimeters. This essentially adds up to a huge volume of wood that can be used for various purposes. Like Paulownia, Oxytree can also grow back using its existing root system. It is estimated that Oxytree can regenerate for about 7-10 times after cutting down. Oxytree leaves also have some applications but the most important and attractive feature of these leaves is its carbon sequestration capability. Oxytree leaves are estimated to absorb 10 times more carbon dioxide than normal plant species. During its lifetime, it absorbs a significant amount of carbon dioxide, hence the name Oxytree-Oxygen tree.[4]

2. Methodology

2.1. Type of samples

Three types of samples were obtained from Oxytree.pl, an Oxytree plantation in Wroclaw. It is to be noted that this plantation is situated in Poland and hence all the climatic and environmental conditions apply to it. These 3 samples were tested for the calorific value, moisture content, organic content: presence of Carbon, Hydrogen, Sulphur, Nitrogen and Chlorine. The following are types of samples that were tested,

2.2. Oxytree Pellets

The first sample was Oxytree in the form of pellets which is used typically for biomass energy generation. All the biomass energy generation plants receive wood in the form of pellets which makes it more suitable for extracting

energy and hence most of energy generation plants are designed in this way to accommodate wood pellets. Figure 2.1 is a picture of the wood pellets as received.

Fig 2.1. Oxytree Pellets

For the ease of testing the wood pellets were grinded using a grinder. After grinding the wood pellets turned into finely grinded wood dust.

2.3. **Oxytree Branch**

The second sample was the branch of an Oxytree. The branch was also obtained from one of the trees from the plantation, it was obtained from a tree which was 3 years old. Figure 2.2 is a picture of the Oxytree branch which was used for testing.

Fig 2.2. Oxytree Branch

Since it is impossible to perform laboratory tests on a whole branch, the branch was sawed using a saw and the dust obtained from sawing the branch was used for the various tests.

2.4.Oxytree Trunk

The third sample was a part of the trunk of an Oxytree. The trunk was obtained from a tree in the plantation which was 3 years old. The sample of the trunk is one of the most important samples as most of the wood that obtained is from the trunk of the tree. A part of the trunk was cut off from the tree for the purpose of our testing. Figure 2.3 is a picture of a part of the trunk from an Oxytree.

Fig 2.3. Oxytree Trunk

The trunk was also sawed using a saw to make the sample more usable for testing. The saw dust obtained from sawing the trunk was used for testing purpose.

3. Summary of results

Identifying the energy potential and presence of organic elements and properties of Oxytree is essential in deciding the possible energy generation techniques. Table 1 depicts the amount of different organic elements, moisture content, ash content, and calorific value present in 3 different samples of Oxytree which were the pellets, branch, and trunk of Oxytree.

Table 1. Summary of results

Results	Pellets	Branch	Trunk
Carbon (%)	46.31	46.89	47.19
Hydrogen (%)	7.36	7.87	8.34
Chlorine (%)	0	0	0
Sulfur (%)	0.039	0	0
Nitrogen (%)	0.47	0.23	0.39
Moisture (%)	6.3	6.87	8.47
Ash (%)	2.51	2.33	2.36
Calorific value (MJ/kg)	18.3	17.3	17.6

Woody biomasses in general have a carbon content of close to 50%, from the above-performed tests, it is proved that Oxytree also has a similar amount of carbon content. [5] Comparing biomass to coal, the carbon content in coal is close to 78%. It also matters that while burning biomass we only alter the terrestrial carbon cycle in which carbon is relatively accumulated only over a short period of time but while burning coal we alter the geological carbon cycle which is accumulated over a much longer period of time. [6]

The hydrogen content present in Oxytree from our results is close to 8%. In comparison to other short rotation woody biomasses, the content of hydrogen in Oxytree is slightly higher. [7] Higher content of hydrogen in the biomass will increase the calorific value of the biomass. [8]

It was determined that there is close to no sulfur present in Oxytree. The presence of sulfur in the biomass will result in sulfur oxide emissions during combustion. Sulfur oxides are considered a threat to the environment as they can contribute significantly to particulate matter pollution and acid rain. In the case of Oxytree, sulfur emissions are negligibly small. [8]

The moisture content in Oxytree is very less. In the pellets and branches, it is approximately about 6%. Although the Oxytree trunk might contain close to 10% of moisture, it is almost always converted into wood pellets before combusting it for biomass. In the wood pellets that are widely used for biomass today, the moisture content is about 7%. Lesser moisture content higher the heating value of the biomass. [8]

From the experiments performed the ash content estimated in Oxytree is approximately 2.5%. Ash is the amount of uncombusted materials that are leftover. Excess ash is a factor that influences erosion in biomass boilers but this problem can be overcome by the use of additives, fuel-leaching, or post-combustion techniques.

Calorific value is one of the most important factors that determine the potential of biomass as it is the energy content of the biomass. As in most cases, biomass is converted into the form of wood pellets before combusting it in the boilers. The moisture present in the wood is removed while converting it into wood pellets. Hence the Calorific value is close to 18.3 MJ/kg. [8]

The content of Chlorine present in Oxytree is very less. The presence of chlorine can lead to fouling in the boiler tubes which is a form of erosion that will eventually lead to the failure of the boiler. Hence for biomass, fuels with less chlorine content are desirable. [8]

The average content of Nitrogen in Oxytree is 0.4%. The presence of nitrogen in the fuels leads to the formation of nitrogen oxides which are considered to be very hazardous to the environment. Lesser content of nitrogen is preferred in the biomass as it reduces the NOx emissions. [9]

4. Comparison

From this paper, it is established that Oxytree is a good source of biomass but let's see how it fares against other sources of biomass. As established earlier several types of biomasses are currently being used for biomass energy generation but it is to be noted that not all sources of biomass are suitable for growth in diverse conditions like Oxytree neither can most of them grow as fast as Oxytree. The closest to Oxytree are hardwood biomasses which are also cultivated as short rotation energy crops. The following are a few hardwood biomasses that are renowned sources of biomasses,

- Willow
- Poplar
- Chestnut
- Maritime Pine

The following are the various aspects in which the biomasses mentioned above compare to that of Oxytree. For uniformity, the data from the pellets of Oxytree are used for this comparison.

4.1. Calorific value

As established earlier, calorific value is one of the most important characteristics for any source of biomass as it determines the energy potential of the biomass. Figure 4.1 depicts the calorific value of the various biomasses,

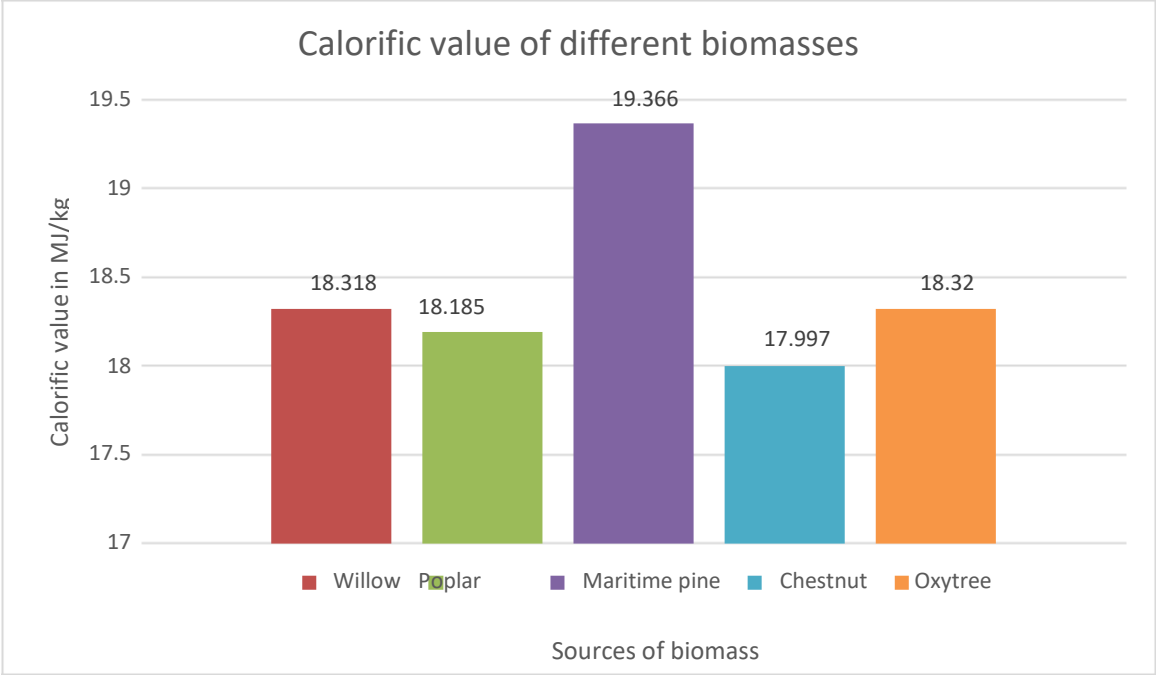

Fig 4.1. The calorific value of woody biomasses. [11]

As you can see from the figure, the calorific value of Oxytree is on par with almost all the renowned woody biomasses even marginally higher than most of them. Maritime pine is the only other woody biomass with a higher calorific value. Hence the calorific value of Oxytree can be deemed good.

4.2. Moisture content

As established earlier, the content of moisture present in the biomass is an important parameter in determining the quality of the biomass. Most biomass energy generation methods require less moisture content to increase the efficiency of energy generated. Figure 4.2 depicts how the moisture content of Oxytree compares to the other biomasses.

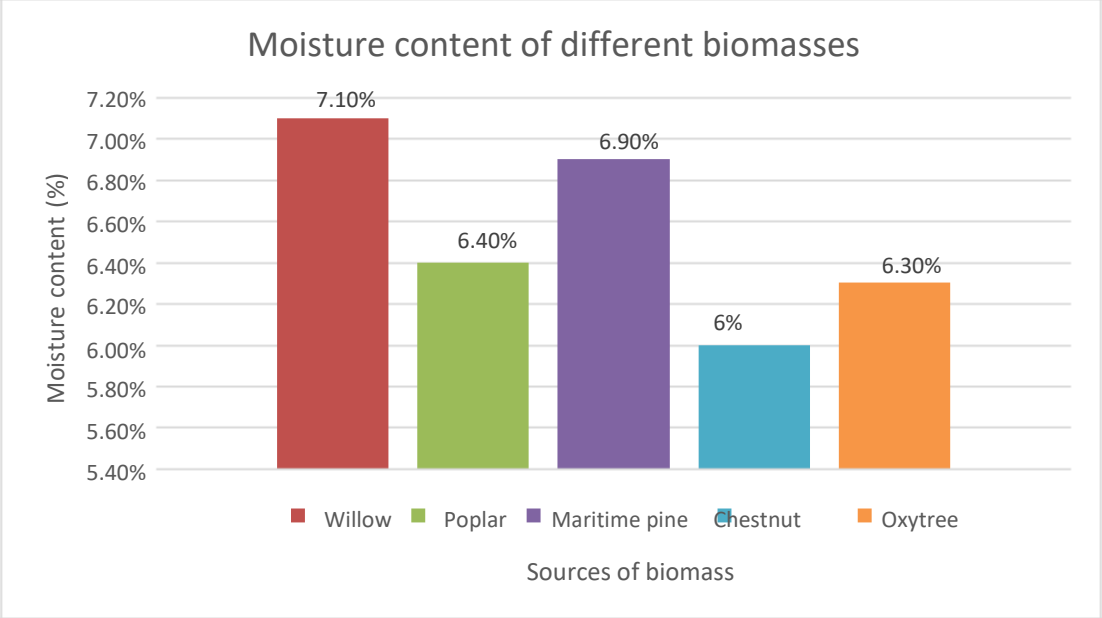

Fig 4.2. The moisture content of different woody biomasses. [11]

From Figure 4.2 it is visible that the moisture content of Oxytree is also quite similar to the other biomass sources. It is also to be noted that the removal of moisture from Oxytree is very easy and does not require any external drying machines to extract the moisture.

4.3.**Ash content**

Also as established earlier, the amount of ash content present in biomass is influential in designing the boiler and taking steps to prevent corrosion. Figure 4.3 depicts the amount of ash in various biomasses.

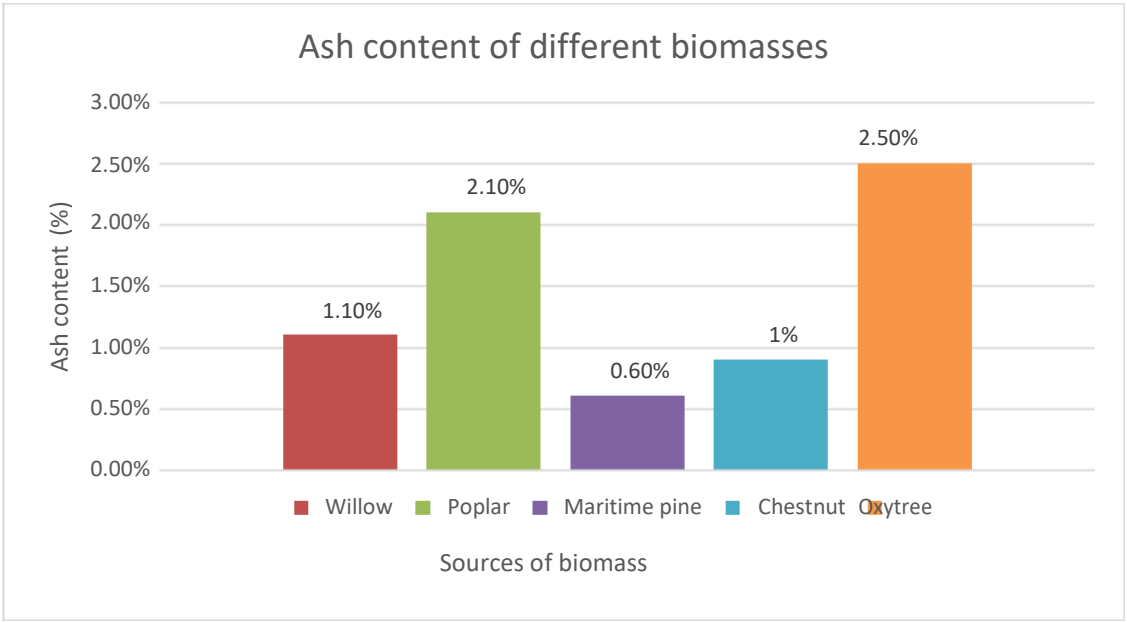

Fig 4.3. Ash content in different woody biomasses. [11]

The ash content after combustion is the highest in Oxytree when compared to other sources. However, the use of additives and other ash clearing methods can prove to be very effective and corrosion of the boiler can be easily prevented.

4.4. Elemental composition

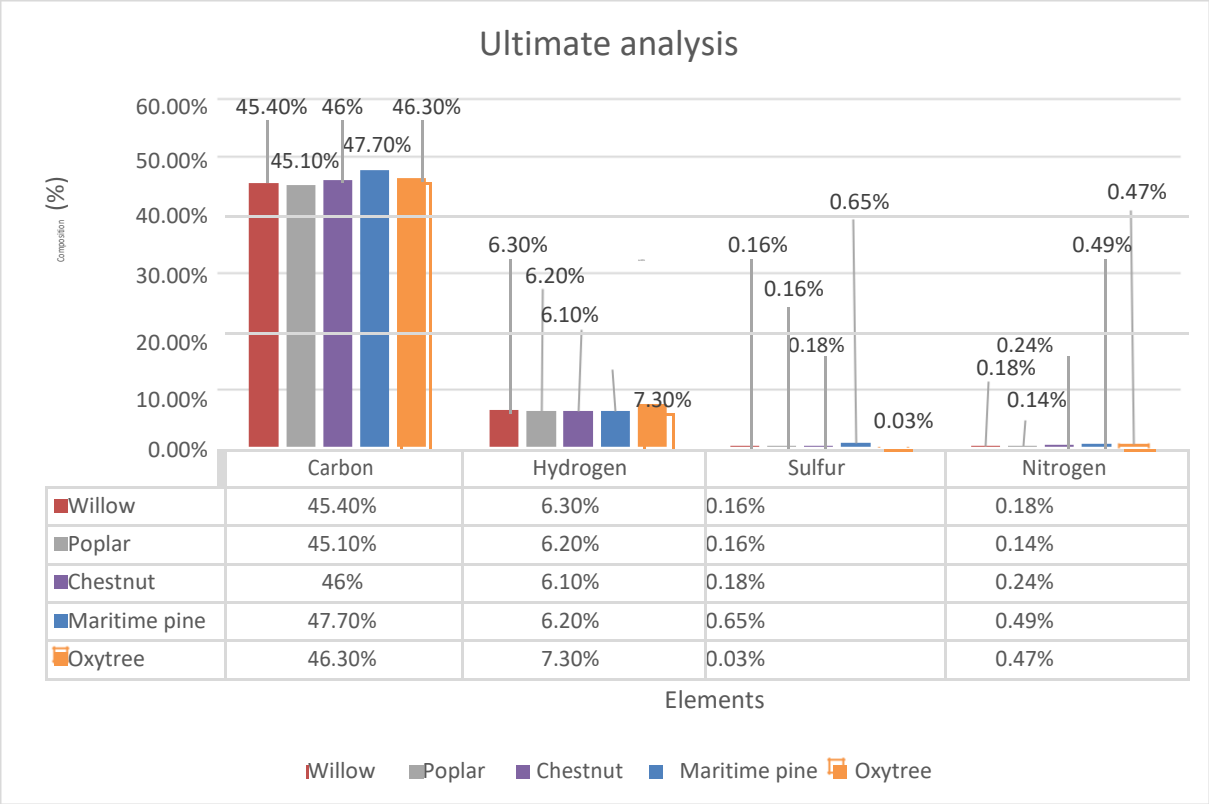

Fig 4.4. Ultimate analysis of different woody biomasses. [11]

From Figure 4.4 it is visible that the elementary composition of the various renowned biomasses is similar to Oxytree. Oxytree has the highest amount of Hydrogen in comparison with the other biomasses. The higher amount of Hydrogen adds value to the biomass by increasing the calorific value. Oxytree also has the lowest amount of sulfur. The presence of sulfur can lead to the emission of sulfur oxides which are considered as a threat to the environment as it increases the particulate matter pollution and increases the chances of acid rain. [8][10][12]

5. Conclusion

With a higher calorific value, lesser ash content, and similar elemental composition, the Maritime pine can appear as a better source of woody biomass, but it is to be noted that Pinus pinaster also known as the Maritime pine is a species that is native to the Mediterranean region and requires Mediterranean climate to grow and flourish. The growth performance of the Maritime pine is highly impacted by climate and is difficult to attain optimal growth in cold conditions and severe winters. Another thing to consider is that there have been cases where the Maritime pine has been considered an invasive species especially because of the invasion in South Africa during the 18th century. The invasion had several negative effects resulting in the loss of biodiversity of the region and water scarcity as the Maritime pine consumes large amounts of water.

Willow and Poplar trees are a more diverse source of woody biomass with similar characteristics to Oxytree but the growth rate of Oxytree is superior to both these trees having the ability to provide higher amounts of biomass within the specified time.

Considering the climatic conditions and growth requirements of Oxytree, it is one of the best sources of energy crop plantations. As established above the energy density, moisture content, ash content and elemental composition are very similar to other successfully grown biomass sources around the world proving the potential of Oxytree as a biomass resource to increase the biomass energy generation.

Acknowledgment

This research was executed under the guidance of Dr. Marcin Landrat and the support offered by Silesian University of Technology.

References

[1] Icka, Pirro & Robert, Damo & Icka, Engjëllushe. (2016). Paulownia Tomentosa, a Fast Growing Timber.

[2] 10. 10.1515/agr-2016-0003.

[3] Yadav, Niraj & Vaidya, Brajesh & Henderson, Kyle & Lee, Jennifer & Shewart, Whitley & Dhekney, Sadanand & Joshee, Nirmal. (2013). A Review of Paulownia Biotechnology: A Short Rotation, Fast Growing Multipurpose Bioenergy Tree. American Journal of Plant Sciences. 4. 2070-2082. 10.4236/ajps.2013.411259.

[4] Innovation for Development of South-South Cooperation - http://www.ideassonline.org/public/pdf/PaulowniaChina-ENG.pdf as on 20/05/2020.

[5] Statement on the CO_2 absorbing capacity of Oxytree. Concerning the CO2 absorption capacity of OXYTREE® (Paulownia Clon in vitro 112®) - http://oxytree.pl/certyfikaty/

[6] Houghton, R. A., Hall, F., and Goetz, S. J. (2009), Importance of biomass in the global carbon cycle, J. Geophys. Res., 114, G00E03, doi:10.1029/2009JG000935.

[7] Harvard University - Jordan Wilkerson and Daniel Utter - Biomass over Coal: Burning Different Carbon to Mitigate Climate Change – April 16, 2018.

[8] Poo Chow, Professor And G.L.Rolfe,Professor and Head Department of Forestry 1 10 Mumford Hall 130 1 W. Gregory University of Illinois, Urbana, IL 6 180 1 (Received September 1987)

[9] S. Clarke, P.Eng., and F. Preto, PhD - Biomass Burn Characteristics - ORDER NO. 11-033 AGDEX 737/120 JUNE 2011.

[10] U.S. National Library of Medicine - https://toxtown.nlm.nih.gov/chemicals-and-contaminants/nitrogen-oxides#:~:text=Nitrogen%20oxide%20pollution%20is%20emitted,especially%20from%20electric%20power%20plants.&text=Nitrogen%20oxides%20and%20sulfur%20dioxide,produce%20rocket%20fuels%20and%20explosives as on 20/07/2020.

[11] MICHAEL TAYLOR - ENERGY SUBSIDIES Evolution in the Global Energy Transformation to 2050 – International Renewable Energy Agency, 2020.

[12] Álvarez-Álvarez, Pedro & Pizarro, Consuelo & Anta, Marcos & Cámara-Obregón, Asunción & Bueno, Julio & Alvarez, Ana & Gutiérrez, Inés & Burslem, David. (2018). Evaluation of Tree Species for Biomass Energy Production in Northwest Spain. Forests. 9. 160. 10.3390/f9040160.

[13] V. C. MORAN1, J. H. HOFFMANN2, D. DONNELLY3, B. W. VAN WILGEN4, and H. G. ZIMMERMANN5 - Biological Control of Alien, Invasive Pine Trees (Pinus species) in South Africa.

Biological properties of soil stimulated by calcium peroxide

Jaspreet Kaur Jandoo[1], Agnieszka Borecka[2], Jolanta Turek-Szytow[3], Anna Gnida[4]

[1]Silesian University of Technology, e-mail: k_jaspreet59@yahoo.com
[2]Silesian University of Technology, e-mail: -
[3]Silesian University of Technology, e-mail: Jolanta.t.szytow@polsl.pl
[4]Silesian University of Technology, e-mail: anna.gnida@polsl.pl

Abstract

Calcium peroxide stimulates soil microbial activity. It provides oxygen and assists in neutralizing an acidic pH. Availability of oxygen increases microbial activity which induces bioremediation of the soil. This experiment aimed to check how the soil behaves after the addition of calcium peroxide. The preparation was applied in two different doses, sequentially increasing the pH of five soil samples taken from different sources in the south of Poland. The soils were incubated for 30 days. In addition to the physio-chemical analyzes, respiration activity and the number of microorganisms were measured. It was observed that calcium peroxide was able to increase the pH of soil for both doses. Moreover, it was observed that the increasing dose resulted in increased respiration rate and microorganism growth.

Keywords: calcium peroxide, soil, bioremediation

1. Introduction

Soil is a very dynamic material. It can sustain the diversity of life forms and has an abundant supply of nutrients, minerals, water, and gases. The soil's inorganic material is modified by the microbial community including bacteria, yeast, and plant roots into the soil. The nutrient supply is maintained by mineral cycling and decomposition and formation of organic matter. These nutrients are scattered in the soil horizontally as well as vertically. Soil composition differs by region and various factors play a role in shaping soil texture and structure. Factors like temperature, pH, humidity, microbial activity, and oxygen help shaping the environment for the microbial community to function. The largest number of microflora is found in the topsoil, but with depth, the diversity and population of microbes decreases. The number of bacteria in one gram of dry weight of the soil can be million to several billion cells. Yeast, however, per gram of soil can spread to several meters with hyphal growth to some hundred meters, fungal cells in the topsoil ranging from 0.001 billion to a billion cells. A change in factors such as pH favours a particular community, for example, acidic pH soil is more conducive for yeast than bacteria [1].

However, the change in factor-like pH can harm the overall soil composition, constituting its microflora. Hence, the treatment of such soils requires an approach which can not only upgrade the quality of the soil but also improve microflora proliferation and their metabolic activities. The scale of soil acidification in Poland has encouraged improving to restore the quality of soil. And hence, many enhancements are being sought to tackle this issue with more reliable treatment and with fewer side effects. Bioremediation of soil through the application of stimulant additives like calcium peroxide (CaO_2) is being utilised to safely adjust and rise the pH of acidic soils [2]. Calcium peroxide in solid form, when administered to the soil, has long-lasting effects as it is less soluble and provides oxygen for bioremediation of soil. CaO_2 is a yellowish colour solid, which is alkaline nature. CaO_2, being less soluble in water, releases oxygen for a long period without being entrapped [3]. A major benefit of utilising CaO_2 is that it can deliver more folds of oxygen in comparison to other additives like magnesium peroxide or hydrogen peroxide which can be toxic in certain doses. Additionally, it is more affordable and can be made by burning lime with hydrogen peroxide [4]. Calcium peroxide can be mixed with cement, sand, fly ash, and peat to develop an oxygen-organic material. This material can provide desirable oxygenation and organic matter releasing properties to the soil [5].

CaO_2 decomposes to hydrogen peroxide and calcium hydroxide in the reaction with water. The former product releases reactive oxygen species which reacts with the metal contaminant and the latter product raises the pH.

Since calcium peroxide is often used to aid in soil bioremediation, this experiment aimed to test its effect on clean soils with low pH.

2. Methodology

2.1. Experiment design

Five different soils were used for the research from different places in the south of Poland: Rachowice (RAC), Plawniowice (PŁA), Zaolszany (ZAO), Palowice (PAL), and Blachownia (BLA). Soil sampling sites have become their working names, therefore they will be called so later in this work.
Because at a later stage, the samples were to be treated with calcium peroxide, the soils were chosen in such a way that their pH was as acidic as possible, so that a change in pH by 1 and 2 under the influence of CaO_2 would not change the pH to alkaline (neutral or slightly acidic pH was desired). The soil was taken from five different places, dried at room temperature, and then sieved through a sieve with a mesh size of approx. 1 mm. This was to unify the soil material and get rid of plant residues, stones, and other undesirable objects. Each of the five soils was divided into three parts and placed in microcosms. Selected doses of calcium peroxide were added to two of them, which were supposed to raise the pH by 1 (microcosm/series 1) and 2 units (microcosm/series 2). The used calcium peroxide was composed of CaO_2 - 15% and CaO - 85%. The third microcosm contained reference soil with no calcium peroxide (microcosm/series 0). The containers were placed at room temperature and covered with cloth to limit excessive water evaporation from the soil. A schematic representation of the experiment is provided in Figure 2.1. The samples were incubated for a period of 30 days (the time during which the processes in the soil should stabilize after the initial rapid changes), ensuring a constant temperature and soil moisture conditions of 65%. The actual doses of calcium peroxide calculated on the previous pH are presented in Table 2.1.

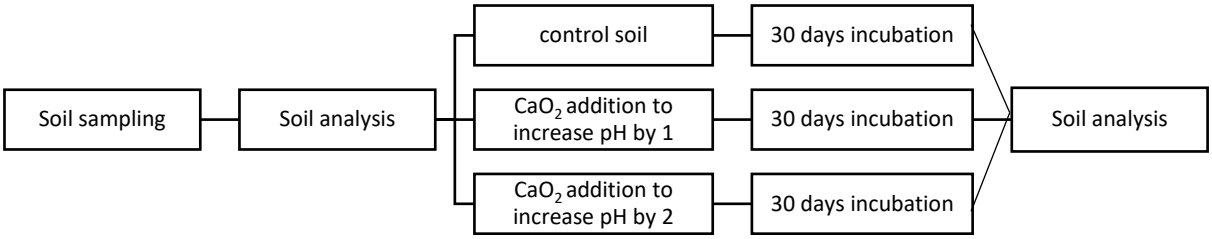

Fig.2.1 Schematic description of the experiment

Table 2.1 Calcium peroxide doses used to raise soil pH by 1 (series 1) or 2 (series 2), in mg CaO_2

	RAC	PLA	ZAO	PAL	BLA
Series 1	3.55	1.58	3.34	4.2	1.54
Series 2	7.05	3.54	7.78	11.94	3.56

2.2. Soil properties determination

The soil pH was determined using probe IJ44C/CX-404 (Elmetron). Absolute dry mass content and water content were measured using the gravimetric method. Turin's method was used to analyze organic carbon content. Hydrolytic acidity (mmol H^+/kg) of the soil was done following the Kappen method.

2.3. Soil microbes activity determination

The soil respiration (SR) tests were determined according to the OECD guidelines for substrate-induced respiration test and by the PN-EN ISO 14240-1: 2011 standard. The above method was modified by resigning from the addition of the substrate because they wanted to recreate the natural conditions present in the field. Measurements were made for 4 (SR4) and 5 (SR5) days.

2.4. Enumeration of soil microbes

The number of microorganisms was determined by the plate method by inoculating soil water extract: bacteria - on an R2A culture medium and yeasts – on Czapek-Dox agar. Water soil solution was prepared according to PN-ISO 14255:2001. Colony-forming units (CFU) were counted and calculated per kg of soil dry mass.

3. Results and discussion

3.1. Soil properties

Soils that were used for the study were taken from five different places in the south of Poland. Table.3.1 shows the properties of soil taken from various places with their initial pH, C: N ratio, and hydrolytic acidity.

Table.3.1 Properties of the soils understudy

Soil sample name	RAC	PŁA	ZAO	PAL	BLA
Soil matter	mineral	mineral	mineral	organic	mineral
Place	mixed forest	young pine forest	mixed forest	mixed forest	-
Vicinity of the place	-	water reservoir	arable fields	breeding pond	chemical plants
Initial pH	4.4	3.8	4	4.1	5.6
Hydrolytic acidity, mol/Kg	0.09 ± 0.004	0.09 ± 0.002	0.13 ± 0.002	0.27 ± 0.024	0.03 ± 0.004
Organic carbon, g/kg	35.4 ± 3.5	18.1 ± 3.8	23.1 ± 0.9	79.3 ± 9.4	8.2 ± 1.7
C:N	7:1	7:1	6.5:1	10:1	5:1

All soils were acidic with a pH in the range of 3.6 to 5.6. Soil from the vicinity of the water reservoir (PLA) showed the most acidic pH among other acidic soil samples. Only one soil was organic in nature, and the rest were minerals. The ratio of the carbon content to the nitrogen content is an important criterion used to assess the degree of risk to the productive function of soil. The carbon to nitrogen ratios for the mineral soils under study were from 5:1 to 7:1, whereas for organic soils it was the highest among all soils (10:1). These values indicate that the tested soil belonged to clean soil. The general assessment of soil according to its sorption capacity proves its ability to store nutrients. The ion content in the sorption complex is different and variable. The share of acidic cations (mainly hydrogen and aluminium) represented by hydrolytic acidity was from 0.3 to 0.13 for mineral soil and 0.27 for the organic one. Hydrolytic acidity is an indicator of the degree of saturation of the sorption complex with hydrogen and aluminium ions.

After the addition of CaO_2 and 30 days of incubation, the pH was higher for all soils (Table 3.2). Organic matter, however, decreased with increasing dose, although its value increased in PAL soil and remained the same in BLA soil. On the other hand, the absolute dry mass remained the same in all soils with slight variation in decimal values. Also, the water content, showed an increase in value for RAC and PLA soil with increasing dose, while it increases in series 1 in the rest of the soils.

Table.3.2 Properties of soil after 30 days of incubation with calcium peroxide

Soil name	Dose of CaO_2	Series 0	Series 1	Series 2
RAC	pH	4.8	6.4	6.9
	Organic matter (%)	8.3 ± 0.62	7.8 ± 0.11	7.7 ± 0.12
	Absolute dry mass (%)	98.8 ± 0.03	98.9 ± 0.05	98.9 ± 0.03
	Water content (%)	27.4 ± 0.16	26.5 ± 0.05	27.1 ± 0.44
PLA	pH	4.4	6.1	7
	Organic matter (%)	3.5 ± 0.09	3.4 ± 0.03	3.2 ± 0.01
	Absolute dry mass (%)	99.5 ± 0	99.6 ± 0.04	99.5 ± 0.06
	Water content (%)	20.7 ± 0.41	18.9 ± 0.11	19.2 ± 1.11
ZAO	pH	4.9	6.6	7.5
	Organic matter (%)	5.8 ± 0.01	5.7 ± 0.14	5.3 ± 0.11
	Absolute dry mass (%)	99.2 ± 0.02	99.3 ± 0.02	99.3 ± 0.11
	Water content (%)	21 ± 0.07	23 ± 0.14	21.5 ± 0.01
PAL	pH	4.5	5.4	6.7
	Organic matter (%)	14.7 ± 0.01	15.8 ± 0.04	16.2 ± 0.14
	Absolute dry mass (%)	98.2 ± 0.1	98.5 ± 0.11	98.6 ± 0.07
	Water content (%)	32.7 ± 0.25	35 ± 0.28	34.7 ± 0.37
BLA	pH	6.7	7.9	8.6
	Organic matter (%)	1.3 ± 0.04	1.3 ± 0.09	1.3 ± 0.1
	Absolute dry mass (%)	99.6 ± 0.12	99.7 ± 0.06	99.8 ± 0.08
	Water content (%)	13.2 ± 0.23	14 ± 0.4	12.5 ± 0.46

3.2. **Soil activity**

Soil activity was measured after 30 days of the experiment. The activity tests represent the average activity for 4 days (SR4) and 5 days (SR5). Fig. 3.1 depicts the soil respiration activity measured in the 5 tested soil samples.

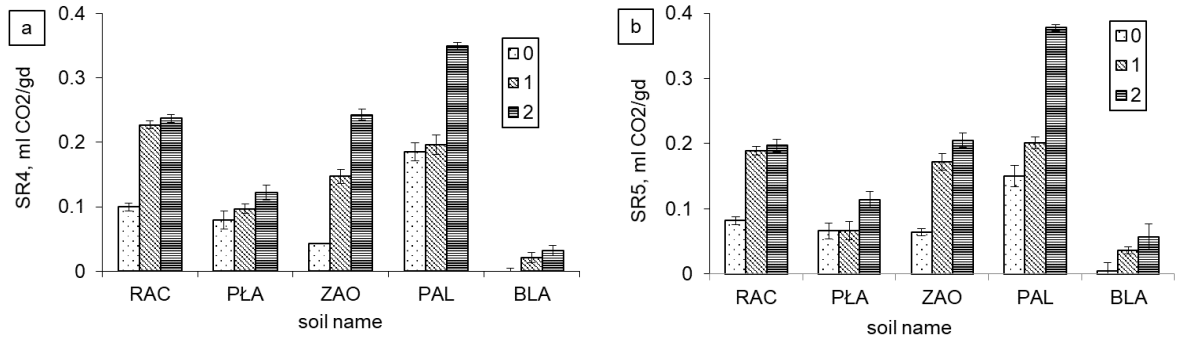

Fig 3.1 Respiration activity of soil after 30 days with calcium peroxide: a) SR4, b) SR5

The respiration during 4 days (SR4) (Figure 3.1a) was for soils without calcium peroxide in the range of 0 – 0.1 and 0.185 ml CO_2/gd for mineral and organic soil, respectively. The soils of series 1 reveal SR4 in the range of 0.097 – 0.227 ml CO_2/gd for soils originated from the forest place and 0.021 ml CO_2/gd for soil from the vicinity of the chemical plant. Similarly, for series 2, SR4 values are similar for soil RAC, PŁA, and ZAO (0.064 - 0.082 ml CO_2/gd), maximal for organic soil PAL (0.349 ml CO_2/gd), and minimal for chemically "touched" BLA soil (0.032 ml CO_2/gd). This trend was likewise that of SR5 (Figure 3.1b).

3.3. **Soil biocoenosis**

Fig.3.2 show the composition of bacteria and yeast after 30 days of application of calcium peroxide. Most of the soils, except BLA, had a similar bacterial count of 0.7 – 8.8 mln cells/kg DM (Figure 3.2a). The BLA soil had almost 35 mln cells/kg DM. The yeast count in series 0 was from 0.7 mln cells/kg DM in PAL soil to 5.4 mln cells/kg DM in ZAO (Figure 3.2b). In series 1, the bacterial count was higher than 10 mln cells/kg DM for RAC, PŁA, and PAL, and higher than 100 and 200 mln cells/kg DM for BLA and ZAO, respectively. In series 2, in all soils except BLA, SR4 value was higher than in other series. The bacterial count in series 2 showed a slight increase for RAC and PLA soil samples, although there was a tremendous increase in the bacterial count for ZAO and PAL as 385 cells/kg DM and 177 cells/kg DM, respectively.

In contrast to the yeast count, an opposite trend was observed for the bacterial count. RAC soil showed the highest fungal count in series 2 by 41 cells/kg DM and with the highest yeast count in series 1, that is, 27 cells/Kg DM. Soils ZAO, PAL, and BLA revealed similar values up to 10 mln cells/kg DM, but in soil RAC and PŁA, the yeast number in series 1 and 2 was higher than 12 and 22 mln cells/kg DM, respectively.

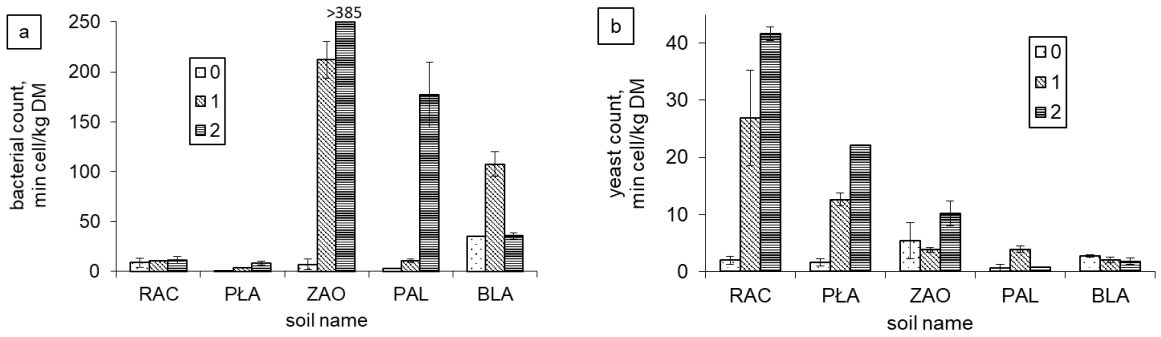

Fig.3.2 Bacterial (a) and yeast (b) soil composition after 30 days of exposure to calcium peroxide

3.4. **Influence of calcium peroxide dose on soil – a discussion of the results**

The addition of calcium peroxide has impacted the soil properties. The soil properties such as pH and organic matter content, microbial activity, and number, have changed within the span of 30 days with the addition of calcium peroxide. The results are shown in Fig. 3.3. The pH increased in all samples amended with calcium peroxide. The lower dose of peroxide (series 1) increased the pH by about 1-1.5, while the higher dose (series 2) by 1.9-2.6. Lower changes in pH of soils from series 1 were observed for mineral soil and soil from the vicinity of the chemical plant. As evidently shown in Fig 3.3, CaO_2 was most effective when administered with a higher dose of calcium peroxide. However, the lower dose also showed a positive impact, although less effective than the higher dose.

During the thirty days of the experiment, the organic matter was slightly reduced (RAC, ZAO, and PAL) or remained at a constant level (PŁA and BLA; the changes were within the standard error). There is a close relationship between the loss and the content of organic matter - in soils, where the loss of organic matter was observed, its content was higher and ranged from 5.7% to 16.4%, while in soils where organic matter was only 1.4% - 3.5% % defect was not observed.

In soils with calcium peroxide, the loss of organic matter was greater, in particular at the higher dose, where the average loss was from 1.7-6.0% and 7.2-8.6%, respectively for series 1 and 2. The loss of organic matter is an unfavourable process that causes soil impoverishment. However, the preparation can be combined with substances

supplementing biogenic elements, thanks to which it is possible to create a fertilizer containing calcium peroxide, which will not adversely affect soil fertility [6].

The organic matter content has great importance for the respiration rate [7]. It was noticed that in soils with a higher content of organics (PAL and RAC), the respiration activity was higher (Figures 3.1 and 3.3). Usually, a rich and well-developed soil microflora is found in fertile soils (with high content and availability of organic matter) [8].

Calcium peroxide stimulated respiratory activity in the studied soils not only by correcting the pH but also by oxygenating the soil [9]. The addition of calcium peroxide increased the respiratory rate by at least once. The higher dose of calcium peroxide resulted in a higher increase in respirometric activity than the lower dose. Higher respiration activity indicates the utilization of oxygen provided by CaO_2 by the heterotrophic microflora for respiration.

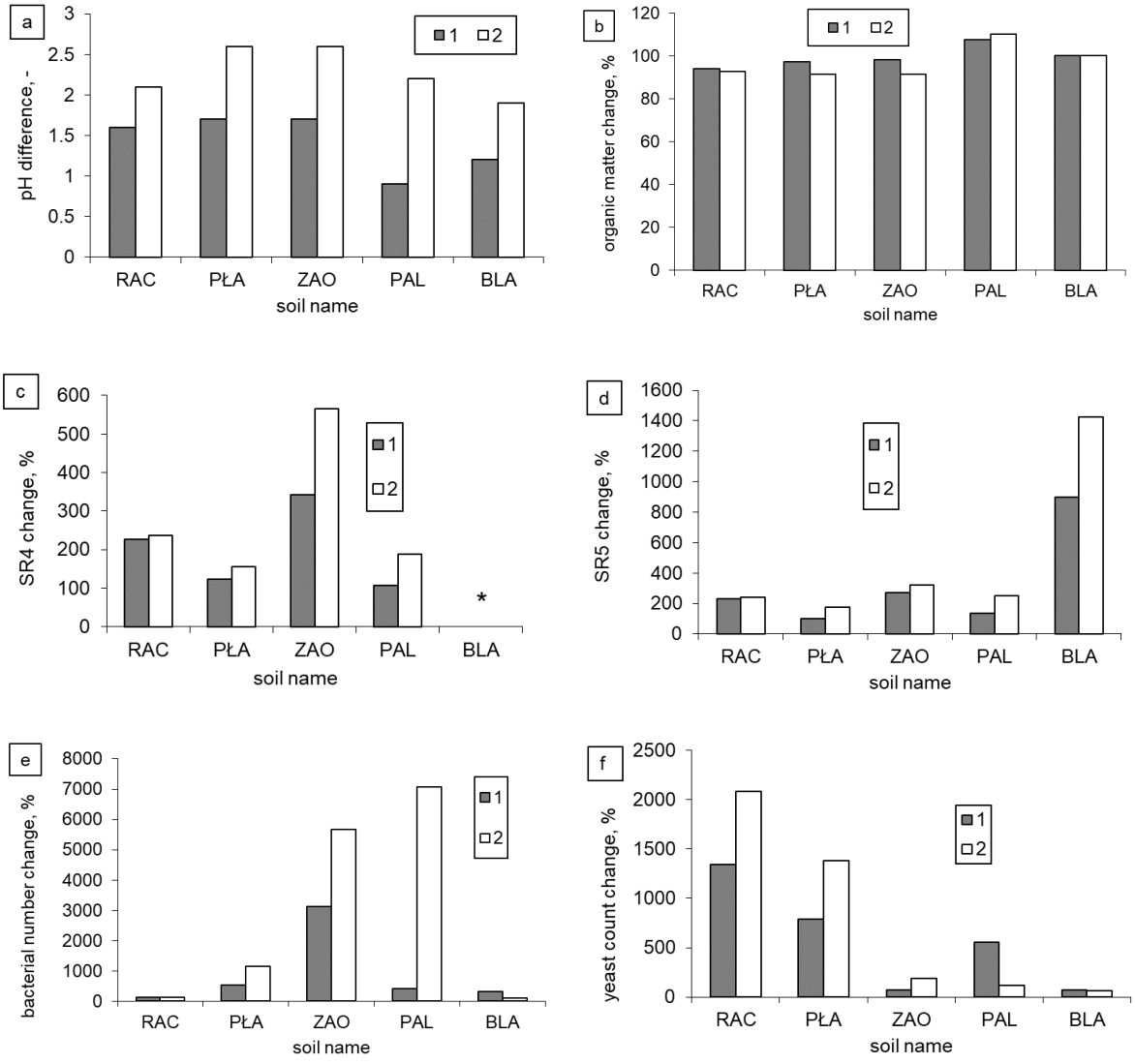

Fig.3.3 Changes in soil properties: pH (a), organic matter (b), respiration activity (c and d), and microbial number (e and f); * as the respirometric activity of soil without calcium peroxide was zero it was not possible to calculate the percentage increase for this soil; 1, 2 - series designations

The negative effect of the preparation on microorganisms occurred in the BLA soil, where the dose increasing the pH by 2 caused the pH to change to alkaline, and also, the added amount of water in this soil was too high, which resulted in inhibition of the growth of the population of microorganisms and a significant reduction in their respiratory activity (inhibition) [10].

Calcium peroxide stimulated the growth of both yeasts and bacteria, but the studies carried out in this study did not show which of these groups of microorganisms had a better effect. Probably the group of organisms that developed more strongly in a given soil under the influence of calcium peroxide was dependent on the initial pool of soil species. Taking into account the sum of bacteria and yeasts in all forest soils, there was a tremendous growth of microorganisms under the influence of calcium peroxide, compared to the sample without this specimen. Only in the soil possibly contaminated with chemicals (BLA) did the levels of each group of microorganisms remain at a similar level.

Soil moisture (Table 3.2) was of key importance for the development of soil microflora. The established level of 65% of full water capacity was to ensure the most favorable conditions. However, in soils with a low organic matter content (PAL and BLA), the determined amount of water turned out to be too high, which had a negative impact on the development and respiration rate of microorganisms. The best results at this level of irrigation were obtained in the PAL soil with the highest organic matter content. The amount of organic matter has a direct and indirect influence on soil properties, including air-water relations. Usually, soils with a higher content of organic matter can retain more water and are more stable and more resistant to changes [8].

4. Conclusion

The conducted research allowed for the formulation of the following conclusions:

- Calcium peroxide stimulates soil microbial activity;
- Increasing the dose of calcium peroxide increases the respiration rate. The peroxide dose changes the soil reaction to neutral resulted in the strongest activity of microorganisms. Exceeding this dose (pH above 7.4) caused a negative effect on the microflora (especially yeasts);
- Calcium peroxide stimulates the growth of bacteria and yeasts;
- Calcium peroxide (in a nontoxic dose) usually stimulates microorganisms to growth;
- The rate of respiration is most influenced by the pH of the environment, humidity and the content of organic matter in the soil;

Acknowledgement

The authors gratefully acknowledge the financial support provided by project MNISW FSB/16/RJP8/2015/512 and 08/080/BK_18/0054 funded by Silesian University of Technology.

References

[1] Willey, J., Sherwood, L., Woolverton, Ch. (2008) *Microbiology*, 7th edition, McGraw-Hill, New York

[2] Hackl, E., Pfeffer, M., Donat, C., Bachmann, G., Zechmeister-Boltenstern, S. (2005) Composition of the microbial communities in the mineral soil under different types of natural forest. Soil Biology and Biochemistry, 37(4), 661-671; doi: 10.1016/j.soilbio.2004.08.023

[3] Lu, S., Zhang, X., Xue, Y. (2017) Application of Calcium peroxide in water and soil treatment: A review. Journal of Hazardous Materials, 337(5), 163-177; doi:10.1016/j.jhazmat.2017.04.064

[4] Cassidy, D.P., Irvine, R.L. (1999) Use of calcium peroxide to provide oxygen for contaminant biodegradation in a saturated soil. Journal of Hazardous Materials, 69(1), 25-39; doi: 10.1016/S0304-3894(99)00051-5

[5] Kao, C. M., Chen, S. C., Su, M. C. (2001) Laboratory column studies for evaluating a barrier system for providing oxygen and substrate for TCE biodegradation. Chemosphere, 44(5), 925-934; doi: 10.1016/S0045-6535(00)00578-6

[6] Miksch K., Walawska B., Turek-Szytow J., Gluzińska J. (2009) Calcium peroxide application into petroleum products biodegradation processes in the environment (in polish). Przemysł Chemiczny 88(5), 520-524

[7] Ryan, M.G., Law, B.E. (2005) Interpreting, measuring, and modeling soil respiration. Biogeochemistry, 73(1), 3-27; doi: 10.1007/s10533-004-5167-7

[8] Turek-Szytow, J., Gnida, A., Marciocha, D. (2013) Soil remediation in theory and practice (in polish). Wydawnictwo Politechniki Śląskiej, Gliwice

[9] Turek-Szytow J. (2016) Calcium peroxide as a chemical stimulator of bioremediation of soil contaminated with persistent organic pollutants (in polish). Przemysł Chemiczny, 95(4), 795-796; doi: 10.15199/62.2016.4.16

[10] Rousk, J., Brookes, P.C., Bååth, E. (2010) Investigating the mechanisms for the opposing pH relationships of fungal and bacterial growth in soil. Soil Biology and Biochemistry, 42(6), 926-934; doi: 10.1016/j.soilbio.2010.02.009

Scientific research of the negative impact of the polluted environment on the mental state

Pitulei Viktoria[1]

[1]*Ivano-Frankivsk National Medical University, e-mail: pituley@ukr.net*

Abstract

Abstract. The article examines the criteria of mental health, the role of psychological resilience and impact polluted environment on the mental health of the individual. Reveals the environmental component of mental health, the impact of environmental catastrophe and environmental crisis on a person's mental health. Highlights the role and significance environmental psychology in dealing with the consequences of the Chernobyl accident. The ecological component of mental health has been studied, in particular the influence of ecological space on the mental state of an individual; the concepts, types and features of the impact of ecological catastrophe and ecological crisis on the mental are revealed personal health; the role of identity crisis as a result of social influence on psychological is considered personal health. The role of ecological psychology in the work with the consequences of the Chernobyl accident is substantiated, the direct and indirect effect of radiation on the mental state of man, the peculiarities of pathology due toecological distress, a description of the "Chernobyl syndrome". The main factors of the human environment that negatively affect his life and health are identified. It is analyzed that air is one of the most important products in human life. A person can go without air for only 5 minutes without any health consequences. Deterioration of air quality violates the right to life and physical and mental health.

Keywords: mental health, ecological space, ecological catastrophe, ecological crisis, ecological psychology.

1. Introduction

Human is a part of nature. From time immemorial, mankind has been interested in the impact on the fate, life and health of unknown forces of the universe and the Earth. This question is still relevant today. Among the many manifestations of human interaction with the environment, usually the greatest attention is paid to the impact of the environment on man, his health, including mental. We have a steady increase in the degree of visual and information load, unfavorable socio-economic situation, as well as destructive in its content for various factors the epochs of social changes that take place have a pronounced negative impact on the leading indicators of the functional state and adaptive resources of the body, the state of physical and mental health man. Numerous scientific studies show that only in the last two decades the prevalence of mental illness of various origins in the world has increased almost 30 times (Ustinov, 2013). However, the dominant position in the structure of pathological changes that occur in the state of mental health, occupy mental shifts of the prenosological maintenance representing a number of intermediates between norm and pathology of qualitatively different in nature psychopathological and psychoneurological phenomena, are marked by the presence of signs of exhaustion and failure of adaptive-compensatory mechanisms, lead to the formation of various manifestations of social and mental maladaptation. The purpose of the article is to theoretically investigate the impact of environmental factors on a person's mental health.

2. The concept of ecological consciousness of the individual. The destructive impact of environmental disasters and environmental crises on environmental awareness.

We will focus on the ecological component of a person's mental health. An integral part of a healthy personality is the formed ecological consciousness is the highest level of mental reflection of the natural, artificial, social environment and one's inner world; reflection on the place and role of man in the ecological world, as well as self-regulation of this reflection.

From birth to death, a person is in a certain ecological space, which in a certain way affects it, but man himself forms this space, builds it or, conversely, destroys it. From how a person will perceive this space, how he will build his relationship with it, his psychological state will depend.

After all, it is known that a poorly constructed ecological space (for example, a cramped or dark room with musty air, poorly chosen colors of living or working spaces) negatively affects the mental state of man. On the other hand, today actively resort to psychotherapeutic interventions,in particular such as art therapy, nature therapy, aromatherapy, which widely use environmental factors (both artificial and natural) for the treatment of mental illness, depression and general improvement of mood and ability to work (Khokhlov, 1997).

However, environmental catastrophes and environmental crises have the most destructive impact on environmental awareness. It is important to note that since the beginning of mankind and until now man has been exposed exposure to environmental factors such as earthquakes, hurricanes, fires, floods, solar eclipses, epidemics, man-made disasters, nuclear weapons, wars, etc. However, today their influence has significantly increased and diversified.

Unexpected disasters (this is the definition given to catastrophes in the reference literature) are of various natures, this anomalous phenomenon is characterized primarily by the presence of two signs: low probability of each case and the special complexity of the consequences. It is also worth it note that since any catastrophe occurs in a certain environment, it will be on its ownstatus of ecological catastrophe.

Research has shown a close linkbetween environmental pollution and the frequency of prematurity, malformations in children and chromosomal diseases, allergic pathology, anemia,mental retardation and behavioral abnormalities and children, their physical development. In children,living in areas of ecological disaster, congenital malformations, recurrent bronchitis, allergic diseases, nephropathy,reduction of mental development rate (IQ), bronchial asthma, immunodeficiency conditions, endocrine pathology, neuropsychiatric diseases, oncopathology, etc.

We will focus on the ecological component of a person's mental health. An integral part of a healthy personality is the formed ecological consciousness. Ecological consciousness is a higher level of mental reflection of the natural, artificial, social environment and one's inner world, reflection on the place and role of man in the ecological world, as well as self-regulation of this reflection.

From birth to death, a person is in a certain ecological space, which in some way affects it, but man himself forms this space, builds it or, conversely, destroys it. His psychological state will depend on how a person will perceive this space, how he will build his relationship with it.

After all, it is known that a poorly constructed ecological space (for example, a cramped or dark room with musty air, poorly chosen colors of living or working spaces) negatively affects the mental state of man. On the other hand, psychotherapeutic interventions are actively used today, in particular such as art therapy, nature therapy, aromatherapy, which widely use environmental factors (both artificial and natural) to treat mental illness, depression and general improvement of mood and performance. However, environmental catastrophes and environmental crises have the most destructive impact on environmental awareness. Environmental crises affect people indirectly, mostly they become a negative psychological factor in the environment or have long-term consequences.

To date, the negative impact of the environment has significantly intensified and diversified. The consequences of the most significant catastrophes (for example, the Chernobyl disaster) are felt far beyond the region where the disaster occurred. According to doctors, the ecological situation in Prykarpattia is very disappointing. The earth is just crying out for help. Prykarpattia, a paradise, already shares the fourth place in terms of air pollution with Zaporizhia. It is clear that the leaders of this rating are Donetsk, Dnepropetrovsk and Lugansk. But it is unbelievable that the lungs of Ukraine - the Carpathians are fourth in this shameful list. To save the environment, it is necessary to make great efforts and protect the cradle in which life originated on our planet.

With the exception of those natural disasters that bypass man-made territories, catastrophes cause a total shock to the vital foundations of certain categories of the population and society as a whole. Except deaths, they lead to a change in the usual way of life (such a change can be instantaneous orrelatively prolonged in time), physical injuries, mass stress, increase in deviant behavior.

The mobilization of efforts and resources to eliminate the consequences of the disaster does not go unnoticed and for those who was not at the epicenter of events. The consequences of the most significant catastrophes (for example, the Chernobyl disaster) are felt far beyond the region where the disaster occurred.

An ecological catastrophe is an acute form of ecological pathology that has severe social and environmental consequences (Levochkina, 2003). According to the level of sociality, ie the level of influence of the social factor that led to ecological catastrophe, A. Prigogine identifies the following types of disasters: natural, environmental or socio-natural, technical, social (Prigogine, 1989).

An ecological crisis is a process that takes place in an ecosystem that threatens the identity of a system or object. An ecological crisis of anthropogenic origin is a state of the ecosystem when it is characteristic the signs are shifted under the influence of the human factor to the point beyond which there is a threat of losing the identity of such a system [ibid.] V. Krysachenko proposes to distinguish the types of environmental crises by the following criteria: by factor (mover), object definition, hierarchical status and the effect (Krysachenko,1996).

An ecological crisis can affect a person in two ways - directly and indirectly. So, when human activity takes place in the ecosystem, which is the source of its existence, and this ecosystem is in crisis, then there is a threat to the existence of man himself. But in modern society, human life takes place mainly in artificial or artificial environment. In this case, environmental crises affect people indirectly, mostly they become a negative psychological factor in the environment or have remote effects.

It should be noted that in modern society in the face of changes in a large part of the population manifests itself in such a psychological phenomenon as the identity crisis. This concept means loss of self-esteem, inability (or difficulty) to adapt to one's role in a changed society. The identity crisis in our current social conditions is determined by the gap between the requirements variable social and economic relations and the rigidity of personal attitudes, stereotypes of behavior. In the course of research, four variants of the identity crisis are identified: anomic (passive departure in myself from difficulties - 40%); dissocial (activation of aggression, destructive style of behavior, intolerance - 12%); negativist or passive-aggressive (hidden, veiled aggression, orthodoxy and rigidity of thinking - 27%); magical (coming into the world of mysticism, irrational - 21%) (Polozhiy,1993).

So today the question is very acute: "As an environment that has undergone fundamental changes under influence of the scientific and technological revolution, affects the human psyche? On the other hand, it appears no less significant question: “How should a person build their relationship with the environment so as not to cause him irreparable damage, which, in turn, will harm humanity? On these, as well as others such questions should be answered by science, which has become particularly acute and relevant in the post-Chernobyl era - environmental psychology.

Ecological psychology is the science of psychological aspects of the relationship between man and the environment (natural, artificial, social, cultural), which is organically included in human life and serves as an important factor in regulating its behavior and social interaction (Levochkina, 2003).

When considering the effects of radiation on a person's mental health, it is important to understand that the direct effects of radiation on a person's mental state are difficult to measure, and that only high doses of radiation can significantly affect a person's mental state. Yes, in the first hours of liquidation of the Chernobyl accident in people who received a dose of 50 Ber, there was nervous excitement, fear, and then - depression. Study of mental development in children who have been exposed to intrauterine radiation as a result of an accident at the Chernobyl nuclear power plant, showed that the intellectual index below 70 is determined in almost 6% of children affected districts and 2% of children from control, unaffected areas (Kozlova,1995).

2.1. **Pathogenic effects of environmental factors on mental health**

The pathogenic effect on the mental health of environmental distress has been studied in the course of transcultural research, in the survey of the population in environmentally unfavorable regions, in extreme situations, in areas of natural and man-made disasters. In these conditions it is determined also (Krasnov,1995) increasing the number of psychosomatosis (somatic diseases and organic, functional disorders in the development of which negative psychological factors or distress are important). Pathology that occurs in environmental distress has features [ibid.]: Combination, synergism a number of factors (including conditionally pathogenic); their somatotropism and, as a consequence, coexistence mental, somatic and neurological changes; conjugation of exogenous and psychogenic reactions, individual and population; sensitization, special vulnerability to new, even ordinary, in including environmental impacts.

Instead, the indirect effect of radiation was much greater not only on individuals but also on society as a whole. For example, people living in areas contaminated by radioactive releases suddenly restructured: they lost not only their health but also their environment,existence, work, friendship, and often family, connections, and at the same time - confidence in the future.

In such cases, scientists trace specific psychological phenomena in the post-Chernobyl space. These phenomena primarily include the so-called "Chernobyl syndrome" (Levochkina, 2003), to which includes: rent guidelines; the position of "victim"; feeling lost health; "Evacuation symptom"; "Symptom of exclusivity", feeling of "lost future"; symptom of helplessness.

However, when considering environmental factors that affect a person's mental health, first of all we it is necessary to narrow the concept of the environment to the definition of "human living environment" - a set of objects, phenomena and environmental factors (natural and artificial),that directly surround a person and determine the conditions of his residence, food, work, rest, training, education, etc. As well as understanding of environmental factors any biological (viral, prion, bacterial, parasitic, genetically modified organisms, biotechnology products, etc.), chemical (organic and inorganic, natural and synthetic), physical (noise, vibration, ultrasound, infrasound) , thermal, ionizing, non-ionizing and other types of radiation), social, food, water supply, living conditions, work, leisure, education, upbringing, etc.) and other factors that affect or may affect human health or the health of future generations (Gushchuk, 212). Among the most common environmental factors that negatively affect or can have a detrimental effect on life and health, the most discussed in society is air pollution, which causes cancer and chronic diseases of the upper respiratory tract, allergies; expansion of the ozone hole, which increases the risk of skin cancer; drinking water pollution that leads to epidemics and chemical poisoning; pollution of surface water bodies; soil pollution waste (solid and liquid, household and industrial); food contamination (causes allergies, mass poisonings and epidemics); use of GMOs; exposure to non-ionizing radiation, including electromagnetic (computer equipment, mobile phones, base stations, etc.); solar activity and magnetic storms, etc. The multiplicity and peculiarity of all the above factors should be taken into account in the context of studying the destructive effects on the mental health of the individual, the formation of preventive measures and interventions in dealing with mental health disorders.

Today, there are many ways to address and prevent environmental threats and challenges. An important place among them is occupied by moral and ethical and environmental health paradigms, according to which health is a matter of personal and social choice of moral values, the relationship between man and the environment, attitude to their health. The human mind should be focused on preserving the environment and their health, on control and responsibility for their own health. A man can be healthy only in a healthy environment.

In the complex of problems of the modern city the problem is of great importance noise. Its intensity in developed countries increases annually by 0.5-1 dB, and this is one of the causes that leads to disease. Noise levels in urban areas streets reach 85-87 dB and cause significant noise in areas, adjacent to highways. The spectrum of noise on the body is very multifaceted. In addition to selective negative effect of noise on the hearing organs, it causes general changes in general body. The negative long-term effect of noise causes noise sickness with phenomena changes in the functional state of the central nervous system. With the dynamics of excitation processes in the cerebral cortex is disturbed, there are phase changes of conditioned reflex activity, slowing down mental reactions

in solving test problems, reduced efficiency, hearing, impaired attention, eventually neurosis. Subjective feelings are reduced to irritability, fatigue, disturbances concentration, pain in the heart and increased blood pressure.

3. Conclusions

Modern ecological the crisis in the world is due to the impact of the complex environmental and occupational factors in combination with stress, neuropsychiatric overload. Environmental education should play an important role in preventing environmental challenges and threats, aimed at the formation of environmental awareness, starting from preschool age and the use of bioprophylaxis. In the article we have considered the criteria of mental health, in particular the criterion of mental balance, the role of psychological resilience and the impact of stress on the mental health of the individual has been studied. The ecological component of mental health has been studied, in particular the influence of ecological space on the mental state of an individual; the concepts, types and features of the impact of ecological catastrophe and ecological crisis on the mental are revealed personal health; the role of identity crisis as a result of social influence on psychological is considered personal health. The direct and indirect effect of radiation on the mental state of a person, the peculiarities of pathology due to environmental distress are revealed. The main factors of the human environment that negatively affect his life and health are identified.

Acknowledgment

Ukraine, Ivano-Frankivsk National Medical University, the department of psychiatry, narcology and medical psychology.

References

[1] Gushchuk, I. (2012),«Estimation of medical and ecological risks in the implementation of the state system of social and hygienic monitoring», Proceedings of the scientific-practical conference "ENVIRONMENT AND HEALTH ” on April 27-28, 2012, Ternopil, pp. 109–110.

[2] Kozlova, I. (1995), «Intrauterine brain damage (consequence of the Chernobyl disaster)», Proceedings of the XII Congress of Psychiatrists of Russia, Moscow, Knowledge, 1995, pp. 151–152.

[3] Krasnov, V. (1995), «Ecological psychiatry: methodology, subject of research and the next practical tasks», Proceedings of the XII Congress of Psychiatrists of Russia, Moscow, Knowledge, pp. 158–160.

[4] Krysachenko, V. (1996), Ecological culture: theory and practice: textbook, Kyiv, Testament, 349 p.

[5] Levochkina, A.(2003), Ecological psychology in the post-Chernobyl era: textbook. Manual,Kyiv, Svichado, pp. 142–148.

[6] Polozhiy, B.(1993), Mental health as a reflection of the social status of society, Review of psychiatry and medicine. Psychology, № 4, pp. 6–11.

[7] Prigogine, A. (1989), Sociodynamics of catastrophes, Sociological research, № 3, pp. 35–45.

[8] Ustinov, O. (2013), Mental health as a component of national security [Electronic resource] /OV Ustinov // Ukrainian Medical Journal. - I / II 2013 - № 1 (93), Mode of access to the article: http: // www.umj.com.ua/article/52851/psixichne-zdorov-ya-yak-skladova-nacionalnoi-bezpeki.

[9] Khokhlov, L (1997) , Mental health of the population and modern ecological, sociocultural influences, Pedagogical Bulletin, № 4, pp. 14–18.Website title, webpage address, date of access (dd/mm/yy).

Parabolic solar trough cooker for outdoor cooking

Ahmed Saber[1]

[1]*Silesian University of Technology, e-mail: aysaber@hotmail.com*

Abstract

Many desgins of solar cookers have been used for cooking as the box type and many concentrator solar cookers bur the parabolic trouph solar cooker is the most effecient one due to the unique desgin that allow it to concentrate all the solar rays to one focal line that allows it to reach higher teperatures that any other design which is is very practrical and suffient for boiling water for cooking, Using this application might help decrease the usage of gas or electricity for cookinh in many hot areas.

At some point, the population of the planet will use up all the coal and oil that lay beneath the surface of the earth. More importantly, using the coal and oil and the by-products of those natural materials creates by-products that pollute our environment from oil spills in the ocean to the scarred earth of strip mining, for generations we have damaged our global environment in our constant quest for more energy sources.

The article is showing results from the inclined cooker facing the sun to measure the thermal performance that depend on heating a vacuum tube filled with therom oil that have high boiling temperature which is acting as heat exchanger fluid that directly transfere heat to the water filled pan on top of the insulated box.

Keywords: Solar energy, CSP, outdoor cooking

1. Introduction

A solar cooker, or solar oven, is a device which uses the energy of sunlight to heat food or drink to cook it or sterilize it. High-tech versions, for example electric ovens powered by solar cells, are possible, and have some advantages such as being able to work in diffuse light. However at present they are very unusual because they are expensive. The vast majority of the solar cookers presently in use are relatively cheap, low-tech devices. Because they use no fuel and cost nothing to operate, many nonprofit organizations are promoting their use worldwide to help reduce fuel costs for low-income people, reduce air pollution and slow deforestation and desertification, caused by use of firewood for cooking. Solar cooking is a form of outdoor cooking and is often used in situations where minimal fuel consumption is important, or the danger of accidental fires is high.

2. Solar power

Concentrating Solar Power (CSP) systems use lenses or mirrors and tracking systems to focus a large area of sunlight into a small beam. The concentrated heat is then used as a heat source for a conventional power plant. A wide range of concentrating technologies exists; the most developed are the parabolic trough, the concentrating linear Fresnel reflector, the Sterling dish and the solar power tower. Various techniques are used to track the Sun and focus light. In all of these systems a working fluid is heated by the concentrated sunlight, and is then used for power generation or energy storage.
Solar power is the conversion of sunlight into electricity, either directly using photovoltaics (PV), or indirectly using concentrated solar power (CSP). CSP systems use lenses or mirrors and tracking systems to focus a large area of sunlight into a small beam. PV converts light into electric current using the photoelectric effect.[1]

2.1. **parabolic trough**

A parabolic trough is a type of solar thermal energy collector. It is constructed as a long parabolic mirror (usually coated silver or polished aluminum) with a Dewar tube running its length at the focal point. Sunlight is reflected by the mirror and concentrated on the Dewar tube. The trough is usually aligned on a north-south axis, and rotated to track the sun as it moves across the sky each day.

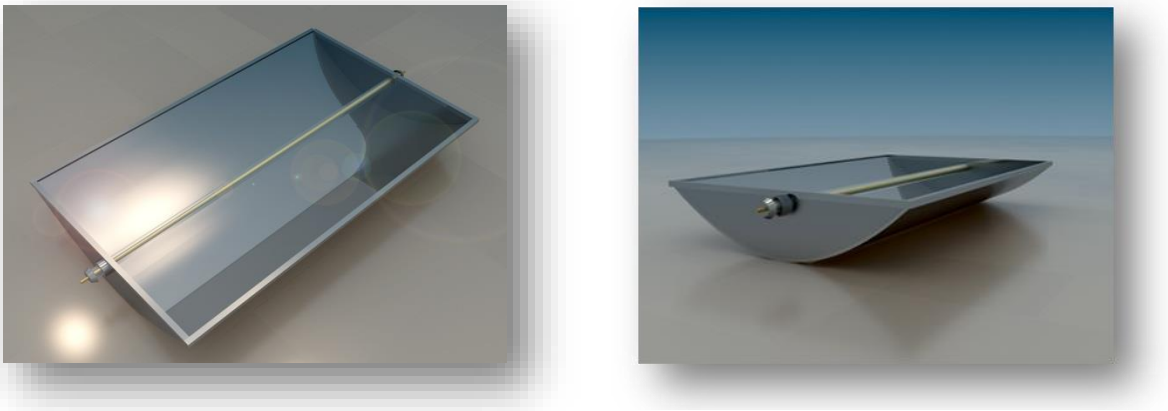

Fig.2.1 The Parabolic Trough

A parabolic trough solar collector uses a mirror in the shape of a parabolic cylinder to reflect and concentrate sun radiations towards a receiver tube located at the focus line of the parabolic cylinder. The receiver absorbs the incoming radiations and transforms them into thermal energy, the latter being transported and collected by a fluid medium circulating within the receiver tube. This method of concentrated solar collection has the advantage of high efficiency and low cost, and can be used either for thermal energy collection, for generating electricity or for both, therefore it is an important way to exploit solar energy directly. [2]

2.2. **Parabolic Dish Systems**

It is the most powerful type of collector which concentrates sunlight at a single, focal point, via one or more parabolic dishes arranged in a similar fashion to a reflecting telescope focuses starlight, or a dish antenna focuses radio waves. Parabolic dish systems consists of a parabolic shaped point focus concentrator in the form of a dish that reflects solar radiation onto a receiver mounted at the focal point (the power conversion unit). This system produces relatively small amounts of electricity (3 to 25 kilowatts of power) compared to other concentrating solar power technologies.[3]

There are two key phenomena to understand in order to comprehend the design of a parabolic dish. One is that the shape of a parabola is defined such that incoming rays which are parallel to the dish's axis will be reflected toward the focus, no matter where on the dish they arrive. The second key is that the light rays from the sun arriving at the Earth's surface are almost completely parallel. So if dish can be aligned with its axis pointing at the sun, almost all of the incoming radiation will be reflected towards the focal point of the dish most losses are due to imperfections in the parabolic shape and imperfect reflection. The resulting beam of concentrated sunlight is reflected onto a thermal receiver that collects the solar heat. The thermal receiver must be mounted in the focus point if the dish.

The engine/generator system is the subsystem that takes the heat from the thermal receiver and uses it to produce electricity. The most common type of heat engine used in dish/engine systems is the Stirling engine. A Stirling engine uses the heated fluid to move pistons and create mechanical power. The mechanical work, in the form of the rotation of the engine's crankshaft, drives a generator and produces electrical power.

Fig.2.2 Parabolic Dish

Fig.2.3 Sterling Engine

Parabolic dish system have a lot of advantges :

- Very high temperatures reached. Conversion efficiency approaching 30% has been achieved. This is the highest conversion efficiency of the concentrating solar power technologies.
- A larger area can be covered by using relatively inexpensive mirrors rather than using expensive solar cells.
- The solar parabolic dish sterling engine system has only a very minimal water requirement. The engine is air cooled, so no cooling water is needed.

Although this model isused for electrical gerneration, there's a small version of it that is used in cooking that concentrates the sun's heat onto the bottom or the sides of a pot -- similar to a stovetop. Temperatures can get so hot that you can fry food or pop popcorn. The advantages are speed and the potential to cook when it is cool outside. The disadvantages are safety concerns (as to eyes and children) and the need to stir the contents of the pot so the food does not stick, just like a stovetop. Temperatures can reach above 400 degrees Fahrenheit in the pot. The parabolic cooker might also need adjustment to keep it faced toward the sun. [6]

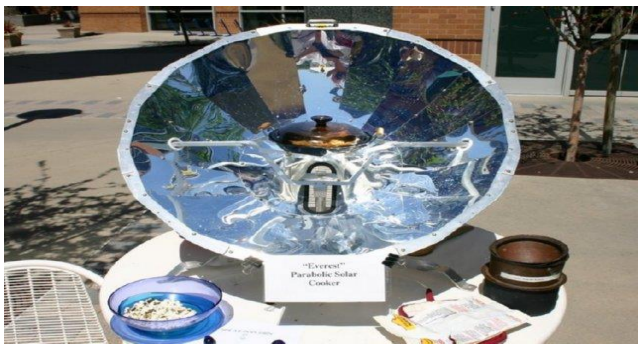

Fig.2.4 Parabolic solar cooker

3. Parabolic trough design

The most obvious features of the parabolic trough solar collector is the parabolic-shaped mirrors or reflectors. It is made of Stainless steel sheet with dimensions (160 cm × 125 cm × 0.07 cm).The stainless steel is curved in the shape of a parabola, which allows it to concentrate the sun's direct beam radiation on the linear absorber as showed in figure (5) along with the support structure that hold the reflector in place. Then there is 58 mm by 180 cm selectively coated, triple cavity vacuum tube holds only 2.5 liters of high heat thermal oil that is used as heat exchanger fluid inside the vacuum tube as in figure (6).

Fig.3.1 real view of PSC

Fig.3.2 vacuum tube

3.1 Absorptivity and emissivity of metal and deposited coating on metals

Table 3.1 (Absorptivity and emissivity of metal)

MATERIAL	Solar Normal Total Absorptivity α_n, solar	Total Hemispherical	Emissivity at Moderate Temperature ε $\left(\frac{\alpha_{n,solar}}{\varepsilon}\right)$
Stainless steel, 301	0.37	0.05 *	7.4

3.2 Design steps

3.2.1 Assumptions

- collector length "l"=160cm
- collector width "l_a" =125 cm
- collector depth “y”= 40 cm
- Irradiance"I"= 950 W/m^2
- $T_{amb=}$ 25 ^{o}C
- T_{abs} =175 ^{o}C

3.2.2 Givens “From tube catalogue”

I. Absorptivity “absorber” = 0.92
II. Emissivity “absorber”=0.08

3.2.3. Equations [5]

1. $y = \frac{1}{4f}x^2$

2. $A_C = \left(\frac{l_a}{2} * \sqrt{1 + \frac{{l_a}^2}{16f^2}} + 2f * \ln\left(\frac{l_a}{4f} + \sqrt{1 + \frac{{l_a}^2}{16f^2}}\right)\right) * l$

3. $A_{ap_c} = l_a * l$

4. $A_{ap_{ab}} = d_o * l$

5. C= $\frac{l_a l}{d_o l} = \frac{l_a}{d_o}$

6. $\tan(\psi) = \frac{\frac{l_a}{f}}{2-\frac{1}{8}(\frac{l_a}{f})^2}$

7. $\frac{l_a}{f} = \frac{4}{tan\Psi} + \sqrt{\frac{16}{tan^2\Psi} + 16}$

8. $Q_{gain} = A_{ap_{ab}}(\alpha CI - \sigma\varepsilon(T_{abs}^4 - T_{amb}^4)) = \frac{m_{oil}C_{p_{oil}}(T_{abs}-T_{amb})}{t}$

9. $\eta_{ab} = \frac{Q_{gain}/A_{ap_{ab}}}{C*I}$

10. $\eta = \frac{Q_{gain}}{A_c*I}$

3.2.4 Calculations

3.2.4.a Focal *point*

From equation "i." we get the focal point (1):

$y = \frac{1}{4f}x^2 \Rightarrow f = \frac{1}{4*(40)} * (62.5^2) = 24.41\ cm$

3.2.4.b Aperture area Surface area

Surface area: The total area of the parabolic trough's faces and curved surfaces.

From equation (2) we get the surface area:

$A = \left(\frac{125}{2} * \sqrt{1 + \frac{125^2}{16*24.41^2}} + 2 * 24.41 * \ln\left(\frac{125}{4*24.41} + \sqrt{1 + \frac{125^2}{24.41^2}}\right)\right) * 160 = 3.0863\ m^2$

Aperature area : the effective area, and the porjection of the surface area.
From equation (3) we get the aperture area:
$2\ A_{ap} = l_a * l = 125 * 160 * 10^{-4} =\ m^2$

3.2.4.c Absorber aperture area [5]

From equation number (4) we get the absorber aperture area:

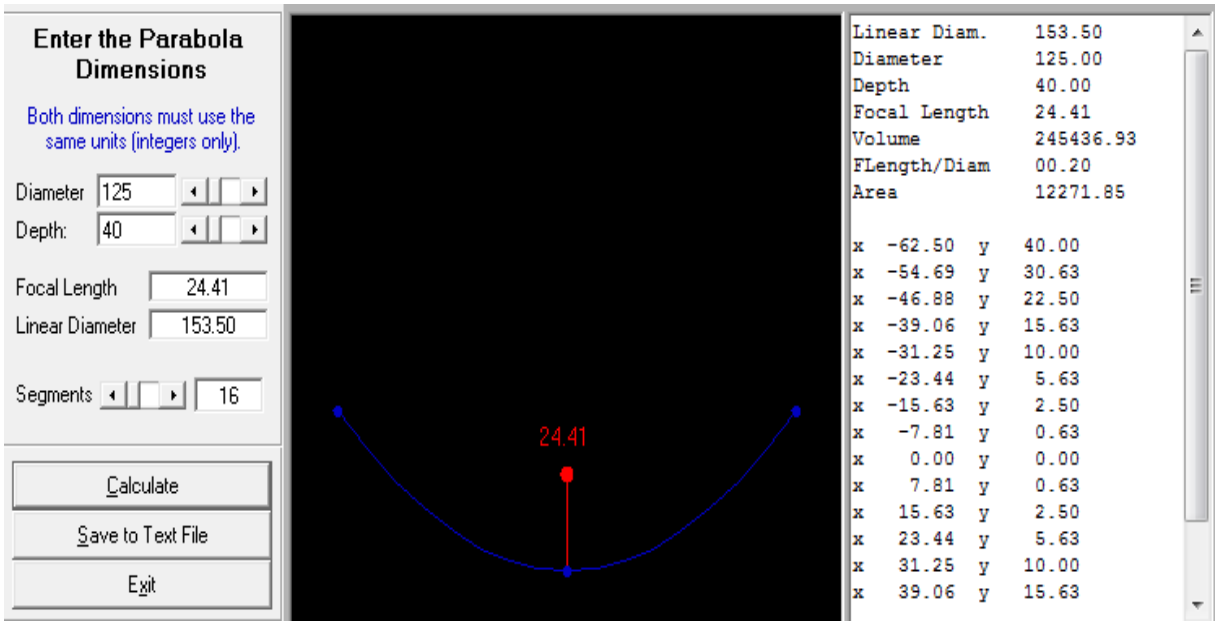

$A_{ap_{ab}} = d_o l = 0.047 * 1.8 = 0.0846\ m^2$

3.2.4.d Concentration ratio [5]

From equation number (5) we get the concentration ratio:

$$C = \frac{l_a l}{d_o l} = \frac{1.6 * 1.25}{1.8 * 0.047} = 23.6$$

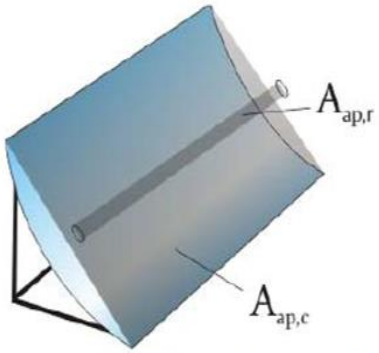

Collector aperture area and receiver aperture area

3.2.4.e Rim angle [5]

From equation number (6) we get the rim angle:

$$\tan(\psi) = \frac{\frac{l_a}{f}}{2 - \frac{1}{8}(\frac{l_a}{f})^2}$$

$$\tan(\psi) = \frac{\frac{125}{24.41}}{2 - \frac{1}{8} * (\frac{125}{24.41})^2} = -4.0073, \qquad (\psi) = -76^\circ = 104^\circ$$

3.2.4.f Inclination angle [5]

It should be noted that the collector was tilted by an angle of inclination to the horizon of 30° to eliminate the shading effect factor caused by the latitude of the site from the equator line, so that the system could have the maximum possible efficiency.

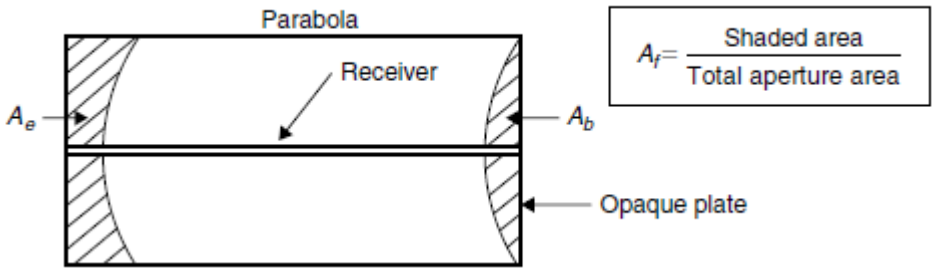

Fig 3.2.4 The shading effect in case 0° tilting angle

3.2.4.g Useful outlet energy

From equation number (8) we get the useful outlet energy:

$$\frac{Q_{gain}}{A_{ap_{ab}}} = \left(\alpha C I - \sigma \varepsilon (T_{abs}^4 - T_{amb}^4)\right) = \left(0.92 * 23.6 * 950 - 0.08 * 5.6704 * 10^{-8} * (175^4 - 25^4)\right)$$

$$= 20622.1472 W/m^2$$

$$Q_{gain} = 0.0846 * 20622.1472 = 1744.634\ watt$$

3.2.4.h Absorber efficiency

From equation number (9) we get the absorber efficiency:

$$\eta_{ab} = \frac{\frac{Q_{gain}}{A_{ab}}}{C * I} = \frac{20622.1472}{23.6 * 950} = 0.919 = 91.9\%$$

3.2.4.i Required time

From equation number (8) we get the time (t) required to heat the thermal oil, m_{oil}=10 liter:

$$\boldsymbol{Q_{gain}} = \frac{\boldsymbol{m_{oil} * C_{Poil} * \Delta T}}{\boldsymbol{t}} \rightarrow \boldsymbol{t} = \frac{\boldsymbol{m_{oil} * C_{p_{oil}} * \Delta T}}{\boldsymbol{Q_{gain}}},$$

Oil properties:

At T=150 °C=423K

From saturated liquids table A.1, Appendix [A]

$$C_{p_{oil}}=2440.2 \text{ J/Kg.k}$$

$$t = \frac{10 * 2440.2 * (150)}{1744.634} = \frac{2098.033}{3600} = 0.583hr = 34.97\ min$$

Then, if the time is 2 hours the output temperature will be:

$$\Delta T = \frac{t * Q_{gain}}{m_{oil} * C_{p_{oil}}} = \frac{2 * 3600 * 1744.634}{10 * 2440.2} = 517.768℃$$

3.2.5 Comparison between different models:

In the follwing table I will describe 3 models where the trough lengh and depth are constant but the trough aperture length will be different thus changing all other parameters as well to choose the best model that have the highest concentration ratio andusefull output energy and the least time to reach 250 ℃.

Table 3.2.5 (models with different Trough aperture width for each case)

Content	***Symbol***	***Case 1***	***Case 2***	***Case 3***
Trough length	l	170 cm	170 cm	170 cm
Trough aperture width	l_a	60 cm	80 cm	125 cm
Trough depth	y	40 cm	40 cm	40 cm
Focal length	f	5.62 cm	10 cm	24.41 cm
Collector surface area	A	1.78 m^2	2.31 m^2	3.0863 m^2
Collector aperture area	A_{ap}	1.02 m^2	1.36 m^2	2 m^2
Absorber aperture area	A_{ab}	0.0799 m^2	0.0799 m^2	0.0846 m^2
Concentration ratio	C	12.76	17.02	23.6
Rim angle	ψ	139˚	126.87˚	104˚
Useful output energy	Q_{gain}	890.7 Watt	1188.2 W	1744.634 W
Absorber efficiency	η_{ab}	91.9 %	91.9 %	91.9 %
Time	t	1.14 hr	0.856 hr	0.583 hr

3.2.6 Relation between time and temperature difference

Table 3.2.6 (results for time (min.)for each case)

ΔT	t "case 1"	t "case 2"	t "case 3"
50Ċ	22.8	17.1	11.66
100Ċ	45.7	34.2	23.31
150Ċ	68.6	51.4	34.97
200Ċ	91.4	68.5	46.62
250Ċ	114.3	85.59	58.29

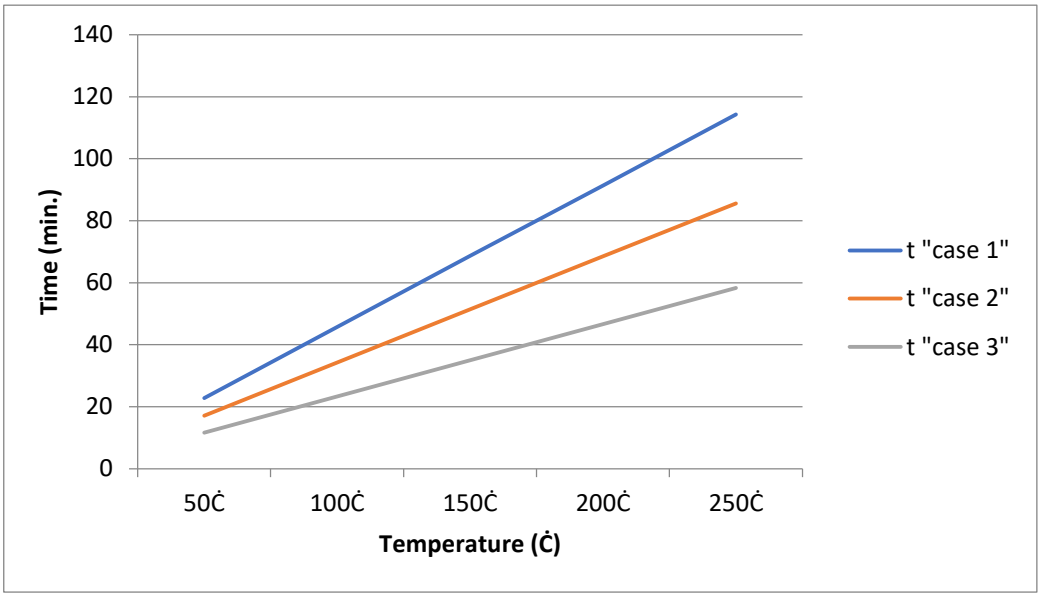

Fig 3.2.6 Time Vs. Temperature

4. Testing the solar cooker

Parameters: 5 liter of Thermal oil, 3 liter was heated in each unit with constant monitoring of the temperatures of oil and water as shown in the figure where oil is given yellow color. Time was noted each 15 min. through thermocouples for both fluids.

Location:
On the rooftop of the old building in Ain Shams University, Cairo, Egypt .it receives an annual average of 950 w/m^2. The roof was in good position of receiving the sun light rays.

Setting:
The cooker was set up facing the sun and was adjusted manually, a few times per hour to optimize that it facing the sun. Testing started in the duration of the sun peak angle to get best results. The following tables show results with the parabola fully proposed to the sun and the one beneath when half the parabola is half shaded to simulate the different weather conditions.

Time frame:

Table 4.1Testing (data collection): 25, 26/June 11:00 to 13:30 with ambient temperature 35 ˚C, 36 C° respectively.

Time (min)	To	Tw
0	50	25
15	58	36
30	68	48
45	75	60
60	86	70
75	95	79
90	106	87
105	120	95
120	129	105
135	130	115
150	129	110

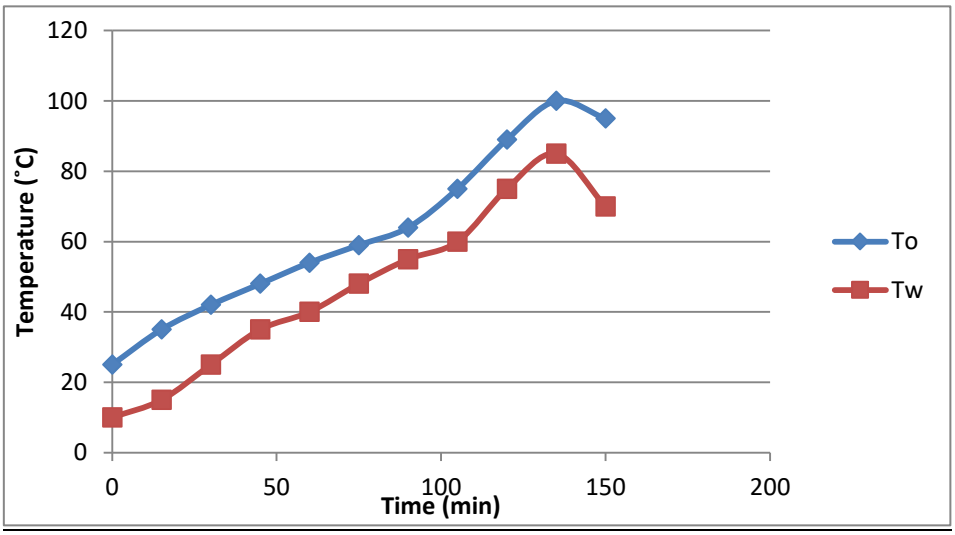

Fig 4.1 Time Vs. Temperature Testing

Table 4.2 When parabola is half shaded

Time (min)	To	Tw
0	25	10
15	35	15
30	42	25
45	48	35
60	54	40
75	59	48
90	64	55
105	75	60
120	89	75
135	100	85
150	95	70

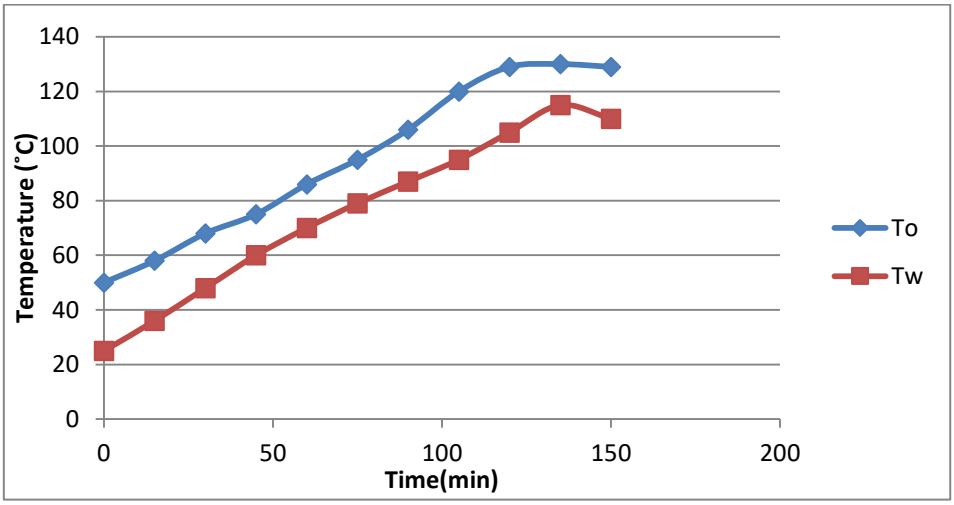

Fig 4.2 Time Vs. Temperature (Half Parabola)

Summary and comments of the tests

Graphic results show more consistent cooking temperatures maintained by the parabolic trough solar cooker Appliance. The unit was less prone to solar variations and achieved more100˚C.

The time taken for the water to reach boiling temperature is almost 2 hours which is relatively high compared with conventional cooking fuels.

The water used in the test was tap water therefore water temperature reach higher values than 100 C° due to the impurities and salts in water.

5. Conclusions

After these results from testing our model in real case scenario we could recognize how efficient it is comparing to any other model used in solar cooking and follow some cons are mentioned :

5.1 benefits of this model

1. Simplicity and low cost. Parabolic trough solar collectors are the only known model for home cooking that gives high Performance without any special tools. Not only the production cost drops to far below the other manufacturing methods of parabolic troughs, but also it makes the solar energy collecting cost substantially lower than any fossil fuel. The economic and social benefits of the method is huge.

2. The biggest advantage of solar cookers is their eco-friendliness. By using a solar cooker, you can be nondependent on gas or electricity for cooking. You can maintain better air quality and reduce the amount of carbon monoxide emissions. You can also enjoy cooler temperatures indoors and conserve more fuel which reduces your energy costs.

3. Solar cooking is free to use once you have bought the cooker itself. For the purpose of operation, all you need is sunlight. You can save a significant amount of money over the long term. As a result, solar cookers are being used increasingly in different parts of the world, especially in poorer communities with limited access to fuel and power.

4. The quality of food cooked in a solar cooker is also notable. There is no danger of burning food and flavors remain intact. Solar cookers can be used for grilling, roasting and baking food. Baked foods also retain moisture and softness if the solar cooker is used properly. Solar cookers are easily accessible to people around the globe. It is very easy to build one from scratch as well.

5.2. Drawbacks of the applied project

1. Cooking with solar cookers requires strong sunlight. This makes the process difficult during winter months and on rainy days. Cooking also takes a significantly longer time as compared to conventional methods. Users must schedule their cooking time and maximize the use of sunlight.

2. Solar cookers are not as efficient at retaining heat as compared to conventional cooking devices. Factors such as wind, rain and snow can seriously hinder the operation of a solar cooker. In such weather conditions, even after the food is cooked, it will lose its warmth very quickly. For most homes, a solar cooker by itself is not a reliable means of cooking. You will need a backup cooking appliance that operates on gas or electricity. It will come handy when the weather is unfavorable and when the sun is hidden.

3. Although solar cookers are easy to build and use, there is a risk of accidental injury or burns if the appliance is not used properly. Eyesight can also be damaged if the concentrated beams of sunlight are reflected back into the eyes from the solar cooker. The use of safety precautions and protective materials is necessary. Unlike parabolic cooker since the cooking area is separate from the heating unit therefore there is no need for the use of sunglasses or possible burns from the reflectors.

Acknowledgment

For acknowledgement, this design was built by me and my team and research activities where held at Ain shames university/renewable energy department faculty of electrical engineering.

References

[1] http://www.powerfromthesun.net/

[2] Gang Xiao. A closed parabolic trough solar collector. 2007. ffhal-00177601v2f

[3] Henry Price et al, Field Survey of Parabolic Trough Receiver Thermal Performance, Proceedings of ISEC2006, July 2006. http://www.nrel.gov/csp/troughnet/pdfs/39459.pdf

[4] David P. Dewitt and Adrienne Levine (2005). “Fundamentals Of heat and mass transfer “; March2, 2, 1934-May 17, 2005.

[5] Harley, E. I., and W. B. Stine (1984), “Solar Industrial Process Heat (IPH) Project Technical Report; October 1982-Septemher 1983” Sandia National Laboratories Report SAND84-1812, March.

[6] Bradford, Travis (2006). *Solar Revolution: The Economic Transformation of the Global Energy Industry*. MIT Press. ISBN 026202604X

[7] Tritt, T.; Böttner, H.; Chen, L. (2008). "Thermoelectrics: Direct Solar Thermal Energy Conversion". MRS Bulletin 33 (4): 355–372.

APPENDIX

Table (6): Properties of Saturated Liquids

T (K)	ρ (kg/m³)	c_p (kJ/kg · K)	$\mu \cdot 10^3$ (N · s/m²)	$\nu \cdot 10^6$ (m²/s)	$k \cdot 10^3$ (W/m · K)	$\alpha \cdot 10^7$ (m²/s)	Pr	$\beta \cdot 10^3$ (K⁻¹)
Engine Oil (Unused)								
273	899.1	1.796	385	4280	147	0.910	47,000	0.70
280	895.3	1.827	217	2430	144	0.880	27,500	0.70
290	890.0	1.868	99.9	1120	145	0.872	12,900	0.70
300	884.1	1.909	48.6	550	145	0.859	6400	0.70
310	877.9	1.951	25.3	288	145	0.847	3400	0.70
320	871.8	1.993	14.1	161	143	0.823	1965	0.70
330	865.8	2.035	8.36	96.6	141	0.800	1205	0.70
340	859.9	2.076	5.31	61.7	139	0.779	793	0.70
350	853.9	2.118	3.56	41.7	138	0.763	546	0.70
360	847.8	2.161	2.52	29.7	138	0.753	395	0.70
370	841.8	2.206	1.86	22.0	137	0.738	300	0.70
380	836.0	2.250	1.41	16.9	136	0.723	233	0.70
390	830.6	2.294	1.10	13.3	135	0.709	187	0.70
400	825.1	2.337	0.874	10.6	134	0.695	152	0.70
410	818.9	2.381	0.698	8.52	133	0.682	125	0.70
420	812.1	2.427	0.564	6.94	133	0.675	103	0.70
430	806.5	2.471	0.470	5.83	132	0.662	88	0.70

NOMENCLATURES

A_C	Collector surface area (m^2)
A_{ap_C}	Collector aperture area (m^2)
$A_{ap_{ab}}$	Absorber aperture area (m^2)
T_{abs}	Absorber temperature (k)
T_{amb}	Ambient temperature (k)
y	depth of parabola (m)
l	Trough length (m)
b	Absorber tube length (m)
l_a	Trough aperture width (m)
f	Focal length (m)
C	Concentration ratio
c_p	Collector fluid specific heat capacity (J/kg-K)
ψ	Rim angle
Q_{gain}	Useful output energy (watt)
m	Mass flow rate (kg/s)
d_o	Absorber tube outer diameter (m)
η_{ab}	Absorber efficiency
η	Solar cooker efficiency
t	time (sec.)
I	Irradiance (W/m^2)
α	Absorber absorptivity
ε	Absorber emissivity
σ	Stefan Boltzmann constant

Implementation of deposit system in Poland

Aleksandra Bratek[1]

[1]*Silesian University of Technology, e-mail: aml.bratek@gmail.com*

Abstract

The amount of wastes is increasing each year and the reason for that is the increased consumption on products. It is connected to an increase in raw material use for packaging which in turn affects badly on the environment. In order to increase the use of already existing packaging the deposit system can be implemented. Within this system the packages, mostly beverage bottles, can be either reused or recycled. The customer pays for the product with the deposit and is given the deposit money back while returning the empty bottle to the collection center. Due to the upcoming regulations voted by EU Poland, as a group member, should consider introducing a deposit system in order to be able to meet the obligations such as e.g. recycling level. Such system is already implemented in 17 countries and some of their best practices are also recommend for Poland.

Keywords: deposit system, reuse, recycle, circular economy

1. Introduction

The deposit-return system aim is to motivate to recycle. Each container is charged with a fee. In deposit system an empty beverage container is returned to a collection point or a unit of trading and the deposit money is given back to the customer. This system is also considered a key point of circular economy. The returned containers can be either reused or recycled. These days, the deposit system is implemented in 17 countries. But twice as many different systems can be found in the world. In order to make those systems work properly, a range of managing methods is implemented. However in most of those systems the beverage containers have barcodes, which enables their tracking and documentation, as well as provides an information on what exactly is returned. [1]

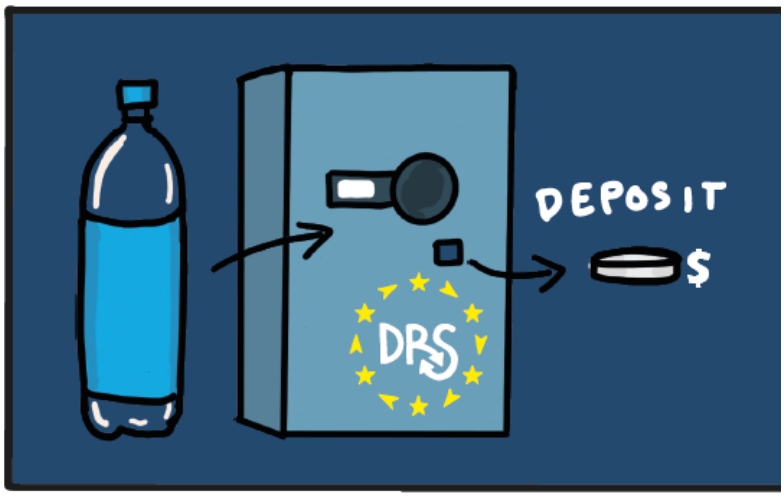

Fig. 1. Deposit Return System (DRS) [2]

Within this article the study on implementation of deposit system has been made. The best practices from other countries have been analyzed and some of them were chosen as good ideas for Poland. The study of need of introducing a deposit system was conducted. Also the “no implementation” scenario and its consequences were studied.

2. Why implementing a deposit system?

These days more and more wastes are produced all over the world. It became a huge problem for some cities or even countries. Often the community generates everyday such amounts of garbage that the services cannot keep up with cleaning them off the streets and dealing with them later. The lifestyle of polish people also changed over the last one even two decades. People generally became wealthier and as the result of they purchase more stuff. This action generates the increase in wastes amounts.

Due to that, the cost for waste management is increasing in each year. The institutions for waste management are forced to follow the law due to constantly changing regulations. The main task for those institutions are to maximize the level of recycling of wastes as well as minimize of the emissions to the environment and minimize the amount of wastes not suitable for recycling. In order to fulfill this task some changes must be made again due to the upcoming restrictions. [3]

2.1. European Union Law

EU countries must meet certain limits and goals for packaging on the market. The limitations put by EU are; reduction of content of hazardous materials and substances, limitation the weight and volume of packaging to the minimum, and design reusable or recoverable packaging. [4] The producer responsibility scheme should also be implemented for all types of packaging. With this scheme the packaging producer has to ensure the channeling and the most appropriate waste management option for the return and/or collection of used packaging and/or packaging waste, as well as for reuse or recycling of the collected packaging and packaging waste.

There are two main directives that EU countries needs to consider and apply in the near future. First of them is Directive (EU) 2019/904 which was voted in 2019 by EU. This directive will have to be a law in EU countries by 3 July 2021. The Extended Producer Responsibility (EPR) will have to be applied from 31 December 2024. Within this document banning of single use plastic by 2021 is described. It also contains a regulations concerning plastic bottles. The EU wants 90% of plastics bottles to be collected in order to be recycled by 2029. Meanwhile the goal is 77% in 2025. Also by 2025 at least 25% of PET bottles should be made from recycled plastic. By 2030 all of the bottles should be made from 30% of recycled material. The other principle described in this directive is so called “polluter pays”. That means that the producers will have to pay for waste management, clean-up, data gathering and awareness raising.

The second Directive (EU) 2018/852 is on packaging and packaging waste. The concept proposed in this document is to reduce the production of packaging waste and to promote the recovery system such as reusing, recycling, and others.[5] This directive encourages EU countries to increase the weight of recycled packaging by 2025 and the amount of reusable packaging. For several materials the recycling levels (by weight) are already defined: 50% for plastic, 70% for ferrous metal, 50% for aluminum, 70% for glass and 75% for paper and cardboard. [5] Therefore a diverse solutions can be applied, such as: setting specific goals, economic incentives, the minimum content of reusable packaging on the market and deposit-return systems.

Table. 1. Brief summaries of responsibilities [4][5]

Government responsibility	Producer responsibility
By 2029 collection of 90% of plastic bottles	By 2025 25% of bottles made from recycled material
Single use plastics banned by 3 July 2021	EPR
Extended producer responsibility implementation for all packaging	Reducing the content of hazardous substances and materials
Increase the weight of recycled packaging	Limit the weight and volume of packaging to minimum
Increase amount of reusable packaging	Design reusable or recoverable packaging

2.2. Polish regulations

Poland, as a member of the European Union, is obligated to restrict any changes introduced by the them. As mention in the paragraph above there are new rules that must be completed before a particular date. In those upcoming regulations the most considered is Extended Producer Responsibility (EPR).

According to this the recycling level of the packaging in Poland should be 65% by 2025 and 70% by 2030, while data on 2019 provides the level of 55%. [6] The minimal amount of recycled material in new PET (polyethylene terephthalate) bottles must be 25% by 2025. However, by 2030 this amount must be at least 30% in all plastic beverage bottles. Furthermore, by 2024 the manufacturers will be obligated to provide the permanent attachment of the caps to the plastic bottles and to cover the costs of cleaning public area from plastic bottles of beverages. In order to be able to fulfill those obligations there can be a deposit system implemented or it can be a voluntary agreement between beverage producers and public authorities or recovery organizations.

In accordance to that directives, the producer responsibility of the product will be extended to the product end-life. Producer/ manufacturer of packaging will be responsible for the selective collection, transport, and processing their packaging. Also the financial contribution must be provided. It should be done in order to support end-life actions decreased by the incomes from the recycle, sale of the secondary raw materials from its products and not received deposit. [6] [10]

To fulfill the obligations, there are three possible ways: recovery organizations, deposit system or establishment of a voluntary agreement between beverage producers and public authorities. If the packaging is not reusable and not recyclable the according to the government, the EPR system should impose sanctions. In general, the EPR would eliminate the problem of overproduction of the packaging. A higher price would discourage consumers from buying them and manufacturers would encourage them to seek alternative materials and eco-design. In their view, reusable packaging should be standardized and, on this basis, exempt from part of the cost to the EPR.

3. Polish government proposal

3.1. EPR system

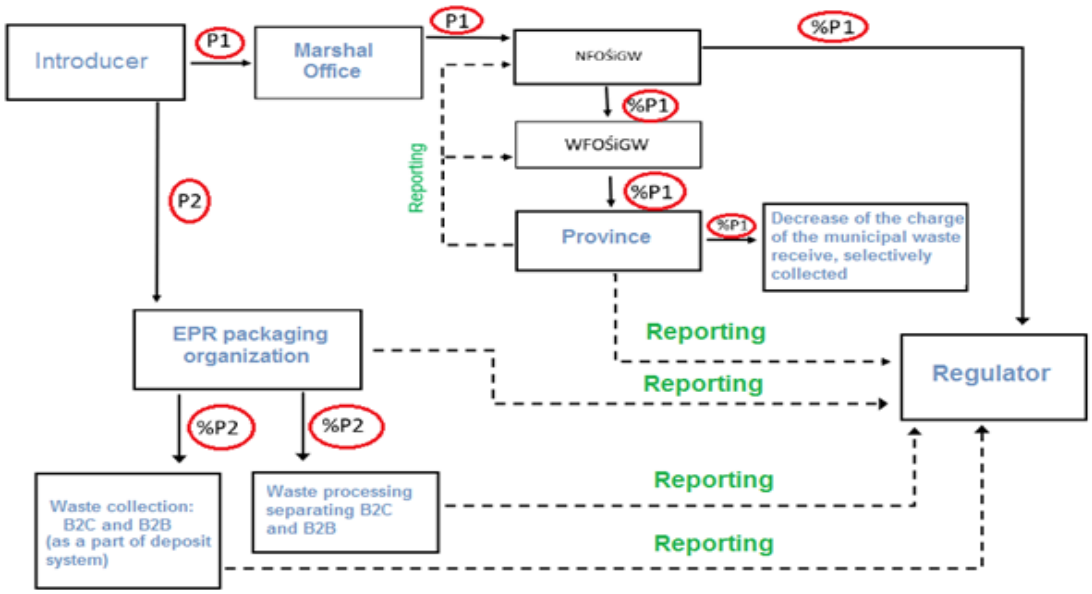

Fig. 2. EPR scheme proposed by Minister of Climate

The packaging introducer will be obliged to pay P1 and P2 charges depending on the type of packaging. P1 will be only for household purposes, while P2 charge will be for all packaging introducers. So P1 will cover plastic

and glass bottles together with caps and labeling and also aluminum cans. Money from P1 will go to the local governments and from P2 to the EPR organization.

On the diagram above the flow of P1 and P2 is shown. P1 would depend on the type of packaging and its recyclability. The value of this charge will be established by the Minister of Climate and controlled by the rule "pay as you throw". It means that the charge will depend on the effectiveness of collection in particular provinces. P1 will be paid by introducer to the Marshal's Office from where it will be forwarded to the National Fund for Environmental Protection and Water Management (NFOŚiGW). Then the reports on the waste management in the municipality and collection effectiveness will be done. Based on them, the P1 charge will be divided between Voivodeship Fund for Environmental Protection and Water Management (WFOŚiGW) and the Regulator (Minister of Climate) in proportions 95% to 5%.

P2 charge will be not lower the minimal rate established by the Regulator. The recyclability and the use of recycled materials in packaging should be considered while deciding. It will be devoted for EPR organization to realize the law obligations such as collection, transportation, recycling but also environmental education and financing a deposit system.

3.2. Deposit system

The deposit system proposed by Minister of Climate is shown on the diagram below. It shows the flow of deposit money and packaging on particular stages of the product's life. The producer introduces the product in packaging on the market after receiving the empty (used) packaging from a Collection Centre. The product then goes to the Unit of Trading. The customer when buying the product in packaging with the deposit, should return the empty package to the Unit of Trading or some Collection Center, and from there the empty bottle goes to the producer who is again introducing the reuse packaging on the market. While the one-use packages goes to the recycler. Customer when returning an empty packaging to a Collection Center or Unit of Trading is given back the deposit. [7] The collection of packages will be realized within the funds from P2 charges and in order to achieve a certain level of recycling rate the producer will be working with the EPR organization responsible for managing the deposit system.

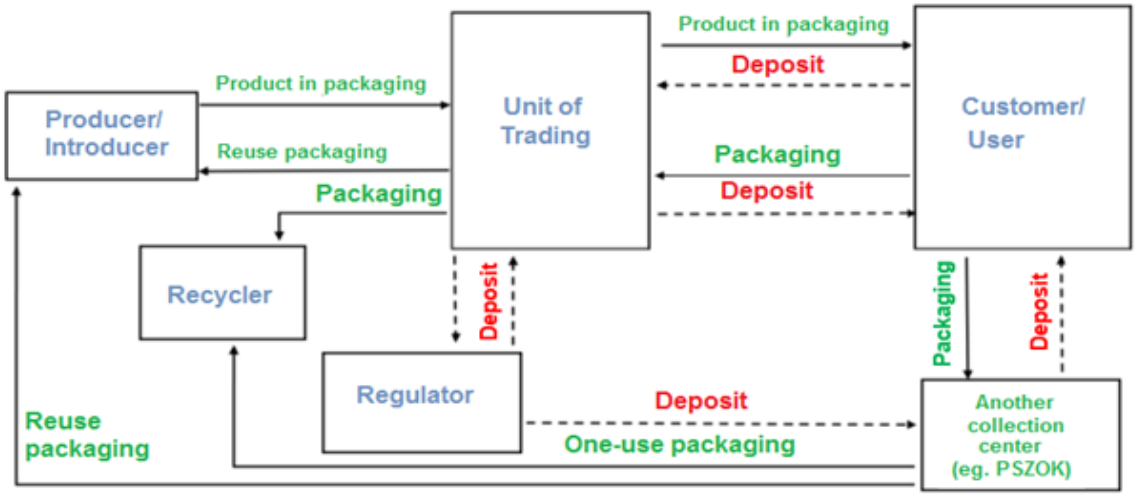

Fig. 3. Deposit system scheme proposed by Minister of Climate

4. Best practices

Poland is not the first planning to implement a deposit system. There is a lot of countries in Europe but also on the other side of the globe like United states, Canada or Australia that had already implemented such system. On the basis of their experience and knowledge the best practices will be described. Their examples might give as a hint which concept would be the best, where the mistakes were done and what ideas were some breakthroughs. In order

to describe those ideas, the concepts of big beverage producing companies were analyzed, as well as two practices from Europe – Germany and Finland.

4.1. Beverage producers

Knowing that the main part of packages in deposit system are beverage bottles it is worth to consider good examples from beverage producers. In the table below there are listed self-goals from 5 of the biggest drink producers in the world.

Table. 2. Producers goals

Producer	Year	Goal
Coca-Cola	2025	100% recyclable packaging and >50% of the plastic bottles made from recycled content [8]
Nestle	2025	100% recyclable or reusable packaging [9]
Danone	2025	Every piece of packaging reusable, recyclable or compostable [10]
Keurig Dr Pepper	2025	100% recyclable or compostable packaging and use of 30% post-consumer material [11]
Unilever	2025	100% of plastic packaging reusable, recyclable or compostable [12]

4.2. Germany

The deposit system for reusable bottles work for almost three decades now in Germany, since the beginning of 90s. However the system for disposable bottles was introduced in the beginning of XXI century (2003). The motivation to do that was a new German law regarding not only beverage packaging but all packaging on market. It also provided information about the recycling rate and packaging taxes, from which the beverage packaging included in deposit system is exempt. [13] The scheme was firstly introduced being a coupon system, but turned out it was uncomfortable solution for people to bring bottles back to the shop and they did not approve it. Then due to the further developments of the system but also the lack of specific requirements so called island-solution was born. It means that the supermarkets were only taking back their own packaging. After implementation more detailed requirements in 2006 the deposit system became the one that it is today. [14]

Joining the deposit system in Germany is mandatory for all producers and importers in Germany. All products introduced on the market are registered in database and marked with a code no matter if the producer sells it to wholesale or retail. The consumer buys a product with a deposit and is given it back when returning empty bottle or can. Small shops (<200 m²) are obliged to take back only the brands they sell while large shops must take back all types of bottles. Even if they only sell certain volume (0.3l) of plastic bottles they need to accept any other given them back. Each bottle generates a record in a database. When it is returned the producer of the packaging must pay the deposit to the store that collected it. The responsibility of the owner of the store is to introduce the packaging into the recycling system. [15]

Not every type of packages are included on German deposit system. Because of the disproportion between economic efforts to ecological benefits excluded are: wine, spirits, milk, and fruit and vegetables juices, cardboard packages and tubular bags.[13] Included to deposit system are mixed drinks containing water, soft drinks carbonated and non-carbonated, alcoholic beverages and beer, with volumes in between 0.1l - 3l.[15] Since there is a lot of exceptions it is difficult for the customer to understand it, remember and therefore use it. The deposit is fixed for all the disposable packaging and its amount is 0.25 €.

The system is constructed in such way that both producer and retailer benefit from it. Due to the fact that beverage producers do not have to pay taxes, according to Nabu Germany they save 225 million € per year. About 410 kilo-tonnes of PET are produced each year and the tax is 550€ per ton. Approximately 4 % of bottles are not returned

in Germany. This percents refers to 720 million bottles, so the overall saving from not paid deposit is 180 million €. As for the retailers, they benefit by selling the recycling material. The amount of the money they earn is approximately 68 million €. [16]

4.3. Finland

Another good example is Finland. Here, joining the deposit system is not obligatory as is Germany. The participation in deposit system is regulated by government through taxes. They set up tax for a packaging which is lower or cancelled for packaging which is included in deposit system.

The history of the system reaches 1990s when Finnish government introduced taxes and civil society set up the DRS (deposit return system) which step by step was including more packages. At first there was only a organization dealing with one-use cans, founded by retailer and beverage producers. Then in early 2000s a second organization for reusable packaging was set up. As the taxes were changing for one-use containers they got included in DRS. In 2012 also the one-way glass bottles were included in DRS and the Finnish deposit system reached todays form. [17]

The deposit system is run by non-profit organization PALPA owned half by half by retailers and by beverage industry. It is mandatory for both, producers and importers to pay a registration fee. An annual fee for their products is obligatory and depend on the type and volume of the products in the system. Since PALPA is non-profit organization the fees are set at rate to cover the cost of running the system (operating costs, administration, transport, sorting costs).[18][19]

The amount of the deposit for certain packaging depend on the material it is made of and its volume. Its level is set by the government. The unclaimed deposit is used by PALPA to cover the system operating costs. The deposit for glass bottle is 0.1 €, for metal can 0.15 €, and for plastic in range between 0.1 €-0.4 € depending on their volume. PET bottles are managed by another organization (Ekopullo).[17][19]

5. Suggestions for Poland

In order to be able to estimate polish deposit rate and need of connected with implementing a deposit system a simple analysis of prices was done. It was conducted by comparing living prices in capitals of Finland and Poland, since the prices in capitals are the highest in whole country.

Table. 3. Prices of living in Helsinki compared to Warsaw [20][21]

-------	2l plastic bottle (Coca-Cola)		0.5l aluminum can (beer)		1l glass bottle (red wine)	
Helsinki	2.75€		2.44€		15€	
Warsaw	1.24€	5.66zł	0.75€	3.42zł	6.56€	30zł

The ratio between those prices (Helsinki-Warsaw in euro) are: 2.22 for plastic bottle, 3.26 for aluminum can and 2.29 for glass bottle which gives the average value of ratio being equal to 2.59. On the basis on this information the forecast for the minimum deposit amount in Poland was made. The prices were recalculated from euro to polish złoty considering the current price of euro to be 1€=4.47zł.

Table. 4 Minimum deposit amount propose for Poland deposit system

Deposit amount	Finland	Poland
Plastic bottle	0.1-0.4 €	0.22-0.8 zł
Aluminum can	0.15 €	0.22 zł
Glass bottle	0.1 €	0.18 zł

As mentioned above the calculated amount of deposit is its minimal value. Especially for the first years it would be convenient for the beverage producers if the customers will pay more money for the deposit. The reason is that then the system would be funded by the customers, but it would also be good for boosting the return rate. If the deposit cost would be high people will return as much as possible and help Poland meet the limits set by EU. In other case, with low amount of deposit people would not be forcing themselves to return which would lead to Poland not meeting the EU targets on time. It might be difficult for the society to integrate with the system but it is a great role of the government to educate, instruct and teach citizens to be more responsible.

5.1. **No implementation scenario**

What if Poland will not implement the deposit system? The forecast for the taxes that will need to be paid if our county will not implement DRS is again estimated on the basis on Finland taxes. To that cost one can add also the fees from EU for not meeting the targets on time. In Finland the fee for each liter of product sold outside the deposit system is 0.51 €. Knowing that Poland population is 37.97 million (data for 2019) and that more or less 35l of juices, nectars and fruit-drink per capita is consumed in year [22] the following estimation has been made:

$$P * A = SA = 37{,}97mln * 35l = 1\ 328\ 950\ 000\ liters\ sold$$

Where,

P	Poland population number,(-),
A	amount of liters consumed per capita in year, (l),
SA	Sold amount of liter during the whole year, (l).

Tax for each liter is 0.51€ in Finland. After recalculating it with the ratio of 2.59 into polish zlotys it is 0.9zł. The overall tax for this amount of liters sold would be almost 1.2 billion zł. That means, not implementing a deposit system will cost beverage producers huge amounts of money.

5.2. **Recommended system**

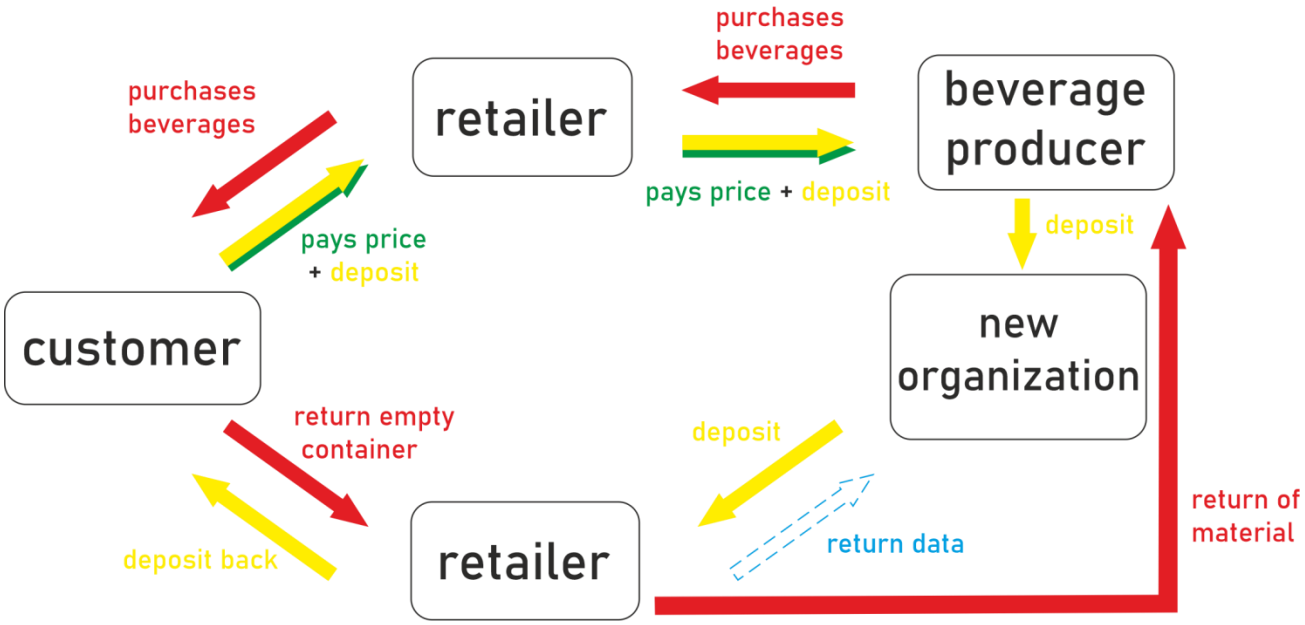

Fig. 4. Scheme of suggested deposit system

As for suggestions for polish deposit system, first of all there should be a non-profit organization created and managed by drink producers (all the stakeholders, with a different share based on the quantity sold). The system should be kept as simple as possible in order to avoid misunderstandings of roles and responsibilities inside. It

should be centralized, that means that the money should not go to government or anywhere else, but remain in the system. In the first years, the costs of installation and management of the system will be supported by the clients, that do not return bottles. It means, that no profit is allowed in the system, each coin from consumers not returning the packaging will fund the organization and system management. The targets and deposit fees will be regulated by EU laws. All the products must be tractable and documented, therefore there should be an identification codes on each packaging (it will also help clients to check what they can return). In big supermarkets there should be installed reverse vending machines.

6. Conclusion

Analyzing best practices from two countries that already use deposit system for more than 20 years, the government driven, two-tax system, that is proposed by Polish politics does not seem to be the best option. According to the experience of Finland, the non-profit organization leading the deposit system and managing it is a great idea. The system suggested within this work would be simple and clear and the loop would be closed. However the concern might be if the customers will accept such system, deposit cost and if they will be responsible enough to return the packaging. Regarding packages best would be if the producers will decide on their own what to recycle, because of the deep knowledge they have on their products. However, it would be good idea to introduce a barcoded packaging in order to be able to track it.

Acknowledgment

The study was performed on Silesian University of Technology in Institute of Waste and Waste Management (KTUiZO).

References

[1] CM Consulting Inc. (2016), Reloop Platform, Deposit systems for one-way beverage containers: Global overview (updated 24 May 2017), [online]. Available: https://www.reloopplatform.org/wp-content/ uploads/ 2017/05/BOOK-Deposit-Global-24May2017-for-Website.pdf (Access: 25/11/2020)

[2] Zero Waste Europe, https://zerowasteeurope.eu/2019/07/deposit-return-systems-an-effective-instrument-towards-a-zero-waste-future/(accesed:26/11/2020)

[3] Rada Ripok, Orli Staw (2020), Zakład Unieszkodliwiania Odpadów Komunalnych, ROP jako element finansowania i rozwoju gospodarki odpadami, [online], 29/10/ 2020.

[4] Eur lex (2019), Single-use plastics ban (Eur lex), [online]. Available : https://eur-lex.europa.eu/legal-content/EN/TXT/?uri=LEGISSUM:4393034 (visited on 20/11/2020)

[5] Eur lex (2018), Packaging and packaging waste (Eur lex), [online]. Available : https://eur-lex.europa.eu/legal-content/EN/TXT/?uri=LEGISSUM:l21207 (visited on 20/11/2020)

[6] Jakub Tyczkowski, Rekpol Organizacja Odzysku Opakowań S.A.(2019), Rozszerzona Odpowiedzialność Producenta, Konferencja: Racjonalizacja Gospodarki Odpadami Komunalnymi, Katowice 13 listopada 2019

[7] PARLAMENT EUROPEJSKI I RADA UNII EUROPEJSKIEJ (2008), Dyrektywa Parlamentu Europejskiego i Rady 2008/98/WE z dnia 19 listopada 2008r. w sprawie odpadów oraz uchylająca niektóre dyrektywy

[8] The Coca-Cola Company (2020), Coca-Cola sets ambitious new sustainable packaging goals for Western Europe, [online]. Available: https://www.coca-cola.eu/news/ambitious-new-sustainable-packaging-goals-western-europe/ (visited on 25/11/2020)

[9] Nestlé (2018), Nestlé aiming at 100% recyclable or reusable packaging by 2025, [online]. Available: https://www.nestle.com/media/pressreleases/allpressreleases/nestle-recyclable-reusable-packaging-by-2025 (visited on 25/11/2020)

[10] Danone HQ (N/A), Circular economy of packaging, Paris, [online]. Available: https://www.danone.com/impact/planet/packaging-positive-circular-economy.html(visited on 05/06/2020)

[11] Keurig Dr Pepper Inc.(2019), Corporate responsibility,[online].Available:https://www.keurigdrpepper.com/en/our-company/corporate-responsibility (visited on 25/11/2020)

[12] Unilever PLC (2017), Unilever commits to 100% recyclable plastic packaging by 2025, London, [online]. Available:https://www.unilever.com/news/press-releases/2017/Unilever-commits-to-100-percent-recyclable-plastic.html (visited on 27/11/2020)

[13] Bundesministerium für Umwelt, Naturschutz und nukleare Sicherheit (BMU) (2020), Mehrweg und Verpackungsgesetz, Berlin, [online]. Available: https://www.bmu.de/faqs/mehrweg-und-verpackungsgesetz/, (visited on 27/11/2020)

[14] Wikipedia Foundation Inc. (2020), Flaschenpfand, San Francisco, [online]. Available: https://de.wikipedia.org/wiki/Flaschenpfand, (visited on 27/11/2020)

[15] DPG Deutsche Pfandsystem GmbH (N/A), Die Pfandpflicht, Berlin, [online]. Available: https://dpg-pfandsystem.de/index.php/de/die-pfandpflicht-fuer-einweggetraenkeverpackungen.html, (visited on 18/04/2020

[16] NABU-Naturschutzbund Deutschland e.V. (N/A), Das Geschäft mit dem Einwegpfand, Berlin, [online]. Available:https://www.nabu.de/umwelt-und-ressourcen/ressourcenschonung/einzelhandel-und-umwelt/mehrweg/21967.html, (visited on 30/11/2020)

[17] Institute for European Environmental Policy, Eunomia, Ettlinger S. (author) (2016), Deposit Refund System (and Packaging Tax) in Finland, [online]. Available: https://ieep.eu/uploads/articles/attachments/9d526526-d22b-4350-a590-6ff71d058add/FI%20Deposit%20Refund%20Scheme%20final.pdf?v=63680923242, (visited on 30/11/2020)

[18] Suomen Palautuspakkaus Oy (2015), Deposit based system, Helsinki, [online]. Available: https://www.palpa.fi/beverage-container-recycling/deposit-refund-system/, (visited on 30/11/2020)

[19] LinkedIn Corporation, Institute for European Environmental Policy (publisher) (2017), Case study: Finnish deposit refund system (DRS), [online]. Available: https://www.slideshare.net/IEEP_eu/case-study-finnish-deposit-refund-system-drs, (visited on 30/11/2020)

[20] Expatistan.com (2020), Cost of living in Finland, [online]. Available: https://www.expatistan.com/cost-of-living/country/finland (visited 01/12/2020)

[21] Expatistan.com (2020), Cost of living in Warsaw, Poland, [online]. Available: https://www.expatistan.com/cost-of-living/warsaw (visited 01/12/2020)

[22] KPMG Sp. (2016), The soft drinks market in Poland, page 40/76" Juices, nectars, and fruit drinks" [online]. Available:https://assets.kpmg/content/dam/kpmg/pl/pdf/2016/09/pl-Rynek-napojow-bezalkoholowych-2016-ENG.pdf, (visited 03/12/2020)

Heat optimization and carbon dioxide utilization in ethylene glycol production: economic and environmental assessment

Mohamad Kasem [1], Abdulkarim Mira [2]

[1,2]Qatar University, e-mail: M.khaledkasem@gmail.com, Abdulkarim.Mira@hotmail.com

Abstract

The aim from the article is to study the change on ethylene glycol production plant in terms of two important aspects: heat optimization, carbon dioxide recycles and reactor injection. The raw materials for ethylene oxide plant are oxygen and ethylene, while the raw materials for the ethylene glycol plant are ethylene oxide and carbon dioxide. The simulation and calculation have been done using Aspen Plus software. Process- Heat optimization is significant and can effect the operating cost of the plant. Heat optimization has been applied to enhance the process by lowering the utility usage and energy consumption by maximizing the exchanged heat between hot and cold process streams after applying heat integration, to produce steam using the excess heat that is produced by the boilers. Furthermore, an environmental impact assessment was accomplished to observe all the change on the environment. The detailed study showed the calculated amount of emission has been reduced by 10.45% after recycling the exist carbon dioxide in the plant. The final step that was performed is the economic evaluation, the plant capital cost was calculated by using the step count method, the cost index, and the inflation rate, the three scenarios were compared to choose the best scenario.

Keywords: Glycol production, Carbon dioxide utilization, Heat optimization

1. Introduction

Ethylene glycol or mono-ethylene glycol (MEG) is a significant chemical compound that is used in different commercial and industrial sectors due to its chemical and physical properties that makes it a versatile intermediate where it is used in different ways such as, a raw material to obtain polyester fibers e.g. Dacron, and since it has low volatility and low corrosive activity it used to manufacture of antifreeze in cooling and heating systems. Di-ethylene glycol (DEG), tri-ethylene glycol (TEG), tetra-ethylene glycol (TETRA EG) are all derivatives of mono-ethylene glycol that are produce as co-products in the production of MEG. Ethylene glycol is a highly toxic compound that cause critical health problems such as central nervous system depression (CNS Depression).

Mono-ethylene glycol (MEG), is a clear, odorless, colorless with sweat taste and it is viscous liquid along with that it's completely miscible with polar solvents such as water and alcohol. It is a highly toxic compound. Ethylene glycol structure is difficult to crystallize when cooled as well as one of its main physical properties is that it lowers freezing point when added to water which make it widely used as anti-freeze.

Ethylene glycol acts like any other alcohol, because of its two-hydroxyl group it is known as dihydric alcohol that have aliphatic carbon chain. Ethylene glycol undergoes different reaction schemes where the OH group results in high water solubility and hygroscopicity and provide a reactive site. Ethylene glycol is used as intermediate in many reactions to produce certain products or other chemicals, these reactions can be taken as a laboratory scale or industrial scale depending on the production capacity needed and final product usage and its demand. Some of these reactions are listed below:

Ethylene glycol reacts with organic acids to produce mono-esters and di-esters.

$$(CH_2OH)_2 + RCOOH \longrightarrow RCOOCH_2\text{-}CH_2OH + H_2O \quad (1)$$

$$(CH_2OH)_2 + 2RCOOH \longrightarrow RCOOCH_2\text{-}CH_2OOCR + H_2O \quad (2)$$

Ethylene glycol reacts with polybasic acids or their derivatives to produce polyesters.

Ethylene glycol reacts with di-alkyl sulfate to form mono-alkyl ether.

Ethylene glycol reacts with ethylene oxide to produce higher glycols such as DEG and TEG, or ether glycols.

Gas phase oxidation of ethylene glycol in presence of air with nitric acid to produce glyoxal

$$(CH_2OH)_2 + O2 \longrightarrow (CHO)2 + H_2O \quad (3)$$

Dehydration of ethylene glycol with zinc chloride to gives acetaldehyde.

$$(CH_2OH)_2 + ZnCl_2 \longrightarrow CH_3CHO + H_2O \quad (4)$$

Ethylene glycol production was based on the hydrolysis of ethylene oxide that was produced by the chlorohydrin process. But that wasn't the only method that was being used to produce EG, from 1940 to 1963 Formaldehyde and carbon monoxide were also used in the commercial production of EG. These methods have been neglected to the emergence of new and advance technologies to produce EG in a much efficient and productive way, these new technologies have higher yield percentage for EG and can be produced in larger capacities. Nowadays, the production of ethylene glycol based on industrial scale comprises of two stages, where the first stage is the production of ethylene oxide by direct oxidation of ethylene with oxygen or air in presence of silver-based catalyst where the product of this plant is send to ethylene glycol plant. The feed of ethylene glycol plant is ethylene oxide with water or CO_2 , in case of water, hydrolysis of ethylene oxide with water, the mixture is send to reactor to converts the feed to EG under certain condition and reactor product is been moved to multi-evaporators where water is recovered and used later in the process, after evaporation section product is send to separation unit to have mono-ethylene glycol (MEG), di-ethylene glycol (DEG), and tri-ethylene glycol. In the other case aqueous ethylene oxide reacted with CO_2 to form ethylene carbonate, subsequently ethylene carbonate reacts with water to form MEG and CO_2 where it is recycled back to feed. The following overall Block Flow Diagram has been schemed using Visio Software that illustrates the initial scheme for the plant.

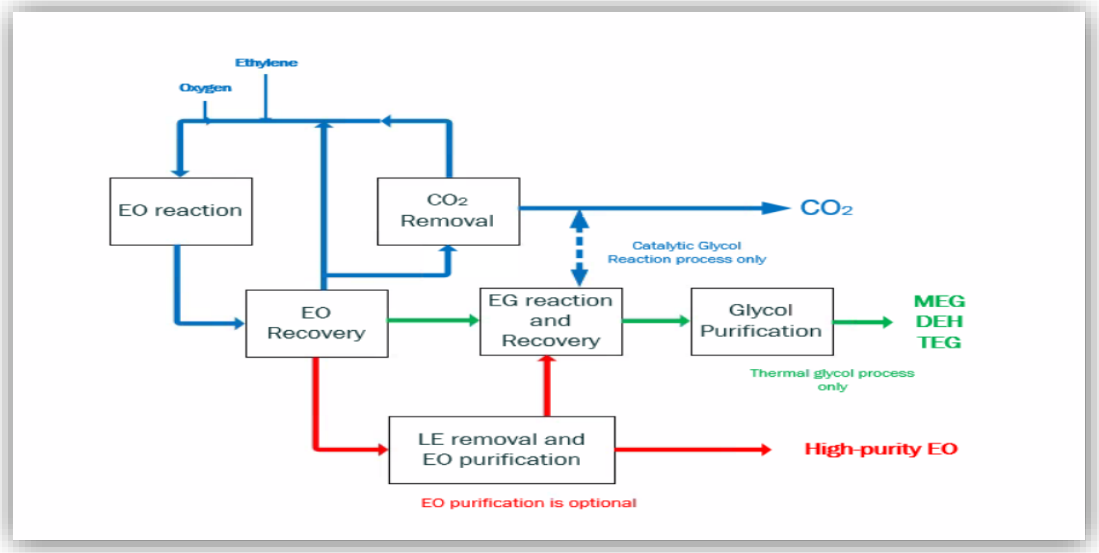

Fig. 1.1. Overall BFD for integrated ethylene oxide-ethylene glycol plant [4].

2. Ethylene glycol process description

The objective from this chapter is to clarify the simulated process in Aspen Plus by preforming the processing sections for each main equipment's were used by general explanation on process flow diagram.

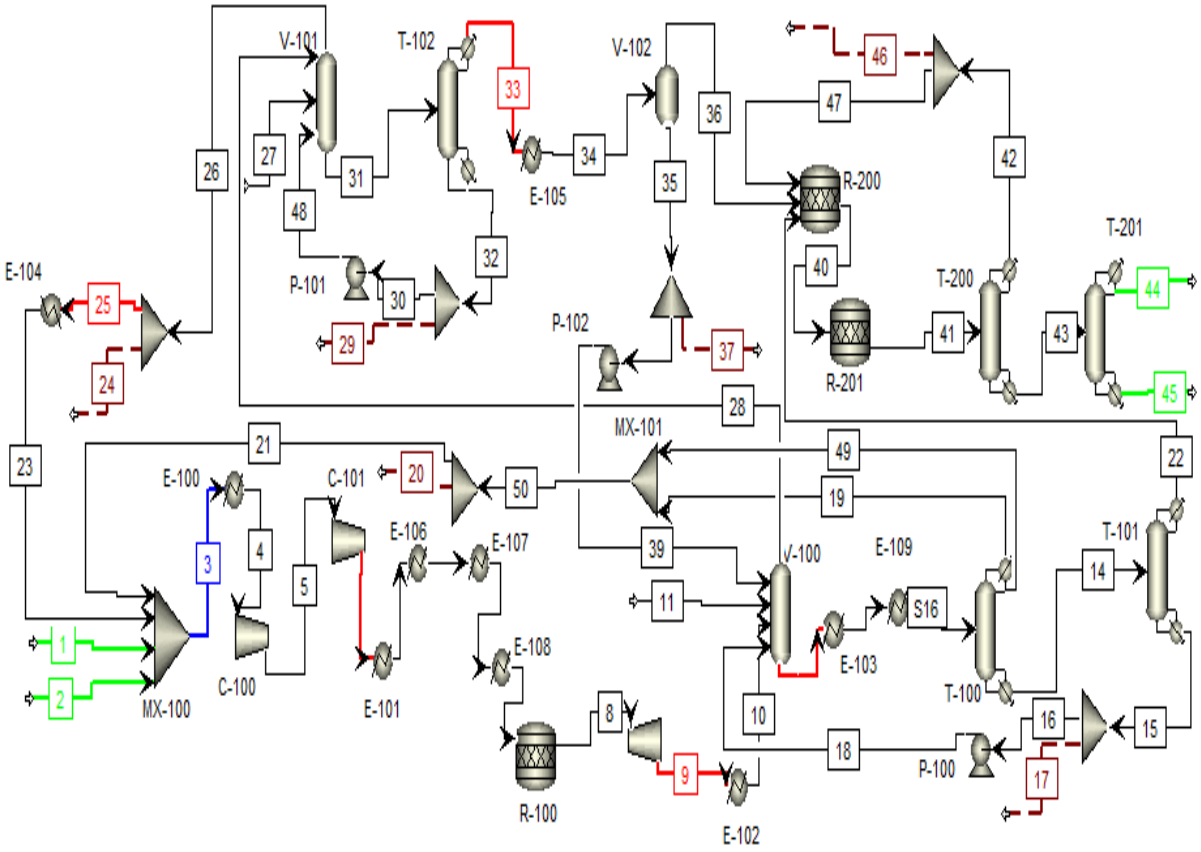

Fig. 2.1. Process flow diagram (PFD) using Aspen Plus [3].

As it can noticed in the above Process Flow Diagram, the raw materials of the ethylene oxide plant are ethylene {1} and oxygen {2} feeds to a mixer and compressor before it enters ethylene oxide reactor maker {R-100}. The mixture then is expanded and cooled before entering the ethylene oxide absorber {V-100} and mixed with water. The gas mixture that is coming up from the column is feed to a carbon dioxide absorber {V-101}, that is mix amine and water with the mixture to separate CO2 and Amine alone and feed it to another separator {T-102} that is finally separate all the CO2 alone from the top to feed it to the Ethylene glycol plant. While, the EO and water liquid that is coming down from {V-100} column is cooled before entering the EO-H2O separator to feed the EG plant reactor with water and the EG mixer with the remaining EO.

The raw materials for the ethylene glycol plant are ethylene oxide and carbon dioxide feeds from the ethylene oxide plant and enters the ethylene carbonate plug flow reactor {R-200}. The ethylene carbonate and water produced by the reactor feed to another reactor that produce ethylene glycol {R-201}. The produced EG feed to the ethylene glycol separator {T-200} to separate the water from the EG. The remaining water and CO2 is recycled back later to the Ethylene carbonate reactor using splitter to control the needed amount. The EG leaves from the bottom EG separator is feed to a distillation column {T-201} to distillate the diethylene glycol from the ethylene glycol and water remained.

R-100(Exothermic)

$$2\ Ethylene + O_2 \rightarrow 2\ Ethylene\ oxide \quad (5)$$

$$Ethylene + 3\ O_2 \rightarrow 2\ CO_2 + 2\ H_2O \quad (6)$$

R-200(Exothermic)

$$\boldsymbol{Ethylene\ oxide\ + CO_2\ \rightarrow Ethylene\ carbonate} \quad (7)$$

R-201(Endothermic)

$$\boldsymbol{Ethylene\ carbonate\ +\ H_2O \rightarrow CO_2 + MEG} \quad (8)$$

$$\boldsymbol{2\ Ethylene\ carbonate\ +\ H_2O \rightarrow 2CO_2 + DEG} \quad (9)$$

3. Case studies

a. Heat Optimization

Process integration can be divided into two main sections: heat integration and mass integration. The main objective of mass integration is to recover some of the mass that is leaving the system and reintegrate it back into the process, and by doing so the amount of waste that the process will be reduced as well as the amount of fresh feed that is needed, while the heat integration focuses on recovering the energy that is leaving the system and reusing it.

To conduct the heat integration, an optimum network of heat exchangers is needed as it connects the hot and cold process streams together and the needed hot and cold utilities. In addition, the trade-off between the capital cost and the energy cost must be considered. As the increase in the number of units used could decrease the need utilities but will increase the capital cost. Therefore, a balance must be found in order to achieve the optimal scenario. Therefore, and after the heat integration analysis and optimization on the process is done, it can be noticed that an overall increase in the process flexibility, reduction in the overall investment, an overall increase in the level of safety, and a reduction in the total amount of waste that is being produced by the plant and environmental footprint would be the result.

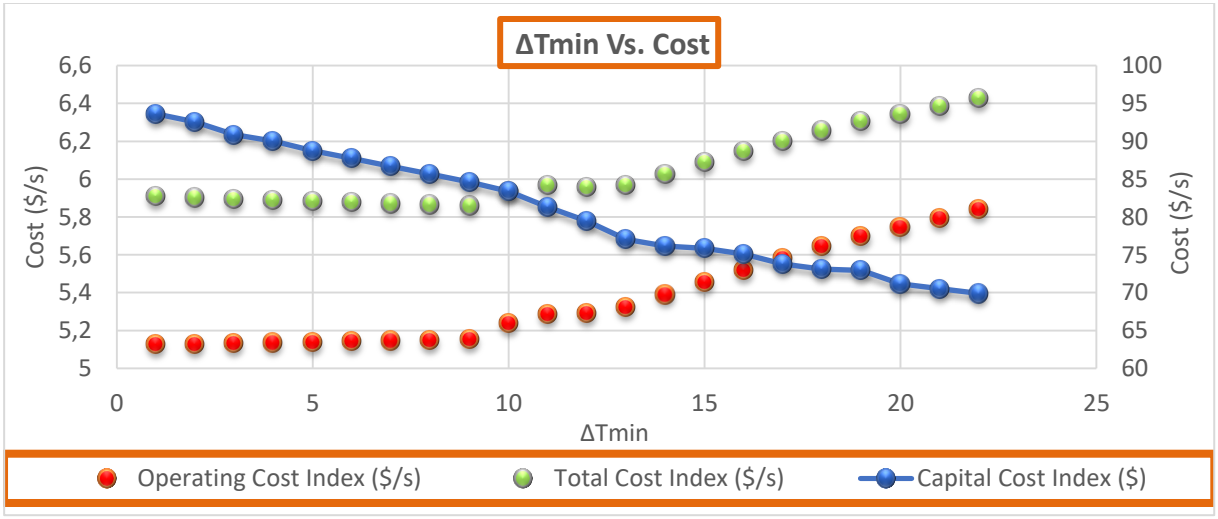

Fig. 3.1. ΔT_{min} vs. Cost

The above figure had been created using Microsoft Excel and illustrates how the operating cost index is increasing at a fixed optimum temperature 10 ºC while at the same time the capital cost index is decreasing at approximately 5,9 $/s, while the total cost is slightly increasing. The optimization outcome highly impacts the cost of utilities and number of heat exchangers used in the plant. These outcomes can significantly reduce the number of utilities needed within the plant where hot and cold streams are fully integrated to further reduce the utilities needed. The ΔT_{min} has carefully handled during the heat exchanger calculation where the temperatures of the inlet and outlet of heat exchanger between hot and cold streams should be above the ΔT_{min} not lower.

b. Carbon dioxide equivalent injection

To start with, ethylene oxide is a major chemical raw material that is used as manufacture derivative for ethylene glycol, surfactants, and ethanolamine's. In this case study an analysis of the ethylene oxide reactor (R-100) has been studied to describe the influence of increasing CO2 equivalent as a raw material to the production of ethylene oxide in an ethylene glycol production plant. This study has been initiated using Aspen plus. In the figure below is the plant section that was analyzed along with the reactor using Aspen Plus simulation software.

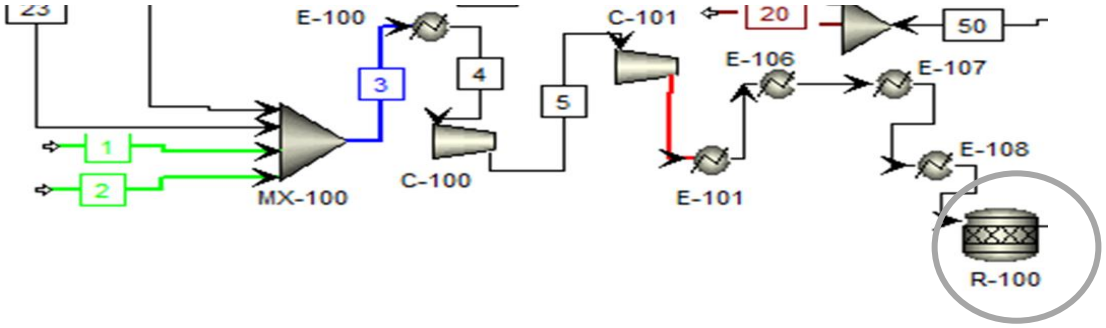

Fig. 3.2. Plant PFD (Selected Reactor) [3].

Epoxidation of ethylene:

$$\boldsymbol{Ethylene + CO_2 \rightarrow Ethylene\ oxide + CO} \qquad \text{(Equation 10)}$$

The results showed a polynomial trend where the produced EO has been increasing with CO2 equivalent tell reaching maximum production of EO, then production has been decreasing dramatically with the increase of carbon dioxide equivalent. The analysis is shown below by the following figure created using Microsoft excel.

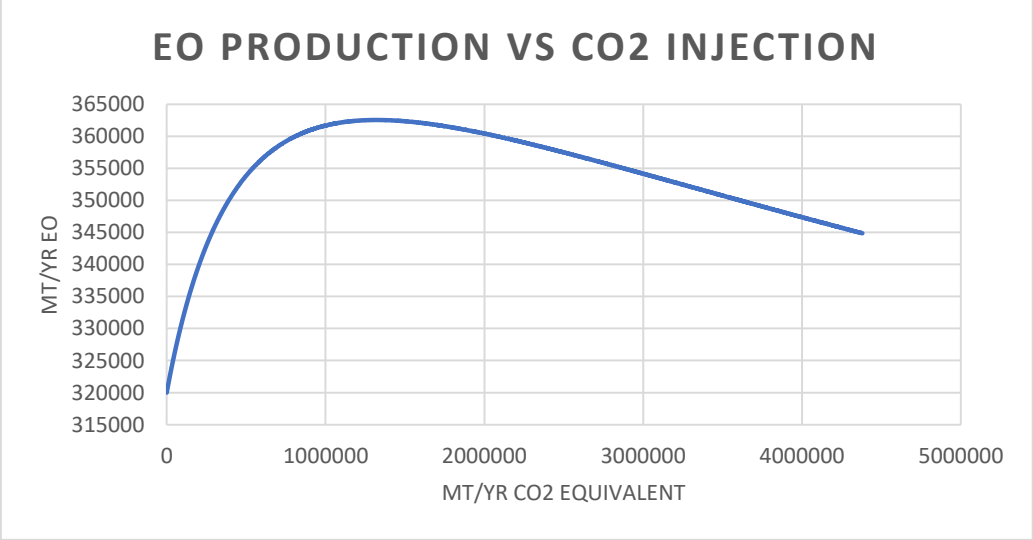

Fig. 3.2.1. Ethylene oxide production vs. carbon dioxide equivalent injection

To sum up CO2 equivalent stored or from other process streams can be injected with ethylene in forming ethylene oxide to reduce environmental emission. However, this could decrease the ethylene oxide production and overall ethylene glycol produced within the plant. So, depending on the desired amount to be produced this parameter can be manipulated to have a positive impact without any economic losses.

c. Carbon dioxide equivalent recycle

For further analysis, a carbon dioxide equivalent recycled stream was introduced into the ethylene carbonate reactor, the stream comes from ethylene glycol purification distillation column (top stream). In which CO2 equivalent reacts with ethylene oxide to form ethylene carbonate.

R-200 (Exothermic)

$$\boldsymbol{Ethylene\ oxide + CO_2 \rightarrow Ethylene\ carbonate} \qquad \text{(Equation 11)}$$

In the next step a comparison between different cases, base case, CO2 equivalent injection case, CO2 equivalent recycle case, and an integrated injection and recycle case, all in relation with the reaction step where at the end will result in overall mono-ethylene glycol production MEG.

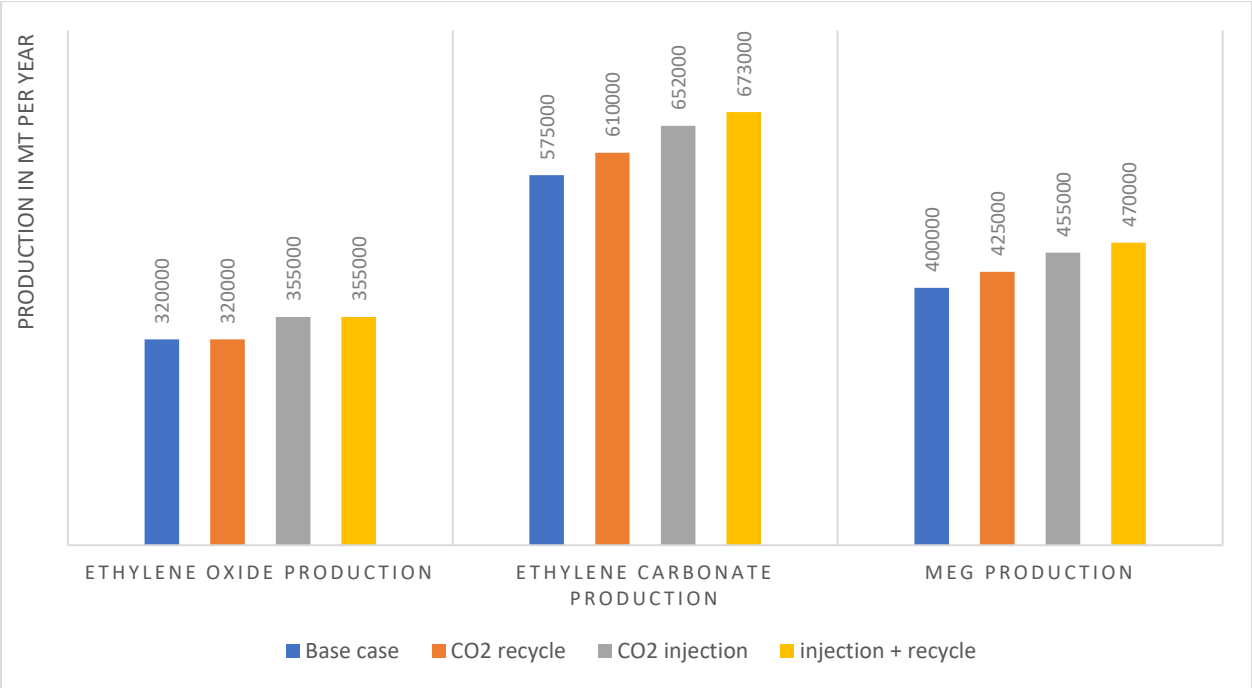

Fig. 3.3. Results of different cases on mono ethylene glycol production

The graph above was generated using excel and it summarizes the different cases that has been analyzed and the goal is to maximize the production of MEG. Starting from base case where the plant has been designed in Aspen Plus according to literature review and according to the material balances that has been done of raw materials, where production is 4,00,000 MT per year of ethylene glycol. In CO2 equivalent recycle case, where CO2 equivalent has been recycled from MEG purification column to ethylene carbonate reactor increased the overall MEG production by 25,000 MT per year. Moreover, is the CO2 equivalent injection case from other process streams where ratio of CO2 equivalent injection has been chosen accordingly with the highest ethylene oxide production as described previously and resulted in higher increase of MEG rather than CO2 equivalent recycle. With an increase from base case of 55,000 MT per year. Last but not least, an integrated case for both CO2 equivalent injection and recycle cases at the same time has the highest MEG production equivalent to 47,000 MT per year. And in such technological process design maximum production has been achieved with lowering the impacts to the environment from CO2 emissions.

4. Environmental Assessment

Environmental impact assessment (EIA) is an encyclopedic study that covers the detrimental effects on environment, living creatures and society from the emissions caused by the chemical process in the plant. The detrimental effects are mitigated by the designers with enforcing the legal by laws and environmental regulations

of the site location and country of the chemical plant. EIA usually done more than once throughout the years of the plant, where the first EIA is the baseline and the ideal calculation to measure the impacts from the process on environment. Therefore, the first EIA is used as a reference for future EIA studies regarding the same chemical plant and location. However, based on the calculations were conducted regarding the emissions, CO_2 equivalent mass emission from the plant decreased by 10.45% when CO_2 equivalent is recycled, where this is not the only method to protect the environment, however, this would be the most beneficial way to reduce the emission and the cost at the same time. The following figure has ben created to show the difference between difference of the Mass CO2 equivalent emitted between the base and recycle cases.

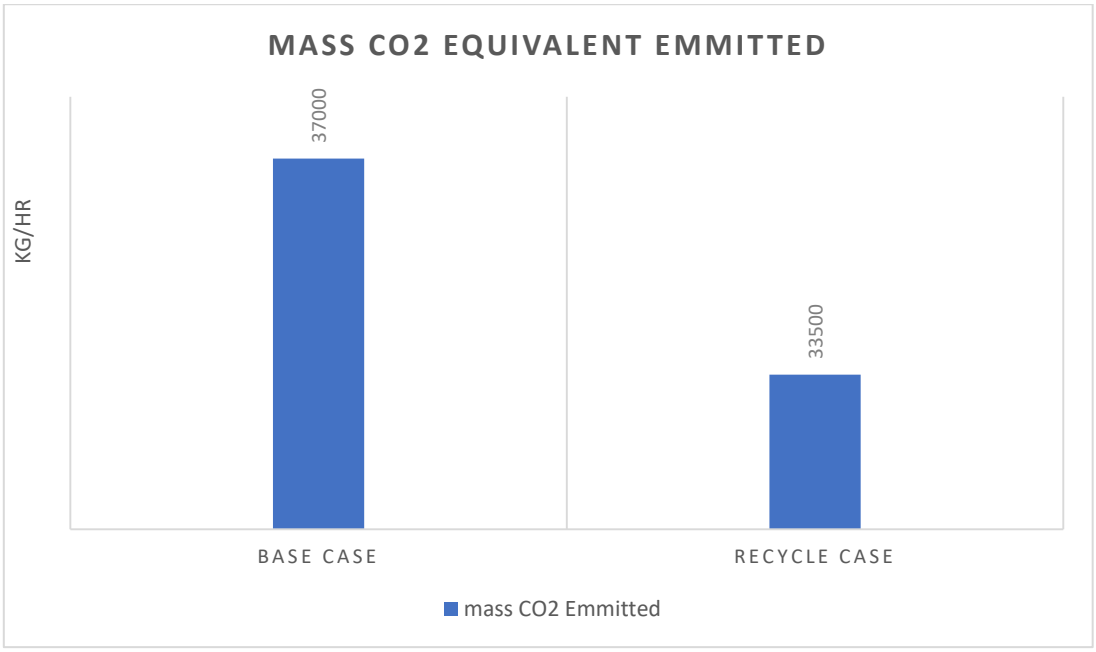

Fig. 4.1. Mass CO2 emitted

5. Economic Evaluation

The following figure illustrates the cumulative cash flow in case of CO2 equivalent recycle or injection or CO2 equivalent recycle plus injection during EG production and its impact on the total revenue. The figure was created using Microsoft Excel. The base case without recycling and injection is considered the worst-case scenario. This scenario is shown to make sure that even if the worst-case scenario will take place the plant would still be profitability attractive with around 5.8×10^9 dollars after 26 years.

After preforming the three scenarios in the economic evaluation, the best scenario was selected based on the profitability, where it will be the CO2 equivalent injection and recycle scenario. In general, some scenarios have a lower revenue than the others even though all of them are attractive. Also, the inflation rate is significant and must be operated into consideration when performing the economic studies because utility, raw material costs, and the product price are going through changes. These considerations can increase or decreases according to the market status.

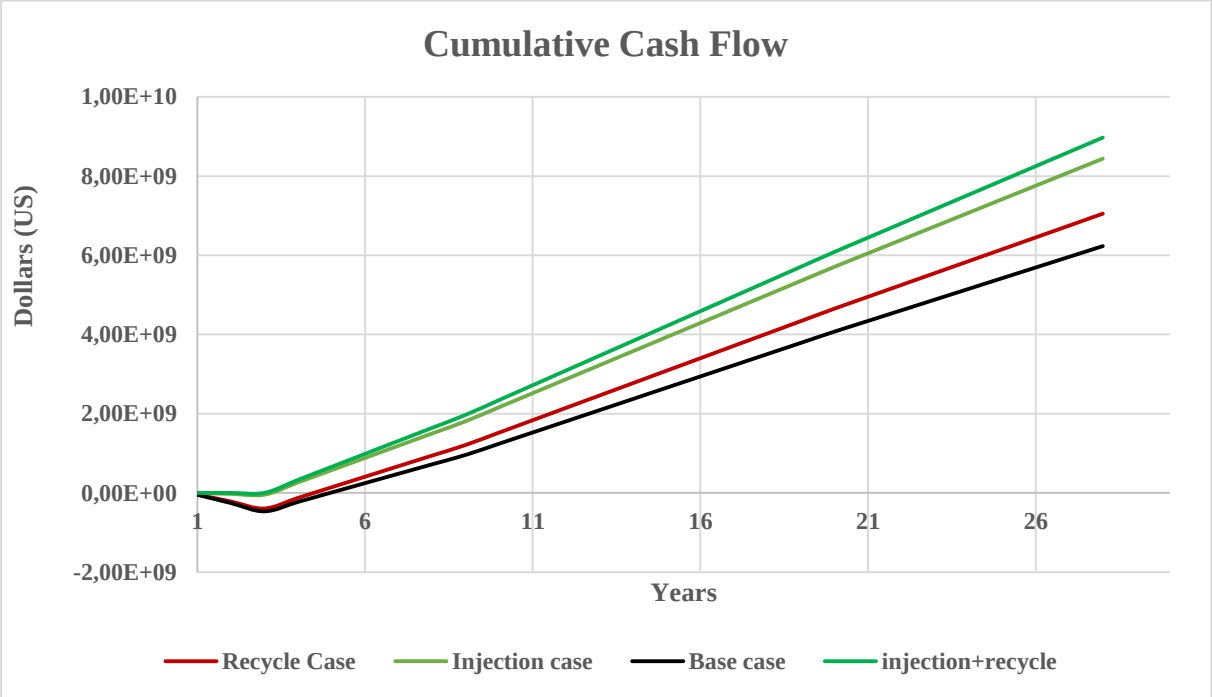

Fig. 5.1. Cumulative cash flow

6. Conclusion

In conclusion, ethylene glycol is a standout amongst the most important commercial and industrial chemical compound used in our daily life. In the other hand a detailed introduction to ethylene oxide was introduced refereeing to its main chemical properties. In the production section, a full overview for the integrated hybrid process plant supported by block flow diagram for ethylene glycol and ethylene oxide, was discussed based on the direct oxidation of ethylene and hydrolysis of ethylene oxide to produce mono-ethylene oxide and its derivatives. Moreover, economic aspects of ethylene glycol were outlined and studied using different references. All feed information and data were obtained using ASPEN PLUS, then it was verified in Excel worksheet to ensure input equal output, at last hand calculation in the report section and appendixes were outlined. Moreover, the environmental impact assessment EIA study was conducted by converting the plant utilities into fuel requirement. EIA calculation was achieved by using a simulation environment in which all fuel was introduced into a Gibbs reactor to undergo a complete combustion reaction as a result amount of nitrogen oxides, sulfur oxides, and carbon mono-oxide were found. In addition, optimizing energy is used introduced. For example, utilizing heat integration study to achieve greater results regarding the efficiency of the process using process streams to cool or heat other streams in order to reduce the amount of utility used within the plant. However, utilizing process streams would save energy and reduce the environmental damages that the plant would cause to the minimum. At the end, Economic evaluation was the final step, in which this step is very important in order to study the difference for different scenarios, where the best scenario was selected, in which the greatest revenue can be achieved after 26 years with approximately 8×10^9 dollars.

Acknowledgment

The design was done during the realization of the senior design course in 2018/19 under the supervision of Prof. Majeda Khraisheh at the Department of Chemical Engineering at Qatar University.

References

[1] Sinnot, R., & Towler, G, Chemical Engineering Design (5th ed.), Oxford: Butterworth-Heinemann, 2009.

[2] Gilbert M. Masters, Wendell P. Ela, Introduction to environmental engineering and science, Upper Saddle River, N.J. : Prentice Hall, c2008.

[3] Aspen Technology, https://www.aspentech.com/en/products/pages/aspen-hysys-dynamics, [Accessed 13 Oct. 2018].

[4] Flowchart Maker and Diagramming Software: Microsoft Visio. (n.d.). Retrieved October 16, 2018, from https://www.microsoft.com/en-us/microsoft-365/visio/flowchart-software.

[5] Dye, R. (2001). Ethylene glycols technology. Korean Journal of Chemical Engineering, [online] 18(5), pp.571-579. Available at: https://www.cheric.org/PDF/KJChE/KC18/KC18-5-0571.pdf [Accessed 18 Oct. 2018].

[6] Batiha, M. (2004). Dynamic Modelling of the Non-Catalytic Process of Ethylene Oxide Hydrolysis. Journal of Science & Technology, 9.

[7] Wan, S. (1953). Oxidation of Ethylene to Ethylene Oxide. Industrial & Engineering Chemistry, 45(1), pp.234-238.

[8] Chems.msu.edu. (n.d.). ASPEN Tutorial | Chemical Engineering and Materials Science. [online] Available at: https://www.chems.msu.edu/resources/tutorials/ASPEN [Accessed 7 Oct. 2018].

[9] Ccsassociation.org. (2018). What is CCS? – The Carbon Capture & Storage Association (CCSA). [online] Available at: http://www.ccsassociation.org/what-is-ccs/ [Accessed 25 Nov. 2018].

[10] Publications.lib.chalmers.se. (2010). Opportunities for improved heat integration in average Scandinavian kraftliner mills: A pinch analysis of a model mill. [online] Available at: http://publications.lib.chalmers.se/records/fulltext/123625.pdf [Accessed 10 Feb. 2019].

[11] Klemes, J. (2013). Handbook of process integration (PI). Oxford: WP, Woodhead Publishing.

[12] Becker, H. (2010). Energy integration of industrial sites with heat exchange restrictions. [online] Infoscience.epfl.ch. Available at: https://infoscience.epfl.ch/record/142506/files/Becker.pdf [Accessed 9 Feb. 2019].

[13] Becker, H. (2010). Energy integration of industrial sites with heat exchange restrictions. [online] Infoscience.epfl.ch. Available at: https://infoscience.epfl.ch/record/142506/files/Becker

Development of battery casing adapted to work in off - grid system in extreme temperature conditions

Mateusz Wiciak[1]; Wojciech Sułkowski[2]; Ida Wilczek[3]; Anna Granieczny[4]; Adam Miliński[5]; Filip Bienek[6]

[1]Silesian University of Technology, e-mail: matewic334@student.polsl.pl
[2]Silesian University of Technology, e-mail: wojcsul374@student.polsl.pl
[3]Silesian University of Technology, e-mail: idawilc924@student.polsl.pl
[4]Silesian University of Technology, e-mail: annagra413@student.polsl.pl
[5]Silesian University of Technology, e-mail: adammil672@student.polsl.pl
[6]Silesian University of Technology, e-mail: filibie860@student.polsl.pl

Abstract

This article provides information about the process of development that took place to create battery casing used in off-grid application for solar lamp. Project is conducted in multidisciplinary fashion that consists of material analysis, durability analysis and thermal conditions of this system, every aspect of this work provided the ability to construct innovative battery casing. In this report large group of possibilities are discussed, that contain methods of use, place of use and the positive aspects of exploring such device.

Keywords: renewable energy sources, solar lamp, off-grid, lithium ion battery

1. Introduction

Growing market for renewable energy sources is the source of creating solutions that are energy efficient and ecological. The first one that comes to mind, is exchanging common sources of light at the streets, represented by sodium lamps, with photovoltaic support. This solution helps with the reduction of energy need within the system and also smaller demand when it comes to fuel used by power plants. Nowadays there is an interesting possibility to choose between solar lamps and hybrid street lighting. Such an infrastructure is a suitable denouement in places located far away from energetic infrastructure, because of high cost of creating one. As an example pedestrian crossing, parking lot, extreme tourism are such cases, where usage of this system is meant to work like the designer created this device [1]. The key element that is responsible for long use in Polish climate, that is known for its four seasons, is the ability to secure the battery against weather conditions. To be sure that those requirements are provided, casing is considered the option to think of. Casing can help with creating conditions (inside of it) that are known to provide high efficiency and effectiveness.

The main target of this project is to create innovative casing, that secures the battery from environmental conditions, such resolution can be made by using broad knowledge, that is a mix of many different science categories and thanks to introducing the engineering software commonly used in the engineering industry. The project is divided in following parts:

Material analysis – this part is responsible for choosing the correct material for the designed casing. Parameters that are creating the array, responsible for eliminating not suitable options, are represented by e. g. thermal conductivity, Poisson ratio, Young modulus, UV ray resistance, and the last but not least possibly the lowest price.

Thermal analysis – thermal map of the inside air conglomeration, provided by CFD simulation;

Strength analysis – stress location, that is connected to used material, its thickness and also the conditions surrounding the system, are all provided by the use of finite element method used by Ansys software;

The main target to secure during the project is to obtain and provide temperatures inside of the casing within the $0 \div 20$ °C range, not depending on external conditions. Another important issue is durability in case of atmospheric

conditions. Enclosure is supposed to be mounted outside (on lantern mast), this is the guarantee for variable conditions.

Casing is designed with support of innovative solutions. The designing method enabled the use of the latest methods of manufacturing industry and energetics. The first aspect is the use of polymer materials, creating self-supporting construction is the next one. Current solutions, that are present on the market, do not serve any values, when it comes to usage and aesthetic parts of this design, although housing provided by the results of this project are going to help with attractive and well thought assembly. Placement of this shell in the upper part of the lantern mast can be beneficial in some ways, such as easy access in case of failure, montage as easy as screwing few bolts into prepared inserts. Another advantage of the housing placing is the shorter distance between solar panel, lighting assembly and the battery, which results in decreasing energy losses.

2. Project stages

2.1. Battery comparison

Very important step in the process of designing street solar lamp is the comparison of batteries. Parameters of the storage compartment are the key elements when it comes to the life span of the whole system. Gel battery is one of the most common choice, because of the high quantity of loading cycles, sometimes in short period, that this type of battery is able to withstand. AGM batteries are recommended to use in this kind of purpose – the electrolyte is enclosed in the separator made from glass fiber matt, this technology is responsible for securing the content from spilling, the main asset is higher current efficiency even considering short drainage period. Its high mass and the impact of variable habitat temperatures suggest, that this kind of battery should be placed in isolated packages underground [1].

Current state of technology market states, that li-ion batteries are getting more popular. This trend is generated by their high efficiency. Another advantage is low mass and small size, that can be supported by flexibility. Considering an off-grid system, maintenance free device is a huge asset, that is one of the merits of li-ion batteries. Durability and fast charging let li- ion storages be the best option when it comes to continuous labor. Drawback happens to be created by low outside temperatures [2].

Array created by the numerous representatives from different battery product lines were considered, all the contestants were chose to be 100 Ah batteries. Compared dimensions and masses of provided storages, some conclusions were created that stated – measurements of li- ion battery were 25% smaller and mass was reduced about three times. The comparison of the batteries is provided in Table 1.

Table 1 Comparison of properties of li-ion [3] and gel batteries [4] of 100 Ah

Akumulator	Wymiary, mm	Masa, kg
Litowo – jonowy	260 x 168 x 212	11,5
Żelowy	338 x 172 x 215	33

Considering pros and cons of batteries used in solar systems, li-ion battery was chosen. Low mass, small size, long life span and high efficiency is strongly supporting this option. All those features are the greatest influence at comfortable usage and ease of duty when it comes to failure, exchange or service.

2.2. Choice of material

Engineering design is very prone to material chosen in the process. Correctly chosen material helps in efficient management of production resources that are technologically most suitable for this manufacturing process. Considering the most important attributes of the material are resilience at extreme temperatures, mechanical

endurance and UV ray resistance. Commonly used material for battery casings is steel or other metal alloys, but considering ecological and economical aspects, different path has been taken.

2.3. **Electrical model of the solar system MATLAB + Simulink**

Matlab is a well-known software for calculations and computer simulations. In this project the Simulink add-on is used in term of control managing and electrical circuits analysis. There is a possibility to construct models using graphic interface and the simulations can be conducted with and without discretization [6].

Model created in Matlab environment provides the ability to acquire results, that are up-close to real system. Provided model helped in the process of analysis when it comes to implementation of certain battery in an off-grid system. Charts containing the characteristics of battery discharge provided by Simulink can be compared to data present at the producer's website. The created model is depicted in the picture (Fig. 3).

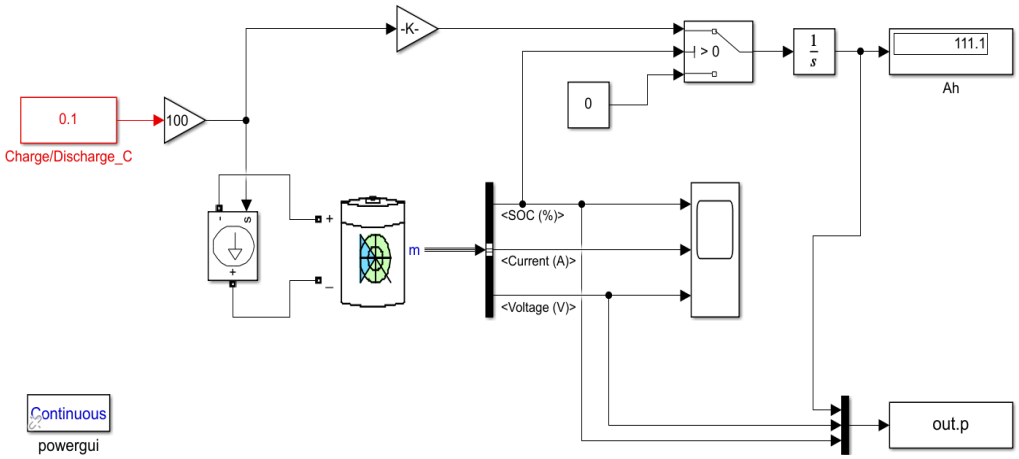

Fig 3 Control model

Comparison of the characteristics of voltage as a function of battery capacity for discharge current equal 0,1 C conducted in Matlab software with characteristics provided by producer's index card shown in the picture (Fig. 4).

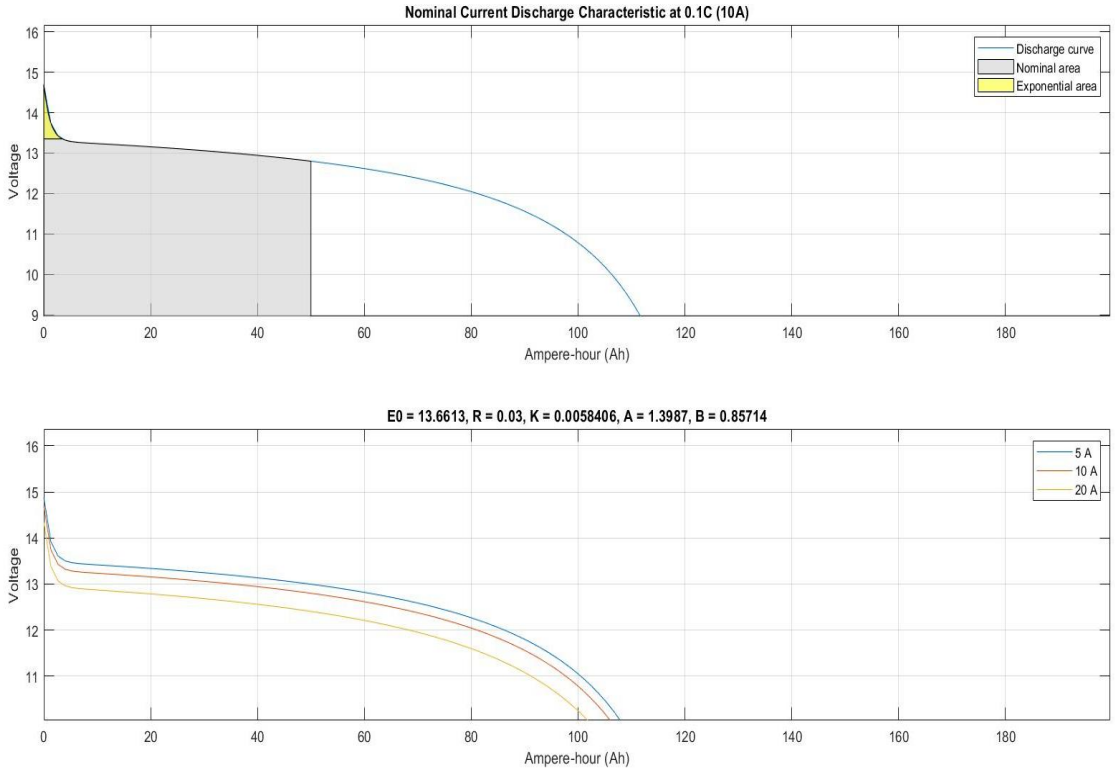

Fig 4. Characteristics of voltage as a function of battery capacity for discharge current 0,1 C

Electrical model of solar system was created (Fig. 5). It contains of charging command module, solar activity simulation, solar panel and part responsible for current usage simulation. This model mimics real usage of solar system in its natural habitat. Modelling helped with obtaining parameters, that were later used as boundary conditions for CFD analysis.

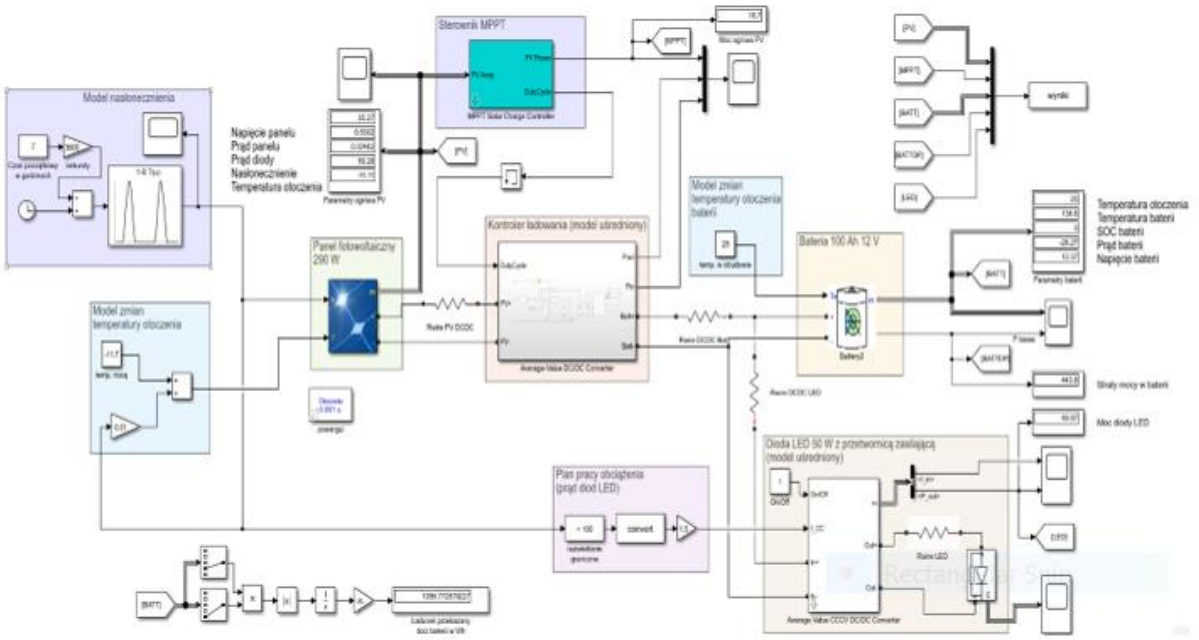

Fig 5. Electrical model of solar system

2.4.**Casing geometry**

The designed casing is primarily intended to perform a protective function and provide conditions that allow the battery to work with high efficiency - regardless of the prevailing weather conditions. In addition, the case will be self-supporting and located at the top of the lamp mast, so a unique, innovative shape of the case was designed that also takes into account its aesthetic qualities. The geometry of the housing is shown below (Fig. 6).

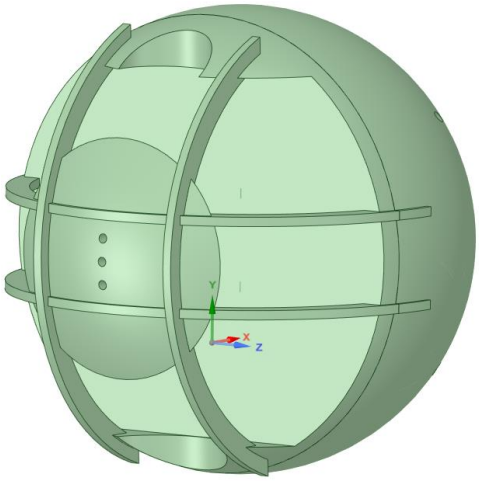

Fig 6. Geometry of the designed casing.

The model shown above has been designed with safety and ease of installation in mind. The model shown above has been designed with safety and ease of installation in mind. This is evidenced by the tapered ends and the use of locking screws to ensure a stable fit and prevent the enclosure from slipping off.

On the other hand, in the section below (Fig. 7.) you can see the use of a mounting rail, which allows for quick and easy installation of the entire set - battery and insulation. At the bottom of the inner wall there is a threshold which will reduce the forces acting on the mounting rail.

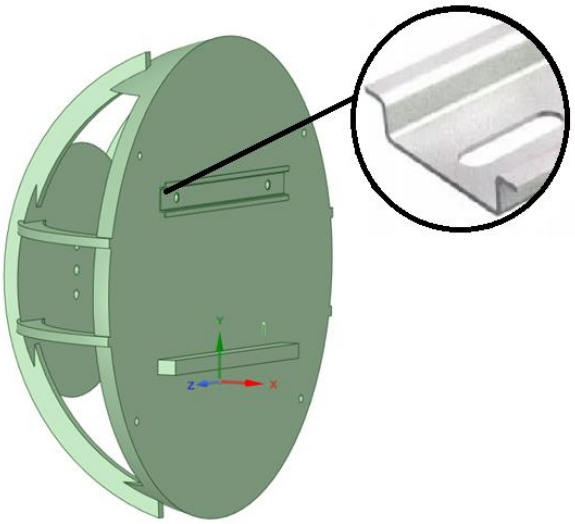

Fig 7. Mounting elements inside the casing.

2.5. **FEM Strength Analysis**

Strength analyses of structures are based on prediction of stress levels and allow for precise determination of the condition of both entire structures and individual elements already at the design stage. They also make it possible to check the deformation of the system depending on the type of loads, the method of fixing and the material parameters of the structure. This makes it possible to predict if the designed structure has enough strength and whether the material from which it is constructed is used economically. Most structures, due to their geometric complexity, need computer methods. The most common method is the Finite Element Method (FEM), in which an object is divided into many simpler pieces (finite elements). The mechanical interactions of these elements are the target of the calculations and are approximated by the computer [7].

The calculations carried out enabled issues relating to the strength properties of the casing to be considered. The total deformations (Fig. 8.), minimum (Fig. 9.), maximum and reduced stresses in the system were checked, caused by the location of the battery in the housing and the forces associated with the attachment of the housing to the mast of the solar street lamp . The values are presented in Table 2.

Table 2: Strength parameters of the casing.

PARAMETER	VALUE	UNIT
Reduced stress	27,8	MPa
Total deformation	2,6	mm
Maximum principal stress	28,5	MPa
Minimum principal stress	7,5	MPa

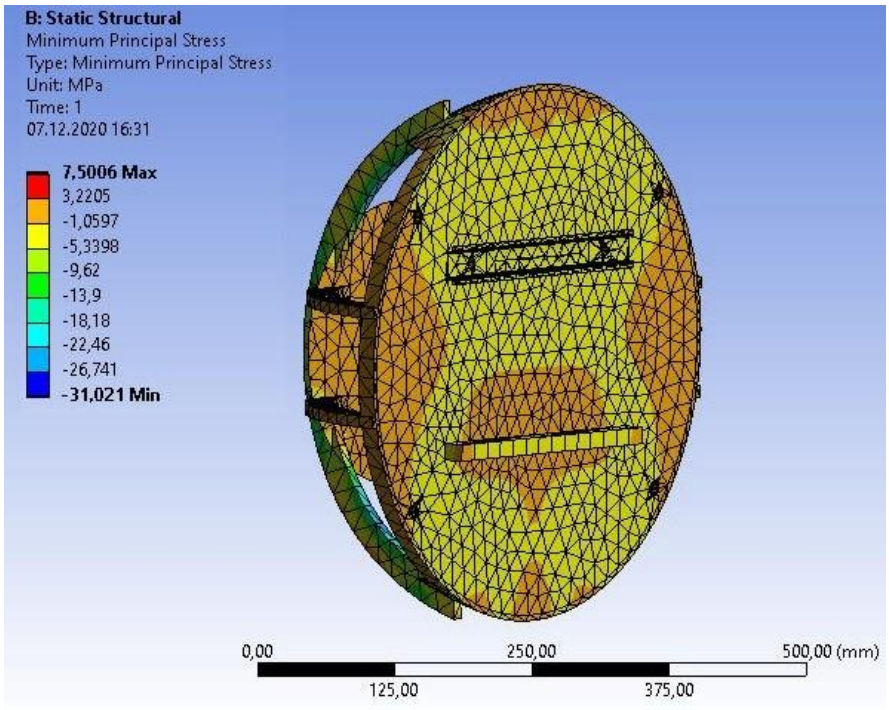

Fig 8. Distribution of the total deformation of the battery case model.

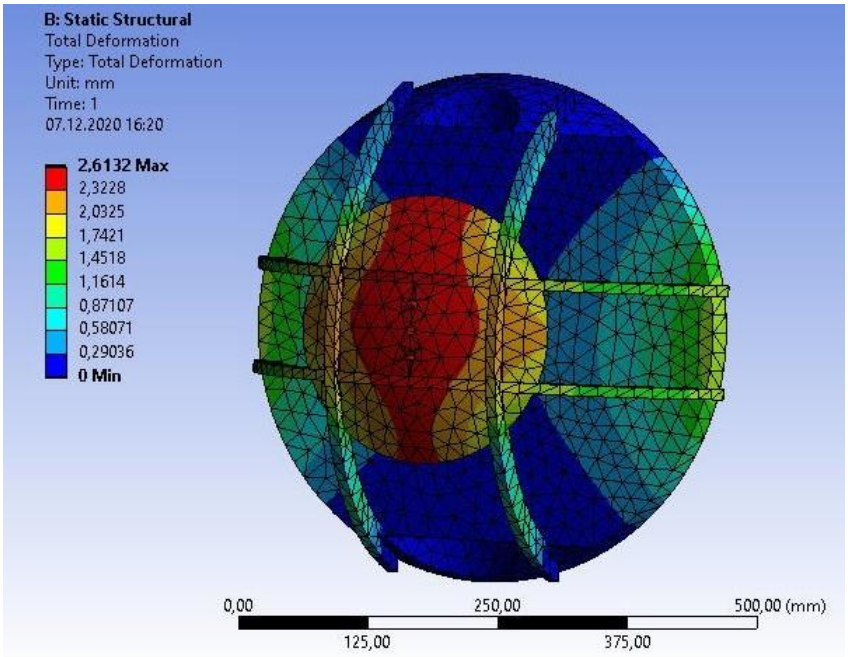

Fig 9. Distribution of minimum stress inside the battery casing model.

2.6. **Thermal analysis CFD**

Computational Fluid Dynamics is a tool for solving equations describing fluid flow using numerical methods. CFD is most often used in cases where the system behavior cannot be calculated using conventional methods, i.e. for complex designs or models that have a specific geometry. Numerical modelling of fluid mechanics is a very useful tool that helps to visualize, what would be difficult to see by other methods. By analyzing the flow of compounds in different sections, it is possible to identify problems that would be impossible to demonstrate on physical models [8].

Thermal testing of the polymer housing is intended to analyse the temperature distribution in the system on both the outside and inside of the enclosure. For this reason, the model geometry was created in Ansys Fluent. There was also a deliberate subdivision of the model geometry into smaller elements to produce a structured numerical mesh. The calculation model for natural convection is used in the system. The reason for this is that battery cooling elements are installed inside the enclosure when extremely high ambient temperatures exist. Preliminary calculations were performed to demonstrate the correct choice of calculation methods and the choice of turbulence model. Temperature boundary conditions on the casing walls were also assumed. Convergence control in the system was based on three points: monitoring residuals, checking the energy balance and monitoring parameters for natural convection at pre-selected locations where the highest temperature gradients and air velocities can be expected. Figure 10 below shows the contour temperature distribution inside the enclosure on the battery walls

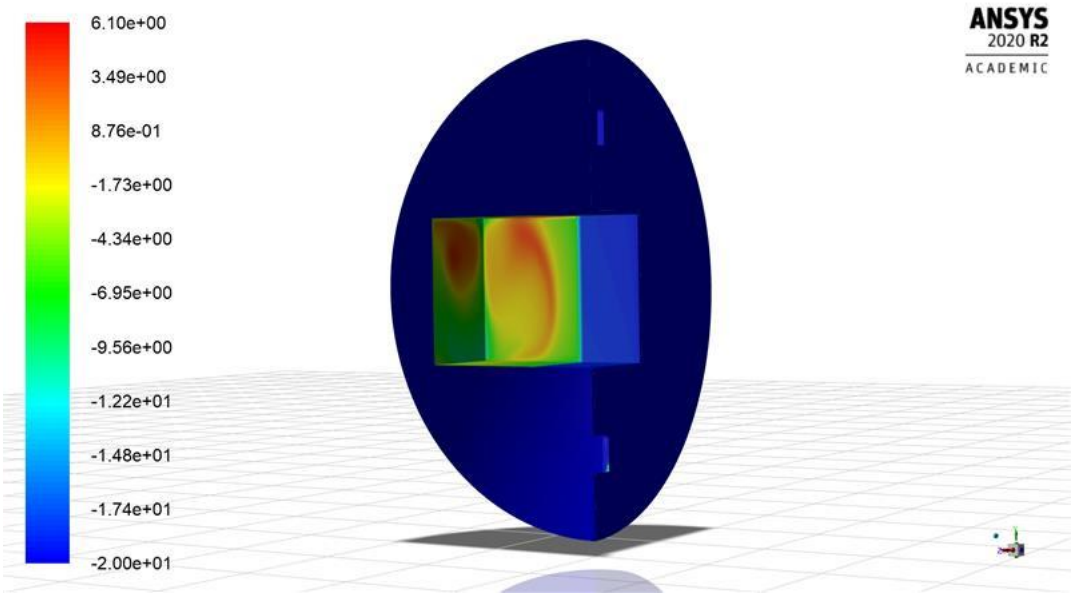

Fig 10. Contour temperature distribution inside the case on the battery walls.

3. **Conclusion**

The aim of the project is to build an innovative, self-supporting battery housing operating off - grid. The algorithm presented in the article for handling the work in the various stages is extremely innovative in terms of functionality, materials used and ensuring the thermal regime. Thanks to the solutions described in the article, it was possible to use a highly efficient lithium-ion battery, select the material and shape of the housing so as to make the project an innovative alternative to existing solar street lamp systems. The project is multidisciplinary and, due to the broad spectrum of research, is additionally carried out in multiple tracks.

The solutions used during the project make it possible to construct an enclosure that can be introduced to the general public and will find its application in the power industry. At the same time, the use of recycled polymer material has a positive impact on the environment.

Acknowledgment

The research reported in this paper was co-financed by the European Union from the European Social Fund in the framework of the project "Silesian University of Technology as a Center of Modern Education based on research and innovation" POWR.03.05.00-00-Z098/17

Special thanks go to Marek Rojczyk, PhD, for creating the project and for his constant support both in terms of content and research.

We would also like to thank the scientific staff consisting of: prof. dr hab. inż. Ireneusz Szczygieł, dr hab. inż. Grzegorz Matula, prof. w Pol. Śl.; dr hab. inż. Grzegorz Nowak, prof. w Pol. Śl; dr inż. Roman Niestrój, za pomoc w realizacji oraz wiele cennych wskazówek pozwalających na przeprowadzenie badań.

References

[1] W. Pabjańczyk, P. Markiewicz, Zasilanie oświetlenia zewnętrznego: zastosowanie systemów hybrydowych; Politechnika Łódzka, 2011

[2] P. Górecki, *Akumulatory litowe,* Elektronika Praktyczna; 3, 2015

[3] https://www.powertechsystems.eu/home/products/12v-lithium-battery-pack-powerbrick/100ah-12v-lithium-ion-battery-pack-powerbrick/

[4] https://www.akumulatory żelowe, AGM, 12V, 12V18ah, 100ah i inne - śląskie - MW Power

[5] J. Hasenauer, D., Küper, J. E. Laumeyer, I. Welsh, 10 Głównych zasad stosowanych w konstrukcji detali z tworzyw sztucznych, 2007

[6] https://www.oprogramowanie Naukowo-Techniczne

[7] G. Rakowski, Z. Kacprzyk, *Metoda Elementów Skończonych w mechanice konstrukcji;* Oficyna Wydawnicza Politechniki Warszawskiej, 2016

[8] D. Kuzmin, *Introduction to Computational Fluid Dynamics*; Institute of Applied Mathematics University of Dortmund, 2018

Fermentation method of utilization waste materials to lactic acid from food, plant and petrochemical industry

Edyta Strzelec[1]

[1]*University of Science and Technology, email: strzelec@agh.edu.pl*

Abstract

In 1780, lactic acid was identified once again as a component of sour milk. It occurs naturally and is produced by many life forms, ranging from bacteria to human cells. It is widely used in food, pharmaceutical, cosmetic and chemical forms in various forms, such as lactic acid, its salts and esters.

While the production of acid, while lactic acid has historically been produced by a chemical process, the production of more than 95% of the production of lactic acid comes from biological resources, and in the end, some of the production is sugar. It comes in various isomeric forms - the L (+) and D (-) forms. The biologically preferred L (+) form is usually obtained by microbial fermentation. Chemical synthesis of lactic acid production for the extraction of crude oil as a raw material. This is inconvenient because taking crude oil as an input material has to be reckoned with fluctuations in its price, fears of environmental aid, and also, what is in the distance from the wallpaper, with a negative source of greenhouse release during processing. These mentioned drawbacks are sufficient to eradicate the chemical formation of lactic acid.

Plastic bio-based products have received considerable attention now. Among them is PLA (Polylactic acid), i.e. a polymer of lactic acid. It is not only biodegradable, but also considered the most economically competitive. The US company Nature Works, a growth producer of PLA, increased its annual production capacity from 70,000 to 140,000 tons in 2008-2009. Compared to the traditional plastics on the petroleum platform, PLA is still more expensive and usually has the desired physicochemical and mechanical tests, which unfortunately checks global commercialization and application.

Keywords: waste, lactic acid, fermentation

1. Introduction

Lactic acid is the raw material for the production of polylactide, i.e. PLA (polylactic acid). There are three routes of lactic acid production. One of them is the body's natural, biological response to exercise. When burning calories, the human body converts substances, namely sugars, into lactic acid during exercise. It then accumulates in the muscles, and the person feels it after all the effort as the so-called "Soreness". The second option is to obtain lactic acid by chemical reaction. Japanese company Mushashino produces lactic acid from lactonitrile. It is currently unknown whether this is used. There is a question here about the profitability of such a process. Because lactic acid can be obtained in a simpler and more cost-effective way through route number three, i.e. lactic fermentation. It is a biotechnologically favorable reaction and, thanks to cooperative microorganisms, it can be carried out on a large-scale scale.

2. Raw materials using to utilization

The commercial production of lactic acid using fermentation technology mainly depends on the cost of raw material used. Therefore, it is compulsory to select a raw material for industrial production of lactic acid with a number of characteristics such as low cost, rapid rate of fermentation, lowest amount of contaminants, high yields of lactic acid production, little or no formation of by-products and availability for whole year.

In order for the biotechnological production of lactic acid to be feasible, cheap raw materials are necessary, because polymer producers and other industrial users usually require large quantities of lactic acid at a relatively low cost. Raw materials for lactic acid production should have the following characteristics: cheap, low levels of contaminants, rapid production rate, high yield, little or no by-product formation, ability to be fermented with little or no pre-treatment, and year-round availability. When refined materials are used for production, the costs for product purification should be significantly reduced. However, this is still economically unfavourable because the refined carbohydrates are so expensive that they eventually result in higher production costs. Therefore, there have been many attempts to screen for cheap raw materials for the economical production of lactic acid. Reports in the literature of recent investigations are listed on table 2.1.

Table 2.1. Literature review about biotechnological production of lactic acid from cheap raw materials [2-6]

Raw material	Organism	γ(lactic acid) g/L	Productivity g/(L·h)
Molasses	*Lactobacillus delbrueckii* NCIMB 8130	90.0	3.8
	Enterococcus faecalis RKY1	95.7	4.0
Rye	*Lactobacillus paracasei* No. 8	84.5	2.4
Sweet sorghum	*Lactobacillus paracasei* No. 8	81.5	2.7
	Lactobacillus paracasei No. 8	106.0	3.5
Wheat	*Lactococcus lactis* ssp. *lactis* ATCC 19435	106.0	1.0
	Enterococcus faecalis RKY1	102.0	4.8
Corn	*Enterococcus faecalis* RKY1	63.5	0.5
	Lactobacillus amylovorus ATCC 33620	10.1	0.8
Cassava	*Lactobacillus amylovorus* ATCC 33620	4.8	0.2
Potato	*Lactobacillus amylovorus* ATCC 33620	4.2	0.1
Rice	*Lactobacillus* sp. RKY2	129.0	2.9
Barley	*Lactobacillus casei* NRRL B-441	162.0	3.4
	Lactobacillus amylophilus GV6	27.3	0.3
Cellulose	*Lactobacillus coryniformis* ssp. *torquens* ATCC 25600	24.0	0.5
Corncob	*Rhizopus* sp. MK-96-1196	24.0	0.3
Waste paper	*Lactobacillus coryniformis* ssp. *torquens* ATCC 25600	23.1	0.5
	Rhizopus oryzae NRRL 395	49.1	0.7
Wood	*Lactobacillus delbrueckii* NRRL B-445	108.0	0.9
	Enterococcus faecalis RKY1	93.0	1.7
Whey	*Lactobacillus helveticus* R211	66.0	1.4
	Lactobacillus casei NRRL B-441	46.0	4.0

Cheap raw materials, such as starchy and cellulosic materials, whey, and molasses, have been used for lactic acid production. Among these, starchy and cellulosic materials are currently receiving a great deal of attention, because they are cheap, abundant, and renewable. The starchy materials used for lactic acid production include sweet sorghum, wheat, corn, cassava, potato, rice, rye, and barley. These materials have to be hydrolyzed into fermentable sugars before fermentation, because they consist mainly of a(1,4)- and a(1,6)-linked glucose. This hydrolysis can be carried out simultaneously with fermentation. Amylase-producing *L. amylophilus* and *L. amylovorus* are often used for the direct fermentation of starchy materials into lactic acid. Cellulosic materials have been used for lactic acid production in similar ways as starchy materials. These materials consist mainly of α-(1,4)-glucan, and often contain xylan, arabinan, galactan, and lignin. The utilization of corncob, waste paper, and wood, has been reported as well. Scientists investigated the production of lactic acid from agricultural residues such as alfalfa fiber, wheat bran, corn stover, and wheat straw. Researcher suggested that, during SSF of alfalfa fiber, lactic acid production was enhanced by adding pectinase and cellulase together. Fermentation of lignocellulosic hydrolyzate is inhibited usually by inhibitory compounds, such as furfural, 5-hydroxymethyl furfural, and acetic acid, which are generated during pre-treatment of lignocellulose. Most studies on methods to decrease this inhibition have been focused on the chemical and physical detoxification of the hydrolyzate.

Some industrial waste products, such as whey and molasses, are of interest for common substrates for lactic acid production. Whey is a major by-product of the dairy industry, and it contains lactose, protein, fat, and mineral salts.

For complete utilization of whey lactose, it is necessary to supplement whey with an additional nitrogen source. For any fermentation process, it is essential to provide nutrients to the fermentation media. Though it results in high production costs, yeast extract is the most commonly used nutrient source for the production of lactic acid.

3. Microorganisms for production of lactic acid

Microorganisms play a pivotal role in the production of lactic acid and they must be readily available and cheap. Lactic acid producing microorganisms are classified into bacteria, fungi, and yeast. Most of the lactic acid production is done industrially by the use of lactic acid producing bacteria. However, the fungal species of Rhizopus have their own advantage as they make use of glucose aerobically to produce lactic acid. But, the production rate of fungal fermentation is low due to mass transfer limitations. The Genetic engineering techniques are exploited to improve the lactic acid yield and optical purity by various microbial producers.

3.1. Fungi

Though majority of the lactic acid production activities are performed by lactic acid bacteria, some fungal species, such as Rhizopus, with their amylolytic enzyme activity, can convert starch into L(+) lactic acid. Some other advantages of fungal fermentation over bacterial fermentation include low-cost downstream process, low nutrient requirements, and formation of fungal biomass, which is an important by-product. Fungal fermentation uses chemically defined medium, and so, the purification of products is simple. This is a major advantage in food industry. Generally, ethanol and fumaric acid are the common by-products formed by fungal fermentation. The organisms of genus Rhizopus are deemed as the best fungal source for lactic acid production by fungal fermentation. Besides Rhizopus, other fungi, like, the organisms of genus Monilia and Mucor are also used in lactic acid production. The main drawback of lactic acid production by fungi is that the lactic yield is reduced as the carbon is utilized for the production of by-products besides lactic acid. The limitations of production of lactic acid by fungi also include mass transfer limitation -which results in low production rate, and requirement of vigorous aeration as it is an aerobic process.

3.2. Yeasts

All the fermentation processes require abundant amount of nutrient supply. In many of the fermentation processes, not only lactic acid, yeast is used as the key nutrient source. The major advantages of using yeast as nutrient source include their tolerance against low pH (1.5), which prevents the regeneration of precipitated calcium lactate, thereby reducing the cost of neutralization by neutralizing agents such as calcium carbonate, and their ability to grow in mineral media. The yield of lactic acid produced by fermentation with wild-type yeast as nutrient source is low. With the advent of genetic engineering, genetically modified yeasts capable of producing high yield of lactic acid have been created and they are being used successfully. The yeast of species Saccharomyces, Candida, Zygosaccharomyces, and Pichia are genetically modified to produce high yield of lactic acid. The main drawback of using yeast as a nutrient source is that it leads to increase in production costs. However, corn steep liquor, rice bran, and wheat bran can be used as alternatives for yeast.

3.3. Bacteria

Lactic acid producing bacteria are classified into four main categories, which are, Lactic Acid Bacteria (LAB), *Escherichia coli*, *Corynebacterium glutamicum*, and *Bacillus* strains. Out of these, Lactic acid bacteria are most commonly exploited. Choosing a proper strain is very important because factors such as yield, productivity, purity and nutrition requirements are dependent on it. Some of the limitations of lactic acid production by bacteria include low yield due to formation of by-product, requirement of nutrient rich medium, high risk of cell lysis, necessity of mixed strains for development of phage-resistant strains to prevent bacterio-phage infection. Lactic acid bacteria can produce lactic acid by anaerobic glycolysis with high yield and productivity. They are present in dairy products, meat, and in plants. Different bacteria grow at different conditions. In general, the optimal pH range for the growth of bacteria is

3.5–9.6 and the optimal temperature is 5–45 °C. Based on the fermentation end product, Lactic acid bacteria are grouped into two types: homofermentative and heterofermentative. Homofermentative lactic acid bacteria glucose exclusively into lactic acid by Embden-Meyerhof pathway. Hence, homo fermentative LAB are used in commercial production of lactic acid. Some of the homo fermentative lactic acid bacteria used in the production of lactic acid are *Lactobacillus delbrueckii*, *Lactococcus lactis*, *Lactobacillus casei*, *Lactobacillus helveticus*, and *Lactobacillus acidophilus*. Heterofermentative LAB produce less yield due to formation of by-products. *Lactobacillus pentosus*, *Lactobacillus bifermentans*, and *Lactobacillus brevis* are some of the examples of heterofermentative bacteria. *Enterococcus mundtii* and genetically engineered *Lactobacillus plantarum* have the capability to convert pentose sugars into lactic acid by homofermentative process. One of the key reasons for usage of lactic acid bacteria in industries is because it does not have any adverse health effects. The properties such as high acid tolerance and the ability to be engineered for selective production of D-or L-lactic acid make lactic acid bacteria commercially useful.

4. Fermentation methods

Batch, fed-batch, repeated batch, and continuous fermentations are the most frequently used methods for lactic acid production. Higher lactic acid concentrations may be obtained in batch and fed-batch cultures than in continuous cultures, whereas higher productivity may be achieved by the use of continuous cultures. Another advantage of the continuous culture compared to the batch culture, is the possibility to continue the process for a longer period of time. Reports in the literature of recent studies on the biotechnological production of lactic acid by different fermentation approaches are listed on table 4.1.

Table 4.1.Examples different fermentation of biotechnological production of lactic acid.

Organism	Fermentation mode	γ(lactic acid) g/L	Productivity g/(L·h)
Lactobacillus casei SU No 22 + *Lactobacillus lactis* WS 1042	fed-batch, coimmobilization	47.0	2.0
Enterococcus faecalis RKY1	batch	95.7	4.0
	repeated batch, cell-recycle *via* membrane	93.2	6.4
Lactobacillus rhamnosus ATCC 10863	batch	~ 120.0	2.1
	continuous, cell-recycle *via* membrane	92.0	57.0
Lactobacillus casei ssp. *rhamnosus* ATCC 11443	continuous, cell-recycle *via* immobilization	22.4	9.0
Lactobacillus delbrueckii NRRL B445	fed-batch, *in situ* removal *via* solvent extraction	~ 23.1	0.2
Lactococcus lactis IO-1 JCM 7638	batch, *in situ* removal *via* electrodialysis	~ 39.0	0.9
Lactobacillus rhamnosus IFO 3863	batch	98.0	1.9
	continuous, *in situ* removal *via* electrodialysis	~ 20.0	8.2
Lactobacillus helveticus CNRZ 303	continuous, cell-recycle *via* membrane	55.0	7.1
Lactobacillus delbrueckii CECT 286	continuous, *in situ* removal *via* ion-exchange resin	26.1	10.4

4.1.Batch fermenter

In batch fermentation, all the required materials such as carbon source, nitrogen source and other components are added prior to beginning of the fermentation process. It is the most commonly practiced fermentation process as it is simple to perform. The major advantage of batch fermentation is that it prevents contamination to a good extent when compared to the other methods as it is a closed system, and so, high concentrations of lactic acid is produced. The drawbacks of batch fermentation include low productivity due to substrate inhibition or product inhibition, and as the amount of nutrients provided is limited, low cell concentrations are obtained. Batch fermentation is mainly of two types, which are, Solid State Fermentation (SSF) and Separate Hydrolysis and Fermentation (SHF). Solid State Fermentation (SSF) is a process that occurs with no water or negligible amount of water. Natural raw materials such as wheat bran, rice bran, barley, fruit pulps, sugarcane bagasse are used as carbon source in this process. This process

is used for the production of pharmaceutical products, industrial chemicals, feed, and fuel. Soccol et al. were able to produce 137.0 g/l of lactic acid at the rate of 1.38 g/l/h by using *Rhizopus oryzae* by SSF. The usage of in solid state fermentation process produced the lactic acid yield of 0.97 g/g of recycled paper. The advantages of using solid state fermentation method include high productivity, single reaction vessel, rapid processing time, and less enzyme loading. In separate hydrolysis and fermentation process, the raw materials are first pre-treated and the unnecessary compounds, such as lignin in the case of lignocellulosic biomass, are eliminated. Then, the raw materials are subjected to enzymatic saccharification and the hydrolysate formed is subjected to fermentation. As SHF is preceded by such a hefty process for pre-treatment of raw materials, the real productivity decreases. It was reported by Marques et al. (2008) that the same *Lactobacillus rhamnosus*, which produced lactic acid yield of 0.97 g/g of recycled paper by SSF produced only 0.81 g/g when done by SHF method.

4.2. Fed-batch fermenter

In Fed-batch fermentation, all the required raw materials such as carbon source, nitrogen source, and other required components are added during fermentation process at regular intervals of time without removal of fermentation broth. This type of fermentation is especially useful to maintain low substrate concentration by supplying nutrients to the fermentation culture which in turn reduces substrate inhibition. Scientists reported that lactic acid production by *Lactobacillus casei* using fedbatch fermentation was found to be more efficient in production of lactic acid than other methods. They used 1% yeast extract and glucose as raw materials and obtained maximum lactic acid concentration of 210 g/l and L-lactic acid concentration of 180 g/l at the rate of production 2.14 g/l/h, and the yield of about 90.3% of L-lactic acid was obtained. Dong-Mei Bai et al. (2003) used *Lactobacillus lactis* for the production of L-lactic acid and obtained about 97% yield of L-lactic acid at the rate of 2.2 g/l/h.

4.3. Continuous fermenter

Continuous fermentation involves addition of fresh medium to the fermenter while withdrawing the already existing broth at the same rate. Due to this, the concentrations of substrates and products is maintained constant (Rahman et al. 2013). The advantages of continuous fermentation include prevention of end-product inhibition, less frequency to shut down, less decrease in productivity during lag phase, inoculation of culture is done once only, high product yield can be obtained, saves time and involves less labour work. Continuous fermentation suffers from a few drawbacks such as contamination, requirement of field operator with expertise, and it is expensive to perform. Shibata et al. reported the production of lactic acid at the rate of 1.56 g/l/h using Enterococcus faecium by continuous fermentation (Shibata et al. 2007). Ahring et al. reported the production of lactic acid using *Bacillus coagulans* (strain AD) at the productivity of 3.69 g/l/h using continuous fermentation (Ahring et al. 2016).

5. Conclusion

From the perspective of an expanding biotechnology, the recovery of products from waste products is becoming an important point in reducing disposal costs in industrial processes. The glycerin market has wide prospects for its use in order to obtain useful products, on the paths of chemical and biotechnological transformation. The many default pathways described in the text for bio-conversion pathways have advantages, but the current mapping solution is considered in the industry as competitive chemical methods. Cost and process economics are an issue. By confronting the possibilities of biotechnology has a significant advantage.

The uses for glycerin waste continue to expand. The above examples show the valuable products obtainable from this process. It is still a research topic that remains largely untapped. An additional aspect is the development of more and more common white biotechnology. In this field of science, microorganisms are used that are involved in the creation of many valuable chemical products. Biotechnological methods largely prevail over chemical methods. The basis is

the possibility of avoiding the disadvantages resulting from the use of catalysts or the purification and preparation of the raw material. This significantly reduces the cost of technology and contributes to conscious waste management.

References

[1] Manandhar A. et al., Processes, 8,199, 2020.

[2] Rahman M. et al., Journal of Biotechnology, Vol. 156, 4, 286-301, 2011.

[3] Dong-Mei Bai et al., Biotechnology Letters, 25, 1833-1835, 2003.

[4] Shibata K. et al., Enzyme Microbiol. Technol., 41, 149-155, 2007.

[5] Marques S. et al., Biochem. Eng Journal, 41, 210-216, 2008.

[6] Ahring K. et al., Biochemical Engineering Journal, 109, 162-169, 2016.

[7] Soccol C. et al., Bioresource Technology, 2002.

[8] Krishna B. S. et al., International Journal of Biotech Research, 1, 1, 2018.

[9] Ghaffar T. et al., Journal of radiation research and applied science, 7, 222-229, 2014.

[10] Wee Y.-J. et al., Food Technol. Biotechnol., 44, 2, 163-172, 2006.

[11] Ogmundarson O. et al., Bioenergy, 12, 19-38, 2020.

[12] Komesu A. et al., Bioresources, 12, 2, 4364-4383, 2017.

Preliminary model of chloride diffusion processes in concrete.

Agnieszka Ciesielska[1], Michał Szeremeta[2]

[1]Silesian University of Technology, email: ines.ciesi@gmail.com
[2]Silesian University of Technology, email: michal.szer@op.pl

Abstract

One of the main causes of reinforced and prestressed structural failure is exposure to high concentrations of chloride ions along with water. It initiates corrosion of the steel rebar placed inside concrete structure. Such failures may be dangerous and require a lot of money to rebuild the damaged construction. To predict the penetration of chloride ions into concrete, the numerical model is developed by means of the Fluent ANSYS software. The mesh is discretized on the 2D geometry of the concrete element which consists of many pores different in size. The boundary conditions are specified on the top of the geometry and at the bottom of the structure. The User Defined Function (UDF) was written in the C language as an auxiliary model used to specify the boundary condition for the chloride ions migration at the bottom of the structure to maintain the homogenous penetration of chloride ions through the whole porous concrete structure. Numerical results were compared with the experimental solutions in order to show the reliability of the numerical model of chloride ions penetration through the porous concrete structure.

Keywords: numerical modelling, corrosion, UDF, concrete

1. Introduction

Depending on the environment conditions, the service time of the unreinforced structure can be long [1]. To enhance the structure, the steel reinforcement is embedded in concrete. Reinforced and prestressed constructions are the basis of the modern construction and offer remarkable strength parameters and relative ease of use.

The concrete structure consists of many pores which are filled with an aqueous solution with different ions. The pH of concrete varies between 12 and 13, which is characteristic for alkaline solutions [2]. Inside the micropores of concrete, high concentration of Ca, Na and Mg hydro- and oxides is observed which create a dense passive layer on the steel reinforcement surface. It is a natural form of the steel protection inside a concrete structure. That passive layer does not stop the corrosion process, it decreases its rates significantly [2].

Concrete with the steel rebar inside is exposed to different environmental stresses such as varying temperature, humidity, carbonation or chloride ions penetration. These can cause the corrosion process which results in the spalling of concrete cover. It happens when the pH of the concrete decreases to around 8. As the pH becomes less alkali, the steel starts to corrode and the passive layer is broken down resulting in the rust on the surface of the steel rebar. The rebar then increases its volume which can reach 10 times higher value than the original one. An increase in volume exerts high stress on the concrete cover which initiates the cracks formation and subsequently falling of that cover [3].

2. Corrosion process

Steel as a not naturally occurring material has some energy, added to the metal during its production. Under normal atmospheric conditions steel is thermodynamically unstable, hence it releases energy resulting in the return to its normal state in the form of iron oxides [2]. Such a process is commonly known as corrosion.

Corrosion is nothing more than an electrochemical process in which negatively charged electrons are exchanged between species or ions.

The first step of a corrosion is a chemical reaction called the redox reaction. Behind that name stands the oxidation of chemical specie(s), during which electrons are released and are transferred in the direction where the reduction reaction is taking place.

2.1. **Redox reaction**

During redox reaction the oxidation state of atoms changes by means of electrons transfer between chemical species (flow of charges). Oxidation reaction does not exist without reduction reaction. Redox reactions take place simultaneously even if there is a lack of current flow. In redox reactions there are two agents, one is called oxidizing agent (oxidizer) the other reducing agent (reducer). Reducer, as the name indicates, reduces the oxidation state of one species, while oxidizer increases that state of another specie.

Place where oxidation takes place is called anode, whereas the one for the reduction is named cathode. Redox reaction occurs in a presence of an electrolyte, being eg. moisture or rainwater trapped in a concrete structure. It is a solution in which a substance is dissolved in a polar solution – water. The dissolved substance splits into positive and negative ions being cations and anions, respectively, spread over the whole solution. Sodium chloride is the simplest example of such substance and it is the main source of steel corrosion in many countries.

In concrete structure some spots behave as anode, hence the metal oxidation occurs. Those spots are the active sites of the steel rebar embedded in a concrete [1, 2].

During oxidation electrons are released from the area of lower electrical potential into the area of higher electrical potential by means of the electrical potential difference. The released electrons are then used to reduce chemical species. The lower the electrical potential (i.e. more negative value) the stronger the reducer is and more active metal (anode), whereas for cathode it happens inversely [4].

2.2. **Mechanism of steel corrosion in concrete**

Corrosion (Figure 1) usually takes place at the anode and occurs in many different steps. During the first step, in a solution present in pores surrounding the rebar, steel is oxidized to a higher oxidation state releasing 2 electrons (Reaction 2.1) [4].

$$Fe_{(s)} \rightarrow Fe^{2+}_{(aq)} + 2e^- \tag{2.1}$$

These electrons are then used in the reduction process which leads to a hydroxide ions formation, OH^- (Reaction 2.2) [4].

$$2e^- + H_2O + \frac{1}{2}O_2 \rightarrow 2OH^- \tag{2.2}$$

The next step for corrosion is the rust formation, which can be shown in one of the commonly known way, where hydrated ferric oxide (so called rust) is formed (Reaction 2.3c) through the formation of ferrous- (Reaction 2.3a) and then ferric hydroxide (Reaction 2.3b).

$$Fe_{(s)} + 2OH^- \rightarrow Fe(OH)_2 \tag{2.3a}$$

$$4Fe(OH)_2 + O_2 + 2H_2O \rightarrow 4Fe(OH)_3 \tag{2.3b}$$

$$Fe(OH)_3 \rightarrow Fe_2O_3 \cdot H_2O + H_2O \tag{2.3c}$$

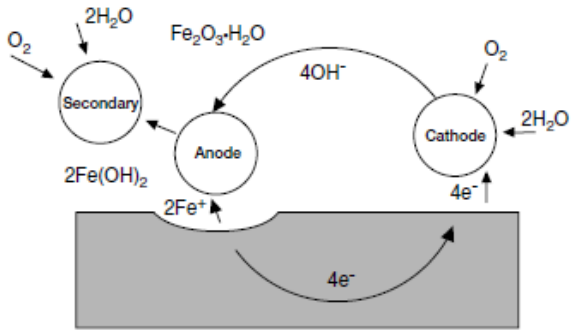

Fig 1. Corrosion occurring on the steel rebar [2].

2.3. **Corrosion products**

As it was mentioned earlier, the corroded steel increases in volume. The result can be seen by virtue of the brittle in color rust in the cracks of concrete. During corrosion, different products are formed by oxy-hydroxide phases. The most common ones are: lepidocrocite (γ-FeOOH), which transforms into geothite (α-FeOOH) and the third is magnetite (Fe_3O_4). The others are maghemite hydrate (γ- $Fe_2O_3 \cdot H_2O$) and hemalite (Fe_2O_3). Both, α-FeOOH and Fe_3O_4 are located in inner layer of the rust layer, while γ-FeOOH is seen more in the outer layers [1, 2].

The first corrosion product $Fe(OH)_2$ is the first diffusion barrier to go through for the oxygen. When the oxygen content is low, lepidocrocite reduces to magnetite (Reaction 2.4) [5].

$$8FeOOH_{(s)} + Fe^{2+}_{(aq)} + 2e^- \rightarrow 3Fe_3O_{4_{(s)}} + 4H_2O \qquad (2.4)$$

The more nonhomogeneous steel rebar structure, the faster the corrosion in microcells/local cells occurs [4]. The corrosion on the rebar stops as soon as FeOOH is consumed completely [6].

2.4. **Corrosion causes**

Chloride ions are the main cause of the steel corrosion. The main source of chlorides in the concrete is the exposure to salt (eg. spread on the roads) and seawater but also chlorides used in the concrete mix with too high concentration than in the specifications. The chlorides migrate deep through the concrete structure and meet the oxygen and moisture causing steel corrosion. The chloride ions content which causes the corrosion in the concrete must be limited. There are different concrete limits around the world. For instance, in the EU the chlorides content must be less than 0.02% for a reinforced one. On the other hand, in the US it should be smaller than 0.07%. There are two values of chloride concentration involved in corrosion, the first one which starts the corrosion, the second after which the concrete cover spall. The concentration equal to 0.1-0.3 % is considered as the critical chlorides concentrations [7].

2.5. **Diffusion coefficient**

Chloride ions migration through the porous concrete structure can be described as a diffusion process. Rate of this process can be described by chloride diffusion coefficient which depends on the concrete quality. Mathematically, the chloride penetration can be described by Fick's second law in a form of the diffusion equation (Eq. 1) [8]:

$$\frac{\partial X}{\partial \tau} = \frac{\partial}{\partial x}\left[\Gamma(X)\frac{\partial X}{\partial x}\right] \qquad \text{(Equation . 1)}$$

Where,

X the chloride concentration, (-),

τ	time, (s),
x	the spatial variable,
Γ(X)	the diffusion coefficient, (m^2/s).

It can be rewritten in a form as follows (Eq. 2 and Eq. 3) [8]:

$$\frac{\partial \rho_{Cl-}}{\partial \tau} = \Gamma \nabla^2 \rho_{Cl-} \quad \text{(Equation . 2)}$$

$$\rho_c \frac{\partial X}{\partial \tau} = \Gamma \nabla^2 \rho_c X \quad \text{(Equation . 3)}$$

Where,	ρ_{Cl-}	the chloride ions concentration in concrete, (kg Cl-/kg of concrete),
	ρ_c	the density of concrete, (kg/m^3),
	$\rho_c \Gamma$	the calculated diffusion coefficient, (m^2/s).

3. ANSYS Software [9]

Corrosion takes some time and to determine its progress and influence on the concrete structure with embedded steel rebar, the numerical modelling using ANSYS software. It allows one to predict the rate of chloride ion penetration into the concrete. To create such numerical model, few crucial steps are required, being:

- Model for the Cl^- transport.
- UDF for the rebar swelling and reaction – written in C language and included in Fluent ANSYS Software.
- UDF in pores to see how the convection process occurs inside the pores, how intensive it will be.
- Final model of all above.

In this paper, only the results of the first step are shown. The rest will be shown in the paper dedicated for the whole project conducted by Zofia Szweda (SUT, Gliwice, Poland).

3.1. Design Modeler

The geometry was created in the Design Modeler. The geometry being investigated is the 2D model with the dimensions equal to 100x100 mm. It is a porous concrete structure with embedded steel rebar of the diameter equal to 12 mm. The number of pores for that model was selected randomly, just for the representation of the porous character of concrete (Figures 1-2).

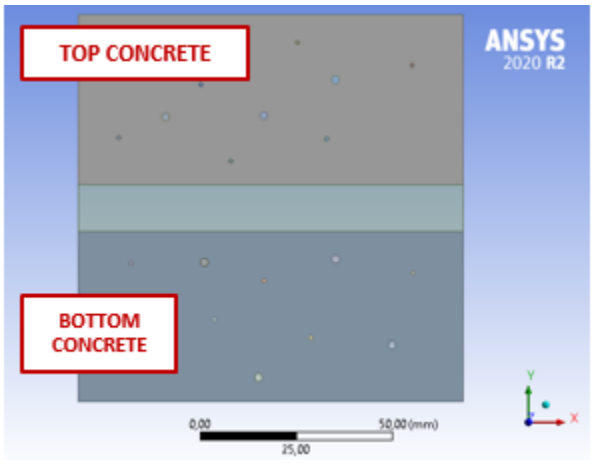

Fig 2. 2D geometry of a segment of reinforced concrete.

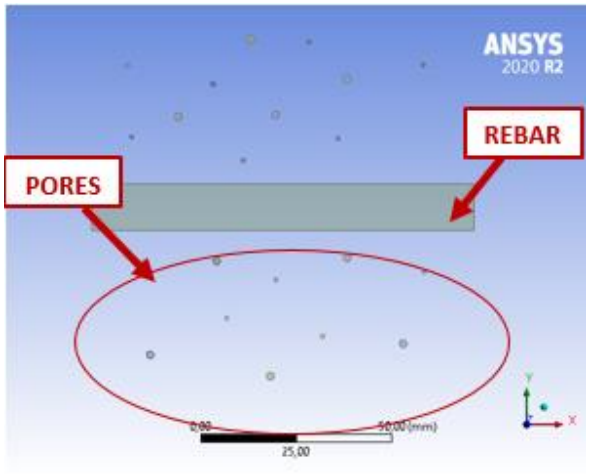

Fig 3. Rebar and pores in the 2D model.

3.2. **Mesher**

Mesh plays an important role for the whole computation process. The geometry being investigated has been discretized into a certain number of elements. The better connected, denser the mesh is, the more exact and reliable are the results and less time a calculation process takes. Due to the fact that we are focused on what happens with the rebar and pores along with the surface of the concrete, in such places the mesh has been made denser. For the top and bottom part of concrete structure, the triangular mesh was used, while for the rebar quadrilateral (Figures 3-4).

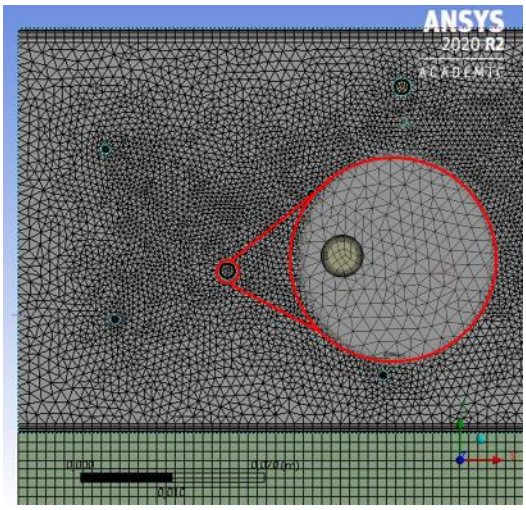

Fig 4. Part of the mesh of 2D geometry (the top of concrete) with pores.

3.3. Fluent

In the Fluent ANSYS software, all required data was assigned. The density for pores, concrete and rebar were set as 1000, 2400 and 8030 kg/m^3 (Fluent Database) respectively.

The diffusion coefficient for the concrete has been taken based on the research [7] and equals 2e-10 m^2/s. The diffusion coefficient in steel was selected to be 5 orders smaller than the value for concrete, whereas for pores it was assumed 5 orders higher.

For the top of the concrete geometry, as a boundary condition, the chlorides concentration was taken as 0.007833 kg Cl/kg of concrete, based on the calculations according to the experimental analysis results.

To set the boundary condition at the bottom part of the concrete, there was a need to create the User Defined Function (UDF) with the help of the Visual Studio which is compatible with ANSYS Fluent. It was required to maintain the migration around the rebar. For that, the DEFINE_PROFILE macro was used with a loop over all faces in the boundary thread and returns modified boundary condition to the algorithm (APPENDIX I).
In the next step, the UDF was compiled with Fluent ANSYS Software, the value of 0.007833 for User Defined Scalar (UDS) at the top boundary condition was set. All calculations were performed and the obtained results were compared with those taken from the experimental analysis supervised by the team of Zofia Szweda. To see the chloride ions penetration progress, calculations were performed for 1 years, 3, 6 and 10 years. The second part was to obtain values and compare them with those obtained experimentally for 35 days (840 h) [7]. Based on that, the simulation time was set for 35 days (840 h) with the time step size equal to 300s.

- **Results**

From each of the numerical calculations, the chloride ions penetration was obtained in order to show its progress within the concrete depth. The contours of the concrete segment for 1 year, 3, 6 and 10 years of the obtained chloride ions penetration can be seen (Figures 5-9) with the closer look to the vicinity of selected pore for 10 years (see Figure 10.). From these contours one may see that the chloride ions reach the steel rebar after 10 years.

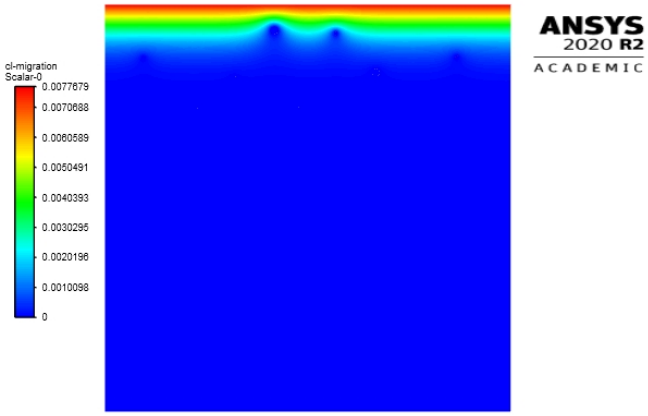

Fig 5. Chloride concentration in concrete segment after 1 year.

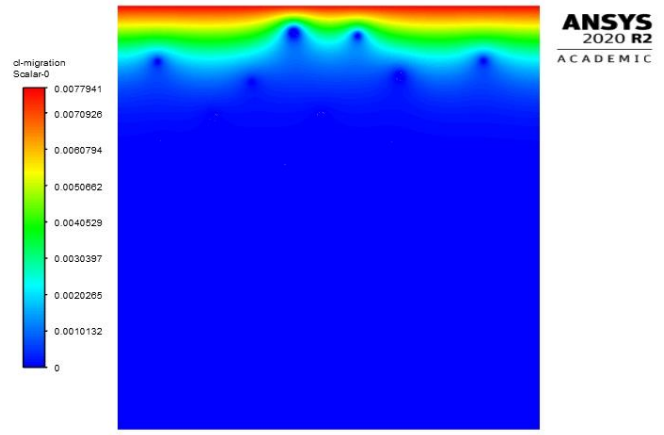

Fig 6. Chloride concentration in concrete segment after 3 years.

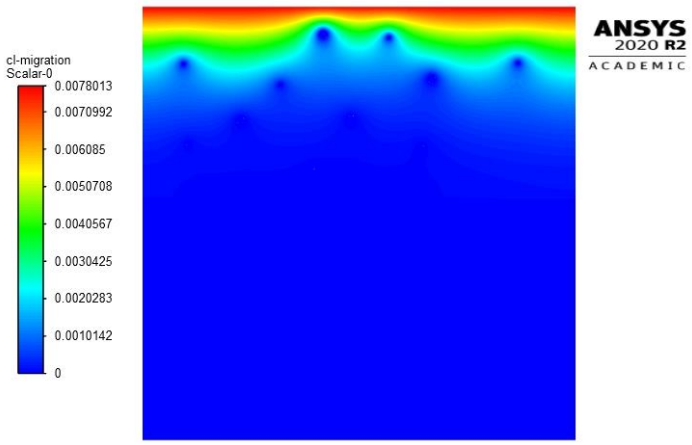

Fig 7. Chloride concentration in concrete segment after 6 years.

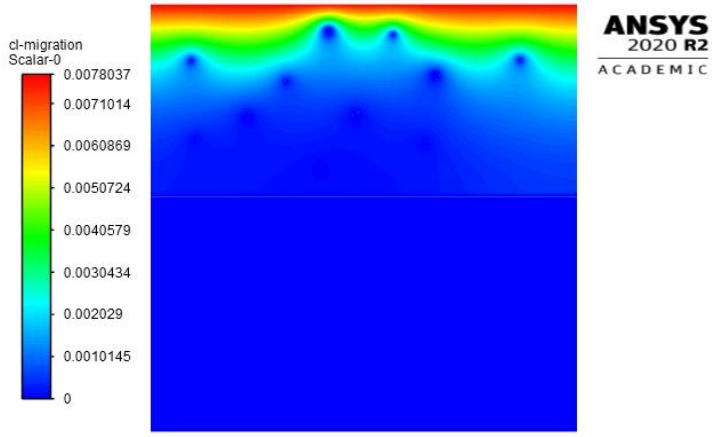

Fig 8. Chloride concentration in concrete segment after 10 years.

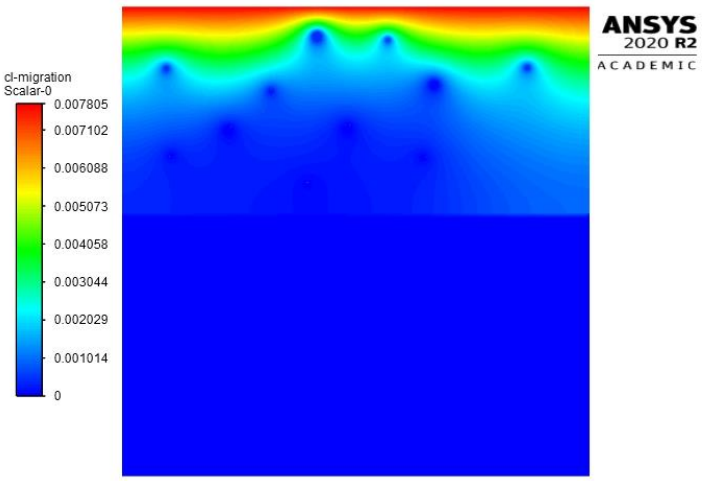

Fig 9. Chloride concentration in concrete segment after 15 years.

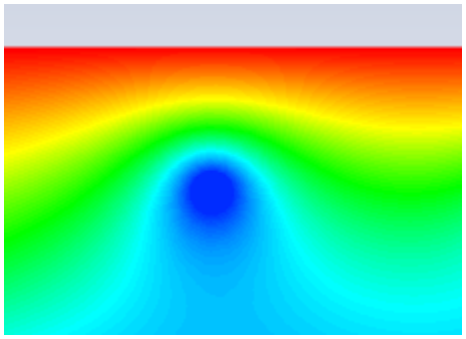

Fig 10. Chlorides concentration in the vicinity of selected pore after 10 years.

The results from the second part were obtained for the vertical line passing the whole geometry structure in half width. For the purpose of this study the experimental results were taken as a good comparison for the numerical results obtained in ANSYS Fluent software. Both were matched and can be seen on the Figure 11. It can be concluded that the tendency of both results is quite similar.

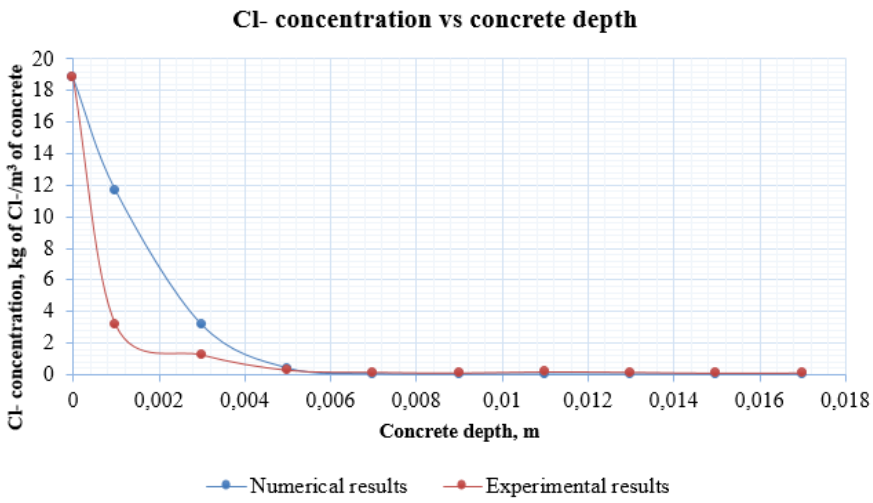

Fig 11. Comparison of obtained chloride concentration at various concrete depth (experimental and numerical results).

4. Conclusion

In this paper the attempts of numerical modelling of 2D geometry of the porous concrete with embedded steel rebar were described. The geometry created in the Design Modeler was shown together with its discretization using the Mesher Software. The User Defined Function for the chloride ions migration was written in C language with the help of the Visual Studio environment.

The simulation for 1 year, 3, 6, 10 and 15 years were done with the compiled UDF in order to check after what time chloride ions will reach the steel rebar. That information is significant for further development of the numerical model to predict the rate of chloride ions penetration through the porous concrete structure. The UDF was then assigned to the bottom wall of the concrete in order to get the homogeneous profile of chloride ions concentration throughout the concrete material in a given time.

The numerical results were extracted and compared with the experimental ones. The values of the chloride ion concentration per cubic meter of concrete within the depth of the structure for both are more likely identical. The small difference may arise due to the fact that not the real geometry of the specimen was taken as a geometry to be discretized used in the numerical analysis performed in the ANSYS Fluent software. Such step can be done in the further step of the project.

That work is important for the next milestones of the project, where the UDF for pores will be implemented to see how intense the convection process would be along with the UDF for the swelling and reaction assigned on the steel rebar.

It is possible to simulate the real chloride ions transport through the porous concrete structure. Such a model can be then used to predict the material failure resulting from the corrosion of a steel rebar in a concrete structure since the ions diffusion might take many years in real life. Consequently, that model could give a fast verification of the material being investigated to avoid corrosion disasters.

Acknowledgment

I would like to thank the project team, especially Zbigniew Buliński, from the Silesian University of Technology (SUT) in Gliwice, Poland, Faculty of Energy and Environmental Engineering and Zofia Szweda from SUT, Gliwice, Poland,

Faculty of Civil Engineering. This study is the part of the project realized as the Project Based Learning (PBL) Vth Edition: Silesian University of Technology as a Center of Modern Education based on research and innovation POWR-03.05.00-00-Z098/17-00 co-financed by the European Union with funds from the European Social Fund.

References

[1] Yuxi Zhao, Weiliang Jin, *Steel corrosion – Induced Concrete Cracking*, 2016, ISBN: 978-0-12-809197-5.

[2] Portland Cement Association (PCA), *Types and Causes of Concrete Deterioration,* Concrete Information, 2002.

[3] R. Winston Revie, Herbert H. Uhlig, *Corrosion and Corrosion Control –An Introduction to Corrosion Science and Engineering*, 4th Edition, 2008, ISBN 978-0-471-73279-2.

[4] V. S. Bagotsky, *Fundamentals of Electrochemistry,* 2nd Edition, ISBN-13 978-0-471-70058-6.

[5] R. Vera, M. Villarroel, A.M. Carvajal, E. Vera, C. Ortiz, *Corrosion products of reinforcement in concrete in marine and industrial environments*, 2008, Elsevier.

[6] Yong-sheng Ji, Meng Wu, Zhongchao Tan, Furong Gao, Fang Liu, *Process control of reinforcement corrosion in concrete. Part 2:Time-dependent dominating factors under different environmental conditions,* 2014, Elsevier.

[7] Zofia Szweda, Zbigniew Buliński, *Application of inverse methodology to estimate chloride diffusion coefficient in precast concrete of HC prestressed concrete slabs.*

[8] Bulinski Z., Orlande H.R.B, *Estimation of the non-linear diffusion coefficient with Marcov Chain Monte Carlo method based on the integral information*, International Journal of Numerical Methods for Heat & Fluid Flow, Vol. 27 Issue: 3, pp.639-659, (2017).

[9] ANSYS User's Guide.

APPENDIX I

```
/* include header file which stores definition of all Fluent specific variables, data and macros*/
#include"udf.h"
DEFINE_PROFILE(cl_bottom, t, i)
{
        real cl = 0.007833;                 /* cl- concentration at the top of the concrete structure*/
        Thread t0;                          /*indicator to the structure of a surface area*/
        cell_t c0;                          /*cell's index*/
        face_t f;                   /*variable of an integer type, face ID*/
        begin_f_loop(f, t)/* loop over all faces in the boundary thread */
        {
        t0 = THREAD_T0(t);          /*ID of cell area*/
        c0 = F_C0(f, t);            /*ID of cell surface */
        cl = C_UDSI(c0, t0, 0);     /* returns value of variable scalar inside the cell*/
        F_PROFILE(f, t, i) = cl;    /*returns modified boundary condition to the algorithm*/
        }
        end_f_loop(f, t)
}
```

The following publication consists of articles presented during the Environmental Protection and Energy Conference at Silesian University of Technology in Gliwice, 11th December 2020

The release is a result of the "learning by doing" approach of students of the Faculty of Energy and Enviromental Engineering.

KTiUZO

Silesian University of Technology

EPAE 2020
Environmental Protection & Energy Conference